

Interrogating novel functions of the I kappa B kinases via CRISPR-Cas9 gene editing and small molecule inhibition

Jack Andrew Prescott

Jesus College, University of Cambridge

The Babraham Institute



This dissertation is submitted for the degree of Doctor of Philosophy

September 2017

Summary

The NF- κ B signalling pathway is a critical mediator of the cellular responses to inflammatory cytokines. The I κ B kinase (IKK) complex, which is composed of two catalytic subunits (IKK α and IKK β) and one regulatory subunit (IKK γ /NEMO) acts as the master regulator of NF- κ B transcription factor activity. Seminal genetic studies in knockout (KO) mouse embryonic fibroblasts (MEFs) have defined two pathways of NF- κ B activation; a canonical pathway, activated in response to cytokines such as TNF α /IL-1 β , that requires NEMO and predominantly IKK β catalytic activity; and a non-canonical pathway, activated in response to a subset of TNF-family cytokines, which requires IKK α and NIK kinase.

We have generated and validated CRISPR-Cas9 IKK α , IKK β and IKK α / β DKO HCT116 colorectal cancer cell lines to interrogate novel functions of the I kappa B kinases in colorectal cancer, including the relative contributions of these kinases to the activation of NF- κ B signalling pathways downstream of TNF α induction. Contrary to the seminal studies in KO MEFs, IKK α appeared to make a more significant contribution to canonical NF- κ B induction in these cells than IKK β . Western blot studies demonstrated that both IKKs contributed to the phosphorylation and degradation of I κ B and the phosphorylation of the NF- κ B subunit, p65 at Serine 536. However, high-content immunofluorescence studies demonstrated that IKK α KO cells were defective in TNF α -induced nuclear translocation of p65 compared to WT and IKK β KO cells. Additionally, NF- κ B-driven luciferase reporter assays showed that IKK α , but not IKK β , KO cells exhibited significantly reduced NF- κ B-dependent gene expression following TNF α stimulation. We also have evidence to suggest that the phosphorylation site at Serine 468 on p65, previously defined as an IKK β -dependent site, is in-fact an IKK α -dependent site in these cells. Furthermore, IKK α knockout revealed a potentially important role for IKK α activity in preventing the stabilisation of NIK protein following prolonged TNF α stimulation.

RNA sequencing analysis of wild-type, IKK α KO, IKK β KO and IKK α / β DKO cells stimulated with TNF α was performed to identify genes whose expression were differentially deregulated by IKK KO. These analyses confirmed the importance of IKK α for canonical NF- κ B gene expression. Furthermore, IKK β knockout had unexpected effects on the expression of a broad range of genes involved in chromatin organisation, cytoskeletal organisation, mitotic cell cycle control and the DNA damage response.

During the characterisation of IKK KO cells it was discovered that the expression of NEMO was downregulated at the protein, but not mRNA level by approximately 50% in IKK α KO cells and 90% in IKK α / β DKO cells. IKK β KO cells, meanwhile, exhibited wild-type NEMO expression. Emetine-chase and radioactive pulse chase labelling experiments demonstrated that the half-life of NEMO in IKK α and IKK α / β DKO cells was significantly shortened due to enhanced proteasomal turnover. Bioinformatics analyses predicted significant regions of intrinsic structural disorder within NEMO, particularly at the N- and C-termini, the former of which overlapped with the IKK binding domain. On this basis, the susceptibility of NEMO to in vitro degradation by the 20S proteasome was examined, with NEMO proving to be a highly effective substrate of the 20S proteasome. Importantly, IKK α and IKK β were both shown to protect NEMO from proteasomal degradation, leading us to propose a model whereby interaction with IKK kinase subunits sequesters/masks intrinsically disordered regions in NEMO that would otherwise make NEMO a highly effective substrate for ubiquitin-dependent and/or ubiquitin-independent proteasomal degradation.

BMS-345541 is a commercially available allosteric inhibitor of IKK β that has been used extensively in numerous studies, including a report that proposed novel functions for IKK β in mitotic cell cycle progression (Blazkova et al., 2007). Similar antiproliferative effects to those reported by Blazkova et al., were observed during the characterisation of a novel ATP-competitive inhibitor of IKK β , AZD2230. In depth characterisation of the selectivity of AZD2230 and BMS-345541, however, revealed that the antiproliferative effects of AZD2230 and BMS-345541 are, in fact, due to off-target inhibition, potentially at the level of RNA Polymerase II C-terminal domain phosphorylation, and hence general transcription.

Collectively, these studies reveal novel functions of the IKK kinases in NF- κ B signalling and inform therapeutic strategies for targeting chronic canonical NF- κ B activation in colorectal cancer.

Declaration

This thesis contains original work that has not previously been submitted for a degree or diploma or other qualifications at the University of Cambridge or any other University or similar institution. It is the result of my own work and contains nothing which is the outcome of work done in collaboration with others, except as specified in the text and acknowledgements. The length does not exceed the limit as stated in the Memorandum to Graduate Students. The dissertation does not exceed the limit of 60 000 words imposed by the Cambridge University Faculty of Biology Degree Committee.

Jack Prescott

Acknowledgements

I would like to extend a huge thank you to my supervisor Simon Cook for his guidance, support, words of wisdom and encouragement over the past four years. Thank you, also, for accommodating my somewhat last-minute approach to thesis draft writing (!), and always being quick to return thoughtful comments/revisions. I could not have asked for a more well-informed supervisor, particularly when it came to the subject of shock-defeats and embarrassing moments in the history of Liverpool FC! Thank you also to my co-supervisor at AstraZeneca, Paul Smith, for his insight throughout my PhD and feedback on this thesis.

A huge thank you to my mentor Kathy Balmanno for all the techniques she taught me and advice she gave me along the way. I am also grateful to all the other fantastic members of the Cook lab, from whom I have learnt a great deal, and who made the many long days running Western blots a touch more bearable! Particular thanks to Becky, Pam and Anne for their patience in answering all my questions and assistance with new techniques over the years. I am also grateful to Simon Walker and Hanneke Okkenhaug for help with various imaging techniques.

I was also lucky to make many great friends at the Babraham Institute and Jesus College over the past four years, who helped keep me from becoming too much of a crazy lab hermit. Special thanks to Steph, for so many reasons, not least for keeping calm when I couldn't. Thanks too to the other Biotech Yes/SYMBLS/grad committee guys, Azad, Joana and Marco; let's never work together again! Thanks to the other Babraham guys, Jo, Stephen, Lina and Michiel, the Jesus Grad football guys, Luke B, Luke S, Tomo, Ricardo, Miles, Dave and everyone else I've made friends with along the way.

Finally, an enormous thank you to my amazing family, Andy, Clare and Emily, and our two dogs, Coco and Tilly, for their endless love and support. I couldn't have made it to where I am today without them.

Acknowledgement of assistance received during the course of this thesis

1. Initial training in techniques and laboratory practice and subsequent mentoring

Annexin V staining – Matthew Sale.
Flow cytometry training – Rachel Walker.
General laboratory practice – Kathryn Balmanno.
InCell high-throughput confocal image analysis – Hanneke Okkenhaug.
Immunoprecipitation – Kate Stuart.
Molecular biology training – Becky Gilley and Pamela Lochhead.
Tissue culture training – Kathryn Balmanno.
Western blotting training – Kathryn Balmanno.

2. Data obtained from a technical service provider

RNA sequencing library preparation, sequencing and raw data analysis (differential gene expression analysis) – Cambridge Genomic Services.

3. Data produced jointly

None.

4. Data/materials provided by someone else

For materials provided by others, see Materials and Methods.

Figure 4.12 was performed by Nadav Myers, The Weizmann Institute, Israel.

Abbreviations

aa	Amino acid
ABIN	A20 binding and inhibitor of NF- kappa B
ABC	Activated B cell
ADP	Adenosine diphosphate
AKT	v-akt murine thymoma viral oncogene homologue 1
ANKR	Ankyrin repeats
ANOVA	Analysis of variance
APC/C	Anaphase promoting complex or cyclosome
AP1	Activator protein 1
ASK1	Apoptosis signal-regulating kinase 1
ATM	Ataxia-telangiectasia mutated
ATP	Adenosine triphosphate
ATR	Ataxia telangiectasia and Rad3 related
BAFF	B-cell activating factor
B-TrCP	Beta-transducin repeat-containing protein
BCL-XL	B-cell leukaemia/lymphoma extra large
BCV	Biological coefficient of variation
BRAF	v-raf murine sarcoma viral oncogene homologue B1
BSA	Bovine serum albumin
C	Cysteine
CAC	Colitis-associated carcinoma
CAF	Cancer associated fibroblasts
Cas9	CRISPR associated protein 9
CC	Coiled coil
CCNA	Cyclin A
CCNB	Cyclin B
CCNE	Cyclin E
CCND	Cyclin D
CD40	Cluster of differentiation 40
CD40L	CD40 ligand
CDH1	Cadherin 1, E -cadherin
CDH2	Cadherin 2, N-cadherin
CDK	Cyclin-dependent kinase
CDS	Coding sequence
ChIP	Chromatin Immunoprecipitation
Chk1	Checkpoint kinase 1
CHUK	Conserved Helix-Loop-Helix Ubiquitous Kinase

CI	Confidence interval
cIAP	cellular inhibitor of apoptosis protein-1
CMA	Chaperone mediated autophagy
COMM1D	Copper Metabolism MURR1 Domain-containing Protein 1
CPM	Counts per million
CRC	Colorectal cancer
CRISPR	Clustered regularly interspaced short palindromic repeats
CSF	Colony-stimulating factor
CTD	C-terminal domain
CV	Coefficient of variance
CYLD	Cylindromatosis
D	Aspartate
DDR	DNA damage response
DE	Differential gene expression/Differentially expressed
DKO	Double knockout
DLBCL	Diffuse large B-cell lymphoma
DMS	Dimethyl sulphoxide
DNA	Deoxyribonucleic acid
dsRNA	Double-stranded RNA
DUB	Deubiquitinase
E	Glutamate
ECM	Extracellular matrix
EDA-ID	Ectodermal dysplasia with Immunodeficiency
EGF	Epidermal growth factor
EGFR	Epidermal growth factor receptor
EMSA	Electrophoretic mobility shift assay
EMT	Epithelial-mesenchymal transition
ERK	Extracellular signal-regulated kinase
EV	Empty vector
FACS	Fluorescence activated cell sorting
FADD	FAS associated death domain protein
FBS	Fetal bovine serum
FC	Fold-change
FGF	Fibroblast growth factor
FLIP	FLICE like inhibitory protein
FOXO	Forkhead box
G1	Growth or gap phase 1
G2	Growth or gap phase 2

GCK	Germinal centre kinase
GFP	Green fluorescent protein
GLUT	Glucose transporter
GO	Gene ontology
GRR	Glycine rich region
gRNA	Guide RNA
GST	Glutathione S-transferase
GSK	Glycogen synthase kinase
GST	Glutathione S-transferase
HAT	Histone acetyltransferase
HCC	Hepatocellular carcinoma
HDAC	Histone deacetylase
HNPCC	Hereditary non-polyposis colorectal cancer
HLH	Helix-loop-helix
HSP	Heat-shock protein
IBD	IKK-binding domain or Inflammatory bowel disease
IDP	Intrinsically disordered protein
IDR	Intrinsically disordered region
IEC	Intestinal Epithelial Cell
IFN	Interferon
IGF	Insulin growth factor
IGF1R	Insulin growth factor-1 receptor
IκB	Inhibitor of NF-κB
IKBKB	IκB kinase β
IKK	IκB kinase
IL	Interleukin
ILR	Interleukin receptor
iNOS	Inducible nitric oxide synthase
IRAK	Interleukin-1 receptor-associated kinase
JNK	c-Jun N-terminal kinase
K	Lysine
KO	Knockout
KD	Kinase dead, Kinase domain
kDa	Kilodalton
KRAS	Kirsten rat sarcoma
L	Leucine
LB	Luria broth

LPS	Lipopolysaccharide
LTβR	Lymphotoxin-beta receptor
LZ	Leucine zipper
M	Methionine
MALT1	Mucosa Associated Lymphoid Tissue-1
MAPK	Mitogen activated protein kinase
mORF	Molecular recognition feature
MCL1	Myeloid cell leukemia 1
MDS	Multidimensional scaling
MEF	Mouse embryonic fibroblast
miRNA	Micro-RNA
MM	Multiple myeloma
MnSOD	Manganese superoxide dismutase
MOMP	Mitochondrial outer membrane permeabilisation
mRNA	Messenger RNA
mTOR	Mammalian target of rapamycin
mTORC	Mammalian target of rapamycin complex
NBD	Nemo-binding domain
NEMO	NF- κ B essential modulator , IKK γ
NES	Nuclear export sequence
NF-κB	Nuclear factor kappa B
NIK	NF-kappa-B-inducing kinase
NK	Natural killer
NLS	Nuclear localisation sequence
NMR	Nuclear magnetic resonance
NSCLC	Non-small cell lung cancer
ODC	Ornithine decarboxylase
P	Proline
p-	phospho-
PAGE	Polyacrylamide gel electrophoresis
PARP	Poly (ADP-ribose) polymerase
PBS	Phosphate buffered saline
PCA	Principle component analysis
PCR	Polymerase chain reaction
PDB	Protein data bank
PEST	Rich in proline [P], glutamic acid [E], serine [S], and threonine [T]
PI	Propidium iodide
PI3K	Phosphatidylinositol-3 kinase

PIAS	Protein inhibitor of activated STAT
PID	Processing inhibitory domain
PIP2	Phosphatidylinositol-3,4-bisphosphate
PIP3	Phosphatidylinositol-3,4,5-trisphosphate
PRR	Proline rich region
PTEN	Phosphatase and tensin homologue
qRT-PCR	Quantitative reverse-transcription PCR
Q-Vd-OPh	Quinoline-Val-Asp-Difluorophenoxyethyl Ketone
RANK	Receptor Activator of Nuclear Factor κ B
RB	Retinoblastoma
RHD	Rel-homology domain
RHIM	RIP homeotypic interactive motifs
RIPA	Radioimmunoprecipitation assay
RIP1	Receptor-interacting protein 1
RNA	Ribonucleic acid
RNAP	RNA polymerase
ROS	Reactive oxygen species
rRNA	Ribosomal RNA
S	Serine
SAPK	Stress-activated protein kinase
SD	Standard deviation
SDD	Scaffold/dimerization regulatory domain
SDS	Sodium dodecyl sulphate
SHARPIN	Shank Associated RH domain Intermediate Protein
siRNA	Small interfering RNA
SCF	Skp, Cullin, F-box
SMRT	Silencing mediator for retinoid or thyroid-hormone receptors
SNAI1	Snail family zinc finger 1
SNAI2	Snail family zinc finger 2
SRR	Signal responsive region
SUMO	Small ubiquitin-like modifier
T	Threonine
TAX1BP1	human T-cell leukemia virus type I binding protein 1
TG	Tris-glycine
T&T	Transcription and translation
TAD	Transcription activation domain
TAK1	Transforming growth factor beta-activated kinase 1
TAM	Tumour-associated macrophage

TBK1	TANK Binding Kinase 1
TBS	Tris-buffered saline
TBST	Tris-buffered saline with Tween
TCA	Trichloroacetic acid
TGF	Transforming-growth factor
Th	T-helper
TLR	Toll-like receptor
TME	Tumour microenvironment
TNF	Tumour necrosis factor
TNFSR	Tumour necrosis factor superfamily
TNFR	Tumour necrosis factor receptor
TPL2	Tumour progression locus 2
TRADD	TNFR associated death domain protein
TRAF	TNF receptor-associated factor 1
Ub	Ubiquitin
UBA	Ubiquitin-associated
UBAN	Ubiquitin binding in ABIN and NEMO
UBD	Ubiquitin-binding domain
ULD	Ubiquitin-like domain
UTR	Untranslated region
WT	Wild-type
Y	Tyrosine
ZEB1	Zinc finger E-box binding homeobox 1
ZNF	Zinc-finger

Contents

Chapter 1. Introduction	2
1.1 Cancer	2
1.1.1 Hallmarks of cancer	2
1.1.2 Cell cycle control and cancer	2
1.1.3 Epithelial to mesenchymal transition and cancer	4
1.1.4 Inflammation and cancer.....	5
1.2 TNF receptor family signalling	7
1.2.1 Overview.....	7
1.2.2 TNFR1 signalling.....	7
1.2.2.1 TNF- α -induced cell death.....	7
1.2.2.2 TNF- α -induced JNK and p38-MAPK signalling.....	10
1.3 NF- κ B signalling.....	11
1.3.1 Overview.....	11
1.3.2 Canonical NF- κ B signalling	12
1.3.2.1 The IKK complex	12
1.3.2.2 Mechanism of IKK activation	15
1.3.2.3 Mechanisms of feedback inhibition	19
1.3.2.4 NF- κ B-independent functions of IKK kinases.....	20
1.3.3 The NF- κ B transcription factor family.....	22
1.3.3.1 Structure, dimerization and binding to DNA	22
1.3.3.2 Transcriptional activity and function.....	23
1.3.3.3 Post-translational modifications of NF- κ B subunits	26
1.3.4 I kappa B proteins	28
1.3.4.1 Overview.....	28
1.3.4.2 The classical I κ B proteins	29
1.3.4.3 The precursor I κ B proteins	31
1.3.4.4 The atypical I κ B proteins	32
1.3.5 The non-canonical NF- κ B pathway	32
1.3.6 Atypical NF- κ B pathways	35
1.4 NF- κ B signalling in cancer	37
1.4.1 Overview.....	37
1.4.2 Mechanisms of constitutive NF- κ B activation in cancer.....	37
1.4.3 Deregulated IKK/NF- κ B is capable of influencing all of the hallmarks of cancer.....	39
1.4.4 NF- κ B and inflammation in colorectal cancer	42
1.4.5 The NF- κ B pathway as a target in cancer therapy.....	45
1.5 Aims	47
Chapter 2. Materials and methods.....	49
2.1 Equipment and reagents	49
2.1.1 Laboratory suppliers	49
2.1.2 Pharmacological inhibitors	51
2.1.3 Solutions	51
2.1.4 Antibodies.....	53
2.1.5 siRNA oligo's	56
2.1.6 qPCR primers	56
2.1.7 Plasmids.....	57

2.2	Cell Lines and culture.....	57
2.2.1	Colorectal cancer cell lines	57
2.2.2	Cell culture medium	58
2.2.3	Routine cell culture.....	59
2.2.4	Cell line storage	59
2.3	Cell treatments	59
2.3.1	Drug treatments	59
2.3.2	RNA interference	59
2.4	DNA and RNA manipulation.....	59
2.4.1	Plasmid recovery and transformation	59
2.4.2	Plasmid preparation	60
2.4.3	Genomic DNA isolation.....	60
2.4.4	Genomic RNA isolation.....	60
2.4.5	cDNA preparation	60
2.4.6	Site-directed mutagenesis.....	60
2.5	Preparation of whole cell lysates.....	61
2.6	SDS-PAGE and Western Blotting.....	61
2.7	Subcellular fractionation	62
2.8	Immunoprecipitation.....	62
2.9	Flow cytometry	62
2.9.1	Propidium Iodide staining and DNA content analysis	62
2.9.2	Annexin V staining	63
2.10	Radioactivity based assays.....	63
2.10.1	Tritiated thymidine Incorporation assay	63
2.10.2	Radioactive pulse-chase assay.....	63
2.10.3	<i>In vitro</i> 20S proteasomal degradation assay	64
2.11	Quantitative Reverse-transcription PCR	64
2.12	Cellular imaging	64
2.12.1	Light microscopy.....	64
2.12.2	Immunocytochemistry.....	64
2.12.3	High-content confocal image acquisition and analysis.....	65
2.13	CRISPR-Cas9 gene knock-out	65
2.13.1	guide RNA design and selection	65
2.13.2	CRISPR-Cas9 plasmid transfection	66
2.13.3	FACS sorting.....	66
2.13.4	Mutant clone screening.....	68
2.13.5	Sequencing gRNA binding site of candidate KO clones	68
2.14	RNA Sequencing.....	69
2.14.1	RNA isolation and quality control.....	69
2.14.2	3' mRNA library preparation and sequencing	69
2.14.3	Bioinformatic analysis.....	69
2.15	Luciferase-reporter assay	70
2.16	Cyquant proliferation assay	70
2.17	Bioinformatic analysis.....	70
2.17.1	Disorder prediction tools.....	70
2.17.1.1	D ² P ² database consensus tools.....	70

2.17.1.2	DisEMBL.....	71
2.17.1.3	PrDOS.....	71
2.17.1.4	DISOPRED3	71
2.17.1.5	MFDp2	71
2.17.2	PEST motif finder	71
2.17.3	mORF prediction tools.....	71
2.17.3.1	DISOPRED3	71
2.17.3.2	ANCHOR.....	71
2.17.3.3	mORFpred.....	72
2.17.3.4	MoRFCHIBI SYSTEM	72
2.17.3.5	DisoRDPbind	72
2.17.4	ChemMapper	72
Chapter 3. Generation, validation and characterisation of CRISPR-Cas9 IKKα, IKKβ and IKKα/β knockout HCT116 cell lines		74
3.1	Introduction.....	74
3.2	Results.....	76
3.2.1	Generation and characterisation of CHUK (IKK α) and IKBKB (IKK β) knockout and IKK α/β double knockout HCT116 CRISPR-Cas9 cell lines.....	76
3.2.2	Validation of IKK knockout reveals a prominent role for IKK α in canonical NF- κ B signalling downstream of TNF α	82
3.2.3	Re-expression of either IKK α or IKK β in IKK α/β DKO cells restores TNF α -inducible NF- κ B transcriptional activity.....	94
3.2.4	IKK α KO cells exhibit a greater defect in TNF α -induced p65 nuclear translocation than IKK β KO cells.....	98
3.2.5	Loss of IKK α is also more detrimental to IL-1 α induced NF- κ B signalling than loss of IKK β	101
3.2.6	IKK kinase knockout has differential effects on the activation of AKT signalling following sustained TNF α treatment.....	106
3.2.7	Colorectal cancer cell lines exhibit basal NIK/IKK α -independent p100 processing.....	113
3.2.8	IKK α KO and IKK β KO cells exhibit differences in the TNF α -dependent regulation of non-canonical NF- κ B pathway signalling components	117
3.3	Discussion	121
3.3.1	IKK knockout has no effect on the growth or survival of HCT116 cells.	121
3.3.2	IKK α plays a major role in canonical NF- κ B signalling in response to TNF α and IL-1 α in HCT116 cells.....	122
3.3.3	The cross-talk between NF- κ B and AKT signalling pathways is altered by knockout of the IKK kinases	125
3.3.4	IKK α knockout results in aberrant TNF α -induced NIK expression.....	126
Chapter 4. NEMO undergoes rapid proteasomal degradation in the absence of the IKKs		130
4.1	Introduction.....	130
4.2	Results	134
4.2.1	Loss of IKK subunits cause a reduction in NEMO expression at the protein, but not mRNA, level	134
4.2.2	NEMO protein has a shorter half-life in IKK DKO cells, potentially due to enhanced proteasomal degradation	139
4.2.3	NEMO is predicted to contain substantial regions of intrinsic disorder, a proportion of which may be stabilised upon protein binding	143
4.2.4	NEMO is susceptible to rapid proteolysis <i>in vitro</i> by the 20S proteasome and is protected from degradation by interaction with IKK α or IKK β	152

4.2.5	Reduced NEMO expression does not account for the lower TNF α -induced NF κ B activation observed in IKK α KO cells or the inability of re-expressed IKK to induce the degradation of I κ B α in DKO cells.....	154
4.2.6	Overexpressed NEMO undergoes less polyubiquitylation when co-expressed with IKK α	157
4.3	Discussion	161
4.3.1	IKK expression is necessary for wild type NEMO protein expression.....	161
4.3.2	NEMO is a protein with significant regions of intrinsic disorder.....	163
4.3.3	The mechanism by which the IKK kinases promote NEMO stability remains to be determined	165
Chapter 5. Assessing the potency and selectivity of I kappa B kinase β inhibitors		170
5.1	Introduction.....	170
5.2	Results	171
5.2.1	The novel, highly potent IKK inhibitor, AZD2230, and the structurally unrelated IKK inhibitor, BMS-345541, induce a proliferative arrest and cell death response in HCT116 cells.....	171
5.2.2	AZD2230 and BMS-345541 induce similar changes in the expression of cell cycle regulators .	174
5.2.3	The observed anti-proliferative and cell-death inducing effects of both AZD2230 and BMS-345541 are off-target effects.	176
5.2.4	AZD2230 and BMS-345541 both inhibit RNA Polymerase II C-terminal domain phosphorylation, possibly due to off-target inhibition of Cyclin-dependent kinases.....	186
5.2.5	Bioinformatic analyses of AZD2230 and BMS-345541 chemical structure highlight additional possible targets of off-target inhibition.....	195
5.3	Discussion	200
5.3.1	AZD2230 and BMS-345541 have off-target effects on cell cycle progression.....	200
5.3.2	AZD2230 and BMS-345541 may block global transcription through off-target inhibition of RNA Polymerase II C-terminal domain phosphorylation.....	202
Chapter 6. RNA-sequencing analysis of TNFα-inducible, IKK-dependent gene expression profiles		207
6.1	Introduction.....	207
6.2	Results	209
6.2.1	Assessment of RNA sample and sequencing quality	209
6.2.2	Assessment of RNA sequencing mapping and counting quality.....	210
6.2.3	Assessment of sample clustering.....	213
6.2.4	Differential gene expression analysis of WT TNF α -treated samples identifies well-characterised patterns of gene expression and putative, novel TNF α -responsive genes.....	215
6.2.5	IKK β knockout causes the downregulation of genes involved in chromosome organisation, mitotic cell cycle progression and DNA damage repair in non-stimulated cells	223
6.2.6	IKK DKO causes additional downregulation in the basal expression of genes involved in microtubule/actin cytoskeleton organisation, cell trafficking, cell junction regulation and cell differentiation.....	229
6.2.7	Minimal differential gene expression was detected in IKK α KO NT samples	230
6.2.8	IKK α KO cells exhibit a greater defect in TNF α -induced gene expression than IKK β KO cells, while DKO cells exhibit minimal TNF α -induced expression changes.....	235
6.3	Discussion	248
6.3.1	A detailed characterisation of the global TNF α -induced expression response in colorectal cancer cells	248
6.3.2	Transcriptome profiling of IKK β KO and IKK DKO cells revealed unexpected changes in the basal expression of genes involved in the regulation of numerous cellular processes	248
6.3.3	Comparison of TNF α -induced expression profiles in WT and IKK KO cells highlights potentially IKK-dependent genes.....	251

Chapter 7. Final discussion.....	254
7.1 Assessing the relative merits of targeting IKK α and IKK β in colorectal cancer.....	254
7.2 Highlighting the discrepancies between NF- κ B signalling in human cells and mouse models.....	256
7.3 Regulation of structural disorder as a possible common mechanistic theme in NF- κ B signalling	257
7.4 Future directions	259
7.5 Conclusions	260

List of figures

Chapter 1.

- Figure 1.1. Overview of cell cycle regulation by cyclin-dependent kinases (CDKs) and cell cycle checkpoints
- Figure 1.2. Overview of the mechanisms by which different forms of inflammation can contribute to tumour development
- Figure 1.3. Overview of TNF-receptor 1 (TNFR1) signalling
- Figure 1.4. Domain organisation of members of the IKK complex
- Figure 1.5. Overview of the canonical NF- κ B signalling pathway
- Figure 1.6. IKK β oligomerization activation model involving sequential TAK1 and trans-autophosphorylation of active site residues
- Figure 1.7. NF- κ B-independent functions of IKK β and IKK α
- Figure 1.8. Domain organisation of the NF- κ B family of transcription factors
- Figure 1.9. Domain organisation of the I κ B family proteins
- Figure 1.10 Overview of the non-canonical NF- κ B signalling pathway
- Figure 1.11. Atypical pathways of NF- κ B activation
- Figure 1.12. Overview of the contribution of NF- κ B-dependent gene expression to the hallmarks of cancer
- Figure 1.13. Overview of tumour-elicited inflammation in the progression of colorectal cancer

Chapter 2.

- Figure 2.1. GENCODE protein-coding transcript annotations for human CHUK and IKBKB genes highlighting the exons targeted by the CRISPR gRNA sequences
- Figure 2.2. Vector map for mammalian pD1301-Ad CRISPR-Cas9 expression plasmid
- Figure 2.3. PCR screening strategy for identifying single cell clones containing indel mutations in gRNA target site

Chapter 3.

- Figure 3.1. Generation of CRISPR-Cas9 IKK knockout HCT116 cells
- Figure 3.2. Representative IKK KO CRISPR-Cas9 cells are completely absent of IKK protein
- Figure 3.3. IKK α / β DKO cells appear to grow in more compact, epithelial-like colonies than WT or IKK α KO and IKK β KO cells
- Figure 3.4. IKK knockout has no significant impact on the growth rate or cell cycle distribution of HCT116 cells
- Figure 3.5. IKK α / β DKO cells exhibit no observable phosphorylation of known IKK substrates in response to TNF α stimulation
- Figure 3.6. IKK α and IKK β have non-functionally redundant kinase activities
- Figure 3.7. Knocking down the remaining IKK subunit in single KO clones drastically reduces the observed TNF α -induced IKK kinase activity and NF- κ B transcriptional activity
- Figure 3.8. Both IKK α and IKK β contribute to the induction of canonical NF- κ B in WT cells
- Figure 3.9. IKK α / β DKO cells exhibit a much greater sensitivity to TNF α -induced apoptosis than single IKK KO cells

Figure 3.10. Reexpressing WT IKK restores WT-like NF- κ B transcriptional activity to IKK KO HCT116 cells, while kinase-dead (KD) IKK α and KD IKK β both act in a dominant-negative fashion

Figure 3.11. Overexpressed S468A p65 induces a moderately increased transcriptional response relative to WT p65

Figure 3.12. IKK α KO HCT116 cells exhibit a greater defect in TNF α -induced p65 nuclear translocation than IKK β KO cells

Figure 3.13. IKK α KO and IKK β KO cells HCT116 cells exhibit similar defects in TNF α -induced c-Rel nuclear translocation

Figure 3.14. IKK α KO and IKK β KO have differential effects on TNF α -induced nuclear translocation of p65 and c-Rel

Figure 3.15. A proportion of IKK α localises to the nucleus of WT HCT116 cells

Figure 3.16. IKK KO has similar effects on the signalling response to IL-1 α as it does for TNF α

Figure 3.17. IKK α KO cells exhibit a greater defect in IL-1 α -induced p65 nuclear translocation than IKK β KO cells

Figure 3.18. IKK α KO and IKK β KO have differential effects on AKT signalling induced by TNF α

Figure 3.19. IKK α KO cells are capable of responding to IGF-1, an activator of PI3K/AKT signalling

Figure 3.20. Colorectal cancer cell lines exhibit basal NIK- and IKK α -independent p100 processing

Figure 3.21. IKK α is more essential than IKK β for blocking the increase in NIK protein levels following prolonged TNF α stimulation

Figure 3.22. IKK α KO cells exhibit enhanced TNF α -induced RelB nuclear translocation

Chapter 4.

Figure 4.1. Domain organisation of NEMO

Figure 4.2. Structures of NEMO and its complexes

Figure 4.3. CRISPR-Cas9 knockout or siRNA-mediated knockdown of IKK causes a significant decrease in NEMO protein levels

Figure 4.4. IKK KO has no statistically significant effect on NEMO mRNA expression

Figure 4.5. Transiently re-expressing IKK α or IKK β in IKK DKO cells partially restores NEMO protein levels

Figure 4.6. Treatment with TNF α decreases levels of NEMO protein to a greater extent in IKK KO cells than WT cells

Figure 4.7. Steady-state NEMO protein levels are partly increased by inhibition of the proteasome but unaffected by inhibition of lysosomal/autophagic degradation

Figure 4.8. NEMO is turned over by the proteasome with a faster rate in IKK DKO cells compared to WT cells following blockage of protein synthesis

Figure 4.9. Newly synthesised NEMO protein has a shorter half-life in IKK DKO cells compared to WT cells

Figure 4.10 Protein disorder prediction methods identify common consensus regions of intrinsic disorder within NEMO

Figure 4.11. mORF predictors identify segments within intrinsically disordered regions of NEMO that might fold upon binding to interaction partners

Figure 4.12. NEMO is rapidly degraded by the 20S proteasome *in vitro*, and protected from degradation by IKK α or IKK β

Figure 4.13. Reduced NEMO protein levels do not explain the reduced TNF α -induced NF- κ B transcriptional activity observed in IKK α KO cells or the absence of I κ B α degradation observed upon TNF α -stimulation in IKK DKO cells reconstituted with WT IKK α

Figure 4.14. Overexpressed IKK α protects co-expressed NEMO from polyubiquitination

Figure 4.15. Putative phosphorylation sites in NEMO

Figure 4.16. Schematic illustrating possible mechanisms of enhanced proteasomal degradation of 'IKK-free' NEMO and mechanisms of protection from degradation by interaction with IKK kinase subunits

Chapter 5.

Figure 5.1. 2D structure of IKK β inhibitors utilised in this work

Figure 5.2. AZD2230 is a potent inhibitor of the IKK kinases

Figure 5.3. AZD2230 and BMS-345541 induce a proliferative arrest in HCT116 cells

Figure 5.4. AZD2230 and BMS-345541 induce changes in protein levels of various cell cycle regulators

Figure 5.5. AZD2230 and BMS-345541 induce a significant cell death response in HCT116 cells

Figure 5.6. IKK β knockdown phenocopies the effects of AZD2230 and BMS-345541 on cell cycle regulator protein levels

Figure 5.7. The highly selective IKK β inhibitor, BIX02514, does not phenocopy the effects of AZD2230 or BMS-345541 on HCT116 cell cycle progression

Figure 5.8. IKK β knockdown with a more selective 'onTARGETplus' siRNA pool does not phenocopy the effects of AZD2230 and BMS-345541 on cell cycle progression

Figure 5.9. IKK α knockdown does not phenocopy the effects of AZD2230 and BMS-345541

Figure 5.10. Double knockdown of IKK α and IKK β does not phenocopy the effects of AZD2230 and BMS-345541

Figure 5.11. The effects of AZD2230 and BMS-345541 on cell cycle progression are due to off-target inhibition

Figure 5.12. Available selectivity data for AZD2230 and BMS-345541

Figure 5.13. AZD2230 and BMS-345541 both inhibit RNA Pol II CTD phosphorylation

Figure 5.14. The kinetics of RNA Pol II CTD phosphorylation by AZD2230 and BMS-345541 correlate with the kinetics of signalling events that trigger a cell cycle arrest

Figure 5.15. The inhibition of RNA Pol II CTD phosphorylation is an off-target effect of AZD2230 and BMS-345541

Figure 5.16. AZD2230 and BMS-345541 induce nucleolar disruption in HCT116 cells

Figure 5.17. Bioinformatics analyses of AZD2230 and BMS-345541 chemical structures

Chapter 6.

Figure 6.1. RNA sequencing quality control

Figure 6.2. RNA sequencing mapping and counting quality control

Figure 6.3. All-sample clustering analysis

Figure 6.4. Characterisation of TNF α -induced gene expression profiles in WT HCT116 cells

Figure 6.5. Expression profiles across a cross-section of well-characterised NF- κ B-dependent genes and putative, novel TNF α -responsive genes

Figure 6.6. TNF α -dependent expression profiles of ID1, ID2, ID3, JunB, ATF3 and SMAD3 in WT, IKK α KO, IKK β KO and DKO cells

Figure 6.7. Identification of DEGs in IKK β KO NT and DKO NT cells relative to WT NT

Figure 6.8. PANTHER GO:term analysis for downregulated and upregulated DEGs in IKK β KO NT samples

Figure 6.9. PANTHER GO:term analysis for downregulated and upregulated DEGs in DKO NT samples

Figure 6.10. Identification of DEGs in IKK α KO NT cells relative to WT NT

Figure 6.11. Identification of DEGs in IKK α KO 2h TNF α and IKK α KO 8h TNF α samples relative to IKK α KO NT

Figure 6.12. RNA sequencing data expression profiles for representative genes that differentially expressed (FDR p-value < 0.05) in IKK α KO TNF α -treated samples, but not WT TNF α -treated samples

Figure 6.13. Identification of DEGs in IKK β KO 2h TNF α and IKK β KO 8h TNF α samples relative to IKK β KO NT

Figure 6.14. qRT-PCR validation of candidate IKK-dependent TNF α -responsive genes

Figure 6.15. Identification of DEGs in DKO 2h TNF α and DKO 8h TNF α samples relative to DKO NT

Figure 6.16. RNA sequencing data expression profiles for genes that are differentially expressed (FDR p-value < 0.05) in DKO TNF α -treated samples, but not WT TNF α -treated samples

List of tables

Chapter 2.

Table 2.1. Sources of general laboratory equipment and reagents

Table 2.2. Source, target and mode of action of pharmacological inhibitors

Table 2.3. General laboratory solutions

Table 2.4. Solutions used for SDS-PAGE and Western blotting

Table 2.5. Solutions used for immunocytochemistry

Table 2.6. Antibodies, blocking solution and dilutions used for Western blotting

Table 2.7. Secondary antibodies used for Western blotting

Table 2.8. Primary antibodies used for immunocytochemistry

Table 2.9. Secondary antibodies used for immunocytochemistry

Table 2.10. Sequences of oligonucleotides used for siRNA

Table 2.11. Primers used for quantitative reverse-transcription PCR

Table 2.12. Cell culture medium and medium supplements for each cell line

Table 2.13. Primer sequences used for site-directed mutagenesis

Table 2.14. Resolving gel composition

Table 2.15. Stacking gel composition

Table 2.16. gRNA sequences designed to target IKK α and IKK β

Chapter 1

Introduction

1 Introduction

1.1 Cancer

1.1.1 Hallmarks of cancer

Tumourigenesis is a multistep process involving the progressive accumulation of genetic alterations, both mutational and epigenetic, at various sites in the genome that drive the transformation of normal cells into malignant derivatives. This multistep evolution towards the neoplastic state is coupled to the acquisition of a number of hallmark capabilities that enable incipient cancer cells to become tumorigenic and ultimately malignant. These six core biological capabilities are defined as: proliferative self-sufficiency, insensitivity to growth-suppressing signals, evasion of cell death, replicative immortality, induction of angiogenesis and activation of invasion and metastasis (Hanahan & Weinberg., 2000). The acquisition of these capabilities is enabled and expedited by the genomic instability of cancer cells, which through random mutation and chromosomal rearrangements facilitates the chance acquisition of rare enabling mutant genotypes, and via tumour-promoting inflammation at the site of pre- and malignant lesions driven by cells of the immune system (Grivennikov *et al.*, 2010; Hanahan & Weinberg., 2011).

Not all mutations acquired during malignant transformation are of equal importance for tumourigenesis. Certain ‘driver’ mutations promote tumour initiation, progression and maintenance while other ‘passenger’ mutations are an incidental consequence of the genomic instability of cancer cells (Haber *et al.*, 2007). Furthermore, numerous studies have demonstrated that despite the many genetic and epigenetic abnormalities present in cancer cells, they are often highly dependent on the activity of one or a few oncogenes for the maintenance of the malignant phenotype. In such cases, the cancer cell is claimed to be ‘addicted’ to the oncogene(s) in question (Weinstein *et al.*, 2008). The excessive dependency on the oncogenic pathway to which the cancer cell is addicted presents the clinician with a ‘therapeutic window’ (Luo *et al.*, 2009). Inhibition of the relevant oncoprotein or pathway may yield dramatic responses with modest, or at least manageable, adverse effects. This provides a strong rationale for molecular targeted therapeutics over traditional cytotoxic chemotherapeutics.

Tumour-promoting chronic inflammation within the tumour microenvironment, sustained proliferation through deregulation of the cell cycle and induction of metastasis by epithelial-mesenchymal transition are particularly relevant cancer hallmarks to this study. The normal regulation of these processes, and their aberrant regulation in cancer, is briefly discussed.

1.1.2 Cell cycle control and cancer

The cell cycle has four sequential phases (Figure 1.1). Arguably the most crucial are S phase (DNA synthesis), when DNA is replicated, and M phase (mitosis), when cell division occurs to generate two daughter cells. Separating S and M phases are two gap phases, G1 and G2. G1 is a phase of cell growth, where cellular contents other than the chromosomes are synthesised and the cell is sensitive to positive and negative signals from growth factor signalling networks. G2 is a period where the cell prepares for cell division and ensures that the newly replicated DNA is free of errors or damage. Progression through each of these phases is controlled via numerous mechanisms that impinge on the cyclin-dependent kinases (CDKs) (van den Heuvel & Harlow, 1993). A major

form of CDK regulation is at the level of the expression of their cognate cyclin interaction partners (Evans *et al.*, 1983; Hunter & Pines 1994). The expression and degradation of cyclins oscillates throughout the cell cycle, thus driving oscillations in the activities of their associated CDKs. CDK-cyclin complex formation contributes to conformational rearrangements in the CDK active site that lead to CDK activation (Jeffrey *et al.*, 1995). Complete activation requires phosphorylation of the activation T loop within the CDK active site (Russo *et al.*, 1996). Cyclins also modulate the subcellular localisation of their cognate CDKs and promote the recruitment of various CDK substrates (Morgan, 1995). Inhibitory phosphorylation of the activation loop must also typically be removed for activation of CDK activity (Lundgren *et al.*, 1995). Active CDKs promote cell cycle progression through the phosphorylation of substrates involved in fundamental cellular processes such as DNA replication initiation and microtubule formation.

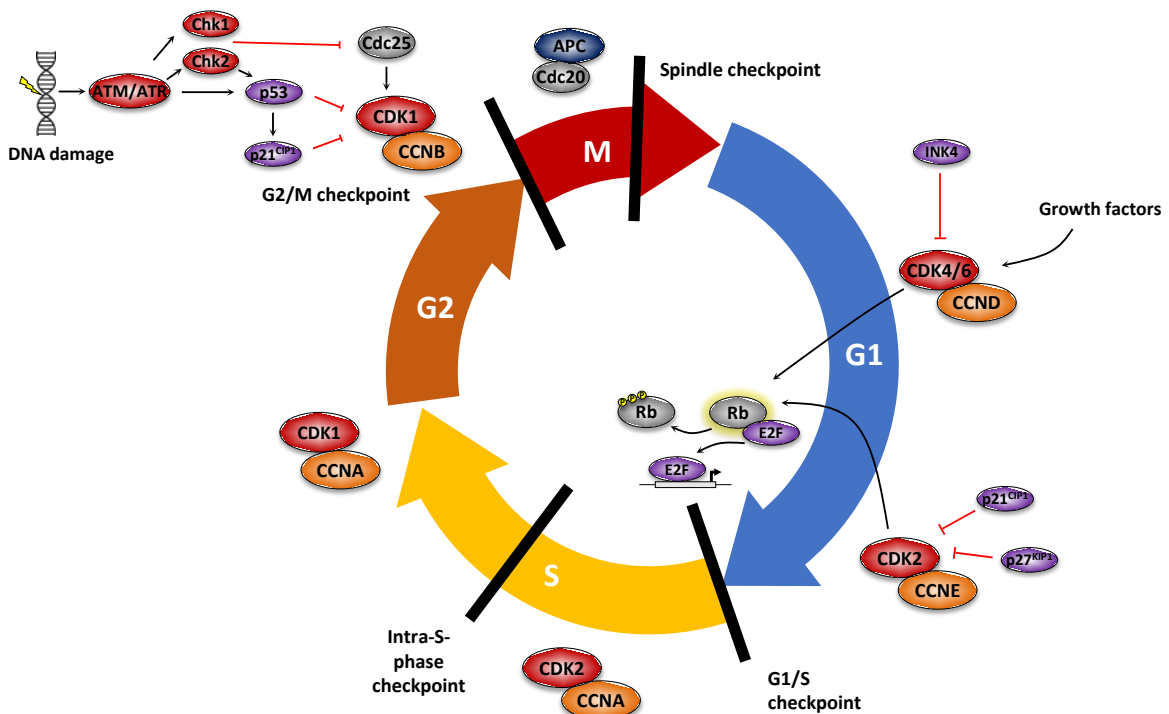


Figure 1.1. Overview of cell cycle regulation by cyclin-dependent kinases (CDKs) and cell cycle checkpoints. Early in G1 phase, CDK4 and CDK6 (CDK4/6) are inactive due to the absence of D-type cyclins (CCND). Their activity is also inhibited by members of the INK4 family of CDK inhibitors. CDK4/6 are activated by growth factors that promote the accumulation of D-type cyclins and assembly of CDK4/6-CCND complexes. Key to progression through the G1/S checkpoint is the activity of the Rb-E2F transcription complex. In G1-phase uncommitted cells, hypo-phosphorylated, active Rb binds to E2F transcription factors, forming an inhibitory complex with HDAC to repress genes required for S phase entry and DNA replication. Commitment to enter S-phase is mediated by sequential phosphorylation and inhibition of Rb, first by CDK4/6-CCND and subsequently by CDK2-CCNE (cyclin E), which permits E2F-dependent transcription. A variety of stimuli, such as DNA damage and replicative senescence, can inhibit CDK2-CCNE activity and hence progression through the G1/S checkpoint, largely through the activity of CIP- or KIP-type inhibitors, such as p21CIP1 and p27KIP1. Progression through S phase is largely driven by CDK2-CCNA (cyclin A) complexes. Detection of DNA damage during DNA replication triggers a pause in S-phase, known as the intra-S-phase-checkpoint, to facilitate damage repair. Progression through G2 and into mitosis (M phase) is controlled by CDK1-CCNA and later CDK1-CCNB (cyclin B1). The G2/M checkpoint serves to prevent the cell from entering M-phase with genomic DNA damage. DNA damage leads to the activation of ATM and ATR kinases, which in turn activate Chk1 and Chk2 and induce the stabilisation of p53, which subsequently mediate three major mechanism controlling entry into G2/M: 1) Inhibition of CDK1 kinase activity; for example, Chk kinases inactivate CDC25 family phosphatases (such as CDC25C) that are required to dephosphorylate inhibitory phosphorylation sites on CDK1. 2) Inhibition of complex formation between CDK1 and cyclin B1; for example, 14-3-3 σ induced by p53 promotes the nuclear export of cyclin B1. 3) Inhibition of the expression of genes required for progression through mitosis.

Throughout the cell cycle there are numerous ‘checkpoints’ at which the cell cycle can be arrested until conditions favourable for continued cell division are met (Murray, 1992). These include the G1/S checkpoint (restriction point), the intra-S-phase checkpoint, the G2/M checkpoint and the spindle checkpoint (metaphase checkpoint). The G1/S checkpoint controls commitment to cell division, is promoted by DNA damage and other stresses, and is primarily controlled by sequential activity of CDK4/6-Cyclin D and CDK2-Cyclin E complexes that relieve the inhibition of E2F transcription factors through the phosphorylation of the retinoblastoma (Rb) protein (Bartek & Lukas, 2001). The intra-S-phase checkpoint is activated in response to DNA damage and/or replication stress to slow DNA replication initiation and elongation and facilitate DNA damage bypass and repair (Bartek *et al.*, 2004). Defects in this checkpoint lead to genomic instability, inability to tolerate DNA damage during DNA synthesis and cancer predisposition. The G2/M checkpoint is also activated in response to DNA damage and prevents initiation of mitosis prior to the repair of DNA damage (Löbrich *et al.*, 2007). Progression through G2 and into mitosis (M phase) is controlled by CDK1-Cyclin A and later CDK1-Cyclin B1 complexes (Nurse, 1990). Numerous mechanisms are activated following the detection of DNA damage to rapidly inhibit CDK1 activity and invoke the G2/M checkpoint. For example, WEE1 kinase is activated and promotes the inhibitory phosphorylation of CDK1 at T14/Y15, while CDC25 phosphatase proteins are inhibited to prevent dephosphorylation of these inhibitory phosphorylation sites (Kumagai & Dunphy, 1991; Lundgren *et al.*, 1991; Strausfeld & Labbe, 1991). Long term arrest at the G2/M checkpoint is mediated by effects of p53 on gene expression (Bunz *et al.*, 1998). For example, p53 represses the expression of various genes required for progression into, and through, mitosis such as CDC20, cyclin B1, Securin and CDC25C, and induces genes such as 14-3-3 σ that promote the nuclear export and degradation of cyclin B1, and p21^{CIP1}, which inhibits CDK1-Cyclin B1 complexes (Taylor & Stark., 2001). Finally, during mitosis a spindle assembly checkpoint delays cell division until accurate kinetochore attachment of the chromosomes to the microtubule spindle apparatus is confirmed (Musacchio & Salmon, 2007). The E3 ubiquitin ligase, anaphase promoting complex, or cyclosome (APC/C) is the main site of regulation for the control of the spindle checkpoint (Li & Zhang, 2009). APC/C promotes the proteasomal degradation of substrates, such as securin and cyclin B1 that promote separation of sister chromatids, and mitotic exit, respectively.

Sustained proliferation is arguably the most fundamental hallmark of cancer cells, and is a direct consequence of cell cycle deregulation. Tumour cells evolve mechanisms to evade normal cell cycle controls and sustain proliferation in the absence of growth factor signals (Hartwell & Kastan, 1994). A common mechanism by which tumour cells acquire constitutive pro-proliferative signals is through the activating mutation of components of signalling pathways, such as RAF-MEK1/2-ERK1/2 and NF- κ B. Furthermore, the intra-S-phase, G2/M and spindle assembly checkpoints all act to maintain genome integrity. Their defective function in cancer contributes to chromosomal rearrangements that promote tumorigenesis.

1.1.3 Epithelial to mesenchymal transition and cancer

Carcinomas, malignancies of epithelial tissue, account for 80-90% of all cancers (CRUK statistics). Epithelial cells exhibit an apico-basal axis of polarity, form tight contacts with each other through specialised cell-cell adhesions and attach to the basement membrane within the epithelial layer (Hay, 1968). In this way, epithelia function as permeability barriers that help to define tissues and organs. Mesenchymal cells, on the other hand, exhibit a spindly, fibroblastic cell morphology and are loosely organised within a three-dimensional extracellular matrix

(ECM). During embryonic development, conversion of cells with an epithelial phenotype to those with a mesenchymal phenotype is a critical process referred to as epithelial-mesenchymal transition (EMT) (Hay *et al.*, 1995; Thiery *et al.*, 2009). Later in life, EMT is also important for wound healing, organ fibrosis and tissue regeneration (Strutz *et al.*, 1995). However, EMT also constitutes a core mechanism of tumour progression and chemoresistance, with tumour cells undergoing EMT characterised by a resistance to apoptosis and an enhanced motility and invasiveness that favours their dissemination and formation of metastases (Brabletz *et al.*, 2001; Thiery *et al.*, 2002). EMT is promoted during tumorigenesis via both cell autonomous mechanisms, such as somatic genetic and epigenetic alterations, including oncogenic BRAF/KRAS mutations (Dong *et al.*, 2003; Shao *et al.*, 2014), and, cell extrinsic mechanisms, such as stimuli from the tumour microenvironment (Talbot *et al.*, 2012). Inflammatory cytokines and growth factors activate several signalling pathways, including phosphoinositide 3-kinase (PI3K)-AKT, RAF-MEK1/2-ERK1/2, Wnt and NF- κ B that initiate the EMT transcriptional program. This is orchestrated by a cohort of master transcription factors, including SNAI1, SNAI2, TWIST1, ZEB1 and ZEB2 that induce EMT in part by repressing *CDH1* (E-cadherin) transcription, and regulating numerous other genes involved in cell-cell contact, motility and cytoskeletal organisation (Yang and Weinberg 2008). Loss of *CDH1*, an important cell-cell adhesion protein, is a defining feature of EMT in tumour development (Hirohashi 1998).

1.1.4 Inflammation and cancer

Chronic inflammation is now widely appreciated to contribute to numerous stages in tumorigenesis, including initiation, promotion, malignant conversion, invasion, metastasis and has impacts on immune surveillance and chemoresistance (Coussens & Werb, 2001). An inflammatory ‘tumour microenvironment’ (TME) consisting of the extracellular matrix, stroma (including cancer-associated fibroblasts (CAFs) endothelial cells and mesenchymal cells), innate immune cells (including macrophages, dendritic cells, neutrophils etc), adaptive immune cells (including T and B lymphocytes) and capillary networks is an intrinsic component of most, if not all, solid tumours (Quail & Joyce, 2013). In the developing TME, antitumorigenic (tissue protective and immune surveillance responses) and protumorigenic immune and inflammatory mechanisms coexist, but over time, and in the absence of tumour rejection, chronic inflammatory conditions enable protumorigenic effects to dominate (Grivennikov *et al.*, 2010). The various types of inflammation, and the mechanisms by which they can contribute to tumorigenesis is highlighted in Figure 1.2. Signalling pathways induced by inflammatory cytokines, such as Tumour-necrosis factor- α (TNF α) and interleukins, which activate transcription factors such as NF- κ B, AP-1 and STAT3, mediate the various protumorigenic effects of inflammation. Many of these pathways operate in feed-forward loops that contribute to increase and sustain inflammation. For example, NF- κ B activation in TME immune cells promotes the secretion of cytokines that activate NF- κ B in cancer cells to induce the secretion of chemokines that draw yet more inflammatory cells into the tumour site. Some of the mechanisms by which inflammatory cytokine-induced NF- κ B signalling can contribute to inflammation-associated tumorigenesis, particularly colorectal cancer, will be discussed in Section 1.4.

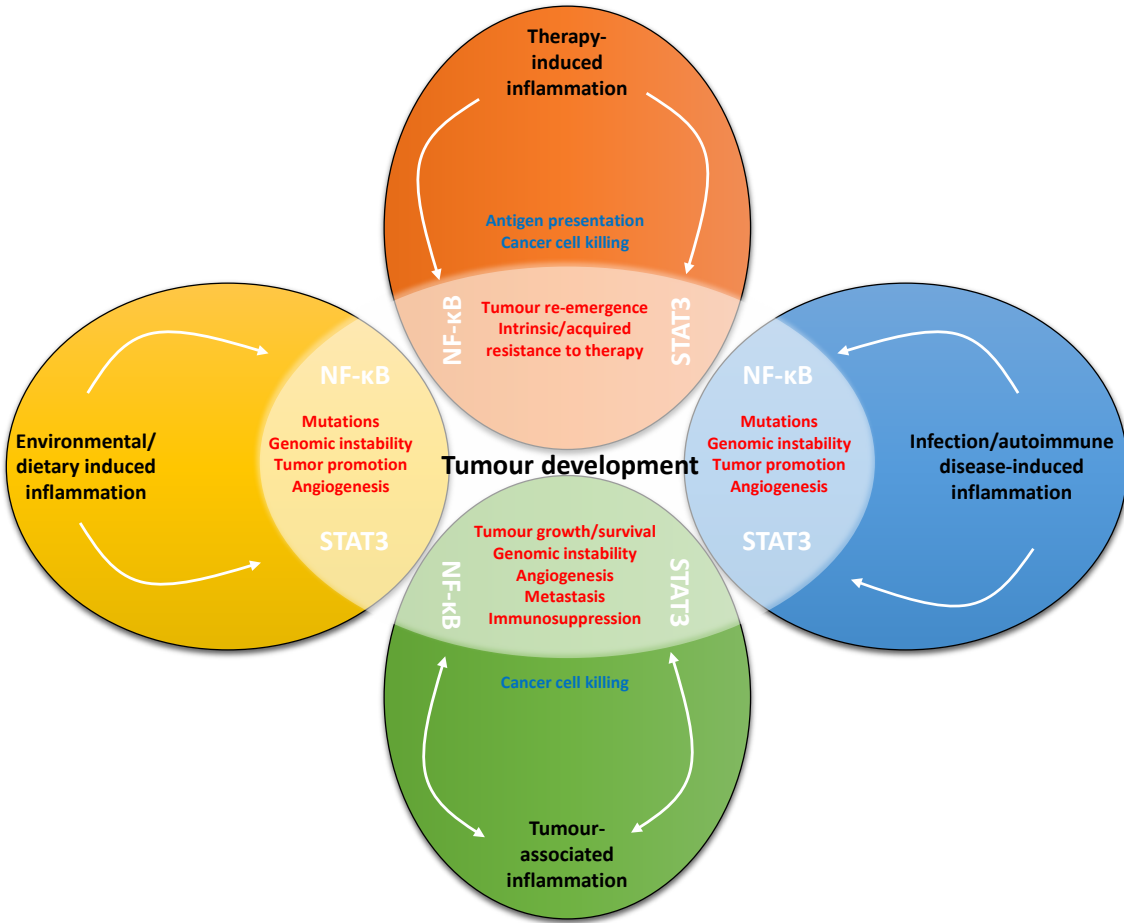


Figure 1.2. Overview of the mechanisms by which different forms of inflammation can contribute to tumour development. Prolonged exposure to various environmental factors, such as particulate matter from tobacco smoke, asbestos and silica particles, and dietary factors such as obesity can contribute to the initiation tumourigenesis through induction of a low-grade chronic inflammatory state that promotes acquisition of oncogenic mutations, genomic instability, early tumour promotion and increased angiogenesis. Similar mechanisms are associated with the chronic inflammatory state induced by certain infectious/autoimmune diseases. For example, persistent Helicobacter pylori infection is associated with MALT lymphoma and gastric cancer, while inflammatory bowel disease greatly increases the chance of colorectal cancer. Following initiation of tumourigenesis, most, if not all, solid tumours develop a protumourigenic microenvironment that contributes to an intrinsic inflammatory response. Various oncogenes, such as RAS and MYC contribute to remodelling the tumour microenvironment. The inflammatory response can contribute to cancer cell killing, but in cases where the tumour survives the chronic inflammatory conditions promote tumour growth/survival, genomic instability, angiogenesis, metastasis and immunosuppression. Finally, cancer therapy can itself trigger an inflammatory response that contributes to resistance to therapy and relapse through tissue trauma/injury and necrosis. In some cases, therapy-induced inflammation can promote antigen presentation, and contribute to cancer cell killing. Protumourigenic mechanisms are in red and antitumourigenic mechanisms are in blue. (Adapted from Grivennikov *et al.*, 2010).

1.2 TNF receptor family signalling

1.2.1 Overview

Tumour necrosis factor (TNF)- α is the prototypic member of a large family of cytokines, the TNF-ligand superfamily, all of which exhibit pro-inflammatory activity. It is a 34 kDa type II transmembrane protein that has signalling potential both as a homotrimeric membrane-integrated protein (mTNF) and as a soluble 17 kDa homotrimeric cytokine (sTNF) released after proteolytic cleavage by the metalloprotease, TNF α converting enzyme (TACE) (Black *et al.*, 1995). sTNF is the endocrine form that circulates in the blood. Both forms mediate their biological functions through binding to members of the TNF receptor (TNF-R) family: TNF-R1, which is constitutively expressed in most tissues and TNF-R2, which is expressed selectively on endothelial cells and immune cells, and whose function is mostly limited to the immune system (Locksley *et al.*, 2001). mTNF is a more potent ligand for TNFR2. TNF- α is mainly expressed by activated monocytes/macrophages and activated natural killer (NK) and T cells, but also by various non-immune cells, including endothelial cells, fibroblasts and neuronal cells. Many cancer cells, including colon, lung, pancreatic, ovarian etc also constitutively secrete TNF α in an autocrine manner (Sati *et al.*, 1999; Petersen *et al.*, 2007; Zins *et al.*, 2007).

TNF- α was initially discovered and named as a result of its antitumour activity, specifically its ability to kill mouse fibrosarcoma cells (Carswell *et al.*, 1975). TNF- α has since been characterized as one of the major pro-inflammatory mediators. Induced by various pathogenic stimuli (including LPS and other bacterial antigens), TNF- α orchestrates multiple aspects of inflammation, and innate and adaptive immunity. The pro-inflammatory effects of TNF- α are primarily due to its ability to activate NF- κ B signalling (see Section 1.5), which leads to the expression of inflammatory genes, cell adhesion molecules, cytokines, chemokines, inducible nitric oxide synthase (iNOS) etc (Pfeffer, 2003). However, deregulated TNF- α signalling is involved in a number of pathological processes, including diseases of chronic inflammation and autoimmunity, and cancer (Körner and Sedgwick, 1996; Aggarwal, 2003).

TNF- α induces TNF-R trimerization and activation leading to recruitment of intracellular adaptor proteins that activate multiple signalling events, including the NF- κ B pathway, the mitogen-activated protein kinase (MAPK) pathways, JNK and p38, and cell death pathways (Figure 1.3). Under certain circumstances, TNFR signalling can also activate the RAF-MEK1/2-ERK1/2 pathway. TNFR1 is the predominant receptor of epithelial cells, and so will be the focus here. Mention of the NF- κ B signalling pathway will be saved for Section 1.2.3.

1.2.2 TNFR1 signalling

1.2.2.1 TNF- α -induced cell death

TNFR1 is classified as a death receptor, due to its cytoplasmic death domains (DD) (Boldin *et al.*, 1995). However, the mechanism of cell death induction by TNFR1 is more complex than other death receptors, such as FAS (Micheau and Tschopp, 2003). The *in vivo* death-inducing capability of TNF-R1 is weak compared to other family members, the kinetics are slower and it typically plays a minor role compared to its predominant functions in inflammation and cell survival (Ashkenazi and Dixit, 1998). This is largely due to the strong, early and concomitant activation of anti-apoptotic NF- κ B signalling that masks the death-inducing capability of TNF- α ; NF- κ B pro-

survival gene products, such as c-FLIP, XIAP, cIAP1/2, GADD45 β , BCL2, BCL-xL and survivin, counteract TNF- α apoptotic signalling (Beg and Baltimore, 1996; Kreuz *et al.*, 2001; Smaele *et al.*, 2001). As evidence of this, mice deficient in the NF- κ B signalling pathway components, p65, I kappa B kinase β (IKK β) or NF-kappa-B essential modulator (NEMO) die early in embryogenesis due to massive TNF α -dependent liver apoptosis (Beg *et al.*, 1995; Li *et al.*, 1999b; Rudolph *et al.*, 2000). Furthermore, inhibitors of NF- κ B signalling are able to unmask the death-inducing capabilities of TNF- α ; luteolin, a plant flavonoid that inhibits TNF- α -induced NF- κ B activation, has been shown to sensitize colorectal cancer (CRC) cells to TNF- α -induced apoptotic cell death (Shi *et al.*, 2004). While other death receptors such as FAS are also able to activate the NF- κ B pathway, apoptosis induction by these receptors is dominant over NF- κ B activation (Lavrik *et al.*, 2005). This is partly due to the fact that the adaptor TNFR-associated factor 2 (TRAF2), which is a major component of the TNF-R1 signalling complex, but not other death receptors, is able to recruit the antiapoptotic, NF- κ B-induced cellular inhibitor of apoptosis proteins (cIAP1/2), which interfere with cell death signalling via TNFR1 (Shu *et al.*, 1996). Receptor-interacting serine/threonine protein kinase (RIP1), is the target of cIAP1/2 regulation, and is the important molecular switch that determines whether cell death or survival predominates (O'Donnell *et al.*, 2007). cIAP1/2-mediated K63-linked polyubiquitination of RIP1 ensures TNF-driven NF- κ B survival signalling predominates (discussed in more detail in Section 1.3) (Ea *et al.*, 2006; Li *et al.*, 2006). Under conditions of low RIP1 ubiquitination, TNF-driven cell death signalling takes over. Two different mechanisms lead to generation of non-ubiquitylated RIP1 kinase (Wang *et al.*, 2008). The deubiquitylase, cylindromatosis (CYLD) associates with TRAF2 and removes K63- and M1-linked polyubiquitin chains from RIP1, causing it to dissociate from the membrane bound TNFR1 signalling complex (Kovalenko *et al.*, 2003; Wang *et al.*, 2008). This dissociated, deubiquitylated RIP1 interacts with TNFR-associated death domain protein (TRADD), FAS-associated death domain protein (FADD), pro-caspase 8 and FLICE-like inhibitory protein (FLIP $_L$) to form the cytosolic complex II a , which subsequently leads to the autocatalytic cleavage and activation of pro-caspase 8, triggering the downstream apoptotic caspase cascade (Micheau *et al.*, 2002; Micheau and Tschopp, 2003). Alternatively, under conditions of cIAP1/2 depletion or inhibition, RIP1 does not become ubiquitylated in response to TNF α and dissociates from the membrane and interacts with RIP3, pro-caspase 8 and FLIP $_L$ to form complex II b , also known as the ripoptosome (Feoktistova *et al.*, 2011). Activation of pro-caspase 8 occurs in a similar manner. cIAP1/2 degradation can be induced by release of second mitochondria-derived activator caspase (SMAC) (Du *et al.*, 2000). In the case of both complex II a and II b , cleavage and inactivation of cytosolic RIP1/RIP3 that is not incorporated into the complexes by pro-caspase8-FLIP $_L$ is essential to prevent activation of necroptosis (Holler *et al.*, 2000; Zhang *et al.*, 2009; Oberst *et al.*, 2011). Under conditions of caspase inactivity, RIP1 and RIP3 form microfilaments called necrosomes, in a process dependent on MLKL kinase activity, and necroptosis dominates as the mechanism of TNF α -induced cell death (Li *et al.*, 2012; Sun *et al.*, 2012).

Many physiological factors can shift the balance of TNF α signalling from NF- κ B-dependent survival in favour of apoptosis. For example, TNF α stimulation can also induce the production of reactive oxygen species (ROS), high, sustained levels of which can promote either apoptotic or necroptotic cell death under certain circumstances (Sakon *et al.*, 2003). TNFR1 engagement activates the NADPH oxidase 1/2 (NOX1/2) complex, which converts extracellular O₂ into O₂⁻, which superoxide dismutase 3 (SOD3) converts into H₂O₂ (Kim *et al.*, 2007). This diffuses into the cell to act as a major source of ROS that preferentially activates necroptosis. Furthermore, as part of cell

death-inducing complex II, activated caspase 8 interacts with ROS modulator-1 (ROMO1) in the mitochondrial outer membrane, which in turn sequesters Bcl-XL to reduce the mitochondrial membrane potential and lead to enhanced ROS production (Kim *et al.*, 2010). The enhanced ROS production can, in turn, activate JNK through inhibition of MAPK phosphatases (Kamata *et al.*, 2005) and activation of the upstream kinase Apoptosis signal-regulating kinase 1 (ASK1) (Liu *et al.*, 2000). The consequent sustained JNK activation promotes mitochondrial outer-membrane permeabilisation (MOMP) via a mechanism involving caspase-independent cleavage of BID to generate the cleavage product jBID (not to be confused with the caspase-8/10 cleavage product, tBID), which leads to SMAC release and subsequent promotion of caspase 8 activation and apoptosis (Deng *et al.*, 2003). ROS might also inhibit NF- κ B activation to promote cell death (Shen *et al.*, 2005; Morgan *et al.*, 2011). However, this is controversial as there is also significant evidence that mitochondrial ROS might promote TNF-mediated NF- κ B activation under certain circumstances (Hughes *et al.*, 2005). Ongoing apoptosis can also interfere with NF- κ B activation due to caspase-mediated cleavage of several NF- κ B pathway components, such as RIP, I κ B α , IKK β and p65 (Staal *et al.*, 2011).

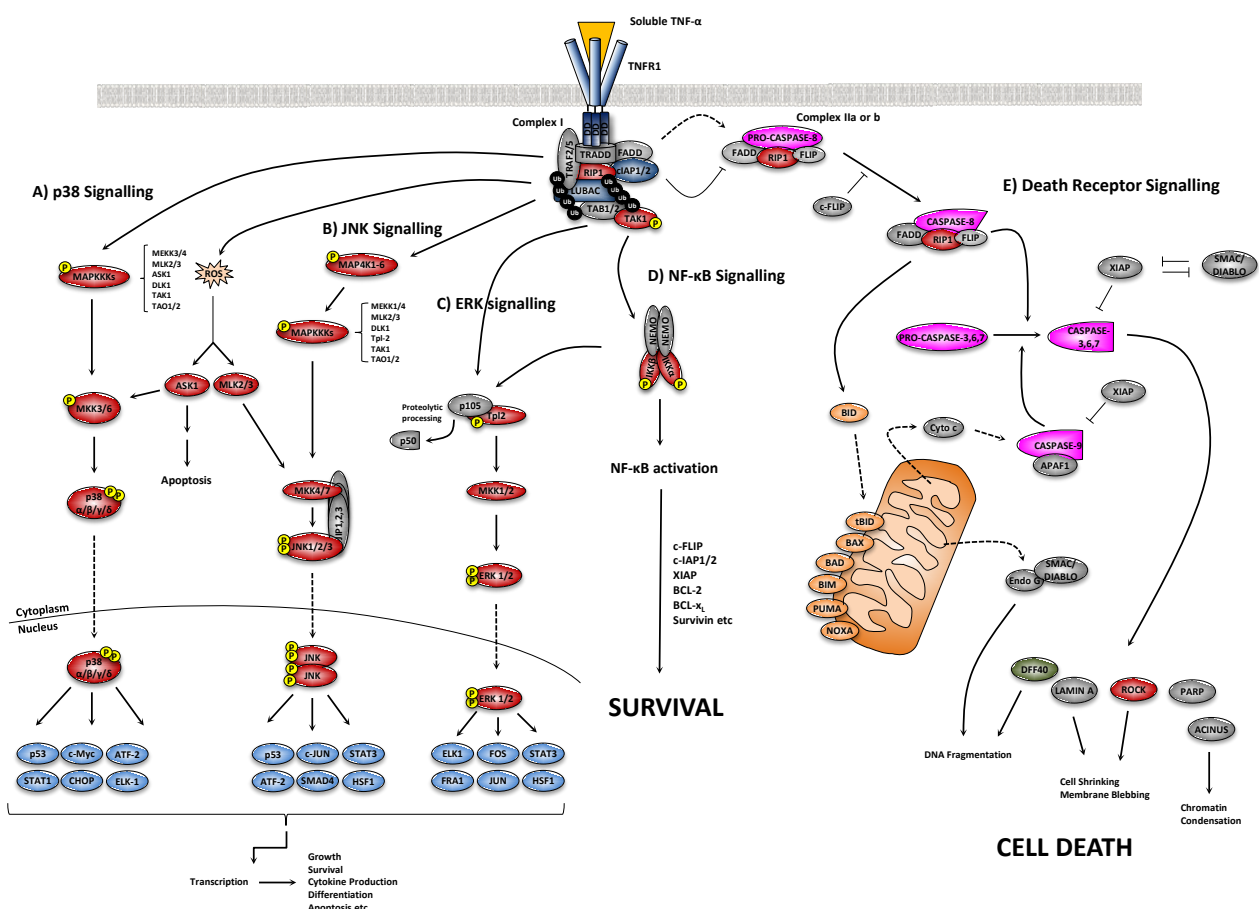


Figure 1.3. Overview of TNF-receptor 1 (TNFR1) signalling. TNF α signalling through TNFR1 is capable of activating p38 (A), JNK (B) and ERK (C) MAPK pathways, the canonical NF- κ B pathway (D), and cell death pathways, both apoptotic (E) and necrotic. TNF α binding to the extracellular domain of the receptor leads to translocation of TNFR1 to lipid rafts and to the recruitment of TNFR-associated death domain protein (TRADD) to the cytoplasmic death domains of TNFR1. TRADD, in turn, recruits the receptor-interacting serine/threonine protein kinase (RIP), and subsequently TNFR-associated factor 2 (TRAF2) or TRAF5 and cellular inhibitor of apoptosis protein 1 (cIAP1) or cIAP2 to assemble the TNFR1 complex I, which directs downstream signalling events to mitogen-activated kinase (MAPK) and NF- κ B pathways. cIAP1 and cIAP2 are E3 ubiquitin ligases that generate K63-linked polyubiquitin chains on RIP1 and other components of the complex. This is necessary to recruit the linear ubiquitin chain assembly complex (LUBAC), which consists of three proteins: heme-oxidized IRP2 ubiquitin ligase 1

(HOIL1), HOIL1-interacting protein (HOIP) and SHANK-associated RH domain-interacting protein (SHARPIN). LUBAC stabilises complex I by catalysing the attachment of linear M1-linked polyubiquitin chains, typically to RIP1. K63-polyubiquitylated RIP1 also recruits TGF β -activated kinase 1 and MAP3K7-binding protein (TAB2) and TAB3 (and possibly TAB1), in addition to its binding partner TGF β -activated kinase 1 (TAK1). TAK1 is the primary mitogen-activated protein kinase kinase kinase (MAPKKK) that activates the p38 and JNK MAPK pathways downstream of TNFR1. Other kinases can also perform this role, including ASK1 and MLK2/3, which are activated by reactive oxygen species (ROS) generated during prolonged TNF α stimulation. In turn, p38 and JNK are activated downstream of MKK3/6 and MKK4/7 respectively, and translocate into the nucleus where they activate various AP-1 family transcription factors. LUBAC-mediated M1-linked linear polyubiquitylation of RIP1, meanwhile promotes the recruitment of NEMO, as part of the IKK complex. The membrane proximal recruitment of the IKK complex leads to the phosphorylation and activation of the IKK kinases, IKK α and IKK β , in a mechanism involving TAK1-dependent phosphorylation, and possibly trans-autophosphorylation of IKK subunits. Activated IKK then phosphorylates I κ B proteins to activate the NF- κ B pathway and promote cell survival, proliferation etc. TNFR1 signalling can also induce cell death under certain conditions. This involves formation of either of two cytosolic complexes containing RIP1, complexes IIa or IIb. The polyubiquitylation of RIP1 by cIAP1/2 is not only important to activate NF- κ B-dependent survival signalling, but also to prevent formation of complex IIa/b and thus death induction. Conditions of low RIP1 polyubiquitylation lead to formation of complex II. For example, activation of the deubiquitylase enzyme cylindromatosis (CYLD), leads to the deubiquitylation of RIP1 and hence triggers formation of complex IIa, which contains TRADD, FAS-associated death domain protein (FADD), pro-caspase 8 and FLICE-like inhibitory protein (FLIP). Conditions where cIAP1/2 activity is depleted, such that RIP1 is not ubiquitylated in the first place, triggers formation of complex IIb (also called the Ripoptosome), which contains RIP1, FADD, pro-caspase 8, FLIP and RIP3. Cleavage of RIP1/RIP3 leads to apoptosis, whereas the absence of RIP cleavage, due to caspase inhibition leads to necroptosis. Pro-caspase is cleaved to generate active caspase8, which is released from complex II to carry out cleavage reactions (e.g. of effector caspases, such as pro-caspase-7) that induce classical apoptosis.

1.2.2.2 TNF- α -induced JNK and p38-MAPK signalling

TNF- α induces a strong activation of the stress-activated protein kinase (SAPK)/c-JUN N-terminal kinase (JNK) group of kinases (Vietor *et al.*, 1993). Such activation occurs via a TRAF2-dependent pathway downstream of TNFR1 (Figure 1.3) (Baud *et al.*, 1999). TRAF2 recruits and activates Mitogen-activated protein kinase kinase kinases (MAP4K1-6) of the germinal center kinase (GCK) family, which in turn activate various MAP3Ks, including TAK1, MEKK1/4, MLK2/3, DLK1 etc (Shi *et al.*, 1997; Yuasa *et al.*, 1998; Shi *et al.*, 1999; Yao *et al.*, 1999). Subsequently, they phosphorylate and activate the downstream kinases MKK4 and MKK7 (Moriguchi *et al.*, 1997). Evidence from knockout mice suggests that MKK7 is essential for TNF-mediated JNK activation, while MKK4 is insufficient alone, but contributes to optimal JNK activation (Lawler *et al.*, 1998; Tournier *et al.*, 2001). Apoptosis signal-regulated kinase-1 (ASK1) can also be activated directly by TRAF2 to activate MKK4/7 (Ichijo *et al.*, 1997; Nishitoh *et al.*, 1998), and independently as a result of increased reactive oxygen species (ROS) of mitochondrial origin that are induced by TNF-R1 stimulation under apoptotic conditions (Goldman *et al.*, 2004). Activated MKK4/MKK7 coordinate to phosphorylate JNKs at T183 and Y185 leading to JNK dimerization and nuclear translocation where they phosphorylate and activate/repress the activity of numerous transcription factors, most notably JUN, but also various other members of the activator protein-1 (AP-1) family (Whitmarsh and Davis, 1996). For example, JNK activates c-JUN, ATF2, SMAD4 and p53 and represses STAT3. As such, JNK activity regulates several important cellular functions including proliferation, differentiation, cytokine production, survival and apoptosis.

TNF- α also activates the p38-MAPK (p38- α , β , γ and δ) signalling cascade (Lee *et al.*, 1994). The mechanism of activation is similar to that of JNK activation, involving TRAF2-dependent recruitment of MAPKKKs, including TGF β -activated kinase 1 (TAK1), as well as activation of ASK1 (Cuadrado *et al.*, 2010). However, the GCK family of MAP4Ks that activate JNK downstream of TNFR1 are unable to stimulate the p38-MAPK cascade, while RIP kinase plays a more prominent role in p38-MAPK activation (Yuasa *et al.*, 1998). The MAPKKKs and ASK1 phosphorylate and activate the downstream kinases MKK3/6, which in turn phosphorylate and activate p38-

MAPKs at T180 and Y182 (Dérijard *et al.*, 1995; Raingeaud *et al.*, 1996). Activated p38 MAPKs subsequently translocate to the nucleus to phosphorylate several TFs involved in regulation of proliferation, differentiation, apoptosis and cytokine production (Kostenko *et al.*, 2011).

1.3 NF-κB signalling

1.3.1 Overview

There are five members of the NF-κB transcription factor family: RelA (p65), RelB, c-Rel, NF-κB1 (p50 and its precursor p105) and NF-κB2 (p52 and its precursor p100). All members share a conserved Rel homology domain (RHD) that enables them to associate with each other to form a diverse array of transcriptionally active homo- and heterodimeric complexes. In most unstimulated cells, NF-κB dimers are generally bound to a member of the IκB family of proteins, which maintain the cytoplasmic steady state localisation of NF-κB dimers and inhibit their DNA-binding activity. The precursor proteins p100 and p105 also contain ankyrin repeat domains, which are cleaved upon processing to p52/p50, such that they comprise internal inhibitors of NF-κB dimers. IKK-dependent phosphorylation of IκB proteins targets them for subsequent proteasomal-degradation/processing and thus liberates NF-κB dimers to translocate to the nucleus and bind to their cognate gene promoters to regulate gene expression.

The activity of NF-κB dimers is regulated by several distinct pathways. The first is the canonical pathway, which is induced by pro-inflammatory cytokines, such as TNF-α and IL-1, engagement of antigen receptors, such as the T- and B-cell receptor, pathogen-associated molecules such as bacterial flagellin and lipopolysaccharides (LPS) and growth factors, such as NGF (see Section 1.3.2 and Figure 1.5). Engagement of this pathway results in the activation of the IKK complex; formed by the catalytic IKK α and IKK β subunits and the regulatory subunit NEMO and primarily regulates p65:p50 and c-Rel:p50 heterodimers (Baldwin, 1996). The non-canonical pathway, meanwhile, is stimulated by a more restricted set of cytokines all belonging to the TNF superfamily, including BAFF, lymphotoxin β , RANKL, TWEAK, LIGHT and CD40L (Sun, 2011) (Section 1.3.5 and Figure 1.10). Engagement of the appropriate receptors leads to the activation of the upstream kinase NF-κB-inducing kinase (NIK), which activates IKK α , leading to the phosphorylation and ubiquitin-mediated proteasome-dependent processing of p100, the predominant RelB inhibitor, and subsequent nuclear translocation of RelB:p52 complexes (Sun, 2011). The canonical and noncanonical NF-κB pathways regulate distinct sets of target genes, in part because IκB α degradation and p100/105 processing regulate different populations of NF-κB dimers, and also because different dimers have different DNA-binding preferences (Wan & Lenardo, 2009). A number of atypical pathways are also capable of activating NF-κB in response to diverse stresses (Section 1.3.6 and Figure 1.11).

1.3.2 Canonical NF-κB signalling

1.3.2.1 The IKK complex

The many stimuli that activate the canonical NF-κB pathway trigger signalling cascades that ultimately lead to the phosphorylation and activation of the I kappa B kinases, IKK α and IKK β , which, together with the regulatory subunit NEMO, make up the IKK complex. IKK α , IKK β , and two other related kinases, TBK1 and IKK ϵ , constitute the IKK family (Pomerantz & Baltimore, 1999; Shimada *et al.*, 1999). The kinase domains of TBK1 and IKK ϵ share approximately 30% sequence identity with IKK α and IKK β , and they exhibit similar domain organisation (Kishore *et al.*, 2002). They also participate in various capacities within the NF-κB pathway, but are not involved in IκB α phosphorylation within the canonical NF-κB signalling pathway (Hacker *et al.*, 2006). As such, the following discussion will be limited to IKK α and IKK β .

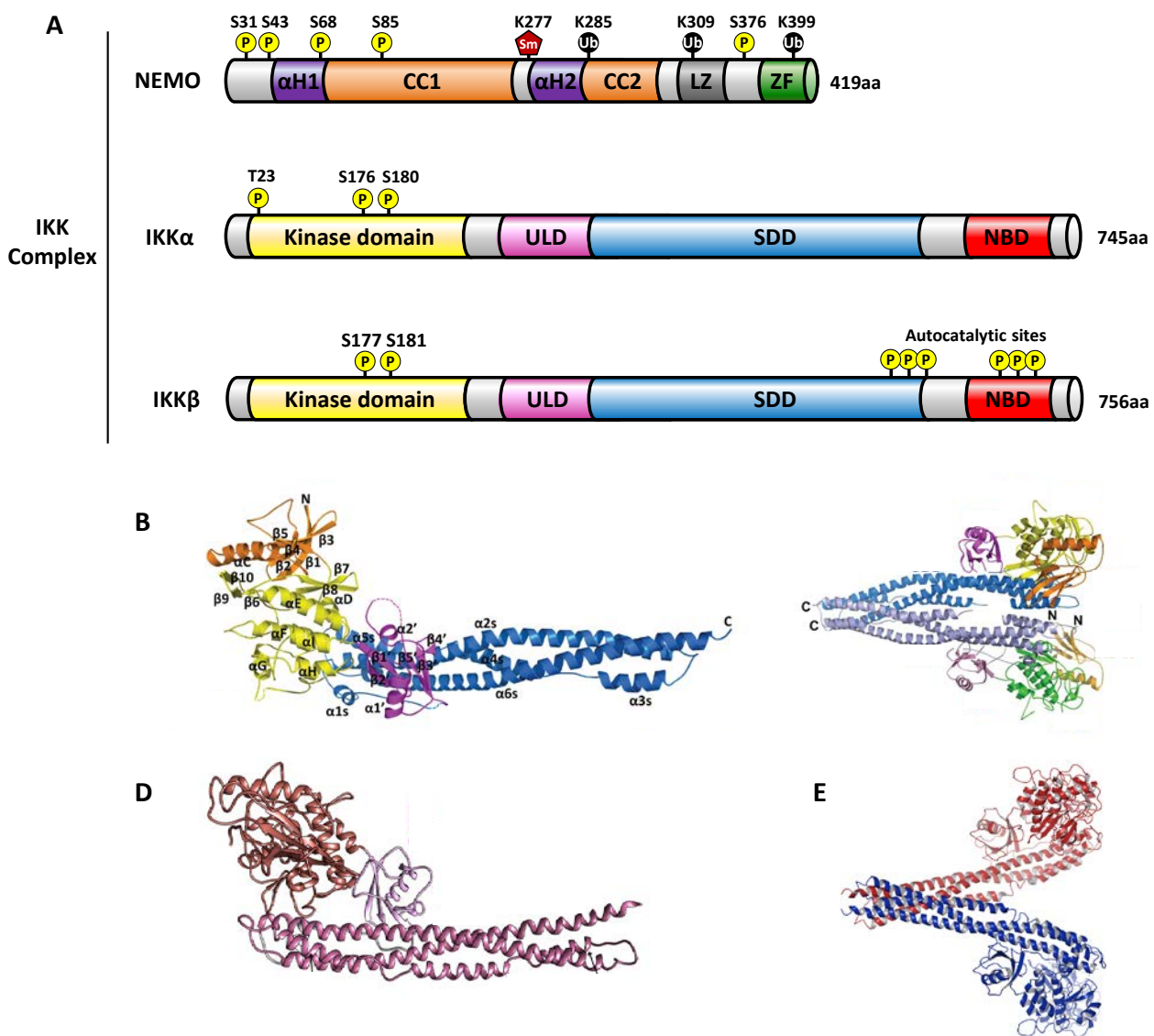


Figure 1.4. Domain organisation of members of the IKK complex. (A) Domain organisation of NEMO, IKK α and IKK β . NEMO contains two alpha helical regions (α H1 and α H2), two elongated coiled coil domains (CC1 and CC2), a leucine zipper (LZ) domain, and a zinc finger (ZF) domain. S31, S43, S68, S85 and S376 are putative IKK β phosphorylation sites. S68 is an ATM phosphorylation site. K277 is a PIASy SUMOylation site. K285, K309 and K399 are well characterised ubiquitin linkage sites. Both IKK α and IKK β contain an N-terminal bilobed kinase domain, a conserved ubiquitin-like domain (ULD) and a

scaffold/dimerization domain (SDD). At the C-terminus, both kinases contain a NEMO-binding domain (NBD). Phosphorylation of the T-loop serines – S176 and S180 for IKK α , S177 and S181 for IKK β – is critical for kinase activity. T23 in IKK α is phosphorylated by AKT downstream of TNFR2. IKK β contains a number of serine residues at its C-terminus that undergo autophosphorylation and decrease IKK activity following stimulation with TNF α . **(B)** Crystallographic structure of Xenopus laevis IKK β (xIKK β) protomer showing tri-modular architecture of KD (N-lobe, orange. C-lobe, yellow), ULD (magenta) and the elongated, α -helical SDD (blue). **(C)** Crystallographic structure of an xIKK β dimer. Dimerization is mediated by the SDD. **(D)** Crystallographic structure of human IKK α (hIKK α) protomer with similar tri-modular architecture as IKK β . **(E)** Crystallographic model of a hIKK α showing highly similar dimer interface mediated by SDD domains compared to IKK β . Crystal structures for IKK α and IKK β taken from Polley *et al.*, 2016, and Xu *et al.*, 2011, respectively.

IKK α and IKK β are ubiquitously expressed serine/threonine kinases with 52% sequence identity and 70% homology (Mercurio *et al.*, 1997). They also share highly similar domain organisation and tertiary structure, as demonstrated by the recent X-ray crystal structures of human IKK α and IKK β (Figure 1.4) (Xu *et al.*, 2011; Polley *et al.*, 2016). The structures demonstrated that both IKK α and IKK β exhibit a trimodular architecture. In each case, the bilobed N-terminal kinase domain (KD) is followed by a ubiquitin-like domain (ULD) and an elongated α -helical scaffold/dimerization domain (SDD). Although not resolved in any structures to date, both IKK α and IKK β contain a NEMO-binding domain (NBD) at their C-termini, which is essential for their ability to activate the NF- κ B pathway (May *et al.*, 2002). Both IKK α and IKK β were predicted to contain a leucine zipper (LZ) and helix-loop-helix (HLH) domain, however these sequences were found instead to be part of the SDD (Kwak *et al.*, 2000). The crystal structures confirmed what was predicted from biochemical techniques; that both IKK α and IKK β form stable dimers (Drew *et al.*, 2007). The SDD of both IKK α and IKK β mediate dimerization (Figure 1.4C and E). IKK α and IKK β are capable of forming both homo- and heterodimers (Huynh *et al.*, 2000). The minimum stable composition of the canonical IKK complex is thought to be an IKK α :IKK β heterodimer bound to a dimer of NEMO subunits, although, as will be discussed in detail in Chapter 4, the exact composition of the IKK complex *in vivo* is still a matter of great debate, and may involve higher order oligomerization (Krappmann *et al.*, 2000; Miller & Zandi, 2001).

Despite having only 21.1% sequence identity with human ubiquitin (in the case of IKK β), the ULD of IKK α and IKK β both exhibit the ubiquitin fold. Curiously, the ULD was not expected from the IKK α sequence (May *et al.*, 2004), but its presence was confirmed by the recent X-ray crystal structure of human IKK α (Polley *et al.*, 2016). Furthermore, deletion of the ULD renders IKK β unable to phosphorylate I κ B α , but deletion of the same region in IKK α seemingly had no effect (May *et al.*, 2004). This discrepancy has not yet been investigated. The crystal structure of IKK β offered some explanation as to the functional significance of the ULD for IKK activity (Xu *et al.*, 2011). Structure-guided deletion mutants demonstrated that the ULD-SDD domains interact with the C-terminal PEST region of I κ B α and may specifically position I κ B α in such a way that only its N-terminal region (and the sites

of S32 and S36 phosphorylated by IKK β) is accessible to the IKK β catalytic site, while the ULD domain itself allosterically potentiates kinase domain activity.

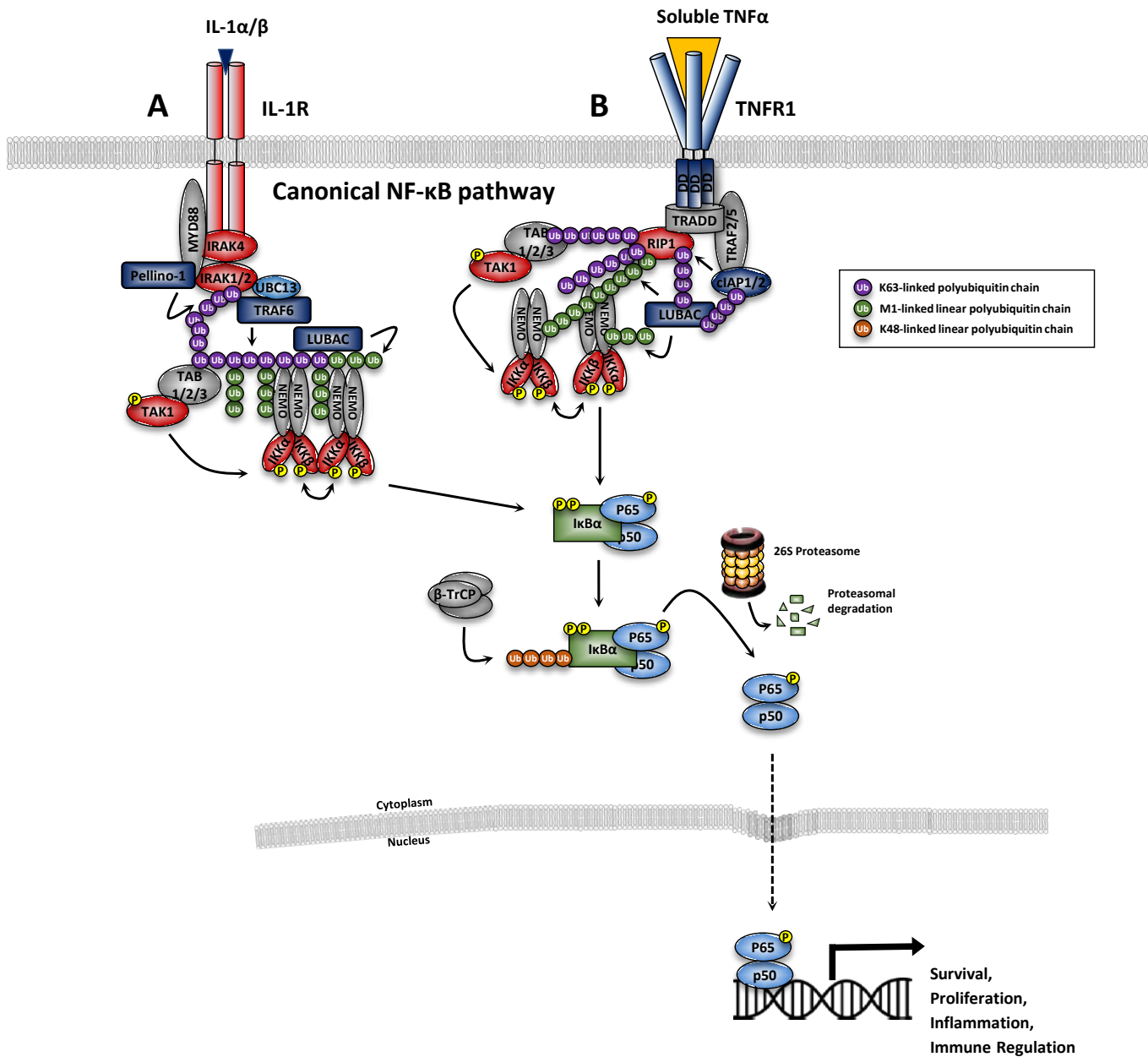


Figure 1.5. Overview of the canonical NF- κ B signalling pathway. The mechanism of activation of canonical NF- κ B signalling pathway is best characterised for inflammatory cytokines, such as IL-1 and TNF α . **(A)** Binding of IL-1 α or IL-1 β to the interleukin-1 receptor (IL-1R) leads to the assembly of the so-called ‘Myddosome’, which is an oligomeric structure consisting of the adaptor protein MyD88, IL-1 Receptor (IL-1R)-Associated Kinase 4 (IRAK4), IRAK1 and IRAK2. IRAK4 activates IRAK1, allowing IRAK1 to autophosphorylate and subsequently phosphorylate the E3-ligase Pellino-1, which in turn causes K63-polyubiquitylation of IRAK1. This leads to the recruitment and activation of TRAF6, which along with the E2-conjugating complex Ubc13-Uev1a, generates K63-linked polyubiquitin chains that serve to recruit and activate the TAK1 complex or TAB1/2/3-TAK1. K63-linked chains also serve as a substrate for the LUBAC complex, which conjugates M1-linked ubiquitin to these oligomers, to generate M1-K63-linked hybrid ubiquitin chains. The IKK complex is recruited to this complex through interaction of NEMO with M1-linked chains. The colocalisation of TAK1 and IKK to ubiquitin chains leads to activation of the IKK complex, which subsequently phosphorylates I κ B α to activate the NF- κ B pathway. **(B)** TNF α binding to the extracellular domain of the receptor leads to translocation of TNFR1 to lipid rafts and to the recruitment of TRADD to the cytoplasmic death domains of TNFR1. TRADD, in turn, recruits RIP kinase, and subsequently TRAF2 or TRAF5 adaptor proteins and CIAP1 or CIAP2 to assemble the TNFR1 complex I. CIAP1 and CIAP2 generate K63-linked polubiquitin chains on RIP1 and other components of the complex. This is necessary to recruit LUBAC, which stabilises complex I by catalysing the attachment of linear M1-linked polyubiquitin chains, typically to RIP1. K63-polyubiquitylated RIP1 also the TAK1:TAB complex. LUBAC-mediated M1-linked linear polyubiquitylation of RIP1, meanwhile promotes the recruitment of NEMO, as part of the IKK

complex. Binding of NEMO to ubiquitin chains is thought to induce a conformational change that contributes to the activation of associated IKK kinases. Membrane proximal recruitment of IKK kinases also contributes to IKK activation through proximity to TAK1, which is thought to prime the activation of IKK via phosphorylation of S176/S177 of IKK α /IKK β , and through oligomerisation of IKK complexes, which is thought to facilitate trans-autophosphorylation of the T loop, leading to full activation. The IL-1 and TNF α signalling pathways converge at the activation of the IKK complex, which subsequently phosphorylates I κ B proteins (at S32 and S36 I κ B α). This promotes the recognition of the PEST motif degron within I κ B α by β -TrCP, which is part of the E3 ubiquitin ligase SCF β -TrCP (S phase kinase-associated protein 1 (SKP1)-cullin 1-F-box protein containing β -transducing repeat-containing protein), and its K48-linked ubiquitylation, which targets I κ B α for proteasomal degradation. This enables NF- κ B complexes, such as p65-p50, to accumulate in the nucleus, where they activate NF- κ B-dependent genes involved in survival, proliferation, inflammation, immune regulation, etc. Adapted from Brenner et al., 2015 and Clark et al., 2013.

Meanwhile, NEMO acts as a scaffold within the IKK complex. An in-depth overview of the structure and function of NEMO will be presented in Chapter 4. In brief, NEMO adopts an elongated, parallel intermolecular coiled coil architecture and is composed of two alpha helical regions (α H1 and α H2), two elongated coiled coil domains (CC1 and CC2), a leucine zipper (LZ) domain, and a zinc finger (ZF) domain (Rothwarf et al., 1998). This elongated domain organisation enables NEMO to interact with multiple partners, often simultaneously. The interaction with IKK subunits is mediated by parts of the α H1 and CC1 domains at the N-terminus of NEMO, while interaction with I κ B α , which it recruits to IKK kinase subunits within the IKK complex, is mediated by the ZF domain at the extreme C-terminus (May et al., 2000; Schröfelbauer et al., 2012). The CC2 and LZ domains constitute a ubiquitin binding domain known as the ‘ubiquitin binding in ABIN and NEMO’ domain (UBAN), while the ZF domain is also able to interact with certain polyubiquitin chains (Cordier et al., 2009; Rahigi et al., 2009). The ability of NEMO to interact with ubiquitin chains is essential for IKK activation, as will be discussed shortly in Section 1.3.2.2.

1.3.2.2 Mechanism of IKK activation

Our understanding of the precise mechanism by which signals are transmitted from receptor to phosphorylation and activation of IKK kinases within the IKK complex is far from complete and remains an area of active research. Furthermore, the exact mechanism and the proteins involved appears to depend on the signalling receptor engaged. The following discussion will be limited to activation of the canonical NF- κ B pathway through ligation of the TNFR1 receptor (Figure 1.4), however, a brief description of the activation mechanism downstream of IL-1R ligation is also provided in the legend of Figure 1.4.

Receptor proximal events

Activation of IKK α and IKK β kinase activity requires the phosphorylation of specific residues in the activation loop of their active sites; S176 and S180 for IKK α and S177 and S181 for IKK β (Mercurio et al., 1997; Delhase et al., 1999). However, the many different receptors that activate IKK, including TNFR1, lack intrinsic enzymatic activity. The receptors rely, therefore, on recruitment to the membrane of a kinase activity capable of phosphorylating and fully activating the IKK kinases. Upon binding of soluble TNF α , TNFR1 redistributes to so-called ‘lipid rafts’ in the plasma membrane, which are enriched in cholesterol and sphingolipids (Legler et al., 2003). This appears to be necessary for TNF α -mediated NF- κ B activation. In addition, a ligand-binding induced conformational change occurs in the cytoplasmic death domains of the receptor complex, which facilitates the binding of the adaptor protein, TRADD (Hsu et al., 1995). Significant evidence suggests that the subsequent recruitment of RIP1, a serine/threonine kinase, is essential for assembly of the signalling complex that activates IKK. For example, RIP1 KOs are deficient in IKK activation (Meylan et al., 2004). Interestingly, however, in most cell types RIP1 kinase

activity is dispensable for IKK activation; NF- κ B activation is restored following reconstitution with a kinase dead mutant (Ting *et al.*, 1996; Devin *et al.*, 2000; Lee *et al.*, 2004). This suggests that RIP1 acts not in a catalytic capacity, but as a scaffold/adaptor. RIP1 is able to interact with various other signalling components, including NEMO and TRAF adaptors, interactions which are important for canonical NF- κ B activation (Hsu *et al.*, 1996). RIP1 has been proposed to facilitate oligomerization-induced activation of IKK as a mediator of induced proximity between kinase and substrate. Indeed, overexpression or enforced oligomerization of RIP1 leads to IKK activation (Hsu *et al.*, 1996; Ting *et al.*, 1996; Inohara *et al.*, 2000). Ubiquitination of RIP1 appears to be integral in the recruitment of downstream signalling components. Initially, K63-kinked ubiquitination of RIP1 was thought to be the key step in assembly of the receptor-proximal signalling complex (Wertz *et al.*, 2004; Ea *et al.*, 2006; Newton *et al.*, 2008). The exact E3 ligase responsible for such ubiquitination has been a matter of debate, but possibly involves the combined, possibly redundant, functions of TRAF2/5 and cIAP1/2 complexes (Li *et al.*, 2006; Bertrand *et al.*, 2008). Consistent with their importance, TRAF2/5 double knockout cells are defective in IKK activation (Yeh *et al.*, 1997; Nakano *et al.*, 1999; Tada *et al.*, 2001), while cIAP1/2 have been shown to be required for TRAF2-dependent K63-linked ubiquitination of RIP1 (Yin *et al.*, 2009). In addition to the controversy surrounding the exact RIP1 E3 ligase, however, there are also question marks surrounding the functional relevance of K63-polyubiquitin linkage. A knock-down and ubiquitin-replacement strategy has demonstrated that TNF α -dependent IKK activation, unlike IL-1 β -dependent activation, was largely unaffected by the absence of K63-linked chains (Xu *et al.*, 2009). This led to the suggestion that other ubiquitin linkages may be important in IKK activation. Indeed, TNF α treatment has since been shown to induce numerous different forms of ubiquitinated RIP1, including K48-, M1-, K63, and K11-linked ubiquitin chains (Haas *et al.*, 2009; Gerlach *et al.*, 2011; Dynek *et al.*, 2010). Curiously, however, only one ubiquitin acceptor site in RIP1, K377, has been determined to date, raising the question of whether TNF α signalling induces different populations of modified RIP1, or whether RIP1 is modified via hybrid chain linkages (Li *et al.*, 2006). The latter has been demonstrated in the IL-1 β -dependent signalling pathway (Figure 1.4), but not in the TNFR1 pathway (Emmerich *et al.*, 2013). Such hybrid chains are an attractive component of a model for IKK activation, as they would enable co-localisation of different signalling components required for IKK complex phosphorylation on the same polyubiquitin chain.

A key step in illuminating the role of ubiquitination in TNFR1 signalling was the identification of a new component of the signalling complex, the ‘linear ubiquitin chains assembly complex’ (LUBAC) (Haas *et al.*, 2009). LUBAC is formed of three subunits; heme-oxidised iron regulatory protein 2 ubiquitin ligase 1 (HOIL1), HOIL-interacting protein (HOIP) and SHANK-associated RH domain-interacting protein (SHARPIN) (Hass *et al.*, 2009; Tokunaga *et al.*, 2009; Ikeda *et al.*, 2011; Tokunaga *et al.*, 2011). Recruitment of this complex to the assembling signalosome depends on the K63-polyubiquitin activity of cIAP1/2, and recruitment is enhanced by, but not entirely dependent on, the presence of RIP1. LUBAC catalyses the attachment of M1-linked polyubiquitin chains to RIP1, and possibly other signalling components including NEMO (Hsu *et al.*, 1996; Haas *et al.*, 2009; Kirisako *et al.*, 2006). Such ubiquitination is thought to contribute to stabilisation of the TNFR1 signalling complex, recruitment of NEMO and, in turn, full activation of NF- κ B by TNF α (Rahigi *et al.*, 2009; Tokunaga *et al.*, 2009). Significant questions remain, however, regarding the relevance of LUBAC, and particularly SHARPIN, to NF- κ B activation. For example, SHARPIN-deficient mice are born normal, unlike core NF- κ B components, exhibit robust NF- κ B gene signatures and exhibit IL-1-dependent inflammatory phenotypes later in life (Gerlach *et al.*, 2011).

The various ubiquitin chains attached to RIP1 by LUBAC/cIAP1/2/TRAF2/5 appear to be important in facilitating the recruitment of NEMO, and hence the IKK complex, to the signalling complex. NEMO is able to interact with linear M1-linked chains via its UBAN domain (Lo *et al.*, 2009; Rahigi *et al.*, 2009), and with K63- and K11-linked chains via UBAN and ZF domains (Cordier *et al.*, 2009; Dynek *et al.*, 2010; Ngadjeau *et al.*, 2013). An L329P mutation in the UBAN domain has been demonstrated to abrogate binding to K63-linked polyubiquitin, binding of NEMO to RIP1, the recruitment of IKK to TNFR1, and the activation of IKK and NF- κ B in TNF α -stimulated cells (Wu *et al.*, 2006a). Notably, however, NEMO interacts with M1-linked ubiquitin with a 100-fold higher affinity than K63-ubiquitin (Rahigi *et al.*, 2009). Interaction of NEMO with ubiquitin chains is essential for activation of IKK in response to TNF α as cells expressing NEMO mutants that are unable to interact with ubiquitin, as well as immune disease patients with mutations in the UBAN domain, fail to induce robust activation of IKK α or IKK β (Ea *et al.*, 2006; Wu *et al.*, 2006a; Hubeau *et al.*, 2011). NEMO itself also undergoes both K63- and M1-linked polyubiquitination within its UBAN domain in response to TNF α and IL-1, although the stoichiometry in cells is low, and the functional significance has not been conclusively demonstrated (Yamamoto *et al.*, 2006; Ni *et al.*, 2008; Tokunga *et al.*, 2009).

Another seemingly integral signalling component, the TAB-TAK1 kinase complex, is recruited to the receptor complex through interaction of TAB2/3 with K63-linked polyubiquitin chains attached to NEMO and RIP1 (Kanyama *et al.*, 2004). An additional layer of complexity comes from reports suggesting that binding of TAB2/3 to unanchored K63-linked polyubiquitin chains facilitates the autophosphorylation and activation of TAK1 (Xia *et al.*, 2009).

Models of IKK kinase activation

At this point it should be clear that there is a great deal of uncertainty surrounding the exact molecular events that follow canonical NF- κ B receptor ligation. This uncertainty extends to the mechanism of IKK phosphorylation and activation itself. We have seen how IKK might be recruited to the signalling complex through NEMO-mediated interaction with polyubiquitin chains, but there are various non-mutually exclusive models for how IKK becomes activated. The key questions that remain unresolved are: 1) the exact function, and nature (attached or unattached), of non-degradative ubiquitination in activation of IKK and 2) whether IKK phosphorylation occurs through autophosphorylation, or through activity of an upstream kinase, such as RIP1 or TAK1. Regarding the former, three potential mechanisms have been proposed for the role of non-degradative ubiquitination: direct activation, induced proximity and complex stabilisation (Hayden & Ghosh 2012). Evidence for the former mechanism is weaker than the latter two. It is proposed that binding of ubiquitin chains by NEMO might induce allosteric conformational changes in the IKK complex that facilitate activation of IKK kinases. For example, the X-ray structures of ubiquitin-bound and free forms of the UBAN domain of NEMO suggest that diubiquitin binding induces a straightening of the upstream coiled coil region which connects to the IKK binding domain of NEMO (Rahigi *et al.*, 2009). However, biophysical approaches have suggested that polyubiquitin-binding induced conformational changes involve subtle changes in the equilibrium of conformational states, rather than large gross structural change (Catici *et al.*, 2016). Non-degradative ubiquitination seems to play a clear role in stabilising the TNFR1 signalling complex, through cross-linking various ubiquitin-domain (UBD) containing

proteins, and through protecting components from K48-linked ubiquitination, as has been shown to be the case for RIP1 (Harhaj & Dixit, 2011).

A mechanism of IKK activation involving ubiquitin-binding-induced proximity and oligomerization effects has received relatively strong experimental support. For example, dimerization of IKK is necessary and sufficient for the constitutive activation observed when IKK is overexpressed (Zandi *et al.*, 1997). Furthermore, enforced oligomerization of NEMO, RIP1 or IKK is capable of activating NF- κ B (Inohara *et al.*, 2000; Poyet *et al.*, 2000). Meanwhile, NEMO mutants that are unable to oligomerise exert dominant negative effects on NF- κ B activation (Tegethoff *et al.*, 2003; Agou *et al.*, 2004). Structural regions of NEMO involved in dimerization and higher order oligomerization have been shown to be essential for reconstituting NF- κ B activity in NEMO deficient cell lines (Marienfield *et al.*, 2006). Free-ubiquitin chains are also able to induce IKK activation via *trans* auto-phosphorylation (Xia *et al.*, 2009). Furthermore, various post-translational modifications of NEMO, such as phosphorylation of S68, which interfere with dimerization/oligomerization of NEMO, also terminate signalling as part of feedback inhibition mechanisms (Palkowitsch *et al.*, 2008). In addition, the existence of NEMO-dependent higher order supramolecular structures has received *in vivo* experimental support in the last few years (Tarantino *et al.*, 2015; Scholefield *et al.*, 2016). Super-resolution microscopy was used to visualise apparent NEMO-dependent lattice structures in non-stimulated cells, whose integrity could be disrupted through abrogation of IKK-binding or non-covalently attached linear/K63-linked polyubiquitin chains (Scholefield *et al.*, 2016).

This evidence for higher-order structures, combined with recent X-ray crystal structures of IKK β dimers in catalytically active conformations, has led to the proposal of a model for IKK activation involving oligomerization-mediated trans-autophosphorylation of IKK subunits (Figure 1.6) (Polley *et al.*, 2013). In contrast to the ‘closed-conformation’ observed in the earlier *Xenopus* IKK β structure, the structure of human IKK β captured IKK β dimers in an open-conformation, where the SDD domains are splayed further apart in a V-shaped interface. This permitted higher order oligomerization within the crystal that was not seen in earlier structures. Such oligomerization might place the kinase domains of neighbouring dimers into close contact in order to facilitate trans-autophosphorylation. Indeed, mutagenesis suggested that oligomer interaction residues are critical for activation of IKK β in cells. The authors speculated that a priming phosphorylation of the one IKK β subunit might increase its propensity to transiently undergo higher order oligomerization that would mediate complete IKK active site phosphorylation. Interestingly, evidence for TAK1 priming phosphorylation of IKK β in response to TNF α and IL-1 has since been presented (Zhang *et al.*, 2014). Zhang *et al* found that TAK1 phosphorylates IKK β at S177 in a priming event that enables IKK β to fully activate itself by phosphorylating S181. This priming event was shown to require interaction between M1-linked chains and NEMO. Whether this mechanism also applies to IKK α remains to be investigated.

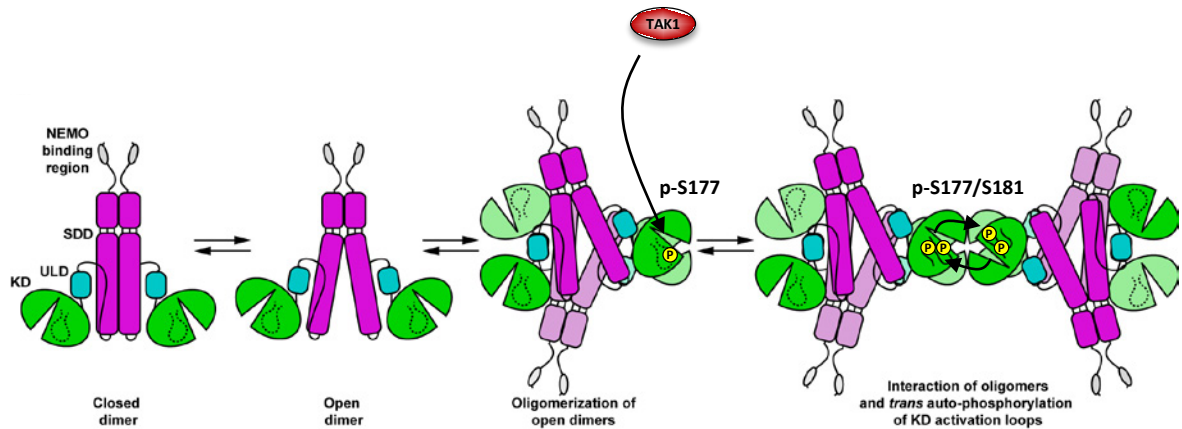


Figure 1.6. IKK β oligomerization activation model involving sequential TAK1 and trans-autophosphorylation of active site residue. The closed dimer conformation was observed in the inactivated Xenopus IKK β structure. Conversely, in the active human IKK β crystal structure, the dimers adopted an open conformation. Flexibility within the SDD permits a transition between closed and open conformations. The open dimeric form of IKK β is able to undergo reversible higher order oligomerization through specific interactions between the KD-ULD and SDD domains of individual protomers. Such higher order oligomerization is sterically unfavourable when the dimers are in the closed conformation, which might explain why they were not observed in the crystal lattice of inactive Xenopus IKK β . Such higher order assemblies would position the catalytic domains of neighbouring subunits in close proximity to enable trans-autophosphorylation. Consistent with this model, mutation of residues involved in higher order oligomerization severely inhibits IKK activation in cells. Shown also is the possible involvement of TAK1 priming phosphorylation of S177, which might promote the subsequent trans autophosphorylation of S181 and full activation of IKK β (as evidenced by Zhang *et al.*, 2014). Figure adapted from Polley *et al.*, 2013.

Activated IKK kinases subsequently phosphorylate I κ B α , as well as NF- κ B subunits themselves, to induce NF- κ B transcriptional activity. As will be discussed in greater detail in Chapter 3, NEMO is absolutely essential for the activation of canonical NF- κ B in response to all stimuli, while the exact requirement for IKK α or IKK β appears to depend on the nature of the stimulus and the cell type.

1.3.2.3 Mechanisms of feedback inhibition

A number of self-regulating mechanisms mediate negative feedback control to restrict and properly terminate activation of the pathway following a stimulus. Each mechanism is induced with a sufficient time delay to enable full NF- κ B pathway activation in the interim. They also poised the system for reactivation in the face of sustained stimulation. The overlap of different negative feedback allows for repeated cycles of reactivation, and leads to oscillatory NF- κ B activity that may enable the fine control of downstream gene expression patterns (see Section 1.3.3.2). Many of these feedback mechanisms are important in the resolution of inflammation, and therefore are important in the pathogenesis of various inflammatory diseases, including cancer (Lee *et al.*, 2000; Kovalenko *et al.*, 2003).

The classic feedback loop that was the first to be defined was the NF- κ B-dependent activation of I κ B α gene expression (Auphan *et al.*, 1995). Indeed, I κ B α is one of the earliest genes to be expressed downstream of NF- κ B activation. Newly expressed I κ B α displaces NF- κ B subunits bound to DNA and shuttles them back into the cytoplasm to inactivate the pathway (Arenzana-Seisdedos *et al.*, 1995). A similar feedback loop involving induction of another classical I κ B protein, I κ B ϵ , also exists, but is invoked with slower kinetics to dampen the induction of late-phase genes (Whiteside *et al.*, 1997) (see Section 1.3.4. for more details).

The expression and/or activity of various deubiquitinase (DUB) enzymes that act to inhibit the signalling complex that activates the IKK complex is also induced by activation of the canonical NF- κ B pathway in an important negative feedback loop. The most prominent example is the DUB, A20, which is induced after NF- κ B activation (Lee *et al.*, 2000). Cezanne is another A20 family member that is induced by NF- κ B activation to downregulate the pathway (Enesa *et al.*, 2008). The N-terminal domain of A20 mediates the deubiquitination of K63-linked polyubiquitin chains on RIP1 and NEMO, thus leading to the disassembly of the signalling complex that activates IKK (Wertz *et al.*, 2004). Interestingly, its C-terminal domain also functions as an E3 ligase to mediate the K48-linked polyubiquitination of RIP1, thus targeting it for proteasomal degradation, which also serves to inhibit the pathway. A20 also inhibits E3 ligase activities of TRAF2 and cIAP1 to further block activation of the pathway (Shembade *et al.*, 2010). Furthermore, phosphorylation of A20 by IKK β has been shown to enhance the activity of A20 (Hutti *et al.*, 2007). A20 also inducibly forms a complex together with the regulatory molecules, TAX1BP1, Itch and RNF11, which is essential for A20 function and recruitment to canonical NF- κ B receptors. Stimulus induced phosphorylation of TAX1BP1 by IKK α was shown to be essential for assembly of the A20 editing complex and thus feedback inhibition of the pathway (Shembade *et al.*, 2011).

Another time-delayed feedback mechanism is intrinsic to the IKK complex itself. A cluster of C-terminal serine residues in IKK β (see Figure 1.4) undergoes cumulative, constitutive auto-phosphorylation upon activation of the IKK complex that is thought to induce a conformation change that decreases kinase activity by 20-30 minutes post-induction (Delhase *et al.*, 1999).

Various feedback mechanisms also occur within the nucleus to inhibit NF- κ B transcriptional output. Some of these are mediated by atypical I κ B family members, as will be discussed in Section 1.3.4.4. Another is thought to involve nuclear IKK α activity. Various inflammatory stimuli, including TNF α , have been shown to lead to IKK α -dependent phosphorylation of the SUMO E3 ligase, PIAS1, which releases PIAS1 to terminate the expression of a subset of NF- κ B-dependent genes through interference of the DNA-binding of p65:p50 dimers (Liu *et al.*, 2007).

Consideration of these feedback mechanisms will be important in developing therapies that target the NF- κ B pathway.

1.3.2.4 NF- κ B-independent functions of IKK kinases

Outside of their direct role in the NF- κ B signalling pathway, both IKK α and IKK β have been proposed to phosphorylate an ever-growing list of substrates involved in a myriad of different biological functions (Figure 1.7). Most of these phosphorylation events are very recently discovered, and thus the level of validation and the associated roles of IKK remain highly putative. However, it is clear that the IKK complex is emerging as a central point of cross-talk between NF- κ B and other signalling pathways. Many of the substrates phosphorylated by IKK α and IKK β , such as FOXO3a and TSC1, are involved in proliferative and pro-survival pathways, and thus these NF- κ B-independent functions of the IKKs may contribute to tumour promotion (see Section 1.4.3).

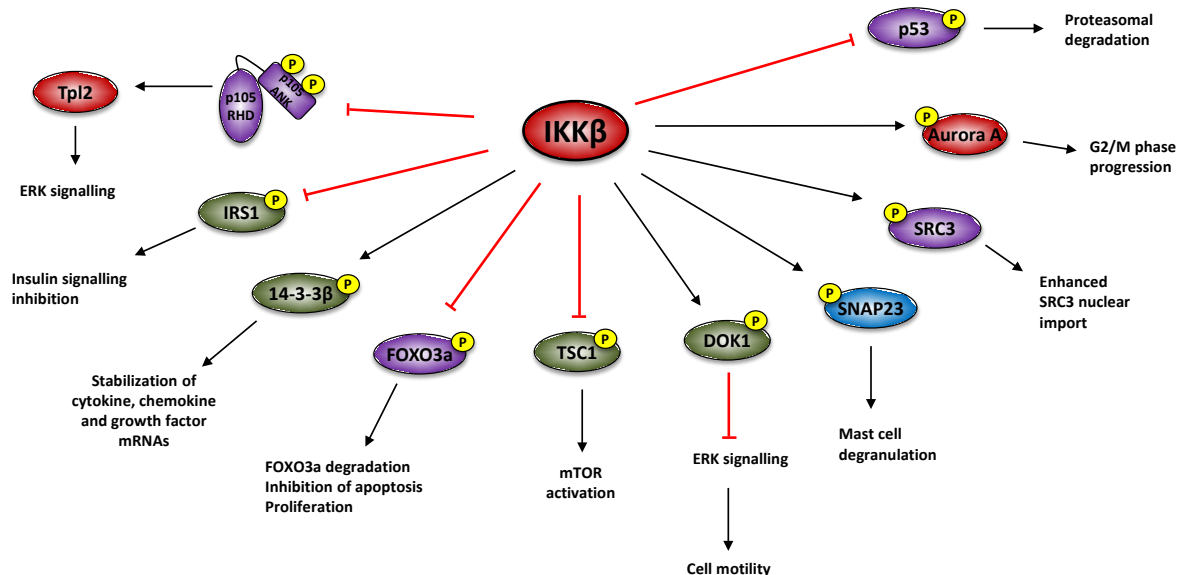
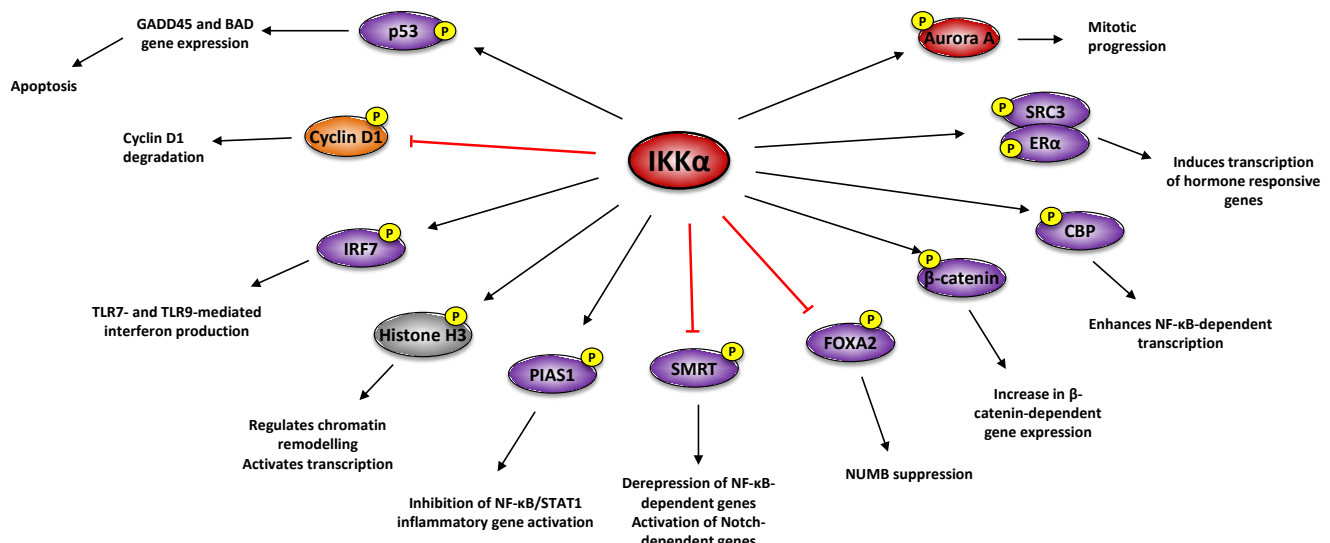
A**B**

Figure 1.7. NF-κB-independent functions of IKK β and IKK α . The IKK kinases phosphorylate a range of substrates, besides those involved in NF-κB activation, and thus mediate cross-talk with a host of other signalling cascades. **(A)** In some cell types p105 is found in a complex with the kinase TPL2. IKK β phosphorylates p105, which triggers processing/degradation of p105, and releases TPL2, resulting in activation of the proliferative ERK1/2 signalling pathway (Waterfield *et al.*, 2004). IKK β phosphorylates insulin receptor substrate 1 (IRS-1), which interferes with its insulin receptor-dependent tyrosine phosphorylation, and thus impairs insulin-dependent signalling pathways. This is thought to be one mechanism by which proinflammatory cytokines can contribute to the development of insulin resistance and type 2 diabetes (Tilg *et al.*, 2008). Downstream of TNF α signalling IKK β phosphorylates 14-3-3 β , which releases the 14-3-3 β -TPP complex from ARE sequences within multiple mRNAs encoding cytokines, growth factors and chemokines, leading to their stabilisation (Gringhuis *et al.*, 2005). IKK β also phosphorylates the transcription factor, tumour suppressor FOXO3a, which leads to its nuclear exclusion and proteasomal degradation, thus inhibiting FOXO3a-dependent cell death and/or cell cycle arrest (Hu *et al.*, 2004). This is one mechanism by which IKK activity can promote tumorigenesis. IKK β also phosphorylates and inhibits tuberous sclerosis 1 (TSC1) downstream of TNF α . This leads to activation of the mTORC1 complex and can promote inflammation-mediated tumour angiogenesis in various tumour types due to consequent enhanced production of VEGF (Lee *et al.*, 2007). IKK β also phosphorylates and activates the MAPK pathway adaptor protein, DOK1 in response to TNF α or IL-1. DOK1 in turn inhibits ERK1/2 activation, and this has been shown to promote cell motility (Lee *et al.*, 2004). IKK β activated downstream of the Fc ϵ RI receptor also phosphorylates SNAP-23, a component of SNARE complexes involved in exocytosis pathways, to promote IgE-mediated mast cell degranulation (anaphylaxis) (Suzuki *et al.*, 2008) and platelet secretion (Karim *et al.*, 2013). IKK β downstream of TNF α also phosphorylates the transcriptional coactivator SRC-3 to promote its nuclear import, where it

regulates gene expression (Wu *et al.*, 2002). IKK β has also been demonstrated to phosphorylate Aurora A, which modulates its stability and prevents hyperactivation of Aurora A during mitosis (Irelan *et al.*, 2007). IKK β phosphorylation of p53 at S362 and S366 has been proposed to lead to its Mdm2-independent ubiquitination and degradation and hence inhibition of p53-dependent gene expression (Xia *et al.*, 2008).

(B) IKK α has been shown to phosphorylate a number of substrates involved in pathways other than NF- κ B. IKK α contains a predicted nuclear localisation sequence (NLS) that enables it to localise to the nucleus. Indeed, any of these phosphorylation events occur in the nucleus. IKK α has been shown to phosphorylate p53 at S20, downstream of Protein kinase Cdelta in response to oxidative stress, which enhances p53-mediated expression of pro-apoptotic genes GADD45 and BAD and leads to induction of apoptosis (Yamaguchi *et al.*, 2007). IKK α phosphorylates cyclin D1 at T286, leading to its nuclear export and degradation (Kwak *et al.*, 2005). In dendritic cells, IKK α activated downstream of TLR7 and TLR9 receptors phosphorylates the adaptor protein IRF7, leading to increased interferon- α (IFN α) production, and thus contributing to antiviral immunity and pathogenesis of disorders of elevated IFN-production (Hoshino *et al.*, 2006). In response to inflammatory cytokines, IKK α has been proposed to phosphorylate Histone H3 at S10 at the promoters of various NF- κ B-target genes to promote chromatin remodelling and increased gene expression (Yamamoto *et al.*, 2003). In response to inflammatory cytokines, IKK α also phosphorylates the transcriptional regulator, Protein inhibitor of activated STAT1 (PIAS1) at S90, which promotes PIAS1-dependent repression of NF- κ B and STAT1 gene promoters (Liu *et al.*, 2007). IKK α has been proposed to phosphorylate the corepressor, SMRT, to trigger its nuclear export along with associated HDAC3, and the proteasomal degradation of SMRT. This allows other transcriptional coactivators, such as CBP to bind to and promote the expression of NF- κ B-dependent genes (Hoberg *et al.*, 2004). Loss of SMRT also leads to derepression of certain Notch-dependent genes Fernandez-Majada *et al.*, 2007). IKK α also contribute to the derepression of Notch-dependet genes through the phosphorylation of FOXA2 transcription regulator, leading to suppression of NUMB expression; a protein that targets Notch1 for lysosomal degradation (Andersen *et al.*, 2012; Liu *et al.*, 2012). This may contribute to inflammation-mediated liver cancer progression. IKK α phosphorylates the transcriptional coactivator β -catenin to block its polyubiquitination and degradation, and thus promote β -catenin-dependent transcription (Lamberti *et al.*, 2001; Carayol *et al.*, 2006). In turn this induces cyclin D1 transcription, such that IKK α plays a key role in mitogenic signalling (Albanese *et al.*, 2003). IKK α also phosphorylates the transcriptional coactivator CBP, to switch the binding preference of CBP from p53 to NF- κ B, and thus promote NF- κ B-dependent gene expression, proliferation and survival, and concomitantly limit cell p53-dependent transcription and apoptosis (Huang *et al.*, 2007). IKK α also phosphorylates the transcriptional coactivators, SRC3 and ER α in breast cancer cells to induce the transcription of estrogen hormone responsive genes, such as cyclin D1 and c-myc (Park *et al.*, 2005). IKK α has also been proposed to phosphorylate Aurora A at T288, to modulate Aurora A kinase activity and promote progression through mitosis. Figure adapted from Perkins, 2007.

Interestingly, NEMO may play a role in restricting the otherwise broader kinase activity of IKK β to I κ B α and other components of the NF- κ B pathway (Schröfelbauer *et al.*, 2012). Expression of C-terminal NEMO mutants that permit activation of IKK β in response to pro-inflammatory cytokines, but that fail to recruit I κ B α to the IKK complex results in hyperphosphorylation of alternative IKK β substrates. These alternative substrates were, however, NF- κ B-dependent (p105, p65 etc), so the relevance of this study to cross-talk with other pathways is unclear.

Many of the NF- κ B-independent functions of IKK α are the consequence of its ability to localise to the nucleus. Numerous studies have demonstrated basal nuclear localisation for IKK α (Lamberti *et al.*, 2001), and some have suggested that the nuclear localisation of IKK α is stimulus dependent (Anest *et al.*, 2003; Yamamoto *et al.*, 2003). IKK β , meanwhile, is detected predominantly in the cytoplasm. Although a handful of studies have proposed a nuclear localisation of IKK β under certain circumstances; for instance, following neutrophil activation (Ear *et al.*, 2005), in the NF- κ B signalling response to UV radiation (Tsuchiya *et al.*, 2010) and following DNA damage (Sakamoto *et al.*, 2013).

1.3.3 The NF- κ B transcription factor family

1.3.3.1 Structure, dimerization and binding to DNA

The NF- κ B family of transcription factors are defined by their conserved 300 amino acids long N-terminal Rel homology domains (RHD), which are responsible for homo- and hetero-dimerization, sequence-specific DNA

binding, nuclear translocation and interaction with I κ B proteins (Figure 1.8) (Sen and Baltimore, 1986; Baldwin *et al.*, 1996; Ghosh *et al.*, 1998). Up to 15 different NF- κ B dimers are possible, although the physiological relevance of all possible dimeric complexes has not been demonstrated; only 12 have been identified *in vivo*, and some of these are limited to specific subsets of cells (Hayden & Ghosh 2004). The p50:p65 dimer is the most abundant and is found in almost all cells as the primary target of canonical NF- κ B signalling; this predominance is due largely to the high affinity with which p50 and p65 interact (Baldwin, 1996). The specific composition of NF- κ B dimers determines their effect on transcription. The NF- κ B family can be subdivided into two groups based on their ability to activate transcription; p65, c-Rel and RelB contain a transcriptional activation domain (TAD) at their C-termini, while p50 and p52 do not. As such, dimers containing at least one of p65, c-Rel and RelB function as activators of transcription, while those made up exclusively of p50 and p52 function as transcriptional repressors (Franzoso *et al.*, 1992). p50 and p52 are unique in that they can also form transcriptionally active complexes with the TAD-containing atypical I κ B proteins, BCL3 and I κ B ζ . RelB is unique in that it can only form complexes with p50 and p52, and it requires its N-terminal leucine zipper region alongside its TAD for full transcriptional activity (Ryseck *et al.*, 1992; Dobrzanski *et al.*, 1993; Dobrzanski et a., 1994).

X-ray crystal structures of NF- κ B dimers revealed that the RHD consists of two domains, each with an immunoglobulin-like fold, joined by a flexible linker; the N-terminal domain of the RHD largely mediates specific interactions with DNA, while the C-terminal domain is predominately involved in dimerization and I κ B interaction.

Once liberated from complexes with I κ B proteins, NF- κ B dimers accumulate in the nucleus and bind to so-called DNA κ B sites within promoters and enhancers. These sites typically have a highly degenerate 10 base pair consensus sequence: 5'-GGGRNWWYCC-3' (where N is any base, R is purine, W is adenine or thymine, and Y is is pyrimidine), such that NF- κ B subunits regulate transcription of a wide variety of target genes (Pahl, 1999). X-ray crystal structures of NF- κ B:DNA complexes revealed that the RHD of two NF- κ B subunits makes intimate contacts within the major groove of a complete turn of DNA (Ghosh *et al.*, 1995; Müller *et al.*, 1995). Each subunit within the dimer recognises half of the DNA consensus sequence (Berkowitz *et al.*, 2002; Escalante *et al.*, 2002).

1.3.3.2 Transcriptional activity and function

The degeneracy of the NF- κ B DNA-binding site means that such sites are found widely dispersed throughout the genome; there are approximately 106 consensus κ B sites in the human genome, and an even greater number of non-consensus sites to which NF- κ B can also bind (Antonaki *et al.*, 2011). However, the majority of signals activating the NF- κ B pathway activate only a specific subset of the genes that NF- κ B dimers are capable of activating. A major question, therefore, is how the NF- κ B pathway can respond to diverse stimuli to mediate specific transcriptional programs in certain physiological contexts. Clearly, DNA binding site specificity alone is not sufficient to confer such complexity.

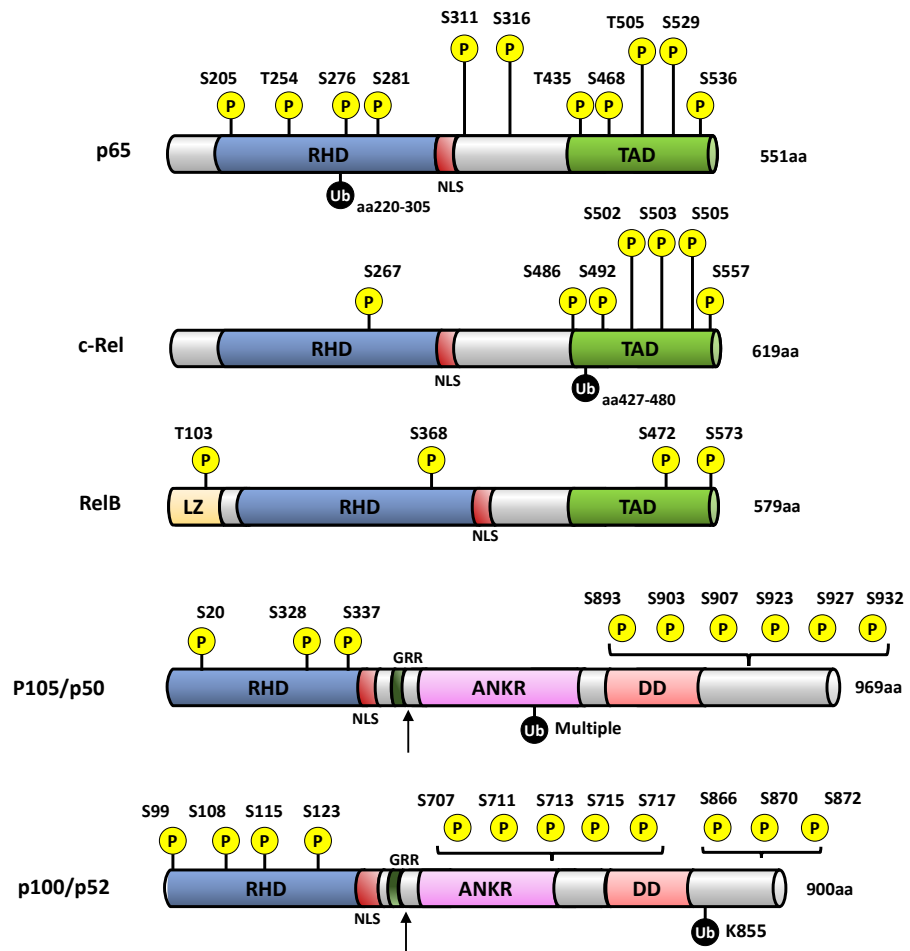


Figure 1.8. Domain organisation of the NF-κB family of transcription factors. The NF-κB proteins are a family of five related transcription factors; p65, c-Rel, RelB, p50 and p52 that may homo- and hetero-dimerise to generate at least 12 different characterised transcriptionally active dimers. Each of the members contains a conserved 300 amino acid long N-terminal Rel homology domain (RHD) that mediates DNA binding, dimerization, IκBα interaction and nuclear translocation (NLS). The family can be divided further into two groups based on their transactivation potential; only p65, RelB and c-Rel contain a C-terminal transactivation domain (TAD) that is responsible for the transcriptional activity of dimers containing these subunits. p50 and p52, which are generated by limited proteolytic processing of the precursor proteins, p105 and p100, respectively, lack a TAD, and thus act as transcriptional repressors in the homodimeric form. p100 and p105 are also classified as IκB proteins due to their C-terminal ankyrin repeats (ANKR), which enable them to bind to other NF-κB subunits and inhibit their nuclear localisation. A glycine rich region (GRR) in p105 and p100 terminates proteolytic processing by the proteasome to prevent complete proteolysis and to generate p50 and p52. An arrow indicates the approximate location of the C-terminal residues of p50 and p52 generated. The C-terminal death domains (DD) of p100 and p105 mediate protein interactions with adaptor proteins involved in regulating apoptosis, NF-κB and AP-1 pathways. In p105 it also mediates interactions with IKK kinases, while in p100 it functions as a processing inhibitory domain (PID) that restricts basal processing to p52. RelB is unique in that it also contains an N-terminal leucine zipper (LZ) region that is required alongside its TAD to be fully active (Dobrzanski *et al.*, 1993). RelB cannot form homodimers, and preferentially binds to p100/p52. Phosphorylations that have been shown to regulate NF-κB are highlighted on each subunit. Numbering corresponds to human amino acid sequence. Ub refers to K48 linked polyubiquitination.

NF-κB subunit dimerization plays a significant role in determining transcriptional specificity. Early *in vitro* binding studies demonstrated that each NF-κB dimer has a degree of preference for a specific subset of κB sites, with some binding to specific sites with a higher affinity than others (Phelps *et al.*, 2000). This was confirmed in studies using NF-κB knockout cell lines, which demonstrated that specific NF-κB-regulated genes have distinct requirements for certain NF-κB dimers (Hoffman *et al.*, 2003). One such example is the mouse B lymphocyte chemokine (BLC) and EBI1-ligand chemokine (ELC) κB sites, which are specifically bound by RelB:p52

heterodimers downstream of non-canonical NF- κ B pathway activation (Bonizzi *et al.*, 2004). A large scale analysis of DNA sites recognized by eight different NF- κ B dimers extended these observations further to define three distinct binding-specificity classes; p50 or p52 homodimers, c-Rel or p65 homodimers; and heterodimers (Siggers *et al.*, 2011). However, c-Rel homodimers bound with much greater affinity than p65 homodimers to all κ B dimers, while NF- κ B heterodimers exhibited very little sequence specificity over one another, highlighting the need for additional specificity determinants in the cell.

Indeed, another key mechanism of transcriptional specificity is imparted by the dynamic, temporal nature of NF- κ B signalling activation kinetics. NF- κ B inducible genes exhibit distinct temporal expression profiles (Hoffmann *et al.*, 2002). For example, microarray studies of cells treated with TNF α have identified distinct expression profiles loosely defined as early, middle, and late, peaking 1, 3 and 6 hours after stimulation, respectively (Tian *et al.*, 2005a). This complexity is thought to emerge from the fact that NF- κ B displays both monophasic and oscillatory activation modes, depending on stimulus duration, brief and tonic, respectively (Nelson *et al.* 2004). Such oscillatory behaviour in NF- κ B nuclear translocation is thought to occur as a result of the various layers of negative feedback induced by IKK activity and NF- κ B-dependent transcription itself; the classic example being the NF- κ B-dependent transcriptional activation of I κ B protein expression (Auphan *et al.*, 1995). The differing kinetics with which the different I κ B family members are induced imparts fine control on the duration of NF- κ B activation oscillations (Hoffmann *et al.*, 2002). Another example is the induction of the deubiquitinase enzyme, A20 by NF- κ B transcriptional activity and the activation of A20 by IKK β -dependent phosphorylation, both of which impart feedback inhibition on the pathway at the level of the IKK activation (see Section 1.3.2.3) (Lee *et al.*, 2000; Hutt *et al.*, 2007). Single cell techniques have been used to study these oscillations and demonstrate that alterations in stimulation interval and duration drive different patterns of NF- κ B-dependent gene expression (Ashall *et al.*, 2009).

An additional mechanism of transcriptional specificity is achieved through interactions between NF- κ B dimers and other heterologous transcription factors and regulators. This further broadens the range of possible NF- κ B target genes and imparts context dependency on NF- κ B-dependent gene expression, enabling cross-talk between NF- κ B and other signalling pathways. For example, transcriptional activation of human interferon B (*IFNB*) necessitates the assembly of an enhanceosome containing p50:p65 NF- κ B dimers, ATF-2:c-Jun dimers and IRF-3/IRF-7 (Panne *et al.*, 2007). Such genes containing promoters requiring simultaneous binding of NF- κ B and other transcription factors will only be expressed when both signalling pathways are activated – so-called ‘coincidence detection.’ NF- κ B proteins are also capable of interacting with various transcriptional coactivators and corepressors, including components of the basal transcription apparatus, such as TATA-binding protein (TBP) and transcription factor IIB (TFIIB), histone acetyltransferases (HATs), such as CBP, PCAF and p300, and histone deacetylases (HDACs), such as HDAC1 and HDAC3, in order to regulate chromatin structure and promote or repress assembly of the pre-initiation complex (PIC) (Xu *et al.*, 1993; Schmitz *et al.*, 1995; Perkins *et al.*, 1997; Ashburner *et al.*, 2001). p50 and p52 homodimers lack a transcription domain and thus are only able to interact with HDACs to repress transcription (Franzoso *et al.*, 1992; Elsharkawy *et al.*, 2010).

The final major mechanism of NF- κ B transcriptional specificity is achieved through post-translational modifications of the NF- κ B subunits themselves.

1.3.3.3 Post-translational modifications of NF-κB subunits

A vast array of NF-κB subunit post-translational modifications have been characterised to date. These regulatory modifications, which include phosphorylation, ubiquitination, sumoylation, acetylation and nitrosylation, can be mediated either by components of the NF-κB pathway itself, particularly IKK α and IKK β , or by components of heterologous signalling pathways. NF-κB subunit modification provides an additional layer of fine control through which NF-κB transcriptional activity can be modulated and represents a key site of cross-talk within the wider signalling network (Perkins, 2007). Some of the best characterised phosphorylation and ubiquitination sites in human NF-κB subunits are highlighted in Figure 1.8. The following discussion will be limited to NF-κB phosphorylation, and particularly phosphorylation of the primary canonical NF-κB subunit, p65, which has been the focus of most studies of NF-κB modification.

NF-κB subunit phosphorylation can occur in the cytoplasm or the nucleus and can influence numerous aspects of NF-κB function, including but not limited to: protein stability and degradation, interaction with IκB subunits, nuclear translocation, DNA binding, transcriptional activity, recruitment of transcriptional coregulators, and termination of the signalling response (Viatour *et al.*, 2005; Perkins, 2006). To-date, eleven well-characterised or putative phosphorylation sites within p65 that span the N-terminal RHD, the interdomain linker and the C-terminal TAD have been identified (Christian *et al.*, 2016). Phosphorylation of p65 in response to pro-inflammatory cytokines has been shown to result in a striking conformational change that impacts its ubiquitination, stability and protein-protein interactions (Milanovic *et al.*, 2014). The two best-characterised phosphorylation sites are Serine 276, within the RHD and Serine 536, within the TAD.

Phosphorylation of p65 at Serine 276 has been proposed to be catalysed by a host of kinases, including protein kinase A (PKAc), MSK1/2, p90-RSK, Pim-1 and protein kinase C (PKC α) (Zhong *et al.*, 1998; Vermeulen *et al.*, 2003; Wang *et al.*, 2010; Wang *et al.*, 2011). Following IκB α degradation, PKAc phosphorylates p65 at S276 within the cytoplasm in a cAMP-independent manner. This promotes the promoter-proximal interaction of p65 with the coactivator CBP/p300, as well as the recruitment of cyclin dependent kinase 9/cyclin T1 complexes, and the recruitment of phosphorylated RNA Polymerase II, leading to the expression of a subset of NF-κB-dependent genes (Zhong *et al.*, 1998; Dong *et al.*, 2008; Nowak *et al.*, 2008; Hochrainer *et al.*, 2013).

Phosphorylation of p65 at Serine 536 has been shown to have both positive and negative effects on NF-κB-dependent transcription and its precise role remains controversial. Both IKK α and IKK β have been shown in numerous studies to phosphorylate p65 at S536 (Sakurai *et al.*, 1999; Sizemore *et al.*, 2002). Various studies have suggested that IKK α / β -dependent phosphorylation of S536 enhances the transcriptional activity of p65 in response to a variety of stimuli (Madrid *et al.*, 2001; Yang *et al.*, 2003; Mahony *et al.*, 2004; Douilette *et al.*, 2006). Furthermore, it has been suggested that S536 phosphorylated p65 is not bound or inhibited by newly synthesised IκB α , such that S536 phosphorylated p65 can evade the feedback inhibition imparted by *de novo* IκB α and translocate into the nucleus to maintain the expression of a subset of genes (Sasaki *et al.*, 2005). TNF α -induced S536 phosphorylation has also been proposed to promote p65 K310 acetylation and p65 transactivation (Chen *et al.*, 2005). In addition, phosphorylation of S536 has been implicated in pathogenic NF-κB activation associated with various inflammatory diseases, including Helicobacter pylori-induced inflammation (Song *et al.*, 2006; Lamb *et al.*, 2009; Kim *et al.*, 2014).

However, a number of studies have found no role or an inhibitory effect of S536 phosphorylation on p65-dependent transcription. Okazaki *et al* observed a complete rescue of TNF α or IL-1-induced IL-6 production in p65 KO MEFs reconstituted with p65 S536A mutants, while Mattioli *et al* suggested that S536 phosphorylation induced by T-cell costimulation is IKK β -, but not IKK α - dependent, occurs in the cytoplasm and negatively regulates p65 nuclear import (Okazaki *et al.*, 2003). Moreover, phosphorylation of S536 by IKK α has been proposed as a major mechanism of pathway inhibition and resolution of inflammation in macrophages through the enhanced turnover of p65 and removal from proinflammatory gene promoters (Lawrence *et al.*, 2005). Independent studies with IKK α KO macrophages, however, have not supported these findings (Li *et al.*, 2005); p65 S536 phosphorylation appeared normal and p65 stability was unaffected. A more recent study attempted to settle these discrepancies through the generation of an S534A- (mouse homolog of human S536) knock-in mouse model (Pradère *et al.*, 2016). The authors reported increased late-phase expression of genes following treatment with LPS, as a result of modest increases in the stability of p65. Such mice exhibited increased mortality following injection with LPS, consistent with the findings of Lawrence *et al.*

Another TAD phosphorylation site, Serine 468, has been shown to be phosphorylated by three kinases, with differing biological outcomes. GSK3 β has been proposed to mediate basal phosphorylation of this site to inhibit p65 transcriptional activity in the absence of stimulation (Buss *et al.*, 2004). In contrast, this site has been shown to be phosphorylated within the nucleus by IKK ϵ following T cell co-stimulation in a manner that enhances p65 transactivation (Mattioli *et al.*, 2006). IKK ϵ also appears to mediate a delayed phosphorylation of this site in response to genotoxic stress to promote apoptotic gene expression (Renner *et al.*, 2010). In response to pro-inflammatory cytokines, such as TNF α and IL-1, S468 phosphorylation has been shown to be mediated by IKK β , but not IKK α , in a range of cell types, including T cell, B cell, breast cancer and cervix carcinoma cells (Schwabe *et al.*, 2005). This phosphorylation event occurs rapidly following stimulation in the cytosol while p65 is in a complex with I κ B α and moderately inhibits cytokine induced NF- κ B-reporter expression, as well as the expression of a subset of genes. A potential explanation for this gene specific inhibition was subsequently provided by the finding that phosphorylation of S468 promotes interaction between p65 and the HDAC, GCN5, which facilitates recruitment of an E3 ligase complex containing Copper Metabolism MURR1 Domain-containing Protein 1 (COMMD1), cullin2 and SOC1 that catalyses the K48-linked ubiquitination and degradation of p65 bound to a subset of promoters, such as *Icam1* (Mao *et al.*, 2009; Geng *et al.*, 2009). Thus, S468 phosphorylation might contribute to selective termination of NF- κ B-dependent gene expression.

In direct contrast to these studies, however, the recent generation of an S467A (mouse homolog of human S468)-knock-in mouse model demonstrated that phosphorylation of this site is actually required for TNF α -inducible expression of a subset of NF- κ B-dependent genes (Riedlinger *et al.*, 2017). Curiously, p65 protein expression was reduced in MEFs and various tissues from S467A mice, a phenotype that was not explained by reduced mRNA expression or reduced protein stability, but by reduced *de novo* protein synthesis. S467 phosphorylation was also proposed to enhance the expression of TNF α , IL- α , ICAM1 and A20 in response to TNF α in MEFs and *in vivo*. Furthermore, S467A MEFs were more sensitive to TNF α -induced apoptosis, while S467A mice were sensitized to weight gain and TNF α - or diet-induced inflammation.

A consensus that emerges from these studies is that the physiological context, stimulus and cell type appear to play a major role in determining the outcome of NF- κ B phosphorylation events.

1.3.4 I kappa B proteins

1.3.4.1 Overview

A defining feature of the NF- κ B pathway is its regulation by I kappa B (IkB) proteins (Figure 1.9). There are currently nine recognised members, split into three groups: the ‘classical’ IkB proteins, IkB α , IkB β and IkB ϵ ; the precursor IkB proteins, p100 and p105; and the atypical IkB proteins, Bcl-3, IkB ζ , IkBNS and IkB η . Family members are defined by the presence of multiple ankyrin repeat domains in their structure, and their ability to bind to and regulate the function of NF- κ B proteins. The crystallographic structure of IkB α in complex with a p50:p65 heterodimer demonstrated that the IkB ankyrin repeat domain mediates an extensive interaction interface with the RHD of the NF- κ B subunits (Huxford *et al.*, 1998; Jacobs and Harrison 1998). Individual IkB proteins preferentially associate with certain NF- κ B dimer subsets. For example, IkB α and IkB β primarily interact with complexes containing p65 and c-Rel (Malek *et al.*, 2003), RelB binds only to p100 (Solan *et al.*, 2001), while Bcl-3 and IkB ζ preferentially interact with p50 and p52 homodimers (Franzoso *et al.*, 1992; Hatada *et al.*, 1992; Nolan *et al.*, 1993). The canonical function of the classical and precursor IkB proteins is to sequester their NF- κ B interaction partners in the cytoplasm in the resting state (Beg *et al.*, 1992; Auphan *et al.*, 1995). IkB α has also been shown to inhibit the DNA-binding ability of NF- κ B subunits; a function mediated by its C-terminal PEST region (Ernst *et al.*, 1995). The proteasomal degradation of classical and precursor IkB proteins upon pathway stimulation imparts signal responsiveness on the NF- κ B pathway and enables NF- κ B subunits to accumulate in the nucleus and to bind to kB promoter elements (Beg *et al.*, 1993; Brown *et al.*, 1995a). The atypical IkB proteins are distinct in that their expression is induced by various stimuli, including NF- κ B activation, and they function within the nucleus to exert both positive and negative effects on NF- κ B-dependent transcription (Schuster *et al.*, 2009).

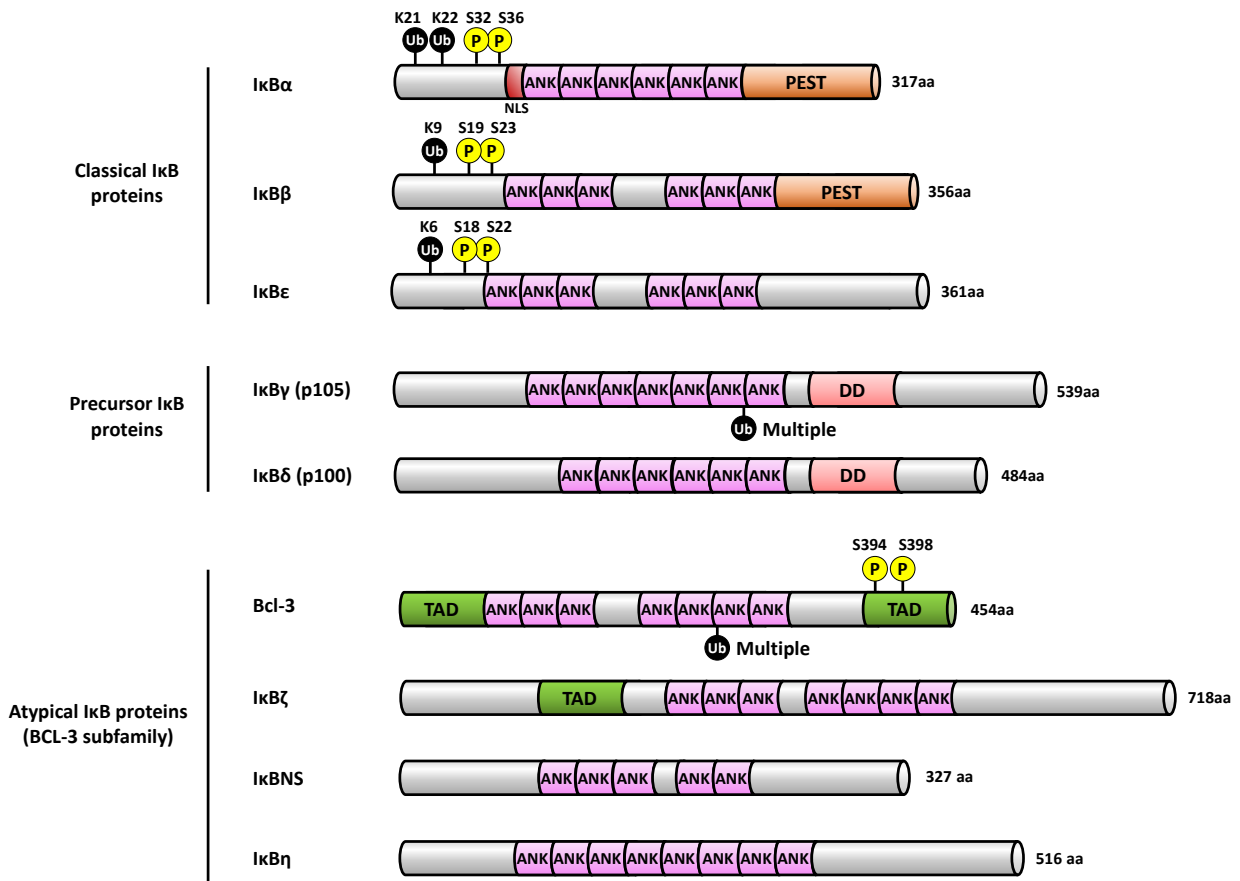


Figure 1.9. Domain organisation of the IκB family proteins. The IκB family consists of nine bona fide members. Each member contains numerous ankyrin repeats, which formally defines the family. The so-called ‘classical’ IκB proteins are; the prototypical member, IκB α ; IκB β ; and IκB ϵ . They function by sequestering NF-κB dimers in the cytosol in unstimulated cells, and are degraded in an IKK-dependent manner upon pathway activation. The sites of IKK-dependent phosphorylation and β-TrCP-dependent K48-linked polyubiquitylation are shown. The precursor IκB proteins are p105 and p100. The unprocessed forms of p105 and p100 act like the classical IκB proteins and sequester NF-κB subunits in the cytosol in the unstimulated state. Proteasomal-dependent limited proteolysis of p105 and p100, however, results in the liberation of p50 and p52 NF-κB subunits, respectively. In the case of p100 this is typically induced in a ubiquitin-dependent manner downstream of activation of the non-canonical NF-κB pathway, while p105 processing is thought to occur largely constitutively, both co- and post-translationally, and in a ubiquitin-independent manner (Lin *et al.*, 1998a; Moorthy *et al.*, 2006). The atypical IκB proteins include BCL-3, IκB ζ , IκBNS and IκB η . Their expression is typically low and is induced by various stimuli, including NF-κB activation. Unlike the other IκB family members, they localise to the nucleus where they bind to DNA-associated NF-κB dimers to exert both positive and negative effects on NF-κB-mediated transcription. Ub, ubiquitin. P, phosphorylation site. ANK, ankyrin domain, PEST, sequence motif rich in proline (P), glutamate (E), serine (S) and threonine (T). DD, death domain. TAD, transactivation domain.

1.3.4.2 The classical IκB proteins

IκB α and IκB β are widely expressed in all tissues, whereas the expression of IκB ϵ is restricted to the hematopoietic system (Whiteside *et al.*, 1997). The classical IκB proteins share a similar signal responsive region (SRR) at their N-terminus that contains conserved serine residues (S32 and S36 in IκB α) that are phosphorylated by IKK kinase subunits upon pathway activation (Traenckner *et al.*, 1993). The DS^PGXXS^P degron motif that is generated is recognised by the receptor subunit βTrCP of the SCF family of E3-ubiquitin ligases and lysine residues within the SRR of the IκB proteins are modified with K48-linked polyubiquitin chains (Alkalay *et al.*, 1995; Baldi *et al.*, 1996; Suzuki *et al.*, 1999). This targets the IκB proteins for proteasomal degradation (Henkel *et al.*, 1993).

Remarkably, whereas the phosphorylation of I κ B proteins is thought to occur in the cytoplasm, the location of I κ B ubiquitination and degradation is still unknown. The majority of cellular β TrCP is sequestered in the nucleus, while many of the other SCF components and the proteasome itself have been reported to function in the nucleus (Davis *et al.*, 2002; von Mikecz *et al.*, 2006). Furthermore, the classical conception of I κ B proteins sequestering NF- κ B proteins in the cytoplasm may not be entirely accurate. Complexes of I κ B α and p50:p65 have been shown to continuously shuttle between the cytoplasm and the nucleus in resting cells due to the presence of a nuclear export signal (NES) in I κ B α , and a nuclear localisation sequence (NLS) in p50 that is not masked by I κ B α (the NLS of p65 is masked, however) (Johnson *et al.*, 1999; Malek *et al.*, 2001; Birbach *et al.*, 2002). Degradation of I κ B α shifts the equilibrium towards nuclear localisation. The physiological relevance of such shuttling is unclear, however, as the experiments supporting this mechanism have relied entirely on leptomycin B treatment, which may have other unforeseen influences on the pathway (Johnson *et al.*, 1999). I κ B β , in contrast, is able to mask the NLS of both NF- κ B subunits it interacts with and, thus, does not undergo nuclear-cytoplasmic shuttling (Malek *et al.*, 2001). I κ B ϵ contains a noncanonical NES, and thus is restricted more to the cytoplasm (Lee and Hannick 2002).

I κ B α , I κ B β and I κ B ϵ exhibit functional differences that are largely due to differences in their rates of degradation and re-expression. I κ B α is degraded rapidly following pathway stimulation; within 5 mins in TNF α -stimulated HeLa cells (Henkel *et al.*, 1993). I κ B β and I κ B ϵ undergo much slower degradation; within 60-90 minutes in LPS-stimulated Jurkat cells in the case of I κ B ϵ (Whiteside *et al.*, 1997). I κ B degradation kinetics are correlated with IKK affinity (Heilker *et al.*, 1999). I κ B α is also rapidly resynthesized following pathway activation as a result of NF- κ B-dependent gene expression (Sun *et al.*, 1993). This negative feedback loop forms an essential mechanism of control of the duration of the canonical NF- κ B signalling response; re-expressed I κ B α translocates to the nucleus and displaces certain NF- κ B dimers from the DNA to terminate specific gene expression. I κ B ϵ , on the other hand, is re-expressed slowly, and hence is thought to inhibit late NF- κ B gene activation by p65:c-Rel dimers (Kearns *et al.*, 2006). I κ B β is also resynthesised slowly downstream of NF- κ B activation and accumulates in the nucleus in a hypophosphorylated form where it is thought to interact with DNA-bound p65 and c-Rel containing dimers in a manner that does not mask their NLS and that blocks interaction with I κ B α ; as such, I κ B β is thought to prolong the expression of certain NF- κ B-dependent genes, such as TNF α (Thompson *et al.*, 1995; Phillips and Ghosh, 1997; Weil *et al.*, 1997; Rao *et al.*, 2010).

Consistent with its central role in the canonical NF- κ B pathway, I κ B α deletion leads to constitutive NF- κ B activation, defective signal termination and postnatal lethality (Klement *et al.*, 1996). I κ B β or I κ B ϵ deletion results in a less striking phenotype suggesting that other I κ B proteins can compensate for their loss (Goudeau *et al.*, 2003; Rao *et al.*, 2010). However, the phenotype of I κ B α knockout can be rescued by reexpressing I κ B β under the I κ B α promoter, indicating that the biochemical properties of I κ B α are less important than the temporal nature of its transcriptional regulation (Cheng *et al.*, 1998). Interestingly, cells deficient for all three classical I κ B proteins exhibit largely normal nuclear/cytoplasmic p65 distribution, but markedly enhanced basal NF- κ B-dependent gene expression (Tergaonkar *et al.*, 2005). This suggests that inhibition of DNA binding is more important than cytoplasmic sequestration in limiting NF- κ B pathway activity.

1.3.4.3 The precursor I κ B proteins

The precursor proteins p100 and p105 are I κ B proteins that undergo proteolytic processing to generate the NF- κ B subunits, p52 and p50, respectively. In the unprocessed form they can dimerize with other NF- κ B subunits via their N-terminal RHDs (Figure 1.8), while their C-terminal ankyrin repeats serve the function of I κ B proteins, enabling them to sequester NF- κ B dimers and inhibit DNA binding activity (Naumann *et al.*, 1993; Scheinmann *et al.*, 1993). Unlike classical I κ B proteins that interact in a 1:1 ratio with NF- κ B subunits, the ability to dimerize with other NF- κ B subunits enables the precursor I κ B proteins to assemble into large multiprotein assemblies containing multiple different NF- κ B subunits (Savinova *et al.*, 2009; Tao *et al.*, 2014). As such, stimulation of p100/p105 degradation can facilitate the release of a range of NF- κ B subunits to encompass a broad spectrum of gene regulatory activities.

The processing of p105 and p100 occurs via different mechanisms. p105 undergoes a high level of constitutive co- and post-translational ubiquitin-independent proteasomal processing to generate p50 (Fan and Maniatis, 1991; Lin *et al.*, 1998a; Moorthy *et al.*, 2006). This may occur via the 20S proteasome *in vivo* (Moorthy *et al.*, 2006). Complete proteasomal processing of both p105 and p100 is prevented by a glycine rich region, C-terminal to the RHD domain, which serves as a stop signal to liberate p50 and p52 (Lin and Ghosh, 1996). Stable p105 that is bound to NF- κ B subunits can also be inducibly degraded following canonical NF- κ B activation as a result of IKK β -dependent phosphorylation of C-terminal residues in p105 (Fujimoto *et al.*, 1995). This targets p105 for polyubiquitination and complete degradation by the 26S proteasome ((Heissmyer *et al.*, 2001; Cohen *et al.*, 2004)).

In contrast, processing of p100 is a predominately stimulus-dependent event (Fong *et al.*, 2002). Constitutive processing occurs only at a very low level in certain cell types, and is inhibited by the C-terminal ARD and death domain, which together constitute a processing-inhibitor domain (PID) (Heusch *et al.*, 1999; Xiao *et al.*, 2001). The PID functions in part through masking the N-terminal NLS, which prevents the nuclear shuttling that is required for constitutive processing (Qing *et al.*, 2005). The importance of this region is highlighted by the fact that oncogenic translocations in the nf- κ b2 gene associated with various leukemias and lymphomas invariably lead to expression of p100 truncation mutants lacking the PID that exhibit nuclear localisation and constitutive processing (Zhang *et al.*, 1994; Thakur *et al.*, 1994; Xiao *et al.*, 2001).

Signal-induced p100 processing forms a fundamental part of the non-canonical NF- κ B pathway (see Section 1.3.5). NIK and IKK α can phosphorylate p100 at a C-terminal degron that targets p100 for polyubiquitination and limited proteolysis by the proteasome to liberate p52 (Senftleben *et al.* 2001; Xiao *et al.*, 2001). This p100 processing most directly effects RelB activity, as RelB-containing dimers (typically RelB:p52) associate exclusively with p100 (Solan *et al.*, 2002). RelB also requires p100 binding for stabilisation (Fusco *et al.*, 2008).

Like the classical I κ B proteins, p100 expression is induced following canonical NF- κ B activation (de Wit *et al.*, 1998). This is a key point of cross-talk between the canonical and non-canonical pathways. This can contribute to complex modulation of gene expression during sequential stimulation events. For example, newly expressed p100 may sequester p65-containing dimers to limit canonical NF- κ B dependent gene expression, with subsequent non-canonical activation liberating a large pool of different NF- κ B complexes (Basak *et al.*, 2007; Shih

et al., 2009). Furthermore, rapidly activated canonical NF- κ B dimers, such as p50:p65 can be displaced by slower activated dimers, such as p52:RelB, to enable fine tuning of temporal gene expression (Saccani *et al.*, 2003).

1.3.4.4 The atypical I κ B proteins

The atypical I κ B proteins, also known as the BCL-3 subfamily, exhibit entirely different nuclear localisations, activation kinetics and functions compared to the classical I κ B proteins (Ohno *et al.*, 1990; Schuster *et al.*, 2013). Unlike the other family members their basal expression is low and they are not degraded following pathway activation as they lack N-terminal signal responsive sequences or C-terminal PEST regions (Michel *et al.*, 2001). Rather, their expression is strongly induced by NF- κ B activation, such that they exert late or secondary-phase functions in the transcriptional response (Eto *et al.*, 2003; Ge *et al.*, 2003). They are also unique in that they interact with NF- κ B proteins within the nucleus, typically while bound to promoters (Nolan *et al.*, 1993; Zhang *et al.*, 1994). They also do not act exclusively as NF- κ B repressors; both BCL3 and I κ B ζ contain a TAD and can, therefore, confer transcriptional activation function to otherwise repressive p50 or p52 homodimers in certain contexts (Bours *et al.*, 1993; Yamamoto *et al.*, 2004). Alternatively, BCL3 may activate transcription indirectly by displacing repressive dimers from promoters and providing access to transcriptionally active NF- κ B dimers (Wulczyn *et al.*, 1992). The function of BCL3 as a transcriptional repressor or activator is tightly regulated by post-translational modifications; unphosphorylated Bcl3 acts as a classical I κ B-like inhibitor and removes p50 and p52 from bound DNA, while phosphorylation by AKT, ERK2 and IKK leads to its activation as a transcriptional coregulatory (Wang *et al.*, 2017).

1.3.5 The non-canonical NF- κ B pathway

Ligation of a subset of TNF-superfamily receptors (TNFSFRs) activates the non-canonical NF- κ B pathway, which displays distinct properties compared to the canonical pathway (Figure 1.10). Whereas the canonical pathway is rapid (< 1h) and transient, is independent of protein synthesis, responds to numerous different stimuli, and mediates diverse functions in a wide range of cells, the non-canonical pathway exhibits an activation mechanism that is slow (~3-4h), persistent, which depends on *de novo* protein synthesis, and that mediates specific functions predominantly in cells of the immune system (Claudio *et al.*, 2002; Saitoh *et al.*, 2003; Liang *et al.*, 2006). Animal model studies have indicated that the major biological functions of the non-canonical pathway depend largely on the activating receptor and the cell type in question. They include B-cell maturation and survival, dendritic cell maturation, secondary lymphoid organogenesis and architectural development, bone metabolism and T cell differentiation (Gerondakis and Siebenlist 2010). The transcriptional program induced by the non-canonical pathway is mediated almost entirely through the activation of p52:RelB dimers (Senftleben *et al.*, 2001). In turn, the activation of p52:RelB dimers is controlled at the level of inducible p100 processing, which itself is regulated by two key kinases, NIK and IKK α , through which all of the non-canonical NF- κ B inducers identified so far are known to signal (Razani *et al.*, 2011).

In the unstimulated state of normal cells, p100 processing is maintained at a minimal level (Heusch *et al.*, 1999). As described in Section 1.3.4.3, unlike p105, p100 is resistant to basal processing due to a processing inhibitory domain (PID) at its C-terminus (Qing *et al.*, 2005). The signalling cascade that results in phosphorylation of sequences in this PID that subsequently target p100 for proteolytic processing requires the accumulation of NIK

protein (Liao *et al.*, 2004). However, in the unstimulated state NIK protein is prevented from accumulating due to basal, proteasomal-dependent degradation (Liao *et al.*, 2004). A complex formed of TRAF2, TRAF3, and cIAP1/2 is responsible for mediating this constitutive NIK degradation (Zarnegar *et al.*, 2008). Upon *de novo* synthesis, the N-terminus of NIK is immediately and tightly bound by TRAF3 (Liao *et al.*, 2004). The importance of this interaction was recently highlighted by the discovery that the API2-MALT1 fusion oncoprotein in mucosa-associated lymphoid tissue (MALT) lymphoma proteolytically cleaves NIK to generate an N-terminally truncated NIK mutant that lacks the TRAF3-binding site and, as such, is resistant to basal degradation, is constitutively expressed and causes deregulation of non-canonical NF- κ B signalling that promotes tumour progression (Rosebeck *et al.*, 2012). TRAF2 heterodimerizes with TRAF3, and recruits the E3 ligases cIAP1 and cIAP2 to the complex (Vallabhapurapu *et al.*, 2008). TRAF3 is unable to bind cIAP1/2 itself (Zarnegar *et al.*, 2008). As such, deficiency of either TRAF3 or TRAF2 leads to constitutive NIK accumulation (He *et al.*, 2006; Grech *et al.*, 2004). cIAP1/2 act as the NIK K48-ubiquitin ligases to catalyse the polyubiquitination of NIK that targets it for proteasomal degradation (Vallabhapurapu *et al.*, 2008). cIAP1 and cIAP2 are redundant in this regard, and as such genetic deficiency of both is necessary to lead to basal accumulation of NIK (Gardam *et al.*, 2008).

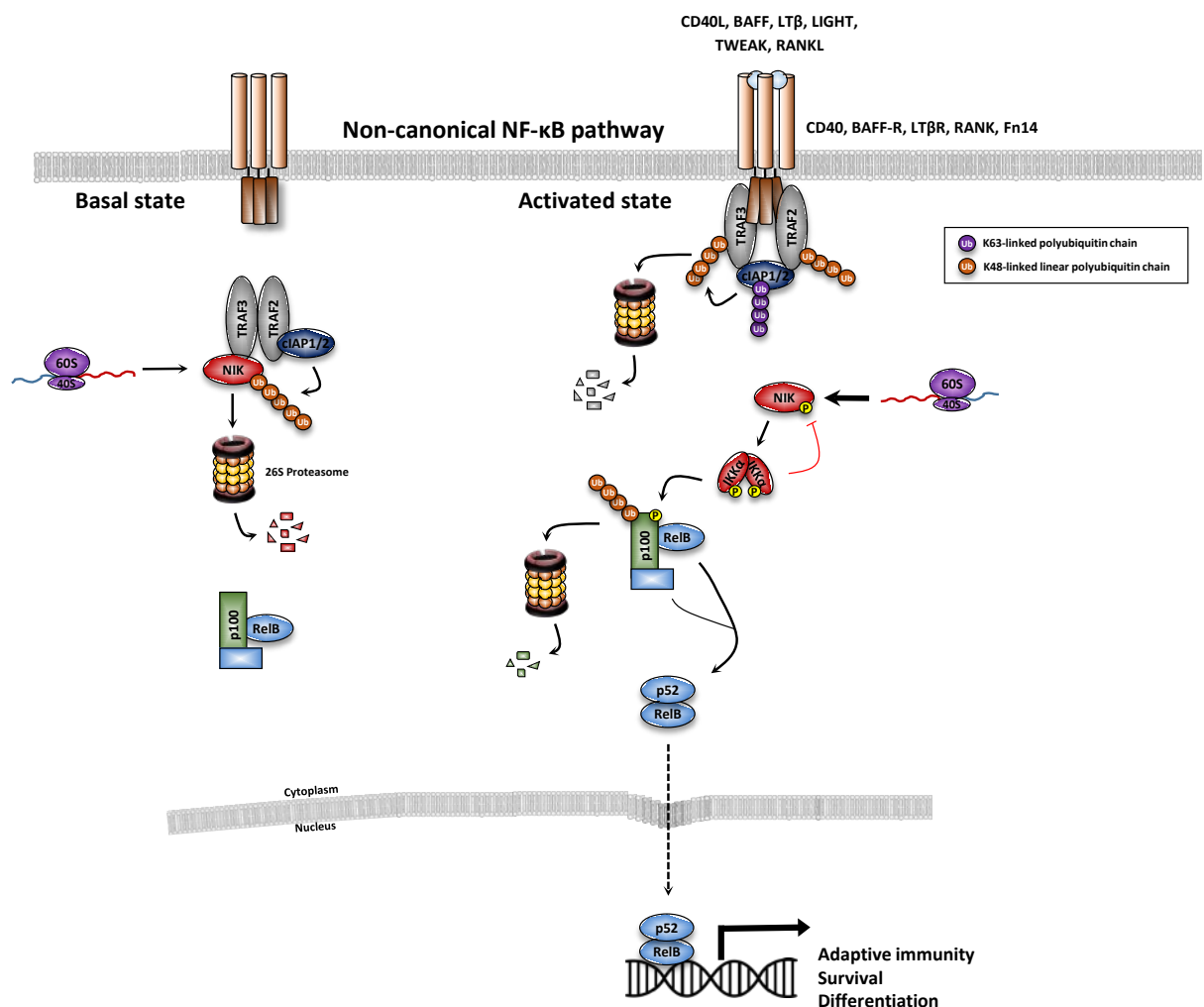


Figure 1.10 Overview of the non-canonical NF- κ B signalling pathway. In the basal state (left-hand side), a TRAF2/3-cIAP1/2 complex immediately catalyses the constitutive degradation of *de novo* synthesised NIK. TRAF3 recruits NIK to the complex via dimerization with TRAF2. cIAP1/2, recruited to the complex by interaction with TRAF2, catalyzes the K48-linked polyubiquitylation of NIK, priming it for proteasomal degradation. This blocks the accumulation of NIK and hence prevents

activation of noncanonical NF- κ B signalling. Receptor ligation of a subset of the TNF receptor superfamily leads to activation of the pathway (right-hand side). Ligands include CD40 ligand (CD40L), BAFF, lymphotxin β (LT β), LIGHT, TNF-like weak inducer of apoptosis (TWEAK), receptor activator of nuclear factor kappa-B ligand (RANKL) and B-cell activating factor (BAFF). Ligand engagement induces the recruitment of TRAF2, TRAF3 and cIAP1/2 to the receptor. Here the K48-specific E3 ligase activity of cIAP1/2 switches from NIK to TRAF3, resulting in TRAF3 degradation. In some cases, TRAF2 is also targeted for degradation. In the absence of TRAF3, de novo synthesised NIK protein is stabilized and accumulates. In turn, NIK phosphorylates IKK α at S176 to activate its kinase activity. NIK also recruits p100 to IKK α leading to IKK α phosphorylating p100. Phosphorylated p100 undergoes K48-linked ubiquitination by β -TrCP and is targeted for limited proteolysis. A glycine rich region in p100 is thought to prevent complete proteasomal degradation. This releases the NF- κ B subunit p52 and enables it to productively dimerize with RelB and translocate into the nucleus to regulate target gene expression.

Receptor ligation promotes degradation of components of the TRAF-cIAP1/2 complex, which leads to NIK stabilisation and accumulation as a result of continuous *de novo* synthesis, and hence pathway activation (Liao *et al.*, 2004). Evidence in support of this model includes the fact that exogenously expressed NIK is active in the induction of p100 processing (Xiao *et al.*, 2001), cIAP1/2 antagonists induce NIK accumulation and pathway activation (Varfolomeev *et al.*, 2007; Vince *et al.*, 2007), and NIK accumulation in TRAF3 KO cells is sufficient for p100 processing (He *et al.*, 2006). The requirement for *de novo* synthesis of NIK explains the slow kinetics of pathway activation. Although the receptor proximal events may be subtly different for each receptor, the general steps are as follows. Receptor ligation leads to the recruitment of the TRAF2/3:cIAP1/2 complex to the cytoplasmic domains of the receptor (Zarnegar *et al.*, 2008). Here TRAF2 promotes the K63 ubiquitination of cIAP1/2, which switches the K48 E3 ligase activity of cIAP1/2 from NIK to TRAF3, such that TRAF3 is targeted for degradation. In some cases, TRAF2 is also targeted for degradation (Sanjo *et al.*, 2010).

Other factors may modulate these steps. One such factor with poorly defined roles in non-canonical signalling is TRAF1. In some circumstances TRAF1 has been demonstrated to positively regulate non-canonical signalling. For example, in response to BAFFR signalling, TRAF1 is recruited to the receptor proximal complex where it promotes TRAF3 degradation and NIK stabilisation (Lavorgna *et al.*, 2009). Another study suggested that following its induction by the canonical NF- κ B pathway TRAF1 disrupts the interaction of NIK with the TRAF2:cIAP1/2 complex, thus promoting its stabilisation (Choudhary *et al.*, 2013). This was proposed as a novel feed-forward mechanism of cross-talk between the canonical and non-canonical pathways. A recent structural study indicated that TRAF1 binding to TRAF2 elevates its affinity for cIAP2, perhaps contributing to the promotion of NIK stabilisation (Zheng *et al.*, 2010).

Early biochemical evidence suggested accumulated NIK requires phosphorylation at T559 within its activation loop for activity (Lin *et al.*, 1998b). However, subsequent structural studies indicated that the NIK kinase domain adopts a constitutively active conformation in the absence of any phosphorylation, and thus newly synthesised NIK is constitutively active (de Leon-Boenig *et al.*, 2012; Liu *et al.*, 2012). Subsequently, accumulated NIK phosphorylates IKK α at S176 to activate its kinase activity (Ling *et al.*, 1998). NIK also recruits IKK α to p100, which IKK α phosphorylates at numerous sites within its N and C-terminus (S99, 108, 115, 123 and 872) (Xiao *et al.*, 2004). This function of IKK α is completely independent of IKK β and NEMO activity (Claudio *et al.*, 2002). Phosphorylation of p100 leads to the recruitment of β TrCP as part of the SCF E3 ubiquitin ligase complex, which targets p100 for K48-linked polyubiquitination at a specific lysine residue in its C-terminus and subsequent proteolytic processing by the proteasome (Fong *et al.*, 2002). The resulting liberation of specific NF- κ B dimers was discussed in detail in Section 1.3.4.3.

As part of a feedback mechanism that limits the duration of non-canonical NF- κ B pathway activation, IKK α phosphorylates NIK at S809, S812 and S815 within the C-terminus of NIK to promote its degradation and terminate the signal (Razani *et al.*, 2010). In the absence of IKK α , NIK expression accumulates continuously over a period of time far beyond that observed in wild-type cells.

Deregulated non-canonical NF- κ B signalling is typically associated with lymphoid malignancies (Cildir *et al.*, 2016). For example, constitutive non-canonical signalling is commonly observed in multiple myeloma as a result of mutations in various components of the pathway, including loss of function mutations in *TRAF2*, *TRAF3*, *CYLD*, *cIAP1* and *cIAP2*, and gain of function mutations in *NFKB1*, *NFKB2*, *CD40*, *LTBR*, *TACI*, and *NIK* (Keats *et al.*, 2007). However, a role for aberrant non-canonical NF- κ B signalling in the progression of solid tumours is starting to emerge. For example, a subset of pancreatic cancer cell lines exhibit constitutive NIK stabilisation, p100 processing and elevated non-canonical NF- κ B target genes (Wharry *et al.*, 2009). Furthermore, non-canonical pathway activation is predictive of poor survival in patients with oestrogen receptor positive breast cancer (Rojo *et al.*, 2016). In addition, deficiency for nucleotide-binding domain and leucine-rich-repeat containing (NLR) protein, NLRP12 increases the susceptibility of mice to colitis and colitis-associated colon cancer (Allen *et al.*, 2012). Polyps isolated from *Nlrp12*^{-/-} mice exhibit elevated noncanonical NF- κ B activation, due to increased NIK stabilisation and p100 processing, and increased expression of target genes, including *Cxcl13* and *Cxcl12*, which contribute to tumourigenesis.

1.3.6 Atypical NF- κ B pathways

In addition to the canonical and non-canonical NF- κ B pathways, there exist various other atypical mechanisms of NF- κ B transcriptional activation that have been proposed to expand the range of stimuli able to impinge on NF- κ B (Figure 1.11). These may be IKK-dependent (Figure 1.11A) or IKK-independent; impinging directly on phosphorylation of I κ B proteins (Figure 1.11B-D). Genotoxic agents, such as doxorubicin, etoposide and camptothecin that generate DNA double-stranded breaks (DSBs), induce increases in nuclear localization of an 'IKK-free' form of NEMO (Huang *et al.*, 2003, Hwang *et al.*, 2015). SUMOylation of NEMO at K277 and K309 by the SUMO E3 ligase protein inhibitor of activated STATy (PIASy) promotes its nuclear localisation, via an undefined mechanism (Mabb *et al.*, 2006). Within the nucleus, poly(ADP-Ribose) polymerase-1 (PARP1), a scaffolding protein that directly senses DNA damage and catalyses the formation of polyADP-ribose chains on itself and target proteins, contributes to the assembly of a nuclear signalosome containing NEMO, PIASy, and the DSB-responsive kinase ataxia-telangiectasia mutated (ATM) that promotes NEMO post-translational modification. Within this complex, NEMO is also phosphorylated on S85 by ATM (Stillman *et al.*, 2009). NEMO SUMOylation and phosphorylation are both required for NF- κ B activation following DNA damage (McCool *et al.*, 2012). Prior phosphorylation at Serine 85 by ATM is also essential for subsequent NEMO monoubiquitylation on K277 and K309, which is possibly catalysed by cIAP1 (Jin *et al.*, 2009). This is thought to promote translocation of a NEMO:ATM complex back into the cytoplasm where TAK1 and the IKK complex are activated, via a poorly defined ATM-kinase dependent mechanism, to induce the canonical NF- κ B pathway (Wu *et al.*, 2006b; Jin *et al.*, 2009; Hinz *et al.*, 2010; Wu *et al.*, 2010). In turn, NF- κ B transcriptional activity induces several cell processes to promote survival, including prolonged cell cycle arrest, DNA damage repair and senescence (McKool and Miyamoto, 2012).

Various other stress-induced pathways have been shown to lead to IKK-independent I κ B α phosphorylation (Figure 1.11B-D). For example, cellular stresses that promote the production of ROS can activate ASK1 and, in turn, JNK, whose sustained activity has been shown to promote β -TrCP expression, and hence promote signal-induced I κ B α degradation (Spiegelmann *et al.*, 2001). I κ B α tyrosine phosphorylation, primarily at Y42, has been shown to be induced by various stimuli, including H₂O₂, pervanadate and hypoxia, possibly through casein kinase II (CK2) activity, downstream of Syk kinase (Schoonbroodt *et al.*, 2000; Takada *et al.*, 2003). Tyr42 phosphorylation does not induce I κ B α degradation, but may promote binding of the p85 α subunit of PI3K, thus freeing NF- κ B subunits to translocate into the nucleus (Beraud *et al.*, 1999). Early in the characterisation of NF- κ B pathways, UV radiation was shown to be an inducer of NF- κ B activity (Liu *et al.*, 1996), though the precise mechanism has remained a topic of debate. It was originally proposed that IKK activity is not required for I κ B α degradation in response to UV (Li and Karin., 1998; Huang *et al.*, 2002), but a more recent study has suggested that IKK β acts as an adaptor within the nucleus to facilitate the p38-CK2-dependent phosphorylation and degradation of I κ B α (Tsuchiya *et al.*, 2010).

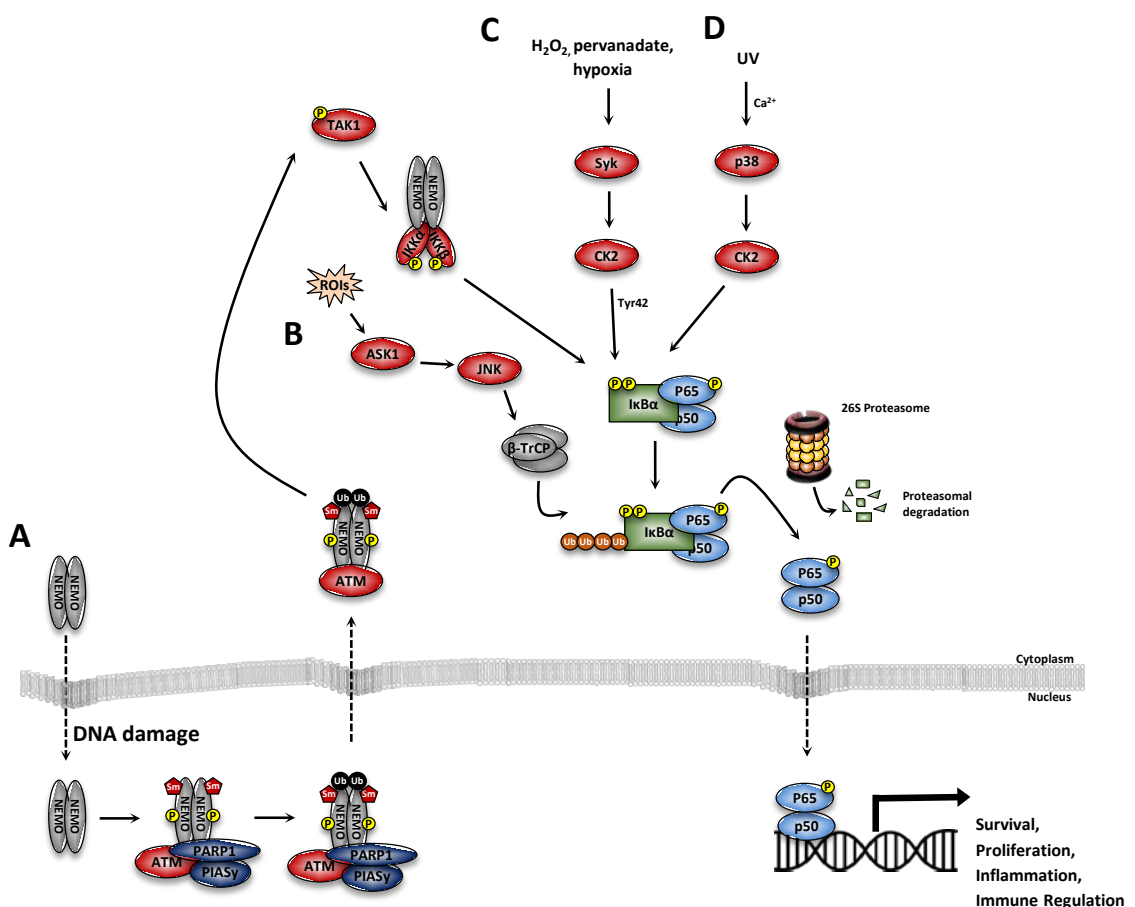


Figure 1.11. Atypical pathways of NF- κ B activation. (A) Genotoxic triggers the nuclear accumulation of 'IKK-free' NEMO. Within the nucleus NEMO forms a complex with PARP1, PIASy and ATM and undergoes a series of post-translational modification. PIASy promotes the sumoylation of NEMO, which promotes its nuclear localisation. ATM phosphorylates NEMO at Serine 85, which is necessary for the subsequent monoubiquitylation of NEMO. This is thought to trigger the nuclear export of the NEMO-ATM complex, which then, in an ill-defined mechanism, activates TAK1 and the IKK complex. (B) Various cellular stresses, including oxidative stress and environmental toxic metal ions result in an increase in the production of reactive oxygen intermediates (ROIs). These are thought to activate ASK1, which in turn activates JNK. JNK has been proposed to contribute to the signal-induced ubiquitination of I κ B α through promotion of β -TrCP accumulation. (C) Various stimuli, including H₂O₂, pervanadate and hypoxia activate NF- κ B through tyrosine phosphorylation of I κ B α . In the case of H₂O₂, this

has been shown to occur at Tyrosine 42 of I κ B α , and possibly mediated by casein kinase II (CK2) downstream of Syk kinase. (D) UV irradiation is proposed to activate NF- κ B via p38-CK2 kinase-mediated I κ B α degradation.

1.4 NF- κ B signalling in cancer

1.4.1 Overview

The NF- κ B signalling pathway is an inducible pathway that is normally tightly controlled by multiple regulatory mechanisms to ensure minimal basal activation. However, given its critical role in promoting cell-survival and proliferation, and regulating genes involved in angiogenesis, metabolism, inflammation and cell adhesion/migration, it is unsurprising that a wide range of haematological malignancies and solid tumours have been shown to exhibit deregulated NF- κ B signalling resulting in constitutive NF- κ B activation (Chaturvedi *et al.*, 2011).

The ability of NF- κ B to induce inflammation places it as one of the crucial links between chronic inflammation and cancer (DiDonato *et al.*, 2012). However, aberrant NF- κ B activation is also capable of promoting tumourigenesis in cancers whose early progression isn't typically associated with inflammation through contributions to almost all of the hallmarks of cancer (see Figure 1.12 and Section 1.4.3).

A consequence of the role of the NF- κ B pathway in promoting cell survival and proliferation is that cancers exhibiting constitutive NF- κ B activation are often intrinsically resistant to both traditional chemotherapeutics and targeted therapeutics. For example, in glioblastoma, the common activating EGFR mutation (EGFRvIII) stimulates mTORC2 activity to promote cancer cell growth, survival and resistance to cisplatin chemotherapy through constitutive activation of NF- κ B signalling (Tanaka *et al.*, 2011).

Given these tumour promoting and chemoresistance-enhancing roles of NF- κ B within cancer cells and cells of the tumour microenvironment, targeting NF- κ B has been a major goal for cancer therapy in recent years.

1.4.2 Mechanisms of constitutive NF- κ B activation in cancer

There are several mechanisms by which NF- κ B transcription factors can become uncoupled from their normal modes of transient and tight regulation, leading to constitutive activation and promotion of tumourigenesis (Staudt, 2010). The discovery of viral oncogenes capable of constitutively activating the NF- κ B pathway, such as v-Rel – the oncogenic avian REV-T virus derivative of c-Rel, generated great anticipation for the discovery of tumour-promoting oncogenic mutations in NF- κ B pathway components in human malignancies (Ballard *et al.*, 1990; Nolan *et al.*, 1991). However, oncogenic mutations that provide p65, c-Rel or other NF- κ B family members with transforming potential have turned out to be rare and mainly occur in lymphoid malignancies (Courtois *et al.*, 2006). Indeed, for the most part, loss-of-function I κ B mutations or gain-of-function IKK mutations are extremely rare in humans. Rather, NF- κ B activation in cancer largely appears to be the result of either oncogenic activation of upstream components of the NF- κ B pathway and oncogenic signalling pathways that activate NF- κ B, such as RAS or PI3K signalling, or chronic autocrine/paracrine exposure to proinflammatory stimuli in the tumour microenvironment (Staudt, 2010).

Many human lymphomas, including but not limited to activated B-cell like (ABC) diffuse large B-cell lymphoma (DLBCL), multiple myeloma (MM), Hodgkins lymphoma and MALT lymphoma, rely on constitutive canonical and/or non-canonical NF- κ B activation for survival (Vallabhapurapu *et al.*, 2009). For instance, constitutive activation of the canonical NF- κ B pathway is the hallmark of ABC DLBCL and contributes to tumourigenesis through the activation of IRF4, which drives plasmacytic differentiation, and the production of IL-6 and IL-10, which activate autocrine tumour promoting STAT3 signalling (Davis *et al.*, 2001; Lam *et al.*, 2005; Lam *et al.*, 2008a). This constitutive NF- κ B activation is the result of oncogenic mutations of upstream signalling components that engage the canonical NF- κ B signalling pathway including Myd88, A20, TAK1, TRAF2, TRAF5, CD79B/A and CARD11 (Compagno *et al.*, 2009). Meanwhile, mutations in NF- κ B pathway components are found in approximately 20% of MM tumours and 40% of MM cell lines (Annunziata *et al.*, 2007; Keats *et al.*, 2007). Such mutations have been shown to lead to constitutive activation of both canonical and non-canonical NF- κ B pathways and enable malignant cells to survive and proliferate away from the survival signals provided by the bone marrow microenvironment (Staudt, 2010).

Constitutive NF- κ B activation has also been observed in a vast number of solid tumours and cancer cell types, including but not limited to pancreatic, lung, liver, breast, prostate and colon (Nakshatri *et al.*, 1997; Tai *et al.*, 2000; Shukla *et al.*, 2004; Sakamato *et al.*, 2009). Various oncogenic mutations in signalling pathways that mediate cross-talk with NF- κ B, such as EGFR, KRAS, PI3K and p53, have been implicated in driving aberrant NF- κ B signalling in epithelial cancers. The link between oncogenic RAS and NF- κ B first became apparent when it was demonstrated that the RAS oncoprotein can regulate the transcriptional activity of NF- κ B (Finco *et al.*, 1993) Subsequently, oncogenic RAS was proposed to require NF- κ B to promote cellular transformation in vitro, in part because of its ability to suppress transformation-associated, p53-independent apoptosis (Mayo *et al.*, 1997) and its ability to promote abnormal proliferation (Jo *et al.*, 2000).

The *in vivo* connection between NF- κ B and KRAS-induced transformation initiation has been strengthened by studies of mouse RAS-driven cancer models. For example, the NF- κ B pathway has been proposed to be important for the development of tumours in a KRAS/p53-mutant mouse model of lung adenocarcinoma (Meylan *et al.*, 2009). Similarly, Bassérès *et al* showed that KRAS activated p65 in an IKK β -dependent manner in lung tumours *in situ*, and that p65 inactivation reduced KRAS-driven tumour formation and resulted in higher levels of tumour cell apoptosis (Bassérès *et al.*, 2010). Furthermore, tumour cell-specific knockout of IKK β in a KRAS-driven mouse model of lung cancer has been shown to significantly attenuate tumour proliferation and prolonged mouse survival (Xia *et al.*, 2012). Such findings are not limited to lung cancer. Conditional knockout of IKK β in an *Ink4a/Arf*-null, HRAS-driven mouse model of spontaneous melanoma blocked tumour formation through a mechanism involving inhibition of Aurora A kinase-mediated cell cycle progression, stabilization of p53, reduction in IL-6 secretion and increased apoptosis (Yang *et al.*, 2010). Meanwhile, pancreas-targeted IKK β inactivation has been shown to inhibit the development of pancreatic ductal adenocarcinoma in a KRAS-driven mouse model (Ling *et al.*, 2012).

The precise mechanisms by which RAS and its downstream effector pathways regulate NF- κ B activation have yet to be conclusively demonstrated. One proposal has been made by Duran *et al* who demonstrated a role for the signalling adaptor p62, transcriptionally induced by KRAS through an ERK- and AKT-dependent pathway, in

coordinating TRAF6 to regulate IKK downstream of oncogenic KRAS-induced signalling *in vitro* and *in vivo* in a model of KRAS-induced lung adenocarcinoma (Duran *et al.*, 2008). This work was subsequently extended in a model of KRAS-driven pancreatic adenocarcinoma by Ling *et al*, who demonstrated that KRAS-activated AP-1 TFs induced an IL-1 α autocrine signalling loop, which in turn activated NF- κ B and its target genes IL-1 α and p62 to initiate a feedforward loop for sustained NF- κ B activity (Ling *et al.*, 2012). Baldwin *et al* identified a link between KRAS and IKK in pancreatic cancer cells via GSK-3 α -mediated stabilization of constitutively active TAK1-TAB complexes to promote IKK activity and constitutive canonical NF- κ B signalling (Bang *et al.*, 2013). GSK-3 α activity downstream of KRAS was also shown to promote noncanonical NF- κ B signalling via promotion of p100-processing. Such findings potentially explain the proposed importance of TAK1 for survival of KRAS-dependent CRC (Singh *et al.*, 2012).

The unconventional I kappa B kinase, TBK1 has also been linked with activation of NF- κ B downstream of mutant KRAS. The GTPase RALB, in complex with a component of the exocyst (SEC5), has been proposed to contribute to cancer cell survival and RAS-induced transformation by directly recruiting and constitutively activating TBK1 to trigger canonical NF- κ B signalling and promote survival (Chien *et al.*, 2006). Separately, TBK1 has been identified in an RNAi synthetic lethality screen for proteins essential for the survival of KRAS-mutant human cancer cells (Barbie *et al.*, 2009). Suppression of TBK1-dependent NF- κ B activation in KRAS-dependent lung cancer cells induced apoptosis.

The pathological relevance of such cell autonomous mechanisms of NF- κ B aberrant activation remains a matter of debate. A more general, and widely accepted mechanism of constitutive NF- κ B activation in tumour cells is via exposure to the pro-inflammatory milieu of the tumour microenvironment. As described in Section 1.1.4 it is well documented that human solid tumours are almost always infiltrated by a host of inflammatory cells that secrete an abundance of pro-inflammatory cytokines and growth factors that activate the NF- κ B pathway in tumour cells (Balkwill and Mantovani, 2001). Interactions with immune cells also induce autocrine cytokine signalling in tumour cells to activate NF- κ B (Spriggs *et al.*, 1995). The generality of this phenomenon has been demonstrated through the observation that conditioned media from a wide range of tumour-derived cell lines and mutant HEK293 derivatives with constitutive NF- κ B activation was highly enriched in numerous cytokines, including TNF α , CSF1, IL-1 β , TGF β 2, FGF5, OX40L, CD27L, RANKL etc that stimulated activation of NF- κ B in naive indicator cells (Lu *et al.*, 2004). The contribution of the proinflammatory microenvironment to the constitutive activation of NF- κ B in colorectal cancer will be discussed in Section 1.4.4.

1.4.3 Deregulated IKK/NF- κ B is capable of influencing all of the hallmarks of cancer

Constitutively active NF- κ B signalling has been shown to play a role in promoting tumour initiation, progression and resistance to therapy in a wide range of cancers. Indeed, NF- κ B-dependent gene targets are capable of influencing all of the hallmarks of cancer (Figure 1.12). The contribution of NF- κ B activation in inducing and maintaining a chronic tumour-promoting inflammatory microenvironment will be discussed in the context of colorectal cancer in Section 1.4.4. Independent of inflammation, deregulated NF- κ B is involved in numerous cancer-associated mechanisms.

One of the most significant is the ability of NF- κ B to protect cancer cells from apoptosis through the induction of anti-apoptotic genes. For example, enterocyte-specific deletion of IKK β in mice has been shown to lead to enhanced apoptosis during tumour promotion in a mouse model of colitis-associated cancer as a result of inhibition of NF- κ B-dependent expression of the pro-survival protein, Bcl-XL (Greten *et al.*, 2004). Furthermore, NF- κ B inhibition leads to apoptotic cell death in certain cancer cell lines, such as Hodgkin's lymphoma (Izban *et al.*, 2001). NF- κ B activation also opposes the induction of cell death through inhibition of persistent JNK signalling. This is achieved in part via the induction of antioxidant genes, such as manganese-superoxide dismutase (MnSOD) and ferritin heavy chain (FHC) that counteract the generation of ROS, which are involved in sustained JNK activation following TNF α stimulation, and also by the induction of genes such as GADD45 β and XIAP, which oppose JNK activation. The latter has been exploited recently to selectively kill MM cells (see Section 1.4.5). Therapy-induced NF- κ B activation of anti-apoptotic genes is also a potential mechanism of resistance to certain chemotherapeutics (Nakanishi & Toi, 2005). For example, paclitaxel sensitivity of breast cancer cells exhibiting constitutive NF- κ B activation is enhanced by inhibition of NF- κ B-dependent survival signalling (Patel *et al.*, 2000). Although certain DNA-damaging agents have been shown to activate apoptosis in an NF- κ B-dependent manner (Strozyk *et al.*, 2006).

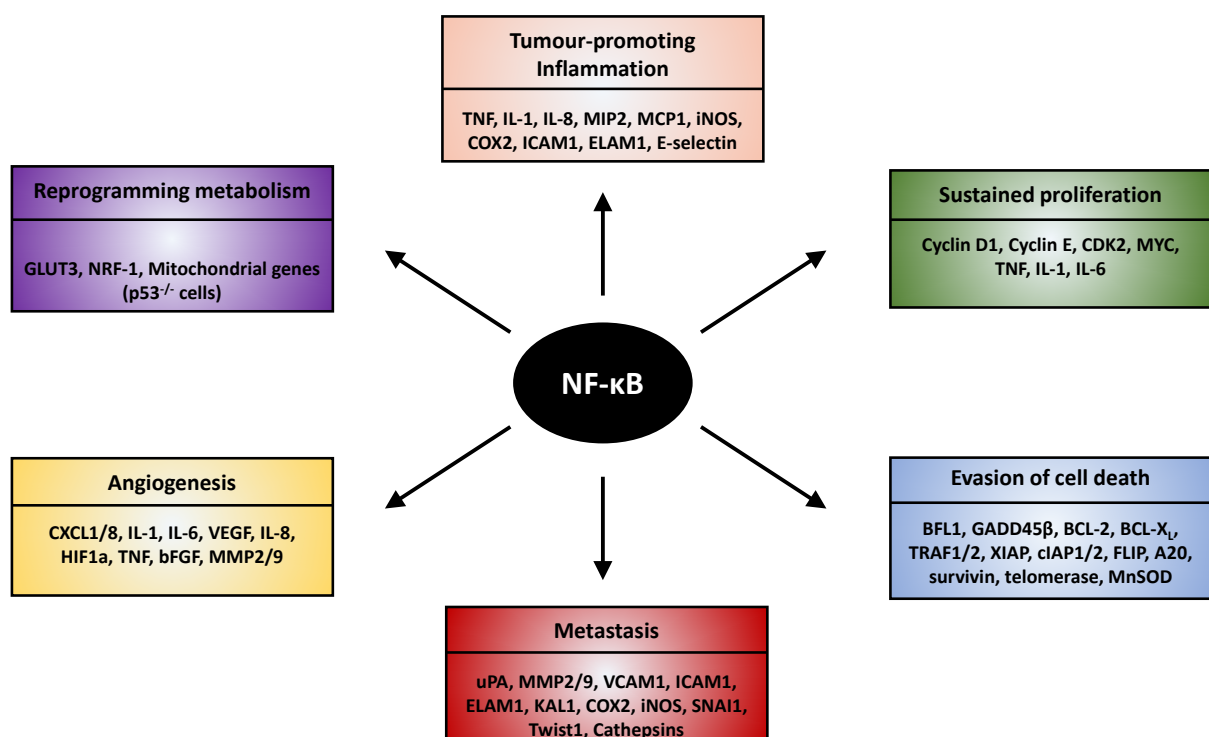


Figure 1.12. Overview of the contribution of NF- κ B-dependent gene expression to the hallmarks of cancer. Activation of NF- κ B-dependent gene expression is capable of influencing the majority of the hallmarks of cancer, including: sustained proliferation, evasion of cell death, metastasis, angiogenesis, tumour-promoting metabolism, and, at least in the case of p53 null cells: tumourigenesis-promoting reprogramming of metabolism. A selection of representative genes involved in each process is summarised. Adapted from Baud, 2009.

Aberrant NF- κ B activation also promotes tumourigenesis through the promotion of autonomous cancer cell proliferation. This has been demonstrated in a mouse lung cancer model; specific IKK β deletion in tumour cells

slowed the growth of tumours due to decreased expression of the NF- κ B target gene, *Timp1*, which promotes ERK-dependent proliferation (Xia *et al.*, 2012).

Constitutive NF- κ B activation has also been linked to tumour maintenance, progression and metastasis through control of angiogenesis and the invasive properties of tumour cells. For example, inhibition of NF- κ B signalling through transfection of an $I\kappa B\alpha$ super-repressor inhibited the expression of the key angiogenic factor, vascular endothelial growth factor (VEGF), the angiogenesis inducing chemokine, IL-8, and matrix metalloproteinase-9 (MMP-9) in human prostate cancer cells and in mice prostate cancer tumours (Huang *et al.*, 2001). Such tumours were slower growing and displayed low metastatic potential. Aberrant NF- κ B may also contribute to tumour metastasis through the induction of genes involved in epithelial-mesenchymal transition (EMT), which is an early event in metastasis. Key EMT genes such as *SNAI1*, *TWIST* and *SNAI2* have been shown to be regulated by NF- κ B in various cancer cell lines. Indeed, NF- κ B has been proposed to be required for EMT and metastasis in a mouse model of breast cancer (Huber *et al.*, 2004).

NF- κ B activation may also play a role in the reprogramming of cellular metabolism that occurs during tumorigenesis; an emerging cancer hallmark. This function of NF- κ B appears to be highly dependent on the p53 status of the tumour cell. In p53 wild-type cells, p65 appears, in fact, to contribute to the suppression of oncogenic transformation through promotion of oxidative phosphorylation and repression of glycolysis in a mechanism dependent on the induction of p53, and in turn, the critical subunit of the mitochondrial respiratory complex IV subunit, cytochrome c oxidase (SCO2) (Mauro *et al.*, 2011). However, loss or mutation of p53 switches the outcome of NF- κ B activation to that of tumour promotion. For example, in the absence of p53 p65 is able to translocate into the mitochondria and repress mitochondrial gene expression, oxygen consumption and cellular ATP, thus switching cancer cells from oxidative phosphorylation to glycolysis and enhancing the Warburg effect (Johnson *et al.*, 2011). In p53^{-/-} p65 activation also induces the expression of the glucose transporter, GLUT3, which might contribute to the maintenance of high glycolytic flux and oncogenic RAS transformation (Kawauchi *et al.*, 2009). Whether these mechanisms function to promote tumorigenesis *in vivo* remains to be clarified.

NF- κ B-dependent gene expression is not the only means through which chronic activation of the pathway may elicit tumorigenesis. Many of the NF- κ B-independent functions of IKK discussed in Section 1.3.2.4 may also be capable of promoting cancer progression. For example, constitutive activation of IKK β has been proposed to promote proliferation and survival in breast cancer tumours through inhibitory phosphorylation of the transcriptional regulator, FOXO3a (Hu *et al.*, 2004). Such phosphorylation excludes FOXO3a from the nucleus and promotes its ubiquitin-dependent proteasomal degradation.

It should be mentioned, however, that there are specific examples where NF- κ B may actually play a tumour suppressive-like role. In some settings NF- κ B has been shown to promote apoptosis. For example, NF- κ B can induce the expression of the proapoptotic gene, Fas in some cells activated by certain stimuli (Chen *et al.*, 1999). p65 activation is also required for induction of apoptosis following serum withdrawal in HEK293 cells (Grimm *et al.*, 1996). Meanwhile, activation of NF- κ B promotes cell death in neural cells (Grilli *et al.*, 1996) and in α -CD3-mediated apoptosis of CD4/CD8 double positive T cells (Hettman *et al.*, 1999). However, to be classed as a tumour suppressor, loss of NF- κ B gene products must lead to development of cancer, and there have only been a few tissue-specific instances where this has been demonstrated to be the case. For example, coexpression of

mutant KRAS and a super-repressor I κ B α mutant that blocks NF- κ B activation in keratinocytes leads to increased squamous cell carcinoma, and implicated NF- κ B in growth arrest upon oncogenic stress in this tissue (Dajee *et al.*, 2003). Furthermore, hepatocyte-specific deletion of IKK β in mice results in the increased initiation of diethylnitrosamine-induced hepatocellular carcinoma (HCC) (Maeda *et al.*, 2005) as well the acceleration of HCC progression that had previously been initiated (He *et al.*, 2010). Interestingly, liver parenchymal cell specific deletion of NEMO or TAK1 lead to spontaneous HCC development in mice (Luedde *et al.*, 2007; Bettermann *et al.*, 2010). In the absence of NF- κ B signalling ROS accumulate, spontaneous liver damage and hepatocyte death occurs, which leads to compensatory proliferation, all of which contribute to HCC development.

More generally, it has been proposed that NF- κ B may act in a tumour suppressive capacity prior to initiation of tumorigenesis, through regulation of DNA damage, cellular senescence and cell death, but is subsequently co-opted to act as a tumour promoter as cancer progresses (Perkins *et al.*, 2004; Rovillain *et al.*, 2011). Support for this model comes from studies showing that precancerous p65-deficient MEFs escape senescence and immortalize earlier than wild-type cells due to increased genomic instability, but upon expression of mutant KRAS p65 deficient MEFs exhibit reduced tumour initiation when transplanted into mice, confirming earlier reports relating to the requirement of NF- κ B for KRAS-induced transformation (Wang *et al.*, 2014a). Importantly, however, p65 deficient MEFs did not give rise to tumours in the absence of mutant RAS transformation, suggesting that loss of p65 alone is not sufficient to promote tumorigenesis. One mechanism by which NF- κ B might promote oncogene-induced senescence is through upregulation of CXCR2 receptor-binding ligands (Acosta *et al.*, 2008).

1.4.4 NF- κ B and inflammation in colorectal cancer

The link between inflammation-induced NF- κ B and tumour promotion is perhaps strongest for colorectal cancer (CRC). A summary of some of the key inflammatory cytokines involved is shown in Figure 1.13. CRC is the third leading cause of cancer-related deaths in the United States, and more than 1 million new cases a year are diagnosed worldwide (Tenesa & Dunlop, 2009). A small proportion of these cases are hereditary; approximately 3-4% due to hereditary nonpolyposis colorectal cancer (HNPCC), 1% due to familial adenomatous polyposis (FAP), and less than 1% due to a range of rare genetic disorders, including hamartomatous polyposis syndromes (Rustigi, 2007). The vast majority of cases are sporadic and are typified by a progressive genetic pathway involving loss of function in the adenomatous polyposis coli (APC) tumour suppressor, activation of β -catenin, and mutations in KRAS, PIK3CA and TP53; this accounts for approximately 80% of all cases in humans (Mundade *et al.*, 2014). Chronic inflammation is a prominent risk factor for CRC development (Terzić *et al.*, 2010). Indeed, patients with pre-existing inflammatory conditions, such as inflammatory bowel diseases (IBD) have a higher risk of developing and succumbing to colorectal cancer, in this case known as colitis-associated CRC (CAC) (Rubin *et al.*, 2012). However, tumour-associated inflammation has also been shown to play an important role in patients with sporadic CRC who exhibited no signs of prior IBD pathogenesis, implicating inflammation as a fundamental general driver of CRC (Reichling *et al.*, 2005; Wood *et al.*, 2007). Both sporadic CRC and CAC can be modelled in mice, and studies with these models have uncovered a prominent role for chronic inflammation in various mechanisms of carcinogenesis, with the NF- κ B pathway playing a central role.

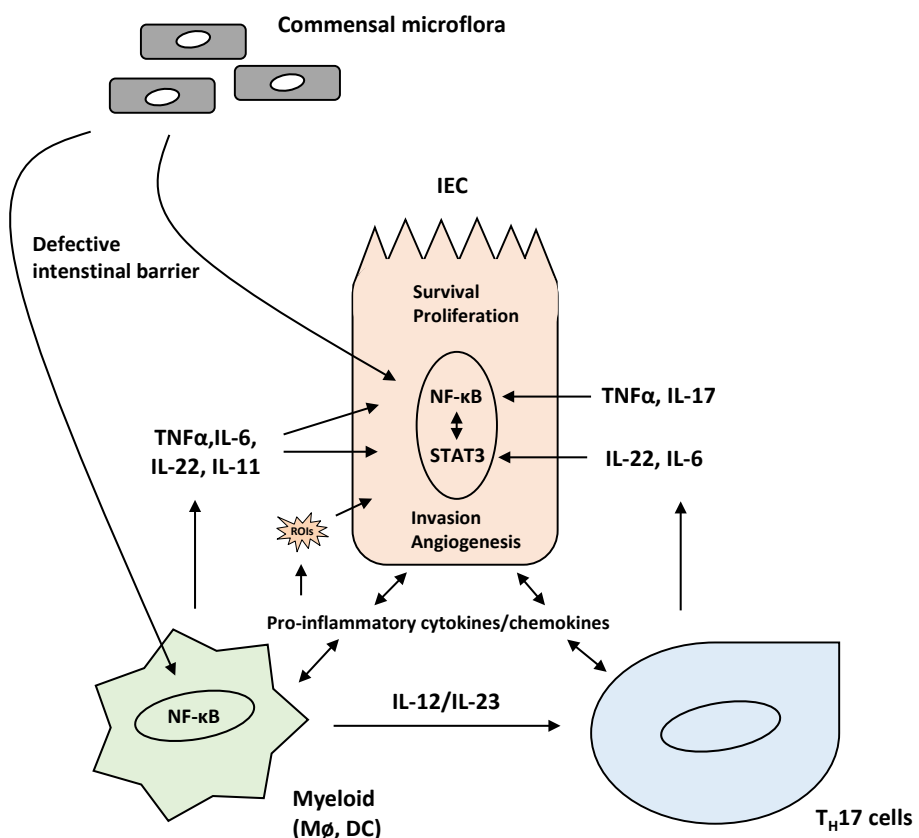


Figure 1.13. Overview of tumour-elicited inflammation in the progression of colorectal cancer. The schematic summarises some of the cytokines and the cell types that produce them that have been proposed to play a role in colorectal cancer progression. NF-κB signalling downstream of pro-inflammatory cytokines from the tumour microenvironment is proposed to be play a role in both tumour-associated myeloid/stromal cells, and intestinal epithelial cells (IECs), both in the promotion of cancer cell survival, proliferation, invasion and angiogenesis, and in the synthesis of pro-inflammatory cytokines and chemokines that attract further immune cells, and induce a pro-tumourigenic phenotype in various host immune cells, including macrophages and T cells. Adapted from Wang & Karin, 2015b.

Indeed, the NF-κB pathway has been demonstrated to be constitutively active in colon carcinoma patient samples. A number of studies have detected increased nuclear localisation and DNA binding activity of p65 in the majority of colorectal adenomas and adenocarcinomas, over that observed in adjacent nonneoplastic tissue (Lind *et al.*, 2001; Yu *et al.*, 2003; Kojima *et al.*, 2004; Sakamoto *et al.*, 2009). The level of expression of p65 has also been shown to significantly increase in the transition from adenoma to adenocarcinoma and occurs concomitantly with an increase in the expression of the pro-survival proteins, BCL-2 and BCL-xL, and a reduction in apoptotic index, implying that increased NF-κB activation may contribute to survival during CRC progression (Yu *et al.*, 2003).

A number of studies have also reported constitutive NF-κB activation in certain CRC cell lines (Dejardin *et al.*, 1999; Sakamoto *et al.*, 2009; Lin *et al.*, 2012). However, the data is unreliable as there are numerous inconsistencies regarding the exact cell lines that have been shown to exhibit constitutive activation and the extent to which they do so. Absence of widespread constitutive NF-κB activation in CRC cell lines is perhaps unsurprising, given that the primary mechanism of aberrant NF-κB activation in colon cancer is thought to be interaction with the pro-inflammatory microenvironment.

Various studies have attempted to stratify CRC into discrete subtypes with distinct biological characteristics to identify biomarker gene expression signatures predictive of the clinical characteristics of each subtype. In one such study, a subtype with poorer disease free survival demonstrated overexpression of a number of genes involved in activation of the NF- κ B pathway (Oh *et al.*, 2012). Another genome wide analysis of patient samples identified five distinct CRC tumour subtypes (Schlicker *et al.*, 2012). One of the poorer prognosis, treatment refractory subtypes exhibited activation of a large number of pathways involved in inflammation, including many that active NF- κ B, such as the TNF- α , Toll-like receptor and IL-1 pathways. A recent largescale approach, combined six independent classification systems to generate four consensus molecular subtypes with distinguishing features (Guinney *et al.*, 2015). The contribution of NF- κ B gene signatures to these subtypes was not addressed specifically, but both the CMS1 and the CMS4 subtypes, accounting for 14% and 23% of tumour samples, respectively, were characterised by high levels of immune/stromal cell infiltration and immune signalling activation, as well as worse relapse-free and overall survival.

The first evidence for NF- κ B signalling as the link between inflammation and colorectal cancer came from work with a CAC mouse mode, where IKK β -driven NF- κ B activation within intestinal epithelial cells (IECs) was shown to provide premalignant progenitor cells with a survival advantage through activation of antiapoptotic genes, such as BCL-XL, whereas IKK β -driven NF- κ B activation in tumour-associated myeloid cells promoted tumour growth and progression through expression of pro-inflammatory cytokines and growth factors (Greten *et al.*, 2004). Subsequent studies demonstrated that these tumour-promoting NF- κ B-induced cytokines include IL-6, TNF α , IL-1 β , IL-11, IL-22 and IL-23. For example, NF- κ B-dependent IL-6 secretion by tumour associated macrophages and dendritic cells has been found to be important in the activation of STAT3-mediated proliferative and survival signalling in IECs and development of CAC (Grivennikov *et al.*, 2009). STAT3 and NF- κ B transcription factors can synergise to enhance expression of survival genes (Greten *et al.*, 2002).

NF- κ B has also been shown to be important in the pathogenesis of sporadic colon cancer. Chronic IKK β activation (using a constitutively active IKK β mutant) in intestinal epithelial cells accelerated APC loss of heterozygocity and tumour initiation when crossed with mice expressing an IEC-specific mono-allelic deletion of APC, possibly through enhanced expression of inducible nitric oxide synthase (iNOS) and nitrosative DNA damage (Shaked *et al.*, 2012). NF- κ B is also extensively involved in another pro-inflammatory cytokine signalling network in sporadic CRC that switches T cells in the tumour microenvironment from a T helper 1 (Th1) anti-tumourigenic phenotype to a pro-tumourigenic T helper 17 (Th17) phenotype. Th17 cells secrete large quantities of cytokines such as IL-17A, IL-17F, IL-21, IL-22, TNF α and IL-6, which have been shown to synergistically activate STAT3 and NF- κ B in IECs to promote CRC growth (Simone *et al.*, 2015). IL-17A mainly signals within transformed IECs to promote their growth and survival during early phases of CRC development through activation of NF- κ B, ERK and p38 signalling (Wang *et al.*, 2014b). High IL-17A expression in stage I/II human colon cancer has also been shown to be associated with poor clinical outcome due to rapid progression to lethal metastasis (Tosolini *et al.*, 2011). Interestingly, the mechanism of Th17 cell activation may involve microbial products from the commensal microflora activating NF- κ B signalling in TME cells. In a mouse model of sporadic colon cancer, microbial products have been proposed to access the tumour microenvironment due to a defective intestinal barrier, whereupon they activate Toll-like receptor (TLR)-dependent NF- κ B signalling in tumour-associated macrophages to stimulate

production of IL-23, which in turn acts on T cells to induce Th17 cell activation (Grivennikov *et al.*, 2012). This is consistent with the separate observation that deletion of the TLR adaptor protein, Myd88, significantly reduces spontaneous APC-loss-driven colon cancer in mice (Rakoff-Nahoum & Medzhitov, 2007). The importance of NF- κ B signalling in tumour-associated macrophages has been further emphasised by the observation that high levels of p50 expression in macrophages promote a pro-tumourigenic M2 phenotype, whereas inhibition of NF- κ B signalling in macrophages induces an M1-like macrophage phenotype to promote tumour killing, reduce angiogenesis, and reduce peritoneal metastasis *in vivo* (Hagemann *et al.*, 2008; Ryan *et al.*, 2015).

NF- κ B may also be involved in the initiation of intestinal tumourigenesis through the reprogramming of post-mitotic IECs into stem cells with tumour-initiating capacity; p65 was proposed to enhance Wnt signalling during stem cell expansion through recruitment of CBP to DNA-bound β -catenin (Umar *et al.*, 2009; Schwitalla *et al.*, 2013).

However, as is typically the case with NF- κ B signalling, there are seemingly contradictory layers of complexity. NF- κ B has been proposed to function in intestinal epithelial cells to control gut epithelial layer and immune homeostasis. Deletion of either IKK β or NEMO in IECs has been shown to lead to chronic inflammation and spontaneous colitis (Zaph *et al.*, 2007; Nenci *et al.*, 2007). The mechanism has been proposed to involve protection from inflammation induced cell death in IECs that leads to invasion of commensal bacteria into the mucosa (Vlantis *et al.*, 2016). However, this mechanism was not proposed to contribute to inflammation-induced carcinogenesis.

1.4.5 The NF- κ B pathway as a target in cancer therapy

The demonstrable role of constitutive or treatment-induced NF- κ B signalling in various aspects of tumour initiation, progression and drug resistance in multiple different cancer types strongly suggests that inhibitors of NF- κ B function would be of benefit in cancer therapy, either as a monotherapy or in combination with general chemotherapeutics. Almost every node in the NF- κ B signalling pathway, from cell surface receptor down to the DNA binding of NF- κ B proteins themselves, has been investigated as a target of pathway inhibition (Gilmore *et al.*, 2006). Hundreds of natural and synthetic compounds have been reported as NF- κ B inhibitors (Gupta *et al.*, 2010). The IKK kinases, however, are perhaps the most attractive targets: they have a druggable, ATP-binding site; the similarity of the kinase domains of IKK α and IKK β with other protein kinases has facilitated large screens of known compounds; and at least one of the IKK family members is required for the vast majority of NF- κ B functions (Miller *et al.*, 2010).

The focus of drug development has historically been IKK β , owing to its purportedly dominant function in canonical NF- κ B signalling over IKK α . Currently, no IKK α selective inhibitors have been developed, partly due to a lack of pharmaceutical interest, and partly due to an intrinsic difficulty to develop inhibitors displaying selectivity over IKK β (Gamble *et al.*, 2012), although this situation is soon to change following the publication of the first potent and selective IKK α selective inhibitors (Anthony *et al.*, 2017). Several reports have documented the efficacy of IKK inhibition in triggering apoptosis in cancer cells as single agents, and in combination either with death-inducing cytokines or chemotherapeutic drugs (Godwin *et al.*, 2013).

Despite promising successes in preclinical models, so far no IKK inhibitors have been clinically approved. The reasons for this lack of clinical application is two-fold; a lack of clinical efficacy and concerns over both real and perceived toxicity issues associated with the chronic inhibition of IKK. The former issue possibly attests to both the lack of highly selective, nanomolar potent IKK inhibitors, and the significant NF- κ B activity that is likely to remain in certain clinical settings when IKK β is the sole target of inhibition. In these regards, the recent high resolution X-ray crystallographic structure of IKK β will likely help facilitate the rational design of novel, highly selective IKK β inhibitors (Liu *et al.*, 2013). Furthermore, more preclinical work is needed to identify relevant clinical settings for the use of dual, or selective IKK α or IKK β inhibition. A recent example of this is the discovery that IKK α -dependent non-canonical NF- κ B signalling is an important driver of castrate-resistant prostate cancer and therefore is the more attractive therapeutic target of the two IKK kinases (Luo *et al.*, 2007; Ammirante *et al.*, 2010).

The latter issue relates to the known toxicity that arises in mouse models following sustained IKK β inhibition. Myeloid-specific deletion of IKK β or sustained pharmacological IKK β inhibition in mice leads to a striking increase in susceptibility to endotoxin-induced shock due to excessive release of IL-1 β and related cytokines; a consequence of an unexpected role for IKK β -dependent NF- κ B activation in the negative control of inflammasome activation (Greten *et al.*, 2007). Myeloid-specific ablation of IKK β has also been observed to lead to lethal IL-1 β -driven neutrophilia and generalized inflammation (Hsu *et al.*, 2010). These effects of IKK β inhibition on innate immune function have clear ramifications for the use of sustained IKK β inhibition in the clinic. It might be possible to mitigate these effects by simultaneously modulating IL-1 receptor function (Hsu *et al.*, 2010), although this is likely to have a severe impact on innate immunity and lead to a high risk of infection (Genovese *et al.*, 2004). Furthermore, another solution to this issue might be the careful evaluation of dosing, scheduling and delivery strategies to ensure transient and reversible IKK β inhibition and to avoid long-term immunosuppression and cytotoxicity.

Another promising strategy to overcome issues of sustained IKK inhibition and systemic toxicity is to target signalling components downstream of chronic IKK/NF- κ B activity that are selectively required for cancer cell survival. Such targets might be downstream components of the NF- κ B pathway, or some of the growing number of NF- κ B-independent substrates of IKK α /IKK β that have been shown in some cases to contribute to tumourigenesis (see Section 1.3.2.4). An example of the former is the recent demonstration that highly cancer-selective targeting of the NF- κ B pathway is possible in multiple myeloma through the use of inhibitors of the interaction between the pro-survival NF- κ B-dependent target, GADD45 β and MKK7, which releases the inhibition of pro-apoptotic JNK activity to kill cancer cells (Tornatore *et al.*, 2014).

Another issue that must be addressed before NF- κ B inhibition can achieve clinical success is rapidly acquired resistance to IKK/NF- κ B inhibition. Such mechanisms of resistance have not been explored, but will likely be a considerable barrier to clinical success. This was highlighted by a study in a mouse mutant-KRAS/p53-driven non-small cell lung cancer (NSCLC) model, where acquired resistance quickly followed an initial period of potent therapeutic efficacy subsequent to administration of the IKK inhibitor, Bay-117082 (Xue *et al.*, 2011).

1.5 Aims

It has evidently been a challenge to manipulate the activity of this pleiotropic and complex pathway. A greater level of insight into the relative functions of IKK α and IKK β in NF- κ B signalling in human cancer cells may help reveal novel avenues for cancer therapy. With this in mind, we have undertaken a study of the relative functions of IKK α and IKK β in a human colorectal cancer cell line using CRISPR-Cas9 gene editing and small molecule inhibition approaches.

We intended to utilise these cell lines for the following purposes:

1. To comprehensively characterise the relative importance of IKK α and IKK β in canonical NF- κ B signalling within a human cancer setting (Chapter 3).
2. To attempt to identify novel NF- κ B-independent functions of IKK α and IKK β (see Chapter 4).
3. To attempt to identify genes regulated in an IKK α - or IKK β -dependent manner (see Chapter 6).
4. To investigate the selectivity of novel and commercially available IKK β inhibitors (see Chapter 5).

Chapter 2

Materials and methods

2 Materials and methods

2.1 Equipment and reagents

2.1.1 Laboratory suppliers

Equipment and reagents were procured from the following companies:

Agilent	
2100 Bioanalyzer	
RNA 6000 Pico Kit	
BD Biosciences	
LSRII Flow Cytometer	
Aria III Cell sorter	
BioRad	
20% Sodium dodecyl sulphate (SDS)	Gel electrophoresis apparatus
30% v/v acrylamide/bis	N,N,N',N'-Tetramethylethylenediamine (TEMED)
BioRad mini transblot	Precision Plus protein markers
Bradford reagent	Protein G-horseradish peroxidase
Freeze 'N Squeeze DNA gel extraction spin columns	
BMG Labtech	
PHERAstar microplate reader	
Calbiochem	
Q-VD-OPh	
Epicentre	
QuickExtract DNA extraction solution	
GE Healthcare	
Enhanced chemiluminescence system	
IN Cell Analyzer 6000	
Hoefer	
Gel casting apparatus	
Mighty small II gel apparatus	
Life Technologies	
Dulbecco's Modified Eagles Medium	Penicillin/Streptomycin
L-glutamine	Secondary antibodies for immunofluorescence
Lipofectamine 2000	Sodium bicarbonate
Lipofectamine RNAiMax	SYBR green PCR master mix
OptiMEM	Trypsin
Marvel	
Non-fat powder milk	
Melford	
4-(2-hydroxyethyl)-1-piperazineethanesulfonic acid (HEPES)	5-Bromo-4-chloro-3-indolyl-β-D-galactoside [X-gal]
Tris	
Millipore	
Immobilon Western Chemiluminescent HRP substrate	
Immobilon P PVDF membrane	
Nikon	
Nikon AR-1 confocal microscope	

PerkinElmer Applied Biosystems	
CellCarrier-96 microplates	
Emulsifier scintillator plus	
1600 TR liquid scintillation analyser	
[methyl- ³ H] thymidine 37MBq	
EasyTag™ Express [³⁵ S] -L-methionine/L-cysteine mix	
Qiagen	
Plasmid plus mini kit	Qiaquick PCR purification kit
Plasmid plus midi kit	QuantiTect reverse transcriptase kit
Plasmid plus maxi kit	RNAeasy Minielute Cleanup kit
Roche	
PhosSTOP™ phosphatase inhibitor tablets	
cComplete™ mini protease inhibitor cocktail tablets	
Sanyo	
CO ₂ incubator	
Sartorius	
150 ml and 500 ml 0.22 µm filter bottles	
Sigma-Aldrich	
Aprotinin	Magnesium chloride
Bovine serum albumin (BSA)	β-Mercaptoethanol
Bromophenol blue	Phenylmethylsulfonyl fluoride (PMSF)
Coomassie brilliant blue	Propidium iodide
Dimethyl sulphoxide (DMSO)	Rabbit serum
Ethanol BioUltra	Ribonuclease A
Ethidium bromide	RIPA buffer
Ethylene glycol bis(2-aminoethyl ether)- N,N,N'N'-tetraacetic acid (EGTA)	Sodium fluoride
Ethylenediaminetetraacetic acid (EDTA)	Sodium orthovanadate
Kanamycin	Triton X-100
Leupeptin	TRI reagent
Goat serum	Thymidine
	Tween-20
Thermo Scientific	
All tissue culture plasticware (Nunc)	
ND-1000 spectrophotometer (Nanodrop)	
Vector Labs	
VectaShield	
VWR	
Acetic acid	Microscope slides
Calcium chloride	Propan-2-ol
Coverslips	Potassium chloride
Disodium hydrogen phosphate	Potassium dihydrogen phosphate
Ethanol	Sodium azide
Glycerol	Sodium bicarbonate
Glucose	Sodium chloride
Haemocytometer	Sodium hydroxide
Magnesium chloride	Trichloroacetic acid
Methanol	
Zymogen Research	
Direct-zol™ RNA Miniprep kit	

Table 2.1. Sources of general laboratory equipment and reagents.

2.1.2 Pharmacological inhibitors

Inhibitor	Targets	Mechanism of action	Supplier	Catalogue number
AZD2230	IKK β , IKK α	ATP competitive	AstraZeneca	N/A
Bafilomycin	Vacuolar-type H ⁺ -ATPase, Ca-P60A/dSERCA	Targets ATP6VOC/VO subunit c	Enzo Life Sciences	BML-CM110-0100
BIX02514	IKK β	ATP competitive	Professor Sir Philip Cohen/AstraZeneca	N/A
BMS-345541	IKK β , IKK α	Allosteric	Tocris	4806
CHIR 99021	GSK3 β and α	ATP-competitive	Selleckchem	S2924
Chloroquine Phosphate	Endosomes/lysosomes	Diprotic weak base that accumulates inside acidic cytoplasmic vesicles (endosomes/lysosomes) causing elevation of pH and inhibition of acid hydrolases	Sigma-Aldrich	PHR1258-1G
Emetine	Ribosome	Binds 40S subunit to inhibit translation	Sigma-Aldrich	E2375
Flavopiridol	CDK9, CDK1, CDK2, CDK4/6	ATP competitive	Cayman Chemical	10009197
MG-132	Proteasome	Competitive inhibitor at chymotrypsin-like site	Sigma-Aldrich	C2211
Roscovitine	CDK7, CDK9, CDK1, CDK2, CDK5	ATP competitive	Stratech	S1153
Selumetinib	MEK1, MEK2	ATP and substrate uncompetitive allosteric inhibitor	AstraZeneca	N/A
SNS-032	CDK9, CDK7, CDK2	ATP competitive	Stratech	S1145-SEL

Table 2.2 Source, target and mode of action of pharmacological inhibitors.

2.1.3 Solutions

All solutions were dissolved in MilliQ deionised water unless specified otherwise.

Solution	Components
Phosphate-buffered saline (PBS)	137 mM NaCl 2.7 mM KCl 1.47 mM KH ₂ PO ₄ 8.1 mM Na ₂ HPO ₄
Tris-buffered saline with Tween (TBST)	50 mM Tris-HCl, pH 7.6 150 mM NaCl 0.1% v/v Tween 20
Coomassie Brilliant Blue solution	50% v/v methanol 0.05% w/v Coomassie Brilliant Blue 10% v/v acetic acid
Western Blot Destain Solution	7% v/v acetic acid 5% v/v methanol
siRNA buffer (GE Pharmacon)	60 mM KCl, 6 mM HEPES pH 7.5

	0.2 mM MgCl ₂
Luria Broth (LB)	10g/L Tryptone 10g/L NaCl 5g/L Yeast extract
Tail Lysis Buffer	100 mM Tris-HCl pH 8.0 5 mM EDTA 0.2% SDS 200 mM NaCl
Annexin assay binding buffer	10 mM HEPES/NaOH pH 7.4 140 mM NaCl 2.5 mM CaCl ₂

Table 2.3 General laboratory solutions.

Solution	Components
SDS running buffer pH 8.3	192 mM glycine 25 mM Tris base 0.1% w/v SDS
Western blot transfer buffer	192 mM glycine 25 mM Tris base 20% v/v methanol
Blocking buffer – 5% milk/TBST	10 mM Tris-HCl, pH 8.0 150 mM NaCl 0.1% v/v Tween 20 5% w/v Marvel dried milk powder
Blocking buffer – 5% BSA/TBST	10 mM Tris-HCl, pH 8.0 150 mM NaCl 0.1% v/v Tween 20 5% w/v BSA
Western Blot Destain Solution	7% v/v acetic acid 5% v/v methanol
4 x Laemmli buffer	200 mM Tris-HCl, pH 6.8 8% w/v SDS 40% v/v glycerol 4% v/v β-mercaptoethanol 0.04% w/v bromophenol blue
TG Lysis Buffer	20 mM Tris-HCl, pH 7.5 137 mM NaCl 1 mM EGTA 1% v/v Triton X-100 10% v/v glycerol 1.5 mM MgCl ₂ 1 mM Na ₃ VO ₄ 1 mM PMSF 10 µg ml ⁻¹ aprotinin 10 µg ml ⁻¹ leupeptin 50 mM NaF
Lysis Buffer (Magalef <i>et al.</i> , 2012)	1 x PBS 0.5% v/v Triton x-100 1 mM EDTA 100 mM Na ₃ VO ₄ 0.25 mM PMSF Roche cOmplete protease inhibitors
Buffer A	10mM Hepes pH7.9 1.5mM MgCl ₂ 10mM KCl 0.1 mM EDTA

Table 2.4. Solutions used for SDS-PAGE and Western blotting.

Solution	Components
Blocking buffer	1 x PBS 5% v/v goat serum 0.2% Tween 20 0.02% w/v sodium azide
Permeabilisation buffer	1 x PBS 0.1% v/v Triton x-100
Antibody dilution buffer	1 x PBS 2% w/v BSA 0.2% v/v Tween

Table 2.5. Solutions used for immunocytochemistry.

2.1.4 Antibodies

The following primary and secondary antibodies were used for Western blotting, immunocytochemistry and other immunofluorescence procedures:

Antibody	Blocking Solution	Dilution	Species of origin	Supplier	Catalogue Number
β-actin	5% milk/TBST	1:10000	Mouse	Sigma	A5441
β-catenin	5% BSA/TBST	1:1000	Mouse	BD Biosciences	610154
p-β-catenin	5% BSA/TBST	1:1000	Rabbit	Cell Signalling Technology	9561
β-Tubulin	5% BSA/TBST	1:5000	Rabbit	Abcam	Ab6046
AKT1	5% milk/TBST	1:1000	Mouse	Cell Signalling Technology	2967
p-AKT1 (S473)	5% BSA/TBST	1:1000	Rabbit	Cell Signalling Technology	9271
p-AKT1 (T308)	5% BSA/TBST	1:1000	Rabbit	Cell Signalling Technology	13038
Aurora A	5% BSA/TBST	1:1000	Rabbit	Cell Signalling Technology	3092
Aurora B	5% BSA/TBST	1:1000	Rabbit	Cell Signalling Technology	3094
Cdc2 (CDK1)	5% BSA/TBST	1:500	Rabbit	Santa Cruz	Sc-747
p-Cdc2 (Y15)	5% BSA/TBST	1:1000	Rabbit	Cell Signalling Technology	9111
Cdc20	5% BSA/TBST	1:1000	Rabbit	Cell Signalling Technology	4823
CDCD25C	5% milk/TBST	1:500	Rabbit	Santa Cruz	Sc-327
CDH1 (E-cadherin)	5% milk/TBST	1:1000	Rabbit	Cell Signalling Technology	3195
cIAP1	5% BSA/TBST	1:1000	Rabbit	Cell Signalling Technology	7065
cIAP2	5% BSA/TBST	1:1000	Rabbit	Cell Signalling Technology	3130
c-Jun	5% BSA/TBST	1:1000	Rabbit	Cell Signalling Technology	9165
c-Rel	5% BSA/TBST	1:1000	Rabbit	Cell Signalling Technology	4727
Cyclin B1	5% BSA/TBST	1:250	Mouse	Neomarkers	MS-868
Cyclin D1	5% milk/TBST	1:200	Mouse	Calbiochem	CC12
FLAG	5% milk/TBST	1:2000	Mouse	Sigma-Aldrich	F-3165
GSK-3β	5% milk/TBST	1:1000	Rabbit	BD Transduction	610201

p-GSK-3 α β (S21/S9)	5% BSA/TBST	1:1000	Rabbit	Cell Signalling Technology	9331
Histone H3	5% milk/TBST	1:1000	Mouse	Abcam	ab24834
I κ B α	5% milk/TBST	1:1000	Rabbit	Cell Signalling Technology	9242
I κ B α (N-terminal epitope)	5% milk/TBST	1:1000	Mouse	Cell Signalling Technology	4814
p-I κ B α (S32/36)	5% BSA/TBST	1:1000	Mouse	Cell Signalling Technology	9246
I κ K α (N-terminal epitope)	5% BSA/TBST	1:1000	Rabbit	Cell Signalling Technology	2682
I κ K α (C-terminal epitope)	5% BSA/TBST	1:1000	Rabbit	Abcam	ab109749
I κ K β (C-terminal epitope)	5% BSA/TBST	1:1000	Rabbit	Cell Signalling Technology	2684
I κ K β (N-terminal epitope)	5% BSA/TBST	1:1000	Rabbit	Abcam	ab124957
p-I κ K α/β (I κ K α S176/180 and I κ K β S177/S181)	5% BSA/TBST	1:1000	Rabbit	Cell Signalling Technology	2697
p-I κ K α/β (I κ K α S176/I κ K β S177)	5% BSA/TBST	1:1000	Rabbit	Cell Signalling Technology	2078
JNK1	5% milk/TBST	1:500	Rabbit	Santa Cruz	Sc-474
p-JNK (T183/Y185)	5% BSA/TBST	1:1000	Mouse	Cell Signalling Technology	9255
Lamin A/C	5% milk/TBST	1:400	Mouse	Santa Cruz	Sc-7292
LC3B	5% milk/TBST	1:4000	Mouse	Sigma	SAB4200361
MCL1	5% milk/TBST	1:500	Rabbit	Santa Cruz	Sc-819
NEMO	5% milk/TBST	1:1000	Rabbit	Abcam	ab178872
NEMO	5% milk/TBST	1:1000	Mouse	Cell Signalling Technology	2695
NIK	5% BSA/TBST	1:1000	Mouse	Cell Signalling Technology	4994
p21 ^{CIP1}	5% BSA/TBST	1:500	Mouse	BD Biosciences	556431
p38	5% milk/TBST	1:2000	Rabbit	In house	N/A
p-p38 (T180/Y182)	5% BSA/TBST	1:1000	Rabbit	Cell Signalling Technology	9211
p53	5% milk/TBST	1:200	Mouse	Calbiochem	OP43
p65	5% BSA/TBST	1:1000	Rabbit	Cell Signalling Technology	8242
p-p65 (S468)	5% BSA/TBST	1:1000	Rabbit	Cell Signalling Technology	3039
p-p65 (S536)	5% BSA/TBST	1:1000	Rabbit	Cell Signalling Technology	3033
p100/p52	5% BSA/TBST	1:2000	Mouse	Millipore	05-361
PARP	5% milk/TBST	1:1000	Rabbit	Cell Signalling Technology	9542
PTEN	5% milk/TBST	1:1000	Rabbit	Cell Signalling Technology	9552

p-Rb (S795)	5% BSA/TBST	1:1000	Rabbit	Cell Signalling Technology	9301
p-Rb (S807/11)	5% BSA/TBST	1:1000	Rabbit	Cell Signalling Technology	9308
RelB	5% BSA/TBST	1:1000	Rabbit	Sigma Aldrich	HPA040506
RIP1	5% milk/TBST	1:1000	Rabbit	Cell Signalling Technology	9493
RNA Pol II	5% milk/TBST	1:200	Rabbit	Santa Cruz	Sc-9001
p-RNA Pol II (S2)	5% BSA/TBST	1:1000	Rabbit	Abcam	Ab5095
p-RNA Pol II (S5)	5% BSA/TBST	1:1000	Mouse	Abcam	Ab5408
TRAF1	5% milk/TBST	1:1000	Rabbit	Cell Signalling Technology	4715
TRAF2	5% milk/TBST	1:1000	Rabbit	Cell Signalling Technology	4724
TRAF3	5% milk/TBST	1:1000	Rabbit	Cell Signalling Technology	4729
Securin	5% milk/TBST	1:1000	Rabbit	Cell Signalling Technology	13445

Table 2.6. Antibodies, blocking solution and dilutions used for Western blotting.

Antibody	Blocking Solution	Dilution	Supplier	Catalogue Number
Goat anti-mouse IgG-HRP conjugate	5% milk/TBST	1:3000	BioRad	170-6516
Goat anti-rabbit IgG-HRP conjugate	5% milk/TBST	1:3000	BioRad	170-6515
Protein G-HRP conjugate	5% milk/TBST	1:3000	BioRad	170-6425

Table 2.7. Secondary antibodies used for Western blotting.

Antibody	Blocking Solution	Dilution	Supplier	Catalogue Number
c-Rel	ICC Blocking buffer	1:100	Cell Signalling Technology	4727
Ki67	ICC Blocking buffer	1:400	Cell Signalling Technology	9129
p65	ICC Blocking buffer	1:400	Cell Signalling Technology	8242
IKK α	ICC Blocking buffer	1:100	Cell Signalling Technology	2682

Table 2.8. Primary antibodies used for immunocytochemistry.

Antibody	Blocking Solution	Dilution	Supplier	Catalogue Number
Alexa Fluor 488 goat anti-rabbit IgG	ICC Blocking buffer	1:1000	Life technologies	A-11008
Alexa Fluor 488 goat anti-rabbit IgG	ICC Blocking buffer	1:1000	Life technologies	A-11008

Table 2.9. Secondary antibodies used for immunocytochemistry.

2.1.5 siRNA oligo's

The following siRNA oligonucleotide sequences were used for RNA interference:

siRNA	Supplier	Catalogue Number	Sense oligonucleotide sequence (5' → 3')
IKK α	Dharmacon (GE LifeSciences)	siGENOME SMARTpool IKK α siRNA M-003473-02-005	CAAAGAACGUGACAAUACU CCAGAUACUUUCUUUACUA GAAGUUCGGUUUAGUAGCC AAAUAUGGCAUCUCUUA
IKK β	Dharmacon (GE LifeSciences)	siGENOME SMARTpool IKK β siRNA L-003473-00-0005	GGAAGUACCUGAACCAGUU CCAAUAUUCUUAACAGUGU GGAAUCAGCUUCUCCUAAA GUGGUGAGCUUAUGAAUG
IKK β	Dharmacon (GE LifeSciences)	ON-TARGETplus SMARTpool IKK β siRNA L-003473-00-0005	AUGAAUGCUCUCGACUUA GAAGAGGUGGGUGAGCUUA GAGCUGUACAGGAGACUAA CCGUAAGCCUGCCACUCA
KRAS	Dharmacon (GE LifeSciences)	siGENOME SMARTpool KRAS siRNA M-005069-00	AUGAAUGCUCUCGACUUA GAAGAGGUGGGUGAGCUUA GAGCUGUACAGGAGACUAA CCGUAAGCCUGCCACUCA
NEMO	Dharmacon (GE LifeSciences)	ON-TARGETplus SMARTpool NEMO siRNA L-003473-00-0005	AUGAAUGCUCUCGACUUA GAAGAGGUGGGUGAGCUUA GAGCUGUACAGGAGACUAA CCGUAAGCCUGCCACUCA
NIK	Dharmacon (GE LifeSciences)	siGENOME SMARTpool NIK siRNA M-003580-04-0005	UCUCAAAGCUCGCGGGACA GGGAAAGCGUCGCAGCAAA CGCCAAAUCAGCCAAUUA GAUCCUGAAUGACGUGAUU
Non-Targeting	Dharmacon (GE LifeSciences)	siGENOME Non-targeting siRNA pool (D-001206-13-20)	UAGCGACUAAAACACAUAA UAAGGCUAUGAAGAGAUAC AUGUAUUGGCCUGUAUUAG AUGAACGUGAAUUGCUCAA

Table 2.10. Sequences of oligonucleotides used for siRNA.

2.1.6 qPCR primers

The following primers were used for quantitative real-time PCR.

Target	Sequence
IKK α	FWD: 5'- TGTACACAGAGTTCTGCCG-3' REV: 5'- TGAAGTCTCCCCATCTTGAGG-3'
IKK β	FWD: 5'-CTTGGGACAGGGGGATTGG-3' REV: 5'-ATTGGGGTGGGTAGCCTTC-3'
NEMO	FWD: 5'-GACAACCACATCAAGAGCAGC-3' REV: 5'-CTTGTAGATATCGCCTGG-3'
UBC	FWD: 5'-CTGGAAGATGGTCGTACCTG-3' REV: 5'-GGTCTGCCAGTGAGTGTCT-3'
YWHAZ	FWD: 5'-TGATCCCCAATGCTTCACAAG-3' REV: 5'-GCCAAGTAACGGTAGTAATCTCC-3'
B2M	FWD: 5'-TGCTGTCGCCATGTTGATGTA-3' REV: 5'-TCTCTGCTCCCCACCTCTAAGT-3'
AKT1	FWD: 5'- CTTCTTGCCGGTATCGTG-3' REV: 5'- TGCTGTCATCTGGTCAGG-3'

CSF1	FWD: 5'- TGGCGAGCAGGAGTATCACC-3' REV: 5'- AGGTAGCACACTGGATCTTCAAC-3'
USP43	FWD: 5'- CTGCAAGGTGGGCATTACAC-3' REV: 5'- AGCTGGTAGAGCCTCTCATGG-3'

Table 2.11. Primers used for quantitative reverse-transcription PCR.

2.1.7 Plasmids

HA-RelA and pGL4.32[luc2P/NF-κB-RE were a kind gift from Prof Neil Perkins (*Institute for Cell and Molecular Biosciences, Newcastle University, UK*). Wild-type FLAG-IKK α and kinase inactive FLAG-IKK α (K44A) plasmids were kind gifts from Prof Lienhard Schmitz (Department of Biochemistry, Justus-Liebig-Universität Gießen, Germany). Wild-type pCMV2TAG IKK β and kinase inactive pCMV2TAG IKK β (K44M) were purchased from Addgene (Plasmid #11103 and 11104, respectively). Wild-type pCMVTAG2B NEMO and mutant pCMVTAG2B NEMO (L329P) were purchased from Addgene (Plasmid # 11970 and #11971, respectively). pD1301-AD Cas9 expression vector was supplied by Horizon Discovery™.

2.2 Cell Lines and culture

2.2.1 Colorectal cancer cell lines

DLD1

DLD-1 cells are an epithelial colorectal adenocarcinoma cell line established between 1977-1979. These cells harbour an activating KRAS mutation (G13D) and an activating PIK3CA mutation (E545K). They were kindly provided by Paul Coffer (University Medical Center, Utrecht, The Netherlands).

HCT116

HCT116 cells are an epithelial colorectal carcinoma cell line established in 1981. These cells harbour an activating KRAS mutation (G13D) and an activating PI3KCA mutation (H1047R). They also harbour mutations in β-catenin (S45del), MLH1 (S252*) and p14^{ARF} (E74fs*). They were kindly provided by Prof Bert Vogelstein (John Hopkins University, Baltimore, USA).

HT-29

HT29 cells are an epithelial colorectal adenocarcinoma cell line established in 1964 from a 44 year old female Caucasian patient. These cancer cells harbour an activating BRAF mutation (V600E), a PI3KCA mutation (P449T), a SMAD4 mutation (Q311*), a TP53 mutation (R273H) and APC mutations (E853* and T1556fs*3). They were purchased from ATCC.

LoVo

LoVo cells are an epithelial colorectal adenocarcinoma cell line This cell line was established from a metastatic site (lymph node). These cells harbour an activating KRAS mutation (G13D), an FBXW7 mutation (R505C), and MSH2 mutation and APC mutations (R1114* and M1431fs*42). They were purchased from ATCC.

SK-CO1

SK-CO1 cells are an epithelial colorectal adenocarcinoma cell lines. This cell line was established in 1972 from a metastatic site (ascites) in a 65-year-old Caucasian male with colorectal adenocarcinoma. These cancer cells harbour an activating KRAS mutation (G12V) and mutations in the APC gene (F1089fs*37 and P1443fs*30). They were purchased from ATCC.

SW620

SW620 cells are an epithelial colorectal adenocarcinoma cell line established in 1976 from a metastatic site in the lymph node of a 51 year old Caucasian male. These cancer cells harbour an activating KRAS mutation (G12V) and were purchased from ATCC.

SW837

SW837 cells are an epithelial colorectal adenocarcinoma cell line established from a 53 year old Caucasian male. These cancer cells harbour an FBXW7 mutation (L403fs*34), a TP53 mutation (R248W), a FAM123B mutation (R497*), a KRAS mutation (G12C) and APC mutations (R1450* and R213*). They were purchased from ATCC.

2.2.2 Lung cancer cell lines

A549

A549 cells are an epithelial-like lung carcinoma cell line established in 1972 from a 58 year old Caucasian male. These cancer cells harbour an activating G12S mutation, an LKB1 mutation (Q37*) and a CDNKA mutation (M1*). They were purchased from ATCC.

2.2.2 Cell culture medium

The following medium was used for routine cell culture:

Cell line	Culture Medium	Supplementation
HCT116 Isogenic HCT116 CRISPR IKK KO cell lines SK-CO1 LoVo A549	DMEM (Life Technologies 41966)	10% (v/v) foetal bovine serum 2mM L-glutamine 100U/ml penicillin 100 µg/ml streptomycin
DLD1	DMEM (Life Technologies 11880)	10% (v/v) foetal bovine serum 1.75 g Glucose 1mM L-glutamine 100 U/ml penicillin 100 µg streptomycin
HT29	McCoy's 5A (Life Technologies 22330)	10% (v/v) foetal bovine serum 2 mM L-glutamine 100 U/ml penicillin 100 µg/ml streptomycin
SW620 SW837	Leibovitz's L-15 Medium (Life Technologies 11415)	10% (v/v) foetal bovine serum 2 mM L-glutamine 100 U/ml penicillin 0.075% (v/v) sodium bicarbonate 100 µg/ml streptomycin

Table 2.12. Cell culture medium and medium supplements for each cell line.

2.2.3 Routine cell culture

Cells were cultured at 37°C in a humidified incubator with 95% air and 5% CO₂ and passaged at ~80% confluence, typically every 3-4 days. For passaging, growth medium was aspirated, cells were washed with pre-warmed 0.05% trypsin/EDTA solution and then incubated at 37°C with fresh 0.05% trypsin/EDTA solution for 5 minutes. Detached cells were resuspended in fresh, pre-warmed culture medium to generate a single-cell suspension, prior to dilution into new tissue culture flasks.

2.2.4 Cell line storage

Cells were trypsinised as above, resuspended in fresh medium and cell pellets collected by centrifugation. The medium was then aspirated and cells were resuspended in 10% v/v FBS/DMSO to yield a cell density of ~1-2 × 10⁶ cells/ml. The resulting suspension was then aliquoted (1 ml per cryovial) and frozen slowly in an insulating box at -80°C. For longer term storage of cells, cryovials were transferred to liquid nitrogen. As required, cells were rapidly thawed at 37°C and placed into a fresh 75 cm² culture flask containing 20 ml pre-warmed medium. The following day, this medium was replaced to remove traces of DMSO.

2.3 Cell treatments

2.3.1 Drug treatments

Stock solutions of drugs were diluted in cell culture medium as appropriate to yield the final drug concentrations. All treatments were adjusted so as to contain the same volume of vehicle (e.g. DMSO or ethanol). Vehicle-only containing medium was used as control. Treated cells were incubated at 37°C, 5% CO₂/95% air for the length of time indicated in the figure legend.

2.3.2 RNA interference

siRNA oligonucleotides were resuspended in 1 x siRNA buffer to generate 20 μM stock solutions. siRNAs were mixed with Optimem media (Invitrogen), and an equivalent volume of Optimem was combined with an empirically determined volume of Lipofectamine RNAiMax (Invitrogen), and both mixtures incubated separately for 5 minutes at room temperature (RT). The two solutions were combined, mixed and incubated at RT for 20 minutes. Cells were trypsinised and plated at the required density in antibiotic-free media, together with siRNA-lipid complexes, to give a final concentration of 5-50 nM siRNA (experiment dependent, see figure legends for details).

2.4 DNA and RNA manipulation

2.4.1 Plasmid recovery and transformation

Plasmid solutions spotted onto 3MM chromatography paper were excised with a sterile razor blade and placed in a sterile tube. 20 μl nuclease free H₂O (Ambion) was added to the paper, tubes vortexed and left to stand for

5 minutes, prior to centrifugation to recover solubilised DNA. 5 µl of this solution was added to 50 µl DH5 α competent E.coli cells (New England Biolabs) and incubated on ice for 30 minutes. Cells were heat shocked for 30 seconds at 42°C, incubated for 15 minutes on ice, mixed with 950 µl Luria Broth (LB) and then grown for 1 h at 37°C shaking at 220 rpm. Transformed bacteria were then streaked onto LB-agar plates containing 100 µg/ml ampicillin or 50 µg/ml kanamycin and incubated overnight at 37°C. Plasmids acquired from Addgene were supplied as transformed bacteria in stab culture format. Bacteria from the stab were streaked onto an agar plate to isolate single colonies.

2.4.2 Plasmid preparation

Individual transformed DH5 α colonies were picked and used to inoculate a 5ml LB starter culture containing 100 µg/ml ampicillin or 50µg/ml kanamycin, which was subsequently incubated at 37°C in a shaking (220 rpm) incubator for 8 h. The culture was then diluted 1:1000 in 500ml LB containing appropriate antibiotic and incubated overnight at 37°C in a shaking (220 rpm) incubator. Plasmid DNA was purified with Qiagen Plasmid Plus Midi kit according to the manufacturer's instructions. DNA concentration and A260/A280 ratio were subsequently determined using a NanoDrop spectrophotometer. DNA was stored at -20°C.

2.4.3 Genomic DNA isolation

For routine genomic DNA isolation cells were lysed with Tail Lysis Buffer and 200 µg/ml Proteinase K added to the lysate prior to incubation at 55°C overnight. An equivalent volume of phenol/chloroform/isoamyl alcohol 25:24:1 v/v saturated with 10 mM Tris. pH 8.0, 1 mM EDTA (Sigma-Aldrich) was added and tubes mixed by inversion. After centrifugation the DNA-containing aqueous phase was collected and precipitated by adding 0.8 volumes of 100% isopropanol (Sigma-Aldrich). The precipitated DNA was pelleted by centrifugation, washed with 70% ethanol and solubilised in nuclease-free water. QuickExtract DNA extraction was used, according to manufacturer's instructions, to isolate PCR-ready genomic DNA from CRISPR clones growing in 96-well plate format.

2.4.4 Genomic RNA isolation

Cells were lysed with 1 ml of TRI reagent per 10 cm² of culture dish surface area and a homogenous lysate generated by pipetting and vortexing. Samples were incubated for 5 minutes at RT to permit complete dissociation of nucleoprotein complexes. Lysates were transferred to sterile Rnase-free tubes, and genomic RNA was isolated using Direct-zol RNA MiniPrep kit according to manufacturer's instructions. Genomic DNA was removed from samples through an in-column DNase I digestion. RNA eluted with DNase/RNase-free water was stored at -80°C for short-term storage.

2.4.5 cDNA preparation

cDNA for qRT-PCR was synthesised from 1 µg of purified RNA using the Quantitech Reverse Transcription kit, according to manufacturer's instructions. cDNA was diluted 1:20 in RNase-free water and stored at -20°C.

2.4.6 Site-directed mutagenesis

S468A and S468D mutant versions of a HA-RelA plasmid were generated using the QuikChange II XL site-directed mutagenesis kit according to manufacturer's instructions. The following primers were used:

Mutant	Primer Sequence
P65 S468A	F – agttgtcgacggctgccaggctgtgaacac R – gtgttcacagacactggcagccgtcgacaact
P65 S468D	F - cggagttgtcgacgtctgcccaggctgtgaacacag R - ctgttgtcacagacacctggcagacgtcgacaactccg

Table 2.13. Primer sequences used for site-directed mutagenesis.

2.5 Preparation of whole cell lysates

The culture medium was either discarded or kept depending on whether non-adherent/floating cells was present. Cells were washed twice in PBS and scraped from the dish in TG lysis or RIPA buffer. To harvest cells from the culture medium, the medium was centrifuged (500 x g), the resulting pellet washed in PBS and then lysed in lysis buffer. Lysates were cleared of non-soluble material by centrifugation (13 000 x g at 4°C for 10 minutes). Supernatant protein concentration was estimated either using the Bradford protein assay (Biorad, in the case of lysis with TG lysis buffer) or the Pierce BCA protein assay kit (Invitrogen, in the case of lysis with RIPA buffer). For the Bradford assay, 5 µl cleared lysate was mixed with 795 µl distilled water and 200 µl Bradford reagent, and absorbance determined at 595 nm using a spectrophotometer. The BCA assay was performed according to manufacturer's instructions and absorbance determined at 562 nm using a spectrophotometer. Samples were prepared for Western Blotting by boiling in 4 x Laemmli sample buffer (SB) for 5 minutes and stored at -20 °C.

2.6 SDS-PAGE and Western Blotting

Resolving and stacking SDS-PAGE gels were assembled as in Tables 2.14 and 2.15.

Component	Resolving gel percentage (%)			
	8	10	12	14
30% Acrylamide/Bis (ml)	16.2	19.8	24	27.6
1.5 M Tris pH 8.8 (ml)	15	15	15	15
ddH ₂ O (ml)	27.6	24	19.8	16.2
20% SDS (ml)	0.6	0.6	0.6	0.6
10% APS (ml)	0.6	0.6	0.6	0.6
TEMED (µl)	60	60	60	60

Table 2.14. Resolving gel composition

Component	Stacking gel percentage (%)		
	4	5	6
30% Acrylamide/Bis (ml)	2.67	3.33	4
1.5 M Tris pH 8.8 (ml)	5	5	5
ddH ₂ O (ml)	11.93	11.27	10.6
20% SDS (ml)	0.2	0.2	0.2
10% APS (ml)	0.2	0.2	0.2
TEMED (µl)	25	25	25

Table 2.15. Stacking gel composition

Equivalent quantities of protein were resolved by SDS-PAGE (Hoefer Mighty Small system) at 25 mA per gel, with protein standards run in one lane as a molecular weight reference. Proteins were subsequently transferred to methanol-activated Immobilon P PVDF membrane at 300 mA for 90 minutes using the Mini Trans-Blot Cell wet blotting system. Membranes were blocked in 5 % (w/v) powdered milk/TBST or 5% (w/v) BSA/TBST for 30 minutes and probed with primary antibodies at 4°C overnight with gentle agitation. Primary antibodies, their origin, and dilution used for Western blotting are shown in Table 2.6. Membranes were washed three times in TBST and probed with appropriate HRP-conjugated secondary antibody diluted at 1:3000 in 5 % (w/v) powdered milk (Table 2.7) for 1 h at RT. Following three TBST washes, antibody-antigen complexes were detected by the enhanced chemiluminescence (ECL) system coupled with an autoradiographic film developer.

2.7 Subcellular fractionation

Cells were harvested by gently scraping in PBS-EDTA (10mM). Cells were then pelleted, and the pellet washed with PBS. The washed cell pellet was subsequently gently resuspended in 5 pellet volumes of ice cold Buffer A, which had been supplemented with 1 mM DTT and protease (cOmplete, Mini, EDTA-free protease inhibitor cocktail, Roche) and phosphatase (PhosSTOP, Roche) inhibitors. Cells were incubated on ice for 15 minutes, then 0.1 % (v/v) NP-40 added to release the cytoplasmic contents. A 1 ml dounce homogeniser was used to ensure complete cell lysis. Nuclei were subsequently pelleted at 800 x g for 10 minutes at 4°C and the cytoplasmic fraction (supernatant) transferred to a fresh tube. This supernatant was centrifuged again 10 000 x g for 5 minutes to pellet any contaminating nuclei. NaCl and glycerol were added to the cytoplasmic fraction to final concentrations of 137 mM and 10% (v/v), respectively. The nuclei pellet was washed at least three times in ice cold buffer A, prior to addition of 0.7 pellet volumes of RIPA buffer (Sigma), supplemented with >250 U benzonase nuclease (Sigma-Aldrich). Samples were incubated at 4°C for 4 h with end-over-end inversion, with occasional vortexing. The nuclear fraction was subsequently cleared by centrifugation.

2.8 Immunoprecipitation

Cells were lysed in TG lysis buffer and the lysates precleared with Protein A-Sepharose beads for 1 h at 4°C. A fraction of this lysate was retained for input blots. Rabbit anti-NEMO monoclonal antibody (ab178872) was subsequently added to the remaining lysate, to a final dilution of 1:100, and antibody-antigen complexes formed during a 3 h incubation at 4°C with end-over-end rotation. Protein A-Sepharose beads were then added to the lysate for a further 4 h incubation at 4°C. Following centrifugation, the beads were washed three times in TG lysis buffer, before elution of the beads in 4 x SB with boiling. The lysate was retained for unbound blots. Eluents and input/unbound fractions were then subjected to SDS-PAGE and Western blotting. To minimise heavy and light chain interference, a mouse anti-NEMO primary antibody and Protein G-HRP secondary antibody (Bio-Rad Laboratories) were used for immunoblotting.

2.9 Flow cytometry

2.9.1 Propidium Iodide staining and DNA content analysis

Following harvest, cells were pelleted by centrifugation (1,500 rpm, 4°C, 5 min), washed in PBS, and then resuspended in 0.2 ml PBS. Cells were fixed in 70% (v/v) ethanol/PBS, and stored at 4°C. On the day of analysis, samples were centrifuged (1,500 rpm, 4°C, 5 min), washed with PBS, and resuspended in 0.25 ml PBS containing 25 µg RNase and 12.5 µg of the DNA-intercalating agent propidium iodide (PI). Following 30 minutes incubation at 37°C, samples were passed through a 25-gauge needle to reduce cell clumping. Cell cycle profiles were acquired with an LSRII flow cytometer (BD Biosciences), using a 488 nm excitation laser line and a 670 nm long pass emission filter to measure binding of PI to DNA, and counting 10,000 cells per sample. Data was analysed using FlowJo v10.

2.9.2 Annexin V staining

Seeded and floating cells were briefly trypsinised and pelleted by centrifugation (1,500 rpm, 5 min). Pelleted cells were washed once in PBS and once in 1x binding buffer (see Table 2.3). After pelleting of cells and aspiration of buffer, cells were resuspended in 200 µl of 1 x binding buffer containing 0.25 µl (1:800) Annexin-FITC conjugate and 2 µl DAPI (final concentration 100 µg/ml). Cells were incubated for 10 min at RT in the dark. Annexin staining was analysed with an LSRII flow cytometer (BD Biosciences), using a 488 nm excitation laser line and a 670 nm long pass emission filter to measure binding of PI to DNA, and counting 10,000 cells per sample. Data was analysed using FlowJo v10.

2.10 Radioactivity based assays

2.10.1 Tritiated thymidine Incorporation assay

Seeded cells were incubated at 37°C, 5% (v/v) CO₂ for 24h, then treated with fresh medium containing the appropriate drug concentrations. Cells were incubated at 37°C, 5% (v/v) CO₂ for a further 24 hours, with the addition of 5 µM thymidine containing 0.5 µCi [³H-methyl]thymidine for the final 6 hours. Medium was aspirated and cells fixed in 5% trichloroacetic acid (TCA) at 4°C overnight. Fixed cells were then washed in H₂O, DNA solubilised with 0.1 M NaOH, and solutions transferred to scintillation vials containing 4 ml scintillation fluid (0.4% TCA), prior to scintillation counting on a Packard Tricarb 4000 series counter.

2.10.2 Radioactive pulse-chase assay

Cells were plated in 10 cm dishes to reach ~75% confluence the following day. Media was aspirated and cells washed three times with prewarmed PBS. PBS was thoroughly aspirated and 1 ml methionine/cysteine-free DMEM, supplemented with 10% dialyzed foetal calf serum, 2mM glutamine and 1 mM sodium pyruvate was added. Cells were incubated at 37°C for 1 h, with occasional shaking. Subsequently, 125 µCi [³⁵S]-L-methionine/[³⁵S]-L-cysteine mixture (EasyTag express protein labelling mix, PerkinElmer) was added to each plate and cells incubated for 40 minutes at 37°C, with occasional shaking, to radioactively label newly synthesised protein. Radioactive media was removed, and for time 0 plates, cells washed once with prewarmed PBS, and lysed in TG lysis buffer. For all other timepoints, cells were washed with prewarmed PBS, and 2.5 ml prewarmed DMEM, supplemented with 10% normal foetal calf serum, 2 mM L-methionine (Sigma-Aldrich) and 2 mM L-cysteine (Sigma-Aldrich) added. At subsequent timepoints, cells were washed with PBS and lysed. NEMO

immunoprecipitation was performed as described in section 2.8. PVDF membrane containing radioactively labelled protein was dried and exposed to a BAS-IP storage phosphor screen (GE LifeSciences) for 72 h. The screen was imaged using a phosphor imager (Typhoon FLA 7000 IP).

2.10.3 *In vitro* 20S proteasomal degradation assay

In vitro transcription and translation was performed in the presence of [³⁵S]-methionine using the TnT Quick Coupled Transcription/Translation System (Promega), according to manufacturer's instructions. Plasmids employed were pCDNA3.1-NFLAG_NEMO, pcDNA3.1-NFLAG_IKK α , pcDNA3.1-CFLAG_IKK β . Purified 20S proteasomes were generated based on a method described in Beyette, Hubbell, & Monaco, 2001. [³⁵S]-methionine-labelled proteins translated *in vitro* were incubated with 0.35 or 1 μ g of purified 20S proteasomes in 150 mM NaCl, 50 mM Tris HCl pH 7.5 and 1 mM DTT at 37°C for a defined time period. Reactions were then resolved by SDS-PAGE and visualized by autoradiography. Experiments kindly performed by Nadav Myers, The Weizmann Institute, Israel.

2.11 Quantitative Reverse-transcription PCR

cDNA was prepared as described in section 2.4.5. Relative mRNA levels within samples were determined by real-time PCR using SYBR green master mix (InVitrogen) and a CFX96 real-time PCR detection system (BioRad), according to manufacturer's instructions. The primer sequences used are detailed in Table 2.11. For each new pair of primers PCR efficiency was calculated from the slope of a calibration curve generated using a dilution series of a pool of all relevant sample cDNAs:

$$E_{amp} = 10^{\frac{1}{[-1/slope]}}$$

Relative quantitation of mRNA levels was performed using the Pfaffl method with normalisation of target-gene expression to two non-regulated reference genes: *UBC* (Ubiquitin C) and *YWHAZ* (Tyrosine 3-Monooxygenase/Tryptophan 5-Monooxygenase Activation Protein Zeta):

$$ratio = \frac{(E_{target})^{\Delta Ct\ target\ (control-treated)}}{(E_{reference})^{\Delta Ct\ reference\ (control-treated)}}$$

Statistical analysis was performed within the REST 2009 software package using an applied two-sided pair-wise fixed reallocation randomization test.

2.12 Cellular imaging

2.12.1 Light microscopy

Light microscopy images of cellular morphology were captured using an Olympus BX41 light microscope.

2.12.2 Immunocytochemistry

Cells were seeded in 6-well plates containing sterilised glass coverslips and treated as indicated in the Figure legends. Media was aspirated and cells fixed with either 4% v/v paraformaldehyde/PBS for 15 minutes at RT or -20°C 100% methanol for 5 minutes on ice, depending on the antigen. Following three washes in PBS, cells were permeabilised with 0.1% v/v Triton X-100/ PBS for 10 minutes. Cells were washed once in PBS and blocked for one hour in blocking buffer (see Table 2.5) at RT. Cells were incubated with primary antibody diluted (as indicated in Table 2.8) in antibody dilution buffer at 4°C overnight. Cells were washed three times in PBS and then incubated with secondary antibody (Table 2.9) diluted in blocking solution for 1 hour at room temperature in the dark. Cells were washed three times in PBS, before being mounted onto microscope slides with VectaShield antifade mounting medium (Vectorlabs) and sealed with nail varnish. Slides were left to dry for 1 hour at room temperature in the dark and imaged using a Nikon A1R confocal microscope. Image analysis was performed using the Fiji X Image J distribution.

2.12.3 High-content confocal image acquisition and analysis

Cells were seeded in triplicate in CellCarrier 96 well plates (PerkinElmer) for 48 h prior to fixation and immunostaining as described in section 2.11.2. High-content image acquisition was performed using an In Cell Analyzer 6000 (GE Healthcare). Confocal images were analysed using the CellProfiler software package.

2.13 CRISPR-Cas9 gene knock-out

2.13.1 guide RNA design and selection

Five different target guide RNA (gRNA) sequences (Table 2.16.) targeted to each of either the *CHUK* or *IKBKB* genes were designed using the GUIDEbook™ software (Desktop Genetics). The exons targeted by each gRNA are highlighted in Figure 2.1. Each gRNA sequence was cloned into a pD1301-AD mammalian Cas9 (double stranded nuclease *Streptococcus pyogenes* Cas9) genome editing vector (see Figure 2.2) by DNA 2.0 (now ATUM). gRNA-directed target cutting efficiency was assessed using the Surveyor Mutation detection assay (Transgenomic) according to manufacturer's instructions. On the basis of these results (data not shown), guide RNAs g24 g25 and g27, and g76, g82 g87 were selected to target IKK α and IKK β , respectively.

Target	gRNA identifier	gRNA sequence	Position in genomic sequence targeted	Exon targeted
IKK α	g24	5' - AGCCGCTCCCGCATCTCCCCA - 3'	121 - 140	1
	g25	5 ' –ACAGACGTTCCCGAAGCCGC - 3'	149 - 168	1
	g26	5' – TGTACCAGCATGGGTGAGG - 3'	170 - 189	1
	g27	5' – TCTTCATAATCTGGATTCA - 3'	3668 - 3687	2
	g28	5' - AGGCCTTACAACATTGGC - 3'	6639 - 6659	3
IKK β	g76	5' – AGCCGCTCCCGCATCTCCCCA - 3'	5873-5892	1
	g79	5' - ACAGACGTTCCCGAAGCCGC - 3'	5904-5923	1
	g82	5' – TGTACCAGCATGGGTGAGG - 3'	23847 – 23866	3
	g85	5' – TCTTCATAATCTGGATTCA - 3'	23876 – 23895	3
	g87	5' – AGGCCTTACAACATTGGC - 3'	23931 - 23950	3

Table 2.16. gRNA sequences designed to target IKK α and IKK β .

2.13.2 CRISPR-Cas9 plasmid transfection

Two pools of 2.5×10^6 early passage (p7), healthy HCT116 cells were each electroporated with 3.75 µg of either the IKK α -targeted Cas9 plasmid DNA, the IKK β -targeted Cas9 plasmid DNA or empty-vector GFP Cas9 plasmid DNA before being combined and incubated at 37°C, 5% (v/v) CO₂ for 48 h. For the double knockout of IKK α and IKK β , 1.875 µg of each plasmid was transfected. Electroporation was performed with Nucleofector™ Kit V (Lonza) using program D-032 on a Nucleofector™ device (Lonza).

2.13.3 FACS sorting

48 h after transfection, cells were harvested by trypsinisation, spun down and resuspended in an appropriate volume of 2% (v/v) FBS in PBS. The cell suspension was subsequently filtered through a 40 µm cell strainer (CellTrics). GFP-positive cells were single-cell sorted into 96-well plates containing 100 µl complete growth media (containing 25% conditioned media) using a FACS Aria III cell sorter (BD) configured with an 85 µm nozzle.

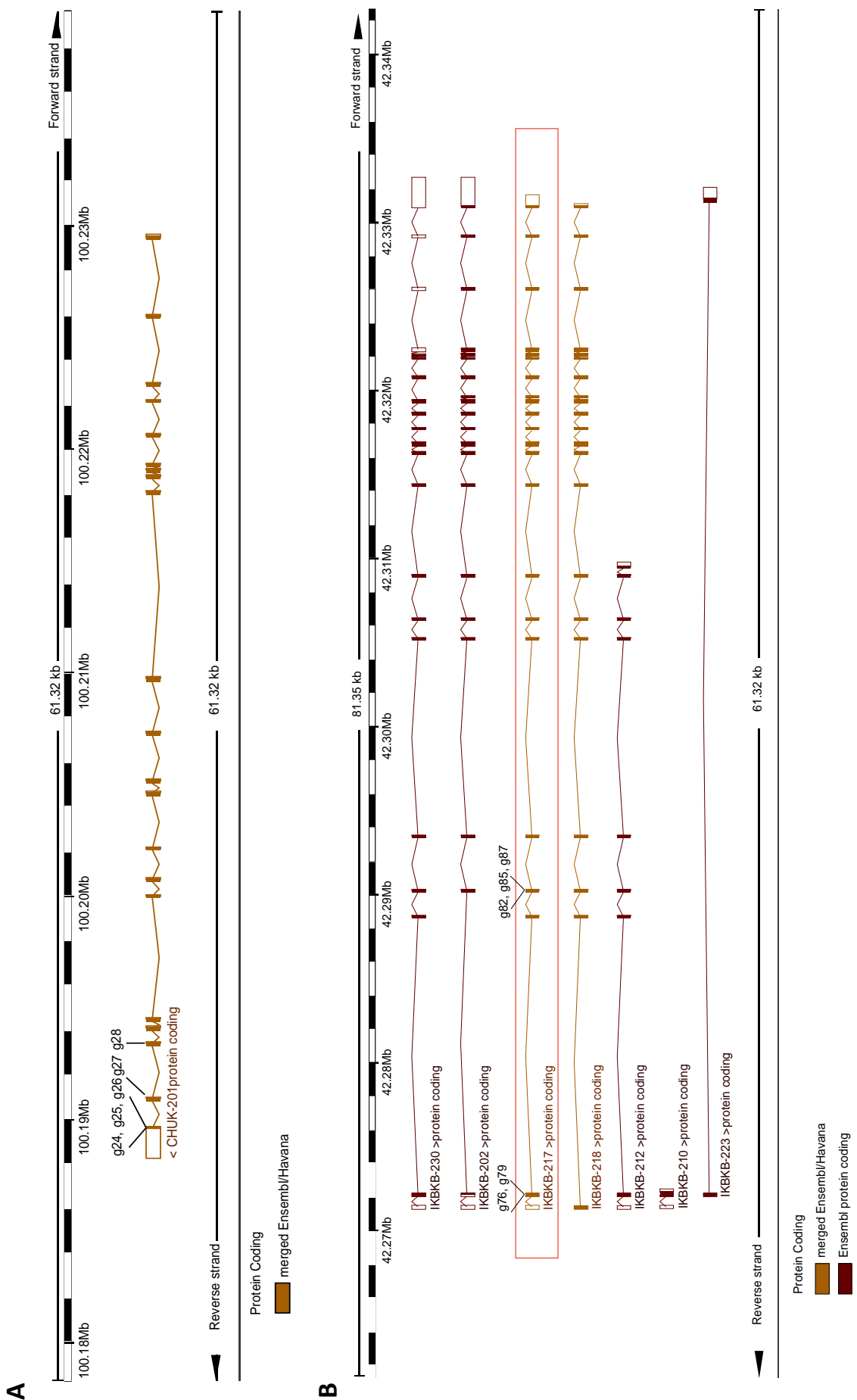


Figure 2.1. GENCODE protein-coding transcript annotations for human *CHUK* and *IKBKB* genes highlighting the exons targeted by the CRISPR gRNA sequences. (A) *CHUK* protein coding transcripts. (B) *IKBKB* protein coding transcripts. Red box highlights the accepted ‘canonical’ transcript that is predominantly expressed.

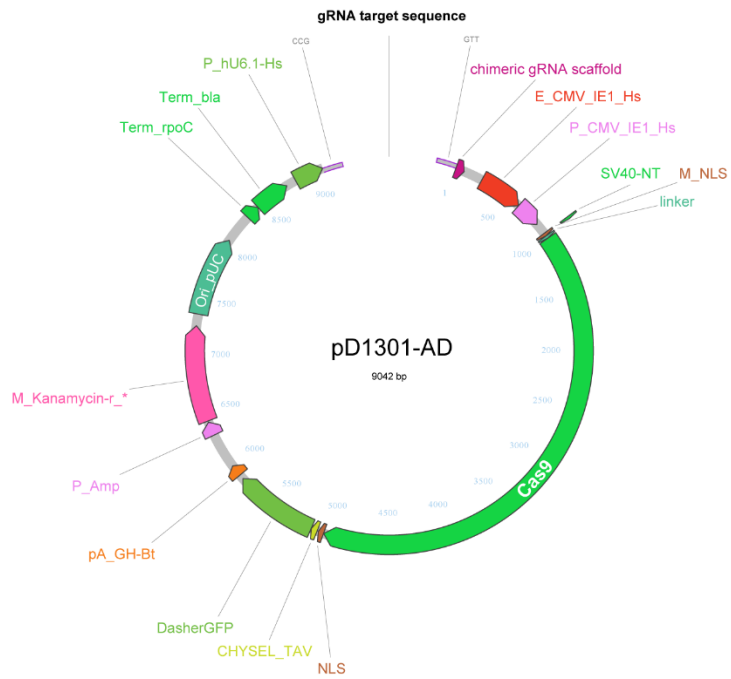


Figure 2.2. Vector map for mammalian pD1301-AD CRISPR-Cas9 expression plasmid. Cas9, *S. pyogenes* Cas9 nuclease gene. NLS, nuclear localisation sequence. CHYSEL_TAV, sequence enabling cleavage of downstream GFP. DasherGFP, IP-Free© green fluorescent reporter protein that is used as a selectable marker for expression monitoring of Cas9 protein. pA_GH-Bt, bovine growth hormone polyadenylation (bgh-PolyA) signal is a specialized termination sequence for protein expression in eukaryotic cells. P_hU6.1-Hs, a type 3 core promoter for RNA expression. Chimeric gRNA scaffold, consists of a ~20-nt target specific complementary region (specific to gene of interest), a 42-nt Cas9-binding RNA structure and a 40-nt transcription terminator derived from *S. pyogenes* that directs Cas9 nuclease to the target site for genome modification. E_CMV_1E1_Hs, strong CMV enhancer. P_CMV_1E1_Hs, strong constitutive mammalian promoter. Ori_pUC, *E.coli*-derived origin of replication.

2.13.4 Mutant clone screening

Single-cell derived colonies were allowed to grow over a 10-14 day period, with fresh media added every 4 days. Upon reaching confluence, cells were split into two 96-well plates: one for clone genotyping and the other for clonal expansion. Genomic DNA for genotyping was extracted as described in section 2.4.3. A PCR-based screening strategy was employed to identify candidate clones with mutated gRNA target sequences (Figure 2.3). Candidate clones were expanded and knockout verified via Western blotting.

2.13.5 Sequencing gRNA binding site of candidate KO clones

The final clones selected for study were sequenced across the guide RNA target sequence to confirm the presence of biallelic Cas9-cleavage-induced indel mutations. In short, genomic DNA was extracted as described in section 2.4.3 and used as a template to PCR amplify an approximately 1 kb region spanning the guide RNA target sequence. Phusion High-Fidelity DNA polymerase (Invitrogen) was used to reduce PCR error. Purified PCR product containing 3' adenose overhangs was cloned into a pCR 2.1 TOPO vector and plasmid DNA transformed into XL1 blue competent cells (Agilent). Multiple individual bacterial colonies were picked, and plasmid insert DNA sent for Sanger sequencing (Beckman-Coulter genomics).

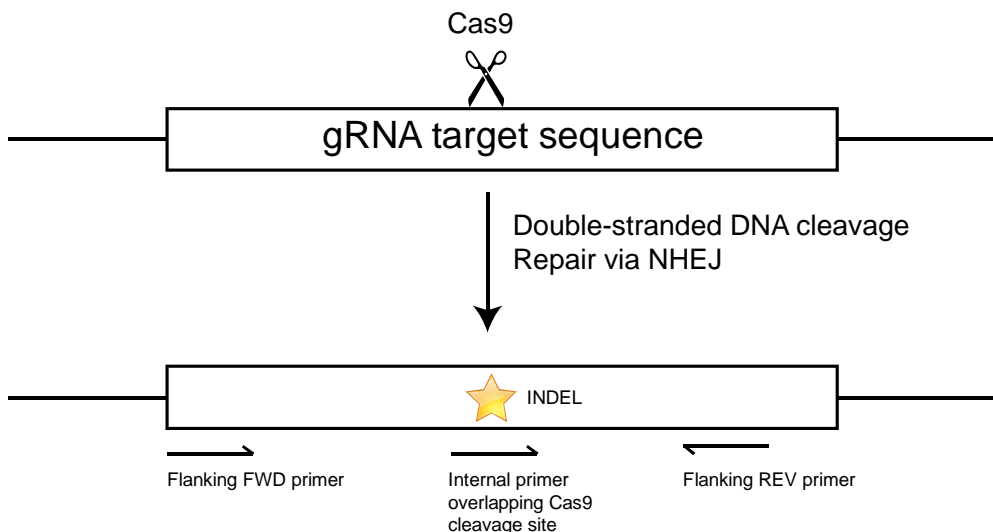


Figure 2.3. PCR screening strategy for identifying single cell clones containing indel mutations in gRNA target site. Involved design of external primers well outside the mutated region and an internal primer whose 3' end spanned the Cas9 cleavage site within the gRNA target sequence.

2.14 RNA Sequencing

2.14.1 RNA isolation and quality control

Total genomic RNA was isolated from each sample on the same day in one batch, as described in section 2.4.4. The quality of each RNA prep was confirmed by measuring A260/A280 and A260/A230 ratios on a Nanodrop spectrophotometer and by measuring RNA integrity number (RIN) using a Bioanalyzer 2100 (Agilent). Each sample sent for sequencing had A260/A280 and A260/A230 ratios above 2 and RIN values >9.5

2.14.2 3' mRNA library preparation and sequencing

RNA library preparation was performed by Cambridge Genomic Services (CGS). A QuantSeq 3' mRNA-Seq Library Prep Kit FWD (Lexogen) was used to generate Illumina compatible, indexed, strand-specific libraries of sequences close to the 3' end of polyadenylated RNA. Libraries were quantified and assessed using an RNA ScreenTape assay (4200 TapeStation, Agilent). Indexed libraries were sequenced with a 75bp single-end protocol on one lane, by the NextSeq 500 system (Illumina).

2.14.3 Bioinformatic analysis

Quality control of reads was done using FastQC v0.11.4. Reads were trimmed using TrimGalore v0.4.1. Reads were mapped using STAR v2.5.2a. Ensembl Homo_sapiens. GRCH38.dna.primary_assembly.fa (release 90) reference genome file was used to do the mapping of reads, using the annotated transcripts from the ensemble Homo_sapiens.GRCH38.90.gtf. The number of reads that mapped to protein-coding genomic features was calculated using HTSeq v0.6.0. Reads with a mapping quality less than 10, that map to multiple loci or to overlapping gene regions were discarded to avoid ambiguity and false positives. Differential gene expression analysis was performed using the counted reads and the R package edgeR v3.16.5 (R version 3.3.3). Genes not

having more than 10 counts per million (cpm) in at least 1 sample were filtered from analysis. Gene ontology analysis was performed using Panther v12.0.

2.15 Luciferase-reporter assay

Cells were seeded in antibiotic-free media in 96 well plate format. The following day cells were transiently transfected with 0.1 µg/well pGL4.32[luc2P/NF-κB-RE luciferase experimental-reporter plasmid DNA and 0.01 µg/well constitutively-expressed pCMV renilla plasmid DNA (used to normalise for inter-well differences in transfection efficiency or cell viability). The following day, the relevant treatments were performed. Luciferase activity was measured using the Dual-Luciferase Reporter Assay System (Promega), and on a MicroLumatPlus LB96V reader, according to manufacturer's instructions.

2.16 Cyquant proliferation assay

Cells in phenol red-free DMEM were seeded in quadruplicate into eight 96 well plates at a density of 2.5×10^3 /ml. Half the culture media was replenished with fresh media every other day during the 8 day incubation. At each 24 h interval following seeding, a 96 well plate was frozen at -80°C. At the end of the 8 days, plates were thawed to RT and 200 µl cell-lysis buffer (containing CyQUANT GR dye at a 2 x final concentration) was added to each well. After a 5 minute incubation in the dark, the sample fluorescence was measured using a 480 nm/520 nm excitation/emission filter set on a PHERAstar plate reader (BMG Labtech).

2.17 Bioinformatic analysis

2.17.1 Disorder prediction tools

2.17.1.1 D²P² database consensus tools

D²P² database contains disorder prediction annotations of all protein sequences from 1765 complete proteomes. Consensus predictions were derived using the following predictors: PONDR VL-XT, PONDR VSL2b, PV2, Espritz (all variants) and IUPred (all variants). PONDR VL-XT integrates three trained neural network predictors of disordered regions on the basis of various sequence factors, including hydropathy, coordination number, flexibility and local amino acid composition (Li *et al.*, 1999c; Romero *et al.*, 2001). PONDR VSL2 is a combination of trained neural network predictors for short and long disordered regions that applies a sequence profile and the weighted result of secondary structure prediction from PHD and PSIPRED, and sequence alignments from PSI-BLAST (Peng *et al.*, 2006). PV2 is a meta-predictor composed of five prediction methodologies: a neural network, a support vector machine, logistic regression, a conditional random field, and the VSL2b predictor (Ghalwash *et al.*, 2012). Espritz uses three variant bidirectional recursive neural networks trained on different datasets: PDB crystallography data of short disorder (Espritz-X), NMR mobility (Espritz-N) and long disorder data from DisProt (Espritz-D) (Walsh *et al.*, 2012). Different probability cut-offs are used for each variant to yield 5% false positive rate. IUPRED variants -S (short) and -L (long) uses amino acid pair-wise interaction energy estimates to predict those stretches of amino acids not significantly contributing to stable, globular structure, and thus likely to be disordered (Dosztányi *et al.*, 2005).

2.17.1.2 DisEMBL

DisEMBL uses two different neural networks trained on different data sets: one enriched in sequences containing coils/loops as defined on DSSP secondary structure assignments, and one enriched in sequences containing missing X-ray coordinates (REMARK 465) (Linding et al., 2003). Probability cut-offs are used for each variant to yield 5% false positive rate.

2.17.1.3 PrDOS

PrDOS makes uses a combination of the results of two predictors (Ishida et al., 2007). The first is a support vector machine with a position-specific profile of local amino acid sequence. The second predictor uses PSI-BLAST and assumes conservation of intrinsic disorder in homologous protein domain families.

2.17.1.4 DISOPRED3

DISOPRED3 uses two independent predictors – a neural network and a nearest neighbour classifier, both trained on evolutionarily conserved sequence features of disordered regions from missing residues in X-ray crystal structures to identify long intrinsically disordered regions. The results are integrated by an addition neural network (Jones et al., 2015).

2.17.1.5 MFDp2

MFDp2 combines residue-level and sequence-level disorder prediction with post-processing filters and sequence alignment via PSI-BLAST (Mizianty et al., 2013).

2.17.2 PEST motif finder

Epestfind uses an algorithm that scans for hydrophilic stretches of at least 12 amino acids, with a high local concentration of proline, glutamate, serine and threonine and an absence of positively charged motifs (arginine, lysine and histidine) (Rogers et al., 1986). Epest find also stringently defines PEST motifs as those flanked by positively charged amino acids. The quality of such identified sequences is refined by means of a scoring parameter based on the local enrichment of critical amino acids, as well as the motifs overall hydrophobicity. PEST scores above the threshold score of + 5.0 are considered biologically significant.

2.17.3 mORF prediction tools

2.17.3.1 DISOPRED3

DISOPRED3 predicts protein-binding sites using a support vector machine (SVM) learning algorithm with classifiers based on sequence profile features that was trained on a positive set of 840 peptides, the structures of which have been solved in complex with globular protein domains and a negative set of unbound protein linker regions in known protein structures (Jones et al., 2015).

2.17.3.2 ANCHOR

ANCHOR predicts mORFs by identifying sequential residues within disordered regions that are unlikely to form enough favourable intrachain interactions with local neighbours to fold on their own. It also tests the feasibility that a given residue can form enough favourable, stabilizing interactions with folded proteins upon binding. The

approach relies on pairwise amino acid interaction energy estimations (Mészáros *et al.*, 2009; Dosztányi *et al.*, 2009).

2.17.3.3 mORFpred

MoRFpred converts an input sequence into a sliding-window feature vector, representing relevant sequence characteristics, such as amino acid indices, predicted disorder (IUPred), solvent accessibility and B-factor flexibility, which is inputted into a linear SVM algorithm trained on a large data set of protein complexes. Propensities are then merged with alignment results of the input protein against the MoRF-annotated proteins in the training dataset (Disfani *et al.*, 2012).

2.17.3.4 MoRFCHIBI SYSTEM

MoRFCHIBI SYSTEM performs a Bayes integration of two SVM algorithms input with local sequence physicochemical properties and sequence similarity, a protein disorder (Espritz/DisProt) prediction score and a range of PSI-BLAST derived conservation scores (Malhis *et al.*, 2016).

2.17.3.5 DisoRDPbind

DisoRDPbind utilizes three logistic regression models inputted with features generated from information from the physiochemical properties of amino acids, putative secondary structure and disorder, sequence complexity and sequence alignment to generate propensity scores for each residue. PSI-BLAST annotations are then merged with these scores (Peng *et al.*, 2015).

2.17.4 ChemMapper

ChemMapper is an online drug-interaction prediction platform that assembles a large repertoire of bioactive chemical database annotated with pharmacological target information (Gong *et al.*, 2013). The chemical structures of AZD2230 and BMS-345541 (in canonical SMILES format) were used as query for a 3D similarity search using the SHAFTS algorithm, which calculates similarity based on molecular shape and chemotype features (Liu *et al.*, 2011). A list of potential protein targets is returned that are ranked based on the number and overall degree of 3D similarity of hits that have annotated binding activity against the target.

Chapter 3

Generation, validation and characterisation of CRISPR-Cas9 IKK knockout cell lines

3 Generation, validation and characterisation of CRISPR-Cas9 IKK α , IKK β and IKK α / β knockout HCT116 cell lines

3.1 Introduction

Early genetic studies identified distinct and non-redundant biological functions for the IKK kinases, IKK α and IKK β , within the context of NF- κ B activation. *IKKb*^{-/-} mice die during embryonic development at approximately day E13, largely as a result of catastrophic liver damage (Li *et al.*, 1999a; Li *et al.*, 1999d). This is highly similar to the phenotype of *rela*^{-/-} (Beg *et al.*, 1995) and *nemo*^{-/-} mice (Rudolph *et al.*, 2000). Crossing *IKKb*^{-/-} mice with *tnfr*^{-/-} mice rescued this lethality until after birth, suggesting the lethal hepatocyte apoptosis is due to TNF signalling during embryogenesis (Li *et al.*, 1999d). IKK α appeared to have insufficient functional redundancy within the canonical NF- κ B pathway to prevent this lethality. This finding was reflected by work with *IKKb*^{-/-} mouse embryonic fibroblasts (MEFs) (Li *et al.*, 2002). These cells are highly defective in the phosphorylation and degradation of I κ B α , NF- κ B DNA binding activity and NF- κ B-dependent transcription following treatment with TNF α or IL-1 (Sizemore *et al.*, 2002). Conditional knockouts have also shown that IKK β protects against apoptosis triggered by TLR signals in macrophages (Park *et al.*, 2005), gut epithelium (Chen *et al.*, 2003) and osteoclasts (Ruocco *et al.*, 2005), while conditional deletion of *IKKb* in gastric epithelial cells accelerates Helicobacter-dependent gastric apoptosis and carcinogenesis (Shibata *et al.*, 2010).

In contrast, the phenotype of *IKK α -/-* mice is less severe; they survive until a month post-birth, but develop distinct morphological defects affecting epidermal and skeletal development (Hu *et al.*, 1999; Li *et al.*, 1999b; Takeda *et al.*, 1999). However, using a catalytically inactive IKK α mouse model these defects were shown to be independent of both IKK α kinase activity and NF- κ B activity (Cao *et al.*, 2001). A similar, yet more severe phenotype was later observed in patients with autosomal recessive loss-of-function mutations in *Chuk* (encoding IKK α) (Lahtela *et al.*, 2010). The essential role of IKK α in non-canonical NF- κ B activation for the development of lymphoid organs and B cell maturation was subsequently demonstrated using the catalytically inactive IKK α mouse model, *IKK α -/-* chimeras and *IKK α -/-* MEFs (Senftleben *et al.*, 2001; Kaisho *et al.*, 2001; Dejardin *et al.*, 2002; Bonizzi *et al.*, 2004).

Whilst *IKK α -/-* MEFs did show defective NF- κ B transcriptional activity and p65 phosphorylation in response to TNF α and IL-1, IKK β homodimers were still capable of phosphorylating I κ B α and inducing NF- κ B nuclear translocation and DNA binding, leading to the conclusion that IKK β is sufficient for canonical NF- κ B pathway activation (Li *et al.*, 1999b; Li *et al.*, 1999d; Hu *et al.*, 2001). Furthermore, the interaction between IKK α and NEMO was shown to be weaker than with IKK β (May *et al.*, 2000; Miller & Zandi., 2001), while IKK β was shown to be a more effective kinase *in vitro* in the phosphorylation of I κ B α (Huynh *et al.*, 2000).

From such studies, a consensus emerged that IKK β is the predominant kinase activating the canonical NF- κ B pathway in a NEMO-dependent manner, while the primary function of IKK α is to act as the regulator of the noncanonical NF- κ B pathway, in a NEMO-independent manner. As such, the primary focus of drug design for targeting the canonical NF- κ B pathway in human disease has been IKK β (Gilmore *et al.*, 2006). No selective IKK α inhibitors are currently commercially available, although this also appears to reflect a greater difficulty in designing potent inhibitors of the IKK α catalytic site (Gamble *et al.*, 2012).

However, a range of evidence suggests that IKK α may play a more significant role in canonical NF- κ B pathway activation than initially appreciated. Although exhibiting defective I κ B α degradation and NF- κ B DNA binding, an appreciable level of NF- κ B dependent gene expression in response to TNF α and IL-1 is still observed in *IKKb* $^{-/-}$ MEFs (Li *et al.*, 1999a; Li *et al.*, 2002). Furthermore, in contrast to the developing liver in *IKKb* $^{-/-}$ mice, mature hepatocytes are not sensitized to TNF α -induced apoptosis following deletion of IKK β , suggesting that IKK α is able to compensate within the canonical NF- κ B pathway of adult mice (Luedde *et al.* 2005). IKK α has also been reported to be obligatory for receptor activation of NF- κ B (RANK)-induced canonical NF- κ B activation in mammary epithelial cells, where it promotes cyclin D1 expression (Cao *et al.*, 2001).

In contrast to earlier studies, IL-1 but not TNF α was later shown to be able to promote I κ B α degradation and NF- κ B nuclear translocation in *IKKb* $^{-/-}$ MEFs in a NEMO-dependent manner (Solt *et al.*, 2007). Catalytically inactive IKK β blocked TNF α but not IL-1-induced I κ B degradation, suggesting that the nature of the stimulus may determine the absolute requirement of IKK β for canonical NF- κ B activation. Subsequent work by the same lab demonstrated that TNF- α and IL-1 induced NF- κ B transcriptional activity was completely defective in *IKK α* $^{-/-}$ MEFs, and that this could be rescued by an IKK α mutant defective for NEMO binding, suggesting that IKK α activates canonical NF- κ B independently of NEMO (Solt *et al.*, 2009), possibly through direct phosphorylation of p65.

IKK α was shown to be able to mediate a compensatory activation of the canonical NF- κ B pathway in response to CARD11 and TNF α signalling to overcome inhibition of IKK β in some, but not all, activated B-cell-like (ABC) diffuse large B-cell lymphoma (DLBCL) cells (Lam *et al.*, 2008b). Furthermore, Adli *et al.*, showed that in contrast to MEFs, both IKK α and IKK β contribute to TNF α -induced I κ B α phosphorylation and NF- κ B activation in HeLa cells, raising the possibility that IKK α may play a more important role in canonical NF- κ B signalling in humans than it does in mice (Adli *et al.*, 2010).

In support of this, patients with homozygous null mutations of *IKBKB* exhibit significantly less severe phenotypes than *IKKb* $^{-/-}$ mice (Pannicke *et al.*, 2013; Mousallem *et al.*, 2014). Such patients are normal at birth and exhibit none of the liver damage or developmental defects of *IKKb* $^{-/-}$ mice, suggesting perhaps that IKK α is better able to compensate within the canonical NF- κ B pathway of human cells. They do, however, develop severe combined immunodeficiency (SCID) due to a lack of T- and B-cell activation (naïve phenotype) and low T-cell and NK-cell numbers. B cells from these patients exhibited defective phosphorylation and degradation of I κ B and defective nuclear p65 translocation in response to PMA (Mousallem *et al.*, 2014). Primary skin fibroblasts from these patients exhibited stimulus-dependent differences in I κ B phosphorylation and NF- κ B DNA binding; responses were drastically reduced in response to TNF α , and only marginally affected in response to IL-1 β (Pannicke *et al.*, 2013). Wild-type response to TNF α was reconstituted by restoring IKK β expression in patient cells.

Overall, these contradictory studies indicate that the IKK subunits might have species-/cell-type-/developmental stage- and stimulus-specific roles in activating the canonical NF- κ B pathway.

Aberrant activation of the canonical NF- κ B pathway contributes to each of the hallmarks of cancer to promote the initiation and progression of various types of cancer (Chapter 1, Section 1.4.3). For instance, there is growing evidence for a connection between chronic inflammatory conditions within the tumour microenvironment and

tumour development, with the NF- κ B pathway potentially acting as a key mechanistic link between the two. This link is well demonstrated in cancers of the gastrointestinal tract, including esophageal, gastric and colorectal. Colorectal cancer (CRC) can be divided into hereditary, sporadic and colitis-associated carcinoma (CAC) forms. The role of NF- κ B as a mechanistic link between chronic inflammation and cancer is most apparent in the progression of two forms of inflammatory bowel disease (IBD), ulcerative colitis and Crohn disease, to CAC (Rubin *et al.*, 2012). For example, intestinal epithelial cell-specific deletion of IKK β decreased tumour incidence, in the case of enterocytes, and tumour size in the case of myeloid cells in a mouse model of CAC (Greten *et al.*, 2004). Furthermore, NF- κ B has been shown to be constitutively active in human tumour samples, representative of both CAC and sporadic CRC (Lind *et al.*, 2001; Kojima *et al.*, 2004). Higher nuclear expression of p65 and p50 has been observed in primary CRC tumour and liver metastases than normal mucosa and is prognostic of worse outcome (Puvvada *et al.*, 2010). Constitutive NF- κ B pathway activation has also been observed in various CRC cell lines, suggesting that cell autonomous mechanisms may lead to aberrant pathway activation, in addition to chronic inflammatory conditions within the tumour microenvironment (Dejardin *et al.*, 1999; Sakamoto *et al.*, 2009).

Interest in IKK and NF- κ B function in colorectal cancer was recently enhanced by a series of studies by the Espinosa/Bigas labs. They initially identified a novel NF- κ B-independent role for constitutively active, nuclear IKK α in colorectal cancer cells (Fernandez-Majada *et al.*, 2007). Nuclear IKK α associates with the chromatin of specific Notch target genes leading to the phosphorylation and release of the nuclear corepressor, SMRT, and the transcriptional activation of these genes. Subsequently, the predominant form of active, nuclear IKK α was demonstrated to be a truncated 45 kDa form of IKK α , which retains the kinase domain but lacks C-terminal regulatory domains (Margalef *et al.*, 2012). p45-IKK α is thought to be phosphorylated downstream of mutant BRAF in CRC cells through an ill-defined mechanism involving endosomal compartment-associated TAK1 (Margalef *et al.*, 2015).

Given the lack of clarity regarding the relative importance of IKK α and IKK β in human canonical NF- κ B signalling, the known importance of inflammatory signalling in driving colorectal tumorigenesis, and the apparent NF- κ B-independent functions of IKK α in colorectal cancer cell lines, we were motivated to generate IKK α , IKK β and IKK α / β double CRISPR-Cas9 knockouts in a HCT116 colorectal cancer cell line background.

3.2 Results

3.2.1 Generation and characterisation of *CHUK* (IKK α) and *IKBKB* (IKK β) knockout and IKK α / β double knockout HCT116 CRISPR-Cas9 cell lines

IKK α and *IKK β* knockout (KO) and *IKK α* / β double knockout (DKO) CRISPR-Cas9 HCT116 cell lines were generated as described in detail in Chapter 2. The rationale for choosing HCT116 cells as the parental cell line was both technical and biological in nature. HCT116 cells are well-characterised, relatively easy to transfect and readily grow out from single cell clones. Furthermore, this cell line was chosen as it has a KRAS^{G13D} mutation and is dependent on this mutation for its malignant properties. It was therefore hoped that this might provide insight into the reported requirement for NF- κ B signalling in KRAS transformation. However, it should be noted that in our hands the NF- κ B pathway was minimally active in HCT116 cells, both at the level of IKK phosphorylation, I κ B

phosphorylation, p65 nuclear localisation and NF- κ B transcriptional activity (Figure 3.12 and Figure 3.6, respectively). The question of whether HCT116 cells are in any way reliant on NF- κ B signalling for cell growth or survival, as is the case for various other cancer cell types (Bhat-Nakshatri *et al.*, 2002; Garner *et al.*, 2013; Abdel-Latif *et al.*, 2015), was, therefore, an interesting one.

In brief, five guide RNAs (gRNAs) targeted to exons N-terminal to the kinase domain and common to all known transcripts of each of both the *CHUK* and *IKBKB* genes were designed using gUIDEbook™ software (Desktop Genetics) and cloned into a pD1301-AD-GFP Cas9 (double-stranded nuclease Cas9 from *Streptococcus pyogenes*) mammalian expression vector. Three guide RNAs specific to each gene were selected on the basis of highest cutting efficiency, as assessed by a preliminary Surveyor mutation detection assay, and transfected into early passage HCT116 colorectal cancer cells, alongside a control transfection with empty vector (EV) Cas9 DNA to generate matched EV clones. High Cas9 expressing cells were single cell cloned on the basis of GFP expression. Clones containing homozygous indel (insertion/deletion) mutations within the gRNA target sequence were identified via a PCR screen and expanded, prior to Western blotting to identify knockout clones. A number of wild type EV clones were also expanded (labelled subsequently as clones A3, A8, C4 and E10). Only two out of the three guide RNA sequences specific to IKK (g24 and g25) and two of the three specific to IKK (g76 and g87) gave rise to knockout clones. From these, three clones of each of IKK α KO, IKK β KO and IKK α / β DKO were selected for further validation and characterisation; IKK α KO clones, F6 (g25), C7 (g25) and A2 (g24); IKK β KO clones, G9 (g87), A7 (g87) and A4 (g76); and IKK α / β DKO clones, C8 (g87 + g25), G1 (g87 + g25) and E9 (g87 + g24). For each of these clones the region surrounding the gRNA target sequence was sequenced via Sanger sequencing and the presence of homozygous frameshift mutations confirmed, and likely premature stop codons identified (data not shown).

Each of the final KO clones selected for further analysis were null for full-length protein expressed from the IKK gene(s) targeted (Figure 3.1A). This was confirmed with two different antibodies against IKK α and IKK β , specific for an N-terminal and C-terminal epitope, respectively. No compensatory changes in the expression of the remaining IKK subunit were observed in any of the targeted clones. The knockouts were also validated at the mRNA level (Figure 3.1B and C). There was on average a greater than 2-fold reduction in IKK α mRNA in the IKK α KO clones and the DKO clones, and, similarly, a greater than 2-fold reduction in IKK β mRNA in the IKK β KO clones and the DKO clones. A statistically significant reduction in IKK β mRNA in the IKK α KO clones was also observed (Figure 3.1C). However, this evidently did not translate into a reduction in IKK β protein in the IKK α KO clones (Figure 3.1A). That a greater reduction in IKK mRNA was not observed was not of great concern; significant amounts of prematurely terminated mRNA can remain in the cell following CRISPR-Cas9 gene editing. The more important observation was the absence of IKK protein in these KO cells.

Colorectal cancer cell lines, including HCT116, have been reported to express a catalytically active, C-terminal proteolytically cleaved form of IKK α , p45-IKK α (Margalef *et al.* 2012). This truncated form lacks the C-terminal scaffold/dimerization regulatory domain (SDD) and the NEMO-binding domain (NBD) but retains the N-terminal kinase domain. p45 IKK α is reported to be constitutively phosphorylated at Serine 176/180 and hence constitutively active and localises almost exclusively to the nucleus. The cell lysis buffer used routinely in this work was a relatively gentle 1% (v/v) Triton X-100-based lysis buffer (TG lysis buffer, see Chapter 2 for

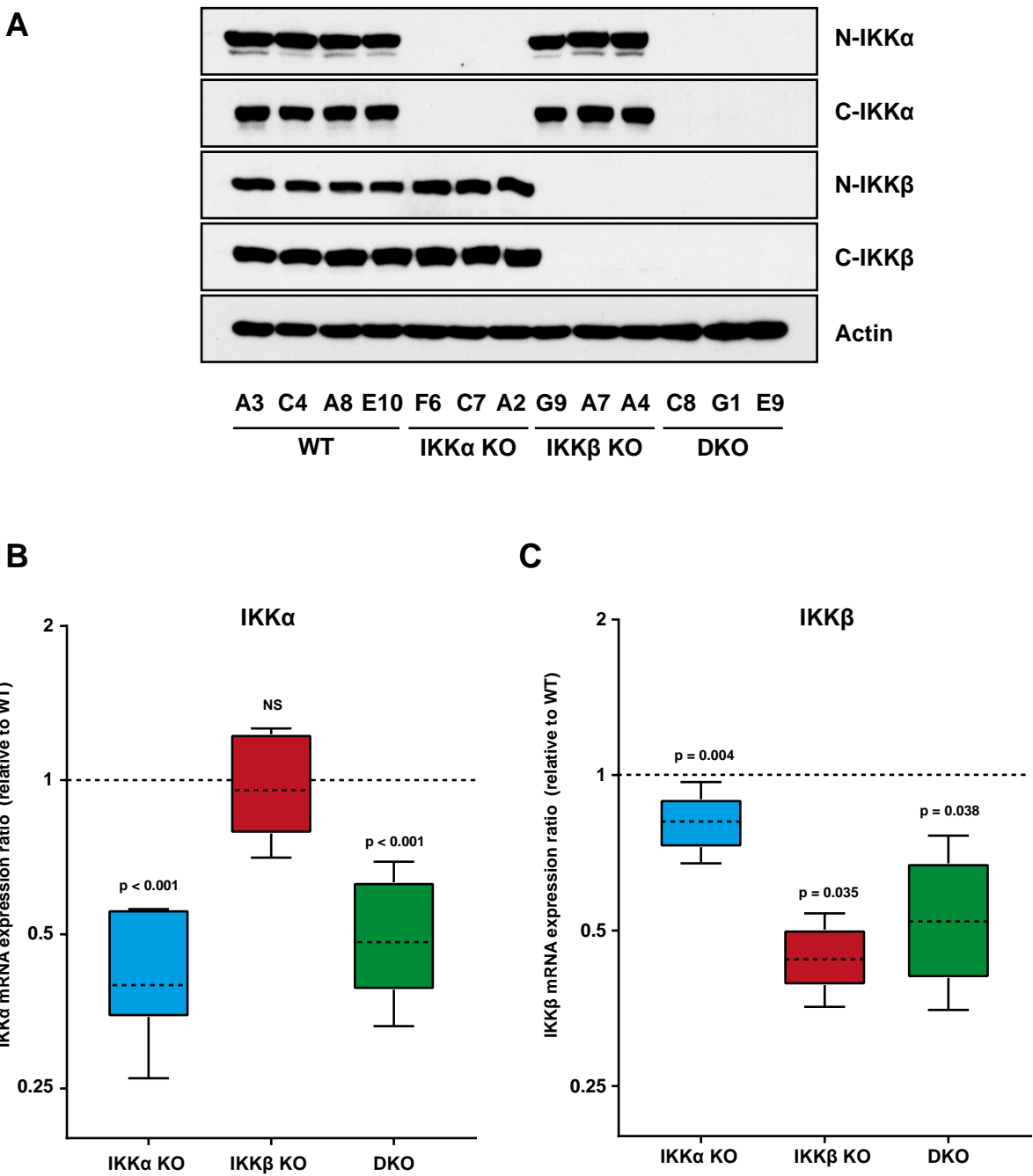


Figure 3.1. Generation of CRISPR-Cas9 IKK knockout HCT116 cells. (A) Best candidate clones were expanded and whole-cell lysates generated for independent, single-cell derived WT, IKK α KO, IKK β KO and IKK α / β DKO CRISPR clones. Lysates were fractioned by SDS-PAGE and Western blotted with the indicated antibodies to confirm absence of expressed protein corresponding to targeted gene. Clones A3, C4, A8 and E10 were confirmed as WT. Clones F6 and C7, derived from cells expressing gRNA 24 and clone A2, derived from cells expressing gRNA 25, were confirmed as IKK α KO. Clones G9 and A7, derived from cells expressing gRNA 87 and clone A4, derived from cells expressing gRNA 76, were confirmed as IKK β KO. Clones C8 and G1, derived from cells expressing both gRNA 25 and gRNA 87, and clone E9, derived from cells expressing both gRNA 24 and gRNA 87, were confirmed as IKK α / β DKO. Data are from a single experiment representative of three independent Western blots giving similar results. (B and C) Three independently derived WT clones and three clones each of IKK α single, IKK β single and IKK α / β double knockout were seeded in normal growth medium for 48 hours prior to RNA extraction. Relative IKK α (B) and IKK β (C) mRNA expression was determined by RT-qPCR, with normalisation to the geometric mean of the reference gene (YWHAZ and UBC) expression. Expression ratios are plotted on a logarithmic scale as median IKK expression ratios relative to the WT control samples. Boxes represent the interquartile range. Whiskers represent the minimum and maximum observations. N, N-terminal specific antibody. C, C-terminal specific antibody.

composition) that efficiently solubilises soluble nucleoplasmic proteins, but which is less stringent than other whole cell lysis buffers such as RIPA, and so is less effective at solubilising chromatin bound proteins. To confirm that the clones were completely absent of IKK protein, and to rule out any residual nuclear expression of p45 IKK α , the most commonly used clones in subsequent analysis were lysed in both TG lysis buffer and RIPA buffer (Figure 3.2). The resulting Western blots confirmed that the clones were entirely absent of full-length and intermediate forms of IKK α and IKK β protein. Efficient whole cell lysis by RIPA buffer was confirmed by the increased Histone H3 protein detected. In addition to an IKK α species of approximately 45 kDa, numerous other putative truncated IKK α species were detected by the N-terminal and C-terminal specific IKK α antibodies in WT and IKK KO cells, all of which were absent in IKK α KO and IKK α/β DKO cells. No other IKK α truncation forms besides p45-IKK α have been reported. At this stage it cannot be confirmed that these are functionally relevant forms of IKK α , and not, for example, degradation artefacts of the cell lysis.

Surprisingly, attempts to detect phosphorylated p45-IKK α in either HCT116 or HT-29 cells with the same antibody used by Margalef *et al* failed when either TG lysis buffer or RIPA buffer was used (Supplementary Figure S1A and B). Only the precise 0.5% (v/v) Triton-X-100-based lysis buffer recipe employed by Margalef *et al* was capable of resolving a band corresponding to 45 kDa. This buffer is highly similar to the TG lysis buffer used predominantly in this work, except for the use of a markedly higher concentration (100 mM vs 1 mM) of the general phosphotyrosyl phosphatase inhibitor, sodium orthovanadate, which is 100-1000 fold more concentrated than routinely used. Other papers published by the same lab confirmed that this high concentration was not wrongly reported. It is difficult to understand how a higher concentration of a phosphotyrosyl phosphatase inhibitor, such as sodium orthovanadate, might enhance the detection of a phosphoserine site on IKK α . Vanadate has been shown to induce NF- κ B through activation of IKK β kinase activity as quickly as 15 minutes post treatment with a concentration as low as 30 μ M (Chen *et al.*, 1999). However, the characterisation of p45-IKK α was relatively thorough, so it is not possible on this basis alone to call into question the findings of Margalef *et al*. The evidence for phosphorylated p45-IKK α was most convincing in BRAF mutant colorectal cancer cells, such as HT-29. KRAS mutant cell lines, such as HCT116, exhibited far less phosphorylated p45-IKK α in their hands. Indeed, in a follow-up study Margalef *et al* proposed that p45-IKK α is phosphorylated downstream of mutant BRAF in an ill-defined mechanism involving endosomal localised TAK1 (Margalef *et al.*, 2015). Given the uncertainty surrounding the detection of phosphorylated p45-IKK α , no further efforts were made to repeat the findings of Margalef *et al*. Regardless of the validity of the reported phosphorylation state of p45-IKK α , no truncated IKK α forms were detected in the *IKK* KO clones, thus confirming their applicability in the study of IKK α function.

HCT116 cells are an adherent cell type with epithelial morphology. The morphology of IKK and IKK KO clones was largely comparable with WT clones (Figure 3.3A). Some subtle heterogeneity between the different clones was apparent, with IKK KO clone F6 subjectively growing in more compact, epithelial-like colonies compared to clones C7 and A2, while the same was true of IKK KO clone A4 relative to clones G9 and A7. These morphological differences were not correlated with the different guide RNA sequences used to generate the clones, and so are unlikely to be due to off-target effects of Cas9 gene editing. There is natural cell morphological heterogeneity within the parental HCT116 cell population, so this heterogeneity amongst the clones could be the result of the single cell cloning process (Singh *et al.*, 2014). Meanwhile, all three of the DKO clones, C8, G1 and E9, appeared

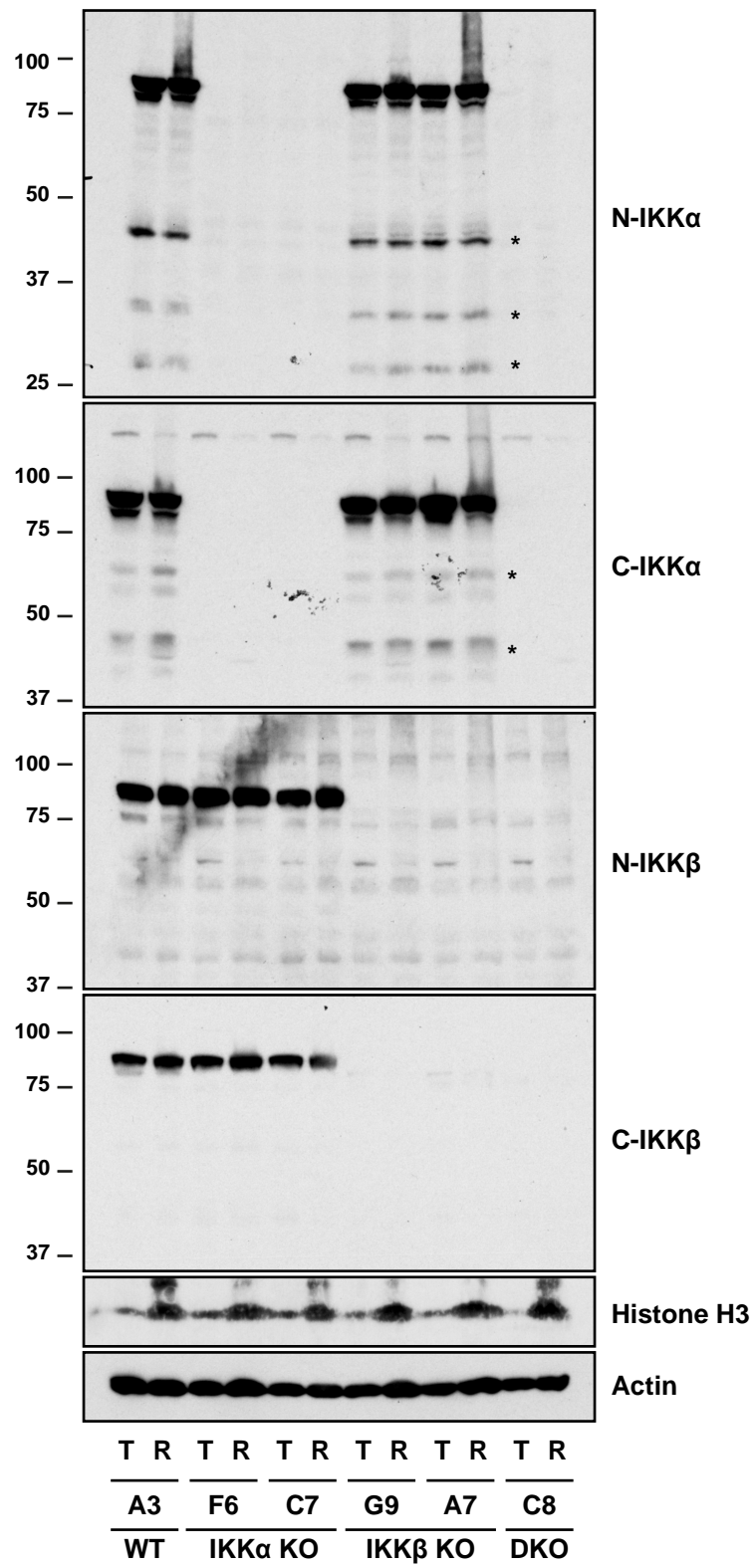


Figure 3.2. Representative CRISPR-Cas9 IKK KO cells are completely absent of IKK protein. (A) Representative WT, IKK α KO, IKK β KO and IKK α/β DKO HCT116 cells were seeded in normal growth medium for 48 hours prior to lysis with either the less stringent TG lysis buffer (T) or the more stringent RIPA buffer (R). Lysates were fractionated by SDS-PAGE and Western blotted with the indicated antibodies to confirm absence of expressed protein corresponding to targeted gene. Data are from a single experiment representative of two showing similar results.
*Possible truncated forms of IKK α .

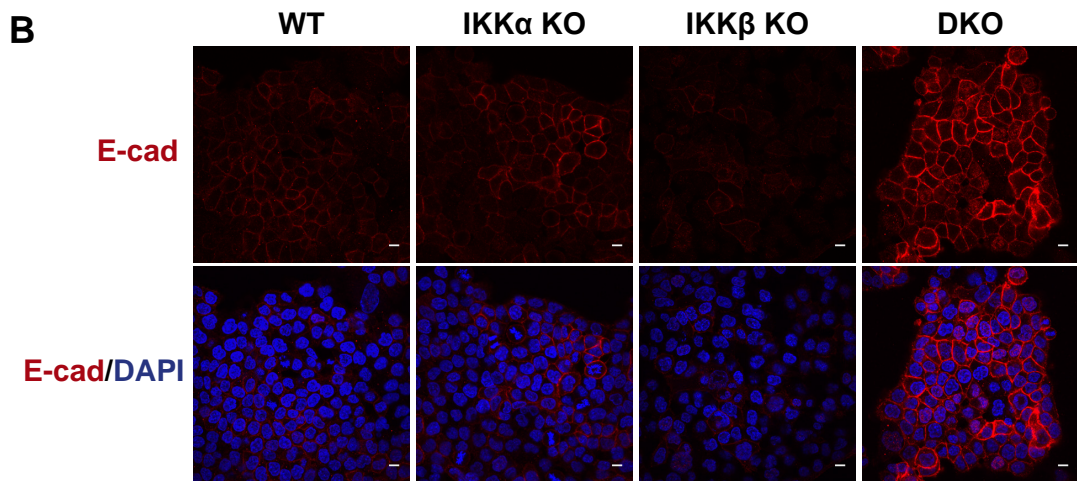
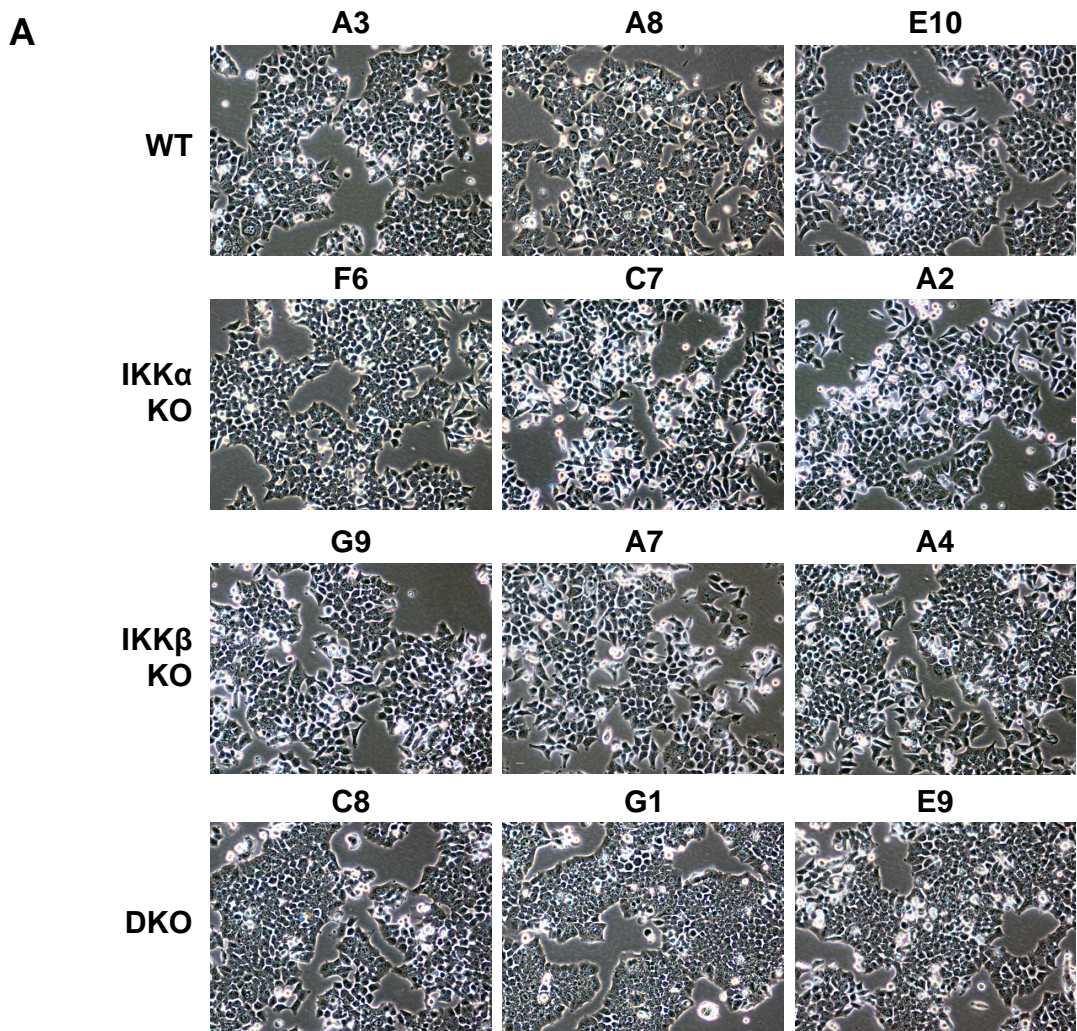


Figure 3.3 IKK α / β DKO cells appear to grow in more compact, epithelial-like colonies than WT or IKK α KO and IKK β KO cells. (A) WT, IKK α KO, IKK β KO and IKK α / β DKO HCT116 cells were seeded in normal growth medium so as to be at similar levels of confluence (~70%) after 48 hours, subsequent to capture of representative light microscopy images. Scale bar, 20 μ m. (B) WT, IKK α KO, IKK β KO and IKK α / β DKO HCT116 cells were seeded in normal growth medium so as to be at similar levels of confluence (~70%) after 48 hours, subsequent to immunofluorescence staining of cells with anti-CDH1 (E-cadherin, red) and nuclei with DAPI (blue). Scale bar, 10 μ m.

substantially more epithelial in nature, growing in tightly packed colonies. In support of this more pronounced epithelial morphology, DKO clone C8 exhibited greater immunofluorescence staining for the epithelial cell-type marker, E-cadherin than WT cells or single IKK KO cells. (Figure 3.3B). However, given the morphological heterogeneity of the IKK KO clones in general, additional DKO clones would need to be examined to confidently conclude that this more epithelial morphology is due to IKK knockout. Whilst this apparent phenotype of the DKO clones is consistent with the known role of NF- κ B transcriptional activity in promoting epithelial-to-mesenchymal transition (EMT) through Snail-dependent repression of E-cadherin expression (Zhang *et al.*, 2011; Pires *et al.*, 2017), no further investigations were made into this observation.

Subsequently, the growth of the KO clones was assayed via a fluorescent, DNA-binding dye-based assay (Figure 3.4A and B). In this assay, DNA content is used as an indirect measure of cell number. The relationship between DNA-binding dye fluorescence and cell number is approximately linear ($R^2=0.991$) over the range of fluorescence intensities observed (Figure 3.4A inset). There were small differences in the exponential phase (day 4 to 6) growth rate of individual clones, but no overall significant difference between the average growth rates of the different genotypes. As with the subtle morphological differences between clones, three independent clones were insufficient to statistically distinguish between clonal heterogeneity and any genuine small effects of IKK knockout on cell growth rate.

Consistent with the lack of an effect of IKK knockout on cell growth, IKK knockout had no significant impact on the cell cycle distribution of the clones (Figure 3.4B). A consistent, small increase in G1 phase content and decrease in S phase content was observed in the IKK α/β DKO clones, but this could reflect the growth of these clones in more compact colonies; cells at the centre of such compact colonies might be more likely to undergo G1 arrest due to nutrient deprivation.

3.2.2 Validation of IKK knockout reveals a prominent role for IKK α in canonical NF κ B signalling downstream of TNF α

Western blotting indicated that the clones were knockout for IKK protein. However, a more important consideration was whether the clones represented genuine functional knockouts. The single cell cloning process might have favoured clones with re-wired cell signalling pathways that compensated for the loss of IKK protein. To investigate this the cell signalling response to TNF α was examined in IKK KO clones (Figure 3.5 and Figure 3.6A and B). Each of the three IKK α/β DKO clones exhibited no observable IKK kinase activity, as assessed by the phosphorylation of known IKK substrates, including I κ B α and p65. The absence of p65 phosphorylation at Serine 536 in DKO clones indicated that in the absence of IKK kinases this site cannot be phosphorylated in response to TNF α by other kinases, such as TBK1 and IKK ϵ , which have been shown to phosphorylate this site under certain circumstances (Buss *et al.*, 2004). In addition to the NF- κ B pathway, TNF α activates the JNK and p38 signalling cascades. Compared to WT clones, IKK α/β DKO clones exhibited a similar phosphorylation of JNK at T183/Y185 in response to TNF α . However, the DKO clones exhibited a small increase in basal p38 phosphorylation at T180/Y182, and a higher level of p38 phosphorylation after 30 minutes treatment with TNF α . A longer time course comparison would be necessary to determine if this reflects a more sustained p38 signalling response in the DKO clones relative to WT.

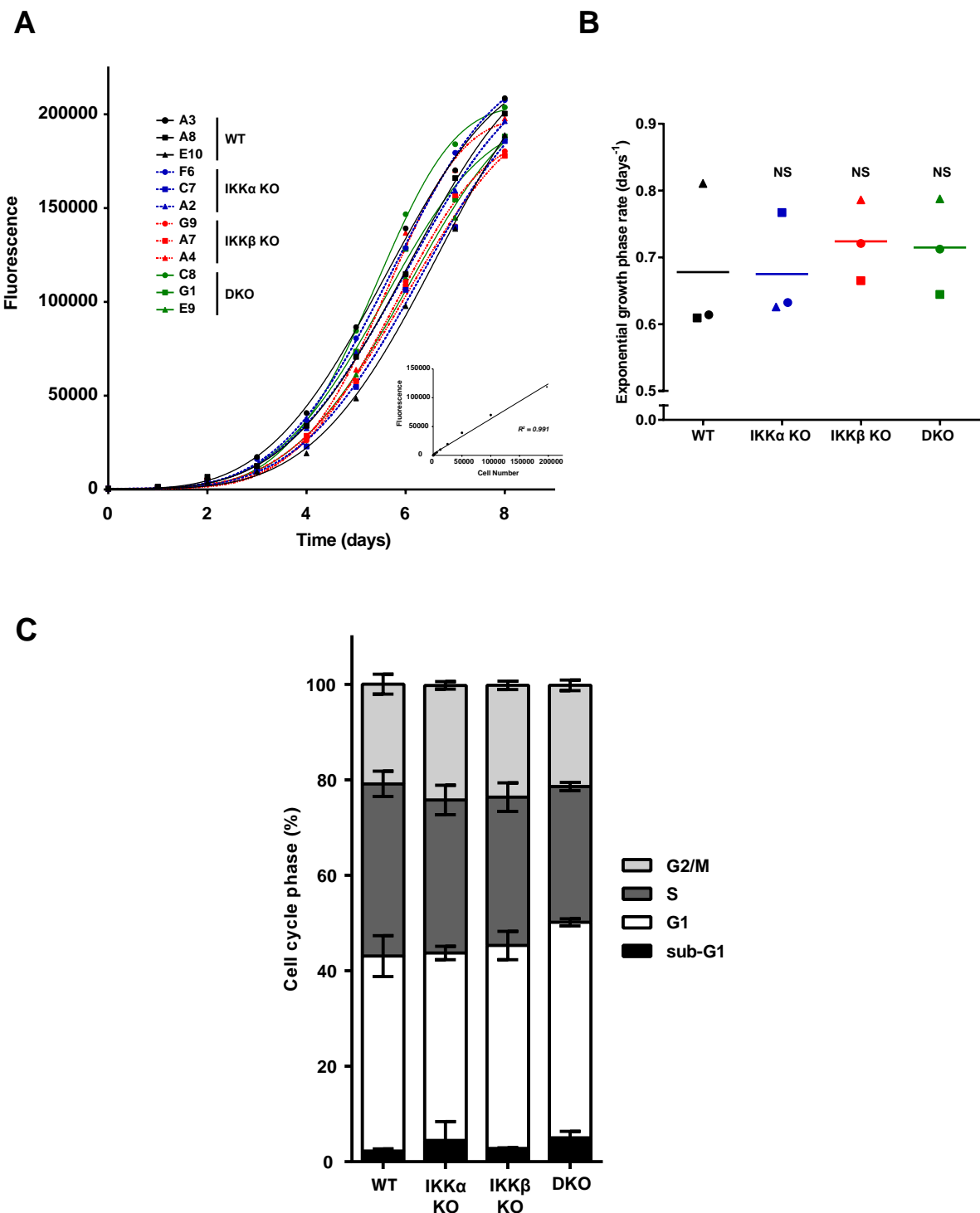


Figure 3.4. IKK knockout has no significant impact on the growth rate or cell cycle distribution of HCT116 cells (A) On day 0, three independent clones of WT, IKK α KO, IKK β KO and IKK α/β DKO HCT116 cells were seeded in quadruplicate at a density of 500 cells per well of seven 96-well plates. The following day for 8 consecutive days, the cells in a plate were washed and frozen at -8 °C an fluorescence of quadruplicates for each independent clone (no error bars shown to prevent over-cluttering the chart). The Weibull growth model of nonlinear regression was used to fit the data. The embedded chart is experimental data highlighting the linear relationship between DNA-binding dye fluorescence intensity and cell number. (B) The growth rate (days^{-1}) of cells during the exponential growth phase (day 4 to 6) was estimated by calculating the slope of the linear regression curve of the natural log transformed fluorescence as a function of time (days). Significance testing was performed by ANCOVA, with post-hoc Dunnett test. (C) Three independent clones of WT, IKK α KO, IKK β KO and IKK α/β DKO HCT116 cells were seeded in triplicate for 24 hours. Cells that were subconfluent at the point of harvest, were fixed, stained with propidium iodide and cell cycle distribution assessed by flow cytometry. Results are mean \pm SD of the three independent clones.

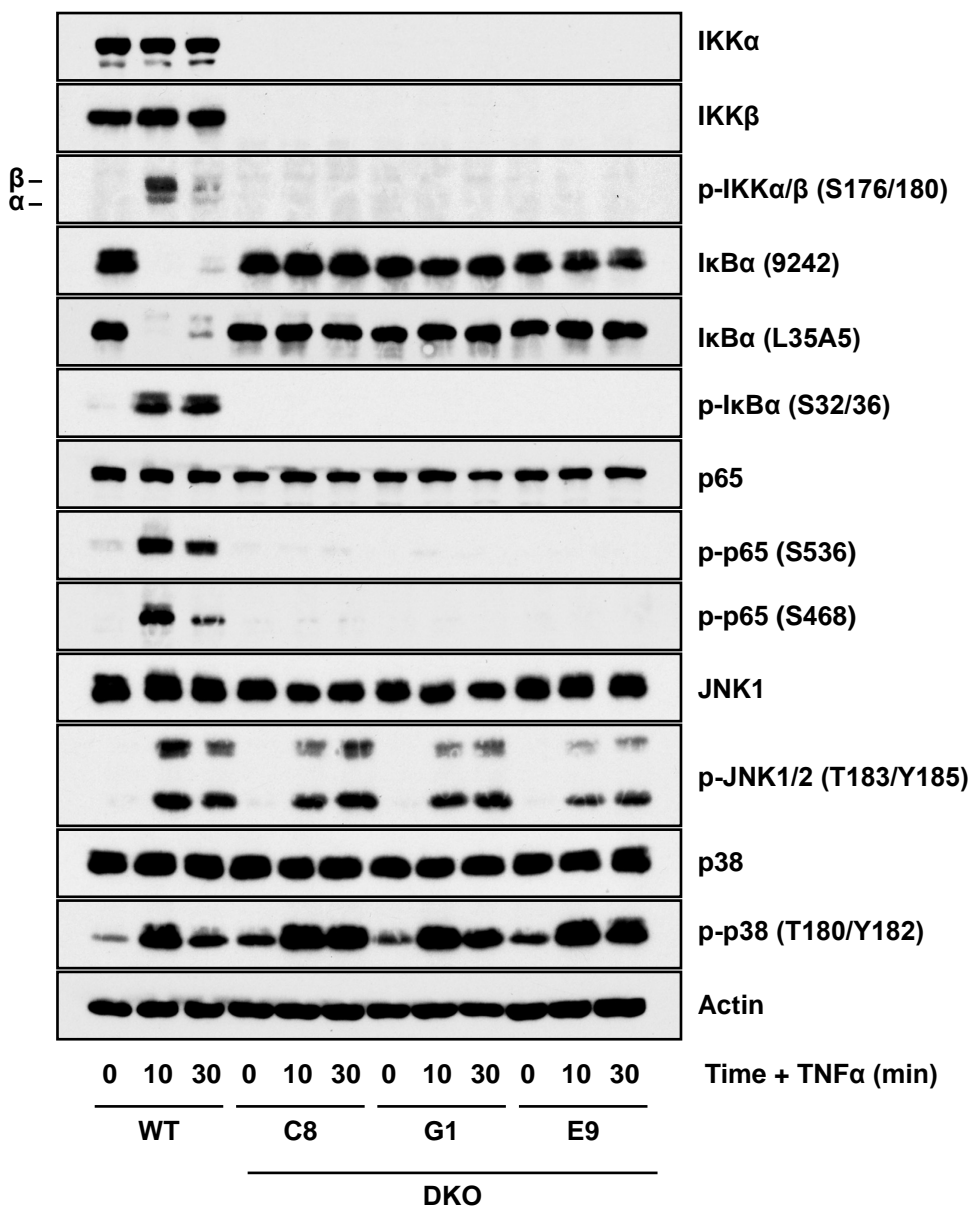


Figure 3.5. IKK α /β DKO cells exhibit no observable phosphorylation of known IKK substrates in response to TNF α stimulation. A single WT clone (A3) and three independent IKK α /β DKO clones were seeded in their normal growth medium for 48 h, prior to treatment with 10 ng/ml recombinant TNF α for the indicated timepoints. Whole cell extracts were prepared, fractionated by SDS-PAGE and Western blotted with the indicated antibodies. Data are from a single experiment. p, phospho-

Meanwhile, western blotting following treatment of IKK α KO and IKK β KO clones with TNF α indicated a degree of functional redundancy between IKK α and IKK β (Figure 3.6A and B). As expected, in WT cells I κ B α was rapidly phosphorylated at Serine 32/36 and targeted for proteasomal degradation within 10 minutes of TNF α treatment. By 60 minutes, downstream activation of NF- κ B transcriptional activity increased the expression of I κ B α to restore I κ B α protein levels as part of the well-characterised negative feedback loop that inhibits the pathway. Two different I κ B α antibodies were used; I κ B α 9242, which binds preferentially to the unphosphorylated form; and I κ B α L35A5, which recognises both phosphorylated and unphosphorylated forms of the protein. IKK α and IKK β are themselves maximally phosphorylated within their activation loops at Serine 176/180 and Serine 177/181, respectively, less than 10 minutes after TNF α treatment. The antibody used (described as S176/180) detects IKK α only when phosphorylated at Ser176/180 and IKK β only when phosphorylated at Ser177/181. The NF- κ B subunit, p65, was also rapidly phosphorylated at the two sites examined, Serine 468 and Serine 536. The NF- κ B pathway was minimally basally activate in WT HCT116 cells. A very low basal IKK α and I κ B α phosphorylation was detectable upon overexposure of blots, whereas basal phosphorylation of p65 at Serine 536 was more routinely detected.

Whilst it is normally undesirable to directly compare blots run on separate gels, an effort was made to make the blots from IKK α KO (Figure 3.6A) and IKK β KO (Figure 3.6B) clones as comparable as possible by loading the same amount of lysate for each, and exposing the blots for identical lengths of time. The WT clones may also be used as a frame of reference for comparison between each set of blots. With this caveat in mind, the IKK α KO and IKK β KO clones exhibited a similar small defect in the degradation of I κ B α following TNF α treatment relative to WT cells. After 10 and 30 minutes TNF α treatment, there was more I κ B α remaining in IKK α KO and IKK β KO clones than in WT cells. I κ B α was restored after 60 minutes in both IKK α KO and IKK β KO indicating that the negative feedback loop and NF- κ B transcriptional activation was intact. The KO clones highlighted the specificity of the phospho-IKK antibody; the upper band being specific to IKK β (Serine 177/181) and the lower band specific to IKK α (Serine 176/180). The remaining IKK kinase was phosphorylated in both the IKK α KO and IKK β KO clones. Interestingly, IKK β appeared to be phosphorylated to a greater extent in the IKK α KO clones relative to WT at each of the time points examined. Whether this indicates enhanced upstream IKK phosphorylation loop kinase activity or weaker phosphatase activity remains to be determined. Conversely, the phosphorylation of IKK α in the IKK β KO clones was largely similar to that observed in WT cells.

As described in Chapter 1, both IKK α and IKK β have been demonstrated to phosphorylate p65 at Serine 536, with IKK β thought to be the more efficient kinase (Sakurai *et al.*, 1999; Sizemore *et al.*, 2002; O'Mahony *et al.*, 2004). Meanwhile, IKK β is thought to be the dominant kinase phosphorylating p65 at Serine 468 in response to inflammatory cytokines, such as TNF α and IL-1, with very little if any contribution from IKK α *in vivo* (Schwabe *et al.*, 2005). The TNF α -induced *phosphorylation* of p65 at Serine 536 was unaffected in either of the IKK α KO or IKK β KO clones, suggesting that both IKK α and IKK β can fully compensate for the loss of the other kinase with regard to phosphorylation at this site. Interestingly, the basal phosphorylation of p65 at Serine 536 was absent in IKK α KO clones but was unaffected in IKK β KO clones, suggesting that basal IKK α kinase activity might be responsible for this phosphorylation. In direct contrast with the literature, p65 phosphorylation at Serine 468 was strongly diminished in IKK α KO clones, but largely unaffected by IKK β KO, suggesting that IKK α , but not IKK β

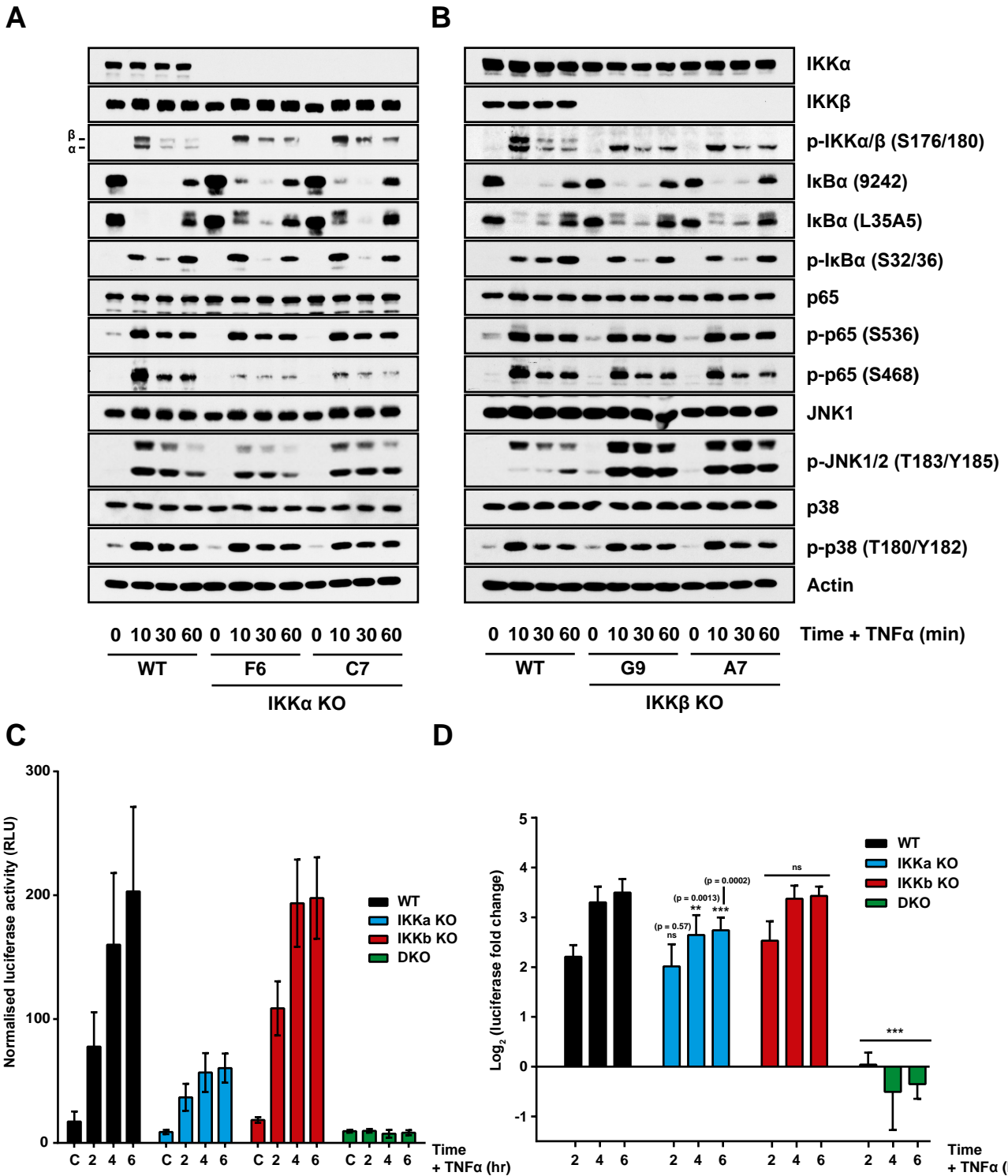


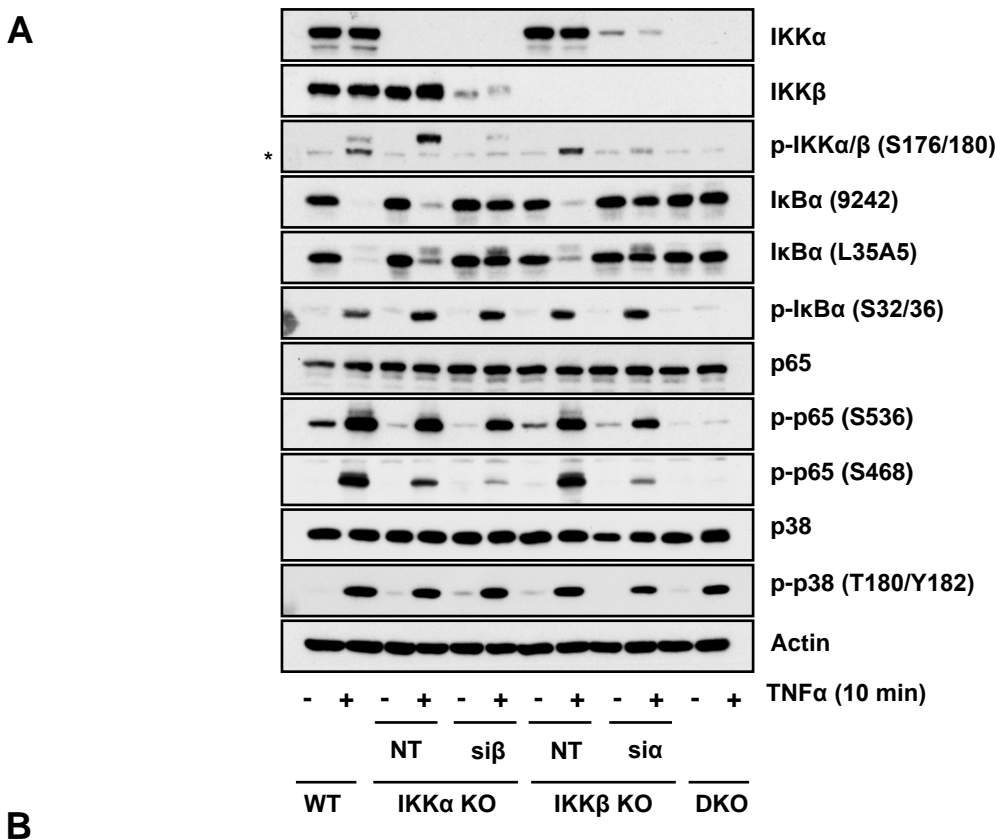
Figure 3.6. IKK α and IKK β have non-functionally redundant kinase activities. (A) A single WT clone (A3) and two independent IKK α KO clones and (B) a single WT clone (A3) and two independent IKK β KO clones were seeded in their normal growth medium for 48 h, prior to treatment with 10 ng/ml recombinant TNF α for the indicated timepoints. Whole cell extracts were prepared, fractionated by SDS-PAGE and Western blotted with the indicated antibodies. Similar results were seen for the two other WT clones (A8 and E10) and the other IKK α (A2) and IKK β (A4) KO clones (data not shown). (C and D) WT, IKK α KO, IKK β KO and IKK α/β DKO HCT116 cells were seeded in antibiotic-free growth medium overnight prior to transient transfection with 0.1 μ g pGL4.32[Luc2P/NF- κ B-RE firefly luciferase (reporter) plasmid DNA and 0.01 μ g renilla luciferase (internal control) plasmid DNA. The following day, cells were treated with 10 ng/ml recombinant TNF α for the indicated time periods. Firefly luciferase luminescence was normalised relative to renilla luciferase luminescence and data expressed as log₂(fold change in TNF α -induced luciferase activity relative to the relevant, matched untreated condition). Results are mean \pm SD of three independent experiments, each of which was performed with three independent clones, seeded in triplicate (WT - A3, A8 and E10. IKK α KO - F6, C7, A2. IKK β KO - G9, A7, A4 and IKK α/β DKO - C8, G1, E9). Significance testing was performed using two-way ANOVA (repeated measures) with Tukey post-hoc test. p values relate to comparison with corresponding timepoint(s) of WT control. P < 0.0001 (***) p-, phospho-. ns = not significant.

is necessary for phosphorylation at this site in response to TNF α in these cells. Whether IKK α activity is sufficient for phosphorylation at this site will be discussed shortly.

Phosphorylation of p38 was unaffected by knockout of either IKK α or IKK β , indicating that the enhanced p38 phosphorylation observed in DKO clones was due to either: a combined effect of loss of any IKK kinase activity; loss of NF- κ B activity in response to stimulus; or a gene expression change in DKO clones that was not present in *IKK α* KO or *IKK β* KO clones that predisposes DKO clones to enhanced p38 activation downstream of TNF α signalling. Meanwhile, stimulatory phosphorylation of JNK1/2 at Threonine 183/Tyrosine 185 in response to TNF α was unaffected by IKK α KO but was enhanced relative to WT cells by IKK β KO.

To examine the effect of IKK KO on downstream NF- κ B transcriptional activity three independent clones of each genotype, WT, IKK α KO, IKK β KO and IKK α/β DKO were transfected with a luciferase reporter construct under the control of a tandem NF- κ B promoter and treated with TNF α for various time periods (Figure 3.6C and D). A plot of luciferase activity normalised to the expression of constitutively induced renilla activity demonstrated that both the basal and stimulus induced NF- κ B transcriptional activity was substantially reduced in IKK α KO clones relative to WT (Figure 3.6C). The fold induction of NF- κ B activity above basal levels was significantly reduced in IKK α KO clones relative to WT (Figure 3.6D). However, there was no significant difference in the basal or TNF α induced fold change in NF- κ B activity in IKK β KO clones relative to WT. IKK α/β DKO clones exhibited no TNF α -induced NF- κ B activity, consistent with the complete absence of IKK activity observed in these cells. As with the prior observations of heterogeneity between clones at the level of cell morphology and growth rate, both the WT and IKK KO clones exhibited a degree of heterogeneity regarding the absolute level of NF- κ B transcriptional induction in response to TNF α . However, this heterogeneity was largely matched by an equivalent degree of heterogeneity in the basal level of NF- κ B activity, such that the fold changes in activity were more consistent between clones of the same genotype. Despite this heterogeneity, the differences between WT and IKK KO clones were of sufficient magnitude to reach statistical significance, thus highlighting the biological significance of this observation.

Given the overlapping functions of IKK α and IKK β it was impossible to rule out any residual expression and activity of the targeted IKK kinase in the single IKK KO clones from the data described up until this point. To confirm that the IKK KO clones were genuinely functionally null for the targeted IKK subunit, IKK α KO and IKK β KO clones were treated with siRNA targeted to the remaining IKK subunit; to knockdown IKK β in the IKK α KO clone and to knockdown IKK α in the IKK β KO clone (Figure 3.7A and B). A knockdown of approximately >60 % was achieved for both IKK α and IKK β . This was sufficient to almost completely block the degradation of I κ B α observed after 10 minutes TNF α treatment in both the IKK α and IKK β KO clones, indicating that the IKK activity observed in these clones was due to the redundant IKK kinase remaining after IKK knockout. The enhanced phosphorylated I κ B α detected under these conditions was potentially due to the residual IKK activity that had escaped siRNA-mediated knockdown, and the accumulation of non-degraded I κ B α in an intermediate phosphorylated form. The phosphorylation of p65 at Serine 536 and Serine 468 was also diminished following the knockdown of the remaining IKK subunit in both the IKK α and IKK β KO clones, although again IKK kinase activity was clearly not entirely abolished. The corresponding luciferase assay demonstrated that knocking down the remaining IKK subunit caused a significant reduction in the TNF α -induced NF- κ B transcriptional activation (Figure 3.7B); by



B

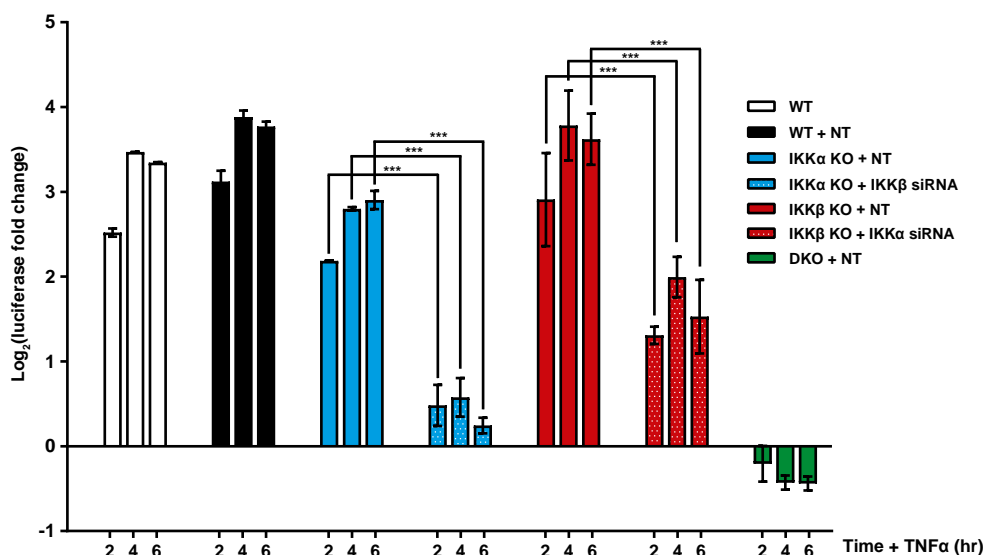


Figure 3.7. Knocking down the remaining IKK subunit in single KO clones drastically reduces the observed TNF α -induced IKK kinase activity and NF- κ B transcriptional activity. (A) WT (A3), IKK α KO (F6), IKK β KO (G9) and IKK α/β DKO (C8) HCT116 cells were transfected with non-targeting (NT) siRNA or transfected with either 20 nM IKK α -specific siRNA (sia) or 20 nM IKK β -specific siRNA (si β). 48 hours after transfection, cells were treated with 10 ng/ml TNF α for 10 minutes, before whole cell lysates were prepared and Western blotted with the indicated antibodies. Data are from a single experiment representative of two giving similar results. (B) WT, IKK α KO, IKK β KO and IKK α/β DKO HCT116 cells were transfected with non-targeting (NT) siRNA or transfected with either 20 nM IKK α -specific siRNA (sia) or 20 nM IKK β -specific siRNA (si β). 24 hours later, cells were transiently transfected with 0.1 μ g pGL4.32[Luc2P/NF- κ B-RE firefly luciferase (reporter) plasmid DNA and 0.01 μ g renilla luciferase (internal control) plasmid DNA. The following day, cells were treated with 10 ng/ml recombinant TNF α for the indicated time periods (2, 4 and 6 hours). Firefly luciferase luminescence was normalised relative to renilla luciferase luminescence and data expressed as log₂(fold change in TNF α -induced luciferase activity relative to the relevant, matched untreated condition). Results are mean \pm SD of two independent experiments using the same KO clones as in (A), each performed in technical triplicate. Significance testing was performed using two-way ANOVA (repeated measures) with Tukey post-hoc test. $P < 0.0001$ (***) p-, phospho-. *faint non-specific band running at similar molecular weight to P-IKK α .

approximately 4-fold in the IKK α cells and 3-fold in the IKK β cells. The greater fold reduction observed in IKK α cells likely reflects the superior siRNA-mediated knockdown of IKK β compared to IKK α .

To further validate the single IKK KO clones, WT, IKK α KO and IKK β KO clones were treated with the highly selective IKK β inhibitor, BIX02514, and the effect on the phosphorylation status of IKK substrates and NF- κ B transcriptional activity examined (Figure 3.8A and B). BIX02514, at a concentration that had been shown previously to maximally inhibit IKK β (10 μ M) in IKK α KO cells (Chapter 5 Figure 3.6A), had only a small inhibitory effect on the TNF α -induced degradation of I κ B α in WT cells. It also had no effect on the phosphorylation of p65 at Serine 536 or Serine 468, suggesting that a kinase other than IKK β , perhaps IKK α , phosphorylates these sites in response to TNF α in the wild type state. Nevertheless, the small inhibitory effect of BIX02514 on I κ B α degradation was apparently sufficient to result in a significant decrease in the TNF α -induced NF- κ B activity (Figure 3.8B). The approximately 2-fold reduction in NF- κ B activity when IKK β is maximally inhibited implies that IKK α and IKK β contribute equally to the induction of NF- κ B in the wild-type state. Meanwhile, BIX02514 completely inhibited I κ B α phosphorylation and degradation in IKK α KO cells with the corresponding effect of fully inhibiting the induction of NF- κ B transcriptional activity. BIX02514 treatment also markedly inhibited the phosphorylation of p65 at Serine 536 and the residual phosphorylation of Serine 468 observed in IKK α KO cells following TNF α stimulation. These results strongly suggest that the IKK activity observed in IKK α KO cells is due to IKK β activity. Furthermore, BIX02514 had no noticeable effect on the TNF α -induced phosphorylation and degradation of I κ B α , or the phosphorylation of p65 in IKK β KO cells, confirming that the IKK activity observed in IKK β KO cells is not due to residual IKK β activity. Indeed, BIX02514 had no significant effect on the induction of NF- κ B transcriptional activity in IKK β KO cells (Figure 3.8B). The small decrease that was observed is likely to be due to off-target inhibition of IKK α at this high concentration of BIX02514.

Two different antibodies specific to phosphorylated IKK were used to investigate TNF α inducible IKK phosphorylation within this experiment. The S176/180 antibody as described earlier detects IKK α phosphorylated on S176/180 and IKK β on S177/181. In other words it detects all phosphorylation events on IKK. The S176/177 specific antibody, on the other hand, only detects IKK α phosphorylated on S176 and IKK β phosphorylated on S177. Interestingly, TNF α treatment in the presence of the IKK β selective inhibitor resulted in a higher level of IKK phosphorylation detected by the S176/177 specific antibody. Whether this represented an increase in the phosphorylation of IKK α or IKK β or both was impossible to tell. Unfortunately, the blot was less clear with the S176/180 antibody. As previously described, the S176/180 antibody detects a higher level of TNF α -induced IKK β activity in IKK α KO cells. Interestingly, this was completely abolished by the IKK β selective inhibitor, suggesting that this phosphorylation was due to IKK β autophosphorylation. However, the S176/177 specific antibody did not detect an enhanced level of IKK β phosphorylation, and no change was observed after treatment with BIX02514; a band shift was detected, however, possibly reflecting the lower overall level of IKK β phosphorylation. This suggests that it is phosphorylation of IKK β at Serine 181, but not Serine 177 that is enhanced in IKK α KO cells, and that Serine 177 is phosphorylated by an ‘upstream’ kinase in an IKK β independent manner, while Serine 181 is phosphorylated by IKK β itself in IKK α KO cells. Interestingly, the phosphorylation of IKK α at Serine 176 was considerably weaker in IKK β KO cells compared to WT cells.

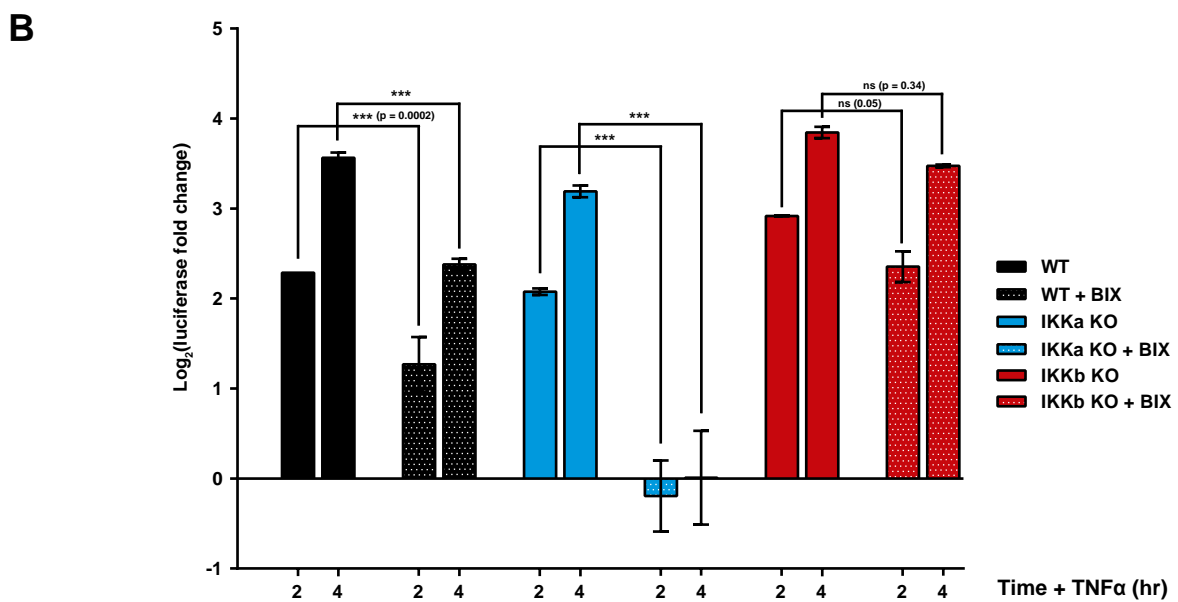
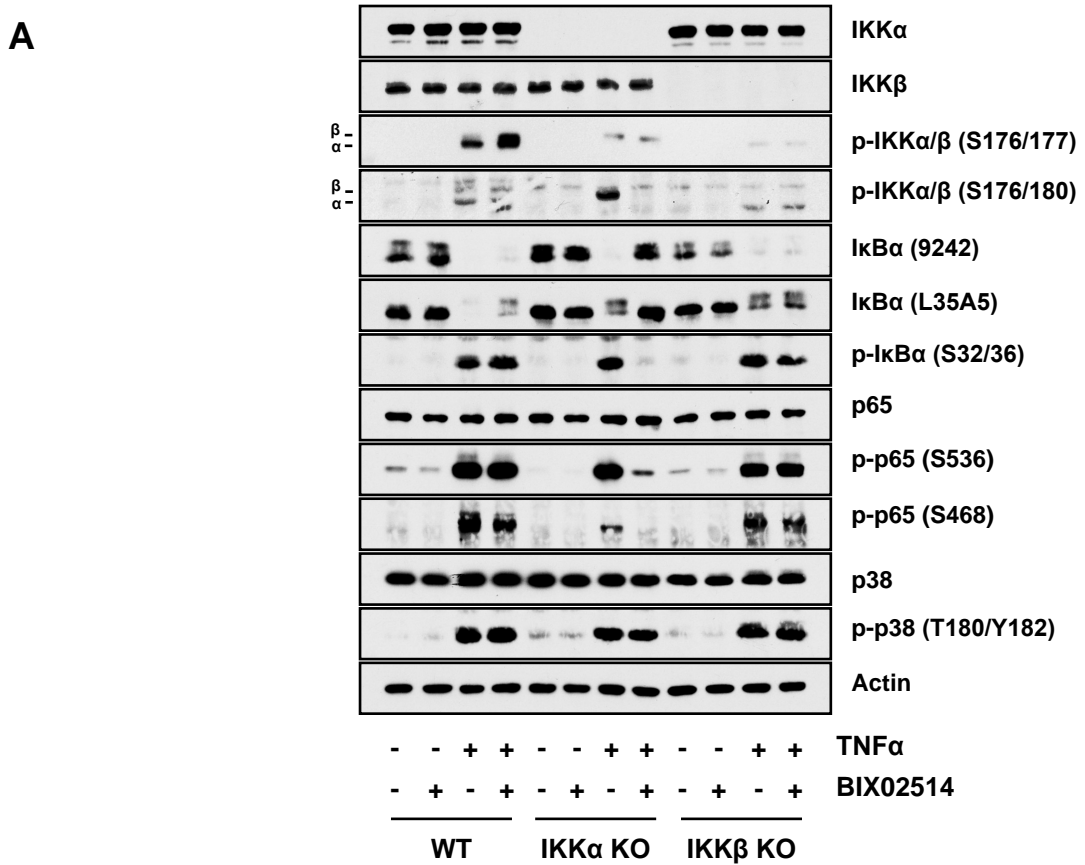


Figure 3.8. Both IKK α and IKK β contribute to the induction of canonical NF- κ B in WT cells. (A) WT (A3), IKK α KO (F6) and IKK β KO (G9) HCT116 cells were seeded for 48 hours prior to treatment with 10 μ M BIX02514 or DMSO vechicle control for 30 minutes. Cells were subsequently treated with 10 ng/ml TNF α for 10 minutes, before whole cell lysates were prepared and Western blotted with the indicated antibodies. Data are from a single experiment. **(B)** WT, IKK α KO and IKK β KO HCT116 cells were transiently transfected with 0.1 μ g pGL4.32[luc2P/NF- κ B-RE firefly luciferase (reporter) plasmid DNA and 0.01 μ g renilla luciferase (internal control) plasmid DNA. The following day, cells were treated with BIX02514 or DMSO vechicle control for 30 minutes, prior to treatment with 10 ng/ml recombinant TNF α for the indicated timepoints (2 and 4 hours). Firefly luciferase luminescence was normalised relative to renilla luciferase luminescence and data expressed as log₂(fold change in TNF α -induced luciferase activity relative to the relevant, matched untreated condition). Results are mean \pm SD of two independent experiments using the same KO clones as in (A) each performed in technical triplicate. Significance testing was performed using two-way ANOVA (repeated measures) with Tukey post-hoc test. P < 0.0001 (**). BIX, BIX02514. p-, phospho-.

The cell death inducing effects of TNF α on WT, IKK α KO, IKK β KO and IKK α/β DKO cells were examined as a final form of functional validation of the knockout cell lines (Figure 3.9). The suppression of TNF α -induced cell death, both apoptotic and necrotic in nature, by concomitant NF- κ B-dependent survival signalling is a well observed effect (Beg & Baltimore, 1996). Conversely, inhibition of NF- κ B activation sensitises cells to the cell death inducing effects of TNF α (Sumitomo *et al.*, 1999 and Chaisson *et al.*, 2002). In agreement with the complete absence of TNF α -induced NF- κ B activation observed, an IKK α/β DKO clone (C8) underwent a pronounced cell death response after 24 hours treatment with TNF α , as indicated by a significant increase in sub-G1 DNA content (Figure 3.9A) and PARP cleavage (Figure 3.9B). This cell death was caspase-dependent and hence apoptotic in nature as it could be significantly inhibited by treatment with the pan-caspase inhibitor, Q-VD-OPh. Neither the IKK α KO (F6) nor IKK β KO (G9) clones exhibited a significant difference in the extent of TNF α -induced cell death compared to the WT clone, consistent with the fact that NF- κ B transcriptional activation is intact in these cells.

However, sub-G1 % DNA content is a relatively crude measure of late-stage cell death. A superior assay for distinguishing early and late apoptosis is the Annexin-V assay. Annexin V binds with high affinity to surface-exposed phosphatidylserine (PS), the presence of which is an early indication of apoptosis, and which precedes the loss of membrane integrity (measured by DAPI staining) that accompanies cell death (Figure 3.9C). Therefore, cells that are considered viable (live) are both Annexin V and DAPI negative, while cells that are in early apoptosis are Annexin V positive and DAPI negative, and cells that are in late apoptosis or already dead are both Annexin V and DAPI positive. Late apoptotic cells are broadly distinguished from necrotic cells on the basis of higher Annexin V-staining intensity, although further assays would be needed to more accurately distinguish apoptosis from necrosis. The Annexin V assay was performed for three independent clones representative of WT, IKK α KO, IKK β KO and IKK α/β DKO treated with TNF α for 24 hours. In agreement with the sub-G1% content results, DKO cells exhibited a marked increase in the percentage of early and late apoptotic cells compared to WT cells. There was a considerable degree of heterogeneity amongst the WT, and particularly the IKK α KO and IKK β KO clones regarding the level of TNF α -induced early and late-phase apoptotic cell death. However, unexpectedly, this heterogeneity at the level of TNF α -induced cell death did not correlate with heterogeneity at the level of TNF α -induced NF- κ B-dependent transcriptional activity (Figure 3.6). For example, WT clone A8 consistently exhibited the highest NF- κ B-dependent transcriptional activation out of the WT clones, but also exhibited the highest level of TNF α -induced cell death. The opposite was true of IKK α KO clone F6, which exhibited the lowest NF- κ B-dependent transcriptional activation of the IKK α KO clones, but also exhibited the smallest increase in cell death (also as observed in Figure 3.9A). The heterogeneity observed in this assay did not appear to be the result of technical issues, as the results for the DKO clones were highly consistent.

The cell death response induced by TNF α in IKK α/β DKO cells was rapid in onset, with significant DNA fragmentation, effector caspase-cleavage and PARP cleavage within 4 hours of treatment (Figure 3.9D and E). This data informed the choice of time points used for RNA sequencing analysis of the response of IKK KO cells to TNF α (as described in Chapter 6); an early time point of 2 hours and a late time point of 8 hours was chosen.

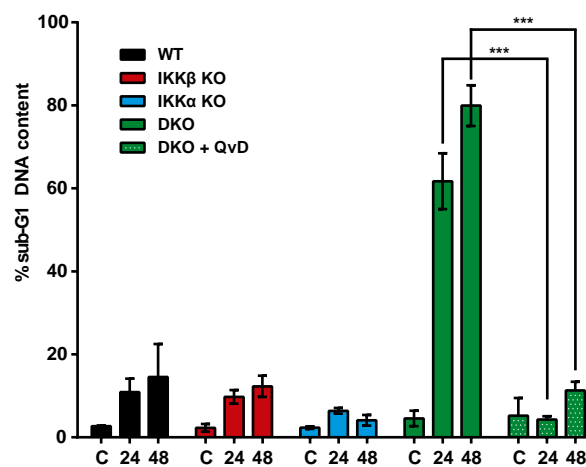
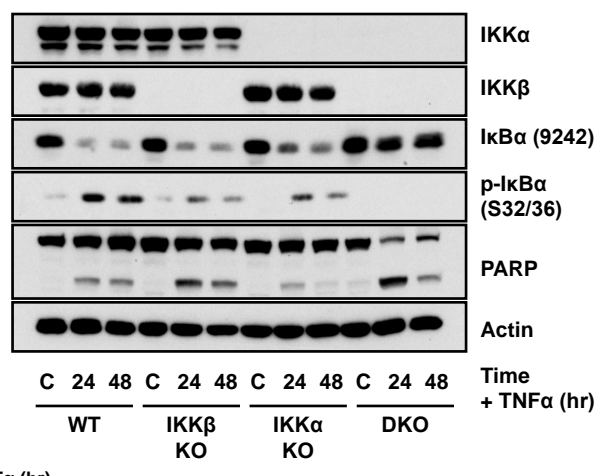
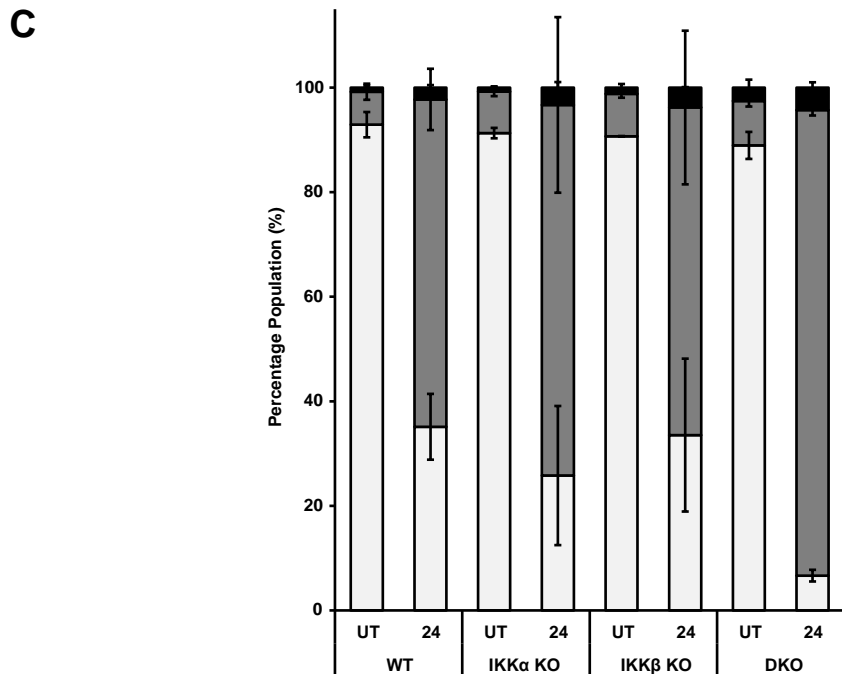
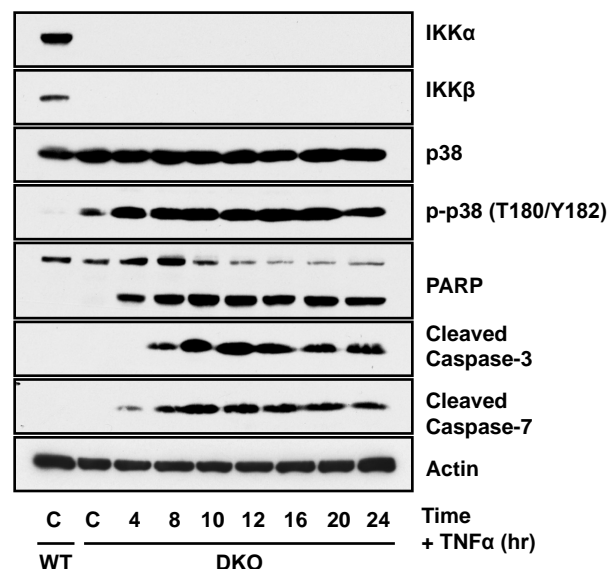
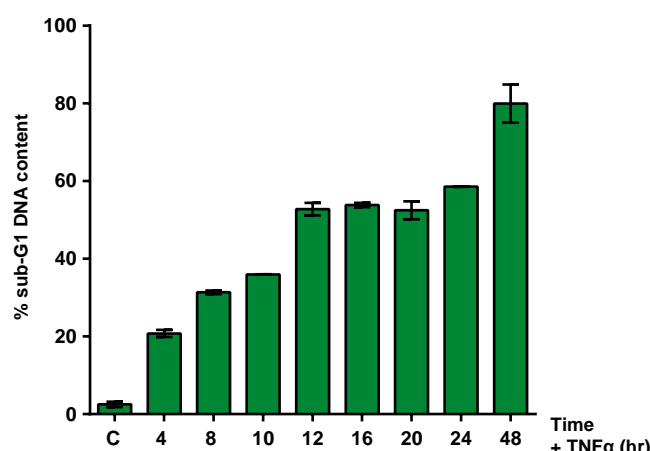
A**B****C****E**

Figure 3.9. IKK α / β DKO cells exhibit a much greater sensitivity to TNF α -induced apoptosis than single IKK KO cells. (A) WT (A3), IKK α KO (F6), IKK β KO (G9) and IKK α / β DKO (C8) HCT116 cells were seeded in triplicate in normal growth medium for 24 hours prior to treatment with 10 ng/ml TNF α for the indicated timepoints (24 and 48 hours). Caspase-dependent cell death was blocked by pretreating cells for 30 minutes with 10 μ M of the pan-caspase inhibitor, QVD-OPh. Cells that were subconfluent at the point of harvest, were fixed, stained with propidium iodide and percentage sub-G1 population (as a crude marker of cell death) assessed by flow cytometry. Results are mean \pm SD of the three independent experiments. (B) The same clones were treated as in (A) and whole lysates prepared and Western blotted with the indicated antibodies. Data are from a single experiment representative of two showing similar results. (C) Three independent clones of each of WT, IKK α KO, IKK β KO and IKK α / β DKO HCT116 cells were seeded in duplicate in normal growth medium for 24 hours prior to treatment with 10 ng/ml TNF α or vector control (UT) for 24 hours. Cells that were subconfluent at the point of harvest, were gently trypsinised, then stained with Annexin V-FITC conjugate and DAPI prior to assessment of populations of live, early apoptotic, late apoptotic and necrotic cells via flow cytometry. Annexin-FITC (488 excitation, 530/30 nm emission), DAPI (355 excitation, 450/50 nm emission). (D) WT (A3) and IKK α / β DKO (C8) HCT116 cells were seeded in triplicate in normal growth medium for 24 hours prior to treatment with 10 ng/ml TNF α for the indicated timepoints (4, 8, 10, 12, 16, 20, 24 and 48 hours). Cells that were subconfluent at the point of harvest, were fixed, stained with propidium iodide and percentage sub-G1 population (as a crude marker of cell death) assessed by flow cytometry. Results are mean \pm SD of a single experiment performed in technical triplicate. (E) The same clones were treated as in (D) and whole lysates prepared and Western blotted with the indicated antibodies. Data are from a single experiment. Significance testing was performed using two-way ANOVA (repeated measures) with Tukey post-hoc test. $P < 0.0001$ (***) . Qvd, QVD-OPH. p-, phospho-

Collectively, these results indicate that CRISPR-Cas9 mediated IKK α , IKK β and IKK α/β knockout was successful in the clones examined and that IKK α plays a significant role in canonical NF- κ B signalling in response to TNF α in HCT116 cells.

3.2.3 Re-expression of either IKK α or IKK β in IKK α/β DKO cells restores TNF α -inducible NF- κ B transcriptional activity

To investigate whether NF- κ B transcriptional activity could be restored to IKK α/β DKO cells, DKO cells were transfected with WT or catalytically inactive (kinase-dead, KD) IKK α or IKK β constructs and the effect of TNF α treatment examined via a luciferase reporter assay (Figure 3.10A). TNF α -dependent NF- κ B transcriptional activity was restored by the expression of either WT IKK α or IKK β , but not KD forms of these constructs. An additive effect of re-expression of both WT IKK α and IKK β was also observed. No conclusions could be made regarding the relative magnitudes of the NF- κ B responses restored by expression of IKK α and IKK β because the relative expression levels of IKK α and IKK β within this experiment were unknown given the lack of a corresponding set of Western blots. Attempts were made to generate lysates from cells transfected in 96 well plates, in a manner analogous to the experimental setup of the luciferase assay, however, it proved difficult to generate sufficient quantities of protein to run Western blots. The relative amounts of the different constructs transfected into the cells in 96 well format in Figure 3.10A were proportionally scaled down from equivalent experiments performed in 6-well plates, such as Figure 3.10B, which demonstrated a similar level of overexpression of IKK α and IKK β relative to their expression in WT cells, and an equal expression of WT relative to KD constructs. WT IKK α re-expression also rescued the reduced TNF α -induced NF- κ B activation observed in IKK α KO cells, whilst overexpression of WT IKK β had no effect. This further highlights the importance of IKK α in activating the canonical NF- κ B in response to TNF α in these cells.

Previous results in WT cells demonstrating a dominant negative effect of kinase inactive IKK β on the stimulus-induced activation NF- κ B have been used as evidence of the dominant involvement of IKK β over IKK α in canonical NF- κ B signalling. More recent evidence in IKK KO MEFs has demonstrated that kinase inactive IKK β also has a dominant negative effect on TNF α -induced canonical NF- κ B signalling in IKK β KO MEFs (Adli *et al.*, 2010), indicating that kinase inactive IKK β can block TNF α -induced IKK α activity. Consistent with these results, KD IKK β strongly inhibited TNF α -induced NF- κ B activation in WT cells and IKK β KO cells, and also inhibited the restored TNF α -inducible NF- κ B activation in DKO cells when co-expressed with WT IKK α . KD IKK β also inhibited the induction of NF- κ B in IKK α KO cells, indicating that KD IKK β acts in a dominant negative fashion towards both WT IKK β and IKK α . Interestingly, similar effects were also seen with KD IKK α . Kinase inactive IKK α inhibited the induction of NF- κ B in WT cells, albeit not to the same extent as KD IKK β . Remarkably, KD IKK α also inhibited the induction of NF- κ B in IKK α and IKK β KO cells, indicating that kinase inactive IKK α also acts in a dominant negative manner to inhibit the activity of both IKK α and IKK β . However, KD IKK α was repeatedly unable to inhibit the NF- κ B activity induced in DKO cells by co-expressed WT IKK β following TNF α treatment. This is difficult to reconcile with the observed inhibitory effect of KD IKK α on NF- κ B activation in IKK α KO cells, which is a seemingly analogous set of conditions. Why KD IKK α should be able to inhibit endogenous but not exogenously expressed IKK β is difficult to ascertain at this point. This result could be explained by a significantly higher overexpression of WT IKK β relative to KD IKK α , such that sufficient active WT IKK β homodimers were present to induce NF- κ B even in

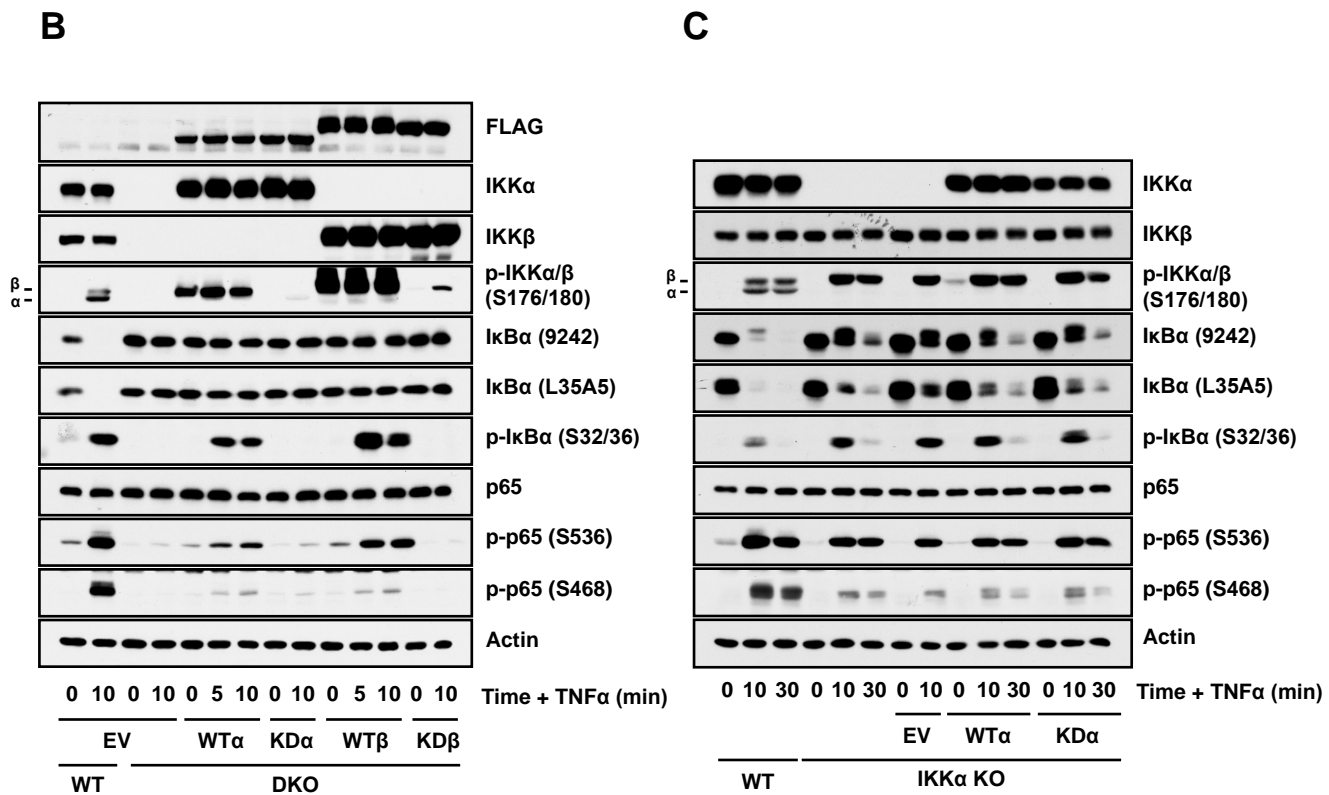
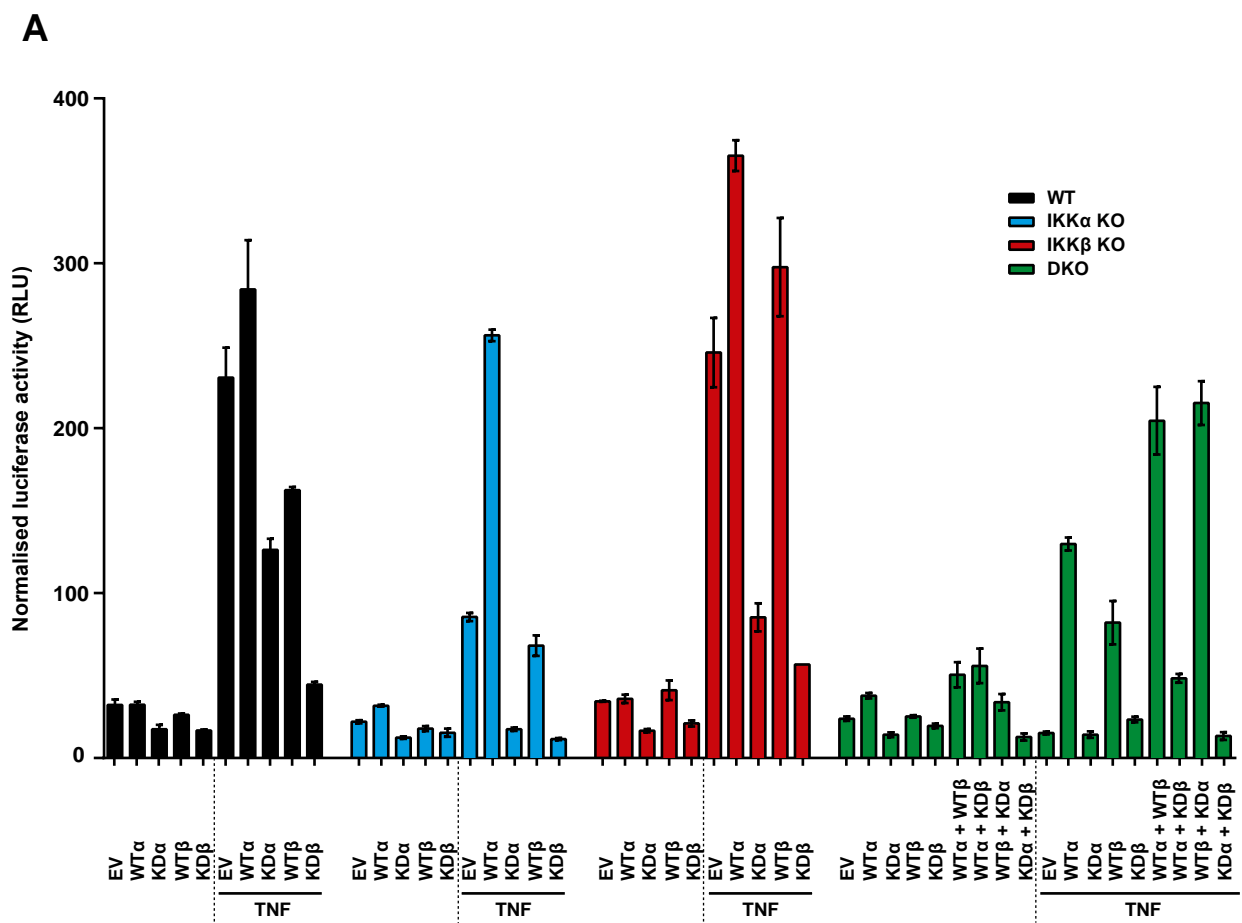


Figure 3.10. Reexpressing WT IKK restores WT-like NF- κ B transcriptional activity to IKK KO HCT116 cells, while kinase-dead (KD) IKK α and KD IKK β both act in a dominant-negative fashion. (A) WT (A3), IKK α KO (F6), IKK β KO (G9) and IKK α / β DKO (C8) HCT116 cells were transiently transfected with the indicated constructs: empty vector (EV), WT IKK α (WT α), KD IKK α (KD α), WT IKK β (WT β) and KD IKK β (KD β), in addition to 0.1 μ g pGL4.32[Luc2P/NF- κ B-RE firefly luciferase (reporter) plasmid DNA and 0.01 μ g renilla luciferase (internal control) plasmid DNA. The following day, cells were treated with 10 ng/ml recombinant TNF α for 4 hours. Firefly luciferase luminescence was normalised relative to renilla luciferase luminescence and data expressed as relative luciferase activity (luciferase/renilla activity), RLU (relative light units). Results are mean \pm SD of two independent experiments performed in technical triplicate. (B) WT and IKK α / β DKO HCT116 cells were transiently transfected with the following quantities of plasmid DNA: 0.28 μ g pCMV-Tag2B empty vector (EV), 0.19 μ g pCMV-Tag2B-WT IKK α , 0.28 μ g pCMV-Tag2B-KD IKK α (K44A), 0.15 μ g pCMV-Tag2B-WT IKK β and 0.26 μ g pCMV-Tag2B-KD IKK β (K44M). Total transfected plasmid DNA was equalized to 0.28 μ g with EV. 24 hours later, cells were treated with 10 ng/ml TNF α for 5 or 10 minutes. Whole-cell lysates were fractioned by SDS-PAGE and Western blotted with the indicated antibodies. Data are from a single experiment representative of two showing similar results. (C) WT and IKK α KO HCT116 cells were transiently transfected with the following quantities of plasmid DNA: 0.25 μ g pCMV-Tag2B empty vector (EV), 0.15 μ g pCMV-Tag2B-WT IKK α , 0.25 μ g pCMV-Tag2B-KD IKK α (K44A). Total transfected plasmid DNA was equalized to 0.25 μ g with EV. 24 hours later, cells were treated with 10 ng/ml TNF α for 10 or 30 minutes. Whole-cell lysates were fractioned by SDS-PAGE and Western blotted with the indicated antibodies. Data are from a single experiment. p-, phospho-.

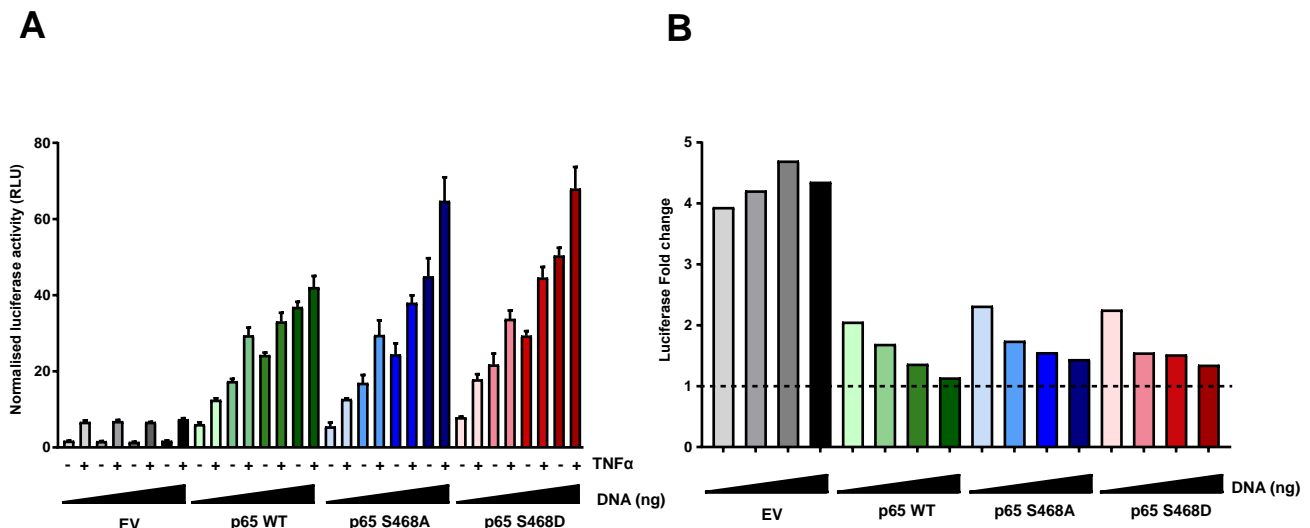


Figure 3.11. Overexpressed S468A p65 induces a moderately increased transcriptional response relative to WT p65. WT HCT116 cells were transiently transfected with increasing amounts (5 ng, 10 ng, 25 ng, 50 ng) of the indicated constructs: empty vector (EV), WT p65, S468A p65 and S468D p65, in addition to 0.1 μ g pGL4.32[Luc2P/NF- κ B-RE firefly luciferase (reporter) plasmid DNA and 0.01 μ g renilla luciferase (internal control) plasmid DNA. The following day, cells were treated with 10 ng/ml recombinant TNF α for 2 hours. Firefly luciferase luminescence was normalised relative to renilla luciferase luminescence and data expressed as relative luciferase activity (luciferase/renilla activity), RLU (relative light units). Plotted in (A) are mean normalised RLU \pm SD of one experiment performed in technical triplicate. Plotted in (B) are the same data, but showing the TNF α -induced fold changes in luciferase activity relative to the untreated state, which for each condition is represented by a dashed line at fold change = 1.

the presence of KD IKK α . Further experiments with better control of the relative expression levels of transfected constructs will be needed to investigate this.

Collectively, these results indicate that both IKK α and IKK β contribute to the induction of NF- κ B in response to TNF α under WT conditions, and that the activity of both IKK α and IKK β homodimers can be disrupted by either kinase-dead IKK α or IKK β .

IKK α/β DKO cells were transfected with equivalent amounts of IKK α and IKK β constructs as used in Figure 3.10A to examine the downstream signalling rescued by IKK re-expression (Figure 3.10B). Under these conditions, IKK β was overexpressed to a greater degree than IKK α . These levels of overexpression were sufficient to trigger the autocatalytic phosphorylation of both WT IKK α and IKK β in the absence of stimulus, an effect that has been previously reported (Li *et al.*, 2001). Despite this IKK autophosphorylation, no downstream IKK activity was observed in the absence of TNF α stimulation, either in the form of I κ B α or p65 phosphorylation. Surprisingly, upon TNF α treatment, both the re-expressed WT IKK α and IKK β phosphorylated I κ B α , however, no concomitant I κ B α degradation was observed. In fact, total I κ B α protein levels appeared completely unchanged. I κ B α phosphorylated at Serine 32/36 is normally tightly coupled to its ubiquitylation by the SCF- β -TRCP E3 ligase complex, which targets it for rapid proteasomal degradation, enabling its NF- κ B transcription factor binding partners to accumulate in the nucleus and activate transcription. This apparent uncoupling of I κ B α phosphorylation and degradation observed here was difficult, therefore, to reconcile with the observed induction of NF- κ B activity under these same conditions (Figure 3.10A), which indicated that transfected WT IKK α and IKK β constructs were capable of activating the NF- κ B pathway. The luciferase assay reports only on those cells that have been successfully transfected with constructs, both luciferase reporter and IKK, whereas the Western blot represents lysate from the entire population of cells, both transfected and untransfected. Therefore, it could be that the proportion of untransfected cells outweighs the proportion of transfected cells with degraded I κ B α , such that no significant difference is observed in the Western blot. However, the transfection efficiency under these conditions was confirmed to be approximately 60 %, which should be sufficient to observe some change in total I κ B α protein levels. Further experiments described in Chapter 4 examined the ubiquitylation of I κ B α under these conditions.

Re-expressed WT IKK α and IKK β also phosphorylated p65 at Serine 536 following TNF α treatment. The level of phosphorylation was higher in the case of IKK β , however, this could simply reflect the greater overexpression of IKK β compared to IKK α . Both WT IKK α and IKK β were able to partly restore TNF α -inducible phosphorylation of p65 at Serine 468, but the levels were much lower than those seen in WT cells. Furthermore, whereas the results described in Figure 3.6 suggested that IKK α might be the predominant kinase phosphorylating this site, re-expressed IKK α did not have a noticeably greater impact than IKK β on TNF α -inducible Serine 468 phosphorylation. To explore the sufficiency of IKK α for phosphorylation of Serine 468 further, WT or KD IKK α was expressed in IKK α KO cells (Figure 3.10C). Surprisingly, re-expressed WT IKK α had no effect on the phosphorylation of p65 at Serine 468, or on the phosphorylation and degradation of I κ B α . This again contrasts with the results of the NF- κ B-driven luciferase reporter assay, which indicated that re-expressed IKK α increases TNF α -inducible NF- κ B activation in IKK α KO cells. The only indications that the transfected WT IKK α construct

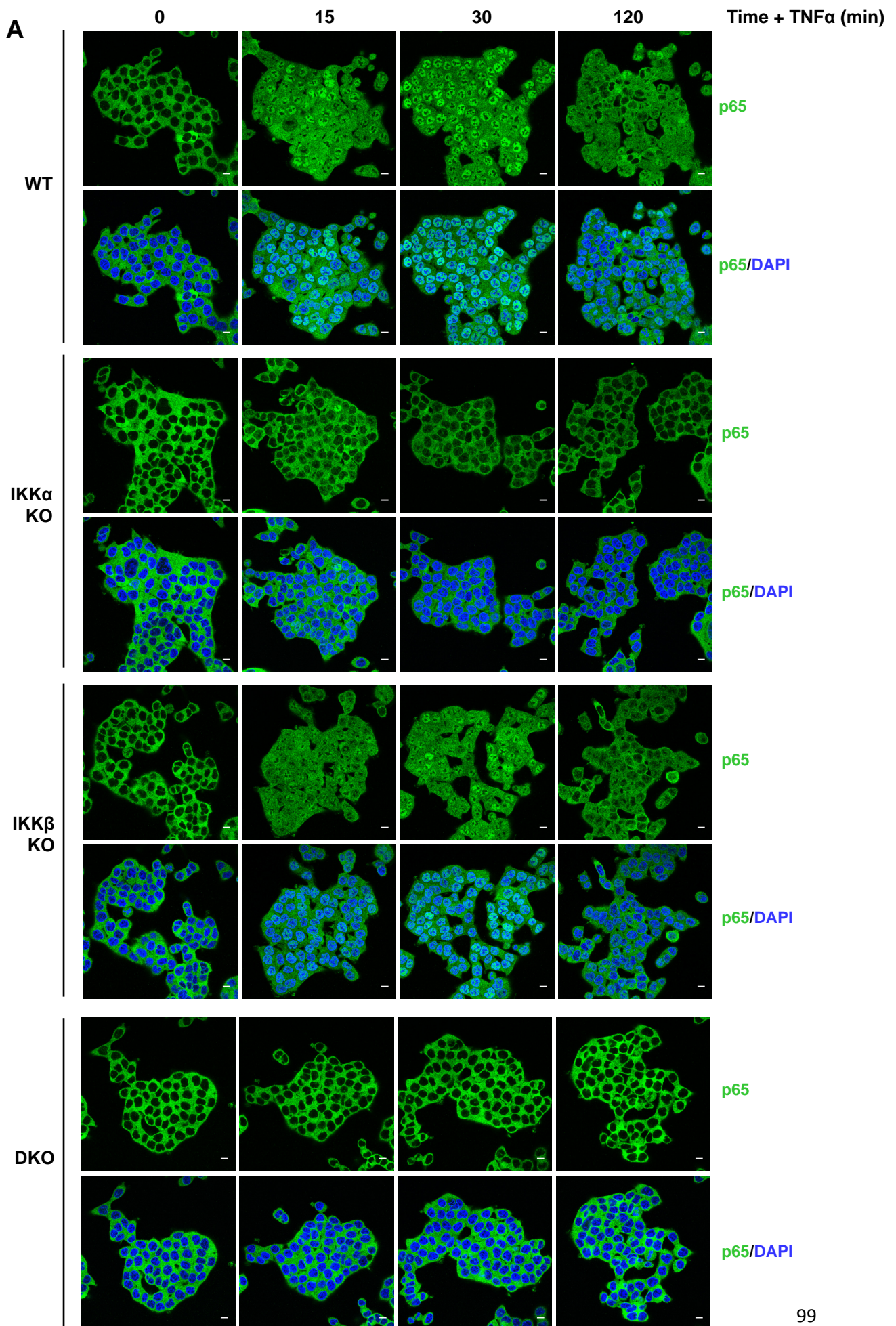
was catalytically active in this experiment was an increased basal phosphorylation of IKK α itself, and p65 at Serine 536, neither of which were observed following transfection with KD IKK α .

As we were unable to rescue the phosphorylation of Serine 468 with IKK α reexpression, we are currently only able to conclude that IKK α activity is necessary for efficient phosphorylation of p65 at Serine 468. Proof of sufficiency will require further experiments. What is clear, however, is that in HCT116 cells IKK β makes only a very small contribution to phosphorylation of this site in response to TNF α and IL-1 α .

The function of stimulus induced p65 phosphorylation at S468 is not as well characterised as that of Serine 536. Its IKK β -mediated phosphorylation was shown to have no effect on p65 nuclear translocation, but a small inhibitory effect on TNF α -induced NF- κ B activation was reported (Schwabe *et al.*, 2005). In a preliminary effort to explore the function of S468 phosphorylation in HCT116 cells, the effect of increased expression of WT, S468A and S468D p65 on untreated and TNF α -induced NF- κ B-dependent transcription was measured (Figure 3.11). All three forms of p65 increased transcription of the luciferase reporter in the absence of TNF α stimulus in a dose responsive manner (Figure 3.11A). However, the mutant forms induced a moderately increased transcriptional response, particularly at the highest amount of transfected DNA. The intended ‘phospho-mimetic’ S468D mutant exhibited similar results to the non-phosphorylatable S468A mutant, suggesting that S468D is actually behaving as a non-phosphorylatable mutant also. The mutant forms also potentially exhibited a slightly higher TNF α -induced fold change than WT p65 (Figure 3.11B). These results are from a single experiment, and we have not yet confirmed that these mutants express at similar levels to WT p65 in the cell, so the results are preliminary and not conclusive. However, the results are consistent with those of Schwabe *et al.*, 2005.

3.2.4 IKK α KO cells exhibit a greater defect in TNF α -induced p65 nuclear translocation than IKK β KO cells

IKK α KO cells exhibited a weaker TNF α -induced NF- κ B transcriptional response than WT or IKK β KO cells. To examine whether these differences were due to defects in the nuclear translocation of NF- κ B subunits, immunostaining for p65 and c-rel was performed in WT, IKK α KO, IKK β KO and IKK α / β DKO cells (Figure 3.12A and B, and Figure 3.13A and B). Representative confocal images demonstrated that in WT HCT116 cells, the vast majority of p65 was localised to the cytoplasm under basal conditions. Although, such static snapshots do not accurately represent the dynamic shuttling of inactive I κ B α :p65 complexes between the cytoplasm and nucleus (Huang *et al.*, 2000). Treatment with TNF α led to the rapid accumulation of p65 within the nucleus, with a peak nuclear localisation after around 30 minutes, followed by a progressive decline. Consistent with the results of the NF- κ B-driven luciferase reporter assay, IKK β KO cells exhibited a comparable p65 nuclear localisation response to TNF α stimulation as WT cells, whereas IKK α KO cells were severely defective at each of the time points examined. Meanwhile, IKK α / β DKO cells exhibited no p65 nuclear localisation in response to TNF α . These observations were quantified across three independent clones of each of the four genotypes; WT, IKK α KO, IKK β KO and IKK α / β DKO, through high-content image analysis (Figure 3.12B). The results confirmed what could be seen by eye; IKK α KO clones exhibited a strong statistically significant reduction in the TNF α -induced nuclear localisation of p65 compared to WT clones. The analysis also indicated that IKK β KO clones exhibited a less pronounced, but nonetheless statistically significant, defect relative to WT clones.



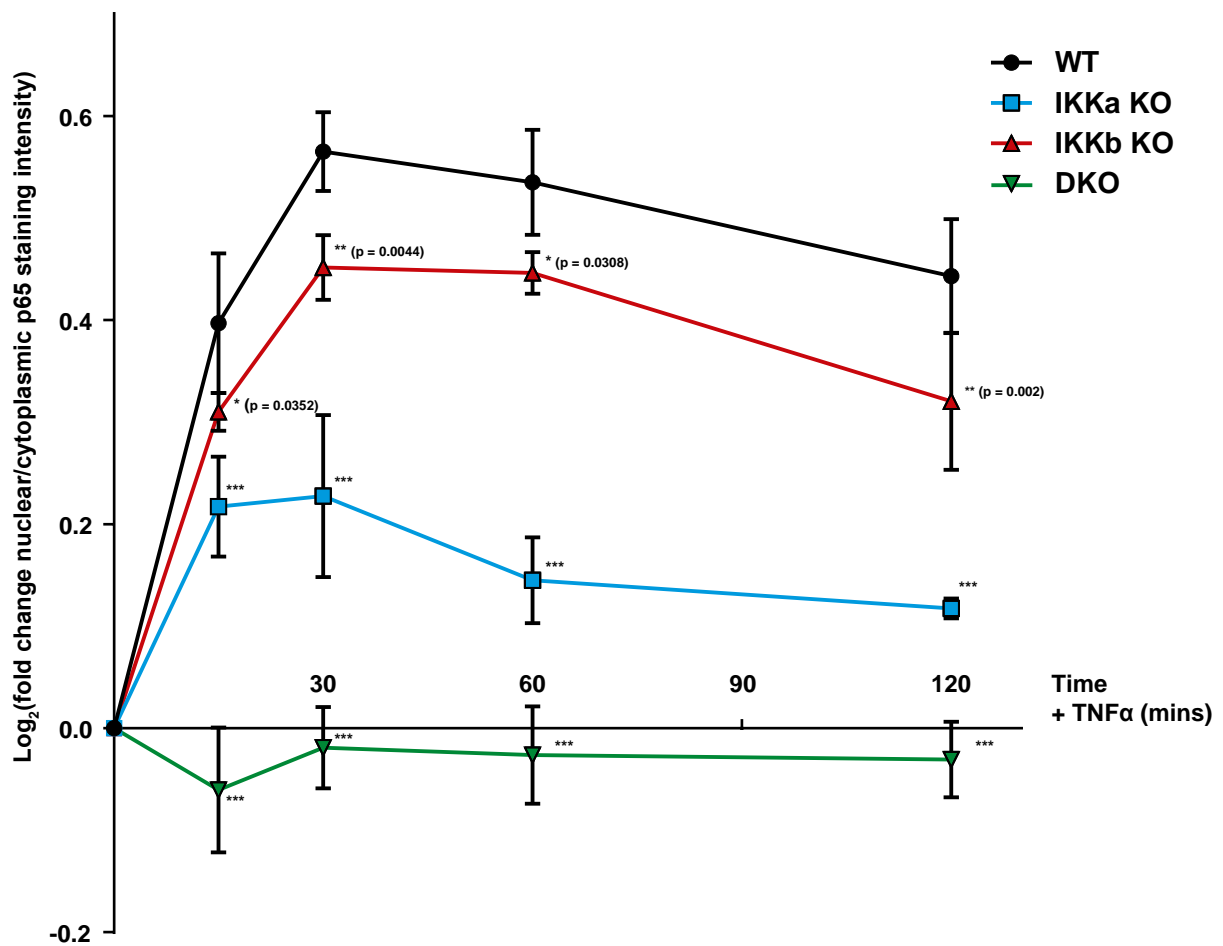
B

Figure 3.12. IKK α KO HCT116 cells exhibit a greater defect in TNF α -induced p65 nuclear translocation than IKK β KO cells. (A) WT, IKK α KO, IKK β KO and IKK α / β DKO HCT116 cells were seeded in normal growth medium for 48 hours, prior to treatment with 10 ng/ml recombinant TNF α for the indicated timepoints (15, 30, and 120 min). Immunofluorescence staining of cells was performed with anti-p65 (green) and nuclei with DAPI (blue). (B) WT, IKK α KO, IKK β KO and IKK α / β DKO HCT116 cells were seeded in 96 well plates in normal growth medium for 48 hours, prior to treatment with 10 ng/ml recombinant TNF α for the indicated timepoints (15, 30, and 120 min). Cells were stained with anti-p65 and nuclei with DAPI and confocal images captured across 30 non-overlapping fields-of-view per well using the In Cell Analyzer 6000 high-content imaging system (20x objective). p65 staining intensity analysis was performed using CellProfiler software. Data presented as the \log_2 transformed fold change in nuclear:cytoplasmic p65 staining intensity. Data are mean \pm SD of three independent CRISPR-Cas9 KO clones. Significance testing performed using two-way ANOVA (repeated measures) with Dunnett post-hoc test. $P < 0.0001$ (**). Scale bar, 10 μ m

Interestingly, when the analysis was repeated with an antibody specific to another NF- κ B subunit, c-Rel, the defect in TNF α -induced nuclear localisation relative to WT clones was comparable between IKK α KO and IKK β KO clones (Figure 3.13A and B). Once again, IKK α/β DKO cells exhibited no c-Rel nuclear localisation in response to TNF α .

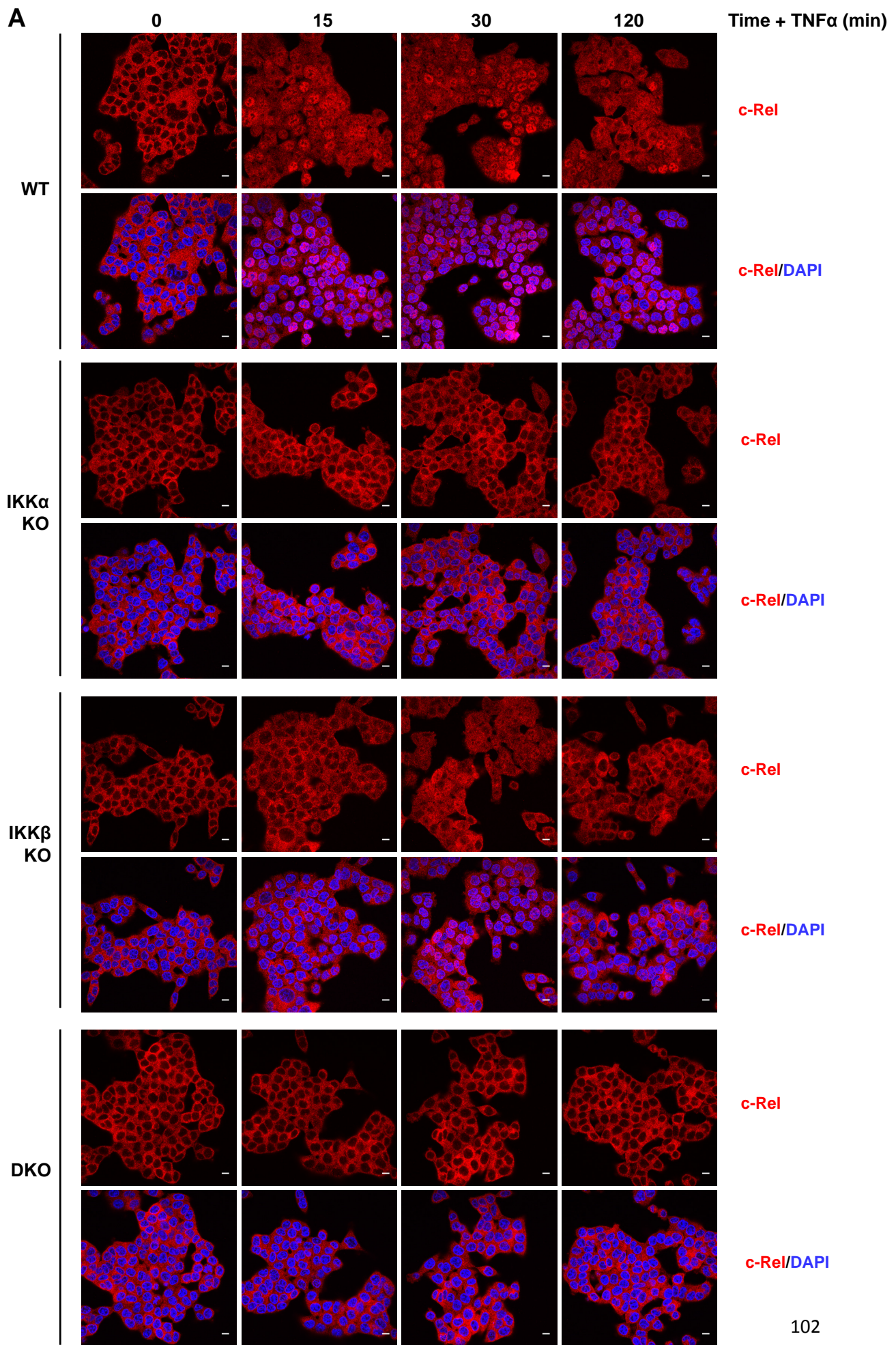
Subcellular fractionation was performed to gain more insight into this apparent differential effect of IKK KO on TNF α -induced nuclear localisation of p65 and c-Rel (Figure 3.14A and B). The cytoplasmic and nuclear fractions were well resolved, as judged by the enrichment of the cytoplasmic and nuclear fraction markers, β -tubulin and Lamin A/C, respectively. Consistent with the p65 immunofluorescence analysis, IKK α KO cells exhibited a drastically reduced TNF α -induced nuclear translocation of p65 relative to WT cells. In contrast, the p65 nuclear translocation observed in IKK β KO cells was more comparable to that seen in WT cells. As before, the caveat here is that the lysates were not run on the same gel. However, the same amount of protein was loaded on each set of gels, the exposure times were identical between the two set of experiments, and the relative protein differences are large enough to be confident that they reflect a genuine biological difference. On the other hand, the TNF α -induced nuclear translocation of c-Rel was defective to approximately the same level in IKK α KO and IKK β KO cells relative to WT, thus confirming the immunofluorescence results. The greater defect in p65 nuclear translocation in IKK α KO cells relative to IKK β KO cells did not appear to be a consequence of a greater defect in I κ B α degradation; as previously observed the defect in TNF α -induced I κ B α degradation was comparable between the two different IKK KO cells. Some other factor, such as reduced IKK α -dependent p65 phosphorylation must explain this difference.

Previous studies have reported a significant proportion of full length IKK α localised to the nucleus of HCT116 cells (Margalef *et al.*, 2012), while others have reported TNF α -inducible nuclear translocation of IKK α (Anest *et al.*, 2003). A proportion of full length IKK α was detected in the nucleus of WT HCT116 cells, but only after over exposure of the blot (Figure 3.15A). This nuclear localisation was confirmed, however, through immunostaining (Figure 3.15B). However, no increase in nuclear translocation of IKK α after TNF α treatment was observed (Figure 3.15A).

Collectively, these results demonstrate that IKK α and IKK β KO cells are similarly defective in TNF α -induced nuclear translocation of c-Rel, whereas IKK α KO cells exhibit a greater defect in p65 nuclear translocation. This is likely to be a major factor accounting for the reduced TNF α -inducible NF- κ B transcriptional activation observed in IKK α KO cells.

3.2.5 Loss of IKK α is also more detrimental to IL-1 α induced NF- κ B signalling than loss of IKK β

The relative importance of IKK α and IKK β in the activation of canonical NF- κ B signalling has been shown to depend, under certain circumstances, on the cytokine stimulating the pathway (Sizemore *et al.*, 2002; Solt *et al.*, 2007). To investigate the generality of the apparent importance of IKK α in canonical NF- κ B signalling in HCT116 cells, the effect of IKK knockout on the response to another inflammatory cytokine, IL-1 α , was examined (Figure 3.16). As with TNF α , both IKK α and IKK β KO cells, but not IKK α/β DKO, cells responded to IL-1 α to activate the canonical NF- κ B pathway. The degradation of I κ B α in response to IL-1 α was less effective in IKK α KO cells



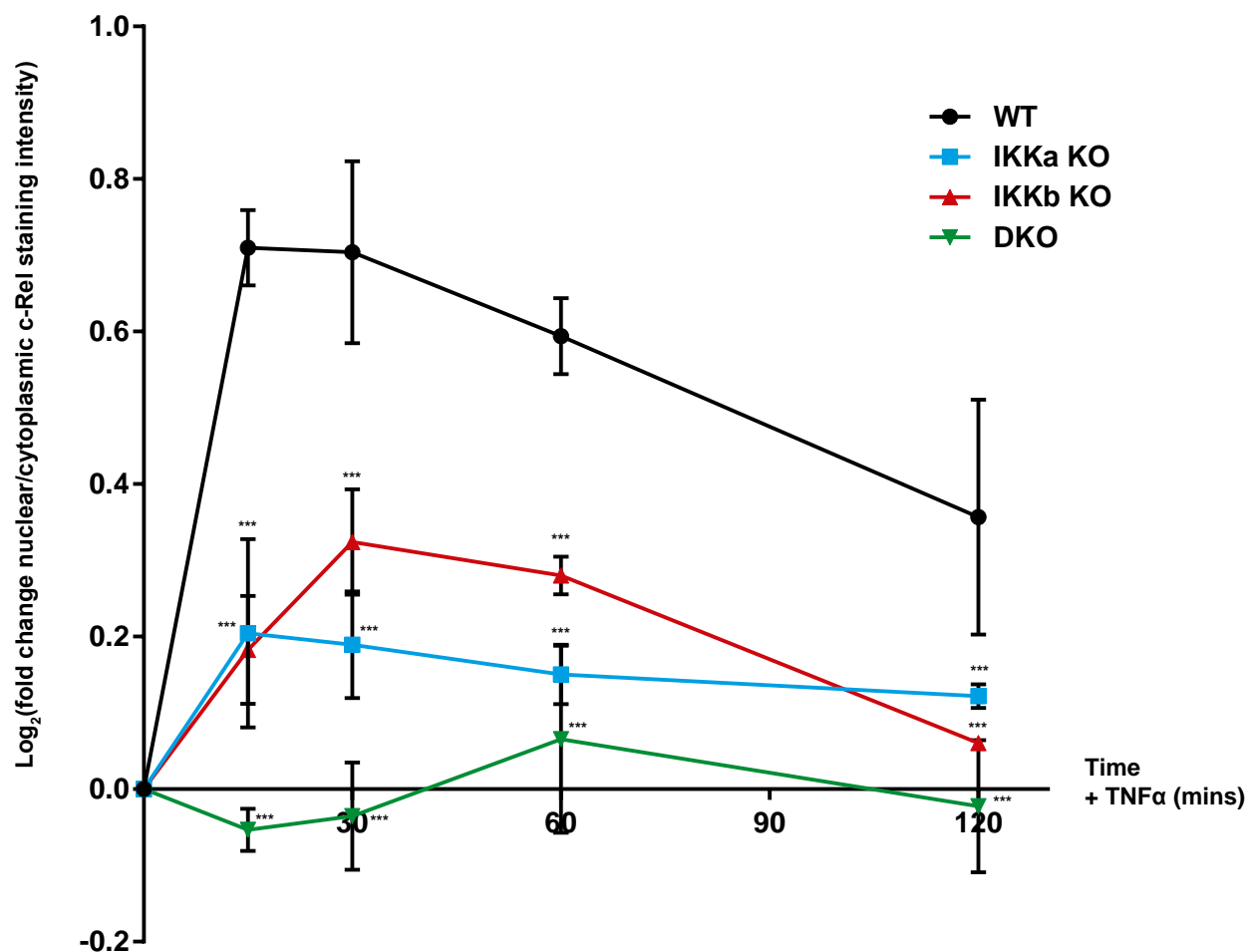
B

Figure 3.13. IKK α KO and IKK β KO cells exhibit similar defects in TNF α -induced c-Rel nuclear translocation. (A) WT, IKK α KO, IKK β KO and IKK α / β DKO HCT116 cells were seeded in normal growth medium for 48 hours, prior to treatment with 10 ng/ml recombinant TNF α for the indicated timepoints (15, 30, and 120 min). Immunofluorescence staining of cells was performed with anti-c-Rel (red) and nuclei with DAPI (blue). (B) WT, IKK α KO, IKK β KO and IKK α / β DKO HCT116 cells were seeded in 96 well plates in normal growth medium for 48 hours, prior to treatment with 10 ng/ml recombinant TNF α for the indicated timepoints (15, 30, and 120 min). Cells were stained with anti-c-Rel and nuclei with DAPI and confocal images captured across 30 non-overlapping fields-of-view per well using the In Cell Analyzer 6000 high-content imaging system (20x objective). c-Rel staining intensity analysis was performed using CellProfiler software. Data presented as the log₂ transformed fold change in nuclear:cytoplasmic p65 staining intensity. Data are mean \pm SD of three independent CRISPR-Cas9 KO clones. Significance testing performed using two-way ANOVA (repeated measures) with Dunnett post-hoc test. $P < 0.0001$ (***)

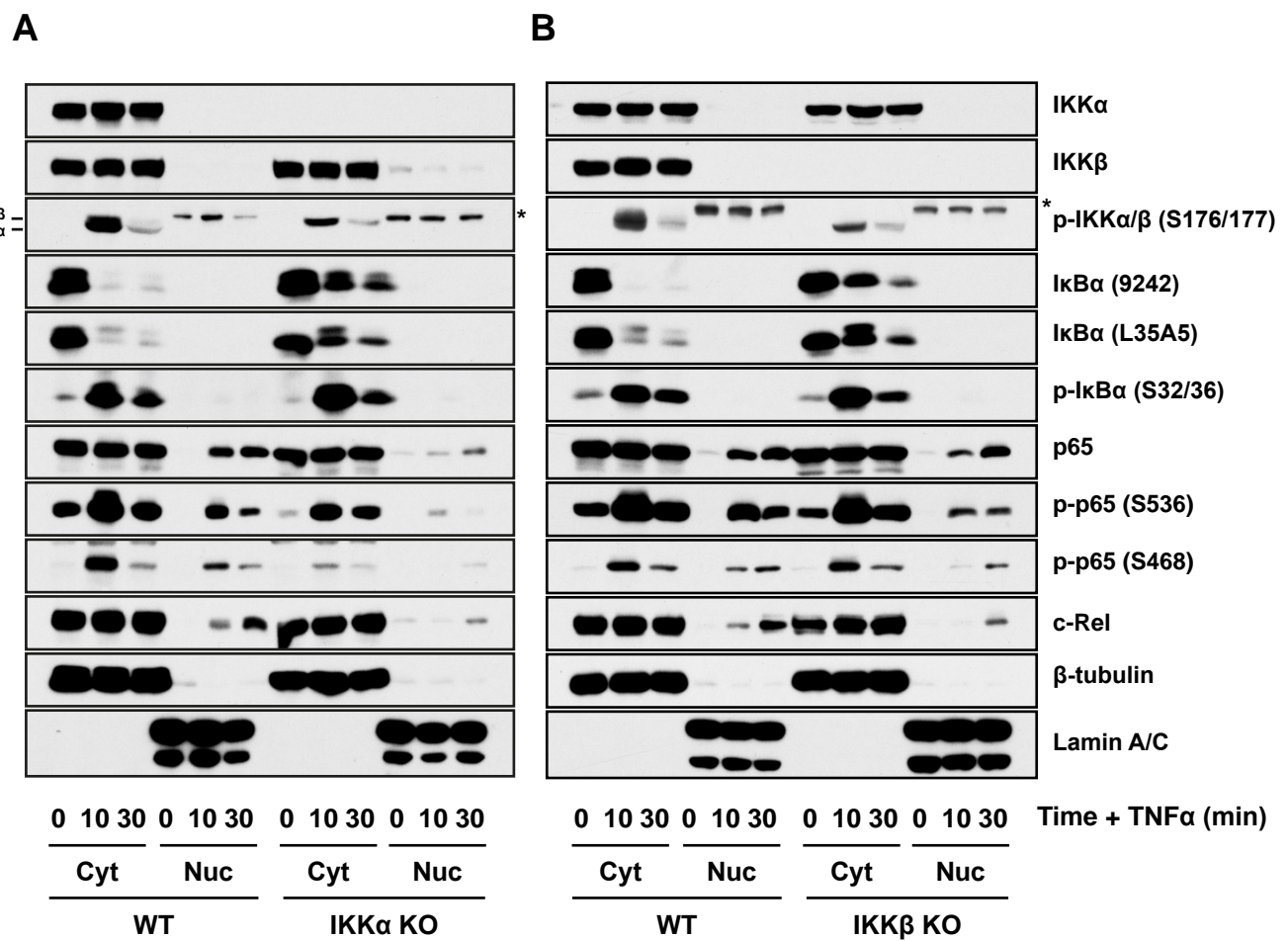


Figure 3.14. IKK α KO and IKK β KO have differential effects on TNF α -induced nuclear translocation of p65 and c-Rel. (A) WT and IKK α KO, and (B) WT and IKK β KO HCT116 cells were seeded in normal growth medium for 48 hours prior to treatment with 10 ng/ml TNF α for the indicated timepoints (10 and 30 minutes). Cytoplasmic (cyt) and nuclear (nuc) lysate fractions were prepared and Western blotted with the indicated antibodies. β -tubulin and Lamin A/C were used as markers of the cytoplasm and nucleus, respectively. Data are from a single experiment representative of two showing similar results. p-, phospho- *unknown band.

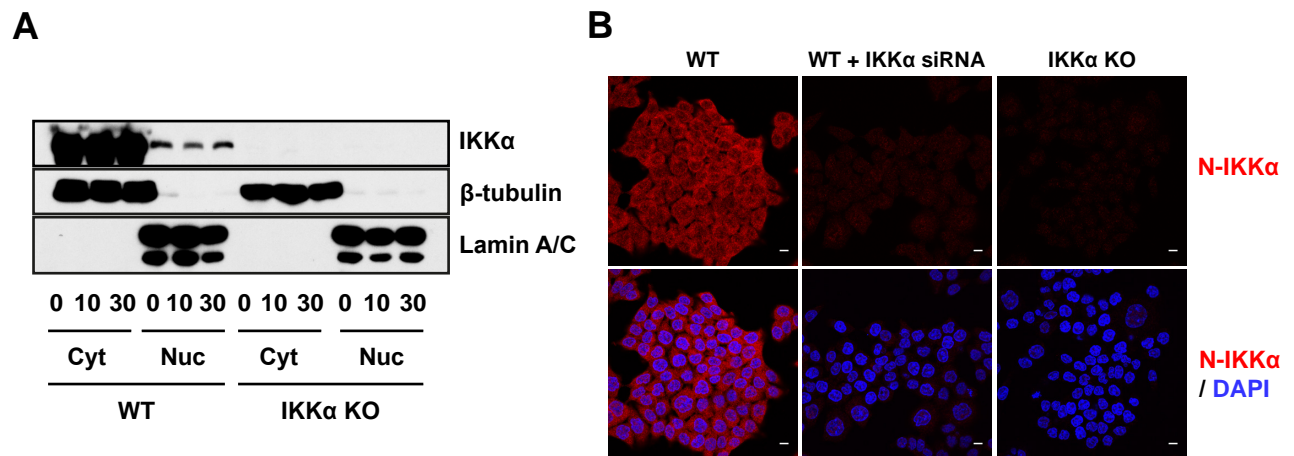


Figure 3.15. A proportion of IKK α localises to the nucleus of WT HCT116 cells. (A) WT and IKK α KO HCT116 cells were seeded in normal growth medium for 48 hours prior to treatment with 10 ng/ml TNF α for the indicated timepoints (10 and 30 minutes). Cytoplasmic (cyt) and nuclear (nuc) lysate fractions were prepared and Western blotted with the indicated antibodies. (B) WT and IKK α KO HCT116 cells were seeded prior to treatment of WT cells with 20 nM siRNA targeted against IKK α . Immunofluorescence staining of cells was performed with anti-IKK α (N-terminal Ab) (red) and nuclei with DAPI (blue). Scale bar, 10 μ m.

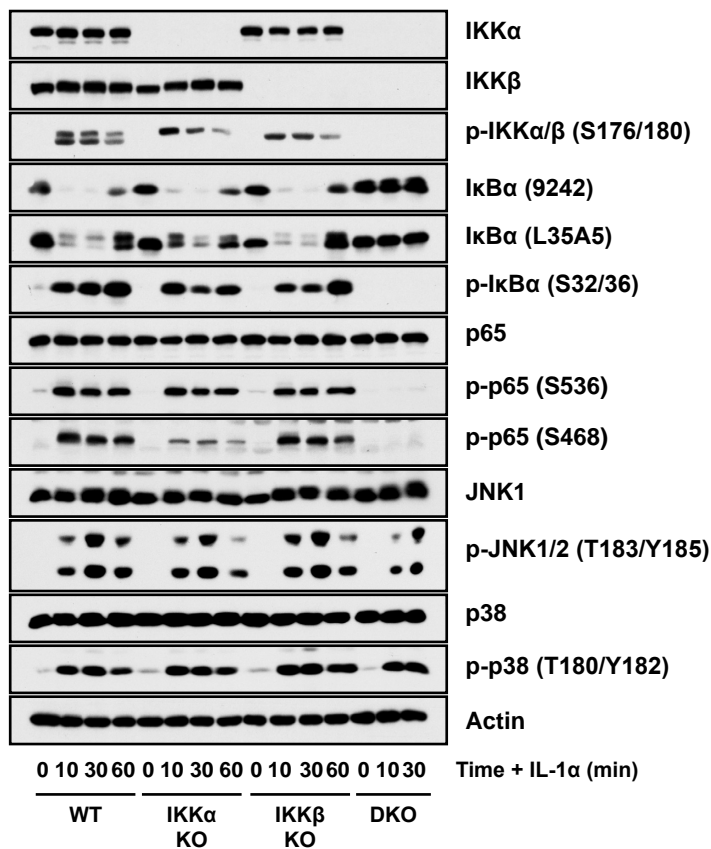
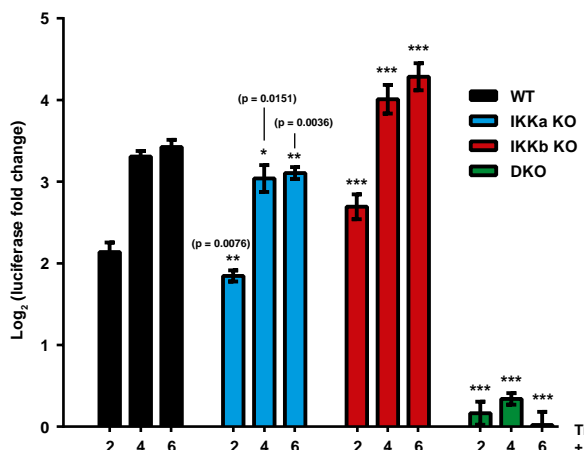
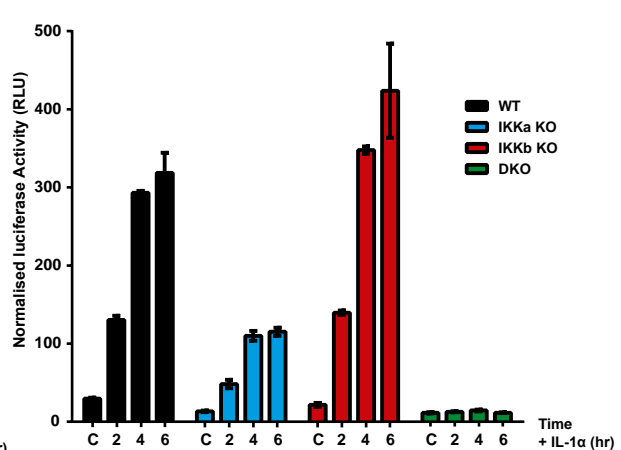
A**B****C**

Figure 3.16. IKK KO has similar effects on the signalling response to IL-1 α as it does for TNF α . (A) WT (A3), IKK α KO (F6), IKK β KO (G9) and IKK α/β DKO (C8) HCT116 cells were seeded in their normal growth medium for 48 h, prior to treatment with 25 ng/ml recombinant IL-1 α for the indicated timepoints (10, 30 and 60 minutes). Whole cell extracts were prepared, fractionated by SDS-PAGE and Western blotted with the indicated antibodies. Data are from a single experiment. (B and C) The same clones as in (A) were seeded in antibiotic-free growth medium overnight prior to transient transfection with 0.1 μ g pGL4.32[Luc2P/NF- κ B-RE firefly luciferase (reporter) plasmid DNA and 0.01 μ g renilla luciferase (internal control) plasmid DNA. The following day, cells were treated with 25 ng/ml recombinant TNF α for the indicated time periods (2, 4 and 6 hours). Firefly luciferase luminescence was normalised relative to renilla luciferase luminescence and data expressed as \log_2 (fold change in IL-1 α -induced luciferase activity relative to the relevant, matched untreated condition). Results are mean \pm SD of three independent experiments, each of which was performed with the same clones as in (A), seeded in technical triplicate. Significance testing was performed using two-way ANOVA (repeated measures) with Tukey post-hoc test. $P < 0.0001$ (***)-, phospho-.

compared to WT or IKK β KO cells, although the difference was marginal. Similar to TNF- α , the IL-1 α induced phosphorylation of p65 at Serine 536 was largely unaffected by either IKK α or IKK β KO, while basal phosphorylation at this site was reduced in IKK α KO cells. Furthermore, IL-1 α induced a lower level of p65 Serine 468 phosphorylation in IKK α KO cells, while IKK β KO cells were largely unaffected. Unlike TNF α , however, IKK KO had no effect on the phosphorylation of JNK or p38 in response to IL-1 α .

IKK α KO also had a similar effect on IL-1 α induced NF- κ B transcriptional activation (Figure 3.16B and C); the fold increase in NF- κ B transcriptional activity was significantly lower in IKK α KO cells relative to WT. Unlike TNF α , however, the transcriptional response to IL-1 α was significantly enhanced in IKK β KO cells relative to WT. As expected, IKK α/β DKO exhibited no response to IL-1 α stimulation. Consistent with these results, IKK β KO cells exhibited no apparent defect in IL-1 α induced p65 nuclear translocation, whereas IKK α KO cells were severely defective relative to WT cells (Figure 3.17).

Collectively, these results indicate that, in a manner similar to TNF α , IKK α is less dispensable than IKK β for the induction of canonical NF- κ B signalling in response to IL-1 α in HCT116 cells.

3.2.6 IKK knockout has differential effects on the activation of AKT signalling following sustained TNF α treatment

The NF- κ B pathway has been shown to promote EMT in a range of cancers, including colorectal (Huber *et al.*, 2004; Wu *et al.*, 2009; Wang *et al.*, 2014a; Pires *et al.*, 2017). A hallmark of EMT is loss of E-cadherin expression (Chapter 1, Section 1.1.3). One of the numerous mechanisms by which the NF- κ B pathway may induce EMT is through the transcriptional upregulation and stabilisation of the transcription factor, Snail; which is a key transcriptional repressor of E-cadherin (Julien *et al.*, 2007; Wu *et al.*, 2009). NF- κ B has also been shown to induce the EMT-promoting transcription factors Zeb1 and TWIST, and to directly repress E-cadherin expression itself (Chua *et al.*, 2007; Li *et al.*, 2012). In colorectal cancer specifically, cross-talk between the AKT pathway and the NF- κ B pathway appears to be important in coordinating the EMT process (Julien *et al.*, 2007; Wang *et al.*, 2013; Suman *et al.*, 2014). GSK3 β has been shown phosphorylate Snail and target it for ubiquitin-dependent proteasomal degradation. AKT-dependent phosphorylation (at Serine 9) and inhibition of GSK3 β results in the stabilisation, nuclear localisation and hence activation of Snail, which in turn represses E-cadherin to promote EMT (Zhou *et al.* 2004). NF- κ B has also been proposed to be activated downstream of AKT, via phosphorylation and activation of IKK α , providing an additional mechanism by which Snail is upregulated and stabilised (Julien *et al.*, 2007). Conversely, TNF α has been shown to activate AKT/GSK3 β signalling in gastric and colorectal cancer cells (Oguma *et al.*, 2008; Wang *et al.*, 2013), and in the case of the latter this has been shown to lead to the stabilisation of Snail (Wang *et al.*, 2013). However, the mechanism by which TNF α activates AKT under these circumstances has not been elucidated. Indeed, other than in endothelial cells, the AKT pathway is not recognised as a classic downstream target of TNF α signalling in most cell types (Madge *et al.*, 2000).

The known involvement of TNF α signalling in the induction of EMT provided a rationale to investigate the effects of sustained (96 hours) TNF α treatment on IKK α and IKK β KO cells; of particular interest were potential NF- κ B-independent effects of IKK α and/or IKK β on the induction of EMT (Figure 3.18A). Consistent with its more epithelial-like morphology and increased E-cadherin immunostaining (Figure 3.3A and B), the IKK α/β DKO clone

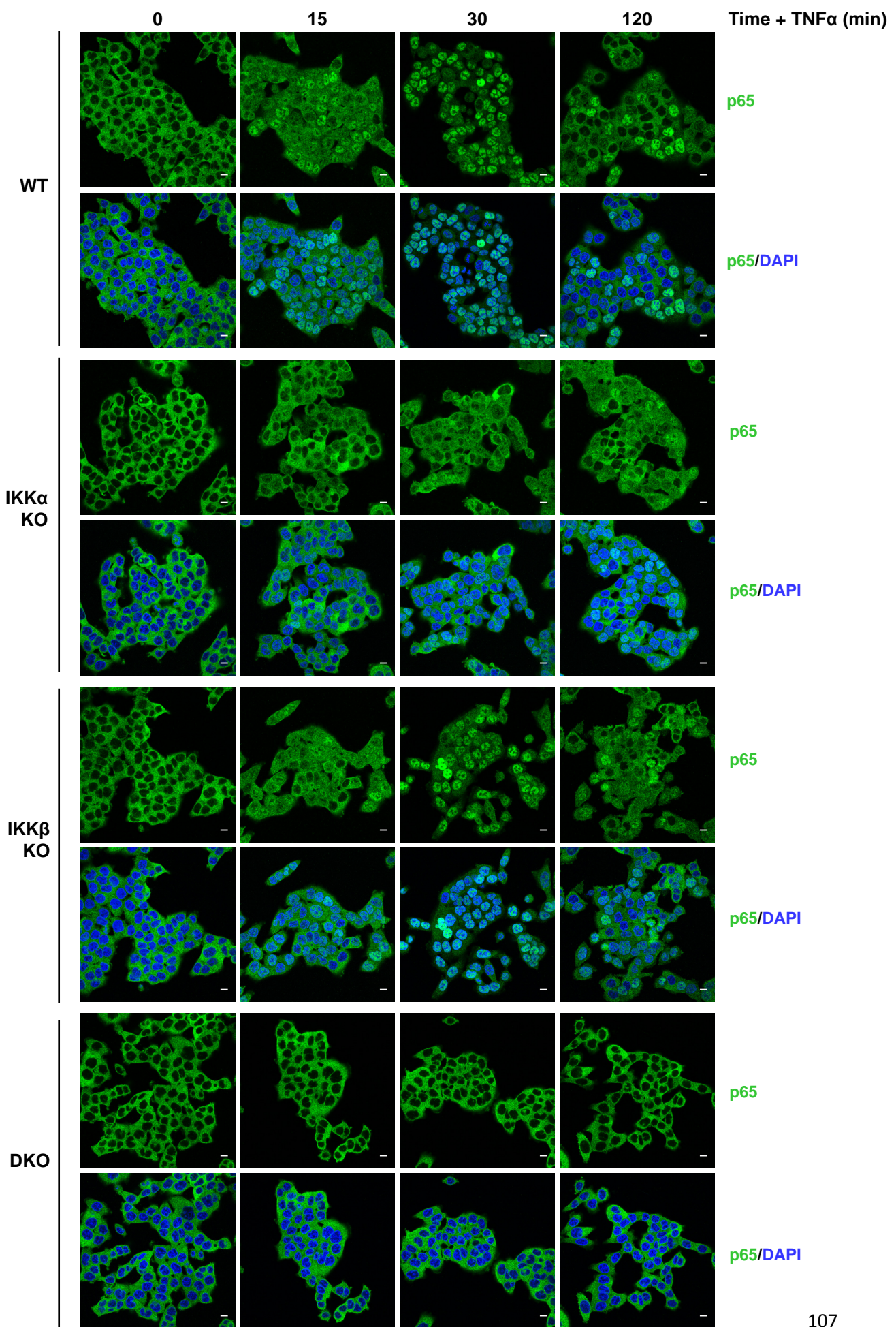


Figure 3.17. IKK α KO cells exhibit a greater defect in IL-1 α -induced p65 nuclear translocation than IKK β KO cells. WT (A3), IKK α KO (F6), IKK β KO (G9) and IKK α/β DKO (C8) HCT116 cells were seeded in normal growth medium for 48 hours, prior to treatment with 25 ng/ml recombinant IL-1 α for the indicated timepoints (15, 30, and 120 min). Immunofluorescence staining of cells was performed with anti-p65 (green) and nuclei with DAPI (blue). Scale bar, 10 μ m.

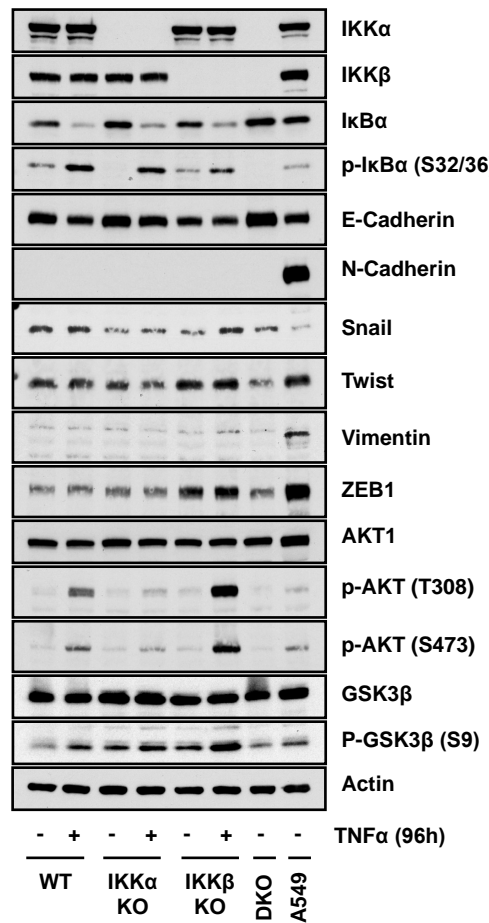
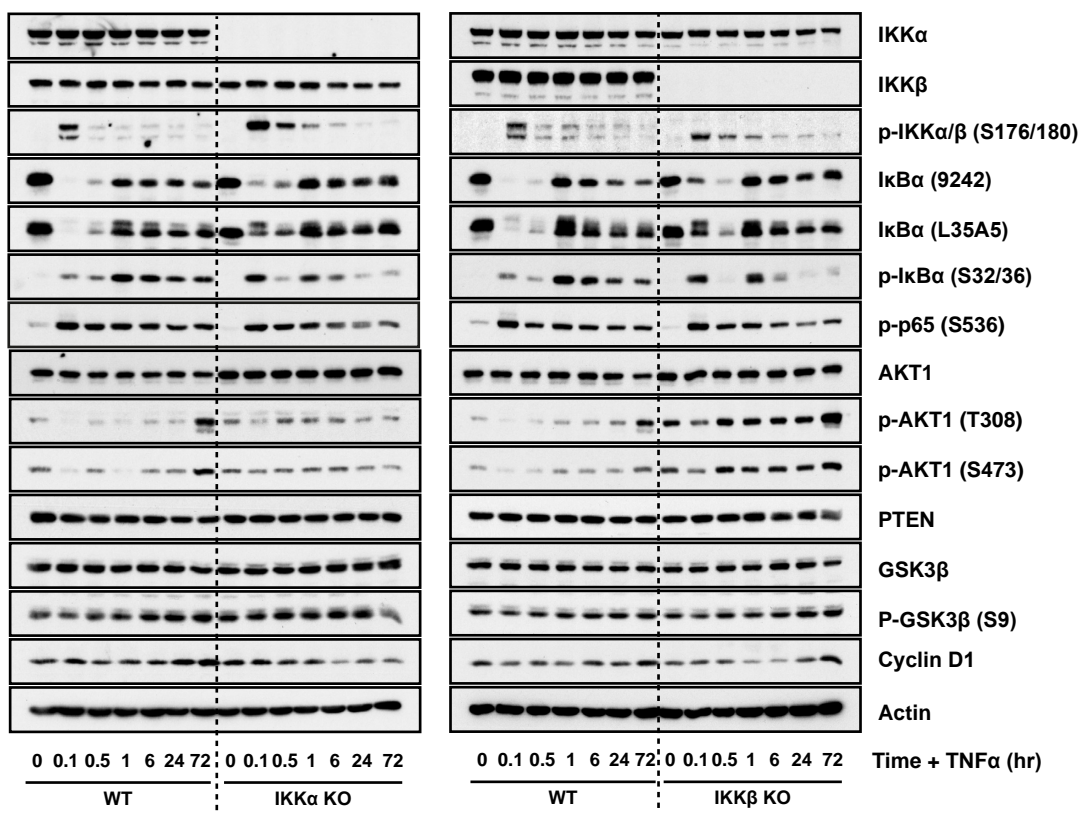
(C8) expressed higher levels of E-cadherin protein. The IKK β clone examined (G9) exhibited a lower expression of E-cadherin than the WT (A3) or IKK α KO (F6) clones, again consistent with the E-cadherin immunostaining results. Interestingly, the IKK β clone also exhibited higher basal expression of Twist and Zeb1, two transcription factors that regulate the transcription of E-cadherin. Similar levels of Twist and Zeb1 expression were observed in the mesenchymal-like breast cancer cell line, A549. In response to TNF α , the WT clone exhibited a decrease in the expression of E-cadherin, consistent with the induction of EMT. However, the expected stabilisation of Snail was marginal, if present at all. The IKK α KO clone exhibited a lower basal expression of Snail than the WT cells and also failed to induce Snail in response to TNF α . The TNF α -induced repression of E-cadherin was also less pronounced in IKK α KO cells than WT cells. An increase in Snail and concomitant decrease in E-cadherin expression was, however, observed in IKK β KO cells. The expression of Twist and Zeb1 was unaffected by TNF α . N-cadherin and vimentin are two mesenchymal markers that are commonly induced during EMT (Nieman *et al.*, 1999; Mendez *et al.*, 2010). Indeed, the switch from E-cadherin to N-cadherin expression is a hallmark of EMT (Tomita *et al.*, 2000; Hazan *et al.*, 2004). Contrary to previous reports in colorectal cancer cells, no induction of these markers was observed in response to TNF α (Wang *et al.*, 2013).

Interestingly, the WT and IKK KO clones exhibited differences in TNF α -induced activation of AKT (Figure 3.18A). AKT is activated in part by activation loop phosphorylation at Threonine 308 by PDK1 (Alessie *et al.*, 1996), and phosphorylation at Ser473 by mTORC2 (Sarbassov *et al.*, 2005; Jacinto *et al.*, 2006). In turn, activated AKT phosphorylates GSK3 β at Serine 9 to inhibit its activity (Cross *et al.*, 1995). AKT was phosphorylated at Thr308 and Ser473 in WT cells following TNF α treatment, which in turn led to an increased phosphorylation of GSK3 β . The activation of AKT was drastically reduced in the IKK α KO clone and no increase in GSK3 β phosphorylation was observed, although a higher basal phosphorylation of GSK3 β was observed relative to WT cells. In contrast, the phosphorylation of AKT was dramatically enhanced in the IKK β KO clone relative to WT cells. The basal phosphorylation of GSK3 β was again higher in IKK β KO cells than WT, but an increase was clearly observed following TNF α treatment.

One caveat with this data is that the effect of long-term TNF α treatment has only been explored for one independent clone representative of each genotype; WT, IKK α KO and IKK β KO. Given the morphological heterogeneity of the KO clones, further work will be needed to confirm the generality of these observations to other KO clones and to rule out clone-specific effects.

To assess the kinetics of the activation of AKT downstream of TNF α signalling, a timecourse of TNF α treatment over 72 hours was performed in WT, IKK α KO and IKK β KO clones (Figure 3.18B and C). TNF α treatment led to an increased, and more sustained, phosphorylation of IKK β in the IKK α KO clone compared to in the WT clone; it took between 6 and 24 hours for the phosphorylation of IKK β observed in IKK α KO cells to decrease to the level observed after 30 minutes in WT cells. Although less striking, a somewhat enhanced and more sustained phosphorylation of IKK α was also observed in the IKK β clone compared to the WT clone.

In WT cells the TNF α -induced degradation of I κ B α occurred in biphasic manner. There was a rapid TNF α -induced degradation phase, before I κ B α protein levels were restored after 1 hour post-treatment. A second slower phase of I κ B α degradation between 1 and 72 hours was also observed. This has been observed before in colorectal cancer cells (Colleran *et al.*, 2011). The first phase of degradation is proteasome-dependent, while the second is

A**B****C**

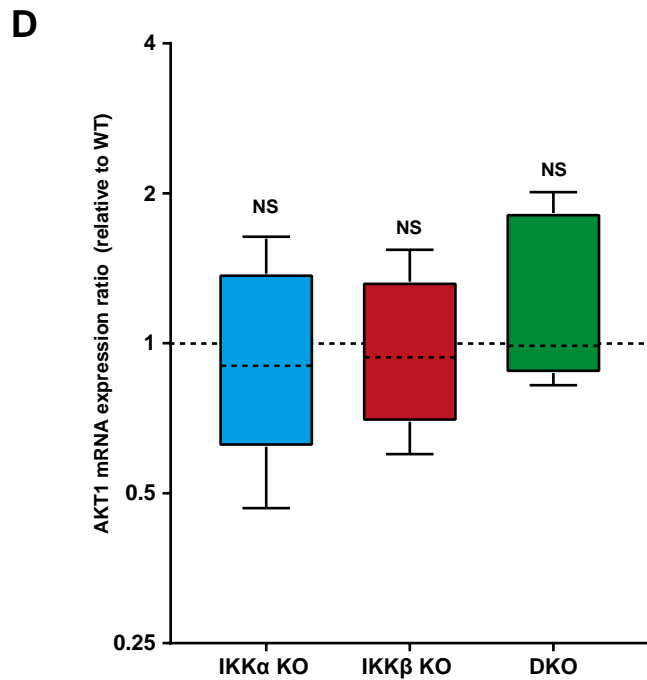


Figure 3.18. IKK α KO and IKK β KO have differential effects on AKT signalling induced by TNF α . (A) WT (A3), IKK α KO (F6), IKK β KO (G9) and IKK α / β DKO (C8) HCT116 cells were seeded in normal growth medium for 24 hours, prior to treatment with 10 ng/ml recombinant TNF α or vehicle control (-) for 96 hours. A549 cells were included as a positive control for a mesenchymal-like cell type. Whole cell extracts were prepared, fractionated by SDS-PAGE and Western blotted with the indicated antibodies. Data are from a single experiment. (B) WT (A3) and IKK α KO (F6) or (C) WT (A3) and IKK β KO (G9) HCT116 cells were seeded in normal growth medium for 24 hours, prior to treatment with 10 ng/ml recombinant TNF α for the indicated timepoints (10 min, 30 min, 1, 6, 24 and 72 hours). Whole cell extracts were prepared, fractionated by SDS-PAGE and Western blotted with the indicated antibodies. Data are from a single experiment. (D) Three independently derived WT clones and three clones each of IKK α single, IKK β single and IKK α / β double knockout were seeded in normal growth medium for 48 hours prior to RNA extraction. Relative AKT1 mRNA expression was determined by RT-qPCR, with normalisation to the geometric mean of the reference gene (*YWHAZ* and *UBC*) expression. Expression ratios are plotted on a logarithmic scale as median AKT1 expression ratios relative to the WT control samples (expression of which is represented by dotted line at expression ratio = 1). Boxes represent the interquartile range. Whiskers represent the minimum and maximum observations. NS, no significant difference between sample and control group. p-, phospho-

proposed to be autophagosome-dependent. Interestingly, the second phase of $\text{I}\kappa\text{B}\alpha$ degradation was less apparent in IKK α or IKK β KO cells. Furthermore, less $\text{I}\kappa\text{B}\alpha$ was in the phosphorylated form at timepoints later than 1 h in IKK α or IKK β KO cells compared to WT. This indicates, that both phases of $\text{I}\kappa\text{B}\alpha$ degradation and NF- κB activation are defective in IKK α and IKK β KO cells. In addition, the phosphorylation of p65 at Serine 536 in response to TNF α was more transient in IKK α and IKK β KO cells than in WT cells. This is despite the prolonged phosphorylation of the IKK subunits in the KO cell lines.

Surprisingly, both the IKK α KO and IKK β KO cells expressed higher levels of AKT1 protein than the WT cells; an observation that was clearer here than in Figure 3.18A. This observation was not pursued any further, beyond confirming that this did not reflect a reduction in AKT1 mRNA expression in IKK KO cells (Figure 3.18D). Regarding the phosphorylation status of AKT, TNF α induced an initial rapid decrease in the phosphorylation of AKT at Threonine 308 and Serine 473 below basal levels in WT and IKK β cells, but not IKK α KO cells. This then rebounded back to basal levels, before increasing drastically after 72 hours TNF α treatment. As observed in Figure 3.18A, the level of phosphorylation was higher after 72 hours in IKK β KO cells than in WT cells. Indeed, the level of AKT phosphorylation was higher at all timepoints measured in IKK β KO cells. This could reflect the apparent higher expression of AKT1 in IKK β KO cells relative to WT cells. The expression of AKT was also higher in IKK α KO cells than WT cells, yet no TNF α -dependent change in the phosphorylation status of AKT from its basal level was observed (Figure 3.18B).

The effects of TNF α on AKT phosphorylation status were mirrored in the phosphorylation status of GSK3 β . In WT and IKK β KO cells, TNF α induced an increase in GSK3 β inhibitory phosphorylation at Serine 9 between 6 and 72 hours post-treatment. No such increase was observed in IKK α KO cells. GSK3 β phosphorylates cyclin D1 at Threonine 286, which induces its nuclear export and proteasomal degradation (Diehl *et al.*, 1998; Alt *et al.*, 2000). Indeed, an increase in cyclin D1 protein expression was observed between 24 and 72 hours TNF α treatment in WT and IKK β KO cells that correlated with the increase in GSK3 β phosphorylation, and hence inhibition. This increase in cyclin D1 expression was not observed in IKK α KO cells; expression of cyclin D1 actually decreased gradually below basal levels. These observations are complicated by the fact that IKK α has also been shown to induce the degradation of cyclin D1 via Threonine 286 phosphorylation (Kwak *et al.*, 2005). Indeed, basal cyclin D1 expression appeared marginally higher in IKK α KO cells than WT cells.

AKT was activated between 24 and 72 hours following stimulation with TNF α . The delayed kinetics of AKT phosphorylation suggests that such phosphorylation is unlikely to be mediated by a kinase directly activated in response to TNF α . TNF α more likely induced gene expression changes that indirectly induced the activation of AKT. For example, NF- κB might have induced the expression of a chemokine/cytokine that activates AKT signalling in an autocrine manner. One mechanism by which TNF α has been demonstrated to activate AKT is through the transcriptional repression of the lipid phosphatase, PTEN (Kim *et al.*, 2004). PTEN antagonises phosphatidylinositol 3 kinase (PI3K) signalling by catalysing the conversion of phosphatidylinositol (3,4,5) trisphosphate (PIP3) to phosphatidylinositol (4,5) bisphosphate (PIP2), which thus inhibits PIP3-dependent processes, such as the membrane recruitment and activation of AKT. Kim *et al.*, observed significant downregulation of PTEN expression between 9 and 24 hours treatment with TNF α in HT 29 colorectal cancer cells. A small decrease in PTEN expression was observed in WT cells after treatment with TNF α for 24 hours

(Figure 3.18A). The effect in IKK β KO cells was made less clear by a possible edge effect within the SDS-PAGE gel (Figure 3.18B). No decrease was observed in IKK α KO cells, indicating that perhaps IKK α activity is important in the repression of PTEN expression. Alternatively, it might be that the weaker induction of NF- κ B transcriptional activity in IKK α KO cells is insufficient to downregulate PTEN.

The absence of AKT activation downstream of TNF α stimulation in IKK α KO cells may have reflected a more general defect in PI3K/AKT signalling in these cells. To examine this, WT, IKK α KO, IKK β KO and IKK α/β KO cells were treated with insulin growth factor-1 (IGF-1), an activator of PI3K/AKT signalling (Figure 3.19). IGF-1 induced the phosphorylation of AKT and GSK3 β in each of the clones, including IKK α KO cells, thus confirming that the PI3K/AKT signalling pathway was intact in these cells. A number of other interesting observations were made, however. Lower amounts of IGF-1 receptor β (IGFR1 β) protein were detected in IKK α and IKK β KO clones relative to the WT and DKO clones. This correlated with a higher level of IGFR1R β phosphorylation at Tyrosine 1316 and 1131 in the WT cells and DKO clones. Three tyrosine residues within the kinase domain of IGFR1R β (Y1131, Y1135, and Y1136) are the earliest major activation loop autophosphorylation sites and are required for kinase activation (Li & Miller, 2006). The autophosphorylation site, Y1316 is important for assembly of signal transduction complexes at the receptor (Tennagels et al., 2000). The higher expression of AKT1 in IKK KO clones compared to WT cells was again observed. Interestingly, the level of phosphorylation of AKT at T308 in response to IGF-1 differed, whereas the level of phosphorylation at S473 was similar between the WT and IKK KO cells. The higher level of T308 phosphorylation in the KO clones likely reflects the higher level of AKT1 protein in these cells compared to WT. The equivalent level of S473 phosphorylation, meanwhile, indicates that a higher proportion of the AKT1 present in the WT cells is in the active, phosphorylated form compared to the IKK KO cells. A third AKT phosphorylation site, Threonine 450 (T450) was examined. T450 is thought to be constitutively phosphorylated on nascent AKT polypeptides by mTORC2 to promote proper protein folding and stabilisation of AKT (Oh et al., 2010). A higher proportion of AKT was phosphorylated at this site in IKK α KO cells compared to WT, IKK β KO or DKO cells. The functional relevance of these observations is currently unclear, but it appears that expression changes induced by knockout of IKK subunits might have contributed to differential alterations in the PI3K/AKT signalling pathway. Importantly, the generality of these observations will need to be extended to other WT and IKK KO clones.

3.2.7 Colorectal cancer cell lines exhibit basal NIK/IKK α -independent p100 processing

The canonical NF- κ B pathway is activated by inflammatory cytokines, involves NEMO-containing IKK kinase complexes and is the predominant mechanism of activation of NF- κ B transcription factor dimers— typically p50/p65 and p50/c-rel - in epithelial cells (Chapter 1, Section 1.3.2). Meanwhile, the noncanonical NF- κ B pathway is activated by a subset of TNFSFR ligands, such as CD40 and BAFF, is NEMO-independent and principally activates p52/RelB dimers is predominant in cells of the immune system (Chapter 1, Section 1.3.5). Central to activation of the non-canonical NF- κ B pathway are the kinases, NIK and IKK α . In the basal, inactive state, NIK is constitutively targeted for degradation through K48-linked ubiquitylation mediated by cIAP1/2, which is part of a complex with TRAF2 and TRAF3. Receptor ligation and recruitment of this complex switches the K48-linked ubiquitylation activity of cIAP from NIK to TRAF3. This destabilises the TRAF:cIAP complex and enables the accumulation of NIK,

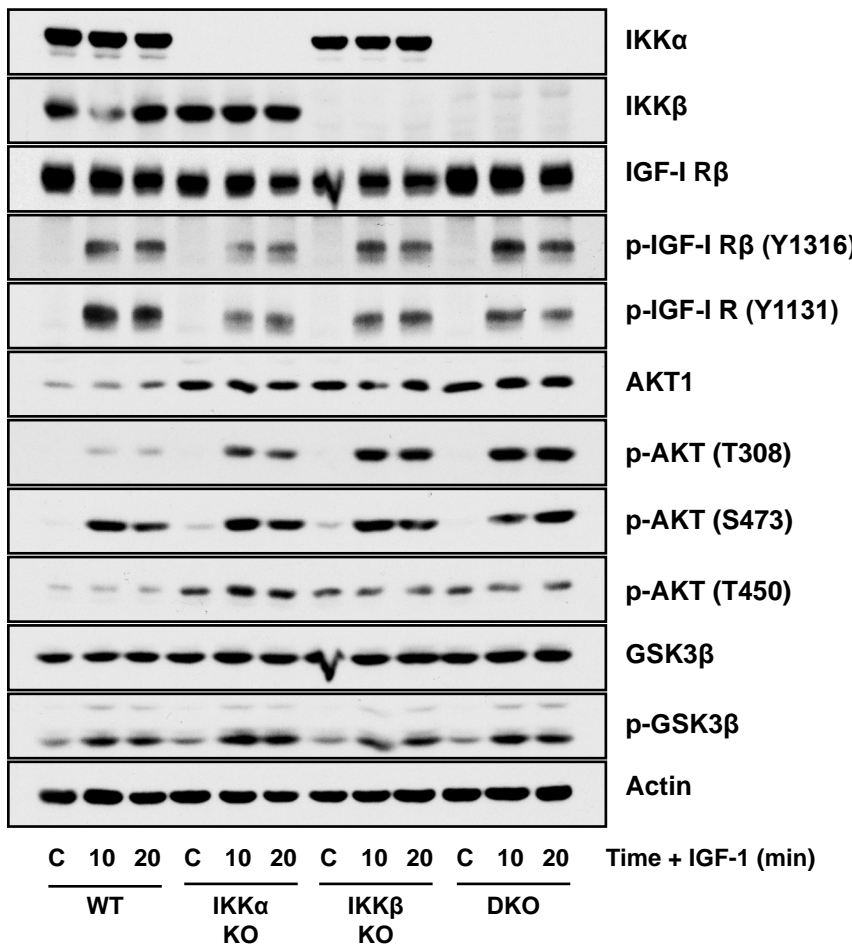


Figure 3.19. IKK α KO cells are capable of responding to IGF-1, an activator of PI3K/AKT signalling. WT (A3), IKK α KO (F6), IKK β KO (G9) and IKK α / β DKO (C8) HCT116 cells were seeded in normal growth medium for 24 hours, prior to treatment with 50 ng/ml recombinant IGF-1 or vehicle control (C) for the indicated timepoints. Whole cell extracts were prepared, fractionated by SDS-PAGE and Western blotted with the indicated antibodies. Data are from a single experiment.

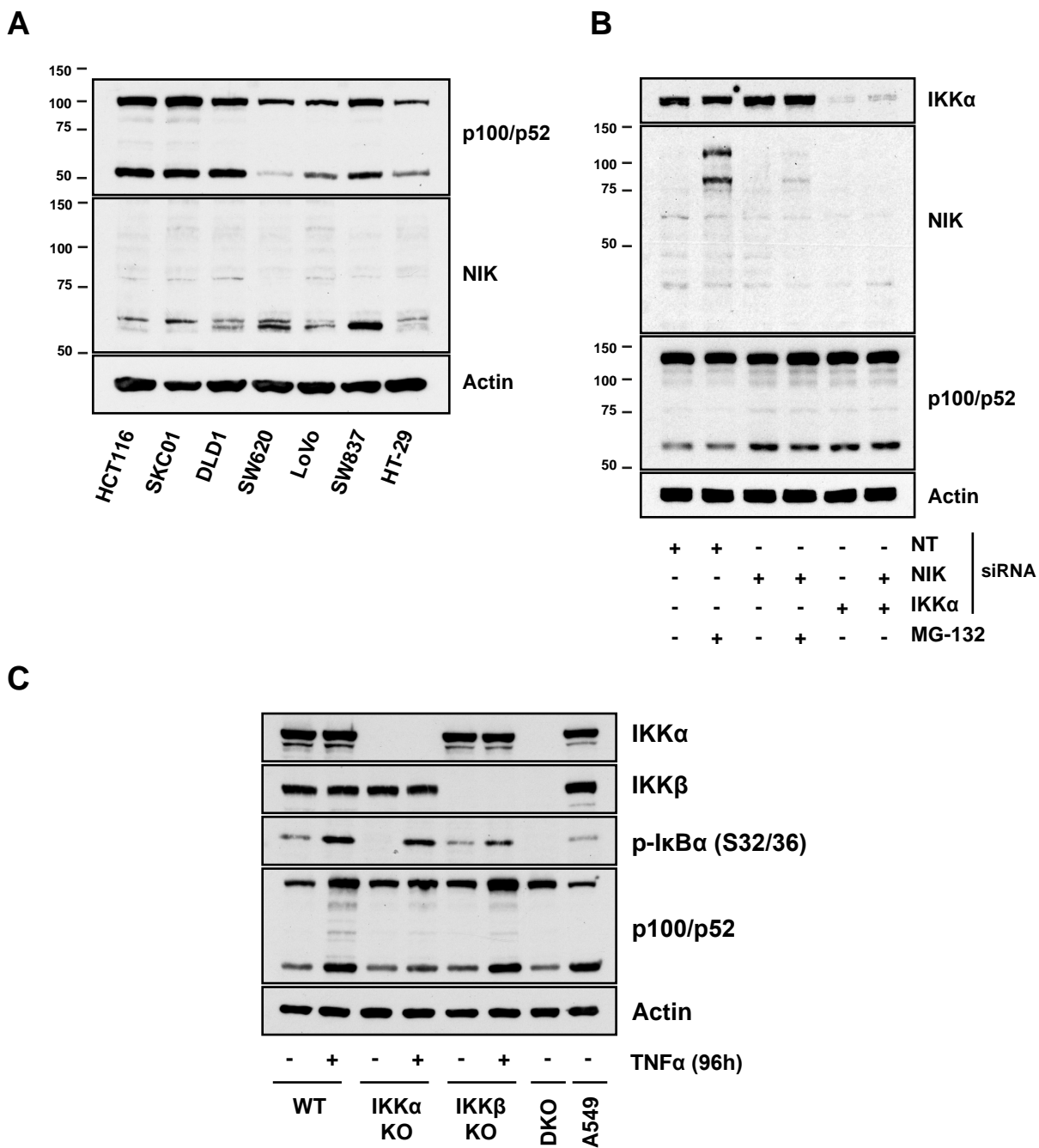


Figure 3.20. Colorectal cancer cell lines exhibit basal NIK- and IKK α -independent p100 processing. (A) Whole cell extracts from a panel of colorectal cancer cell lines were fractionated by SDS-PAGE and Western blotted with the indicated antibodies. Data are from a single experiment. (B) HCT116 cells were reverse-transfected with 20 nM of the indicated siRNA (NT, NIK and IKK α) for 48 hours prior to treatment with 10 μ M MG-132 or vehicle control (DMSO) for 6 hours. Whole cell extracts were generated and fractionated by SDS-PAGE and Western blotted with the indicated antibodies. Data are from a single experiment. (C) WT (A3), IKK α KO (F6), IKK β KO (G9) and IKK α / β DKO (C8) HCT116 cells were seeded in normal growth medium for 24 hours, prior to treatment with 10 ng/ml recombinant TNF α or vehicle control (-) for 96 hours. Whole cell extracts were prepared, fractionated by SDS-PAGE and Western blotted with the indicated antibodies. Data are from a single experiment.

which is constitutively expressed and constitutively active. In turn, NIK phosphorylates and activates IKK α , which then phosphorylates the NF- κ B subunit precursor, p100, targeting it for proteolytic processing, and releasing active, processed p52 to interact with RelB and translocate into the nucleus to regulate a subset of NF- κ B-dependent genes.

The processing of p100 is tightly regulated to ensure a minimal expression of active p52 in the cell. Indeed, when p100 is expressed in mammalian cells, p52 is barely detectable (Xiao *et al.*, 2001). The importance of maintaining tight control over p100 processing is highlighted by the various lymphomas and leukemias associated with chromosomal translocations of the *nf- κ b2* gene encoding p100. In almost all cases studied these rearrangements lead to the expression of p100 truncation mutants lacking the C-terminal processing inhibitory domain (PID) that undergo constitutive processing. The constitutive processing of these p100 mutants is associated with their active nuclear shuttling (Liao & Sun, 2003). Furthermore, multiple myeloma is associated with the aberrant accumulation of NIK resulting from cleavage of TRAF-binding sequences by the API2-MALT1 fusion oncoprotein (Rosebeck *et al.*, 2011). Constitutive activation of the non-canonical NF- κ B pathway has also been observed in some solid tumours. For example, a subset of pancreatic cancer cell lines exhibit constitutive NIK stabilisation, p100 phosphorylation and degradation, and expression of non-canonical NF- κ B target genes (Wharry *et al.*, 2009).

During the characterisation of the basal NF- κ B activation status of HCT116 cells it was observed that these cells expressed significant amounts of processed p52 (Figure 3.20A). This was also observed in a number of other CRCs, including SK-CO1, DLD1, LoVo, SW837 and HT-29. The non-canonical NF- κ B has not been reported to be constitutively active in colorectal cancer. Despite this apparent basal processing of p100, NIK protein was not observed to be constitutively stabilised in these cell lines. Full-length NIK protein is typically resolved on an SDS-PAGE gel at an apparent molecular weight of \sim 100-125 kDa. No species of this size was detected in the cell lines examined. Bands of \sim 60 kDa were detected by the NIK antibody in each of the cell lines, but the expression of these species did not correlate with the amount of p100 processing, and so were unlikely to be functionally relevant. Treatment of HCT116 cells with the proteasome inhibitor, MG-132, induced the expression of two species detected by the NIK antibody, one of \sim 80 kDa in size and the other of \sim 110 kDa (Figure 3.20B). This suggested that *NIK* mRNA was constitutively expressed and translated in these cells, and that NIK protein was basally turned over by the proteasome. It will be interesting to investigate how the expression of NIK in HCT116 cells compares with other CRC lines as well as normal, untransformed colon tissue. MG-132-induced expression of NIK protein had no effect on the processing of p100, which is unsurprising as the processing of p100 itself requires proteasomal activity. siRNA-mediated knockdown of NIK had no effect on the basal processing of p100. Neither did siRNA-mediated knockdown of IKK α , or combined knockdown of IKK α and NIK. Basal p100 processing was also detected at similar levels in IKK α KO cells relative to WT (Figure 3.20C). Collectively, these results indicated that the basal processing of p100 to p52 in CRCs is independent of NIK or IKK α activity.

Unfortunately, colorectal cancer cells were completely unresponsive to any non-canonical NF- κ B pathway activators tested, including LPS or CD40L, regardless of pre-stimulation with interferon-gamma (data not shown). As such, it was not possible to compare the level of basal p100 processing observed with the level induced upon

activation of the pathway. As such, whether the level of basal p52 expression is biologically relevant remains unclear.

One of the mechanisms through which there is cross-talk between the canonical and non-canonical NF- κ B pathways is the induction of the *nfkb2* gene. In the case of non-canonical ligands that induce both canonical and non-canonical NF- κ B activity, such as lymphotoxin- β receptor (LT β R), this positively regulates non-canonical signalling by supplying more precursor for p52 generation (Dejardin *et al.*, 2002). In the case of ligands such as TNF α that induce only the canonical NF- κ B pathway, the accumulated p100 functions as an I κ B inhibitor to inhibit both canonical and non-canonical NF- κ B transcription factors, including RelB and p65 (Sun *et al.*, 1994; Derudder *et al.*, 2003). Consistent with this, long-term TNF α treatment increased the expression of p100 in WT and IKK β KO HCT116 cells (Figure 3.20C). An approximately proportional increase in the processed p52 form was also observed. However, this increase in p100/p52 expression was markedly reduced in IKK α KO cells. This provides further evidence of the significant defect in NF- κ B dependent transcription in IKK α KO cells relative to IKK β KO cells.

3.2.8 IKK α KO and IKK β KO cells exhibit differences in the TNF α -dependent regulation of non-canonical NF- κ B pathway signalling components

Under normal circumstances, soluble TNF α binding to TNFR1 activates the canonical but not the non-canonical NF- κ B pathway (Kim *et al.*, 2011). To confirm that this was the case, lysates from WT, IKK α KO and IKK β KO cells treated with TNF α were blotted for NIK. As expected, TNF α treatment had no effect on the levels of NIK protein in WT cells (Figure 3.21A and B). Surprisingly, however, TNF α induced a delayed increase in the expression of NIK protein in IKK α KO, and to a lesser extent, IKK β KO cells. Whether this reflected an increase in NIK mRNA expression, or an increase in NIK protein stability has yet to be confirmed. However, RNA sequencing data, described in Chapter 6, suggested that TNF α treatment for 8 hours had no effect on the expression of the map3k14 gene encoding NIK in WT, IKK α KO or IKK β KO cells. Furthermore, the functionality of this stabilised NIK protein is difficult to assess. No phosphorylation is needed for NIK activation, such that newly synthesised and stabilised NIK is constitutively active (de Leon-Boenig *et al.*, 2012). However, activation of the non-canonical pathway downstream of NIK stabilisation requires IKK α -mediated phosphorylation of p100 that targets it for proteasomal processing. This function cannot be mediated by NIK alone. As such, the stabilisation of NIK in IKK α KO cells is potentially of no consequence for the activation status of the non-canonical pathway. Indeed, no increase in p100 processing was observed following NIK stabilisation. Nevertheless, this result hinted at a possible involvement of IKK α in inhibiting the induction of NIK expression downstream of TNF α signalling.

To investigate the possible mechanism of TNF α -induced NIK accumulation in IKK α KO cells, Western blots were performed for the key components of the non-canonical NF- κ B signalling machinery (Figure 3.20C and D). IKK α / β DKO cell lysates were blotted alongside those of WT and single IKK KO cells as a control for TNF α stimulation in the complete absence of IKK or canonical NF- κ B signalling. The strong cell death response induced by prolonged TNF α stimulation necessitated the treatment of DKO cells with the pan-caspase inhibitor, QvD-OPh. Unfortunately, WT and single IKK KO cells were not treated in an equivalent manner, therefore, the results are not directly comparable and caution must be taken when interpreting these results. Nevertheless, the

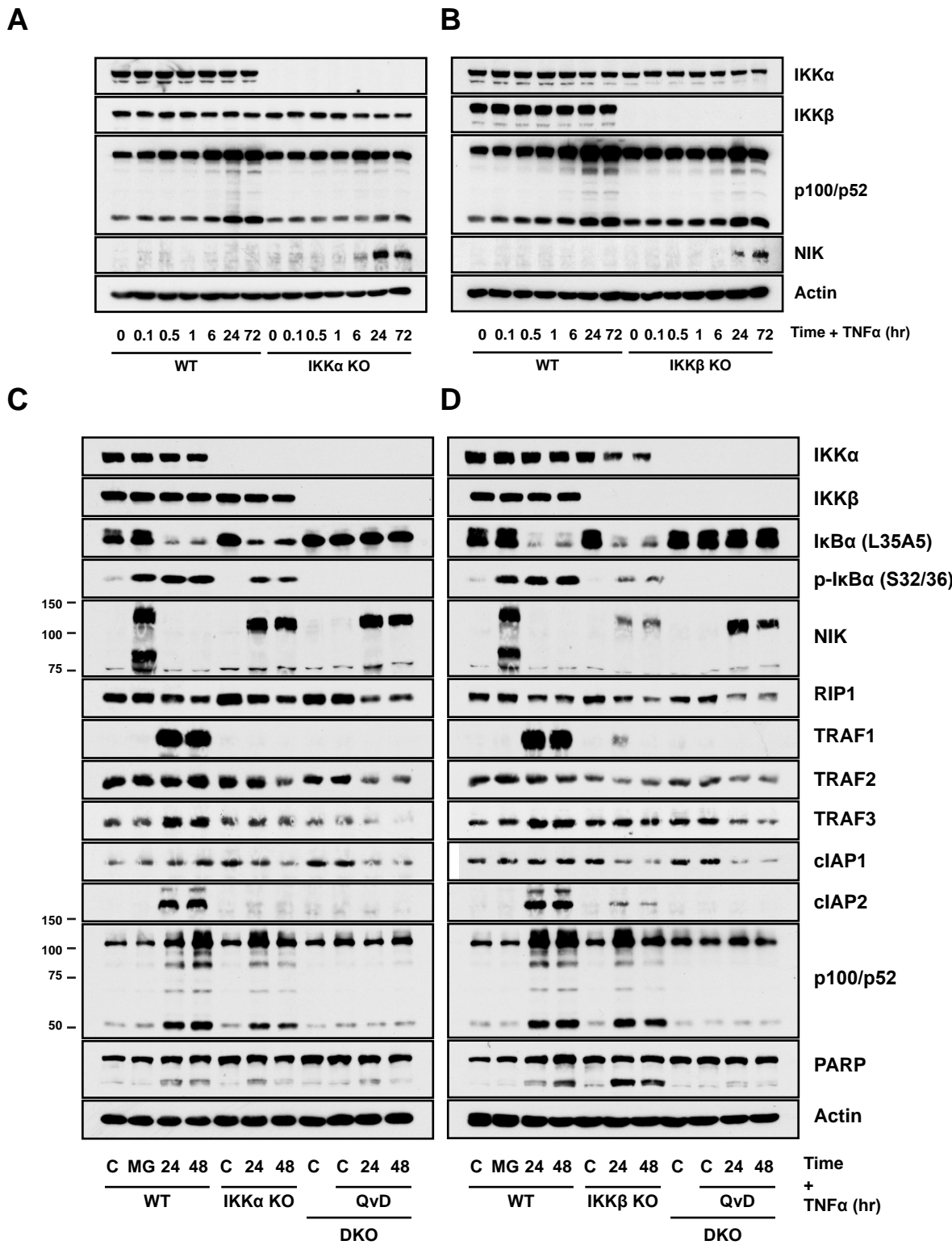


Figure 3.21 IKK α is more essential than IKK β for blocking the increase in NIK protein levels following prolonged TNF α stimulation. (A) WT (A3) and IKK α KO (F6) or (B) WT (A3) and IKK β KO (G9) HCT116 cells were seeded in normal growth medium for 24 hours, prior to treatment with 10 ng/ml recombinant TNF α for the indicated timepoints (10 min, 30 min, 1, 6, 24 and 72 hours). Whole cell extracts were prepared, fractionated by SDS-PAGE and Western blotted with the indicated antibodies. Data are from a single experiment. (C) WT (A3), IKK α KO (F6), and IKK α / β DKO (C8) HCT116 cells or (D) WT (A3), IKK β KO (G9) and IKK α / β DKO (C8) HCT116 cells were seeded in normal growth medium for 24 hours, prior to treatment with 10 ng/ml recombinant TNF α for 24 or 48 hours. WT cells were treated with 10 μ M of the proteasome inhibitor, MG-132 (MG) for 4 hours to induce the stabilisation of NIK protein. DKO cells were treated with 10 μ M of the pan-caspase inhibitor QvD-O-Ph to prevent TNF α -induced cell death. p-, phospho.

observation of TNF α -induced NIK accumulation in DKO cells, but not IKK β KO cells, to a level comparable to that in IKK α KO cells was interesting. It indicated three main possible explanations; that TNF α -induced NIK accumulation is normally suppressed by an NF- κ B-independent function of IKK α , which is more effective when IKK α is part of a WT IKK α :IKK β heterodimer; that IKK α -dependent gene expression is required to limit TNF α -induced NIK accumulation; or that a certain threshold of canonical NF- κ B-dependent gene expression is required to suppress TNF α -induced NIK accumulation, which is met in WT cells, but not in IKK α KO cells, and to a lesser extent IKK β KO cells.

Interestingly, whereas inhibition of the proteasome induced the accumulation of two NIK species of 80 and 120 kDa in size, TNF α stimulation of IKK KO cells induced a single 110 kDa form of NIK protein. The functional differences between these different NIK species warrants further investigation. The expression of RIP1 was similar in the untreated state between WT, IKK α KO, IKK β KO and DKO cells. TNF α treatment for 24 and 48 hours induced a decrease in RIP1 protein expression in WT, IKK α KO, IKK β KO and DKO cells. Although the mechanism behind this decreased expression was not confirmed here, RIP1 has been shown to undergo K48-linked polyubiquitylation and proteasomal degradation following prolonged TNF α stimulation in a manner dependent on the NF- κ B inhibitory protein, A20 (Wertz *et al.*, 2004). This acts as part of a series of negative feedback mechanisms to restrain canonical NF- κ B activation. The TNF α -induced decrease in RIP1 protein expression was slightly enhanced in IKK KO cells relative to WT, but this did not correlate with the induction of NIK.

In WT cells, TNF α strongly induced the expression of the known NF- κ B targets; TRAF1, TRAF3 and cIAP2, all of which are involved in the cross-talk with non-canonical NF- κ B signalling. In contrast, the induction of TRAF1, TRAF3 and cIAP2 was absent in IKK α KO or DKO cells, and was severely reduced in IKK β KO cells. Furthermore, whereas in WT cells the expression of TRAF2 and cIAP1 was maintained following sustained TNF α stimulation, in IKK α KO, IKK β KO and DKO cells their expression was reduced. TRAF2 and cIAP1 are involved in the constitutive turnover of NIK. Their downregulation in IKK KO cells following TNF α stimulation thus likely contributes to the observed accumulation of NIK protein. Furthermore, the marginally higher induction of cIAP2 and TRAF3 in response to TNF α stimulation in IKK β KO cells compared to IKK α KO cells potentially explains their lower accumulation of NIK protein (Figure 3.21D). Collectively, these results indicate that a functional IKK heterodimeric complex is more effective than either IKK α or IKK β homodimers at inducing and/or maintaining the expression of signalling components that act to limit the accumulation of NIK protein in response to TNF α stimulation.

The moderate stabilisation of NIK in IKK β KO cells following TNF α treatment raised the possibility that the non-canonical NF- κ B pathway may be more active in these cells. Unlike IKK α KO cells, these cells expressed functional IKK α and thus expressed all of the components required to activate the non-canonical pathway. To investigate the activation status of the non-canonical NF- κ B pathway, the nuclear localisation of the non-canonical NF- κ B subunits, RelB and p52, was examined following treatment with TNF α for 24 hours (Figure 3.22). 24 hours was chosen as it reflected the timepoint after which NIK was stabilised in IKK KO cells treated with TNF α (Figure 3.21). Over a short time course of TNF α treatment, IKK α KO cells had exhibited a much greater defect in p65 nuclear translocation than IKK β KO cells relative to WT (Figure 3.12). Interestingly, after 24 hours treatment the level of nuclear p65 was lower, relative to WT, to a similar degree in both IKK α and IKK β KO cells. This suggests that IKK α and IKK β KO cells are both defective in maintaining sustained canonical NF- κ B activation in response to TNF α .

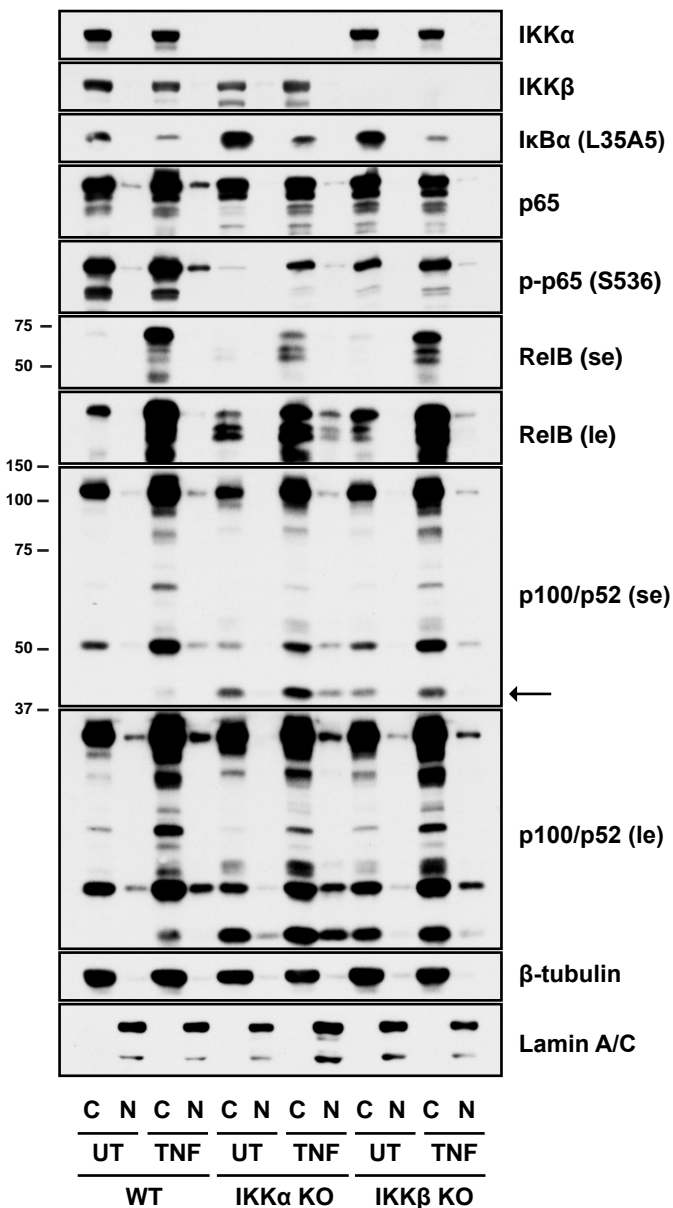


Figure 3.22. IKK α KO cells exhibit enhanced TNF α -induced RelB nuclear translocation. WT (A3) and IKK α KO (F6) and IKK β KO (G9) HCT116 cells were seeded in normal growth medium for 48 hours prior to treatment with 10 ng/ml TNF α for 24 hours. Cytoplasmic (cyt) and nuclear (nuc) lysate fractions were prepared and Western blotted with the indicated antibodies. β -tubulin and Lamin A/C were used as markers of the cytoplasm and nucleus, respectively. Data are from a single experiment representative of two showing similar results. C, cytoplasmic fraction. N, nuclear fraction. se, short exposure. le, long exposure. p-, phospho-

This is consistent with the weaker ‘second phase’ of I κ B phosphorylation and degradation observed in IKK α and IKK β KO cells relative to WT (Figure 3.18B and C).

RelB and p100 were strongly induced in response to TNF α in WT cells as part of the well-characterised cross-talk between the canonical and non-canonical NF- κ B pathways (Sizemore *et al.*, 2002). This induction was weaker in IKK α KO cells, consistent with their weaker NF- κ B transcriptional response. In WT cells under basal conditions, RelB was exclusively cytoplasmic, as was the vast majority of p100 and p52. Therefore, despite a constitutive level of p100 processing, the non-canonical pathway was inactive under basal conditions in WT cells. Treatment with TNF α had no effect on the cytoplasmic localisation of RelB, whilst a small increase in the nuclear localisation of both p100 and p52 was observed. Interestingly, the banding pattern of RelB in the untreated state was different in IKK α and IKK β KO cells compared to WT cells. IKK α KO cells expressed a greater proportion of lower molecular weight RelB species than WT or IKK β KO cells. Whether these represent different RelB phosphorylation states, isoforms or degradation products will be the subject of future investigation.

Surprisingly, despite a lower level of TNF α -induced RelB expression, IKK α KO cells exhibited a greater level of TNF α -induced RelB nuclear translocation than WT or IKK β KO cells. In other words, a greater proportion of total RelB was localised to the nucleus in IKK α KO cells following TNF α treatment. This was the direct opposite of our hypothesis; IKK β KO cells exhibited only a small increase in RelB nuclear translocation relative to WT cells. Interestingly, the slower migrating RelB species was the predominant form that translocated into the nucleus.

No difference was observed in the level of p100/p52 nuclear translocation between WT and IKK KO cells following TNF α treatment. Of note, however, was an approximately 40 kDa species detected by the p100/p52 antibody that was expressed at a higher level in IKK α KO and IKK β KO cells relative to WT cells (arrow, Figure 3.22). The expression of this species was induced by TNF α in WT and IKK KO cells. Interestingly, IKK α KO but not IKK β KO cells, exhibited basal nuclear localisation of this 40 kDa species, and a striking TNF-induced nuclear translocation. The biological relevance of this previously undescribed species and the mechanism behind its selective nuclear translocation in IKK α KO cells will be a source of further investigation. It will be important to determine whether this species is present in a complex with RelB in the nucleus of IKK α KO cells.

Collectively, these results indicate that IKK α might play an important role in restricting the nuclear translocation of RelB and p52-related NF- κ B transcription factor subunits in response to TNF α in WT cells.

3.3 Discussion

3.3.1 IKK knockout has no effect on the growth or survival of HCT116 cells.

We have successfully knocked out IKK α , IKK β and the combination of both in a human cancer cell line; the first time such human IKK KO cells have been reported. Furthermore, these cell lines were thoroughly validated as true knockouts. Neither the IKK α KO, IKK β KO nor IKK α/β DKO cells exhibited an obvious growth defect or reduced viability. This was perhaps surprising, given that various reports have suggested IKK α and IKK β have both NF- κ B-dependent and NF- κ B independent roles in cell cycle progression. For example, NF- κ B can promote the G1/S progression through regulation of cyclin D1 expression (Hinz *et al.*, 1999; Guttridge *et al.*, 1999). Furthermore, both IKK α and IKK β have been proposed to promote the mitotic cell cycle phase by regulating the

phosphorylation and degradation of Aurora A, respectively (Prajapati *et al.*, 2006; Irelan *et al* 2007). In these same studies, depletion of IKK α and IKK β was shown to lead to G2/M arrest and cell-cycle delay, respectively. Although the progression of IKK KO cells through mitosis was not specifically examined, the absence of any obvious growth defect, difference in cell cycle phase distribution or difference in ploidy compared to WT cells suggested that cell cycle progression was largely unperturbed in the KO cells. However, synchronisation experiments will be necessary to confirm that the KO cells exhibit normal progression through different cell cycle phases. The lack of significant basal NF- κ B activity in HCT116 cells might provide an explanation for the absence of a growth defect in IKK KO cells; HCT116 cells may not be ‘addicted’ to IKK/NF- κ B activation, and thus might not rely on these pathways for sustained proliferation. While there is a possibility these cells adapted in culture to the loss of IKK expression, we find this unlikely given that siRNA-mediated knockdown of IKK α and IKK β also showed no significant impact on HCT116 cell cycle progression (Chapter 5). However, it should be mentioned that all experiments were performed in 10% fetal bovine serum (FBS), where growth factors are not limiting. It would be interesting to investigate whether a greater dependence on NF- κ B signalling for growth or survival is revealed in these cells when growth factor signalling is limited.

A consistent theme throughout the characterisation of both the WT and IKK KO clones was an inherent small degree of clonal heterogeneity. This was observed at the level of clonal morphology, growth rate, the magnitude of NF- κ B transcriptional induction and the magnitude of TNF α -induced cell death. The fact that this heterogeneity was seen at an equal level in the WT, single-cell derived clones suggested that this heterogeneity arose as a by-product of the single-cell cloning process and was not related to differences in the extent of on-target or off-target gene editing. However, this heterogeneity limited the power to observe subtle IKK knockout-induced phenotypes, as will be discussed in relation to RNA sequencing analysis in Chapter 6. To account for this heterogeneity, wherever possible the phenotypes of IKK knockout were confirmed in multiple clones generated using independent guide RNA sequences. Future work will benefit from increasing the number of clones of each genotype examined to help mitigate against this clonal heterogeneity and improve the power of statistical analysis.

3.3.2 IKK α plays a major role in canonical NF- κ B signalling in response to TNF α and IL-1 α in HCT116 cells

One of the central dogma’s of the NF- κ B signalling pathway that is repeatedly stated within the literature is that IKK β is the dominant kinase for the canonical pathway and that IKK α plays a marginal role, with a greater importance in the non-canonical NF- κ B pathway. However, we have demonstrated that IKK α plays a significant role in the phosphorylation and degradation of I κ B α , the phosphorylation of p65 at Serine 536 under basal conditions, the phosphorylation of p65 at Serine 468 in response to stimulation, the nuclear translocation of p65 and the NF- κ B-dependent transcriptional response to both TNF α and IL-1 α . IKK β homodimers were far less efficient at compensating for the loss of IKK α than IKK α homodimers were able to compensate for the loss of IKK β . Experiments using a highly selective IKK β inhibitor and kinase dead IKK α confirmed that these observations were not specific to KO cells, and that IKK α plays a significant role in canonical signalling in the WT state. Future work with IKK α selective inhibitors could confirm this further.

Other studies have demonstrated that IKK α plays a role in canonical NF- κ B signalling under certain circumstances and in response to certain stimuli, but this work demonstrates a fundamental role for IKK α in the response to both TNF α and IL-1 α in these cells. A limitation of this work, imposed by the nature of CRISPR-Cas9 experiments and the lack of IKK α selective inhibitors, was that these observations have only been made in HCT116 cells. Future work will therefore attempt to confirm this importance of IKK α in other CRC cells.

One of the interesting observations from this work was the higher level of stimulus-induced activation loop phosphorylation of the remaining IKK subunit in both IKK α and IKK β KO cells. This higher level of phosphorylation did not seem to reflect a compensatory increase in the expression of the remaining IKK subunit. Not only was the level of phosphorylation higher, but it was also sustained for a longer period of time after treatment. The deubiquitinases CYLD and A20 inducibly cleave K63-linked polyubiquitin chains of signalling intermediates upstream of IKK to terminate the NF- κ B signalling response. A20 KO MEFs exhibit more sustained TNF α induced IKK activity. Interestingly, IKK α has been shown to play an important role in this feedback inhibition by phosphorylating the regulatory molecule, TAX1BP1 in response to TNF α /IL-1 α , which promotes the assembly of the A20 ubiquitin-editing complex (Shembade *et al.*, 2011). Determination of the basal and stimulus-induced expression of A20 in WT and IKK KO cells will inform whether this mechanism might be relevant to the results observed. A20 is typically expressed at very low levels in most cell types, but is induced within 30-60 minutes upon NF- κ B activation (Dixit *et al.*, 1990; Krikos *et al.*, 1992). If this is the case in IKK KO cells, it is unlikely that reduced feedback inhibition will explain the higher initial phosphorylation of the remaining IKK subunits.

The greater stimulus induced phosphorylation of the remaining IKK subunit in IKK KO cells could reflect a different IKK activation mechanism for IKK homodimers compared to the wild type IKK heterodimer. The mechanism of IKK activatory phosphorylation has been a source of controversy for many years. It has been found to require phosphorylation by one or multiple upstream kinases, including TAK1, in some studies (Wang *et al.*, 2001; Ninomiya-Tsuji *et al.*, 1999), and by IKK autophosphorylation in others (Xia *et al.*, 2009). Crystal structures of IKK β suggested that such autophosphorylation might proceed through IKK β oligomerisation and trans-autophosphorylation. A more recent study proposed to tie together these seemingly disparate observations by demonstrating that TAK1 phosphorylation of IKK β at Serine 177 primes the subsequent autophosphorylation of IKK β on Serine 181 (Zhang *et al.*, 2014). Our observations with an IKK β selective inhibitor are consistent with this study (Figure 3.8). The observation of enhanced IKK β -dependent autophosphorylation at Serine 181 in IKK α KO cells might reflect the fact that IKK β is more active in the absence of IKK α , or it could reflect a simple stoichiometry effect. However, the observation that IKK β Serine 177 phosphorylation does not increase in IKK α KO suggests that IKK β was not phosphorylated more readily by TAK1 in the absence of IKK α . The lower level of TNF α -induced IKK α Serine 176 phosphorylation in IKK β KO cells also warrants further investigation.

Serine 468 of p65 has been characterised as an IKK β -dependent phosphorylation site (Schwabe *et al.*, 2005). Schwabe *et al* demonstrated that recombinant IKK β phosphorylated this site with a much higher efficiency than IKK α in a GST-p65 kinase assay. Furthermore, a dominant negative IKK β construct, but not an equivalent IKK α construct, inhibited the TNF α and IL-1 α induced phosphorylation of this site in HeLa cells. It was surprising, therefore, that we observed a much greater defect in the TNF α and IL-1 α induced phosphorylation of this site in IKK α KO cells compared to IKK β KO cells. This suggested that IKK α homodimers were better able to compensate

for the loss of IKK β in terms of the phosphorylation of this site than IKK β homodimers were for the loss of IKK α . The minimal role for IKK β in phosphorylating this site in WT HCT116 cells in response to TNF α was also demonstrated with a highly selective IKK β inhibitor. Unfortunately, although knockout and siRNA-mediated knockdown of IKK α interfered with the phosphorylation of this site, we were unable to convincingly demonstrate sufficiency by rescuing the phosphorylation with IKK α re-expression. This could simply reflect a technical limitation of the transient transfections; transiently transfected FLAG-tagged IKK α and endogenous IKK α may not be functionally equivalent. Alternatively, perhaps IKK α facilitates the recruitment of another kinase to phosphorylate p65 at Serine 468 in response to TNF α . Indeed, other kinases such as GSK3 β and IKK ϵ , have been shown to phosphorylate this site under certain circumstances (Buss *et al.*, 2004; Mattioli *et al.*, 2006). An attempt was made to answer the uncertainties surrounding the results of these transient transfections through the generation of WT and KD IKK α and IKK β stable cell lines in an IKK α/β DKO background. Unfortunately, however, this experiment failed to generate successful stable cell lines. First in class IKK α selective inhibitors have recently been described (Ho *et al.*, 2014) and may be made commercially available in the near future. Such inhibitors would be a valuable tool to help resolve the importance of IKK α in the direct phosphorylation of Serine 468 in response to TNF α and IL-1 α .

It will also be interesting to characterise the function of this phosphorylation site in more detail in these cells. Phosphorylation of this site by IKK β has been shown to occur in the cytosol while p65 is bound to I κ B α and appears to moderately inhibit TNF α and IL-1 β induced NF- κ B activation of certain genes (Schwabe *et al.*, 2005). This has been proposed to reflect the fact that phosphorylation of p65 at this site enhances binding of the histone deacetylase, GCN5, which in turn recruits a COMMD1 containing E3 ligase complex that targets p65 bound to specific genes for proteasomal degradation (Mao *et al.*, 2009; Geng *et al.*, 2009). Consistent with this, a preliminary experiment did suggest that a non-phosphorylatable S456A mutant form of p65 was able to induce a moderately greater activation of NF- κ B-dependent transcription in WT HCT116 cells. These results also suggest that the reduced phosphorylation of p65 S468 probably does not account for the reduced nuclear translocation of p65 in IKK α KO cells.

The markedly reduced TNF α -induced nuclear translocation of p65 in IKK α KO cells is likely to have made a significant contribution to the observed lower NF- κ B transcriptional activation in these cells. However, there are other factors that could have influenced the lower NF- κ B transcriptional activation observed, which we have yet to explore. It would be informative, for example, to define the relative DNA binding activities of different NF- κ B dimers in IKK α and IKK β KO cells using electrophoretic mobility shift assays (EMSA). Furthermore, the promoter occupancy of different NF- κ B dimers on specific genes could be defined using chromatin immunoprecipitation (ChIP). Given that the IKK α KO cells exhibit reduced p65 S468 phosphorylation, which has been suggested to promote the proteolytic removal of p65 from the promoters of certain genes, it would be interesting to define the kinetics of promoter occupancy in these cells relative to WT. The overall level of p65-driven expression of certain genes might be lower but perhaps more sustained in these cells for this reason. Furthermore, IKK α has been proposed to have various nuclear-specific roles in both the enhancement and termination of NF- κ B-dependent gene expression, such as the phosphorylation of Histone H3 at S10 and CBP at the promoters of specific genes. The contributions of these proposed nuclear functions of IKK α to the observations made here

have yet to be explored. However, an RNA sequencing approach was undertaken to explore the effect of IKK α and IKK β KO on global gene expression in response to TNF α at an early (2h) and a late (8h) timepoint to attempt to address the impact of each kinase subunit on NF- κ B-dependent transcription (Chapter 6).

Kinase inactive variants of IKK β have been used in many previous studies to propose that IKK β is highly dominant in canonical NF- κ B activation. Indeed, we observed that kinase inactive IKK β inhibited TNF α -induced NF- κ B activation in a dominant negative manner in WT, IKK α KO and IKK β KO cells (Figure 3.10A). However, we observed that kinase inactive IKK α also inhibited TNF α -induced NF- κ B activation in a dominant negative manner in WT, IKK α KO and IKK β KO cells. This is consistent with the hypothesis that IKK α and IKK β are both integral to the activation of the canonical NF- κ B pathway.

3.3.3 The cross-talk between NF- κ B and AKT signalling pathways is altered by knockout of the IKK kinases

TNF α is capable of activating AKT via the PI3K pathway in a cell-type specific manner (Ozes *et al.*, 1999; Sandra *et al.*, 2002; Gustin *et al.*, 2004). We observed an activation of AKT upon treatment with TNF α , but it was so delayed, occurring between 24 and 72 hours post-stimulation, that it was highly unlikely to be a direct effect of the TNF α signalling cascade. Rather, the activation of AKT was likely indirectly induced following NF- κ B-dependent gene expression changes. This could explain the absence of AKT activation in IKK α KO cells, which we have characterised to exhibit significantly weaker TNF α -induced NF- κ B dependent gene expression. The absence of TNF α -induced AKT activation in IKK α KO cells was shown not to be due to a general defect in PI3K signalling in these cells. We observed a small TNF α -stimulated decrease in the expression of PTEN at the protein level in WT and IKK β KO cells, consistent with a previous study that identified this as a possible mechanism of feedforward activation of AKT signalling by TNF α (Kim *et al.*, 2004). Whether this small decrease in PTEN was sufficient to account for the observed activation of AKT will require further investigation. It may also be interesting to characterise the TNF α -induced cytokine/growth factor secretion profile of IKK α KO cells in comparison to WT and IKK β KO cells. NF- κ B is capable of inducing the expression of a host of growth factors, such as EGF, IGF-1, MET, FGF etc, that could activate PI3K signalling in an autocrine fashion (Yang *et al.*, 2016).

Interestingly, tumour-associated macrophage (TAM)-derived IL-1 β has been proposed to activate AKT signalling, and downstream Wnt signalling (due to inactivation of GSK3 β) in an NF- κ B-dependent manner (Kaler *et al.*, 2009a; Kaler *et al.*, 2009b). The authors demonstrated that co-culture with HCT116 cells induced the release of IL-1 β from macrophages, which in turn activated AKT/Wnt signalling in the HCT116 cells in a manner dependent on NF- κ B-dependent signalling. Activated macrophages have also been shown to promote Wnt signalling in gastric tumour cells in a TNF α -dependent manner (Oguma *et al.*, 2008). The data presented here is consistent with these findings. The delayed activation of AKT observed in WT and IKK β KO cells in response to TNF α may reflect the slow secretion and accumulation of factors (such as IL-1 β) expressed in an NF- κ B-dependent manner that are capable of activating AKT in an autocrine signalling mechanism. Wnt signalling is an important tumour-promoting pathway in colorectal cancer. Although Wnt signalling was not specifically assessed in the IKK KO cells, the absence of AKT activation in IKK α KO cells might predict that AKT-driven Wnt signalling is also reduced in

these cells. This will be investigated in future experiments. Provided this assumption is correct, IKK α inhibition may be a therapeutic approach to block TAM-driven Wnt signalling and tumour progression in colorectal cancer.

The higher protein expression of AKT1 in IKK KO cells compared to WT cells was puzzling. This observation will first need to be replicated in additional WT clones to rule out any confounding clonal effects. Taken at face value, however, this observation suggests that an intact IKK α / β heterodimer may play some role in the stability of AKT1. The regulation of AKT1 degradation and stability is a relatively understudied aspect of AKT biology. AKT1 is a client protein of the HSP90 chaperone. Dissociation of AKT from the HSP90 complex enhances its dephosphorylation and subsequent degradation (Basso et al., 2002). Indeed, the stability of AKT is particularly sensitive to the HSP90-specific inhibitor, 17-AAG (Basso et al., 2002). The IKK kinase subunits are also client proteins of the HSP90 chaperone (Chen et al., 2002). One can speculate, therefore, that in the absence of IKK subunits, as in IKK KO cells, there might be a greater pool of HSP90 chaperone available to bind to and stabilise AKT1. However, as yet we have no evidence to support this hypothesis.

3.3.4 IKK α knockout results in aberrant TNF α -induced NIK expression

Basal processing of p100 in colorectal cancer cells has been observed before (Dejardin et al 1999; Arabi et al., 2012), but the mechanism and functional significance of this processing has not been investigated. Constitutive p100 processing is classically due to chromosomal rearrangements that lead to the expression of p100 truncations that undergo basal proteolytic processing. This is highly unlikely to be the case in CRC cells as they expressed p100 of the expected full-length size; C-terminal truncation mutants that undergo constitutive processing are typically resolved at an apparent molecular weight of < 80 kDa (Qing et al., 2005). Constitutive, pathogenic processing of p100 truncation mutants has been shown to be independent of NIK and β -TrCP, but requires IKK α and nuclear shuttling of p100 (Qing et al., 2005). Basal processing of p100 in HCT116 cells was shown to be IKK α -independent. The nuclear shuttling of p100 was not explored. Despite this basal level of p52 expression, the expression of p100 was still significantly higher than p52, and thus likely sufficient to maintain the basal cellular pool of RelB within the cytoplasm. Indeed, nuclear fractionation studies demonstrated that there was minimal RelB and p52 present in the nucleus in the unstimulated state, suggesting that the noncanonical pathway was inactive despite this basal p52 processing.

TNF α induced the expression of p100 in HCT116 cells. This is a well-characterised mechanism of crosstalk between the canonical and noncanonical NF- κ B pathways. However, this induction of p100 is typically not accompanied by a concomitant increase in p52 (Mordmüller et al., 2003; Kim et al., 2011). It is interesting therefore that the expression of p52 increased approximately proportional to that of p100 in HCT116 cells treated with TNF α . Whatever the mechanism of p100 basal processing in HCT116 cells, it was not inhibited by increases in p100 expression.

Multiple species of varying molecular weight were detected by the p100 antibody in HCT116 cells and the expression of most of these species were increased upon TNF α stimulation. These species could reflect a high level of non-specific partial processing by the proteasome. Interestingly, an approximately 40 kDa species was highly expressed in IKK α and IKK β KO cells, but not WT cells, and translocated into the nucleus of IKK α KO cells

following TNF α stimulation. This was accompanied in IKK α KO cells by an increase in the nuclear localisation of RelB. It will be important to validate this apparent TNF α -induced nuclear translocation of RelB by other means. Attempts were made to follow RelB translocation via immunofluorescent staining, but a suitable, specific antibody was not found. Provided the TNF α -induced nuclear translocation of RelB and the unidentified p52-like species are confirmed, it would be interesting to determine if they form a functional complex and bind to promoters.

The differing banding patterns of RelB in IKK α and IKK β KO cells relative to WT was intriguing. The faster migrating bands present in IKK KO but not WT cells could represent different phospho-forms of RelB. Indeed, both IKK α and IKK β have been shown to phosphorylate nuclear RelB at Serine 472 in response to TNF α leading to its dissociation from I κ B α and binding to promoters of migration-associated genes (Authier *et al.*, 2014). Furthermore, RelB undergoes phosphorylation-dependent degradation in lymphoid cells (Marienfield *et al.*, 2001; Neumann *et al.*, 2011), although the identity of the kinase is unknown. Interestingly, such degradation proceeds first through an N-terminal cleavage intermediate that resolves at a similar molecular weight to the species detected in IKK α KO cells (Neumann *et al.*, 2011). Numerous other putative phosphorylation sites exist throughout RelB but none have been validated (Baud & Collares, 2006).

It should be noted that the contribution of p105 processing to the phenotypes observed in IKK KO cells has not yet been explored. p105 is an I κ B-like inhibitor of NF- κ B transcription factors that is constitutively processed by the proteasome to p50. IKK β phosphorylates p105 at multiple sites (Ser921, 923, 927, and 932) in response to TNF α . This enhances the targeting of p105 to the proteasome, but favours the complete degradation of p105 rather than the increased generation of processed p50. Whether this is also the case in HCT116 cells will need to be confirmed.

The TNF α -induced expression of NIK in IKK α KO and IKK α/β DKO cells was unexpected. Although it does not typically activate the non-canonical NF- κ B pathway, TNFR1 has been shown to have an intrinsic capability to do so, which is normally suppressed by the adapter kinase, RIP1 (Kim *et al.*, 2011; Gentle *et al.*, 2011). RIP1 inhibits TNF α -stimulated proteasomal degradation of TRAF2 and cIAP1, which normally promote the destabilisation of NIK protein, in an ill-defined mechanism that is independent of its kinase activity. The TNF α -induced degradation of TRAF2 and cIAP1 in the absence of RIP1 leads to the accumulation of NIK and subsequent processing of p100. However, the level of RIP1 downregulation in WT and IKK KO cells did not correlate with the level of NIK protein induced, suggesting a different mechanism of NIK expression/stabilisation from the RIP1-dependent mechanism identified by Kim *et al.* The expression patterns of TRAF1, TRAF3 and cIAP2 inversely correlated with the expression of NIK and the importance of each in the observed NIK expression will be worthwhile investigating. There are conflicting reports on the function of TRAF1 in NF- κ B activation. It appears to have a dual role as a negative or positive modulator downstream of different TNF family receptors, possibly in a cell-type dependent manner (Lee & Choi *et al.*, 2007). It has been proposed that following its induction by TNF α TRAF1 stabilises NIK by disrupting its association with the TRAF2:cIAP2 complex to facilitate a feedforward coupling between the canonical and non-canonical pathways (Choudhary *et al.*, 2013). However, our data is entirely inconsistent with

this model. TRAF1 has also been shown to protect TRAF2 from cIAP2-mediated degradation downstream of membrane-bound TNF α signalling through TNFR2 (Wicovsky *et al.*, 2009). Furthermore, a crystal structure of TRAF1 in a complex with TRAF2 and cIAP2 indicated that TRAF1 would be more optimally positioned for cIAP2-mediated ubiquitination within this complex, providing a potential mechanism for TRAF1-dependent inhibition of TRAF2 degradation (Zheng *et al.*, 2010). Whether the absence of TNF α -dependent TRAF1 induction in IKK α KO cells explains the greater reduction in TRAF2 and TRAF3 expression, and hence the stabilisation of NIK will be the subject of future investigation. The drastically reduced TNF α -dependent induction of TRAF1 and cIAP2 in IKK β KO cells is surprising given the apparently normal NF- κ B transcriptional response in these cells suggested from NF- κ B reporter experiments. qRT-PCR of TRAF1 and cIAP2 over a timecourse of TNF α treatment will clarify whether this reflects a defect at the transcriptional or protein stability level.

Key to understanding the mechanism behind the greater NIK expression in IKK α KO cells will be to determine whether it is the absence of TNF α -induced IKK α kinase activity or the absence of TNF α -induced NF- κ B gene expression that is most significant. Following sustained non-canonical NF- κ B signalling IKK α has been shown to phosphorylate NIK in a manner that promotes its proteasomal degradation, thus terminating the signal (Razani *et al.*, 2010). The absence of such inhibitory phosphorylation could contribute to the NIK stabilisation in IKK α KO cells, but is unlikely to be the sole explanation given that it does not explain the other observations, such as reduced TRAF/cIAP expression. Interestingly, classical NF- κ B activity has been shown to play a crucial role in the suppression of basal noncanonical NF- κ B signalling; IKK β KO, NEMO KO and p65 KO MEFs as well as NEMO defective human peripheral blood mononuclear cells exhibit enhanced basal NIK stabilisation (Gray *et al.*, 2014). How these findings relate to the canonical stimulus induced increase in NIK expression described here is difficult to say, but clearly NIK is subject to multiple layers of regulation by IKK kinases that are only beginning to be elucidated.

In summary, this is the first report of IKK α KO, IKK β KO and IKK α/β DKO human cells. Our results challenge the prevailing dogma by showing that IKK α is equally, if not more, important than IKK β for mediating the activation of canonical NF- κ B signalling in response to TNF α and IL-1 α . These results were confirmed by the use of selective IKK siRNA and IKK β selective small molecule inhibition and should refocus efforts towards the development of IKK α selective inhibitors. Furthermore, these cells will provide a valuable research tool for future studies into both NF- κ B-dependent and NF- κ B-independent functions of IKK α and IKK β .

Chapter 4

**NEMO undergoes rapid proteasomal degradation
in the absence of the IKKs**

4 NEMO undergoes rapid proteasomal degradation in the absence of the IKKs

4.1 Introduction

The canonical IKK complex is the master regulator of the NF- κ B signalling pathway. It is minimally composed of the three components: the homologous kinases IKK α and IKK β , and a regulatory protein, NF- κ B essential modulator (NEMO/IKK γ) (Rothwarf *et al.*, 1998; Yamaoka *et al.*, 1998; Mercurio *et al.*, 1999). Although catalytically inactive, cell lines lacking NEMO fail to induce the canonical NF- κ B pathway in response to almost all pro-inflammatory, immune regulatory and pro-survival stimuli (Schmidt-Supprian *et al.*, 2000). NEMO-deficient mice die early in embryogenesis due to substantial liver apoptosis resulting from their inability to activate NF- κ B in response to TNF α stimulation (Rudolph *et al.*, 2000). Furthermore, point mutations and deletions in the *IKBKG* gene encoding NEMO cause a number of X-linked genetic disorders, including; incontinentia pigmenti, a severe form of dermatitis (Schmidt-Supprian *et al.*, 2000; Smahi *et al.*, 2000); and anhydrotic ectodermal dysplasia with immunodeficiency (EDA-ID) (Döfing *et al.*, 2001), characterised by severe bacterial infections of the respiratory, gastrointestinal tracts, bones, soft tissues and skin. Collectively, these studies highlight the fundamental importance of NEMO in facilitating activation of canonical NF- κ B signalling.

NEMO is a 48 kilodalton (kDa) multi-domain polypeptide (Rothwarf *et al.*, 1998). Early structural predictions, recently confirmed by X-ray crystallography structures, indicated that NEMO is predominantly an elongated, parallel intermolecular coiled coil (Rothwarf *et al.*, 1998; Tegethoff *et al.*, 2003; Rushe *et al.*, 2008). NEMO contains two coiled coil (CC) domains, CC1 and CC2, two small α -helical regions (α H1, α H2) located either side of the CC1 domain, a leucine zipper (LZ), a proline rich region (PRR) and a zinc-finger domain (ZNF) at the extreme C-terminus (Figure 4.1). In addition, parts of CC2 and LZ, together with a conserved ubiquitin binding sequence (amino acids (aa) 285 – 315), make up the so-called ubiquitin binding in ABIN and NEMO (UBAN) domain (Rahig *et al.*, 2009). The ZNF domain of NEMO is also thought to mediate interactions with polyubiquitin chains (Cordier *et al.*, 2009; Ngadjeua *et al.*, 2013), in addition to I κ B α (Schrofelbauer *et al.*, 2012). A region spanning the α H1 and CC1 domains, known as the IKK-binding domain (IBD) and minimally defined as aa 44-111, mediates interaction with IKK α and IKK β (May *et al.*, 2000, Marienfeld *et al.*, 2006). The interaction with NEMO is mediated by a short C-terminal sequence in IKK α and IKK β known as the NEMO-binding domain (NBD), and is required for IKK activation (May *et al.*, 2000).

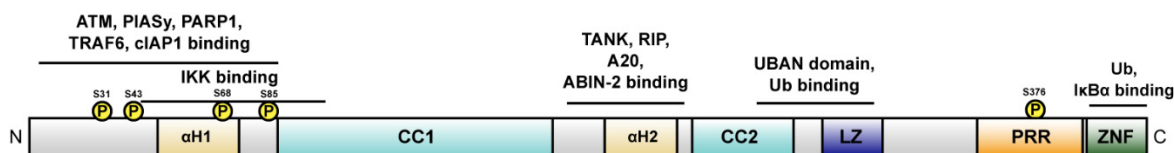


Figure 4.1. Domain organisation of NEMO. NEMO contains several domains essential for its function as a regulatory hub of the NF- κ B signalling pathway. The N-terminus contains an α -helical region (α H1) and a coiled-coil domain (CC1) that function as the binding site for numerous interaction partners, including the canonical IKKs (IKK α and IKK β), ATM, PIASy, PARP1, TRAF6

and cIAP1. There are a number of putative IKK phosphorylation sites (S31, S43, S68 and S85) within this region. Another α -helical region (α H2) forms a binding interface for TANK, RIP, A20 and ABIN-2. A coil-coiled domain (CC2) and the adjacent leucine zipper (LZ) forms the ubiquitin-binding domain (UBAN). At the far C-terminus NEMO contains a proline-rich region, containing an additional IKK β phosphorylation site (S376) and a zinc-finger (ZNF) domain that may be involved in interaction with I κ B α , as well as certain polyubiquitin chains.

The precise *in vivo* composition of the IKK complex and the stimulus-dependency of this composition are areas of continued investigation and debate. Biochemical assays with purified IKK complexes suggest the minimal canonical IKK complex is composed of an IKK α :IKK β heterodimer bound to a dimer of NEMO subunits (Krappmann *et al.*, 2000; Miller and Zandi., 2001). Multiple forms, however, including IKK α or IKK β homodimers, associated with or distinct from NEMO may be possible *in vivo* (Khoshnani *et al.*, 1999; Huynh *et al.*, 2000; Senftleben *et al.*, 2001). NEMO-dependent functionality of IKK β in IKK α KO cells is evidence of this (Li *et al.*, 1999b; Hu *et al.*, 2001). A region spanning the α H1 and CC1 domains that overlaps the IKK binding domain has been implicated in NEMO dimerization (Tegethoff *et al.*, 2003), while a region spanning CC2 and the LZ has been described as a minimal oligomerization domain (Agou *et al.*, 2004). Mutations in this domain greatly reduce NF- κ B activation, highlighting the importance of NEMO oligomerisation for function of the NF- κ B pathway (Marienfeld *et al.*, 2006). The full-length NEMO protein has been described as existing in a dimeric, trimeric or tetrameric state (Fontan *et al.*, 2007). The latter, whereby the canonical IKK complex would be predicted to consist of two IKK α , two IKK β and four NEMO molecules, is consistent with early biochemical studies indicating the apparent molecular mass of endogenous, basal IKK complexes to be in the 700-900 kDa range (Tegethoff *et al.*, 2003). However, this large apparent mass may be an overestimate caused by the elongated nature of NEMO and the IKK complex as a whole (Ivins *et al.*, 2009). Indeed, recent hydrodynamic studies have proposed that apo-NEMO (in the absence of IKK) is a dimeric protein that is in weak equilibrium with a tetrameric assembly, and that interaction with IKK is mutually exclusive with tetramerization (Ivins *et al.*, 2009).

The recent crystallisation of *Xenopus* and human IKK β has provided new insights into the possible composition of IKK complexes (Xu *et al.*, 2011; Liu *et al.*, 2013; Polley *et al.*, 2013). The structures indicated IKK β forms a stable dimer, with dimerization required for IKK β activation (via phosphorylation) but not activity. However, different higher-order oligomeric states, including tetramers, trimers and dimers of IKK dimers, were observed in the asymmetric unit of the crystal lattice through specific contacts between kinase domains (Liu *et al.*, 2013; Polley *et al.*, 2013). Dimerization of IKK β dimers was proposed as a mechanism of IKK activation via *trans* auto-phosphorylation, and a potential explanation for the high level of signal amplification observed within the pathway (Liu *et al.*, 2013; Polley *et al.*, 2013). Subsequently, a recent study attempted to characterise putative higher-order IKK structures using super-resolution microscopy (Scholefield *et al.* 2016). A higher order NEMO lattice extending from 400 nm to over 1 μ m was observed in untreated cells, and was speculated to be composed of NEMO dimers linked through dimeric IKK subunit and polyubiquitin chain binding. Consistent with this model, abrogation of non-covalent polyubiquitin chains or IKK:NEMO binding lead to collapse of the lattice. IL-1 stimulation altered the arrangement of this lattice, resulting in dense, smaller NEMO aggregates visible by conventional confocal microscopy.

NEMO is the regulatory hub of the IKK complex, integrating multiple signals and acting as a scaffold to bring various proteins into the IKK signalosome; protein microarrays have identified over 100 NEMO interactors (Fenner *et al.*, 2010). Indeed, this scaffold function of NEMO has been shown to be important in directing the stimulus-specific substrate specificity of IKK β ; otherwise a functionally pleiotropic kinase (Schröfelbauer *et al.*, 2012). Two characteristics of NEMO are vital for this role as a central scaffold: its ability to bind to non-degradative ubiquitin chains, and its elongated, modular structure.

Regarding the former, NEMO interacts with linear Met1-linked ubiquitin chains via its UBAN domain (Lo *et al.*, 2009; Rahigi *et al.*, 2009), and K63-linked ubiquitin chains via both the UBAN and the ZNF domains (Cordier *et al.*, 2009; Ngadjeua *et al.*, 2013). Such interactions are important for induction of the canonical IKK complex, because IL-1 and TNF α fail to robustly activate IKK α or IKK β in cells expressing NEMO mutants that are incapable of binding ubiquitin chains (Ea *et al.*, 2006; Wu *et al.*, 2006a; Windheim *et al.*, 2008). Multiple explanations for the mechanistic importance of ubiquitin binding have been proposed. They include; facilitating the stimulus-induced recruitment and colocalisation of upstream signalling components (such as TAK1) to promote IKK activation (Wang *et al.*, 2001; Xu *et al.*, 2009); inducing allosteric conformational changes in NEMO that promote the activity of bound IKK (Bloor *et al.*, 2008; Rahigi *et al.*, 2009; Catici *et al.*, 2015); and, as previously discussed, facilitating the formation of higher-order NEMO-dependent structures that promote IKK trans-activation (Fujita *et al.*, 2014).

To date, a handful of partial NEMO solution structures have been determined, summarised in Figure 4.2. (Rushe *et al.*, 2008; Bagneris *et al.*, 2008; Cordier *et al.*, 2008; Lo *et al.*, 2009; Yoshikawa *et al.*, 2009; Cordier *et al.*, 2009). Collectively, they suggest a structural model whereby NEMO subunits within the IKK complex form two entwined predominantly helical rods that act as an extended linear platform for the binding of multiple interaction partners along its length (Zheng *et al.*, 2011). However, no structure for the full-length form of NEMO has yet been solved, and only two structures of fragments of apo-NEMO (in the absence of bound interaction partners), that of a CC2-LZ fragment and the ZNF domain, have been determined (Cordier *et al.*, 2008; Lo *et al.*, 2009). This likely reflects both the elongated nature and conformational heterogeneity of full-length NEMO, as well as a high degree of conformational flexibility in the absence of binding partners (Catici *et al.*, 2015). For example, apo-NEMO constructs of any length encompassing the IKK-interaction domain produce nuclear magnetic resonance (NMR) spectra that are poor in quality, indicating structural instability and conformational heterogeneity (Rushe *et al.*, 2008). In support of this, the crystal structure of a NEMO-IBD/IKK complex fragment demonstrated that hydrophobic residues in the IKK-binding specificity pocket of NEMO would be water-exposed if the IKK peptides were stripped from the structure, suggesting that the aa44–111 region (minimal IKK binding sequence) could be disordered, in a different conformation, or masked in the absence of IKK (Rushe *et al.*, 2008).

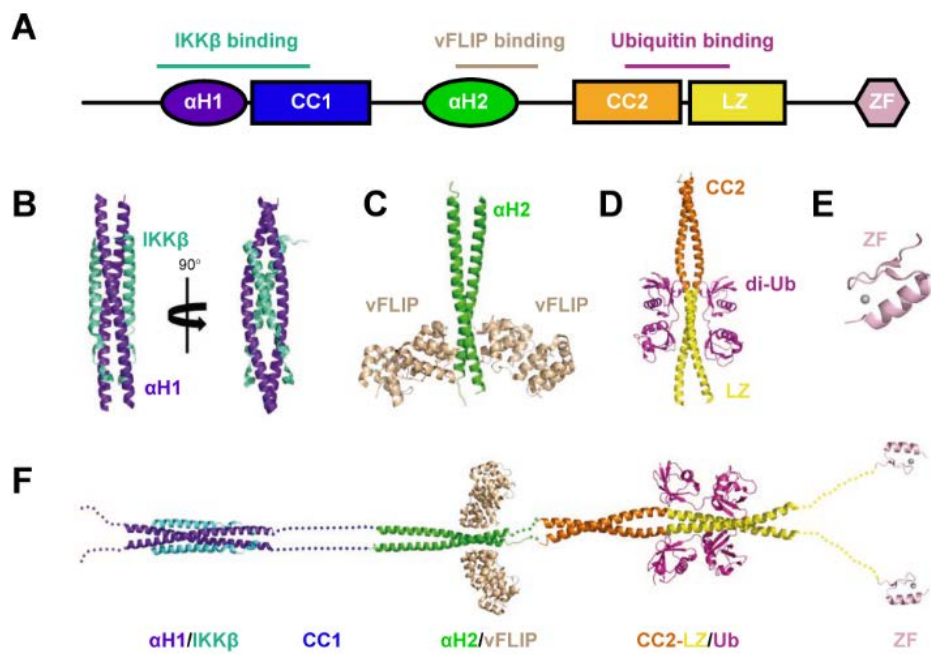


Figure 4.2. Structures of NEMO and its complexes. (A) Simplified domain organisation of human NEMO with highlighted binding sites of interaction partners, the complexes of which have been structurally characterised. (B) Crystal structure of NEMO IKK-binding domain (IBD, purple) in complex with an IKK β peptide (cyan) (PDB code 3BRT). Two orthogonal views of the NEMO dimer are shown. (C) Crystal structure of NEMO α H2 (green) in complex with vFLIP (brown) (PDB code 3CL3). (D) Crystal structure of NEMO CC2-LZ domain (orange-yellow) in complex with linear di-Ub (magenta) (PDB code 2ZVN). (E) NMR structure of NEMO ZNF (pink) (PDB 2JVX). Zinc ion shown as grey sphere. (F) Proposed model of full-length NEMO as an elongated coiled coil dimer. (Rushe *et al.*, 2008; Bagneris *et al.*, 2008; Cordier *et al.*, 2008; Lo *et al.*, 2009; Yoshikawa *et al.*, 2009; Cordier *et al.*, 2009). Figure adapted from Zheng *et al.*, 2011.

Despite these indications, the potential conformational flexibility of NEMO has been an understudied aspect of its function as a signalling platform. Three studies, have attempted to address this problem using various biophysical techniques (Catici *et al.*, 2015; Bagnères *et al.*, 2015; Catici *et al.*, 2016). Collectively, they suggest that NEMO has a significant degree of native structural disorder and is in a dynamic equilibrium between well-folded (coiled coil) and locally unfolded (random coil) states, which can be differentially stabilized upon ligand (IKK, I κ B α , polyubiquitin chains) binding.

Although poorly studied in the case of NEMO, there is an increasing general realization that the molecular mechanism of many proteins, particularly those involved in signalling or protein-interaction networks, is governed by molecular flexibility and protein structural disorder (Haynes *et al.*, 2006; Cortese *et al.*, 2008). These so-called intrinsically disordered proteins (IDPs), examples of which include p53 and p21^{CIP1}, are proteins containing extensive disorder that is important for function (Bell *et al.*, 2002; Asher *et al.*, 2005; Yoon *et al.*, 2012). Some of the physical characteristics of well-defined IDPs that benefit their central role as signalling hubs include; conformational flexibility, enabling promiscuous interactions with numerous targets; accessible sites for post-translational modifications; conserved sequence motifs and recognition elements that fold upon partner

binding; high-specificity, low-affinity transient and dynamic protein interactions; and allosteric regulation of binding partner activity (van der Lee *et al.*, 2014).

Another characteristic feature defining many IDPs is a susceptibility to ubiquitin-independent degradation by the core 20S proteasome, so-called ‘degradation by default’ (Tsvetkov *et al.*, 2009). The common consensus is that proteins must undergo prior ubiquitin modification in order to be targeted to and degraded by the 26S proteasome, which consists of the 20S proteolytic core and two 19S regulatory capping complexes (Hochstrasser *et al.*, 1996). A range of accumulating evidence, however, suggests that ubiquitin-independent proteasomal degradation has been greatly underestimated and is an important regulatory process, particularly in the destructive removal of ‘aged’, oxidised or unfolded proteins (Erales *et al.*, 2014). IDPs represent the predominant targets of the ubiquitin-independent pathway identified to date, and is thought to be because uncapped 20S proteasome particles exhibit basal degradative activity towards protein substrates with complete or regionally localised intrinsic disorder, without the requirement of prior modification (Tsvetkov *et al.*, 2008). A ‘nanny’ model has been proposed to explain the protection of newly synthesised IDPs from ‘degradation by default’ via the 20S proteasome (Tsvetko *et al.*, 2009). An interaction partner(s), the ‘nanny’ would bind to recognition motifs within intrinsically disordered segments of newly synthesised IDPs, shifting the conformational equilibrium to a more discrete, ordered state and thus protecting the IDP from recognition and degradation by the 20S proteasome. For example, the protein NQO1 has been described as a general ‘nanny’ that protects numerous regulatory proteins, such as p53, p73, p33, c-Fos and eIF4GI from 20S-mediated ubiquitin-independent degradation *in vivo* (Asher *et al.*, 2002; Asher *et al.*, 2005; Adler *et al.*, 2010; Alard *et al.*, 2010; AT Dinkova-Kostova *et al.*, 2010).

During the characterisation of IKK α KO, IKK β KO and IKK α/β DKO CRISPR-Cas9 HCT116 cells, an IKK KO-selective decrease in NEMO protein was observed. Here, preliminary evidence is presented that this decrease in NEMO protein reflects enhanced proteasome-dependent degradation and may reflect the fact that NEMO is an IDP that is unstable in the absence of IKK interaction partners.

4.2 Results

4.2.1 Loss of IKK subunits cause a reduction in NEMO expression at the protein, but not mRNA, level.

WT, IKK α KO, IKK β KO and IKK α/β DKO isogenic HCT116 CRISPR-Cas9 cell lines were generated as described in Chapter 3. Whilst examining the effect of IKK knockout on the function of the NF- κ B pathway it was observed that the expression of NEMO protein was significantly lower in IKK α and IKK α/β DKO clones than WT clones (Figure 4.3A). This was observed with two different specific monoclonal antibodies against NEMO, so was unlikely to be due to an epitope-masking effect. Densitometry analysis of the blots confirmed what could be seen by eye (Figure 4.3B and C). IKK α knockout resulted in an approximately 50-60% decrease in NEMO protein, while knockout of both IKK α and IKK β caused a striking >90% decrease in NEMO protein. A small, but significant, decrease in NEMO protein was also seen in IKK β KO cells with one of the antibodies tested.

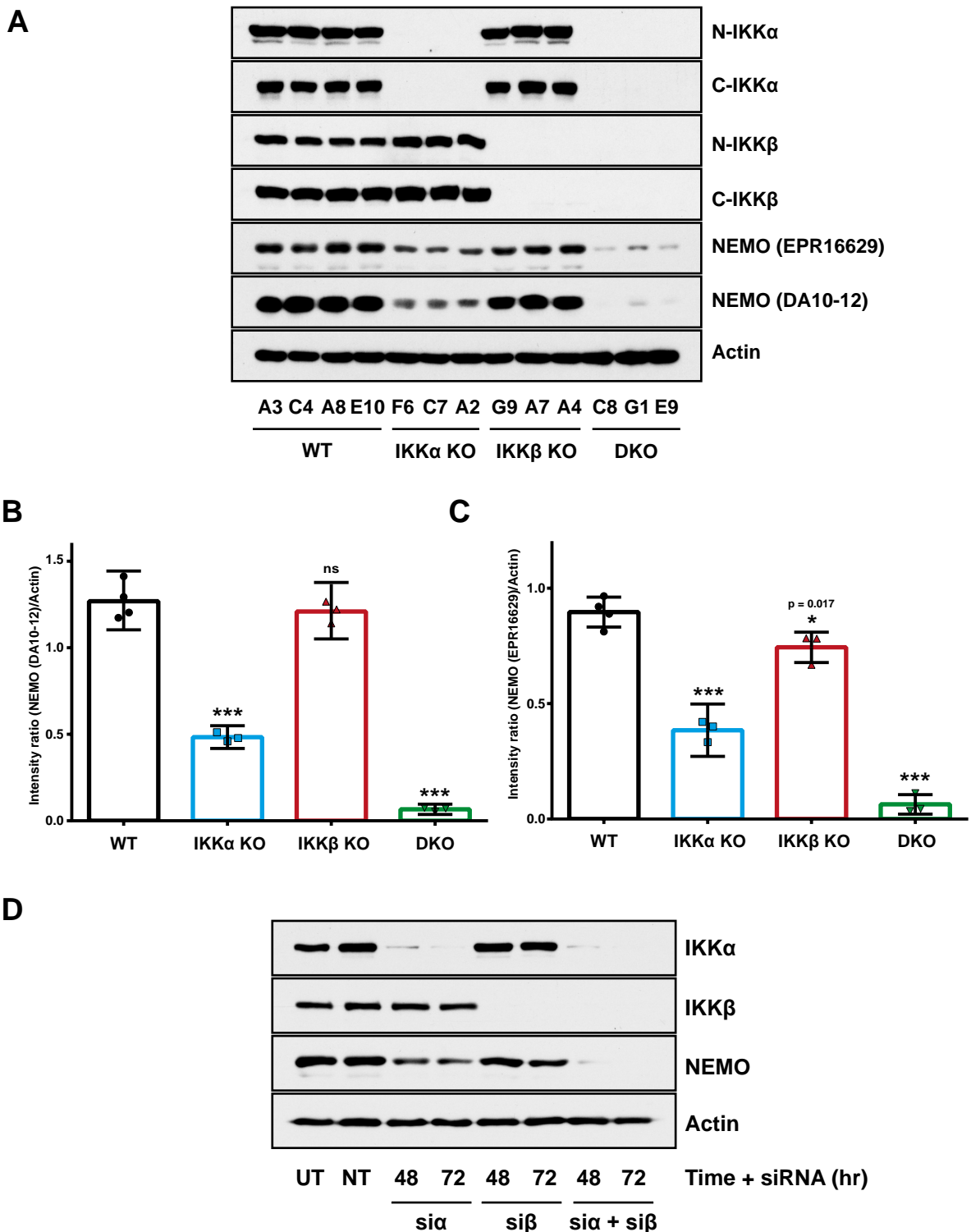


Figure 4.3. CRISPR-Cas9 knockout or siRNA-mediated knockdown of IKK causes a significant decrease in NEMO protein levels. (A) Whole-cell lysates were generated for independent, single-cell derived WT, IKK α KO, IKK β KO and IKK α / β DKO HCT116 CRISPR clones, fractionated by SDS-PAGE and Western blotted with the indicated antibodies. Data are from a single experiment representative of at least two giving similar results. (B and C) Densitometry plots for western blot data shown in (A). Intensities of bands were calculated using ImageJ, verifying for non-saturation and subtracting background. Intensity ratios after normalising against Actin loading control were plotted. Data in (B) corresponds to Western blot data using NEMO (CST) antibody. Data in (C) corresponds to Western blot data using NEMO (Abcam) antibody. Data points correspond to individual clones in (A). Statistical testing performed using one-way ANOVA between WT and KO samples, with Dunnett's multiple comparisons test (**p < 0.001). (D) HCT116 cells were left untransfected (UT), transfected with non-targeting (NT) siRNA or transfected with either 20 nM IKK α -specific siRNA (si α), 20 nM IKK β -specific siRNA (si β) or 20 nM of both si α and si β siRNA. Total siRNA was equalized to 40 nM with NT siRNA for all transfected conditions. 48 or 72 hours after transfection, whole cell lysates were prepared and Western blotted with the indicated antibodies. Data are from a single experiment representative of two showing similar results. N, N-terminal. C, C-terminal.

One potential issue with inferring protein function from the phenotype of knockout cells is the possibility of adaptation to loss of the knocked out protein over a period of time by rewiring gene expression. To confirm that the decreased NEMO expression observed in IKK KO cells was a direct result of loss of IKK, the effect of siRNA-mediated knockdown of IKK subunits on NEMO expression was investigated (Figure 4.3D). The results were consistent with those seen with the KO cells. IKK α knockdown caused a greater reduction in NEMO expression than IKK β knockdown, while knockdown of both IKK α and IKK β caused a reduction in NEMO that was greater than the effect of the single KOs combined. Collectively, the data suggest that IKK is necessary for continued expression of NEMO protein, and that IKK α is of greater importance than IKK β for maintaining wild-type levels of NEMO expression.

Reverse-transcription quantitative PCR (RT-qPCR) was used to determine if the reduced NEMO expression in IKK KO cells was the result of decreased mRNA expression or a post-transcriptional effect (Figure 4.4). IKK knockout had no significant effect on NEMO mRNA levels. In contrast to the levels of NEMO protein, IKK α/β DKO cells exhibited a small increase in NEMO mRNA expression relative to WT. Although, this difference did not reach significance for the three DKO clones examined. The effect of IKK knockdown on NEMO mRNA expression was not examined.

IKK appeared, therefore, to be necessary for normal NEMO protein expression. To examine whether IKK was also sufficient to promote NEMO expression, and the requirement of IKK kinase activity, WT and kinase dead (KD) IKK α and IKK β constructs were re-expressed in IKK α/β DKO cells. Re-expression of either WT IKK α or IKK β led to a partial, but significant, restoration of NEMO expression back towards WT levels (Figure 4.5A and B). The same effect was seen with KD IKK α or IKK β , indicating that kinase activity was not necessary for IKK to promote an increase in NEMO protein. Interestingly, treatment with TNF α had the effect of reducing NEMO expression back towards the level observed prior to IKK re-expression. This was not observed in WT cells. More repeats are needed to gain statistical power and hence confidence in the significance of the subtle differences in NEMO expression observed between timepoints for WT compared to KD IKK.

Co-expression of KD IKK α and IKK β had a greater effect on NEMO expression than expression of either construct alone, suggesting that both IKK α and IKK β normally act to promote NEMO expression in the WT state (Figure 4.5C and D). However, the increase in NEMO following re-expression of either or both IKK α and IKK β was relatively modest, and did not come close to restoring WT levels of NEMO expression. Despite the apparent overexpression of IKK α and IKK β , the transfection efficiency achieved in HCT116 cells was typically relatively low; approximately 50 – 60% after optimization (data not shown). Therefore, approximately 50% of cells might have remained IKK DKO after transfection, and hence 50% of the lysate might have contained NEMO protein expression representative of DKO cells. Unfortunately, initial attempts to generate stable WT and KD IKK-expressing cell lines failed. However, this approach will be necessary to confirm the sufficiency of IKK in promoting NEMO expression.

NEMO expression decreased following TNF α treatment in cells transfected with a single IKK subunit (Figure 4.5B). The same effect was also observed in IKK β and IKK α KO cells treated with TNF α (Figure 4.6A). NEMO protein decreased in WT cells following treatment with TNF α , but the decrease was more pronounced in IKK β and IKK α .

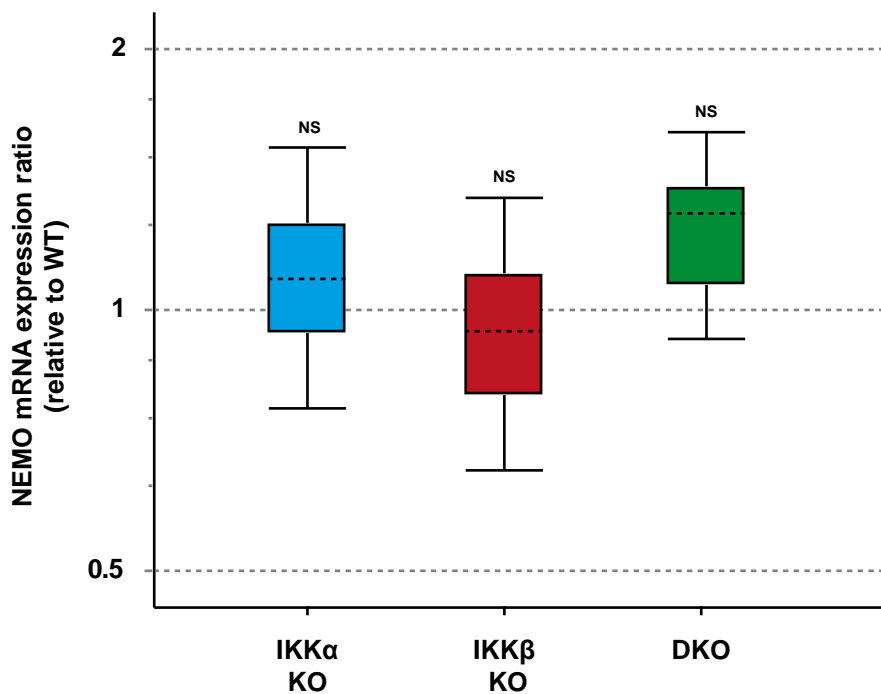


Figure 4.4. IKK KO has no statistically significant effect on NEMO mRNA expression. Three independently derived WT clones and three clones each of IKK α single, IKK β single and IKK α/β double knockout were seeded in normal growth medium for 48 hours prior to RNA extraction. Relative NEMO mRNA expression was determined by RT-qPCR, with normalisation to the geometric mean of the reference gene (*YWHAZ* and *UBC*) expression. Data are plotted on a logarithmic scale as median NEMO expression ratios relative to the WT control samples (expression of which is represented by dotted line at expression ratio = 1). Boxes represent the interquartile range. Whiskers represent the minimum and maximum observations. NS, no significant difference between sample and control group.

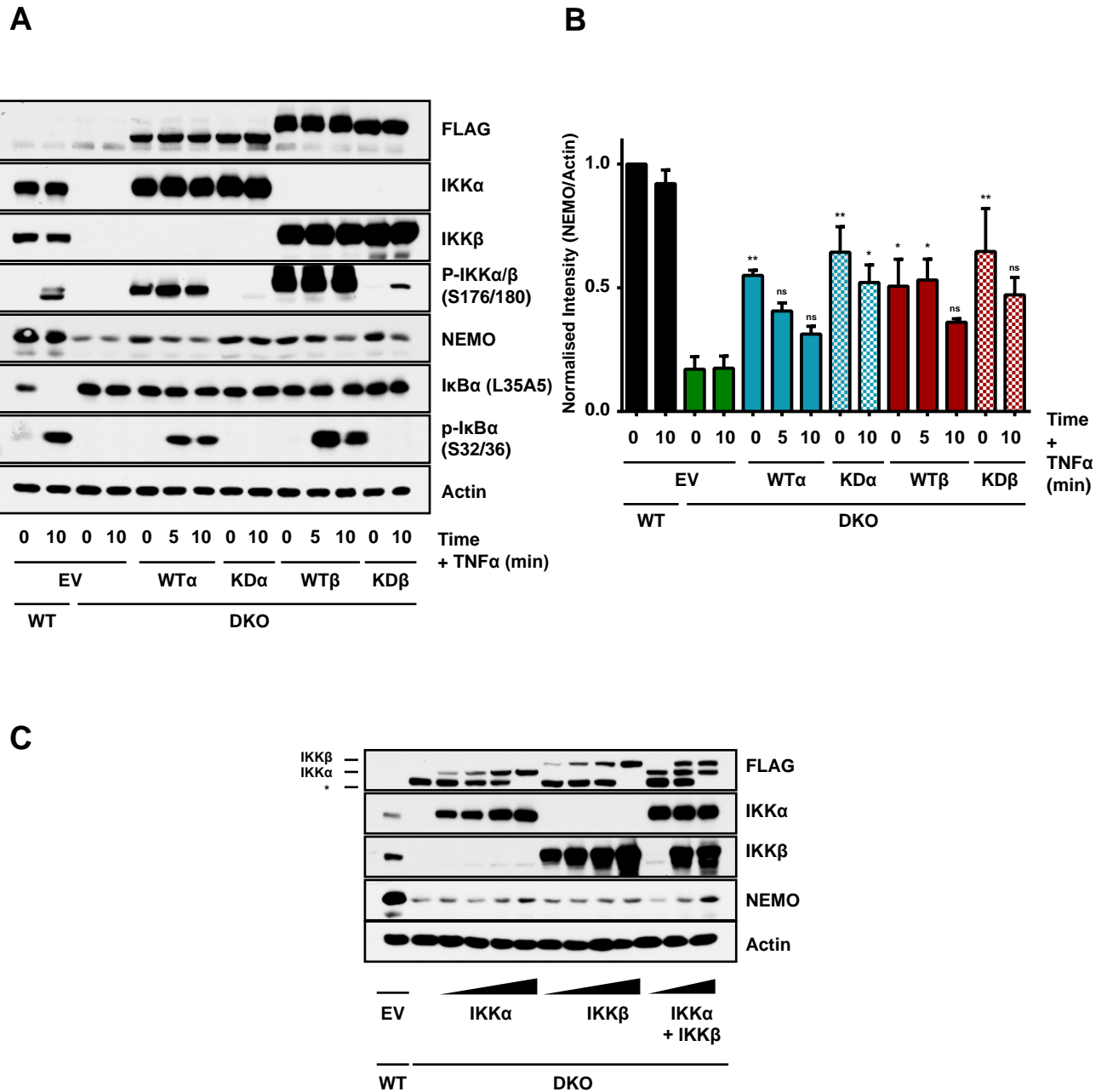


Figure 4.5. Transiently re-expressing IKK α or IKK β in IKK DKO cells partially restores NEMO protein levels.

(A) WT and IKK α/β DKO HCT116 cells were seeded in 6-well plates in normal growth medium for 24 hrs prior to transient transfection with the following quantities of plasmid DNA: 0.28 μ g pCMV-Tag2B empty vector (EV), 0.19 μ g pCMV-Tag2B-WT IKK α , 0.28 μ g pCMV-Tag2B-KD IKK α (K44A), 0.15 μ g pCMV-Tag2B-WT IKK β and 0.26 μ g pCMV-Tag2B-KD IKK β (K44M). Total transfected plasmid DNA was equalized to 0.28 μ g with EV. 24 hours later, cells were treated with 10 ng/ml TNF α for 5 or 10 minutes. Whole-cell lysates were fractionated by SDS-PAGE and Western blotted with the indicated antibodies. Data are from a single experiment representative of two showing similar results. (B) Densiometry plots for western blot data shown in (A). Intensities of bands were calculated using ImageJ, verifying for non-saturation and subtracting background. Intensity ratios after normalising against Actin loading control were plotted. Statistical testing performed using one-way ANOVA between WT and KO samples, with Tukeys multiple comparisons test. Displayed significance summaries correspond to comparisons with untreated DKO condition (* = p < 0.033, ** = p < 0.002). (C) WT and IKK α/β DKO HCT116 cells were seeded in 6-well plates in normal growth medium for 24 hrs prior to transient transfection with increasing quantities of pCMV-Tag2B-WT IKK α (0.25, 0.5, 0.1 and 2 μ g), pCMV-Tag2B-WT IKK β (0.25, 0.5, 0.1 and 2 μ g) or a combination of both (0.25, 0.5 and 1 μ g of each). Total transfected plasmid DNA was equalized to 2 μ g with EV. Whole-cell lysates were fractionated by SDS-PAGE and Western blotted with the indicated antibodies. Data are from a single experiment representative of two giving similar results. WT, wild-type. KD, kinase dead. EV, empty vector. *unspecified band.

KO cells (Figure 4.6B). This data is preliminary in nature due to the lack of replicates, but the trend is apparent and worthy of further investigation.

4.2.2 NEMO protein has a shorter half-life in IKK DKO cells, potentially due to enhanced proteasomal degradation

By definition, the steady state expression of a protein is reached when its rate of synthesis (mRNA translation) and degradation are balanced, and unchanging with respect to time. The lower steady state NEMO protein abundance in the absence of lower mRNA expression indicated that IKK knockout might have shifted the equilibrium between the rates of NEMO mRNA translation and protein degradation. Protein degradation occurs mainly through the ubiquitin-dependent or ubiquitin-independent proteasome system, and autophagic pathways, including autophagosome-dependent macroautophagy, autophagosome-independent chaperone-mediated autophagy (CMA) and endosomal microautophagy (Dunn 2003). Other proteases also play a minor role in protein degradation, including calpains and caspases.

MG-132 is a tripeptide aldehyde inhibitor of the catalytic core of the 26S proteasome (Rock *et al.*, 1994). At concentrations of 50-100 µM it inhibits all three proteasomal peptidase active sites: chymotrypsin-like (ChT-L), trypsin-like (T-L) and postacidic. Concentrations of ≤ 10 µM are sufficient to specifically inhibit the ChT-L activity, which is considered to be the most important proteolytic activity (Patterson *et al.*, 2005). Treatment of IKK DKO cells with 10 µM MG-132 for 6 hours led to a modest increase in steady state NEMO protein (Figure 4.7A). This effect was not as clear in the IKK α KO cells. Accumulation of phosphorylated I κ B α due to decreased basal turnover of I κ B α was used as a positive control for inhibition of the proteasome. Increasing the concentration of MG-132 to 20 µM or 50 µM had no additional stimulatory effect on steady state NEMO protein abundance over that observed with 10 µM. In fact, NEMO abundance appeared lower in WT, IKK α KO and DKO cells treated with 50 µM MG-132. The concomitant decreased in phosphorylated I κ B α and IKK α abundance could indicate a toxicity effect at this high MG-132 concentration. Unfortunately, no quantitative assessment of cell viability was made.

To explore the contribution of autophagosome-dependent autophagy and endosomal/lysosomal degradation pathways to decreased steady state NEMO protein, WT, IKK α KO, IKK β KO and IKK α / β DKO cells were treated with bafilomycin A1, chloroquine and ammonium chloride (NH₄Cl). Bafilomycin A1 is an inhibitor of the vacuolar H⁺ ATPase (V-ATPase) that blocks fusion between autophagosomes and lysosomes and hence inhibits delivery of proteins targeted for lysosomal degradation (Yoshimori *et al.*, 1991; Yamamoto *et al.*, 1998). Chloroquine is a lysosomotropic agent (Steinman *et al.*, 1983). It accumulates in acidic compartments of the cell, including endosomes and lysosomes where it causes acidification that inhibits lysosomal hydrolases and prevents fusion of lysosomes and autophagosomes/endosomes. Ammonium chloride causes a similar acidification of the lysosomes/endosomes (Gordon *et al.*, 1980). These inhibitors had no effect on the steady state level of NEMO protein (Figure 4.7B). The activity of these inhibitors was confirmed by treatment-induced accumulation of LC3B-II.

The partial accumulation of NEMO observed following MG-132 treatment (Figure 4.7A) might indicate that the rate of nascent NEMO protein synthesis is slow, such that only a small amount of protein accumulated within the 6 hour period that proteasomal degradation was inhibited. As such, inhibition of lysosomal degradation for 6

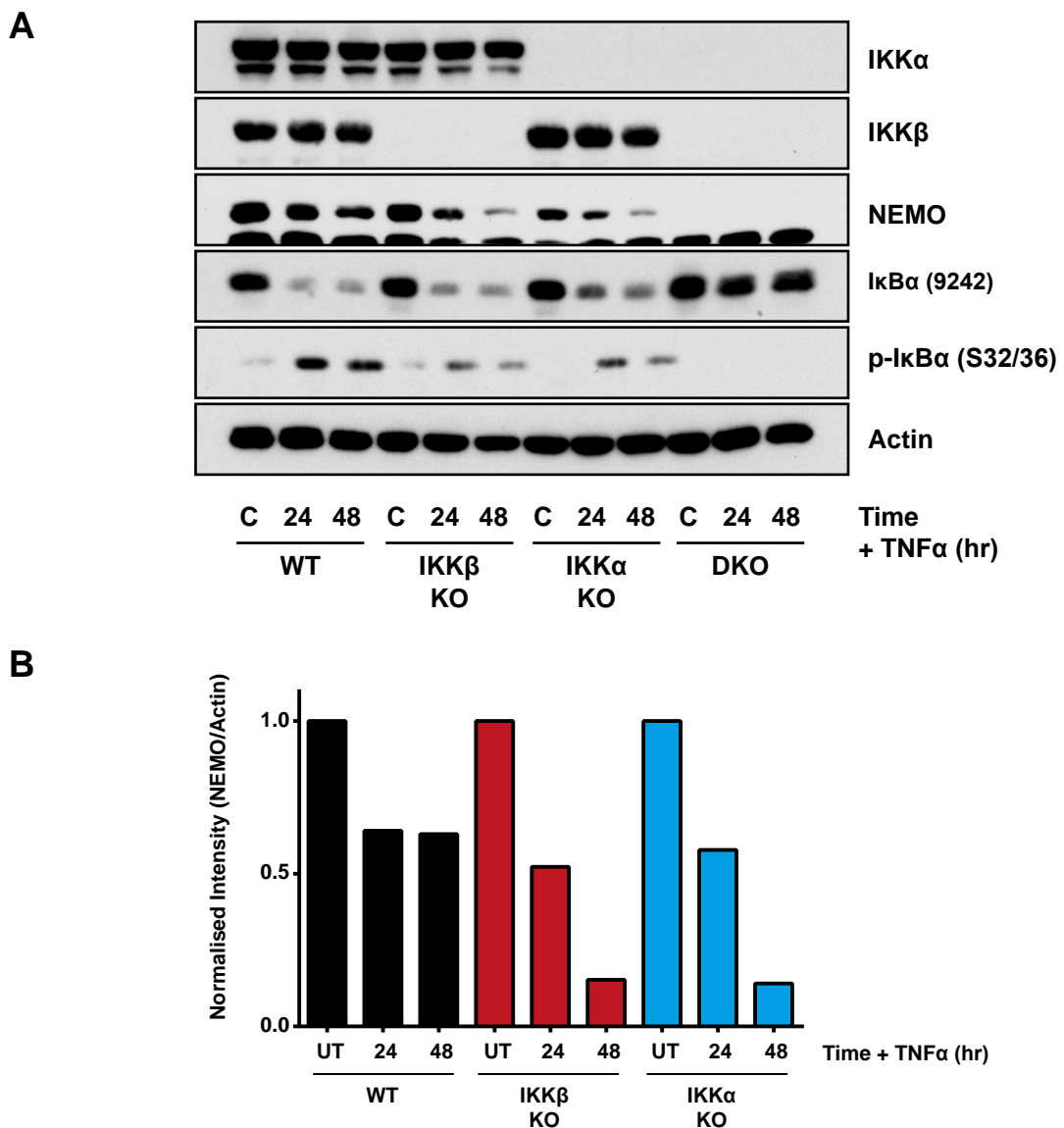


Figure 4.6. Treatment with TNF α decreases levels of NEMO protein to a greater extent in IKK KO cells than WT cells. (A) WT (A3), IKK α KO (F6), IKK β KO (G9) and IKK α / β DKO (C8) HCT116 cells were seeded in normal growth medium for 24 hours prior to treatment with 10 ng/ml TNF α for the indicated timepoints (24 and 48 hours). Whole lysates prepared and Western blotted with the indicated antibodies. Data are from a single experiment. (B) Densiometry plots for western blot data shown in (A). Intensities of bands were calculated using ImageJ, verifying for non-saturation and subtracting background. Intensity ratios after normalising against Actin loading control were plotted. p-, phospho-

hours may not have been sufficient to observe a substantial increase in NEMO protein. To attempt to address this, the effect of MG-132 and chloroquine on NEMO abundance over a 16 hour period was examined (Figure 4.7C). To mitigate against effects on cell viability, the concentrations of both inhibitors were lowered. MG-132 again induced the accumulation of NEMO protein in both the IKK α KO and IKK DKO cells. Interestingly, whereas chloroquine treatment decreased the expression of NEMO further in DKO cells, it induced a small increase in the IKK α KO cells. Whether this observation is significant awaits further repeats.

GSK3 β has been proposed to stabilise NEMO protein through the phosphorylation of residues at the N-terminus of the protein; S8, 17, 31 and 43 (Medunjanin *et al.*, 2016). Although a convincing mechanism by which GSK3 β phosphorylation protects NEMO from degradation was not proposed, Medunjanin *et al* claimed to rule out proteasomal degradation. It is possible, therefore, that in the absence of IKK, GSK3 β is no longer able to interact with and phosphorylate NEMO to promote its stability. To investigate whether GSK3 β phosphorylation contributes to the stability of NEMO in this context, WT, IKK α KO and DKO cells were treated with the highly selective GSK3 α/β inhibitor, CHIR 99021 for 4 or 8 hours. (Figure 4.7D). Potent inhibition of GSK3 β was confirmed through blotting for phosphorylation of β -catenin at the GSK3 β phosphorylation sites, S33, S37 and T41. In direct contrast to the conclusions made by Medunjanin *et al*, inhibition of GSK3 β kinase activity actually appeared to promote a moderate stabilisation NEMO in WT, IKK α KO and DKO cells, suggesting that the reduced NEMO protein in IKK KO cells is not due to reduced GSK3 β function. All experiments performed by Medunjanin *et al* to investigate NEMO stability and degradation were performed using GFP-tagged NEMO constructs, rather than endogenous NEMO. This is of concern because multiple studies have demonstrated that tagged proteins, particularly those fused to large tags such as GFP and TAP, have artificially shorter half-lives than the untagged form of the protein (Belle *et al.*, 2006; Yewdell *et al.*, 2011). Multiple mechanisms have been proposed to account for this. For example, GFP expressed alone or as fusion proteins has been shown to inhibit K48 and K63 polyubiquitylation, resulting in NF- κ B and JNK pathways being less responsive to activation (Baens *et al.*, 2006).

A new steady-state level of a protein after treatment with a proteasome inhibitor can be reached kinetically by changes in its degradation rate with a constant rate of protein synthesis, by changes in its rate of protein synthesis, or by both changes in synthesis and degradation (Alvarez-Castelao *et al.*, 2012). Therefore, in the absence of measuring the effect of MG-132 on NEMO mRNA expression it was not possible to conclude with any certainty that the lower steady state NEMO protein observed in IKK α KO and DKO cells was due to a greater rate of proteasomal degradation. The observed trend, however, was sufficient to explore the effect of proteasome inhibition on NEMO protein half-life in a series of emetine-chase and radioactive pulse-chase kinetic experiments. Emetine dihydrochloro hydrate (hereafter described as emetine), is an alkaloid that blocks protein synthesis in eukaryotic cells by binding to the 40S ribosomal subunit and inhibiting the translocation step of the elongation cycle (Grollman, 1968). WT cells treated with 10 μ M emetine for up to 8 hours exhibited a small decrease in existing NEMO protein by Western blot that could be reversed by treatment with MG-132 (Figure 4.8A and C). MCL1 is a protein with a short half-life of approximately 30 minutes (Yang *et al.*, 1996). The complete depletion of MCL1 protein over the 8 hour timecourse indicated that protein synthesis had been fully inhibited at this saturating emetine concentration. MG-132 treatment alone induced a marked accumulation of MCL1 protein. The partial reduction in MCL1 observed following 8 hours combined treatment with emetine and MG-132

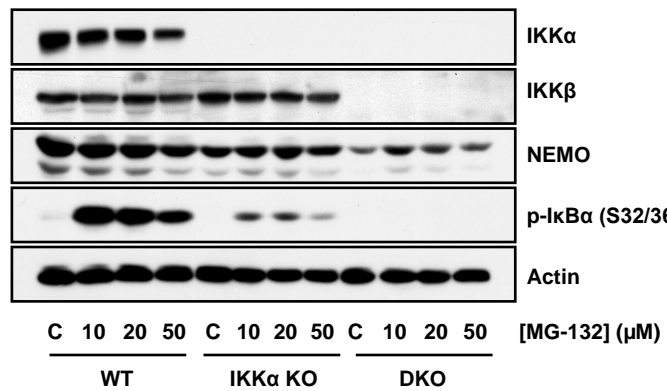
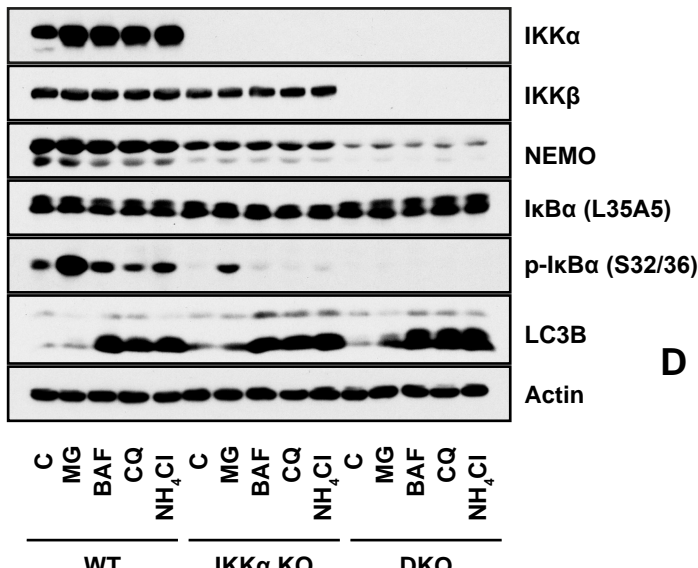
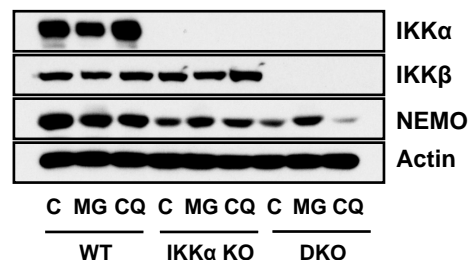
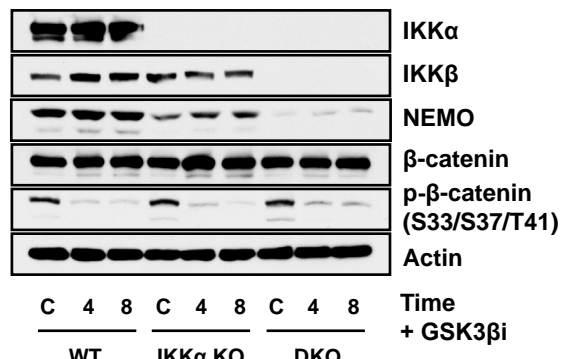
A**B****C****D**

Figure 4.7. Steady-state NEMO protein levels are partly increased by inhibition of the proteasome but unaffected by inhibition of lysosomal/autophagic degradation. (A) WT, IKK α KO and IKK α/β DKO cells were seeded in normal growth medium for 48 hours prior to treatment with the indicated concentrations of MG-132 (10 to 50 μ M) for 6 hours. Whole-cell lysates were fractionated by SDS-PAGE and Western blotted with the indicated antibodies. Data are from a single experiment representative of two giving similar results. (B) WT, IKK α KO and IKK α/β DKO cells were seeded in normal growth medium for 48 hours prior to treatment with either 10 μ M MG-132 for 6 hours, 100 nM Baflomycin-A1 for 2.5 hours, 50 μ M Chloroquine for 2.5 hours or 10 mM NH₄Cl for 2.5 hours. Whole-cell lysates were fractionated by SDS-PAGE and Western blotted with the indicated antibodies. Data are from a single experiment. (C) WT, IKK α KO and IKK α/β DKO cells were seeded in normal growth medium for 48 hours prior to treatment with either 7.5 μ M MG-132 for 16 hours or 25 μ M Chloroquine for 16 hours. Whole-cell lysates were fractionated by SDS-PAGE and Western blotted with the indicated antibodies. Data are from a single experiment. (D) WT, IKK α KO and IKK α/β DKO were seeded in normal growth medium for 48 hours prior to treatment with the GSK3 β inhibitor, CHIR 99021 for 4 or 8 hours. Whole-cell lysates were fractionated by SDS-PAGE and Western blotted with the indicated antibodies. Data are from a single experiment. C, vehicle control (DMSO). p, phospho-

indicated that the proteasome may not have been completely inhibited under these conditions, although this could also reflect a toxicity effect or an effect at the mRNA level.

NEMO protein decayed at a small but significantly faster rate in the IKK α KO cells than the WT cells (Figure 4.8A and B). The emetine-induced depletion of NEMO protein in both the WT and IKK α KO cells could be significantly reversed through treatment with MG-132. As seen earlier, IKK α/β DKO cells under steady state conditions exhibited considerably less NEMO protein than WT cells. NEMO in DKO cells also decreased in abundance at a significantly faster rate than in WT cells upon perturbation of the steady state with emetine; NEMO protein decayed to almost undetectable levels after 8 hours (Figure 4.8C and D). The rate of decay of NEMO protein in DKO cells could be significantly reversed through treatment with MG-132. As with MCL1, the absence of complete rescue by MG-132 could reflect incomplete inhibition of the proteasome, reduced cell viability, changes in mRNA synthesis/degradation, or the effect of additional non-proteasome dependent degradation pathways. As before, further experiments are needed to rule out contributions of changes at the mRNA level to the observed effects on NEMO protein. In addition, it is important to note that additional timepoints will be required to more accurately compare half-lives. Nevertheless, the data is consistent with a reduced NEMO protein half-life in IKK α KO and DKO cells compared to WT, and suggests that a contributing factor to such reduced half-lives might be enhanced proteasomal degradation.

A limitation of emetine-chase experiments is that the disruption of global protein synthesis may affect the stability and abundance of proteolytic enzymes themselves or regulators of the transcription/translation/post-translational modification of the protein of interest. As such, the protein half-life is measured under conditions that may not accurately reflect normal growth conditions. Radioactive pulse-chase labelling is an alternative method for estimation of protein half-life that imposes minimal perturbation on normal cell growth or metabolism. However, it does only measure the turnover rate of newly synthesised protein, which may or not be identical to the rate of degradation of the pre-existing protein in the cell. The two rates will be similar when the rate of protein folding, post-translational modifications, protein interactions and subcellular localization (all of which modulate protein stability) are significantly faster than the rate of protein degradation. Although preliminary in nature due to the absence of replicates, a [35 S]-methionine/cysteine pulse chase experiment indicated that the half-life of newly synthesised NEMO protein was considerably reduced in DKO cells compared to WT (Figure 4.9B and C). Unfortunately, due to technical issues the data for IKK α KO was incomplete (Figure 4.9A and B). The available data points, however, indicated that the half-life of newly synthesised NEMO in IKK α KO cells might be approximately close to that in WT cells. The effect of proteasomal inhibition was not examined and so no conclusions could be made about the cause of this apparent shorter half-life in DKO cells.

4.2.3 NEMO is predicted to contain substantial regions of intrinsic disorder, a proportion of which may be stabilised upon protein binding

The factors that determine the half-life of a protein are complex and varied. Although an oversimplification, the rate at which a protein undergoes proteasomal degradation will be considered here as the dominant factor influencing protein half-life (Belle *et al.*, 2006). The degron model of ubiquitin-dependent proteasomal degradation suggests that the signal for degradation consists of three parts: a primary degron (peptide motif)

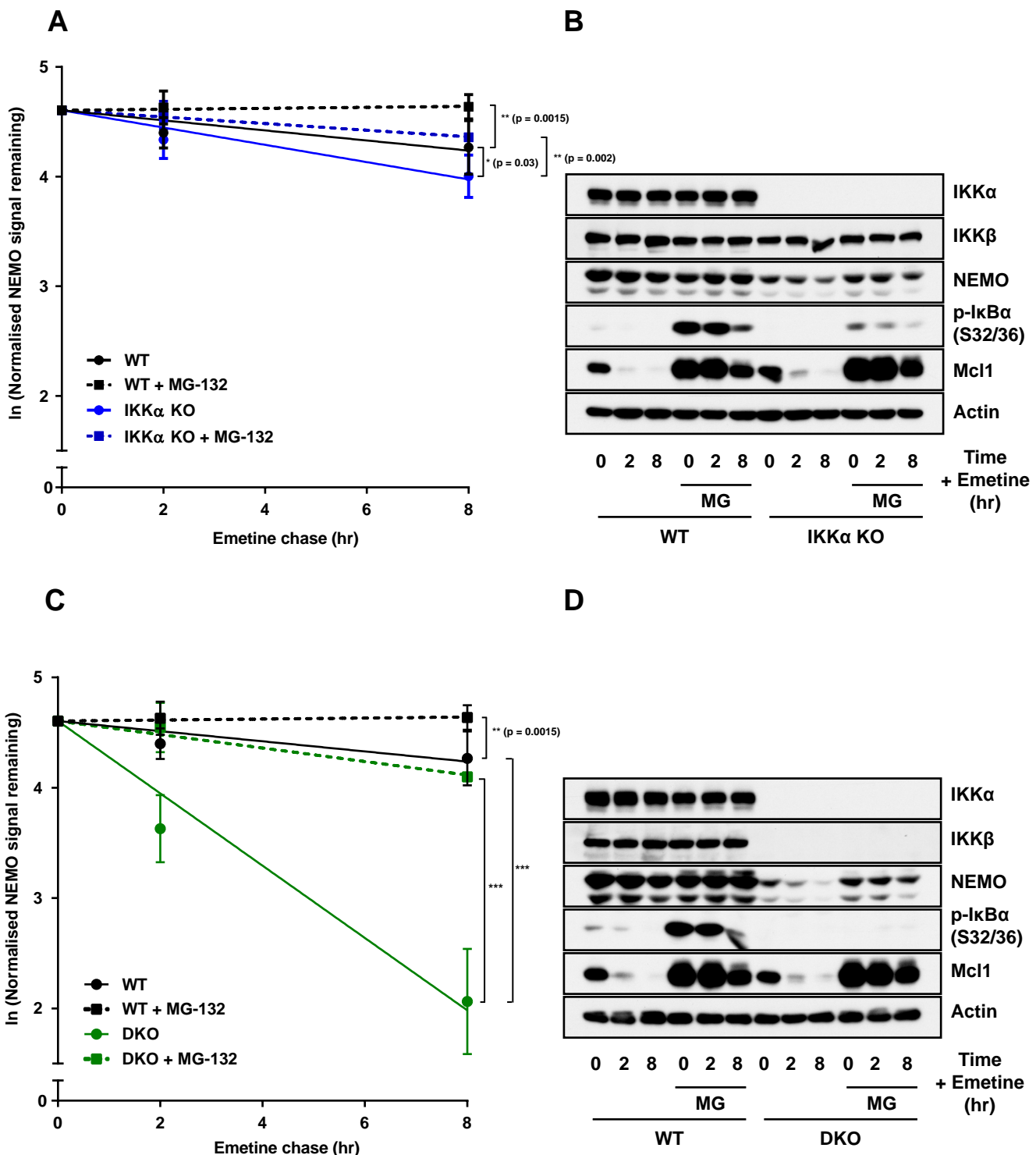


Figure 4.8. NEMO is turned over by the proteasome with a faster rate in IKK DKO cells compared to WT cells following blockade of protein synthesis. (A and D) WT and IKK α KO HCT116 cells (A) or WT and IKK α/β DKO HCT116 cells (D) were seeded in normal growth medium for 48 hours prior to treatment with 10 μ M emetine for 2 or 8 hours, and in the presence or absence of 10 μ M MG-132. Whole-cell lysates were fractionated by SDS-PAGE and Western blotted with the indicated antibodies. Data are from a single experiment representative of three giving similar results. (B and C) Densiometry plots for western blot data shown in (A and D). Intensities of bands were calculated using ImageJ, verifying for non-saturation and subtracting background. Intensity values for NEMO protein bands were normalised against Actin loading control and plotted as a percentage of the intensity signal present at time = 0 hours. Results are mean \pm SD of three independent experiments. Statistical testing performed using one-way ANOVA of comparison of slopes with Tukeys multiple comparisons test (** = $p < 0.01$, *** = $p < 0.001$).

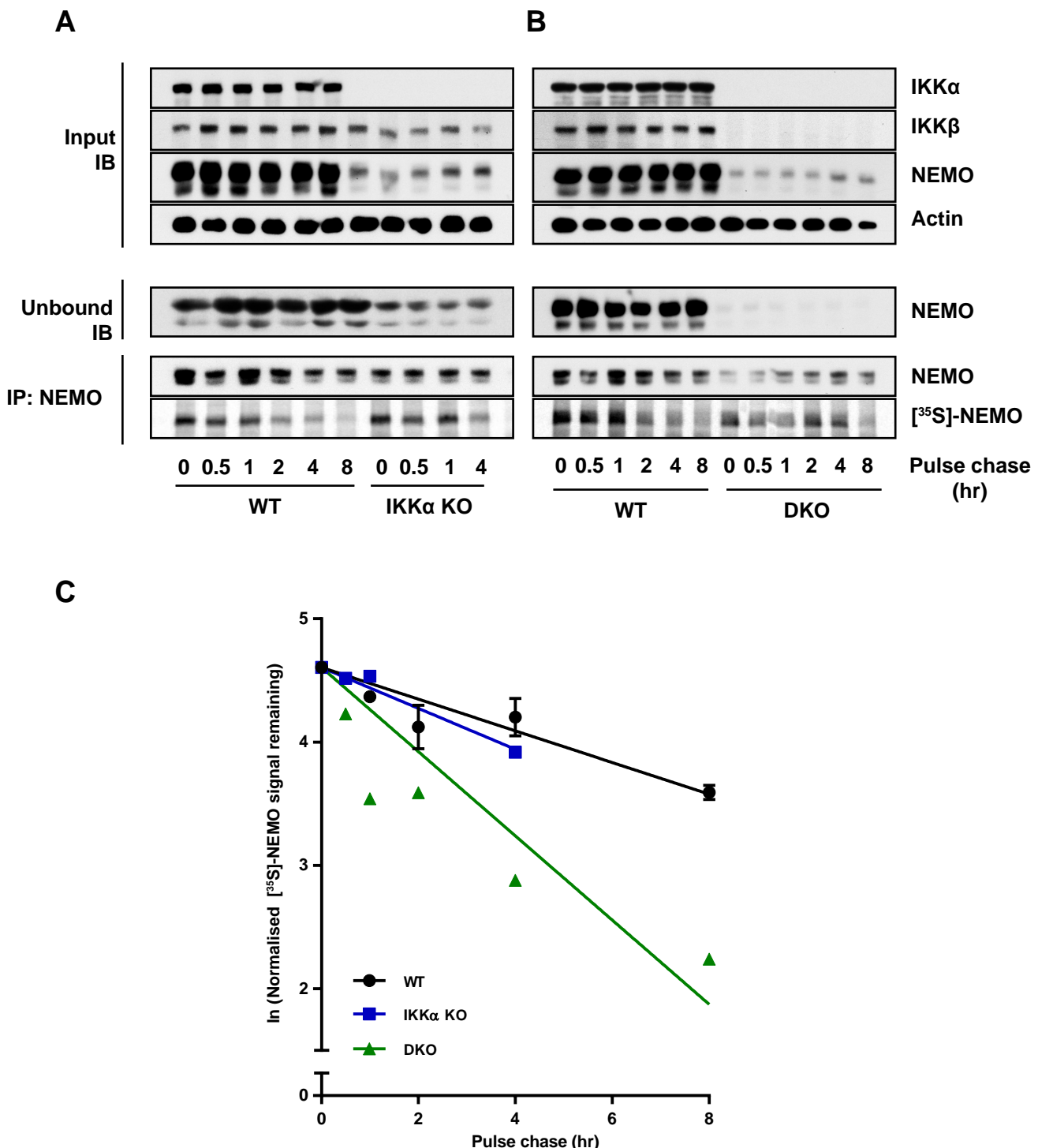


Figure 4.9. Newly synthesised NEMO protein has a shorter half-life in IKK DKO cells compared to WT cells. (A and B) WT and IKK α KO HCT116 cells (A) or WT and IKK α/β DKO HCT116 cells (B) were seeded in normal growth medium for 24 hours prior to starvation in L-methionine/L-cysteine-free growth medium for 1 hour. Newly synthesised proteins were radioactively labelled with 125 μ Ci/ml [35 S]-methionine/cysteine for 40 minutes. At t=0, radioactive media was removed and cells resupplemented with normal growth media containing 2 mM L-methionine and 2 mM L-cysteine. Whole-cell lysates were collected at the indicated timepoints. Input, unbound, and NEMO IP-blot fractions of whole cell lysates were fractionated by SDS-PAGE and Western blotted with the indicated antibodies. Immunoprecipitated [35 S]-labelled NEMO protein was detected using a phosphorimager. Results are from a single experiment. (C) Densiometry plots for [35 S]-labelled NEMO protein bands shown in (A and B). Intensities of bands were calculated using ImageJ, verifying for non-saturation and subtracting background. Intensity values for [35 S]-labelled NEMO protein bands were normalised against NEMO IP intensity values and plotted as a percentage of the intensity signal present at time = 0 hours. Data for WT samples are mean \pm SD derived from (A) and (B), whilst IKK α and DKO are from a single experiment.

that confers substrate recognition by E3 ubiquitin ligases; a reversibly attached ubiquitin tag that is recognised by adaptor proteins that deliver the protein to the 26S proteasome; and an unstructured initiation site within the target protein that facilitates recognition by the proteasome and subsequent unfolding and proteolysis of the entire polypeptide chain (Guharoy *et al.*, 2016a). Regarding the former, the minimal signal necessary for proteasome targeting is a chain of four K48-linked ubiquitin molecules, although numerous other ubiquitin linkages have also been shown to target proteins for degradation (Thrower *et al.*, 2000; Ciechanover *et al.*, 2014). However, ubiquitin modification of a folded protein alone is not sufficient for rapid proteasomal degradation; an intrinsically disordered region (IDR), either terminal or internal, to which the proteasome binds and initiates degradation, is also required (Prakash *et al.*, 2004). This initiation region must be of a certain minimal length and must be sufficiently separated in space from the proteasome-binding tag (Prakash *et al.*, 2004; Inobe *et al.*, 2011). In the case of terminal IDRs, this length appears to approximately 20 – 40 aa for efficient targeting, which corresponds to a random coil conformation span of 50-70 Å (Miller *et al.*, 1968; Inobe *et al.*, 2011). This is similar to the predicted distance between the entrance to the ATPase ring of the 19S regulator cap (the motor of the proteasome thought to catalyse unfolding) and loops protruding into pore of the ring that are thought to bind and pull on the unstructured initiation region (Djuricic *et al.*, 2009).

Although the physiological relevance remains unclear, many IDPs, such as p53, p21^{CIP1}, Rb, c-Fos and BIM_{EL} have been demonstrated to undergo ubiquitin/ATP-independent degradation by the 20S core proteasome both *in vitro* and, in some cases, *in vivo* (Kaletjea *et al.*, 2003; Li *et al.*, 2007; Baugh *et al.*, 2009; Adler *et al.*, 2010; Wiggins *et al.*, 2011). Susceptibility to this form of proteolysis has been proposed as a general property of IDPs (Tsvetkov *et al.*, 2008). Such proteins typically have IDRs at their termini, which can target the whole protein for degradation without the need for ATP-dependent unfolding (Peña *et al.*, 2009). Indeed, the N-terminal unstructured domains of various IDPs, such as ornithine decarboxylase (ODC), Rpn4 and IκBα have been shown to function as transplantable ubiquitin-independent degrons to mediate degradation of otherwise globular proteins (Gödderz *et al.*, 2011; Ha *et al.*, 2012; Fortmann *et al.*, 2015). The mechanism by which this occurs is poorly defined, but may involve unstructured termini entering through the narrow gate of the 20S catalytic core during stochastic gate openings (Osmulski *et al.*, 2000; Religa *et al.*, 2010). These unstructured termini may contain sequence/conformational features that allow them to function as particularly effective initiation sites (Suskiewicz *et al.*, 2011).

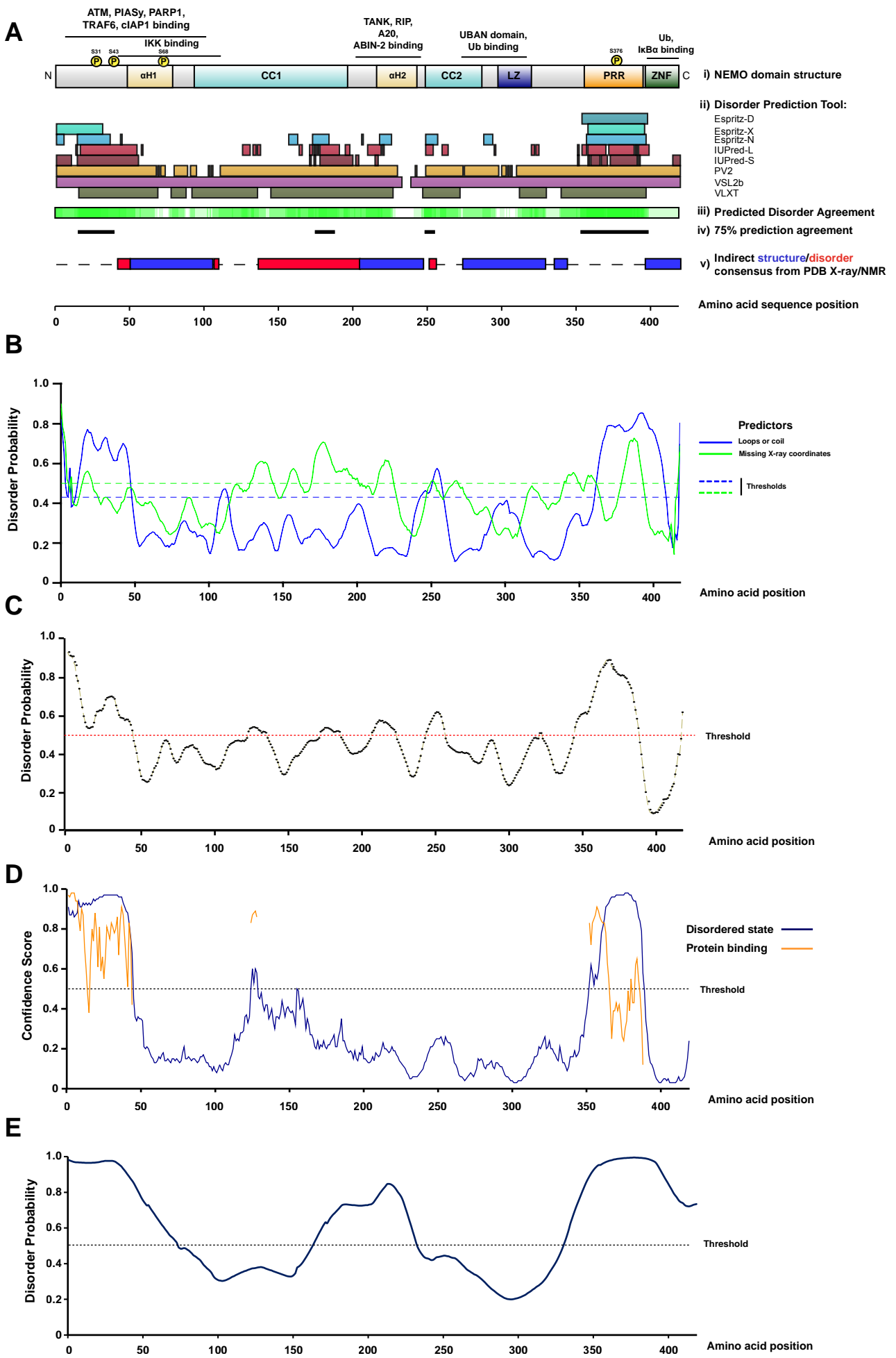
The presence of significant regions of intrinsic structural disorder appears, therefore, to be a common factor promoting both ubiquitin-dependent and ubiquitin-independent proteasomal degradation. Indeed, a recent large-scale analysis demonstrated that yeast, mouse and human proteins with terminal or internal IDRs had significantly shorter half-lives than proteins without such features (van der Lee *et al.*, 2014).

A range of protein disorder prediction algorithms were used to investigate the potential degree of intrinsic disorder in NEMO ((Figure 4.10, see Materials and Methods Section 2.17 for details). Such algorithms display a degree of inherent inaccuracy (5% false positive rate in trained data sets at the probability thresholds used) that can be partly mitigated through the use of a combination of predictors. Confidence in this common consensus can be further increased by using tools with different prediction strategies. Overall, the NEMO amino acid sequence predicted major regions of intrinsic structural disorder, with a striking level of agreement between the

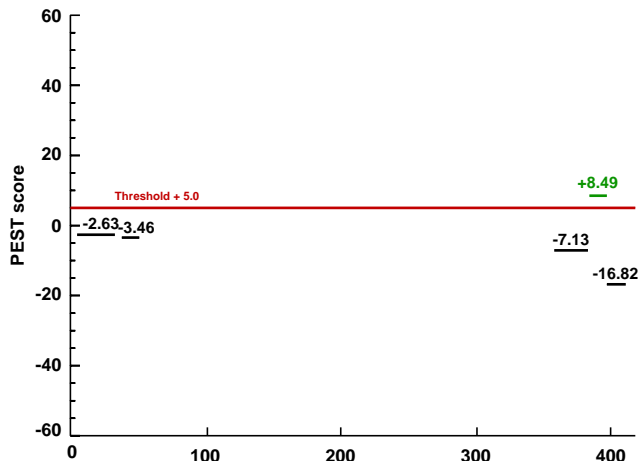
various predictors. The consensus prediction indicated two long (> 30 aa) high confidence regions of disorder, one at the extreme N-termini, and one near the C-terminus. This pattern of disorder was reminiscent of that observed in the well-characterised IDP, p53, which has highly disordered termini (Figure 4.10G). A number of shorter, internal regions of disorder were also predicted, although there was less agreement on their location. However, seven out of the eleven predictors predicted a high confidence disordered region of approximately 20 amino acids centred on aa 180, while six out of the eleven predictors, predicted a high confidence disordered region of approximately 20 amino acids centred on aa 250. The structure/disorder consensus taken from the Protein data bank (PDB) structures available for NEMO indicated that the predicted regions of disorder were found approximately between the regions of solved structure (Figure 4.10Av). This is also reflected in the plot of non-assigned X-ray structure coordinates, as defined by REMARK-465 entries in the PDB (Figure 4.10B). The failure to date to crystallize full-length NEMO protein is perhaps due to these significant regions of intrinsic disorder.

The predicted N-terminal disordered region partially overlapped the IBD of NEMO (Figure 4.10Ai). Furthermore, IKK β phosphorylates two residues, Serine 31 and Serine 43, *in vitro*, that lie within this N-terminal disordered region (Carter *et al.*, 2003). The function of these phosphorylation sites have not been identified. A third IKK β phosphorylation site, Serine 376 sits within the predicted C-terminal disordered region, which aligned with the PRR of NEMO and is thought to be important in feedback inhibition of IKK activity (Prajapati *et al.*, 2002). Interestingly, the PRR of NEMO was predicted to contain a potential PEST motif (Figure 4.10F). PEST motifs were originally identified as enriched sequences in proteins with short half-lives (Rogers *et al.*, 1986). They are proposed to act as conditional proteolytic signals, although the mechanism by which they do so has remained elusive. PEST motifs lack a common consensus, but are typically C-terminal hydrophilic stretches of ≤ 12 residues rich in proline, glutamate, serine and threonine, flanked by lysine, arginine or histidine, and uninterrupted by positively charged residues (Rechsteiner and Rogers *et al.*, 1996). A cross-species alignment of this sequence demonstrated a high degree of sequence conservation.

As mentioned earlier, proteins with significant regions of intrinsic disorder are thought to be inherently sensitive to proteasomal degradation, but are often protected from ‘degradation by default’ by interaction with binding partners, which either promote order in, or mask, the IDRs. Such interactions typically occur with functional elements known as molecular recognition features (MoRFs) (Oldfield *et al.*, 2005). These are short amino acid sequences within longer disordered regions that undergo disorder-to-order transitions (folding) upon binding to their interaction partners. A selection of the most accurate MoRF identification tools with differing prediction strategies were used to predict the location of potential MoRFs within NEMO (Figure 4.11. See Materials and Methods Section 2.21.3 for details). All of the prediction tools identified at least one high confidence mORF within the N-terminal 50 amino acids of NEMO. There was also strong agreement on the presence of at least one high confidence mORF within the C-terminal 50 amino acids. This pattern is also found in p53, which contains multiple validated mORFs within its terminal disordered regions (Figure 4.11G). There was less agreement between predictors on the location of other internal mORFs, possibly reflecting the different sensitivities of each algorithm; some are more accurate at predicting long mORFs than short mORFs and *vice versa*. However, there was agreement between two predictors, ANCHOR and moRFpred (Figure 4.11A and B), on the presence of a high



F



Human	385 RRSPPEPPDFCCPK 399
Chimpanzee	RRSPPEPPDFCCPK
Gorilla	RRSPPEPPDFCCPK
Orangutan	RRSPPEPPDFCCPK
Vervet	RRSPPEPPDFCCPK
Macaque	RRSPPEPPDFCCPK
Mouse	RRSPPEPPDFCCPK
Rat	RRSPPEPPDFCCPK
Pig	RRSPPEPPNFCCPK
Cat	RRSPPEPPDFCCPK
Horse	RRSPPEPPDFCCPK
Platypus	RRSLPDEQPDFCCPK

G

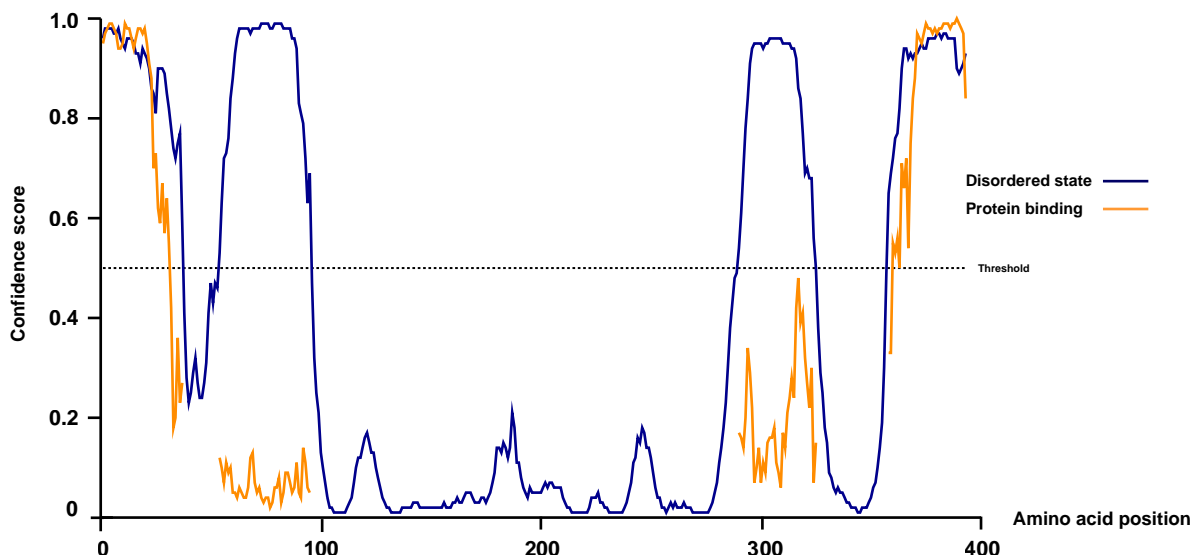
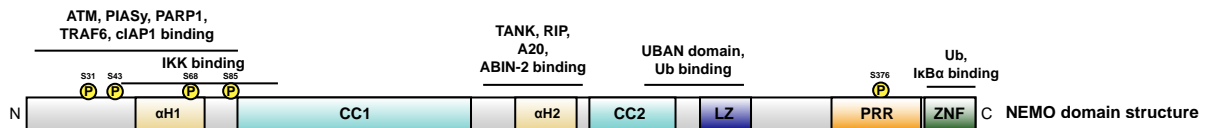
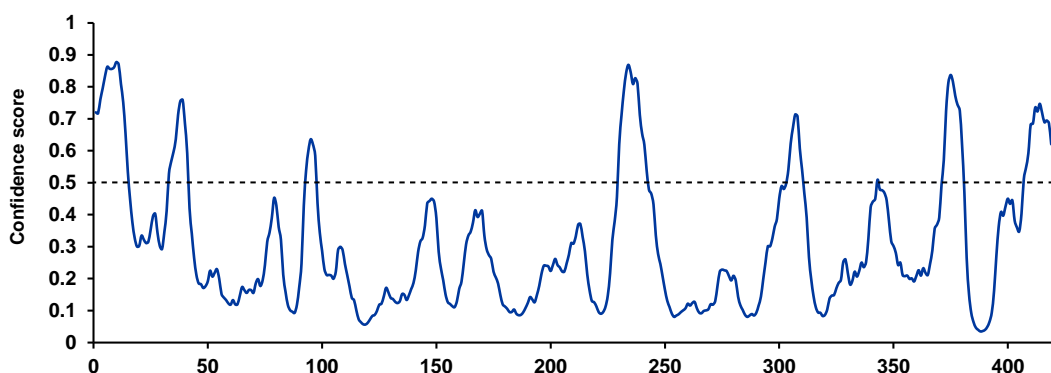


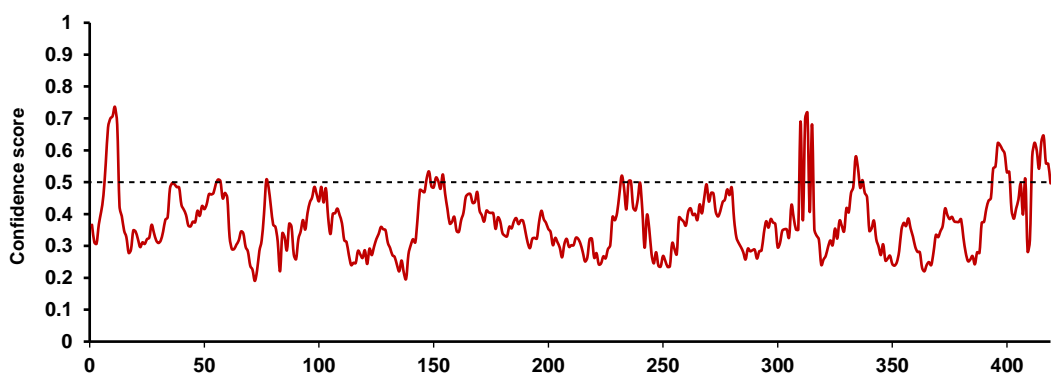
Figure 4.10. Protein disorder prediction methods identify common consensus regions of intrinsic disorder within NEMO. (A) NEMO domain structure is displayed with a selection of highlighted key known/predicted protein interaction sites and identified (either *in vitro* or *in vivo*) IKK β -specific phosphorylation sites. On the same amino acid sequence scale are the results of a selection of protein disorder predictors (Espritz, IUPRED, PV2, PONDR VLXT and PONDR VSL2b) taken from the D²P² database. Coloured blocks represent disordered regions having a confidence score higher than 0.5, with a 5% false positive rate. The level of agreement between all of the disorder predictors is shown as color (green) intensity in an aligned gradient bar below the stack of predictions. Directly beneath this is clear indication of sequence positions for which there is 75% agreement between all predictors in the database for the region being disordered. Below this is a representation of consensus regions of defined structure or disorder provided by the various X-ray and NMR structures of NEMO within the PDB (consensus data obtained from MobiDB database). (B) Intrinsic disorder probability plot for NEMO generated using DisEMBL. Loops/coils (in blue) as defined by DSSP - alpha-helix, 3-10 helix or beta-strand defined as ordered, and all other states as loops/coils. Missing X-ray coordinates (green), as defined by REMARK-465 entries in PDB. Dashed lines mark the threshold above which amino acids are regarded as disordered according to the two separate prediction definitions. (C) Intrinsic disorder probability plot for NEMO generated using PrDOS. Threshold with 5% false positive rate shown as red dashed line. (D) Intrinsic disorder probability plot for NEMO generated using DISOPRED3. Blue line indicates residue disorder confidence levels. Threshold with 5% false positive rate shown as black dashed line. For disordered residues, the orange line shows the confidence of disordered residues being involved in protein-protein interactions. (E) Intrinsic disorder probability plot generated using MFDP2. Threshold with 5% false positive rate shown as black dashed line. (F) Potential PEST motifs in NEMO identified by epestfind and a cross-species alignment of the PEST motif (shown in bold) with a score of +8.49. Blue residues are flanking positively charged residues. Red highlights non-conserved residues. (G) DISOPRED3 prediction of intrinsic disorder and residues involved in protein binding for the well-characterised IDP, p53. CC, coiled coil. α H, alpha-helix. LZ, leucine zipper. ZNF, zinc-finger domain. PRR, proline rich region. P, phosphorylation



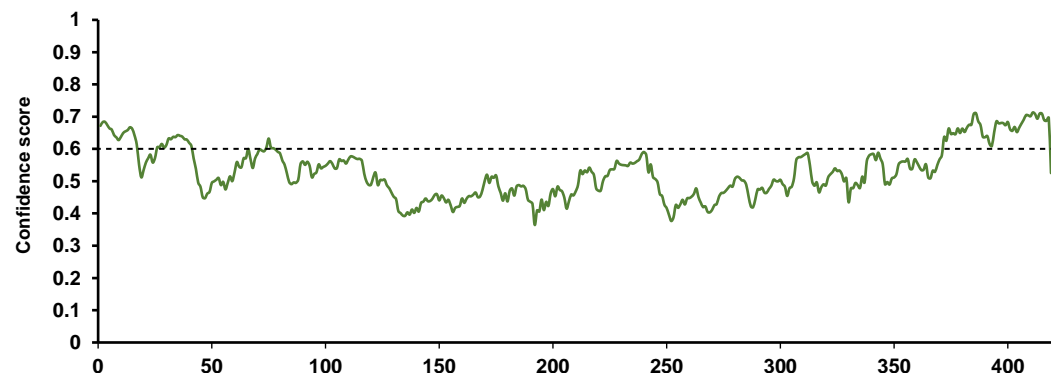
A



B



C



D

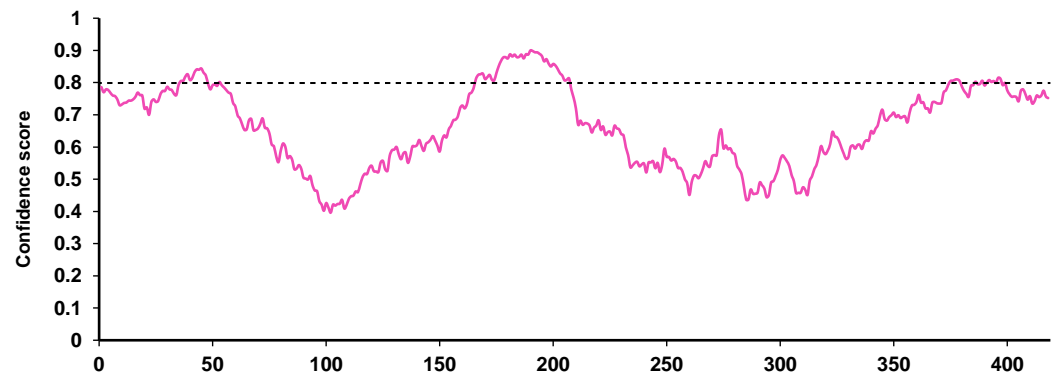


Figure 4.11. mORF predictors identify segments within intrinsically disordered regions of NEMO that might fold upon binding to interaction partners. **(A)** Plot of confidence scores derived from ANCHOR predictor that residues within NEMO are within molecular recognition features (mORFs). Residues with confidence scores above threshold = 0.5 are predicted to be within mORFs. **(B)** Plot of confidence scores derived from mORFpred predictor that residues within NEMO are within molecular recognition features (mORFs). Residues with confidence scores above threshold = 0.5 are predicted to be within mORFs. **(C)** Plot of confidence scores derived from mORFCHIBI SYSTEM predictor that residues within NEMO are within molecular recognition features (mORFs). Residues with confidence scores above threshold = 0.6 are predicted to be within mORFs. **(D)** Plot of confidence scores derived from DisoRDPbind predictor that residues within NEMO are within molecular recognition features (mORFs). Residues with confidence scores above threshold = 0.8 are predicted to be within mORFs.

confidence mORF within the leucine zipper (LZ) domain of NEMO. Interestingly, each of the prediction tools identified at least one potential, albeit relatively low confidence, mORF within the minimal IKK binding domain of NEMO (aa 44-111).

4.2.4 NEMO is susceptible to rapid proteolysis in vitro by the 20S proteasome and is protected from degradation by interaction with IKK α or IKK β

It must be stressed that the in silico predictions of potential intrinsic disorder and mORFs in NEMO were performed in order to guide further investigation, and should not be taken as definitive. Collectively, the predictions indicated that NEMO is a candidate IDP, with significant regions of disorder at the extreme N terminus and within the PRR that might make NEMO susceptible to ‘degradation by default.’ The presence of mORFs within the N terminal disordered region suggested that this region might undergo folding upon interaction with binding partners, thus preventing recognition of this potentially effective proteasomal degradation initiation site. To investigate this, the susceptibility of NEMO to in vitro 20S-mediated proteasomal degradation was assessed (Figure 4.12). Sensitivity to 20S proteasomal degradation has been proposed as an operational definition for IDPs (Tsvetkov et al., 2008). [³⁵S]-methionine labelled NEMO was synthesised in an in vitro coupled transcription and translation (T&T) reaction and incubated with purified 20S proteasomes. NEMO was rapidly degraded within 60 minutes incubation with 20S proteasomes (Figure 4.12A, B and C). As described earlier, a ‘nanny’ model has been proposed to account for the protection of IDPs from degradation by default within the cell; interactions with partner proteins mask and/or induce folding of IDRs that would otherwise target IDPs for degradation by the 20S proteasome (Tsvetkov et al., 2009). The disorder predictions highlighted a potential N-terminal IDR overlapping the IKK binding site of NEMO. N-terminal IDRs are known to facilitate rapid 20S-dependent turnover of other well-characterised IDPs, such as P53. This N-terminal IDR was also predicted to contain at least one mORF, suggesting that this region may be stabilised through protein interactions. To investigate whether interaction with IKK might protect NEMO from degradation, NEMO was incubated with or without IKK α and/or IKK β in the presence of purified 20S proteasomes. Both IKK α and IKK β significantly protected NEMO from 20S-dependent degradation (Figure 4.12D and E). The greater protection mediated by IKK β compared to IKK α was at odds with the observation that IKK α KO cells exhibited a greater reduction in NEMO protein than IKK β KO cells. There are numerous technical explanations for why this might be the case. For example, the greater band smear observed when IKK α was expressed with NEMO compared to IKK β may indicate that IKK α was also partially degraded by the 20S proteasome under these conditions. Further experiments are needed to confirm this. Also, the differing location of the FLAG-tags in IKK α (N-terminal) and IKK β (C-terminal) might have had an impact on the results, particularly given that the NEMO-binding domain is located at the extreme C-terminus. These experiments will be repeated with un-tagged versions of IKK to test this.

Collectively, the in silico predictions and in vitro 20S proteasome assay results highlighted that NEMO contains significant regions of intrinsic disorder that might act as highly effective initiation sites for proteasomal degradation in the absence of binding partners, such as IKK α and IKK β .

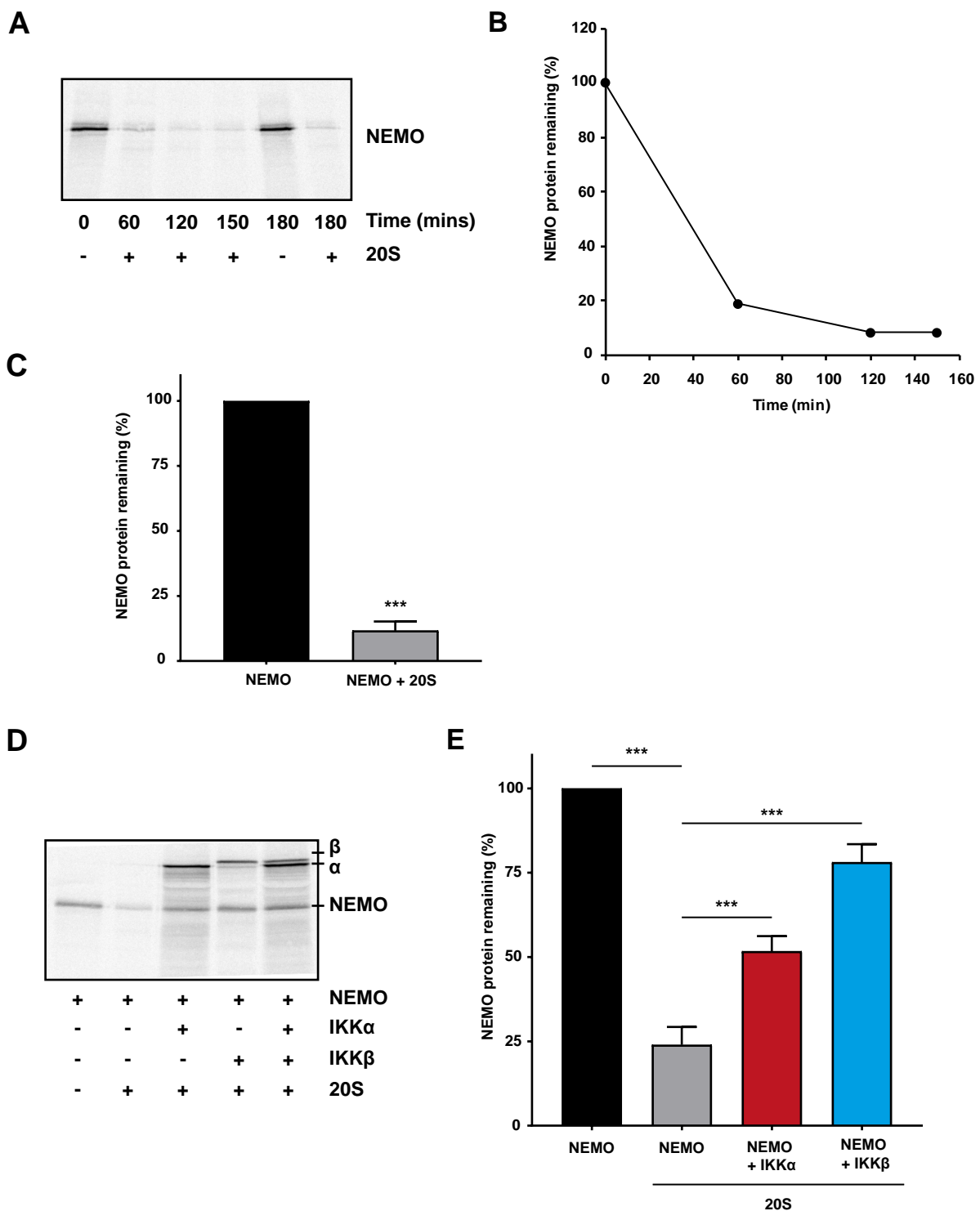


Figure 4.12. NEMO is rapidly degraded by the 20S proteasome *in vitro*, and protected from degradation by IKK α or IKK β . (A) FLAG-NEMO was synthesized *in vitro* using a T&T reaction in the presence of [35 S]-methionine, followed by incubation with purified 20S proteasomes for the indicated time intervals. Samples were subjected to SDS-PAGE and detected by autoradiography. (B) Quantification of this data is shown graphically, where the amount of protein is represented as a percentage of protein present at time zero. Data are from a single experiment. (C) Results quantified from three independent experiments in which FLAG-NEMO was incubated with 20S proteasomes for 2 hours. Statistical testing performed using unpaired, two-tailed Student's t-test (** = $p < 0.001$). (D) FLAG-NEMO, FLAG-IKK α and FLAG-IKK β were synthesized *in vitro* using a T&T reaction and [35 S]methionine. FLAG-NEMO was then incubated with purified 20S proteasomes for 1 hour with or without FLAG-IKK α or FLAG-IKK β . The degradation reaction was stopped, samples were subjected to SDS-PAGE and detected by autoradiography. (E) Results quantified from three independent experiments. Statistical testing performed using one-way ANOVA with Tukeys multiple comparisons test (** = $p < 0.001$). Experiments performed by Nadav Myers, The Weizmann Institute, Israel.

4.2.5 Reduced NEMO expression does not account for the lower TNF α -induced NF κ B activation observed in IKK α KO cells or the inability of re-expressed IKK to induce the degradation of I κ B α in DKO cells.

As discussed in Chapter 3, IKK α KO cells exhibited reduced induction of NF- κ B transcriptional activity in response to TNF α compared to WT cells. This could be reversed by re-expressing WT, but not kinase-dead (KD), IKK α (Chapter 3, Figure 3.10). IKK α KO cells also exhibited reduced NEMO expression compared to WT (Figure 4.3A). To investigate whether the reduced NEMO expression might contribute to the weaker induction of NF- κ B in response to TNF α , the effect of re-expression of WT or L329P mutant NEMO on TNF α -induced NF- κ B activity in IKK α KO cells was examined (Figure 4.13A). The L329P mutation within the leucine zipper (LZ) domain abrogates the ability of NEMO to bind to K63-linked polyubiquitin chains such that L329P NEMO is defective in mediating IKK and NF- κ B activation (Wu *et al.*, 2006a). As observed previously, re-expression of WT, but not kinase-dead (KD), IKK α , reversed the effect of IKK α knockout on the induction of NF- κ B activity. However, the reduced NF- κ B transcriptional activity in IKK α KO cells could not be reversed by overexpressing WT NEMO. WT NEMO, in fact, had a dose-responsive inhibitory effect on TNF α -induced NF- κ B activation. This was even more pronounced for L329P mutant NEMO. A dominant negative effect of NEMO overexpression on NF- κ B activation has been seen before (Krappmann *et al.*, 2000; Ye *et al.*, 2000). An equivalent Western blot was not performed to demonstrate the relative protein expression achieved in this experiment, however, the ratio of IKK α and NEMO constructs expressed were proportionally scaled down from amounts expressed in Figure 4.13B, which demonstrated approximately wild-type levels of IKK α and NEMO construct re-expression.

As discussed in Chapter 3, IKK constructs re-expressed into DKO cells activated NF- κ B transcriptional activity and phosphorylated IKK substrates, such as I κ B α and p65, in response to TNF α , but were seemingly incapable of inducing I κ B α degradation. To investigate if the low level of NEMO protein expression in DKO cells might explain these observations, WT and KD IKK α were re-expressed, with or without NEMO, in DKO cells, and cells treated with TNF α (Figure 4.13B). In WT cells, 10 minutes TNF α treatment induced the complete phosphorylation and degradation of I κ B α . As seen previously, DKO cells exhibited no response to TNF α and expressed lower levels of NEMO protein. Re-expression of WT, but not KD, IKK α partially restored phosphorylation of p65 and I κ B α , but had no effect on I κ B α expression, as seen previously. Re-expressed IKK α was phosphorylated within its activation loop (S176/180) in response to TNF α , albeit to a lower level than observed in WT cells. Re-expressed WT or KD IKK α both moderately increased the expression of NEMO. NEMO was re-expressed to levels similar to those seen in WT cells. Interestingly, co-expression of WT IKK α and NEMO increased the expression of NEMO above that observed following transfection of an equal amount of NEMO construct alone. This is further evidence in support of the stimulatory effect of IKK α expression on NEMO protein levels. KD IKK α also had a stimulatory effect on the expression of the NEMO construct, although it is difficult to compare the magnitude of this effect with that of WT IKK α because the two IKK α constructs were not expressed to the same level. Expression of WT IKK α alone did not induce phosphorylation of IKK α , unlike in other similar experiments (Figure 4.14). This is most likely because a lower amount of IKK α plasmid DNA was transfected into cells in this particular experiment. Overexpressed IKK subunits are known to induce their autophosphorylation (Poyet *et al.*, 2000). Interestingly, overexpressed NEMO had the effect of inducing the constitutive phosphorylation of WT, but not KD, IKK α in the

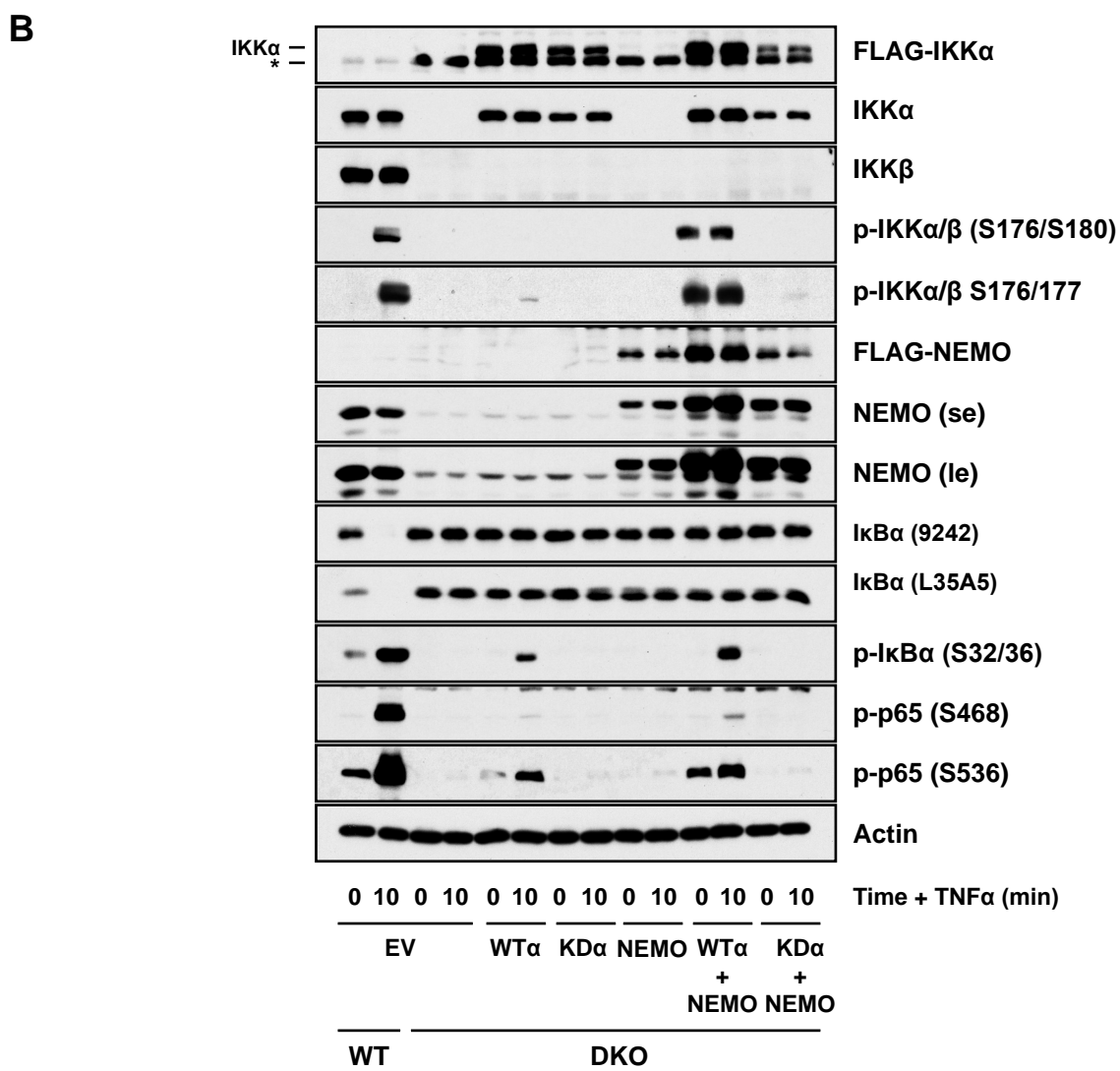
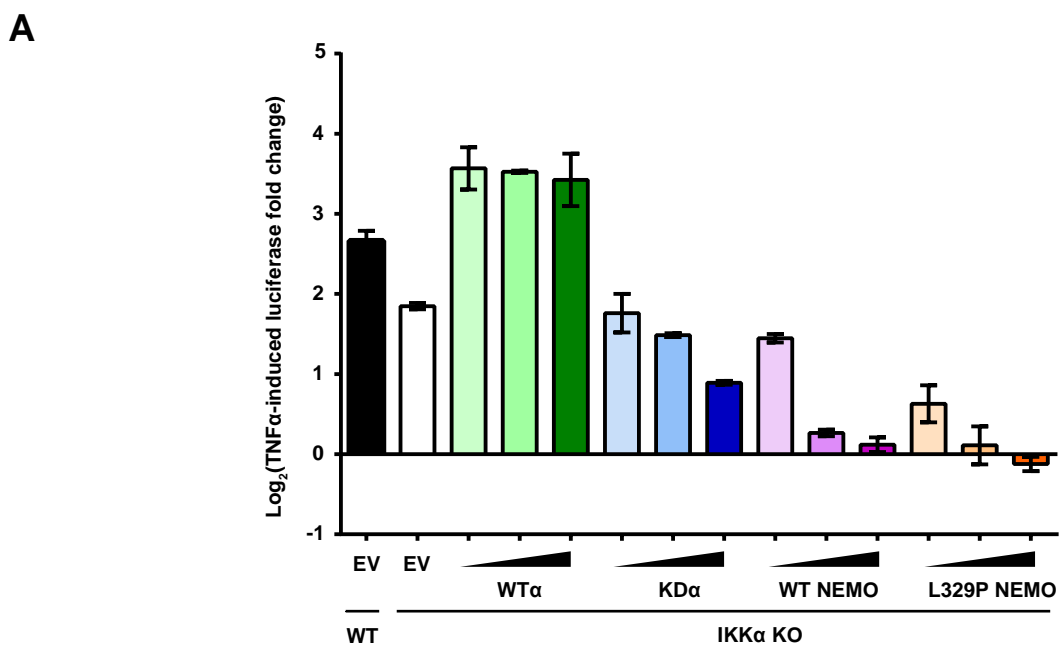


Figure 4.13. Reduced NEMO protein levels do not explain the reduced TNF-induced NF- κ B transcriptional activity observed in IKK α KO cells or the absence of I κ B α degradation observed upon TNF α stimulation in IKK DKO cells reconstituted with WT IKK α . (A) WT and IKK α KO HCT116 cells were seeded in antibiotic-free growth medium overnight prior to transient transfection with 0.1 μ g pGL4.32[luc2P/NF- κ B-RE firefly luciferase (reporter) plasmid DNA and 0.01 μ g renilla luciferase (internal control) plasmid DNA, in addition to the following quantities of plasmid DNA: 20 ng EV, 5, 10 and 20 ng WT IKK α , 5, 10 and 20 ng KD IKK α , 5, 10 and 20 ng WT NEMO and 5, 10 and 20 ng L329P NEMO. Total transfected plasmid DNA was equalized to 20 ng with EV. The following day, cells were treated with 10 ng/ml recombinant TNF α for 4 hours. Firefly luciferase luminescence was normalised relative to renilla luciferase luminescence and data expressed as log₂(fold change in TNF α -induced luciferase activity relative to the relevant matched untreated condition). Results are mean \pm SD of two experiments performed in cell culture triplicate. (B) WT and IKK α / β DKO HCT116 cells were seeded in 6-well plates in antibiotic-free growth medium for 24 hrs prior to transient transfection with the following quantities of plasmid DNA: 0.45 μ g pCMV-Tag2B empty vector, 0.15 μ g pCMV-Tag2B-WT IKK α , 0.25 μ g pCMV-Tag2B-KD IKK α (K44A) and 0.2 μ g pCMV-Tag2B-NEMO. Total transfected plasmid DNA was equalized to 0.45 μ g with EV. 24 hours later, cells were treated with 10 ng/ml TNF α for 10 minutes. Whole-cell lysates were fractioned by SDS-PAGE and Western blotted with the indicated antibodies. Data are from a single experiment. WT, wild-type. KD, kinase dead. EV, empty vector. *unspecified band. p-, phospho-.

absence of stimulus. This suggests that the IKK α phosphorylation observed was a result of IKK α kinase activity, possibly through trans-autophosphorylation. Overexpression of NEMO possibly activates IKK activity through an enforced oligomerization effect, also known as a ‘proximity activation effect’ as has been shown with RIP1 (Ting *et al.*, 1996; Poyet *et al.*, 2000).

This constitutively phosphorylated IKK α induced a higher level of p65 phosphorylation at Serine 536, but not Serine 468, in the absence of TNF α stimulation. However, no increase in basal I κ B α phosphorylation or degradation was observed. TNF α treatment caused a negligible increase in IKK α phosphorylation. P65 and I κ B α were phosphorylated to higher levels than observed with WT α single expression, however, degradation of I κ B α was not restored.

4.2.6 Overexpressed NEMO undergoes less polyubiquitylation when co-expressed with IKK α

Collectively, the preliminary data described up until this point suggest that in the absence of IKK α or IKK β NEMO protein has a shorter half-life, possibly due to enhanced proteasomal degradation. *In vitro* 20S proteasome assays suggest that in the absence of IKK interaction partners, NEMO undergoes enhanced ATP- and ubiquitin-independent degradation, possibly due to greater exposure of terminal IDRs. Whether this is the case for endogenous NEMO remains to be seen. However, terminal IDRs are also known to be highly important for effective recognition and initiation of ATP- and ubiquitin-dependent degradation by the 26S proteasome; they are thought to facilitate interaction of the targeted substrate with the ATPase ring that initiates unfolding (Guharoy *et al.*, 2016b). An overall higher degree of disorder may also shorten a protein’s half-life due to a higher processivity of degradation upon engagement by the 26S proteasome; ATPase subunits may spend less time and energy unfolding IDPs compared to highly structured proteins of similar length (van der Lee *et al.*, 2014). Furthermore, an analysis of 171 primary degrons showed that approximately 80% are present in disordered regions, while degradation-linked, ubiquitinated lysines are often predicted to fall into locally disordered regions (Guharoy *et al.*, 2016a). In addition, IDPs are highly susceptible to ubiquitylation and degradation by the 26S proteasome following heat-shock induced misfolding stress (Ng *et al.*, 2013).

As such, it is plausible that interaction of NEMO with IKK subunits protects it from degradation by the ubiquitin-dependent 26S proteasome pathway, either through sequestration of highly efficient disordered initiation sites, or through promotion of proper folding. In a preliminary step towards addressing this, the effect of IKK α overexpression on basal and TNF α -induced ubiquitylation of transiently transfected NEMO was examined using a GST-Dsk2 pulldown (Figure 4.14). Dsk2 is a UBA domain-containing protein from *S. cerevisiae* that acts as a ‘shuttle factor’ by binding to K48-linked polyubiquitinated proteins and delivering them to the 26S proteasome for subsequent degradation (Rao *et al.*, 2002). However, *in vitro*, Dsk2 has been shown to strongly interact with unanchored K48-, K63- and K29-linked polyubiquitin and monoubiquitin in a largely linkage-independent manner (Ohno *et al.*, 2005; Raasi *et al.*, 2005, Tsuchiya *et al.*, 2017). The Dsk2 pull-down was thus used as a general indication of the ubiquitylation status of overexpressed NEMO in the presence or absence of overexpressed WT IKK α . As seen previously, co-transfection of IKK α and NEMO led to an increased expression of NEMO protein compared to transfection of NEMO alone. Interestingly, an increase in a NEMO species corresponding to a

molecular weight of approximately 110 kDa was also observed upon co-transfection of IKK α and NEMO. A species of this size has been demonstrated to represent dimeric NEMO (Marienfield *et al.*, 2006). Whether NEMO dimerization was actually enhanced by co-expression of IKK α or whether the apparent increase in dimeric NEMO was due to a stoichiometric increase in monomeric NEMO expression is difficult to assess without additional controls.

Interestingly, a greater amount of NEMO protein was pulled-down by GST-Dsk2 when WT IKK α and NEMO were co-expressed compared to NEMO alone, but less polyubiquitylated NEMO was detected, suggesting that interaction with IKK α might protect NEMO from polyubiquitylation. The greater overall pull-down of NEMO in the absence of IKK α might indicate that a greater fraction of the NEMO protein in the cell under these conditions is in a monoubiquitylated form, indicated by the thicker NEMO banding pattern. Although non-specific interaction of NEMO with GST-Dsk2 cannot currently be ruled out. An increase in the ubiquitylation of endogenous NEMO upon treatment with TNF α for 10 minutes was observed as expected. A similar increase was not observed for overexpressed NEMO, either alone or in the presence of co-expressed IKK α . The discrete banding pattern of ubiquitylated NEMO, separated by intervals of approximately 8 kDa (i.e. the molecular mass of ubiquitin), in contrast to the ‘smear’ of ubiquitylated material observed in the p-IkB α GST-Dsk2 pull-down, is more consistent with small homotypic ubiquitin oligomers of a particular chain type (Emmerich *et al.*, 2015). However, these results are very preliminary in nature. The specificity of the pull-down for ubiquitylated NEMO will need to be confirmed using mutant Dsk2 that is unable to bind to ubiquitin. Furthermore, the linkage identity of the polyubiquitin chains will need to be confirmed. Various immobilised ubiquitin-binding domains (UBDs) with differing specificity for ubiquitin chains, as well as linkage-specific antibodies could be used to identify the specific ubiquitin chain linkages that IKK α appears to protect NEMO from receiving.

The GST-Dsk2 pull-down was also blotted for phosphorylated IkB α (Serine 32/36) to understand why IkB α phosphorylated by IKK α re-expressed into IKK DKO cells did not appear to undergo degradation (as observed in Chapter 3 Figure 3.10B). Following 10 minutes TNF α treatment, polyubiquitylated p-IkB α was detected in WT cells. A larger amount of polyubiquitylated p-IkB α was detected after 10 minutes in IKK β KO cells, consistent with the slightly defective degradation of IkB α observed in these cells. As observed previously, the phosphorylation of IkB α by overexpressed IKK α in DKO cells was not accompanied by the expected degradation of IkB α . However, the phosphorylation of IkB α was accompanied by an increase in the polyubiquitylation of p-IkB α . This leaves two explanations. Either the phosphorylated and ubiquitylated IkB α is somehow unable to be recognised by β -TrCP and degraded under these conditions, or as described in Chapter 3, the efficiency of IKK α transfection into DKO cells is not high enough to detect a significant decrease in total IkB α . The latter appears most likely, as a small decrease in overall expression of IkB α is consistently observed.

As observed previously (Figure 3.10B and Figure 4.13B), IKK α expressed alone induced only a small increase in S468 phosphorylation of p65 following TNF α treatment. This observation had called in to question the sufficiency of IKK α activity for phosphorylation of this site. However, here we observed that the phosphorylation of p65 at S468 was significantly enhanced when IKK α was co-expressed with NEMO in IKK DKO cells, even in the absence of TNF α stimulation (Figure 4.14). The markedly enhanced phosphorylation and hence activation status of IKK α co-expressed with NEMO potentially explained this difference. IKK α activity alone, therefore, appeared to be

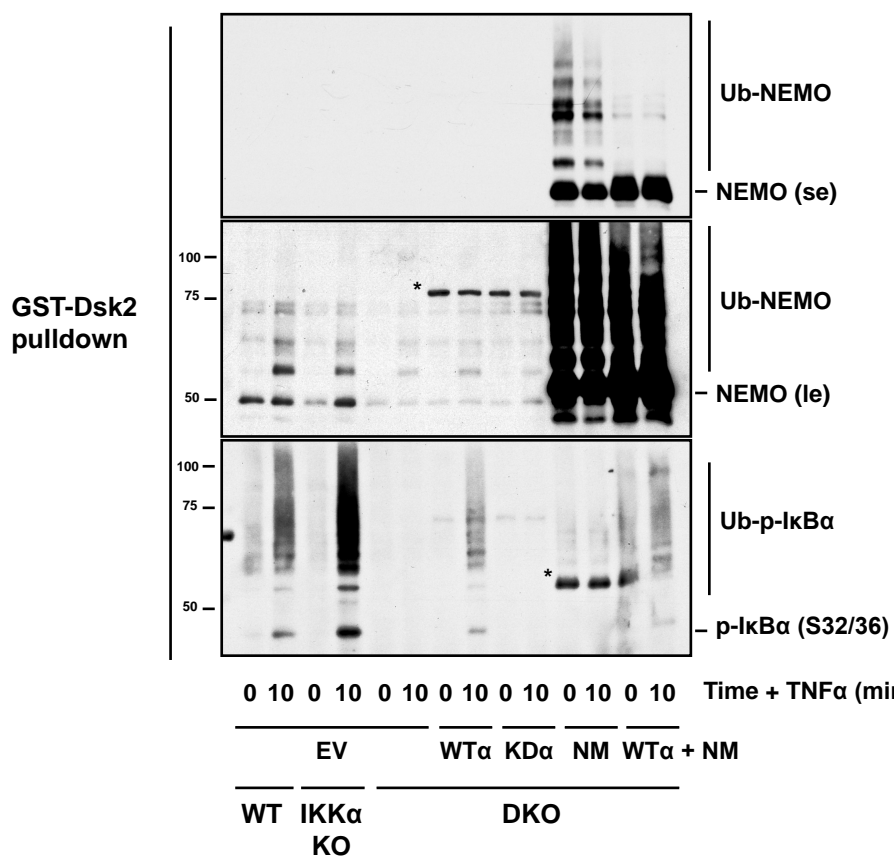
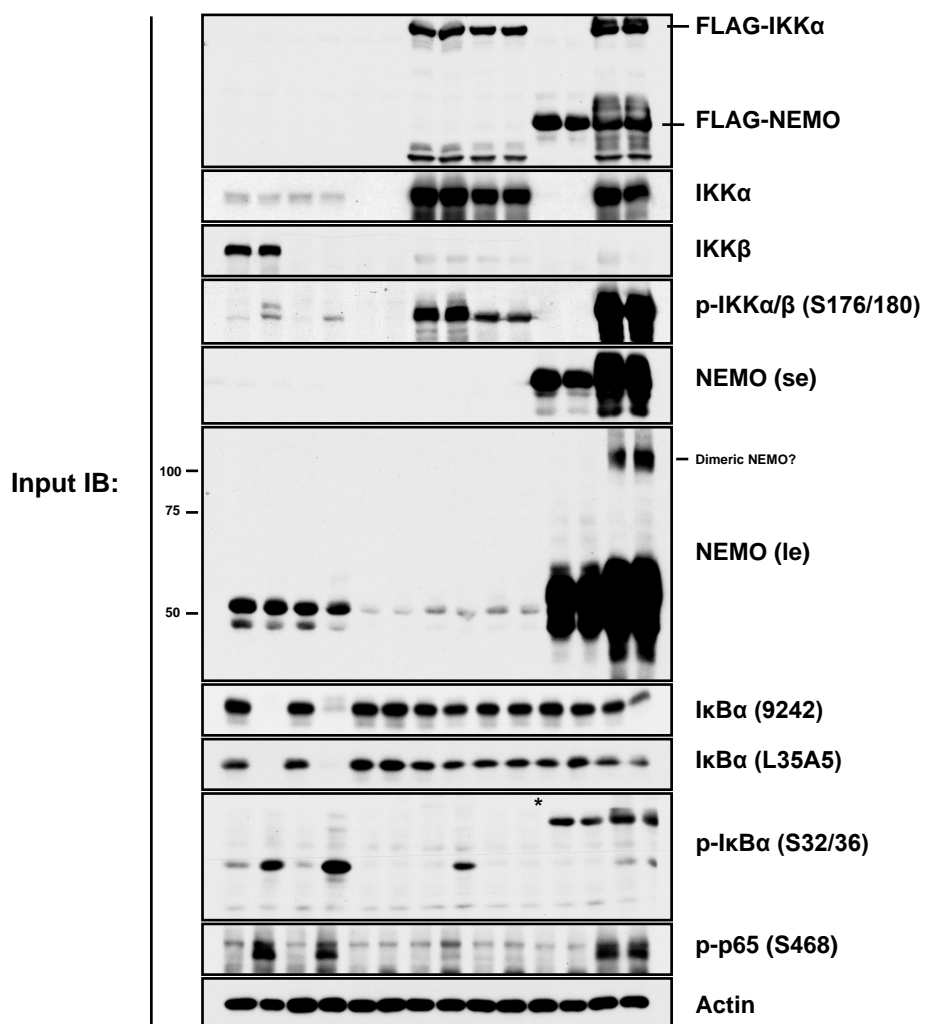


Figure 4.14. Overexpressed IKK α protects co-expressed NEMO from polyubiquitination. WT, IKK α KO and IKK α/β DKO HCT116 cells were seeded in 10 cm dishes for 24 hours prior to transient transfection with the following quantities of plasmid DNA: 8.5 μ g pCMV-Tag2B empty vector, 4 μ g pCMV-Tag2B-WT IKK α , 8.5 μ g pCMV-Tag2B-KD IKK α (K44A) and 4 μ g pCMV-Tag2B-NEMO. Total transfected plasmid DNA was equalized to 8.5 μ g with EV. 24 hours later, cells were treated with 10 ng/ml TNF α for 10 minutes. A proportion (input) of whole-cell lysates were fractioned by SDS-PAGE and Western blotted with the indicated antibodies. The remaining whole cell lysates were subject to pre-clearing with GST beads, followed by immunoprecipitation using GST-Dsk2 beads to pull-down ubiquitinated proteins. Eluted lysate was then fractionated by SDS-PAGE and Western blotted with the indicated antibodies. Data are from a single experiment. WT, wild-type. KD, kinase dead. EV, empty vector. NM, NEMO construct *cross-reactive FLAG bands. p-, phospho-. se, short exposure. le, long exposure.

sufficient to phosphorylate this site. The much higher overexpression of IKK α and NEMO in this experiment may explain the discrepancy with Figure 4.13B, where a similar effect was not observed. As with the detection of IkB α degradation, the issue of poor transfection efficiency may have played a role in confounding the results of IKK α expression on S468 phosphorylation.

4.3 Discussion

4.3.1 IKK expression is necessary for wild type NEMO protein expression.

The evidence presented here suggested that in the absence of IKK kinase expression the steady-state expression and half-life of NEMO protein were substantially reduced; in the case of IKK DKO NEMO protein expression was approximately 90% lower than in WT cells. Preliminary evidence was presented that the shorter half-life in the absence of IKK expression was due to enhanced proteasomal degradation. Labs working with IKK α and IKK β knockout mouse embryonic fibroblasts (MEFs) have not reported a similar effect of IKK knockout on NEMO protein expression (Li *et al.*, 2000; Kwak *et al.*, 2005; Solt *et al.*, 2009). A simple potential explanation for this discrepancy could be biological differences in the NF- κ B pathway between MEFs and human cancer cell lines. Despite a remarkable degree of conservation of function between humans and mice that makes mice excellent preclinical models of human disease, there does exist significant biological differences, particularly in immune system development and activation (Mestas *et al.*, 2004). Studies that have performed siRNA-mediated knockdown of IKK α and/or IKK β in human cell lines have generally neglected to probe for NEMO expression (Huang *et al.*, 2007, Adli *et al.*, 2010, Jiang *et al.*, 2010, Nottingham *et al.*, 2014). Given that this work has focused on a single human cancer cell line - HCT116 cells - it cannot presently be ruled out that the observed phenotypes of IKK knockout are not cell line specific. Future experiments will probe the effect of IKK knockdown on NEMO protein expression in a range of human cell lines. However, evidence for the generality of our observations comes from the characterisation of the expression of IKK signalling components in patients with a rare form of severe combined immunodeficiency (SCID) caused by a loss of function mutation in the *IKBKB* gene encoding IKK β (Pannicke *et al.*, 2013). Fibroblasts and peripheral-blood mononuclear cells (PBMCs) from these patients exhibited a complete loss of IKK β protein expression, accompanied by a significant loss of IKK α and NEMO protein expression. Pannicke *et al.*, showed that this was not due to reduced mRNA expression, but did not explore this observation further. This provides great confidence in the physiological relevance of our results.

The molecular basis of the apparent greater importance of IKK α in maintaining wild-type NEMO protein expression, implied from the differential effects of IKK α and IKK β knock out, is currently unclear. The results of other experiments were not entirely consistent with this observation. For example, IKK α did not offer greater protection than IKK β within an *in vitro* 20S proteasome assay. Although, this could reflect the fact that an *in vitro* transcription and translation system is far from a true reflection of the *in vivo* state. Within the cell, IKK α may enhance NEMO folding and/or stability through phosphorylation events or by mediating interaction with other proteins. In addition, IKK re-expression studies did not reveal a clear difference in the ability of IKK α or IKK β to increase NEMO protein expression. Indeed, the sufficiency of IKK to promote NEMO protein expression was not conclusively proven, nor was the importance of interaction between IKK and NEMO. IKK subunits may promote NEMO expression through facilitating interaction with another protein, for example. Generation of re-expressed

IKK α and IKK β stable cell lines will provide a clearer understanding of the relative importance of the IKK subunits, while the use of IKK NEMO-binding domain truncation mutants will provide insight into the importance of interaction with NEMO. Furthermore, compared to WT cells, IKK α KO cells exhibited only a small, albeit statistically significant, reduction in NEMO half-life following inhibition of protein translation. The half-life of NEMO in IKK β KO cells was not examined. It remains to be determined, therefore, whether the magnitude of this decrease in half-life is sufficient to account for the lower steady state NEMO protein observed in IKK α KO cells compared to IKK β KO cells.

Nevertheless, the finding that NEMO protein expression is lower in IKK α KO cells compared to IKK β KO cells is interesting in the context of what is known about the interaction between IKK subunits and NEMO. IKK α has been reported to bind NEMO with a weaker affinity *in vitro* than IKK β (May *et al.*, 2002). However, the crystal structures of NEMO in complex with either an IKK β NBD peptide or an IKK α/β hybrid NBD peptide indicate a structurally equivalent binding mode of key IKK α and IKK β NBD residues to the specificity pocket of NEMO (Rushe *et al.*, 2008). Curiously, the authors did not solve the structure of a true NEMO:IKK α complex and so were left to speculate that the reduced affinity of IKK α might result from sequence differences in the helical region N-terminal to the NBD residues. The vast majority of studies relating to interaction between NEMO and IKK have focused on IKK β , with very little attention given to IKK α . This might be related to the historical greater importance placed on IKK β for regulation of canonical NF- κ B; a dogma that has been called into question in more recent years (Adli *et al.*, 2010, and see Chapter 3). Differences in NEMO binding may be key to understanding differences in IKK α and IKK β function *in vivo* because swapping the C-termini of IKK α and IKK β confers IKK α with IKK β -like activity (Kwak *et al.*, 2000). Evidently, more work is needed to understand the functional consequences of structural differences in the interaction between IKK α /IKK β and NEMO.

Unlike the effect of IKK knockout on NEMO expression, this is not the first report of regulation of NEMO protein stability. A handful of studies have indicated that NEMO degradation is a mechanism by which the NF- κ B can be regulated under certain circumstances (Ammirante *et al.*, 2010; Fliss *et al.*, 2012; Shibata *et al.*, 2012; Medunjanin *et al.*, 2016). Ammirante *et al* demonstrated that the HSP70 co-chaperone, BAG3, influences the levels of NEMO protein in human osteosarcoma and melanoma cell lines, possibly through inhibiting interaction of HSP70 and blocking HSP70-mediated delivery of NEMO to the proteasome, although this later conclusion was made without strong supporting evidence. Furthermore, the majority of the work by Ammirante *et al* relied on siRNA-mediated knockdown of Bag3 using a single siRNA oligonucleotide at 200 nM, a concentration at which off-target effects are highly likely. Nevertheless, HSP70 has been shown to interact with NEMO and to inhibit NEMO oligomerization *in vitro* (Agou *et al.*, 2002; Ran *et al.*, 2004), although HSP70-mediated delivery of NEMO to the proteasome has yet to be demonstrated. Another co-chaperone, HSP90, has been shown to be required for IKK complex formation and NF- κ B activation, and is believed to stabilize nascent IKK α and IKK β during biosynthesis and prevent their proteasomal degradation (Chen *et al.*, 2002; Broemer *et al.*, 2004). However, Broemer *et al* found that HSP90 was not important for the stability of nascent or existing NEMO protein folding or stability. Meanwhile, Fliss *et al.*, showed that murine cytomegalovirus inhibits NF- κ B activation through interaction of the viral protein M45 with NEMO, which, via an undefined mechanism, targets NEMO to autophagosomes and

subsequent lysosomal degradation. This mechanism of NEMO degradation, however, is limited to the pathogenic state.

NEMO has also been proposed to be targeted for lysosomal degradation during the normal function of the NF- κ B pathway (Shibata *et al.*, 2012). Shibata *et al* demonstrated that the Golgi protein, p47 binds to K63-linked and linear chain polyubiquitylated NEMO following stimulation of cells with TNF α or IL-1. Unconvincing evidence was presented that p47 targets polyubiquitinated NEMO for lysosomal degradation, thereby inhibiting the NF- κ B pathway. Proteasomal degradation of NEMO was ruled out on the basis of treatment with MG-132 for 2 hours, which is likely to be insufficient to observe a significant accumulation of proteasomally-degraded NEMO. p47 also had no effects on the basal stability of NEMO. Nevertheless, IKK knockout might increase the susceptibility of NEMO to p47-mediated lysosomal degradation in the absence of stimulus. Furthermore, we observed a greater TNF α -induced reduction of NEMO expression in IKK KO cells compared to WT. It will be interesting to investigate whether this reflected enhanced lysosomal degradation of NEMO.

The observation that NEMO protein is significantly less stable in the absence of both IKK α and IKK β is potentially interesting in the context of the known role of NEMO in the response to genotoxic stress (Chapter 1, Section 1.3.6). The observation that NEMO is unstable in the absence of IKK α or IKK β raises the question of how 'IKK-free' NEMO is able to perform its function during DNA damage repair and avoid rapid turnover. One possibility is hinted at by the fact that ATM, PIASy and PARP1 have all been shown to interact with NEMO within its disordered N-terminus, in a region overlapping the IKK binding domain of NEMO (Mabb *et al.*, 2006; Wu *et al.*, 2008; Stilmann *et al.*, 2009). Furthermore, the interactions between NEMO and ATM, PIASy and PARP1 have been shown to be mutually exclusive with interaction with IKK β . This suggests that during 'hand-over' of NEMO from IKK β to components of the DNA damage response machinery, the N-terminal disordered region of NEMO might remain masked through interaction with DNA damage response proteins. This may protect IKK-free NEMO from turnover, on the assumption that exposure of the N-terminal IDR is the signal for NEMO degradation. It will be interesting to determine whether ATM, PIASy and PARP1 protect NEMO from *in vitro* 20S-dependent proteasomal degradation in a similar manner to IKK α and IKK β .

Numerous other proteins have been shown to bind to the N-terminal region of NEMO, some in a mutually exclusive manner with IKK β , including SENP2 (Lee *et al.*, 2011), NESCA (Napolitano *et al.*, 2009) cIAP1 (Jin *et al.*, 2009) and TRAF6 (Gautheron *et al.*, 2010). The apparent conformational flexibility of the N-terminal region of NEMO may be important for mediating such promiscuous protein interactions.

4.3.2 NEMO is a protein with significant regions of intrinsic disorder.

Previous studies have highlighted that NEMO exhibits significant conformational flexibility (Agou *et al.*, 2002; Catici *et al.*, 2015; Catici *et al.*, 2016). However, this is the first report that this structural disorder may be linked to turnover of NEMO protein. Agou *et al* first highlighted that recombinant monomeric NEMO has a circular dichroism profile consistent with a secondary structure of 44% α -helix, 0% β -sheet/turn and 56% random coil. Catici *et al* refined these estimates to 48% α -helix, 11% β -sheet/turn and 41% random coil, and extended this work to demonstrate that molecular flexibility and ligand-induced conformational change are central to the function of NEMO. Catici *et al* propose that NEMO exists in a broad equilibrium of interchangeable conformation

states, between well-folded (coiled coil) and locally unfolded (random coil) states, and this equilibrium can be differentially stabilized upon binding of ligands, such as $\text{I}\kappa\text{B}\alpha$, IKK and polyubiquitin chains. Intrinsic/extrinsic fluorescence measurements suggested that binding of an $\text{I}\kappa\text{B}\alpha$ peptide was coupled to the burial of hydrophobic residues in NEMO, consistent with the adoption of a more ordered conformation. In contrast, binding of either an IKK β NBD peptide or polyubiquitin was coupled to exposure of hydrophobic residues in NEMO, consistent with the adoption of a more disordered conformation. These conclusions appear difficult to reconcile with our hypothesis that IKK binding to the IBD of NEMO induces a more ordered conformation of the intrinsically disordered N-terminus, which protects NEMO from turnover by the proteasome. However, the fluorescence emissions measured by Catici *et al.* were, by their nature, global metrics of NEMO conformational change. Therefore, IKK binding could, in principle, induce a local ordering of the disordered N-terminus concomitant with induction of a greater overall degree of conformational disorder elsewhere in NEMO. Furthermore, disordered termini generally function more effectively than internal IDRs as proteasomal initiation sites (Prakash *et al.*, 2004), such that masking of the disordered N terminus by IKK binding may be sufficient to inhibit proteasomal degradation irrespective of an enhanced structural disorder elsewhere in the protein. Finally, Catici *et al.* did not investigate the effect of IKK α binding on the conformational heterogeneity of NEMO.

The conclusions of Catici *et al.* are also difficult to reconcile with other experimental evidence. For example, an apo-NEMO₄₄₋₁₁₁ minimal IKK binding domain fragment displayed an NMR spectra indicative of a high level of conformational heterogeneity, whereas an NEMO₄₄₋₁₁₁/IKK NBD peptide complex displayed a spectra more consistent with a single, folded species (Rushe *et al.*, 2008). Furthermore, the crystal structure of this complex indicated that the hydrophobic residues present within the specificity pocket of the IBD would be exposed to water if the IKK peptides were stripped from the structure, suggesting that this N-terminal region of NEMO may be disordered, masked or in a different conformation in the absence of IKK binding (Rushe *et al.*, 2008). However, recent evidence suggests that the structural instability of the short NEMO₄₄₋₁₁₁ construct may be an artefact of construct truncation (Guo *et al.*, 2014). Engineering of a homodimeric coiled-coil adaptor sequence from GCN4 to the C-terminal end of the NEMO₄₄₋₁₁₁ construct increased the stability of the NEMO IBD and increased IKK β binding affinity.

The predicted C-terminal disordered region aligned with the PRR of NEMO. This is perhaps not that surprising; well-characterised IDPs contain, on average, 1.7-1.8 times more prolines than other proteins in the Uniprot database (Theillet *et al.*, 2013). This is a higher fold-enrichment than any other amino acid. Proline-rich motifs have high propensities for assuming non-classical conformations, such as the polyproline type II (PPII) helix, which are extended, open structures with no internal hydrogen bonding that often act as unique binding interfaces for protein-protein interactions within scaffolding proteins and/or linkers between structured domains (Adzhubei *et al.*, 2013). Little is known about the function of the PRR of NEMO. To date, only CYLD, a deubiquitinase that cleaves K63 linked chains has been reported to bind within this region (Saito *et al.*, 2004). NEMO mutants with deletions in this region were not defective for activation of NF- κ B or binding to K63-linked polyubiquitin (Laplantine *et al.*, 2009). The functional significance of intrinsic disorder in this region has not been investigated. The presence of numerous putative phosphorylation sites with unknown functions (Figure 4.15) suggest this region may be important for regulation of NEMO activity. The function of the putative IKK β

phosphorylation site within the PRR, S376, has yet to be well-defined, although expression of S376A NEMO mutants has been shown to increase the ability of NEMO to simulate IKK β activity.

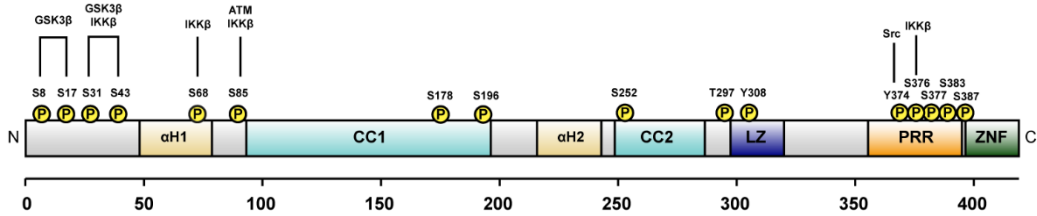


Figure 4.15. Putative phosphorylation sites in NEMO. All identified validated or putative phosphorylation sites on NEMO. Highlighted are those phosphorylation sites for which a putative kinase has been proposed. (Carter *et al.*, 2003; Wu *et al.*, 2006b; Palkowitzsch *et al.*, 2008; Lee *et al.*, 2012; Medunjanin *et al.*, 2016).

The significant regions of intrinsic disorder predicted from the NEMO protein sequence, particularly at the N- and C-termini, prompted us to examine the sensitivity of NEMO to *in vitro* degradation by the 20S proteasome. Susceptibility to degradation in this assay has been proposed as an operational definition for IDPs. Indeed, NEMO was a highly efficient substrate for 20S proteasomal degradation. Such was the efficiency with which NEMO was degraded that the amount of recombinant 20S proteasome had to be lowered for this assay relative to the amount typically used in such assays. Unfortunately, due to time constraints positive and negative controls for 20S proteasomal degradation were not completed, so it is not possible to compare the rate of NEMO degradation to that of structured proteins, such as PCNA, which typically exhibit very little degradation, and highly disordered proteins, such as p21^{CIP1}, which typically undergo levels of degradation comparable to the levels seen with NEMO. Nevertheless, IKK α and IKK β were both shown to protect NEMO from 20S-dependent degradation, consistent with our hypothesis that interaction with IKK stabilises NEMO. Future work will seek to confirm the importance of the interaction with IKK subunits for this protection, through the utilisation of IKK constructs with mutant/deleted NBDs.

4.3.3 The mechanism by which the IKK kinases promote NEMO stability remains to be determined.

The preliminary nature of the data presented here makes it impossible to draw definitive conclusions about the mechanisms by which IKK kinase subunits might stabilise NEMO and protect it from rapid turnover. However, a number of testable, alternative hypotheses can be proposed (Figure 4.16). Firstly, the N-terminal disordered region of NEMO may serve as a highly efficient initiation sequence for proteasomal degradation that is sequestered and/or conformationally altered through binding of IKK to the IBD of NEMO, thus preventing recognition and targeting to the proteasome. NEMO, in the absence of IKK, is a highly efficient substrate of *in vitro* 20S proteasomal degradation, but further work is needed to determine the relative contributions of the 20S and 26S proteasomes to the short half-life of NEMO in IKK KO cells. Indeed, terminal IDRs promote efficient degradation by both the 26S and 20S proteasome (Prakash *et al.*, 2004). Proteins with IDRs have, on average, shorter half-lives than proteins lacking appropriate initiation regions (Erales *et al.*, 2014). On the other hand, proteins with ubiquitin-like domains that bind to, but are not degraded by, the proteasome lack accessible disordered regions that permit the 26S proteasome to initiate degradation (Yu *et al.*, 2016). For example, the

yeast proteasome ‘shuttling factors’, Rad23 and Cdc34, escape degradation when targeted to the proteasome, but are rapidly degraded following the fusion of a disordered ~50 aa tail to their termini (Fishbain *et al.*, 2015). It will be interesting to investigate whether the 50 aa N terminal region of NEMO is capable of destabilizing normally stable proteins, such as a GFP reporter. Not all IDRs influence half-life; disordered polypeptides with repetitive compositions, such as polyglutamine and glycine-alanine repeats, actually impede proteasomal degradation (Shapiro *et al.*, 1998). However, this may be explained by a recent study that demonstrated a pronounced preference of the proteasome for initiation regions with unbiased sequences (Fishbain *et al.*, 2015).

Key to understanding the mechanism involved in NEMO degradation will be further characterisation of the effect of IKK interaction on the K48-linked polyubiquitylation of NEMO. Furthermore, use of IKK NBD mutants will be vital to confirm that interaction with IKK subunits rescues the shorter half-life of NEMO *in vivo*, and protects NEMO from degradation by the 20S proteasome.

IKK β has been shown to phosphorylate Serine 31 and 43 within the N-terminal disordered region *in vitro* (Carter *et al.*, 2003). It will be interesting to investigate whether these phosphorylation events are absent in IKK KO cell lines and whether this may influence NEMO stability. Indeed, phosphorylation of these residues by GSK3 β has previously been linked to NEMO stability (Medunjanin *et al.*, 2016). The observation that re-expressed kinase dead IKK has a stabilising impact on steady state NEMO protein expression, however, suggests that this may not be the case.

Alternatively, IKK may regulate the availability and/or conformation of the C-terminal disordered proline rich region, which was identified as containing a potential PEST motif. In some cases, deletion of PEST regions significantly affects protein half-life (Ramakrishna *et al.*, 2011; Li *et al.*, 2012). Typically, however, PEST motifs act as conditional proteolytic signals; the presence of a PEST motif alone is insufficient to target a protein for degradation (Rechsteiner *et al.*, 1996). The mechanism by which PEST motifs conditionally confer rapid proteasomal degradation is unclear. Interestingly, PEST motifs appear to be enriched in disordered regions of proteins, compared to globular domains (Singh *et al.*, 2006). One proposed mechanism therefore involves modulation of the conformational stability of the region containing the motif, through either protein interaction or phosphorylation, which might promote recognition of the motif by the U2/U3 ligase system, and lead to the subsequent rapid degradation of the protein containing it (García-Alai *et al.*, 2006; Sandhu *et al.*, 2006). The close proximity of the PEST motif to the potential IKK β phosphorylation site, Serine 376, makes this region of NEMO worthy of further investigation.

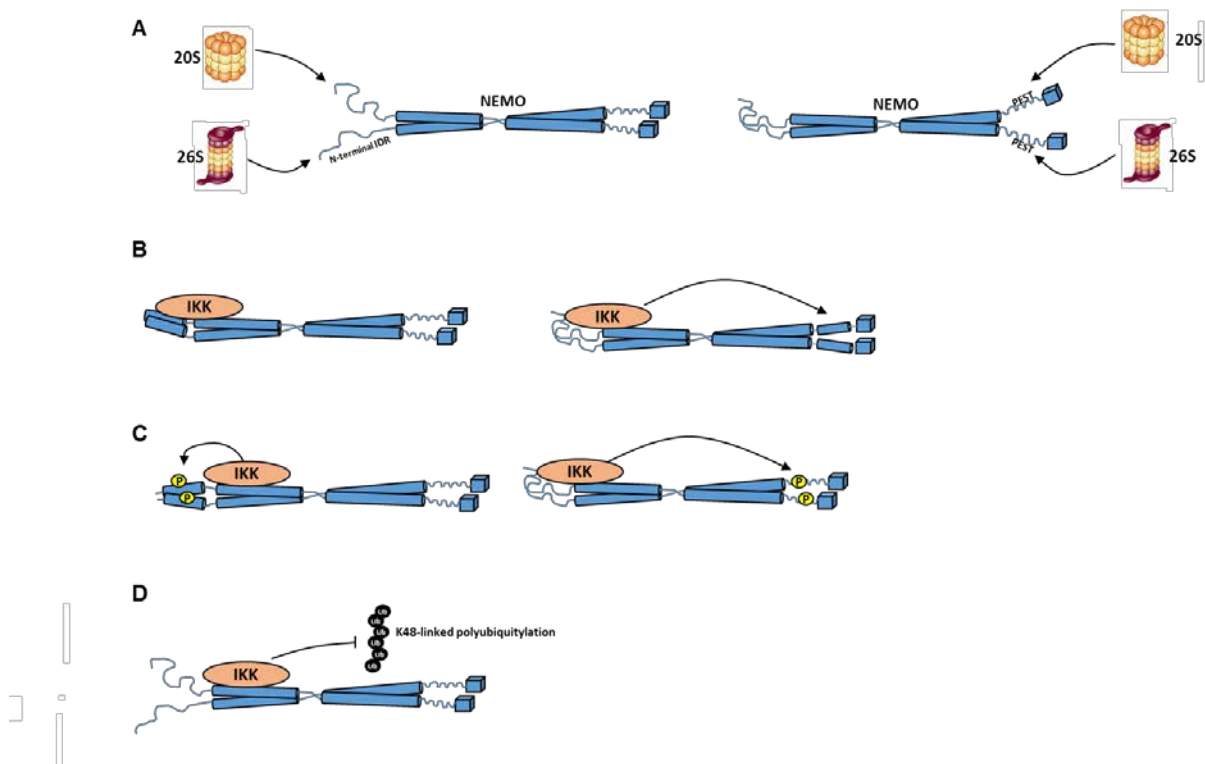


Figure 4.16. Schematic illustrating possible mechanisms of enhanced proteasomal degradation of ‘IKK-free’ NEMO and mechanisms of protection from degradation by interaction with IKK kinase subunits. (A) ‘IKK-free’ NEMO protein exhibited a shortened half-life due to enhanced proteasomal degradation. Highly efficient proteasomal degradation of IKK-free NEMO might be mediated by either its intrinsically disordered N-terminus, or a putative PEST motif within its intrinsically disordered proline rich region (PRR), or a combination of both. Whether the 20S or 26S proteasome mediates degradation of NEMO *in vivo* has yet to be determined, however, IKK-free NEMO was a highly effective substrate of the 20S proteasome *in vitro*. Three non-mutually exclusive hypothetical mechanisms may be proposed to account for the stabilisation of NEMO by IKK subunits (B-D). (B) Through interaction-coupled folding, IKK may stabilise either the disordered N-terminus (which overlaps the IKK binding domain of NEMO) or the PEST-motif containing PRR, and thus mask the recognition of these sites by the proteasomal machinery. How IKK binding at the N-terminus might stabilise the PRR region at the C-terminus is unclear. However, IKK can clearly interact with this region as it is able to phosphorylate S376 within the PRR of NEMO. (C) The conformational state of the N-terminal region and/or the PRR may be altered through IKK-dependent phosphorylation events. IKK β has been shown to phosphorylate S31 and S43 at the N-terminus and S376 within the PRR of NEMO. Such phosphorylation events could modulate the recognition of NEMO by the proteasomal machinery. This appears less likely than (B) given that re-expressed kinase-dead IKK rescued NEMO protein expression as effectively as WT IKK. (D) Interaction of NEMO with IKK subunits may protect NEMO from a higher basal rate of K48-linked polyubiquitylation that would target NEMO for 26S-dependent proteasomal degradation.

The observation that NEMO in the absence of IKK has a shorter half-life might have important physiological relevance. NEMO is a scaffolding protein with an elongated structure that facilitates simultaneous interaction with numerous different protein interaction partners as well as different forms of ubiquitin chain (Ivins *et al.*, 2009; Schröfelbauer *et al.*, 2012). Such interaction promiscuity is a primary characteristic of IDPs and benefits their common function as hubs within protein interaction networks (van der Lee *et al.*, 2014). However, this interaction promiscuity can be harmful for the cell if it is not tightly regulated (Babu *et al.*, 2011). Indeed, 79% of oncogenes contain predicted IDRs of 30 residues or longer (Iakoucheva *et al.*, 2002), while an altered abundance of IDPs is commonly associated with several disease states; most notably α -synuclein and tau proteins in Parkinson’s and Alzheimer’s disease (Brion *et al.*, 1986; Polymeropoulos *et al.*, 1997; Xie *et al.*, 2007). ‘Degradation by default’ represents one mechanism by which the availability of proteins with significant IDRs that have become uncoupled from their normal functional complexes can be tightly controlled (Gsponer *et al.*,

2008). In this context, the rapid turnover of 'IKK-free' NEMO would prevent any undesirable exogenous interactions with NEMO. It may also contribute to fine-tuning of NEMO protein stoichiometry in relation to the IKK subunits, such that a downregulation of IKK expression is quickly matched by an enhanced degradation of NEMO protein. This model would dictate that functional interactions with NEMO would necessitate protection of NEMO from basal degradation. It is intriguing, therefore, that numerous proteins, including ATM, PIASy and PARP1, have been shown to interact with the N-terminal disordered region of NEMO in a manner mutually exclusive with IKK β .

In summary, NEMO appears to be a protein with significant regions of intrinsic disorder that in the absence of interaction with IKK kinase subunits as part of the canonical IKK complex make NEMO an effective substrate of the proteasome and contribute to its short half-life.

Chapter 5

Assessing the potency and selectivity of I kappa B kinase β inhibitors

5 Assessing the potency and selectivity of I kappa B kinase β inhibitors

5.1 Introduction

The NF- κ B pathway plays a crucial role in the normal cellular response to environmental changes. However, there is abundant evidence that dysregulation of the pathway is associated with a multitude of disease states, including chronic inflammation, immunodeficiency and cancer (Smahi *et al.*, 2002, Xia *et al.*, 2014). Regarding the latter, the NF- κ B pathway has been shown to be constitutively active in various lymphoid malignancies and solid carcinomas, including but not limited to: breast, lung, pancreatic, prostate and colon (Nakshari *et al.*, 1997, Huang *et al.*, 2001, Lind *et al.*, 2001, Liptay *et al.*, 2003, Tang *et al.*, 2006). Such uncontrolled NF- κ B activation contributes to tumour initiation, development and metastasis through the deregulation of genes involved in processes such as proliferation, survival, metabolism, angiogenesis and epithelial-to-mesenchymal transition (Hoesel *et al.*, 2013). In addition, there is compelling evidence for a prominent role of both chronically active and therapy-induced NF- κ B activity in modulating the efficacy of cancer therapies (Godwin *et al.*, 2013). As such, inhibitors of NF- κ B activity, either as stand-alone therapies or as adjuvants to existing treatments, have been actively pursued by the pharmaceutical industry (Lee *et al.*, 2007).

The focus of drug development to date has been IKK β , owing to its purportedly dominant function in canonical NF- κ B signalling over IKK α (Li *et al.*, 1999, Gamble *et al.*, 2012). More than 150 compounds that inhibit IKK activity have been reported, although many have poorly defined mechanisms, only sub-micromolar potency, and/or poor selectivity profiles (Gilmore *et al.*, 2006). Typically, such small molecule IKK inhibitors are of three general types: non-hydrolysable ATP analogs with selectivity for the IKK ATP-binding site, compounds that interact with a specific cysteine residue (C179) in the activation loop of IKK β , and compounds with allosteric effects on IKK structure.

An example of the latter is the synthetic compound, BMS-345541 (Burke *et al.*, 2003) (Figure 5.1). BMS-345541 exhibits approximately 10-fold selectivity for IKK β ($IC_{50} = 0.3 \mu M$) over IKK α ($IC_{50} = 4 \mu M$) in *in vitro* kinase assays and inhibits the TNF α -induced phosphorylation of I κ B α in THP-1 cells with micromolar potency ($IC_{50} = 4 \mu M$). A model has been proposed in which BMS-345541 binds to similar, as yet unidentified, allosteric sites on both IKK α and IKK β , which differentially affects the ability of the active sites of the subunits to bind I κ B α and ADP. This unique binding mechanism was proposed by the authors to explain the compounds apparent high selectivity; BMS-345541 failed to inhibit a panel of 15 other kinases, including p38, ERK1/2, PKC and PKA, at concentrations as high as 100 μM .

BMS-345541 has been routinely employed to dissect the function of IKK/NF- κ B in numerous pre-clinical studies since it was made commercially available (Wu *et al.*, 2013, Ping *et al.*, 2016, Battula *et al.*, 2017). Notably, in a study pointing towards a potentially novel role of IKK in cell cycle progression, BMS-345541 was shown to block entry into, and progression through, mitosis and cytokinesis in hTERT-RPE-1 and COS-7 cells (Blazkova *et al.*, 2007). The mechanism was poorly defined, but nonetheless shown to be independent of a direct inhibitory effect of BMS-345541 on mitotic kinases such as Cdk1, Aurora A/B, Plk1 or NEK2.

Despite some of the better-characterised compounds, such as BMS-345541, showing promising inhibitory effects in *in vitro* and *in vivo* studies, so far none have progressed beyond the pre-clinical development stage (Karin *et al.*, 2004, Diwali *et al.*, 2015). As such, there is still a need for the development of new, highly potent and selective IKK inhibitors. Here, the novel, ATP-competitive IKK inhibitor, AZD2230 (IKK β IC₅₀ = 6 nM, IKK α IC₅₀ = 0.1 μ M) (Figure 5.1), was examined for its potency, IKK-selectivity and effect on the viability of HCT116 colorectal cancer cells, alongside the structurally-independent inhibitor, BMS-345541. This also provided the opportunity to assess the reproducibility of the findings of Blazkova *et al.*, and to extend upon this work to identify the mechanism underlying the importance of IKK activity in cell cycle progression through mitosis.

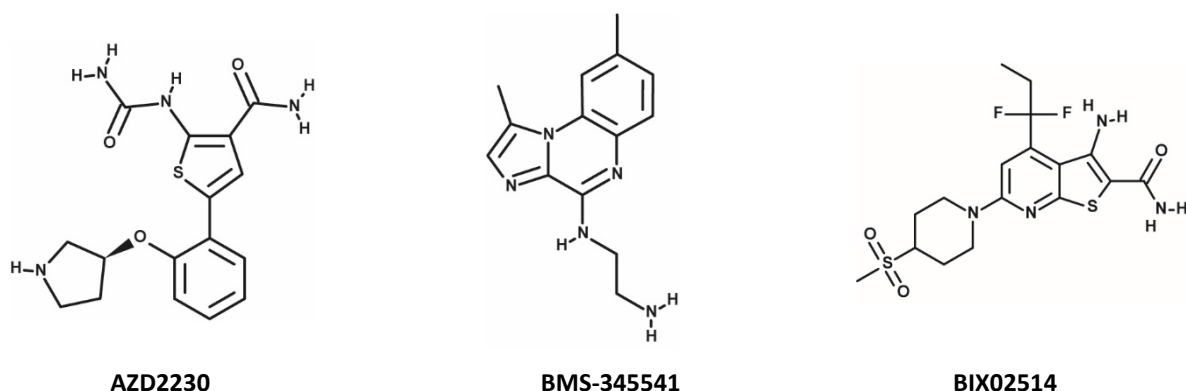


Figure 5.1. 2D structure of IKK β inhibitors utilised in this work.

5.2 Results

5.2.1 The novel, highly potent IKK inhibitor, AZD2230, and the structurally unrelated IKK inhibitor, BMS-345541, induce a proliferative arrest and cell death response in HCT116 cells.

WT and IKK α KO isogenic HCT116 CRISPR-Cas9 cell lines (the generation and validation of which is described in Chapter 3) stimulated with TNF α were employed to assess the potency and IKK-selectivity of AZD2230 and BMS-345541. TNF α -induced, NF- κ B-dependent transcriptional activity was employed as an indirect measure of IKK activity (Figure 5.2A and B). AZD2230 inhibited such IKK-dependent activity with approximately 100-fold greater potency in IKK α KO cells (IC₅₀ = 0.014 μ M, 0.012 to 0.016 μ M 95% CI) compared to WT cells (IC₅₀ = 1.48 μ M, 1.06 to 2.06 μ M, 95% CI). BMS-345541 inhibited TNF α -induced IKK activity with approximately 30-fold greater potency in IKK α KO cells (IC₅₀ = 0.127 μ M, 0.099 to 0.162 μ M, 95% CI) compared to WT cells (IC₅₀ ~ 3.6 μ M). The ambiguous fit of the nonlinear regression to the BMS-345541 data in WT cells precluded an accurate estimation of the IC₅₀ and, as such, the confidence interval for the IC₅₀ is undefined. However, from the data it is clear that AZD2230 was the more potent IKK inhibitor, and that it exhibited a greater degree of selectivity for IKK β over IKK α than BMS-34554. The enhanced sensitivity of IKK α KO cells to both AZD2230 and BMS-345541 observed here is consistent with the known greater *in vitro* kinase potency of both inhibitors for IKK β over IKK α and is evidence in

support of significant TNF α -induced IKK α activation in the WT cells (in agreement with the results described in Chapter 3).

AZD2230 and BMS-34541 inhibited both TNF α -induced I κ B α degradation and p65 phosphorylation at the transcriptional transactivation site, Serine 536, over a similar dose range to the inhibition of NF- κ B transcriptional activity in WT and IKK α KO cells (Figure 5.2C and D). Both AZD2230 and BMS-345541 also inhibited IKK β phosphorylation at the kinase activation loop, on Serine 177/181, at a lower concentration in IKK α KO cells than in WT cells. This could indicate that IKK β autophosphorylation is the more dominant mechanism of kinase activation in the absence of IKK α . Unlike AZD2230, BMS-345541 failed to inhibit IKK β phosphorylation in WT cells at the highest concentration used in the assay.

BMS-345541 has been observed to inhibit cell cycle progression (Blazkova *et al.*, 2007). To assess the reproducibility of these observations, the effect of BMS-345541 and AZD2230 on the proliferation of HCT116 cells was assessed using the [3 H]-thymidine incorporation assay (Figure 5.3A and B). AZD2230 inhibited HCT116 proliferation with an IC₅₀ = 2.72 μ M (2.30 to 3.27 μ M, 95% CI), while BMS-345541 inhibited proliferation with an IC₅₀ = 2.26 μ M (1.96 to 2.61 μ M, 95% CI). The dose-response curve fit to the data for BMS-345541 displayed a larger Hill slope (~4.76) than that of AZD2230 (~1.88). Given that the steepness of the Hill slope is an approximate measure of the cooperativity of a binding process, this difference could reflect the differing target inhibition mechanisms of AZD2230 and BMS-345541; ATP-competitive and allosteric, respectively. (Prinz., 2010). Alternatively, the large Hill slope may indicate that multiple inhibitor molecules bind to one enzyme molecule, or that the inhibitor undergoes a physical phase transition as its concentration is raised that promotes target inhibition, or that the enzyme concentration significantly exceeds the K_d value of the inhibitor (Shoichet *et al.*, 2006). A steeper Hill slope is also observed for the dose response curve fit to the IKK inhibition data for BMS-345541 compared to AZD2230 in WT cells (Figure 5.3A and B).

The proliferative arrest induced by both AZD2230 and BMS-345541 coincided with an accumulation of cells in the G2/M phase and a decrease in the proportion of replicating, S-phase cells. A greater proportion of cells in G1 phase was observed following AZD2230 treatment, compared to BMS-34541. BMS-345541 induced a larger proportion of cells with sub-G1 DNA content than AZD2230. Sub-G1 content is a marker of cell death (Telford *et al.*, 1991), but does not distinguish between apoptotic and necrotic cell death (Mattes., 2007). In support of apoptotic cell death, numerous cells with condensed, and/or fragmented nuclear DAPI staining were also detected following treatment with AZD2230 and BMS-345541 (asterix, Figure 5.3E). However, this effect was not quantified, and as such, it was not possible to conclude that AZD2230 and BMS-345541 induced apoptotic cell death. A specific assay of apoptosis, such as Annexin V staining, would be required to make this conclusion.

Consistent with the findings of Blazkova *et al.*, both inhibitors induced a significant decrease in the mitotic index (Figure 5.3E), suggesting that the increased proportion of cells with 4n DNA content reflected an arrest at the G2/M checkpoint. However, a specific assay to quantitate the proportion of mitotic cells, such as phospho-Histone H3 Serine-10 flow cytometric staining, would be necessary to make this conclusion. In contrast to Blazkova *et al.*, however, only a very small increase in the number of multinucleate cells (cells with >4n DNA content) in response to treatment with BMS-345541 was observed (Figure 5.3C and D).

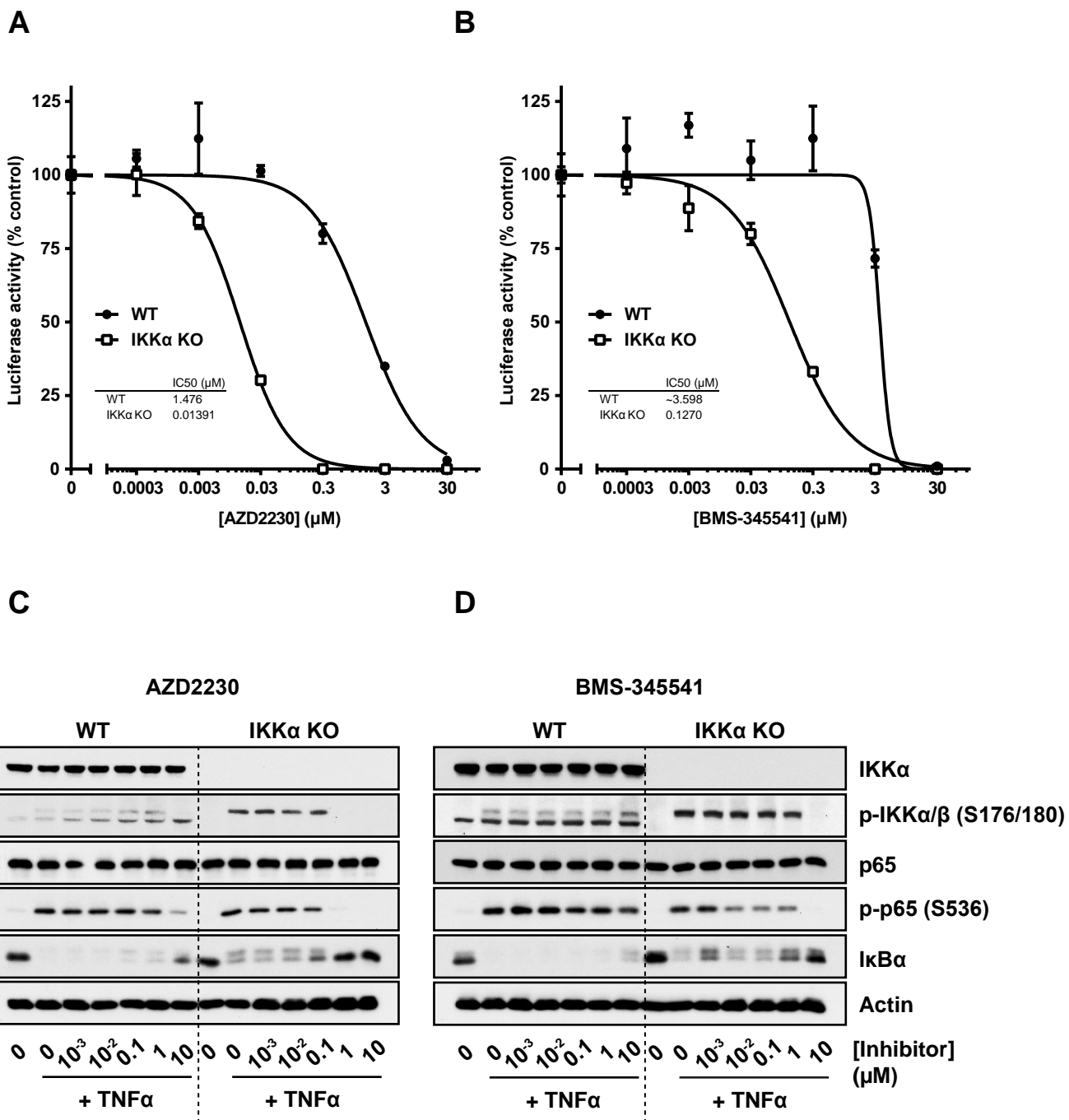


Figure 5.2. AZD2230 is a potent inhibitor of the IKK kinases. (A) WT and IKK α KO isogenic HCT116 CRISPR-Cas9 cells were seeded in their normal growth medium, prior to treatment with the indicated concentrations of AZD2230 or BMS-345541 for 30 minutes. Indicated samples were then treated with 10 ng/ml recombinant TNF α for 10 minutes. Whole cell extracts were prepared, fractionated by SDS-PAGE and Western blotted with the indicated antibodies. Data are from a single experiment representative of two giving similar results. (B) WT and IKK α KO isogenic HCT116 CRISPR-Cas9 cells were seeded in antibiotic-free growth medium overnight prior to transient transfection with 0.1 μ g pGL4.32[Luc2P/NF- κ B-RE firefly luciferase (reporter) plasmid DNA and 0.01 μ g renilla luciferase (internal control) plasmid DNA. The following day, cells were treated with the indicated concentrations of AZD2230 or BMS-345541 for 30 minutes, then treated with 10 ng/ml recombinant TNF α for 2 hours. Firefly luciferase luminescence was normalised relative to renilla luciferase luminescence and data expressed as percentage activity relative to control cells treated with TNF α and vector control (DMSO). Results are mean \pm CV of two independent experiments performed in cell culture triplicate. p-, phospho-.

Blazkova *et al.*, employed a high concentration of BMS-345541 (25 µM) throughout their study, having observed that partial cell cycle inhibition started between 10 and 15 µM, whilst a complete block was seen between 20 and 25 µM. The authors interpreted this as an indication that IKK α , rather than IKK β , was the target through which the effects of BMS-345541 were induced. In contrast, we observed substantial proliferative arrest at concentrations as low 2 µM, and complete proliferative arrest at > 5 µM (Figure 5.3B and D).

5.2.2 AZD2230 and BMS-345541 induce similar changes in the expression of cell cycle regulators

To investigate the cause of the proliferative arrest induced by AZD2230 and BMS-345541, the expression of various proteins with known functions in regulating the G2/M checkpoint and progression through mitosis were measured (Figure 5.4). Largely identical expression changes were observed for AZD2330 and BMS-345541, with the exception of p21^{CIP1}. The expression of p21^{CIP1} increased after 24 hours treatment with > 2.5 µM AZD2230, but was only induced within a narrow range of BMS-345541 concentrations (2.5 - 5 µM), above which it's expression was not induced. However, the induction of p21^{CIP1} also appeared to be weaker at 25 µM AZD2230 compared to 10 µM, suggesting this paradoxical effect might also be seen at higher concentrations of AZD2230. For all other proteins examined, the dose ranges of AZD2230 and BMS-345541 over which expression changes were observed correlated closely with the dose ranges over which proliferation was inhibited.

HCT116 cells express wild-type p53, and are thus capable of inducing a G2/M checkpoint following DNA damage (Taylor *et al.*, 2001). The observed G2/M arrest and induction of p53 in response to AZD2230 and BMS-345541 is consistent with the activation of a DNA-damage induced G2/M checkpoint. The *Cyclin B1* and *cdc25C* genes are known targets of p53 transcriptional repression in response to DNA damage (Krause *et al.*, 2000, Krause *et al.*, 2001). Indeed, both Cyclin B1 and CDC25C protein expression was downregulated in response to AZD2230 and BMS-345541. C-JUN protein expression also increased following AZD2230 and BMS-345541, consistent with the known role of c-Jun in regulating cell death following genotoxic stress (Picco & Pagés, 2013).

Interestingly, the protein expression of the essential mitotic regulators, CDC20, Securin, Aurora A and Aurora B were also decreased following AZD2230 and BMS-345541 treatment (Figure 5.4). P53 has been shown to transcriptionally repress *Cdc20* following genotoxic stress (Banerjee *et al.*, 2009). In addition, CDC20, Aurora A, Aurora B, Securin and Cyclin B1 have all been shown to be downregulated in HCT116 cells in response to sustained doxorubicin-induced genotoxic stress (Weibush & Hagemeier, 2010). This occurs because of premature activation in G2 of the ubiquitin ligase anaphase-promoting complex or cyclosome (APC/C)-Cdh1, which subsequently targets many of its substrates for degradation. Blazkova *et al.*, also observed premature, anaphase degradation of Cyclin B1 and Securin in BMS-345541-treated cells released from a nocodazole-block, but did not attribute this to a DNA-damage response.

An important step in initiation of the G2/M checkpoint is activation of Wee1, which phosphorylates CDK1 at the inhibitory Tyr15 site and prevents entry into mitosis until DNA damage has been repaired (Watanabe *et al.*, 1995). It was surprising, therefore, to observe a decrease in this phosphorylation in response to AZD2230 and BMS-345541 treatment. A similar observation was made by Weibush & Hagemeier who attributed the loss of Tyr15 phosphorylation following sustained genotoxic stress to APC/C-Cdh1-dependent degradation of Wee1.

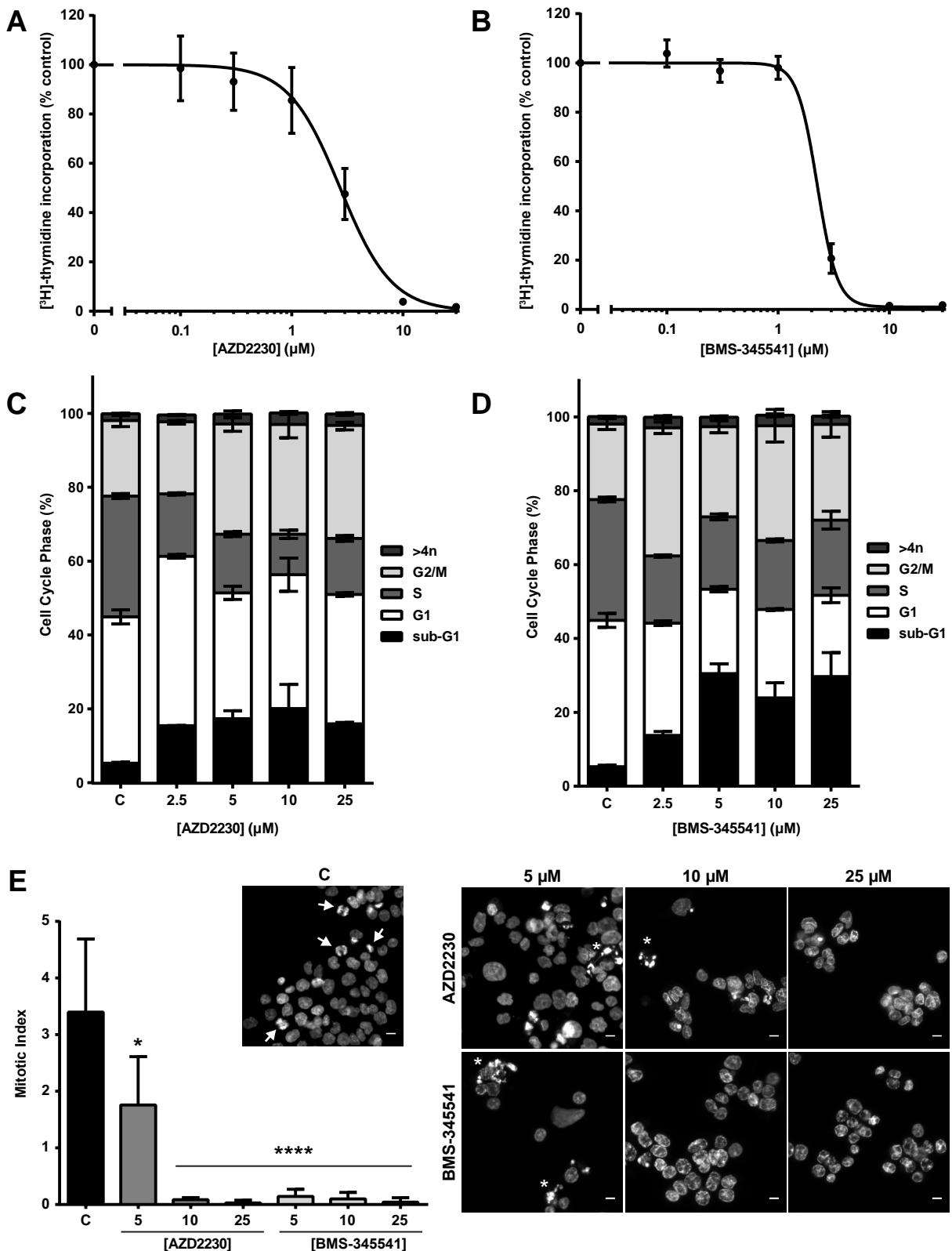


Figure 5.3. AZD2230 and BMS-345541 induce a proliferative arrest in HCT116 cells. (A and B) HCT116 cells cultured in normal growth medium were treated with the indicated concentrations (0.1 to 30 μM) of AZD2230 or BMS-345541 for 24 hours, and DNA synthesis assayed by [³H]-thymidine incorporation. Results are mean ± CV of three independent experiments performed in cell culture triplicate. (C and D) HCT116 cells cultured in normal growth medium were treated with the indicated concentrations (2.5 to 25 μM) of AZD2230 or BMS-345541 for 24 hours, and cells, which were subconfluent at the point of harvest, were fixed, stained with propidium iodide and cell cycle distribution assessed by flow cytometry. Results are mean ± SD of three independent experiments, each performed in cell culture triplicate. (E) HCT116 cells cultured in normal growth medium were treated with the indicated concentrations (5 to 25 μM) of AZD2230 or BMS-345541 for 24 hours, confocal images taken with a 10x objective, and mitotic index (mitotic cells/mitotic + interphase cells) estimated across 1000 cells. Arrows indicate mitotic cells with condensed chromosomes. Asterisk indicates cells with fragmented DNA. Results are mean ± SD of one experiment, performed in cell culture triplicate. Scale bar = 20 μm. C, DMSO vehicle control.

Unfortunately, we did not measure the expression of Wee1. Theoretically, loss of this inhibitory phosphorylation could permit inappropriate CDK1 activity. However, this is unlikely to occur in response to AZD2230 or BMS-345541 given the observed concomitant decrease in Cyclin B1 expression, which would deprive CDK1 of the cyclin binding partner required for its activation. Nevertheless, it would be interesting to characterise the effect of AZD2230 and BMS-345541 on other determinants of CDK1 activity, such as Tyrosine 14 phosphorylation status, Myt1 kinase expression and the expression and cellular localisation of CDC25A and B.

AZD2230 and BMS-345541 also inhibited the phosphorylation of RB at Serine-795 (Figure 5.4) and Serine-807/811 (Figure 5.13). As with p21^{CIP1}, this effect occurred at lower concentrations of BMS-345541 (5 to 10 µM), but was partly reversed at higher concentrations (>25 µM). Rb is dephosphorylated as cells exit mitosis and hyperphosphorylated by CDK4/6-Cyclin D1 and CDK2-Cyclin E as cells progress through the G1/S checkpoint (Lundberg *et al.*, 1998). Rb dephosphorylation is typically associated with a G1/S checkpoint arrest (Weinberg, 1995), however, Rb hypophosphorylation has also been observed in HCT116 cells downstream of the p53-dependent G2/M arrest after genotoxic stress (Flatt *et al.*, 2000).

In addition to their anti-proliferative effects, AZD2230 and BMS-345541 both induced a cell death response in HCT116 cells after 24 hours, as indicated by the increase in the proportion of sub-G1 DNA content (Figure 5.3C and D) and the cleavage of PARP (Figure 5.4). The level of cell death increased dramatically between 24 and 72 hours treatment with AZD2230 and BMS-345541 (Figure 5.5A, B, C and D). Interestingly, the percentage cell death induced was highest at intermediate concentrations of both AZD2230 (5 µM) and BMS-345541 (5 µM), suggesting that the cell cycle arrest may be more stable at higher concentrations of inhibitor.

5.2.3 The observed anti-proliferative and cell-death inducing effects of both AZD2230 and BMS-345541 are off-target effects.

The results presented thus far appear largely to support the findings of Blazkova *et al.* In addition, the observation of the same effects with two structurally unrelated small molecule inhibitors was strong initial evidence that these effects were due to on-target inhibition of IKK. However, the disparity between the potencies of AZD2230 and BMS-345541 determined in the proliferation assay (Figure 5.3A and B) and those determined in the IKK activity assays (Figure 5.2A, B, C and D) were of concern; AZD2230 is the more potent IKK inhibitor, yet BMS-345541 appears to be the more potent inhibitor of proliferation. To attempt to resolve this discrepancy, and to determine the IKK kinase (IKK α or IKK β) mediating the apparent effects on cell cycle progression, the effect of IKK β siRNA-mediated knockdown on cell cycle distribution and cell cycle regulator protein expression was investigated (Figure 5.6A and B). The protein expression changes induced by IKK β knockdown matched closely those induced by AZD2230 and BMS-345541 (Figure 5.6B). However, despite inducing a cell death response, IKK β knockdown did not induce a G2/M arrest (Figure 5.6A). In addition, IKK β siRNA had a dose-responsive effect on the expression of some of the proteins examined, including Cyclin B1, p-CDK1 (Y15), CDC25C, Cdc20, Securin and PRb, despite each concentration of the siRNA dose response knocking down IKK β protein to comparable levels. This lack of correlation between the level of IKK β knockdown and the expression of the proteins examined indicated that the siRNA might have had off-target effects that contributed to these expression changes.

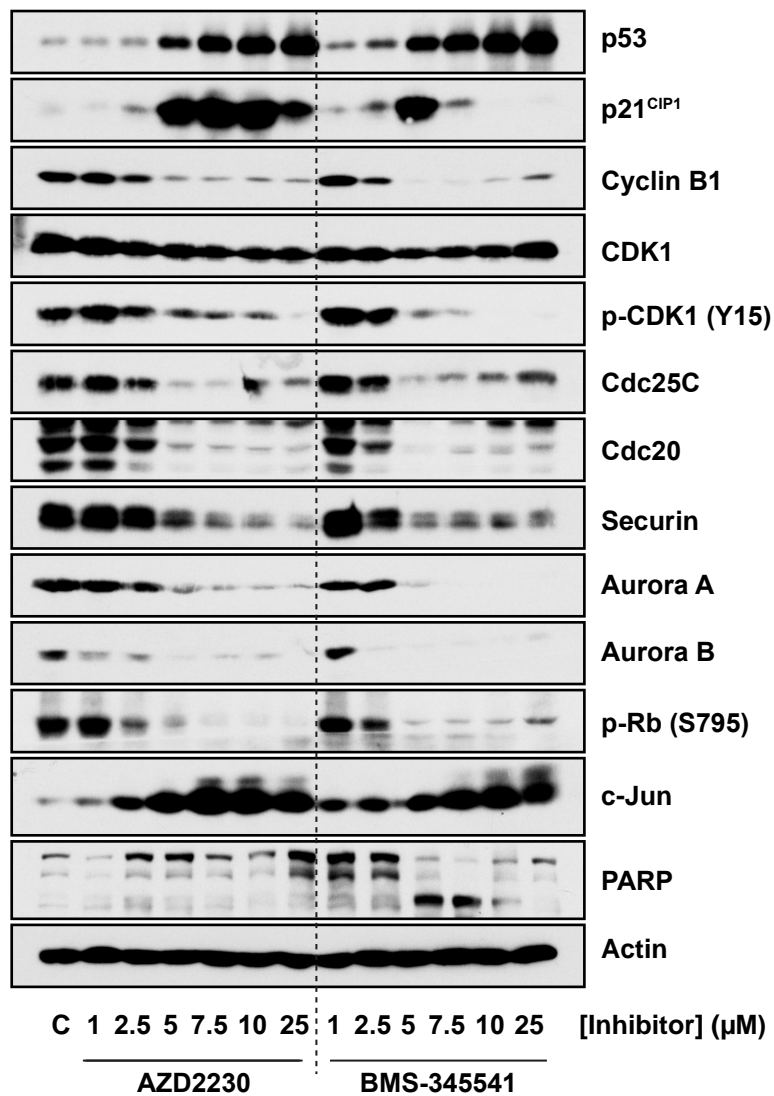


Figure 5.4. AZD2230 and BMS-345541 induce changes in protein levels of various cell cycle regulators.
HCT116 cells seeded in normal growth medium were treated with the indicated concentrations (1 to 25 μ M) of AZD2230 and BMS-345541 for 24 hours. Whole cell extracts were prepared, fractionated by SDS-PAGE and Western blotted with the indicated antibodies. Data are from a single experiment representative of two giving similar results. p-, phospho-. C, DMSO vehicle control.

Given such contradictory findings, it was important to further investigate the selectivity of the observed effects of AZD2230 and BMS-345541 on proliferation. The IKK β -selective inhibitor, BIX02514 (Figure 5.1) has emerged as a class-leading compound in terms of selectivity (Clark *et al.*, 2011). It inhibits IKK β with an IC₅₀ value of 0.38 μ M, and inhibited only IGF1 (insulin-like growth factor 1) receptor (IC₅₀ = 7.6 μ M) out of over 100 protein kinases tested in a large selectivity screen. Here, BIX02514 inhibited TNF α -induced IKK β activity in IKK α KO cells with an IC₅₀ = 0.198 μ M, (0.1595 to 0.2466 μ M, 95% CI, Figure 5.7A). Despite displaying a similar potency towards IKK β as BMS-345541 (IC₅₀ = 0.13 μ M), BIX02514 had no effect on the proliferation of HCT116 cells (Figure 5.7C). Similarly, over a range of concentrations that fully inhibited IKK β , BIX02514 had no effect on the cell cycle distribution of HCT116 cells (Figure 5.7D), and matched none of the effects of AZD2230 and BMS-345541 on the protein expression of cell cycle regulators. Such data strongly suggest that the effects of AZD2230 and BMS-345541 are not due to direct inhibition of IKK β .

In light of this data, the IKK β knockdown was repeated with a different siRNA pool (Figure 5.8). The data described in Figure 5.6 was generated with ‘siGENOME SMARTpool’ siRNA (Dharmacon), a pool of four unmodified siRNA designed to target IKK β (Chapter 2 Table 2.10). The data described in Figure 5.7 was generated with ‘ONTARGETplus’ siRNA (Dharmacon), a pool of four dual-strand modified siRNA designed to target IKK β . The sense strand of ‘ONTARGETplus’ siRNA contains a 5'-O-methyl modification of the terminal ribose, which blocks the phosphorylation of this strand, preventing its uptake by RISC and favouring antisense strand loading, thus eliminating the off-target silencing signature of the sense strand (Chen *et al.*, 2008). The antisense (guide) strand, meanwhile, contains a 2'-O-methyl modification of position 2 of the seed region, which reduces silencing of most off-target transcripts with complementarity to the seed region of the guide strand. (Jackson *et al.*, 2006). In addition, ONTARGETplus’ siRNAs, unlike ‘siGENOME SMARTpool’ siRNAs, are filtered at the design stage to exclude siRNAs with common microRNA seed-region motifs or high frequency seed regions. This is informed by the finding that matches between an siRNA seed region (positions 2-7 of antisense strand) and an mRNA 3' untranslated region (UTR) are associated with off-target silencing (Birmingham *et al.*, 2006). The combined effect of these technological improvements is a reported drastic reduction in off-target silencing (Anderson *et al.*, 2008).

IKK β knockdown with this more selective ‘ONTARGETplus’ siRNA did not phenocopy any of the effects of AZD2230, BMS-345541 or the ‘siGENOME SMARTpool’ siRNA on cell cycle distribution or cell cycle regulator protein expression, despite a similar level of knockdown (Figure 5.8A and B)

AZD2230 and BMS-345541 both exhibited substantially higher potency against IKK activity in WT HCT116 cells (Figure 5.2C and D) than BIX02514 (Figure 5.7A). This likely reflects the fact that TNF α activates both IKK α and IKK β activity in WT cells and the greater selectivity of BIX02514 for IKK β over IKK α . As a result, it was impossible to rule out the possibility that the anti-proliferative effects of AZD2230 and BMS-345541 were due to the inhibition of IKK α . However, siRNA-mediated knockdown of IKK α did not phenocopy the effects of AZD2230 or BMS-345541 (Figure 5.9). Nor did combined siRNA-mediated knockdown of IKK α and IKK β (Figure 5.10A and B).

To confirm the off-target nature of the effects of AZD2230 and BMS-345541, both inhibitors were tested on IKK β KO and IKK α / β DKO CRISPR-Cas9 isogenic HCT116 cell lines (Figure 5.11), which lack the direct targets of these compounds. AZD2230 and BMS-345541 inhibited proliferation with similar potencies in WT, IKK β KO and IKK α / β

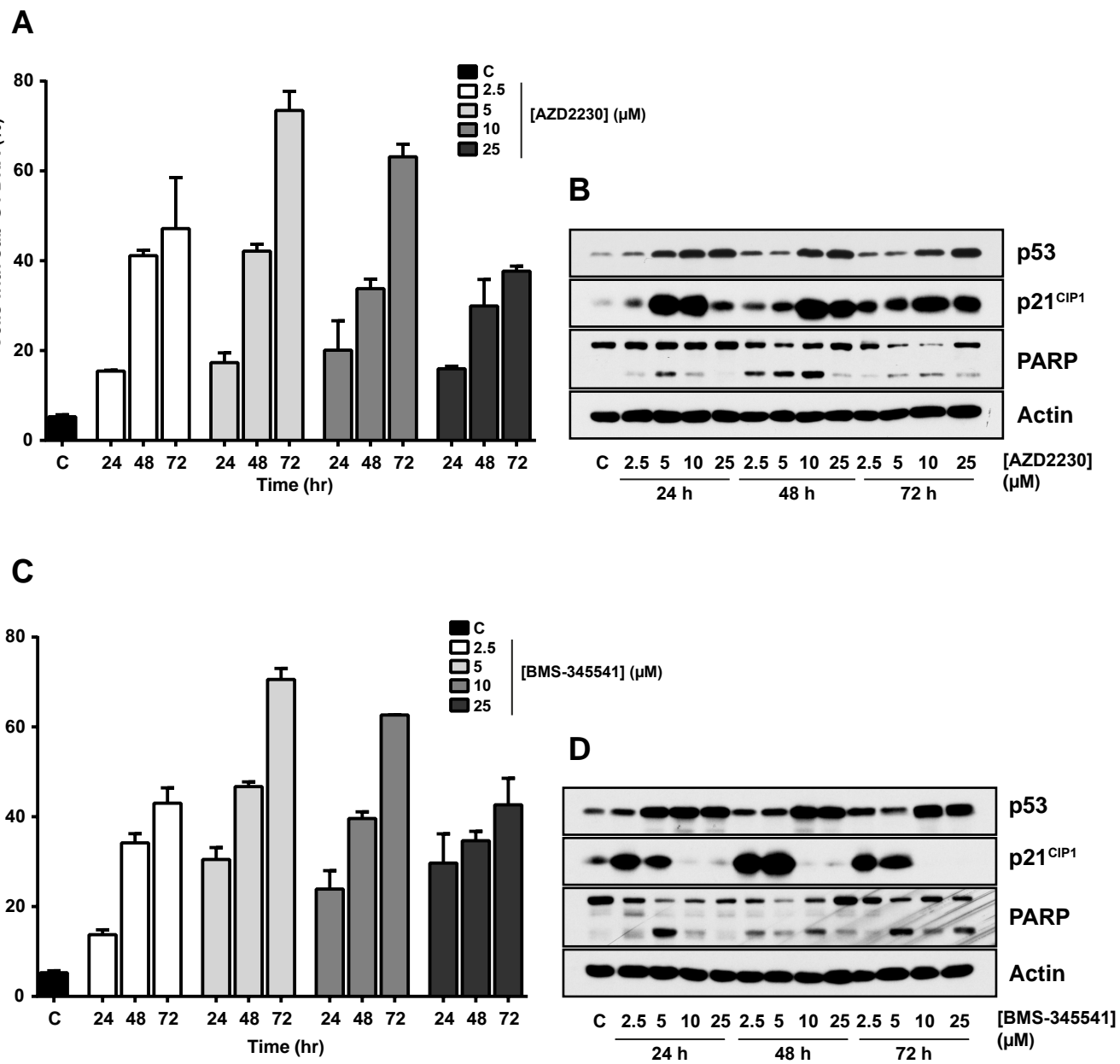


Figure 5.5. AZD2230 and BMS-345541 induce a significant cell death response in HCT116 cells. (A and C) HCT116 cells cultured in normal growth medium were treated with the indicated concentrations (2.5 to 25 μ M) of AZD2230 or BMS-345541 for 24, 48 and 72 hours, and cells, which were subconfluent at the point of harvest, were fixed, stained with propidium iodide and cell cycle distribution assessed by flow cytometry. Results are mean \pm SD of two independent experiments, each performed in cell culture triplicate. (B and D) HCT116 cells cultured in normal growth medium were treated with the indicated concentrations (2.5 to 25 μ M) of AZD2230 or BMS-345541 for 24, 48 and 72 hours. Whole cell extracts were prepared, fractionated by SDS-PAGE and Western blotted with the indicated antibodies. Data are from a single experiment representative of two giving similar results. C, DMSO vehicle control.

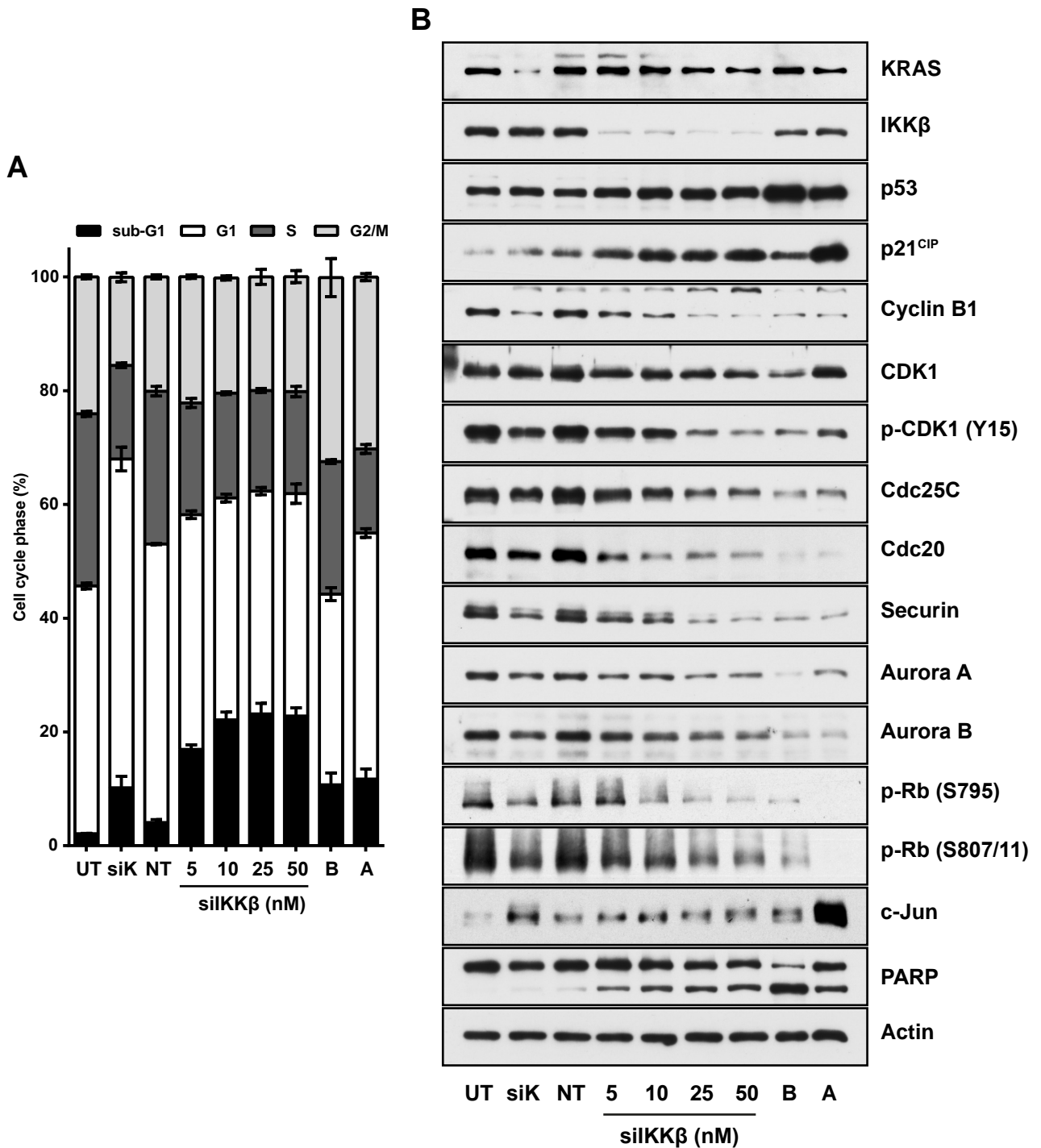


Figure 5.6. IKK β knockdown phenocopies the effects of AZD2230 and BMS-345541 on cell cycle regulator protein levels, but not at the level of cell cycle distribution. (A) HCT116 cells were left untransfected (UT), transfected with KRAS-specific siRNA (siK, positive control), transfected with non-targeting (NT) siRNA or transfected with increasing concentrations of siGENOME IKK β -specific siRNA (siIKK β) (A) 48 hours after transfection, cells, which were subconfluent at the point of harvest, were fixed, stained with propidium iodide and cell cycle distribution assessed by flow cytometry. Results are mean \pm SD of two independent experiments, each performed in cell culture triplicate. (B) 48 hours after transfection whole cell lysates were prepared and Western blotted with the indicated antibodies. Lysates were also generated for HCT116 cells treated with 10 μ M BMS-345541 (B) and 10 μ M AZD2230 (A). Data are from a single experiment representative of two giving similar results. p-, phospho-. UT, untreated.

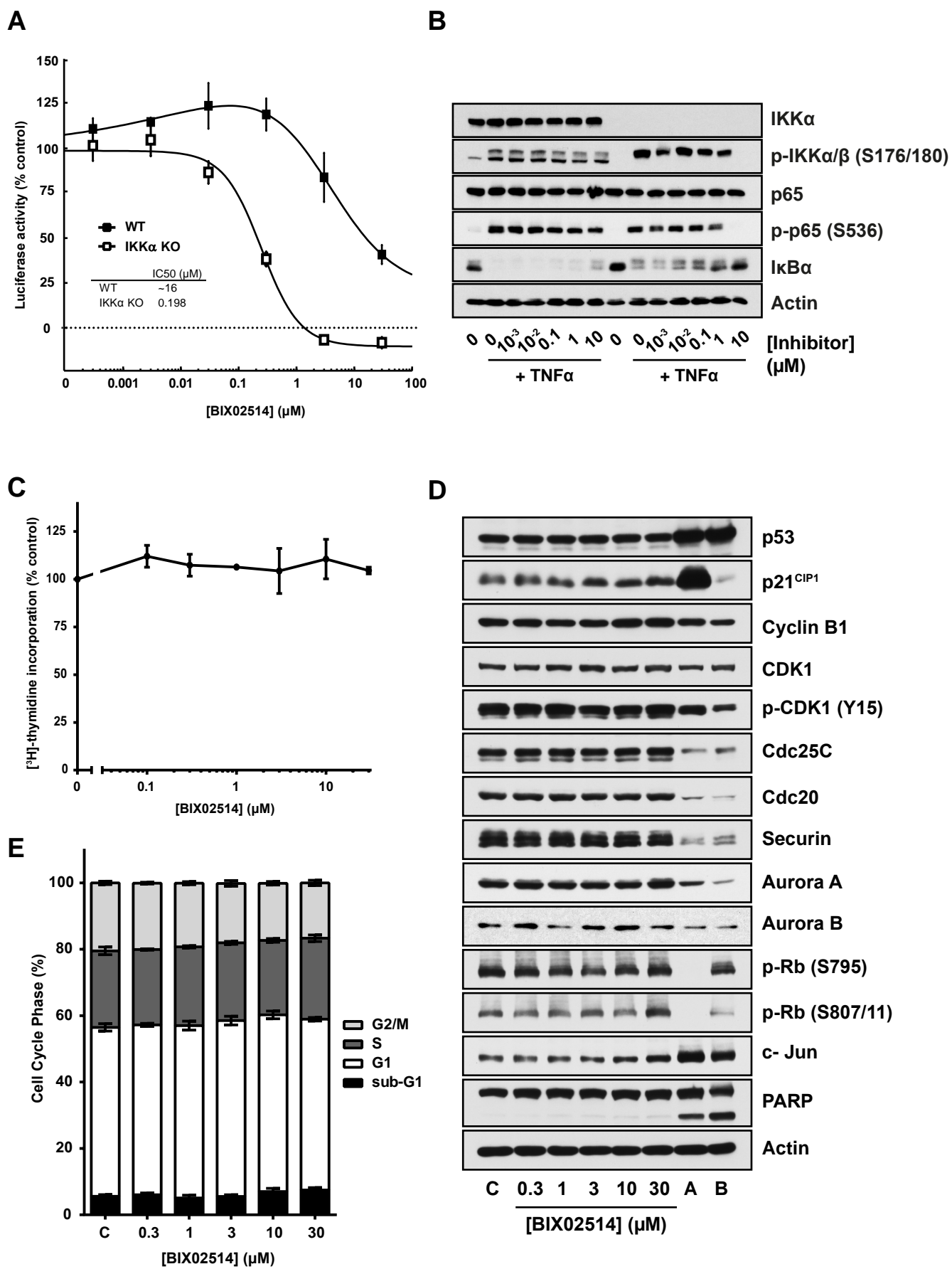


Figure 5.7. The highly selective IKK β inhibitor, BIX02514, does not phenocopy the effects of AZD2230 or BMS-345541 on HCT116 cell cycle progression. (A) WT and IKK α KO isogenic HCT116 CRISPR-Cas9 cells were seeded in antibiotic-free growth medium overnight prior to transient transfection with 0.1 μ g pGL4.32[Luc2P/NF- κ B-RE firefly luciferase (reporter) plasmid DNA and 0.01 μ g renilla luciferase (internal control) plasmid DNA. The following day, cells were treated with the indicated concentrations of BIX02514 for 30 minutes, then treated with 10 ng/ml recombinant TNF α for 2 hours. Firefly luciferase luminescence was normalised relative to renilla luciferase luminescence and data expressed as percentage activity relative to control cells treated with TNF α and vector control (DMSO). Results are mean \pm CV of single experiments performed in cell culture triplicate. (B) WT and IKK α KO cells were seeded in their normal growth medium, prior to treatment with the indicated concentrations of BIX02514 for 30 minutes. Indicated samples were then treated with 10 ng/ml recombinant TNF α for 10 minutes. Whole cell extracts were prepared, fractionated by SDS-PAGE and Western blotted with the indicated antibodies. Data are from a single experiment representative of at least two giving similar results. (C) HCT116 cells cultured in normal growth medium were treated with the indicated concentrations (0.1 to 30 μ M) of BIX02514 for 24 hours, and DNA synthesis assayed by [3 H]thymidine incorporation. Results are mean \pm CV of three independent experiments performed in cell culture triplicate. (D) HCT116 cells seeded in normal growth medium were treated with the indicated concentrations (0.3 to 30 μ M) of BIX02514 or 10 μ M AZD2230 (A) or 10 μ M BMS-345541 (B) for 24 hours. Whole cell extracts were prepared, fractionated by SDS-PAGE and Western blotted with the indicated antibodies. Data are from a single experiment representative of two giving similar results. (E) HCT116 cells cultured in normal growth medium were treated with the indicated concentrations (0.3 to 30 μ M) of BIX02514 for 24 hours, and cells, which were subconfluent at the point of harvest, were fixed, stained with propidium iodide and cell cycle distribution assessed by flow cytometry. Results are mean \pm SD of two independent experiments, each performed in cell culture triplicate. C, DMSO vehicle control.

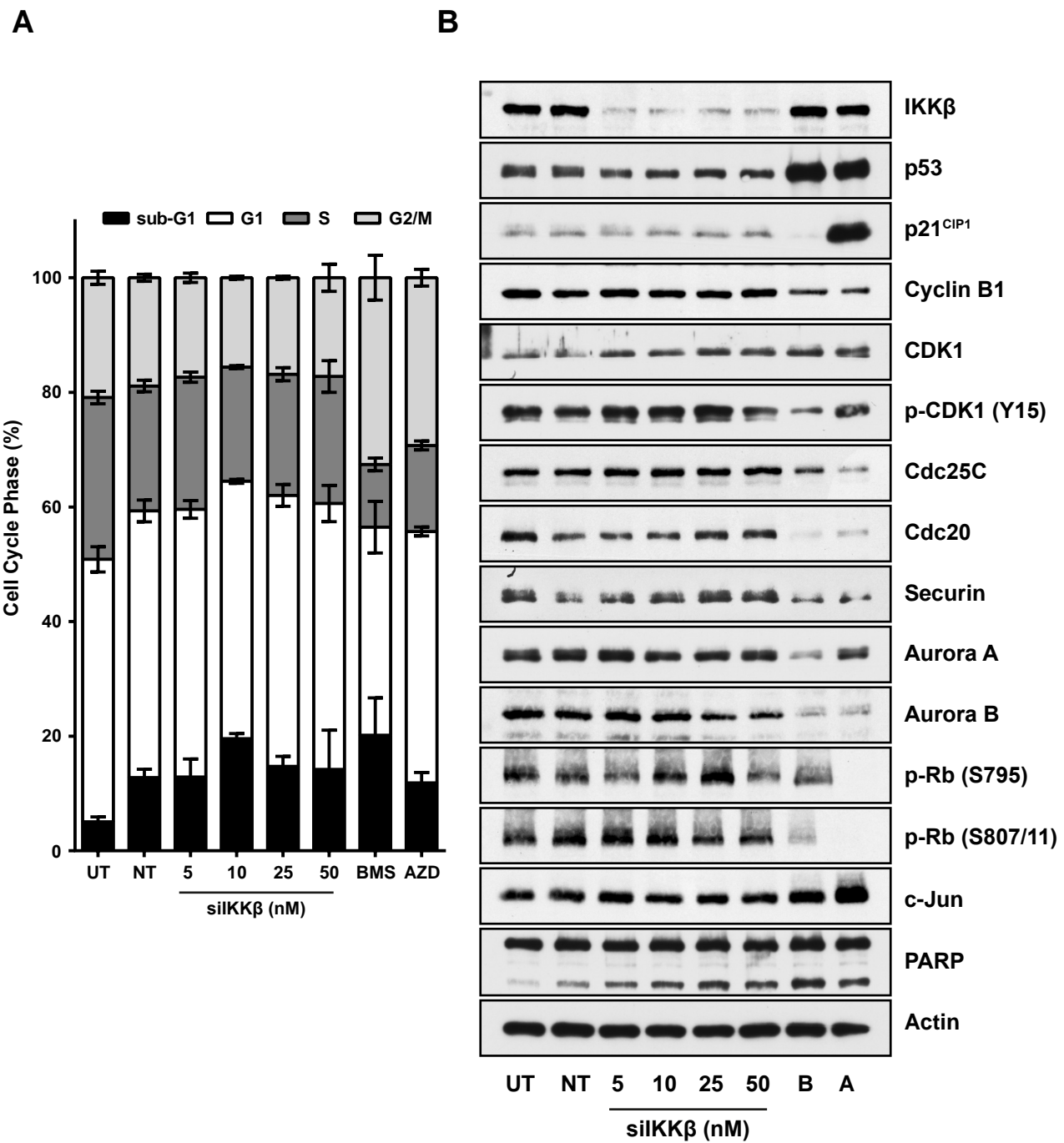


Figure 5.8. IKK β knockdown with a more selective ‘onTARGETplus’ siRNA pool does not phenocopy the effects of AZD2230 and BMS-345541 on cell cycle progression . (A) HCT116 cells were left untransfected (UT), transfected with non-targeting (NT) siRNA or transfected with increasing concentrations of on-TARGETplus IKK β -specific siRNA (siIKK β), and 48 hours after transfection, cells, which were subconfluent at the point of harvest, were fixed, stained with propidium iodide and cell cycle distribution assessed by flow cytometry. Results are mean \pm SD of two independent experiments, each performed in cell culture triplicate. (B) HCT116 cells were left untransfected (UT), transfected with 50 nM non-targeting (NT) siRNA or transfected with the indicated (5 to 50 nM) concentrations of on-TARGETplus IKK β -specific siRNA (siIKK β). 48 hours after transfection whole cell lysates were prepared and Western blotted with the indicated antibodies. Lysates were also generated for HCT116 cells treated with 10 μ M BMS-345541 (B) and 10 μ M AZD2230 (A). Data are from a single experiment representative of two giving similar results. p-, phospho-. UT, untreated.

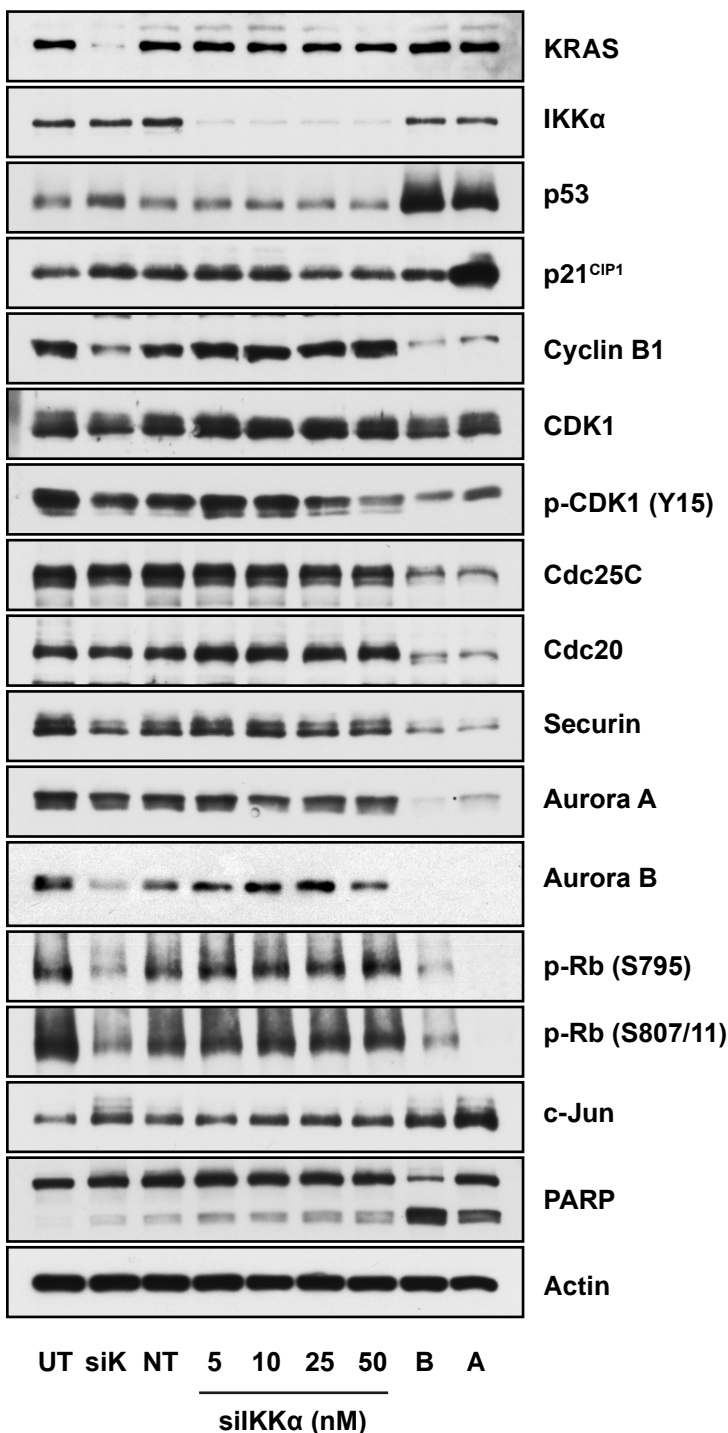


Figure 5.9. IKK α knockdown does not phenocopy the effects of AZD2230 and BMS-345541. HCT116 cells were left untransfected (UT), transfected with 5 nM KRAS-specific siRNA (siK), 50 nM non-targeting (NT) siRNA or transfected with the indicated (5 to 50 nM) concentrations of IKK α -specific siRNA (siIKK α). 48 hours after transfection whole cell lysates were prepared and Western blotted with the indicated antibodies. Lysates were also generated for HCT116 cells treated with 10 μ M BMS-345541 (B) and 10 μ M AZD2230 (A). Data are from a single experiment representative of two giving similar results. p-, phospho-. UT, untreated.

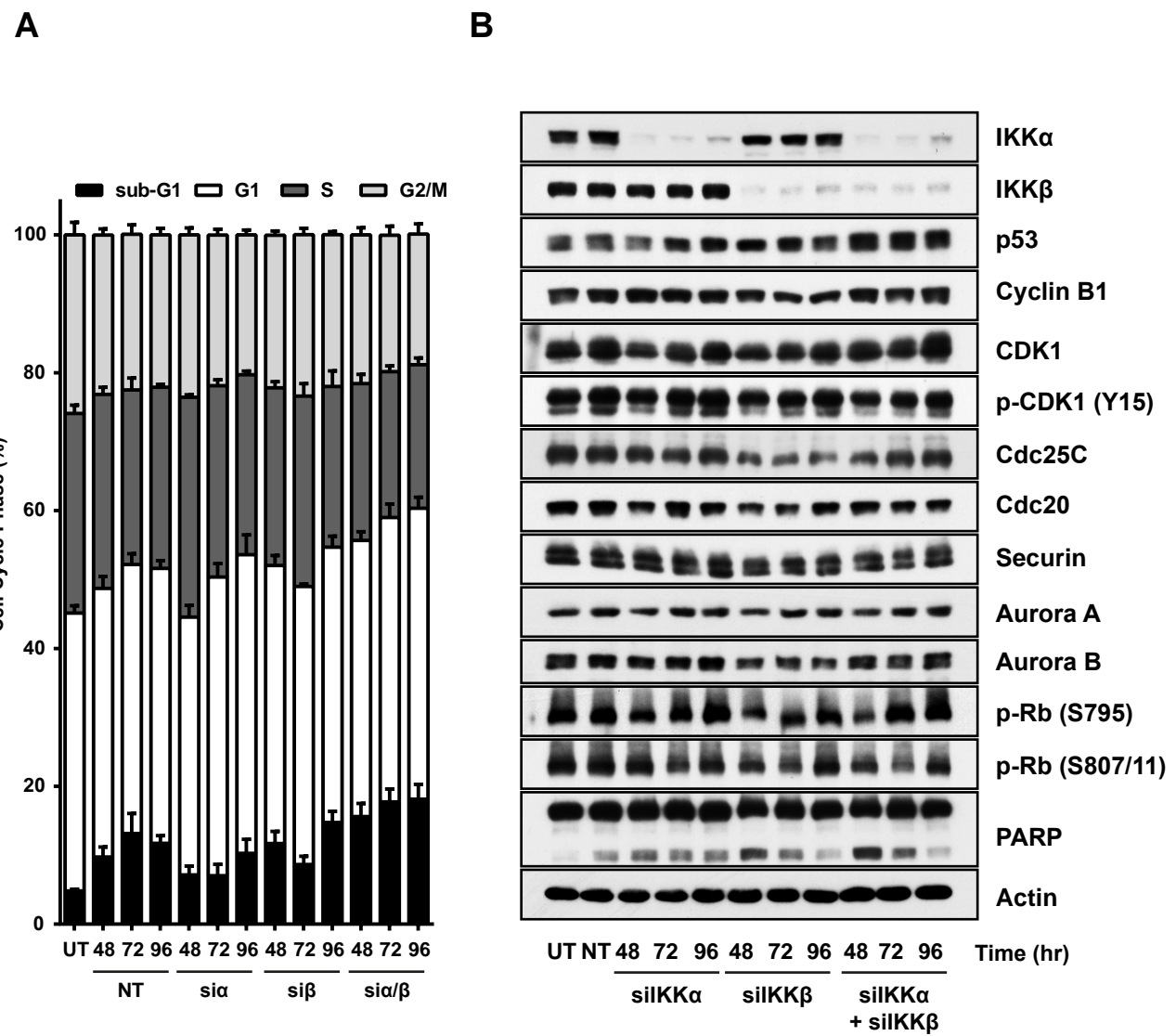


Figure 5.10. Double knockdown of IKK α and IKK β does not phenocopy the effects of AZD2230 and BMS-345541. (A) HCT116 cells were left untransfected (UT), transfected with 40 nM non-targeting (NT) siRNA or transfected with 20 nM IKK α -specific siRNA (silIKK α), 20nM onTARGETplus IKK β -specific siRNA, or a combination of both (20 nM each). The total nM siRNA was made up to 40 nM in all samples with NT siRNA. 48, 72 or 96 hours after transfection whole cell lysates were prepared and Western blotted with the indicated antibodies. Data are from a single experiment. p-, phospho-. (B) HCT116 cells were left untransfected (UT), transfected with 40 nM non-targeting (NT) siRNA or transfected with 20 nM IKK α -specific siRNA (silIKK α), 20nM onTARGET IKK β -specific siRNA, or a combination of both (20 nM each). The total nM siRNA was made up to 40 nM in all samples with NT siRNA. 48, 72 or 96 hours after transfection, cells, which were subconfluent at the point of harvest, were fixed, stained with propidium iodide and cell cycle distribution assessed by flow cytometry. Results are mean \pm SD of one experiment performed in cell culture triplicate. UT, untreated.

DKO cells (Figure 5.11A and B), confirming that this is an off-target effect of both compounds. The slight reduction in potency observed for AZD2230 here compared to that observed in Figure 5.3A is possibly due to the use of a batch of older compound, or the fact that the single-cell derived WT and IKK β KO clones have a reduced sensitivity to AZD2230 compared to the parental HCT116 cell line. Both AZD2230 and BMS-345541 also induced similar changes in the cell cycle distribution of IKK β KO cells and WT cells (Figure 5.11C and D). A similar increase in the proportion of cells in G2/M and cells with sub-G1 DNA was observed, as was the decrease in cells in S phase. However, there were interesting differences between the cell cycle distributions of WT and IKK α/β DKO cells. In response to both AZD2230 and BMS-345541, a smaller proportion of cells accumulated in the G2/M phase, and a larger proportion exhibited sub-G1 DNA, indicative of greater cell death. This may indicate that IKK α/β DKO cells underwent a more transient arrest that more quickly transitioned into a cell death response. However, this did not appear to be accompanied by a strikingly greater degree of PARP cleavage in the DKO cells (Figure 5.11E and F). The difference in the extent of drug-induced cell death between the IKK β KO and DKO cells could indicate that residual DNA damage-induced IKK α kinase activity, and hence NF- κ B transcriptional activity, was involved in promoting survival during inhibitor-induced G2/M arrest in IKK β KO cells. This is consistent with reports that indicate that NF- κ B activity, induced in response to ionizing radiation or etoposide, is important for promoting cell cycle re-entry and survival; cells that fail to activate NF- κ B undergo transient arrest and extensive cell death (Wuerzberger-Davis *et al.*, 2005). However, more evidence is needed to confirm this.

The effects of AZD2230 and BMS-345541 on the protein expression of cell cycle regulators was highly similar in WT, IKK β KO and IKK α/β DKO cells (Figure 5.11E and F). However, there was a small, but replicable, increase in basal p21^{CIP1} protein expression and a small decrease in Serine 795 phosphorylated Rb in the DKOs compared to WT. As neither is seen in the IKK β KO cells, this could be a consequence of IKK α knockout, but this possibility has not been investigated in IKK α KO cells.

5.2.4 AZD2230 and BMS-345541 both inhibit RNA Polymerase II C-terminal domain phosphorylation, possibly due to off-target inhibition of Cyclin-dependent kinases.

The off-target protein(s) mediating the effects of AZD2230 and BMS-345541 inhibition remained an outstanding, and potentially interesting, question given the differing mechanisms of action of AZD2230 and BMS-345541: ATP-competitive and allosteric, respectively.

A search for BMS-345541 kinase selectivity data revealed that it had been included in a comprehensive analysis of 72 kinase inhibitors tested against 442 kinases, covering >80% of the human kinome (Davis *et al.*, 2011). Interestingly, BMS-345541 bound to numerous other CMGC group kinases (Figure 5.12A and B), albeit with approximately 3 to 15 fold weaker affinity compared to IKK β ($K_d = 130$ nM). These included several cyclin-dependent kinases, including CDK7 ($K_d = 680$ nM), CDK9 ($K_d = 1900$ nM), CDK11A ($K_d = 390$ nM), CDK11B ($K_d = 420$ nM), CDK13 ($K_d = 800$ nM) and CDK16 ($K_d = 890$ nM). Only a small amount of selectivity data across a narrow set of kinases was available for the AstraZeneca developmental compound, AZD2230 (Figure 5.12C). However, CDK2 did feature within this list.

The largest subunit Rpb1 of the RNA polymerase II (RNAPII) contains a C-terminal extension, termed the C-terminal domain (CTD), which is composed of multiple heptad-repeat motifs, Y₁S₂P₃T₄S₅P₆S₇, and acts as a binding

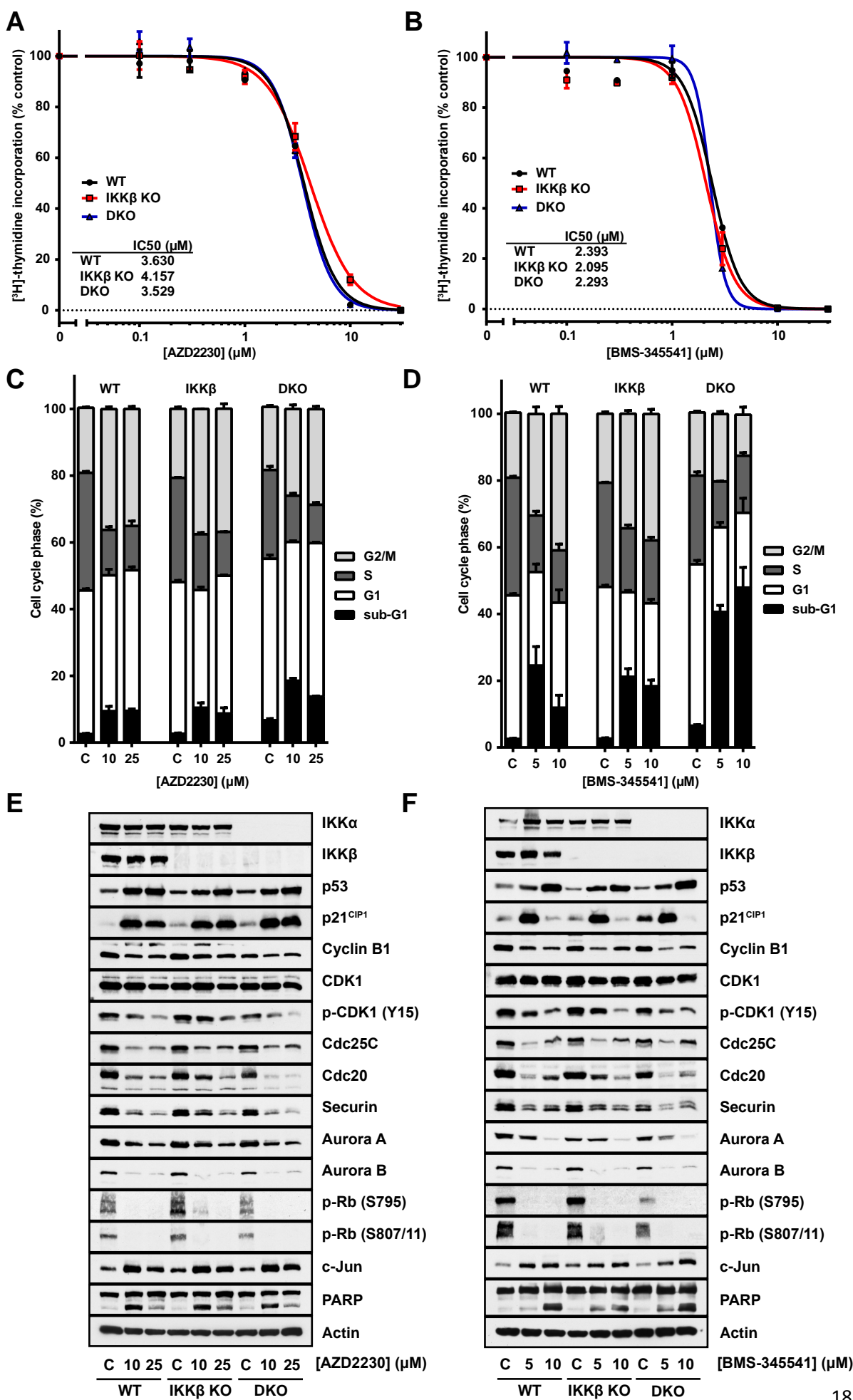
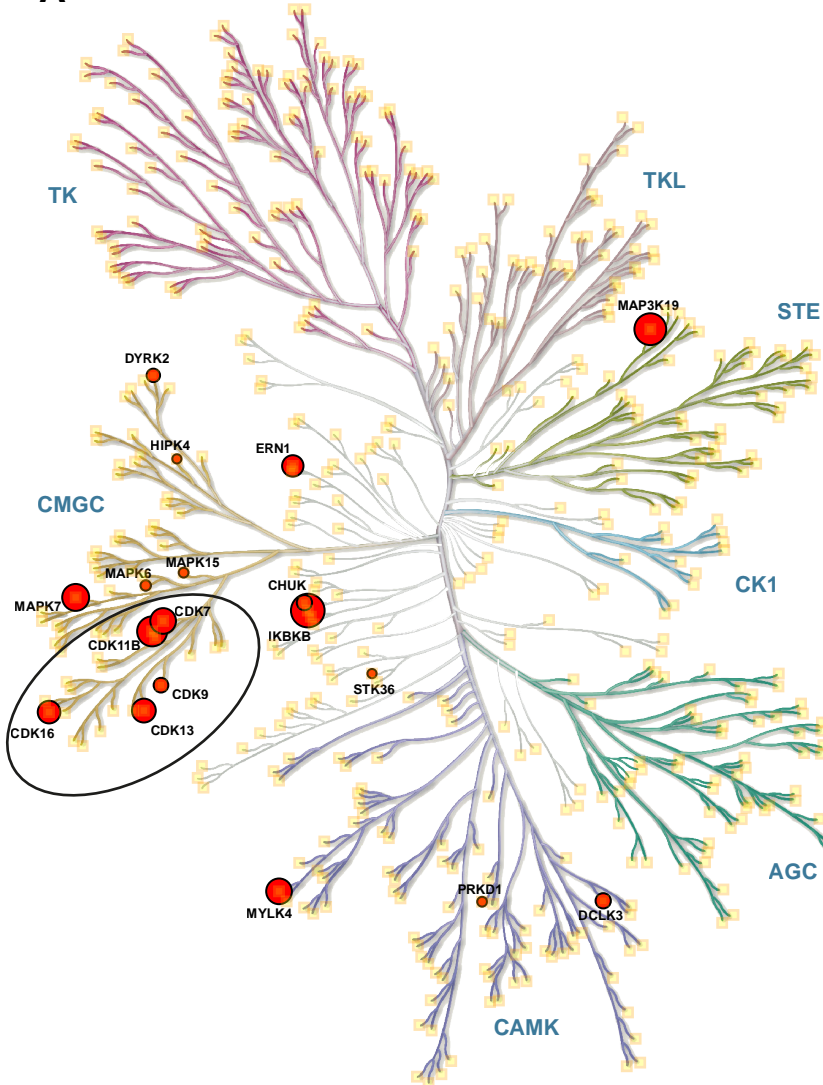


Figure 5.11. The effects of AZD2230 and BMS-345541 on cell cycle progression are due to off-target inhibition. (A and B) WT, IKK β KO and IKK α/β DKO isogenic HCT116 CRISPR-Cas9 cells were seeded in their normal growth medium, prior to treatment with the indicated concentrations (0.1 to 30 μ M) of AZD2230 or BMS-345541 for 24 hours, and DNA synthesis assayed by [3 H]thymidine incorporation. Results are mean \pm CV of three independent experiments performed in cell culture triplicate. (C and D) WT, IKK β KO and IKK α/β DKO isogenic HCT116 CRISPR-Cas9 cells cultured in normal growth medium were treated with the indicated concentrations of AZD2230 or BMS-345541 for 24 hours, and cells, which were subconfluent at the point of harvest, were fixed, stained with propidium iodide and cell cycle distribution assessed by flow cytometry. Results are mean \pm SD of two independent experiments, each performed in cell culture triplicate. (E and F) WT, IKK β KO and IKK α/β DKO isogenic HCT116 CRISPR-Cas9 cells seeded in normal growth medium were treated with the indicated concentrations of AZD2230 or BMS-345541 for 24 hours. Whole cell extracts were prepared, fractionated by SDS-PAGE and Western blotted with the indicated antibodies. Data are from a single experiment representative of two giving similar results. p-, phospho-. C, DMSO vehicle control.

A**B**

Kinase	Kd (nM)
IKK β	130
MAP3K19	260
CDK11A	390
CDK11B	420
MAPK7 (ERK5)	620
CDK7	680
MYLK4	700
CDK13	800
CDK16	890
ERN1	1000
IKK α	1700
DCLK3	1700
CDK9	1900
TYK2	2000
DYRK2	2100
RPS6KA4	2300
PKNB	2400
MAPK6 (ERK3)	4300
MAPK15 (ERK8)	4500
PRKD1	4600
STK36	6500
HIPK4	8100

C

Kinase	IC ₅₀ (nM)
IKK β	6
IKK α	100
CDK2	222
SRC	295
ERK2	353
SIK1	525
IRAK4	576
EGFR	628
TAK1	1100
SIK2	1550
INSR	4310
CDK12	7000

Figure 5.12. Available selectivity data for AZD2230 and BMS-345541. (A) Human kinase tree map with annotated available kinase selectivity data for BMS-345541. Data compiled from Davis et al 2011. Circle diameter is proportional to K_d . Larger circles indicate higher affinity interaction. Kinase targets labelled according to HGNC gene nomenclature. (B) Tabulated form of K_d data presented in (A). (C) Available kinase selectivity data for AZD2230. Data provided by AstraZeneca. Values represent *in vitro* IC₅₀'s derived from various assays; ELISA, ADP-glo luminescence assay etc.

scaffold for transcription factors. The phosphorylation state of the three Serine residues within the CTD heptad motifs is closely linked to the phases of RNAPII-mediated transcription. Broadly speaking, phosphorylation of Serine 7 converts the pre-initiation complex into a transcription-permissive complex, Serine 5 phosphorylation (S5P) is essential for transcription initiation and Serine 2 phosphorylation (S2P), which increases towards the transcription termination site, is required for maintenance of the elongation phase and 3' RNA processing. Importantly, five mammalian CDKs have been described to date as transcription regulating kinases that phosphorylate the RNAPII CTD, three of which exhibit affinity for BMS-345541: CDK7, CDK9 and CDK13 (Figure 5.12A and B). Furthermore, a number of the cell cycle regulators whose expression was inhibited by BMS-345541 and AZD2230, such as Cyclin B1, Cdc20 and Securin (Figure 5.4) are proteins with short half-lives. The expression of such proteins would thus be expected to be highly sensitive to global inhibition of transcription.

In light of this, the effect of AZD2230 and BMS-345541 on the expression of cell cycle regulators and the phosphorylation status of S2P and S5P of the RNAPII CTD was compared with that of three small molecule inhibitors, SNS-032, Flavopiridol and Roscovitine, each with varying potencies towards CDK7, 9 and 13 (Figure 5.13A). SNS-032 inhibits CDK7, CDK9 and CDK2 with IC_{50} = 62 nM, 4 nM and 48 nM, respectively (Chen *et al.*, 2009; Conroy *et al.*, 2009). Flavopiridol is a broad-spectrum CDK inhibitor with selectivity for CDK9 (IC_{50} = 6.4 nM), and potent activity towards CDK1 (IC_{50} = 62 nM), CDK2 (IC_{50} = 40 nM), CDK4/6 (IC_{50} = 40 nM), CDK7 (300 nM), CDK11 (IC_{50} = 57 nM) and CDK13 (IC_{50} = 430 nM) (Losiewicz *et al.*, 1994; Senderowicz *et al.*, 2000); Chao *et al.*, 2001, Davis *et al.*, 2011). Roscovitine is also a broad-spectrum CDK inhibitor with activity towards CDK1 (IC_{50} = 65 nM), CDK2 (IC_{50} = 70 nM), CDK5 (IC_{50} = 70 nM), CDK7 (IC_{50} = 600 nM) and CDK9 (IC_{50} = 600 nM). (McClue *et al.*, 2002).

We have not tested the specific reactivity of the different antibodies used here against hyper- (II_o) and hypophosphorylated (II_a) forms of RPB1, the largest subunit of RNAP, and the CTD. However, the RNAPII antibody (clone H224) is reported to bind to the amino-terminus of RPB1 independently of phosphorylation status, and has been reported to detect II_o and II_a forms of RPB1 (Stock *et al.*, 2007). The antibody against Serine 5P CTD (clone 4H8) is reported to recognise the II_o and intermediately phosphorylated forms of Serine 5P CTD, with no cross-reactivity against Serine 2P CTD, but some evidence of cross-reactivity with unphosphorylated CTD (II_a). The antibody against Serine 2P CTD is reported to recognise the II_o form of Serine 2P CTD, with no cross-reactivity against Serine 5P CTD but some evidence of cross-reactivity with unphosphorylated CTD (II_a).

As expected, SNS-032, Flavopiridol and Roscovitine strongly inhibited phosphorylation of RNAPII CTD at Serine 2 after 24 hours treatment (Figure 5.13A). Inhibition of S5P was also evident, but was less sensitive to the three inhibitors than S2P, consistent with previous reports (Stock *et al.*, 2007). Both AZD2230 and BMS-345541 also strongly inhibited Serine 2 phosphorylation, while AZD2230, and to a lesser extent BMS-345541, inhibited Serine 5 phosphorylation. Both inhibitors also decreased total RNA Pol II protein expression, an effect that was more clearly observed in Figure 5.14A and B & 5.15D and E. This could account for some of the observed decrease in S2P and S5P. MCL1 is frequently used as a protein marker of global transcriptional repression due to its short half-life of approximately 30 minutes (Adams & Cooper, 2007). MCL1 protein expression was strongly repressed by SNS-032, Flavopiridol and Roscovitine. Consistent with inhibition of global transcription and the observed

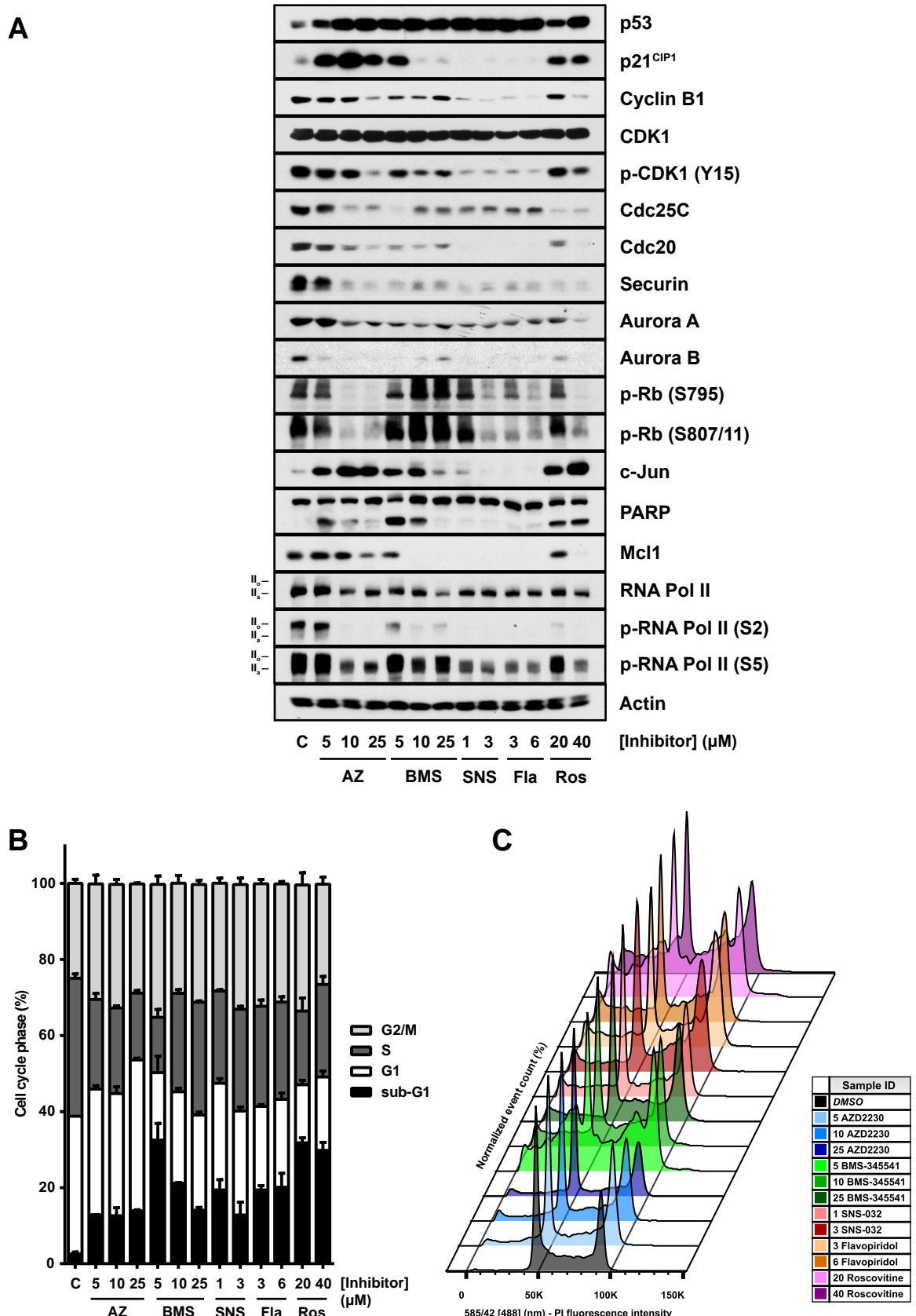


Figure 5.13. AZD2230 and BMS-345541 both inhibit RNA Pol II CTD phosphorylation. (A) HCT116 cells seeded in normal growth medium were treated with the indicated concentrations of AZD2230 (AZ), BMS-345541 (BMS), SNS-032 (SNS), Flavopiridol (Fla) and Roscovitine (Ros) for 24 hours. Whole cell extracts were prepared, fractionated by SDS-PAGE and Western blotted with the indicated antibodies. Data are from a single experiment representative of two giving similar results. (B) HCT116 cells were treated with the indicated concentrations of AZD2230, BMS-345541, SNS-032, Flavopiridol and Roscovitine for 24 hours, and cells, which were subconfluent at the point of harvest, were fixed, stained with propidium iodide (PI) and cell cycle distribution assessed by flow cytometry. Results are mean ± SD of a single experiment performed in cell culture triplicate. (C) Overlay of representative histogram profiles of FACS data presented in (B). p-, phospho-. C, DMSO vehicle control.

inhibition of RNA Pol II phosphorylation, BMS-345541, and to a lesser extent, AZD2230, inhibited MCL1 expression.

Significantly, SNS-032, Flavopiridol and Roscovitine induced strikingly similar changes in the expression of cell cycle regulators that are induced by AZD2230 and BMS-345541. In particular, Roscovitine matched the effects of AZD2230 and BMS-345541 on all proteins examined. These results are consistent with microarray data for HT29 colorectal cancer cells treated with 40 µM Roscovitine, which demonstrated decreased expression of mitotic genes, including *Aurora A/B*, *Cdc25c*, *Cyclin B1*, induction of *c-Jun* expression, decreased phosphorylation of Rb at Serine 795 and 807/11, and decreased phosphorylation of CDK1 at Tyrosine 15 (Whittaker *et al.*, 2007). Interestingly, neither SNS-032, nor Flavopiridol induced p21^{CIP1} expression, despite the fact that both strongly induced p53 expression. In fact, p21^{CIP1} protein expression was decreased by SNS-032 and Flavopiridol to levels lower than the vehicle control. The same effect was seen for C-JUN.

SNS-032, Flavopiridol and Roscovitine also induced changes in the cell cycle distribution of HCT116 cells that mirrored closely those induced by treatment with AZD2230 and BMS-345541 (Figure 5.13B and C). All three CDK inhibitors induced G2/M arrests and cell death responses of similar magnitudes to AZD2230 and BMS-345541. As seen previously (Figure 5.3C and D), the proportion of cells in G1 phase following treatment with AZD2230 was higher than with BMS-345541. Here, it was also higher than observed with either of the CDK inhibitors. The cell cycle profiles of cells treated with Roscovitine and BMS-345541 were highly similar, consistent with previous reports demonstrating arrest of HT29 colorectal cancer cells in G2 following treatment with Roscovitine (Whittaker *et al.*, 2007). This includes the presence in both of a distinct late S-phase peak (Figure 5.13C), which was also seen in other flow cytometry experiments with BMS-345541 (Figure 5.3D and 5.11D). The nature of this peak is unclear on the basis of propidium iodide cell cycle analysis alone. BrdU labelling is required to determine whether this population of cells represents replicating cells that have undergone an intra-S-phase arrest, or perhaps cells in G2/M phase that have lost a proportion of their DNA content due to DNA fragmentation during cell death or aberrant mitosis.

Direct inhibition of RNA Pol II CTD phosphorylation by AZD2230 and BMS-345541 could explain the observed cell cycle arrest. However, RNA Pol II CTD phosphorylation status and transcriptional activity are also regulated during the cell cycle (Oelgeschläger, 2002). For instance, the CTD becomes hyperphosphorylated during mitosis (Akoulitchev & Reinberg, 1998). Furthermore, modulators of CTD phosphorylation are common to both the regulation of global transcription and the cell cycle. For example, the CDK-activating complex (CAK), which in vertebrates is composed of CDK7/cyclin H, regulates CTD phosphorylation and global transcription as part of the TFIIH complex, but also promotes cell cycle progression through phosphorylation of the activation loops of CDK1, CDK2, CDK4 and CDK6 (Wallenfang & Seydoux, 2002). Furthermore, CTD phosphorylation and RNAPII ubiquitination/degradation are regulated in response to transcription-coupled DNA repair (Ratner *et al.*, 1998, Bregman *et al.*, 1996). BRCA1, which plays an important role in DNA repair, has also been shown to inhibit RNAPII CTD phosphorylation levels (Moisan *et al.*, 2004). Therefore, inhibition of RNAPII CTD phosphorylation by AZD2230 and BMS-345541 could be an indirect consequence of an off-target effect of these compounds on cell cycle control and/or DNA damage repair.

To investigate the kinetics of CTD dephosphorylation, a timecourse of AZD2230 and BMS-345541 treatment was performed (Figure 5.14). In response to both 10 and 25 μ M AZD2230, the hyperphosphorylated form (II₀) of RNAPII was rapidly inhibited between 2 and 4 hours. A gradual decrease in the expression of the hypophosphorylated (II_a) form of RNAPII was also observed between 4 and 48 hours post treatment. Roscovitine treatment also decreased the level of RNAPII protein and induced the appearance of a lower molecular weight form of RNAPII, which may represent a degradation intermediate of Rpb1 (Wang *et al.*, 2011). However, we did not confirm whether this band represented RNAPII that had undergone proteasome-dependent degradation. This lower molecular weight band was not seen in response to AZD2230. Serine 2 phosphorylated CTD decreased rapidly after 2 hours treatment with 10 μ M AZD2230 to reach a minimum expression after 16 hours. Intriguingly, the II₀ form subsequently increased between 16 and 48 hours. This correlated well with the expression pattern of MCL1 protein. The rebound of S2P was not observed to the same extent following treatment of 25 μ M AZD2230. This was not due to differences in the expression of total RNAPII. Interestingly, the rapid inhibition of MCL1 was more pronounced after treatment with 25 μ M compared to 10 μ M AZD2230, but the increase of MCL1 protein between 16 and 48 hours was still observed, despite the almost complete inhibition of S2P and low levels of total RNAPII. AZD2230 had similar effects on Serine 5 phosphorylation; an early decrease followed by a late rebound at the lower concentration of drug, and a permanent decrease at the higher concentration.

The effects of BMS-345541 on RNAPII expression were quite different. 5 μ M BMS-345541 induced a gradual increase in RNAPII expression over 24 hours, which subsequently decreased after 48 hours. A large increase in a slower migrating form of RNAPII between 16 and 24 hours was also observed. Whether this band reflects hyperphosphorylated or ubiquitinated RNAPII was not investigated. An increase in the lower molecular weight form of RNAPII was observed after 24 hours. It should be noted that inefficient protein transfer of RNAPII during Western blotting cannot be ruled out as a contributing factor to these observations, as this data was from a single experiment. However, similar, repeatable observations were made in other experiments (Figure 5.15E). Treatment with 10 μ M BMS-345541 caused a substantial and sudden decrease in the II_a form of RNAPII between 16 and 24 hours that was accompanied by a large increase in the lower molecular weight form of RNAPII. No full length RNAPII was detectable under these conditions after 48 hours treatment.

Similar to AZD2230, the lower concentration (5 μ M) of BMS-345541 induced a rapid, initial decrease in S2P. However, the rebound in S2P between 8 and 24 hours was even more pronounced for BMS-345541; the expression of S2P observed after 24 hours was higher than that in the vehicle control. This pattern of S2P expression again correlated well with MCL1 expression. As with AZD2230, the higher concentration (10 μ M) of BMS-345541 rapidly and permanently inhibited S2P. Unlike AZD2230, however, this was associated with a more permanent inhibition of MCL1 expression, although a small rebound in MCL1 expression was detected after 24 hours. Interestingly, this pattern of MCL1 expression correlated with that of p21^{CIP1}. BMS-345541 had similar effects on Serine 5 phosphorylation; an early decrease followed by a late rebound at the lower concentration of drug, and a permanent decrease at the higher concentration.

The expression of the cell cycle regulators examined changed at earlier timepoints when cells were treated with a higher concentration of AZD2230 and BMS-345541. Significantly, the initial decrease in S2 phosphorylation observed after 2 to 4 hours treatment with AZD2230 and BMS-345541 proceeded the expression changes of the

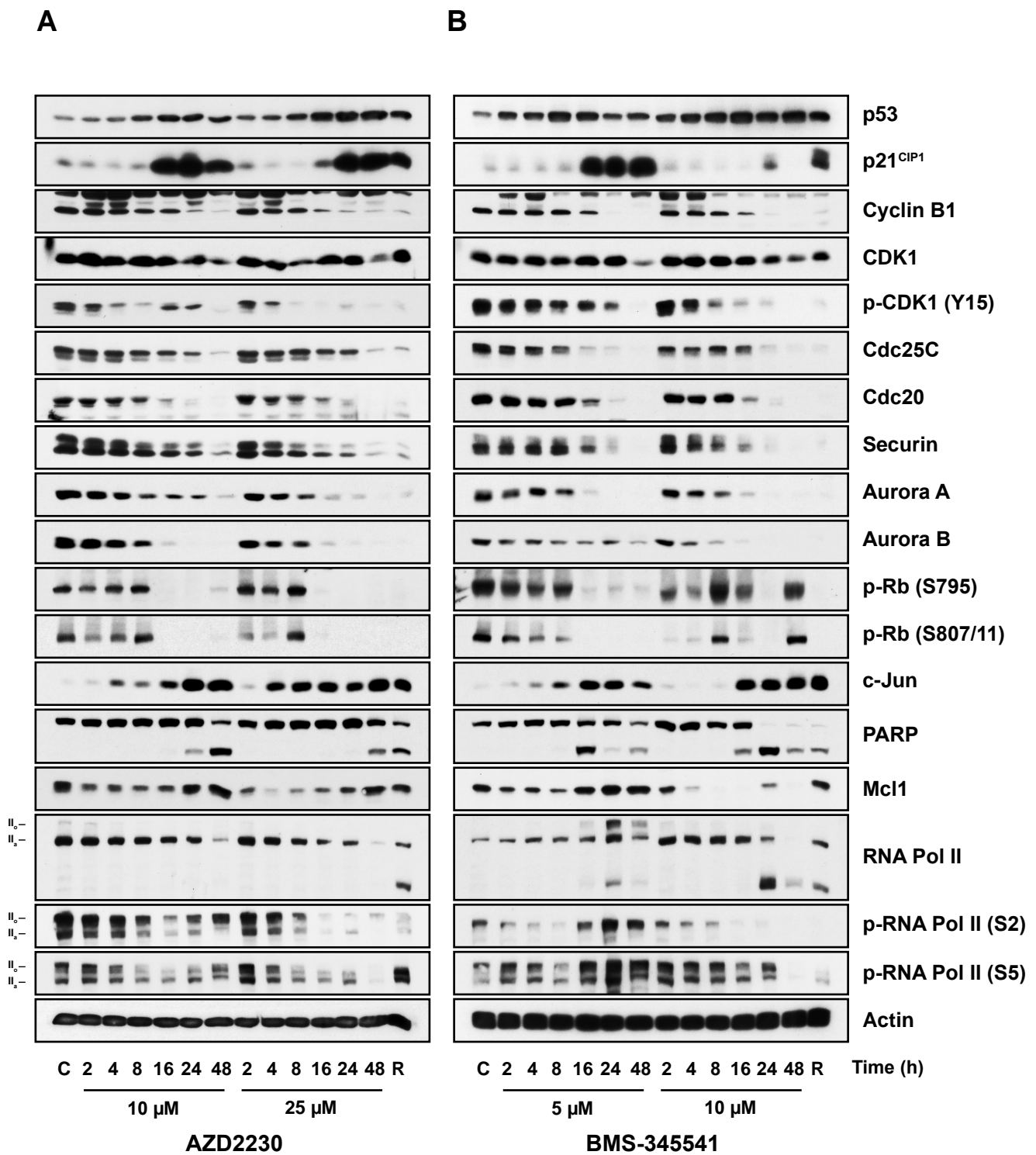


Figure 5.14. The kinetics of RNA Pol II CTD phosphorylation inhibition by AZD2230 and BMS-345541 correlate with the kinetics of the signalling events triggering a cell cycle arrest. (A and B) HCT116 cells seeded in normal growth medium were treated with the indicated concentrations of AZD2230 (10 and 25 μ M) and BMS-345541 (5 and 10 μ M) and whole cell extracts collected at the indicated timepoints (2 to 48 hours). A 24 hour treatment with 40 μ M Roscovitine (R) was used as a positive control for CDK7/9 inhibition. DMSO was used as vehicle control (C). Whole cell extracts were fractionated by SDS-PAGE and Western blotted with the indicated antibodies. Data are from a single experiment. C, DMSO vehicle control.

majority of cell cycle regulators. Besides S2P and MCL1, the earliest expression changes observed were those of p53, PRB S795, PRb 807/11, p-CDK1 (Y15) and C-JUN. p21CIP1 induction between 8 and 16 hours was comparatively delayed. PARP cleavage was a relatively late event for both inhibitors, but occurred earlier at lower concentrations of both AZD2230 and BMS-345541. PRB displayed interesting changes in phosphorylation status in response to AZD2230 and BMS-345541. In the case of 10 µM BMS-345541, a four-phase response was observed; phosphorylation of Serine-795 and Serine-807/11 decreased rapidly in the first 4 hours of treatment, increased back to close to untreated levels after 8 hours, decreased again between 8 and 24 hours, before increasing back to untreated levels after 48 hours. The complexity of such expression changes complicate any conclusions that can be made about the mechanism of cell cycle arrest. Our understanding will be improved by correlating these expression changes with the kinetics of cell cycle arrest.

The inhibition of RNAPII CTD phosphorylation was an off-target effect of AZD2230 and BMS-345541, based on several observations (Figure 5.15). No change in S2P or S5P was observed following treatment of cells with the IKK β inhibitor, BIX02514 (Figure 5.15A) or following siRNA-mediated knockdown of IKK β (Figure 5.15B). siRNA-mediated knockdown of IKK α and combined siRNA-mediated knockdown of IKK α and IKK β had no effect on S2P or S5P expression (Figure 5.15C). Finally, the same changes in S2P and S5P induced by AZD2230 and BMS-345541 in WT HCT116 cells were also induced in IKK β and IKK α/β DKO cells (Figure 5.15D and E).

Global transcription inhibition results in significant changes in nuclear structure. For example, the CDK9 inhibitors, Flavopiridol and Roscovitine disrupt early rRNA processing, which impairs ribosome biogenesis and causes nucleolar disintegration (Burger *et al.*, 2010). Ki67 is constitutively expressed in cycling mammalian cells and localises to nucleoli during late G1, S and G2 phase of the cell cycle, where it promotes heterochromatin organisation (Kill, 1996, Sobecki *et al.*, 2016). Disruption of nucleolar integrity following CDK9 inhibition results in Ki67 nucleoplasmic relocalisation (Kill, 1996). Ki67 expression and localisation was investigated in HCT116 cells treated with AZD2230 and BMS-345541 (Figure 5.16). In agreement with the findings of Blazkova *et al.*, BMS-345541 and AZD2230 induced a decrease in Ki67 staining intensity. Numerous cells expressed no detectable Ki67 protein, consistent with their cell cycle exit. However, these conclusions are preliminary in nature in the absence of Ki67 staining quantitation. AZD2230 and BMS-345541 also induced Ki67 relocalisation from the nucleolus to the nucleoplasm. A similar effect was seen following Flavopiridol treatment. The IKK β inhibitor, BIX02514 had no effect on the cellular localisation of Ki67. A positive control for G2/M arrest and/or DNA damage in the absence of CDK9 inhibition would be informative in defining the mechanism of cell cycle arrest induced by AZD2230 and BMS-345541. Overall, however, the data is consistent with the anti-proliferative effects of AZD2230 and BMS-345541 being due to off-target inhibition of global RNAPII-dependent transcription through inhibition of CDK7, CDK9 and/or CDK13.

5.2.5 Bioinformatic analyses of AZD2230 and BMS-345541 chemical structure highlight additional possible targets of off-target inhibition.

It is difficult to rationalise how AZD2230 and BMS-345541 might exhibit such a similar spectrum of off-target effects, given their differing mechanisms of action; ATP-competitive and allosteric, respectively. Indeed, the allosteric mechanism of BMS-345541 inhibition was proposed as an explanation for the apparent high selectivity

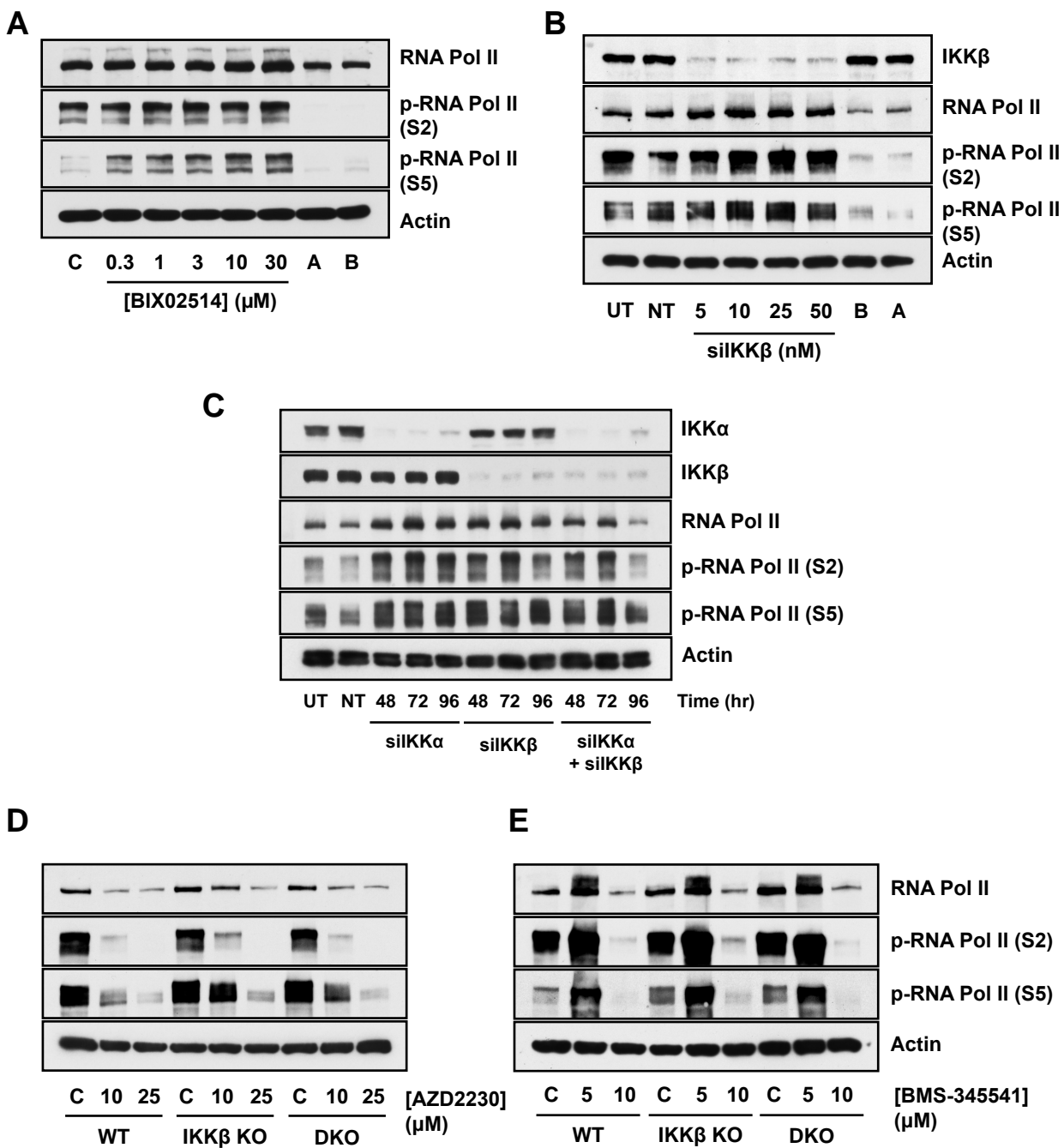


Figure 5.15. The inhibition of RNA Pol II CTD phosphorylation is an off-target effect of AZD2230 and BMS-345541 (A) HCT116 cells seeded in normal growth medium were treated with the indicated concentrations (0.3 to 30 μM) of BIX02514 or 10 μM BMS-345541 (B) and 10 μM AZD2230 (A) for 24 hours. Whole cell extracts were prepared, fractionated by SDS-PAGE and Western blotted with the indicated antibodies. Data are from a single experiment representative of two giving similar results. (B) HCT116 cells were left untransfected (UT), transfected with 50 nM non-targeting (NT) siRNA or transfected with the indicated (5 to 50 nM) concentrations of on-TAR-GETplus IKKβ-specific siRNA (siKKβ). 48 hours after transfection whole cell lysates were prepared and Western blotted with the indicated antibodies. Lysates were also generated for HCT116 cells treated with 10 μM BMS-345541 (B) and 10 μM AZD2230 (A). Data are from a single experiment representative of two giving similar results. (C) HCT116 cells were left untransfected (UT), transfected with 40 nM non-targeting (NT) siRNA or transfected with 20 nM IKKα-specific siRNA (siKKα), 20nM onTARGET IKKβ-specific siRNA, or a combination of both (20 nM each). The total nM siRNA was made up to 40 nM in all samples with NT siRNA. 48, 72 or 96 hours after transfection whole cell lysates were prepared and Western blotted with the indicated antibodies. Data are from a single experiment. (D and E) WT, IKKβ KO and IKKα/β DKO isogenic HCT116 CRISPR-Cas9 cells seeded in normal growth medium were treated with the indicated concentrations of AZD2230 or BMS-345541 for 24 hours. Whole cell extracts were prepared, fractionated by SDS-PAGE and Western blotted with the indicated antibodies. Data are from a single experiment representative of two giving similar results. p-, phospho-. C, DMSO vehicle control. UT, untreated.

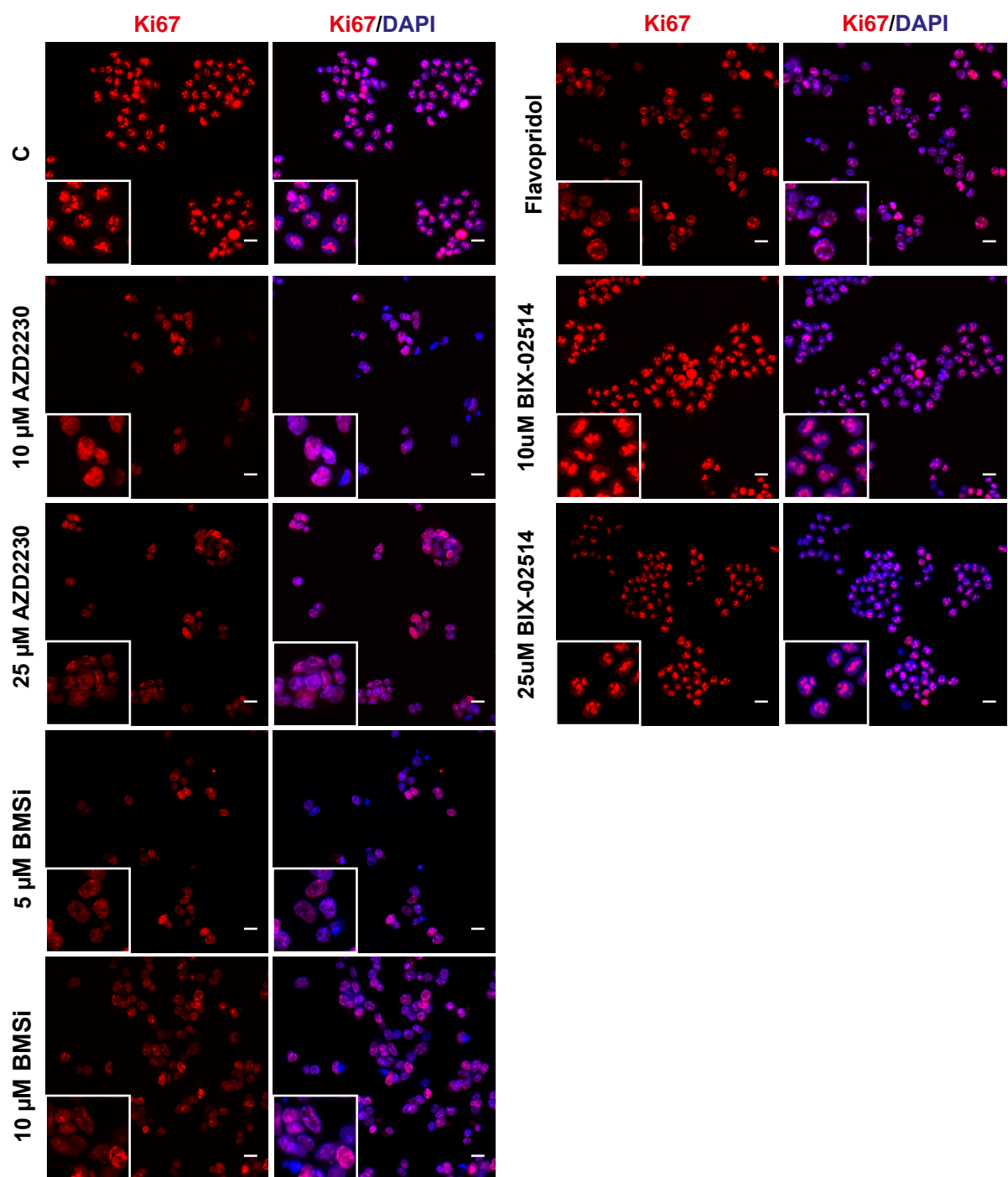


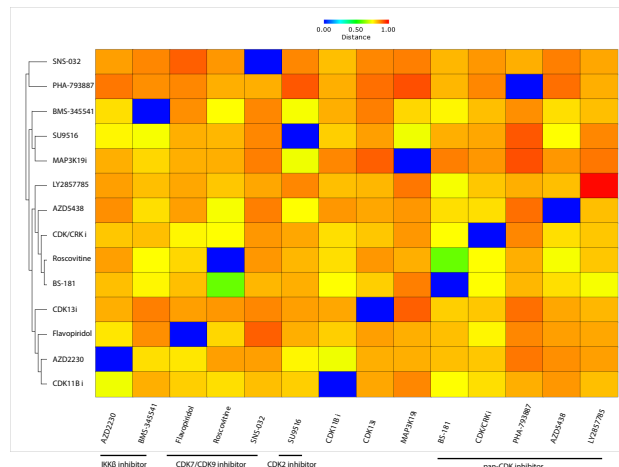
Figure 5.16. AZD2230 and BMS-345541 induce nucleolar disruption in HCT116 cells (A) HCT116 cells seeded onto coverslips in normal growth medium were treated with the indicated concentrations of AZD2230, BMS-345541, BIX02514 for 24 hours. Cells were treated with 3 μ M Flavopiridol as a positive control for nucleolar disruption. Cells were fixed and stained with anti-Ki67 antibody (red) and nuclei with DAPI (blue). Confocal images were taken at 10 \times objective magnification. Scale bar = 20 μ m. C, DMSO vehicle control.

of this compound. How well-conserved the proposed IKK β allosteric binding pocket is within the kinase is unclear. This also assumes that BMS-345541 interacts with all potential targets in the same manner; it might be able to inhibit other kinases in an ATP-competitive manner. Furthermore, despite inducing very similar effects on the cell cycle and expression of cell cycle regulators, it must be stressed that AZD2230 and BMS-345541 need not inhibit the exact same off-target kinase. As will be discussed shortly, the effects of AZD2230 and BMS-345541 are quite generic and could be explained by disruption of a range of cellular processes, including induction of DNA damage, inhibition of cell cycle CDKs and inhibition of transcriptional CDKs.

Bioinformatics approaches can provide an indirect approach to examine structure-activity relationships for compounds with similar phenotypic effects. For example, as part of a supervised approach to assessment of 2D structure similarity, a set of pairwise compound similarity analyses using atom pair descriptors and Tanimoto coefficients were performed using a set of inhibitors chosen to reflect the possible off-target effects of AZD2230 and BMS-345541 (Figure 5.17). BMS-345541 shared the greatest level of structural similarity with a CDK13 inhibitor, whilst AZD2230 shared the greatest level of similarity with the pan-CDK inhibitor, PHA-793887. However, overall AZD2230 and BMS-345541 did not share a substantial level of 2D structural similarity with each other, or with other CDK inhibitors.

In an unbiased approach, the PubChem repository of chemical structures was searched for compounds with > 80% Tanimoto similarity to AZD2230. This yielded 12391 compounds. The Pubchem database stores any available bioassay data for each of the compounds it contains. In other words, potency and selectivity data are available for any given compound wherever this compound has been utilised in a kinase screen. Analysis of the bioassay data for these compounds with structural similarity to AZD2230 is presented in Figure 5.17B. The identification of compounds exhibiting activity towards IKK β is evidence of the structural similarity between AZD2230 and compounds within this list. These compounds also exhibited the highest potency within the bioassays identified. Interestingly, a number of the compounds with structural similarity to AZD2230 exhibited activity towards Chk1, in two independent bioassay screens. Chk1 coordinates the DNA damage response and cell cycle checkpoint activation in response to genotoxic stress. Inhibition of Chk1 is associated with induction of DNA strand breaks (Syljuasen *et al.*, 2005). Half of the members of the list that were tested in a screen for CDK1 inhibitors exhibited micromolar activity, providing further indication of potential CDK inhibition by AZD2230. A similar analysis for BMS-345541 identified 8382 compounds with > 80% structural similarity. A number of these structurally similar compounds appeared as hits in screens for inhibitors of IKK or NF- κ B activity, such as sensitizers of TRAIL-induced cell death. Many of the compounds assayed for inhibition of CDKs, including CDK1, CDK4, CDK6 and CDK5 were defined as active, again supporting the claim that compounds with structural similarity to BMS-345541 may inhibit a variety of CDKs. However, there are a number of issues with this sorts of analysis. For instance, it is difficult to know how many of the ‘structurally similar’ compounds identified are just a chemical series of essentially identical structures. Furthermore, it is likely that not all potential kinases mediating the off-target effects of AZD2230 and BMS-345541 have been screened with a large enough number of compounds to appear as results in this analysis.

An independent approach to identification of potential protein off-targets was taken in the form of the ChemMapper online computational tool (Gong *et al.*, 2013). ChemMapper hosts a database of over 300 000

A**B**

BioAssay Description	No. Compounds Tested	No. Compounds Active	Activity Concentration Range (μM)
Inhibition of tyrosyl-DNA phosphodiesterase (TDP1)	165	34	0.12 – 33
Inhibition of Histone Lysine methyltransferase	162	26	0.32 – 100
Inhibition of Chk1	16	16	0.82 – 29
Inhibition of PLK1	79	7	5.32 – 27
Inhibition of JNK1	6	6	1.9 – 11.9
Inhibition of Inflammasome signalling (IL-1 β)	79	5	N/A
Inhibition of IKK β	4	4	0.05 – 0.3
Inhibition of CDK1	6	3	3.6 – 100
Abrogation of DNA damage induced G2/M arrest (via Chk1 inhibition)	7	3	0.017 – 12.5
Inhibition of GST-IkB α phosphorylation	2	2	0.05 – 0.302

C

Target	Top similarity Score	Overall 3D similarity score
Chk1	1.515	1
PARP1	1.519	0.493
IKK β	1.466	0.406
Adenosine receptor A2a	1.473	0.22
Adenosine receptor A1	1.43	0.186
Adenosine receptor A3	1.624	0.164
JAK2	1.352	0.07
CDK2 associated protein 1	1.395	0.063
GSK3 β	1.59	0.052
GSK α	1.624	0.05
CDK5	1.223	0.004
CDK1	1.341	0.004
CDK2	1.241	0.003

D

BioAssay Description	No. Compounds Tested	No. Compounds Active	Activity Concentration Range (μM)
Inhibition of Fibroblast growth receptor 3	139	138	0.00046 – 4.1
Inhibition of Vascular endothelial growth receptor 2	132	128	0.00779 – 30
Inhibition of CDK4	885	119	0.0501 – 36
Inhibitors of IL- β signalling	937	66	N/A
Inhibition of CDK6	59	59	0.00036 – 0.406
Identification of TRAIL - induced death sensitizers	945	29	N/A
Small molecule activators of BRCA1 expression	946	25	0.5012 – 35
Inhibition of CDK5	25	25	0.05 – 2.3
Inhibition of IRAK4	25	25	0.004 – 8.1
Inhibition of PLK1	947	21	1.68 – 38
Inhibition of JAK1	19	19	N/A
Inhibition of DYRK1A	25	19	0.5 – 10
Inhibition of Aurora A	13	13	0.079 – 10
Inhibition of IKK β using GST-IkB α as a substrate	11	11	0.00708 – 0.046
Inhibition of CDK1	10	10	0.085 – 0.7

E

Target	Top similarity Score	Overall 3D similarity score
Lck kinase	1.515	0.96
Histamine H4 receptor	1.519	0.83
PDE10A	1.466	0.819
Adenosine receptor A3	1.473	0.609
PARP1	1.43	0.322
IKK β	1.624	0.307
Neutrophil elastase	1.352	0.281
Lyn kinase	1.395	0.211
Chk1	1.59	0.193
IKK α	1.624	0.176
CDK1	1.341	0.115
CDK2	1.345	0.041
CDK9	1.329	0.03
CDK5	1.301	0.014

Figure 5.17. Bioinformatics analyses of AZD2230 and BMS-345541 chemical structures (A) Hierarchical cluster map based on pairwise compound similarities between input compounds. The required distance matrices are calculated by all-against-all comparisons of compounds using atom pair similarity measures and transforming the generated similarity scores into distance values. (B) Table of Bioassay data hits for compounds with >80% similarity (as defined by Tanimoto coefficient) to AZD2230. (C) Top 10 hits from a ChemMapper search for candidate AZD2230-binding targets, based on 3D structure similarity to annotated drug-like molecules from the ChEMBL database. (D) Table of Bioassay data hits for compounds with >80% similarity (as defined by Tanimoto coefficient) to BMS-345541. (E) Top 10 hits from a ChemMapper search for candidate BMS-345541-binding targets, based on 3D structure similarity to annotated drug-like molecules from the ChEMBL database.

chemical structures and their associated pharmacology annotations. For the user-provided chemical structure, 3D structure similarity searching, ranking and superposition are performed against each compound in the database, and the top most similar structures are returned. A chemical-protein network is constructed from the pharmacology annotations of these top hits, and a random walk algorithm is used to compute the probabilities of interaction between the query structure and proteins associated with hit compounds. A set of similarity scores between the query and hit compounds are calculated, and scaled from 0 to 2; the closer to 2.0 the score the higher the potential of pharmacological association between the molecules. A threshold of 1.2 was used to report hits. The reported similarity scores in Figures 5.17C and E are those of the top hit. An overall 3D similarity score out of 1.0 is also generated, which factors in the highest 3D similarity score, the number of similar hits, and the average similarity scores of these hits. The list of target hits were filtered for those from *Homo sapiens*. The top 10 hits are presented, along with any CDK's that were hits.

The identification of IKK β amongst the top target hits and exhibiting the highest similarity score for its associated hit compounds, in the case of both AZD2230 and BMS-345541, is evidence that this approach generated meaningful results (Figure 5.17C and D). Interestingly, the top hit for AZD2230 was Chk1, which was also a top hit from the 2D structure similarity approach described earlier (Figure 5.17B). This is perhaps not that surprising, as an overlapping set of structural similar compounds was likely to be identified regardless of whether the search was based on 2D or 3D similarity. Nevertheless, it is additional evidence in support of a potential off-target effect of AZD2230 on Chk1. Chk1, PARP1 and Adenosine receptor A3 appeared in searches for compounds similar to AZD2230 and BMS-345541, potentially indicating a degree of functionally relevant structural similarity between these two inhibitors. The computational search also identified CDK-binding compounds with some structural similarity to AZD2230 and to BMS-345541, although the low number of identified compounds caused the overall similarity score to be low.

Overall, these results indicate that whilst AZD2230 and BMS-345541 display a lack of structural similarity with each other, they both share structural similarity with other compounds that exhibit activity towards targets whose inhibition could account for the off-target effects of AD2230 and BMS-345541.

5.3 Discussion

5.3.1 AZD2230 and BMS-345541 have off-target effects on cell cycle progression.

The novel IKK inhibitor, AZD2230, and siRNA-mediated knockdown of IKK β had effects on proliferation and protein expression that appeared to confirm the role of IKK β in cell cycle progression proposed in a study using the commercially available IKK inhibitor, BMS-345541 (Blazkova *et al.*, 2007). However, the potencies of AZD2230 and BMS-345541 towards IKK did not correlate with their potencies observed in assays of proliferation. Subsequently, the anti-proliferative effects of AZD2230 and BMS-345541 could not be phenocopied using either a highly selective IKK β inhibitor, BIX02514, siRNA-mediated knockdown of IKK β with a selective pool of siRNA, siRNA-mediated knockdown of IKK α , or siRNA-mediated knockdown of both IKK α and IKK β . Furthermore, AZD2230 and BMS-345541 were equally potent in WT, IKK β KO and IKK α/β DKO HCT116 cell lines. This confirmed that the effects of AZD2230 and BMS-345541 on cell cycle progression were off-target. IKK β KO and IKK α/β DKO HCT116 cells exhibited no growth defects (Chapter 3, Figure 3.4A) and asynchronous populations exhibited highly

similar cell cycle profiles (Chapter 3 Figure 3.4B). Overall, these findings cast serious doubt on the role of IKK β in cell cycle progression proposed by Blazkova *et al.* More generally, these findings call into question the validity of other studies that have utilised either BMS-345541 or IKK β -targeted siGENOME SMARTpool siRNA. BMS-345541 has been used as an inhibitor of IKK activity in over 100 publications since it was made commercially available in 2003 and these publications have been cited over 2000 times (Figure 5.18). BMS-345541 was used at a concentration of 3 to 30 μ M in all ten of the most-cited articles referencing this compound. At these concentrations, significant off-target inhibition was observed in HCT116 cells (Figure 5.10B). In some of these studies, BMS-345541 was used to confirm IKK β or NF- κ B activation in response to a given stimulus. Of more concern, however, a number of studies used high concentrations of BMS-345541 to propose novel functions of IKK β or NF- κ B. For example, BMS-345541 was used extensively at a concentration of > 5 μ M in a study that proposed a novel role for IKK β in regulating repair of ionizing radiation-induced DNA double-strand breaks (Wu *et al.*, 2011), and in a study that proposed an important function for the IKK complex in interferon-induced gene expression and antiviral activity (Du *et al.*, 2012).

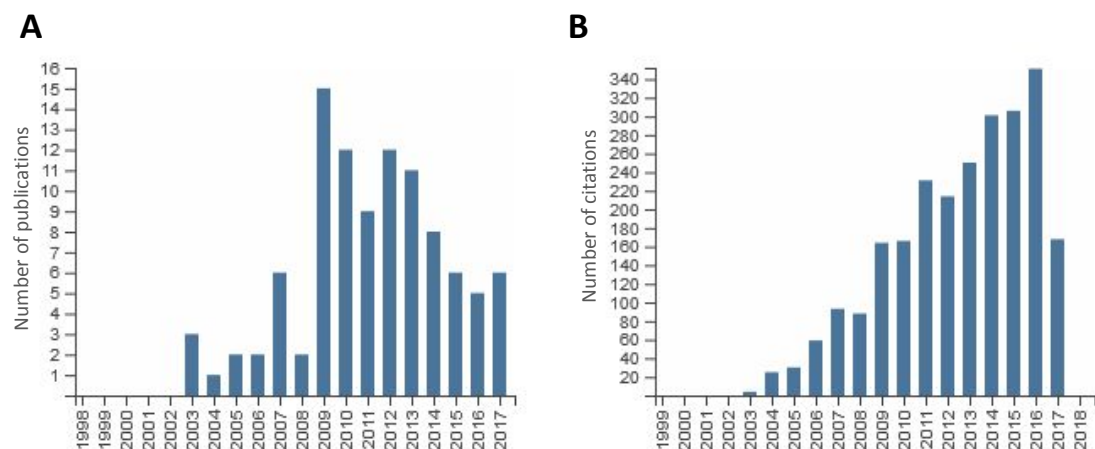


Figure 5.18. Publication statistics for the IKK β inhibitor, BMS-345541. (A) Total yearly publications featuring BMS-345541. **(B)** Sum of times BMS-345541 cited by year. Data sourced from Web of Science

siGENOME SMARTpool siRNA-mediated knockdown of IKK β phenocopied the off-target effects of AZD2230 and BMS-345541 on the protein expression of various cell cycle regulators. This was perhaps not as remarkable a coincidence as it first appeared. A growing body of evidence suggests that siRNA specificity is not absolute, and that there are various mechanisms of off-target gene silencing. For example, global, nonspecific, siRNA concentration-dependent stimulation and repression of gene expression has been observed in numerous RNAi genome-wide screens (Persengiev *et al.*, 2004). Transfected siRNAs have also been shown to induce global upregulation of interferon-stimulated genes through direct activation of the dsRNA-dependent protein kinase, PKR (Sledz *et al.*, 2003). siRNA-specific gene expression changes may also be induced by off-target mRNA degradation mediated by partial sequence complementation (Jackson *et al.*, 2003). High concentrations of certain siRNAs have been shown to induce a ‘toxic’ phenotype through off-target effects that are independent of siRNA sequence (Fedorov *et al.*, 2006). In addition, siRNAs with partial sequence complementarity to the 3'

untranslated region (3' UTR) of endogenous mRNAs can efficiently silence gene expression by repressing translation via a micro-RNA (miRNA)-like mechanism (Zeng & Cullen, 2003, Saxena *et al.*, 2003). miRNA-like translation inhibition was proposed as the mechanism underlying off-target upregulation of p53 and p21^{CIP1} in response to siRNA-mediated knockdown of a functionally unrelated gene, *MEN1* (Scacheri *et al.*, 2003). Importantly, miRNA-like off-targets can be reduced by introducing modifications to the guide strand of the siRNA (Birmingham *et al.*, 2006). Such modifications are made to ONTARGETplus siRNA. IKK β knockdown with a pool of ONTARGETplus siRNA had no effect on the protein expression of cell cycle regulators, confirming the off-target nature of the effects of knockdown with siGENOME SMARTpool siRNA. This highlights the need for caution when interpreting results using high concentrations of unmodified individual or pooled siRNA.

The data presented here is also inconsistent with reports of a role for IKK α in regulating progression through mitosis (Prajapati *et al.*, 2006). Prajapati *et al* demonstrated that siRNA-mediated knockdown of IKK α in HeLa cells induced an accumulation of cells in the G2/M phase and proposed that IKK α regulates Aurora A activity through phosphorylation of Threonine 288 to promote progression through mitosis. In contrast, neither IKK α knockdown (Figure 5.8 and 5.9A) nor IKK α knockout (Chapter 3 Figure 3.4) had any effect on the cell cycle distribution or expression of cell cycle regulators in HCT116 cells. This may reflect differences in cell type specific functions of IKK α .

5.3.2 AZD2230 and BMS-345541 may block global transcription through off-target inhibition of RNA Polymerase II C-terminal domain phosphorylation

Publically available selectivity data showed that BMS-345541 binds to numerous CDKs *in vitro* with similar dissociation constants to IKK β . This included three CDKs (CDK7, 9 and 13) with essential functions in controlling global RNA Pol II-dependent transcription through CTD phosphorylation. AZD2230 and BMS-345541 rapidly inhibited the phosphorylation of the RNAPII CTD at Serine-2 and Serine-5 with kinetics that preceded the changes in protein expression of cell cycle regulators. This was shown to be an off-target effect of both inhibitors. Pan-CDK inhibitors with common activity towards CDK7 and CDK9 induced changes in protein expression and cell cycle distribution that were similar to AZD2230 and BMS-345541. Finally, both AZD2230 and BMS-345541 induced pronounced nucleolar disruption, characteristic of CDK9 inhibition. Overall, these data suggest that CDK7, CDK9 and/or CDK13 may be the targets of AZD2230 and BMS-345541 mediating their inhibitory effects on cell cycle progression.

Further evidence is needed to prove a causal link between off-target inhibition of CDKs and the observed cell cycle arrest. For example, it will be important to directly demonstrate drug induced inhibition of transcription and correlate this with the kinetics of decreases in RNAPII CTD phosphorylation and cell cycle regulator expression. This could be done through quantitation of ³H-uridine incorporation into nascent RNA over a timecourse of treatment with AZD2230 or BMS-345541. Another common method of measuring transcription inhibition is monitoring inducible reporter genes, such as luciferase. This calls into question the accuracy of the NF- κ B-driven luciferase reporter assays used to estimate the IKK inhibition potencies of AZD2230 and BMS-345541 (Figure 5.1C and D). Confounding off-target inhibition of luciferase reporter transcription may have led

to overestimation of the IC₅₀'s for IKK inhibition of both AZD2230 and BMS-345541. However, the results of the luciferase assay correlated well with Western blots for markers of IKK activity (Figure 5.1A and B).

The observed G2/M arrest and many of the protein expression changes caused by AZD2230 and BMS-345541 treatment are consistent with DNA-damage induced G2/M checkpoint activation. For example, various sources of DNA damage in G2 phase trigger an ATM/ATR-protein response that stabilises p53, which in turn transcriptionally activates p21^{CIP1} and represses various genes, such as Cyclin B1, Cdc20 and CDC25C (El Deiry, 1998; Krause *et al.*, 2000; Krause *et al.*, 2001; Taraswi *et al.*, 2008). C-JUN is also activated in response to DNA damage, and is thought to promote expression of DNA repair genes and cell survival as part of AP1 transcription factor complexes (Potapova *et al.*, 2001). Furthermore, genotoxic stress-induced long-term G2 arrest (over 12 hours) is accompanied by premature activation of the APC/C, and results in a pattern of protein expression and degradation that closely matches that induced by AZD2230 and BMS-345541 (Weibusch *et al.*, 2010). Furthermore, DNA damage has been reported to induce nucleolar disruption, independently of CDK9 inhibition (Rubbi *et al.*, 2003). Some reports suggest that nucleolar disruption mediates stabilisation of p53 as a unifying response to DNA damage and other stresses, such as RNA Pol II inhibition (Boyd *et al.*, 2011).

It will be important, therefore, to determine if AZD2230 and BMS-345541 induce DNA damage directly, and the kinetics of any DNA damage response induced compared to the observed inhibition of RNAPII phosphorylation. Deciphering cause and effect will be complicated by the interconnectivity of DNA damage repair processes and global transcription; close coordination is critical for safeguarding genomic integrity. Following DNA damage within transcribed genes, global RNAPII-dependent transcription is arrested, providing the opportunity for DNA damage response (DDR) proteins to access and repair the damage. Interestingly, sustained RNAPII arrest is commonly associated with hyperphosphorylation of the RNAPII CTD, which may serve to inhibit new transcriptional initiation (Rockx *et al.*, 2000). There is some debate regarding the site of this phosphorylation and the kinase responsible; both seem to depend on the nature and extent of the DNA damage. In the case of UV-induced DNA damage, CDK9 has been shown to hyperphosphorylate Serine-5, while topoisomerase inhibitors, such as camptothecin, induce Serine-5 hyperphosphorylation via activation of CDK7. Regardless, hyperphosphorylation of stalled RNAPII elongation complexes appears to be a signal for polyubiquitylation and proteasome-dependent degradation of the RPB1 subunit. This 'last-resort' response to sustained transcriptional arrest results in disassembly of the stalled RNAPII complex, and facilitates access to and repair of damaged DNA.

Importantly, RPB1 hyperphosphorylation, polyubiquitylation and degradation occur under a number of other conditions that lead to persistent transcriptional arrest, including nucleotide triphosphate (NTP) depletion and RNAP II inhibition. For example, the direct RNAPII inhibitor α -amanitin induces RPB1 ubiquitylation and degradation. As such, one can speculate that the lower concentrations of AZD2230 (10 μ M) and BMS-345541 (5 μ M) may have partially inhibited transcriptional CDKs (CDK7, 9 and/or 13), leading to an initial dephosphorylation of RNAPII CTD. In turn, this may have caused stalling of RNAPII elongation complexes, which were subsequently hyperphosphorylated and targeted for degradation by CDKs that had escaped inhibition at these doses. The higher concentrations of AZD2230 and BMS-345541 may have fully inhibited transcriptional CDKs and thus prevented the late-phase hyperphosphorylation of RNAPII. This cannot explain, however, the apparent degradation of RNAPII observed after 24 hours treatment with 10 μ M BMS-345541.

Conversely, CDK inhibition itself may directly elicit a DNA damage response via a variety of mechanisms. For example, CDK2 inhibition during S-phase leads to DNA re-replication, which elicits an intra-S-Phase checkpoint that shares components of the pathway activated by DSBs. Reduced CDK activity may also slow or stall DNA replication forks – this block is detected by ATR, which primarily activates Chk1. However, sustained CDK inhibition has been shown to lead to downregulation of Chk1, perhaps part of a negative feedback loop promoting cell cycle recovery. As such, this may explain the increased frequency of DSBs and cytotoxicity observed when CDK inhibitors (such as Roscovitine) are combined with DNA damaging treatments such as topoisomerase inhibitors. Off-target CDK2 inhibition may contribute to the effects of AZD2230 and BMS-345541. Publically available kinase selectivity data shows that 60% CDK2 activity remains in an *in vitro* assay at 10 µM BMS-345541 (compared to 16% IKK β activity).

Of the binding targets identified in a broad kinase selectivity screen, CDK11A and CDK11B had BMS-345541 dissociation constants most comparable to IKK β ($K_d = 130$ nM): CDK11A $K_d = 390$ nM and CDK11B $K_d = 420$ nM (Davis *et al.*, 2011). *Cdk11a* and *Cdk11b* are duplicated genes that encode highly homologous protein kinases of 110 kDa, CDK11 p110 . CDK11 p110 is expressed throughout the cell cycle and is involved in transcription regulation and mRNA splicing (Trembley *et al.*, 2004). CDK11 p110 activity is required for ovarian, liposarcoma, osteosarcoma and breast cancer cell growth and survival (Duan *et al.*, 2012; Jia *et al.*, 2014; Zhou *et al.*, 2015; Liu *et al.*, 2016). Interestingly, during G2 and M phases, activation of an internal ribosome entry site present in CDK11 mRNA, results in expression of the truncated kinase, CDK11 p58 , which has roles in centrosome maturation, centriole duplication and protection of sister chromatid cohesion at centromeres during mitosis (Rakkaa *et al.*, 2014). Taken together, the antiproliferative effects of BMS-345541 observed here, and by Blazkova *et al.*, could have been mediated, in part, by off-target inhibition of CDK11A and/or CDK11B.

The synergistic effect of BMS-345541 and IKK α/β DKO on cell death is worthy of further investigation. The absence of synergy in response to AZD2230 likely reflects the different off-target profile of BMS-345541. Why this synergy is not observed in the IKK β KO cells is unclear, however. The effect of AZD2230 and BMS-345541 on IKK α KO cells was not explored. The difference could be explained by a greater importance of IKK α over IKK β in protecting against cell death induced by BMS-345541. Alternatively, it could reflect the importance of drug-induced NF- κ B pathway activation in protecting against cell death. Unlike IKK α/β DKO cells, IKK β KO cells are capable of inducing NF- κ B in response to stimulus due to the redundant activity of IKK α (Chapter 3 Figure 3.6). Both of these possibilities require that IKK α activity was not fully inhibited at 5 – 10 µM BMS-345541. The IKK activity data (Figure 5.1B) indicated that IKK α was likely to be significantly inhibited at these concentrations. As previously discussed, however, these results may not be entirely accurate due to off-target inhibition of luciferase expression by BMS-345541. Nonetheless, these results could reflect an important role for IKK α activity and/or NF- κ B signalling in promoting survival following cell cycle arrest induced by CDK inhibition and/or DNA damage. Consistent with this, both IKK α - and IKK β -mediated NF- κ B pathway activation has been shown to protect against doxorubicin-induced cell death (Bednarski, 2008). Furthermore, Bortezomib, which inhibits the NF- κ B pathway as part of its mechanism of action, synergises with Flavopiridol to induce apoptosis in chronic myeloid leukemia cells (Cosimo *et al.*, 2013). It will be interesting to compare the sensitivity of WT, IKK α , IKK β and IKK α/β DKO cells to CDK inhibitors such as SNS-032 and Flavopiridol.

In conclusion, it is likely that a combined off-target inhibition of multiple cell cycle and transcriptional CDKs, with a possible associated induction of DNA damage, explains the inhibitory effects of AZD2230 and BMS-345541 on cell cycle progression. This negates their use in assessing the effects of IKK inhibition on cell proliferation. Furthermore, since NF- κ B is a major transcription factor in immune and inflammatory signalling, off-target inhibition of CDKs involved in RNA Pol II regulation also negates their use in studies of IKK- and NF- κ B-dependent gene expression.

Chapter 6

**RNA Sequencing defines IKK-dependent NF-κB
gene expression profiles**

6 RNA-sequencing analysis of TNF α -inducible, IKK-dependent gene expression profiles

6.1 Introduction

The CRISPR-Cas9 cell line data presented up until this point suggested that IKK α and IKK β have both complementary and non-redundant functions in the activation of canonical NF- κ B in response to pro-inflammatory cytokines and in mediating cross-talk with other signalling pathways. On the basis of these results we decided to perform RNA-sequencing analysis on three independent clones of WT, IKK α KO, IKK β KO and IKK α/β DKO cell lines treated with TNF α for 0, 2 and 8 hours to assess the impact of IKK knockout on basal and TNF α -induced gene expression. There were several reasons for taking this genome-wide approach. It was hoped that comparison of the expression profiles of WT, IKK α KO, IKK β KO and IKK α/β DKO cells in the absence of stimulus might reveal novel functions of the IKK kinases, either in maintaining the basal expression of NF- κ B-dependent genes, or in NF- κ B independent processes. In this way the RNA sequencing analysis might uncover phenotypes of the KO cell lines that had been missed during basic characterisation of the cells (Chapter 3). We were also seeking explanations for some of the observations we had made during the characterisation of these cell lines. For example, the greater epithelial morphology and E-cadherin expression in IKK α/β DKO cells (Figure 3.3), as well as the greater basal activation of p38 in these cells (Figure 3.5).

It was also hoped that characterisation of the expression profile of WT cells treated with TNF α might reveal potential novel NF- κ B-dependent genes with significance in colorectal cancer progression. Numerous genome-wide expression analyses have characterised thousands of NF- κ B-dependent genes across different species, cell types and stimuli (Li *et al.*, 2002; Schwamborn *et al.*, 2003; Zhou *et al.*, 2003; Andela *et al.*, 2005; Massa *et al.*, 2005; Tian *et al.*, 2005a; Tian *et al.*, 2005b; Viemann *et al.*, 2006; Bunting *et al.*, 2007; Hao & Baltimore, 2009; Raskatov *et al.*, 2012; Chen *et al.*, 2016). Indeed, a thorough and up-to-date database of 1667 distinct NF- κ B target genes has recently been compiled (Yang *et al.*, 2016). However, the majority of the studies that have sought to identify NF- κ B-dependent genes have employed DNA microarray approaches. Compared to microarray technologies, RNA sequencing is a more sensitive technique and enables a broader dynamic range of differential gene expression to be assessed. Furthermore, the majority of previous genome-wide expression analyses have been performed in MEFs or in HeLa cells. This is the first reported genome-wide approach to the identification of TNF α -inducible genes in a colorectal cancer cell line. Given the potential importance of TNF α signalling to the progression of colorectal cancer (Chapter 1, Section 1.4.4), it was hoped that this RNA sequencing approach would generate a clinically relevant profile of NF- κ B-dependent genes.

Most significantly, it was hoped that characterisation of the expression profiles of WT, IKK α , IKK β KO and IKK α/β DKO cells treated with TNF α might address the relative contribution of IKK α and IKK β to the expression of NF- κ B-dependent genes. On the basis of the data presented in Chapter 3, we had sufficient reason to believe that the expression profiles of IKK α KO and IKK β KO cells might differ significantly from each other and from that of WT cells, both in terms of the identity of the differentially expressed genes themselves and the fold-changes in the expression of differentially expressed genes common to each cell type. For example, we had observed that IKK α KO and IKK β KO cells exhibited differential defects in TNF α -induced fold-changes in nuclear translocation of

c-Rel and p65; IKK α KO cells exhibited a striking defect in the nuclear translocation of both p65 and c-Rel, while IKK β KO cells were primarily defective in c-Rel nuclear translocation (Figure 3.15). We were interested in how this difference might manifest as differences in the expression pattern of genes that are regulated by p65- and c-Rel-containing NF- κ B dimers. In relation to this, a recent study proposed that TNF α -induced transcriptional output, both in terms of fold expression changes and the identity of the genes induced, correlates most closely with the fold change in nuclear NF- κ B, not the absolute nuclear NF- κ B abundance (Lee *et al.*, 2014). We expected that the expression of well-characterised NF- κ B target genes would be, on average, lower in the IKK α KO clones compared to WT and IKK β KO cells, given that these cells had exhibited markedly reduced TNF α -induced expression of an NF- κ B-dependent reporter (Figure 3.6). But we were also curious as to how this weaker overall induction of NF- κ B gene expression might translate into differences in the profile of genes induced. Furthermore, IKK α KO and IKK β KO cells exhibited differences in the post-translational modification of p65; IKK α KO cells exhibited reduced basal phosphorylation of S536 and reduced TNF α -induced phosphorylation of S468 compared to IKK β KO and WT cells (Figure 3.6). We were interested in how these, and other potential differences in the post-translational modification of NF- κ B subunits that we didn't measure might impact the TNF α -induced expression profile in IKK α KO and IKK β KO cells. In addition, IKK α and IKK β have been proposed to phosphorylate other components of NF- κ B signalling pathway to influence feedback inhibition (Chapter 1, Section 1.3.2.3). For example, IKK α has been proposed to phosphorylate PIAS1 and TAX1BP1, while IKK β has been proposed to phosphorylate A20. Although we have not assessed the status of these specific phosphorylation events in our IKK KO cells, we had reason to believe that feedback mechanisms might have been generally defective given the more prolonged IKK phosphorylation and the weaker second phase of I κ B degradation observed in the KO cells compared to WT (Figure 3.18). This is significant given the apparent importance of feedback mechanisms in setting the precise oscillations in NF- κ B signalling that contributes to define the NF- κ B target gene expression profile (Nelson *et al.*, 2004; Tian *et al.*, 2005a).

A previous study described a similar approach to the one taken here in order to define the IKK-dependence of the NF- κ B gene expression response to inflammatory cytokines (Li *et al.*, 2002). The authors characterised gene expression patterns in IKK α and IKK β KO MEFS treated with TNF α using DNA microarrays, and identified a subset of genes that were dependent on either IKK α or IKK β for expression. Indeed, this was some of the earliest evidence to question the established dogma of the time that IKK β is the predominant canonical NF- κ B pathway kinase and IKK α is the non-canonical NF- κ B kinase. We hoped to extend this work to a more clinically relevant human cancer cell model. Indeed, we have already observed numerous fundamental differences between the regulation of canonical NF- κ B in human HCT116 cells compared to reports that relied on the use of IKK KO MEFs; the IKK dependence of p65 S468 phosphorylation being one example.

Within the tumour microenvironment, colorectal cancer cells that are part of developed tumours are likely to be constantly exposed to pro-inflammatory cytokines, such as TNF α . We therefore examined cells continuously exposed to TNF α , rather than those treated with a short pulse of TNF α . This was also consistent with the treatment method employed in all other experiments we performed. The significance of this decision is that the NF- κ B-dependent gene expression profile has been proposed to differ depending on the length of the stimulation interval (Ashall *et al.*, 2009). Furthermore, TNF α -induced genes have been shown to broadly segregate into three

kinetically distinct groups: an ‘early’-induced group whose expression peaks at ~ 0.5 hours, an ‘intermediate’-induced group whose expression peaks at ~ 2 hours, and a ‘late’-induced group whose expression peaks at ~ 12 hours (Hao & Baltimore, 2009). For this reason we decided to measure genome wide gene expression at two different timepoints. Budget constraints prevented the examination of further timepoints, so we opted for 2 hours as the early timepoint to attempt to capture a proportion of both early and intermediate genes and 8 hours as the late timepoint as this was the latest timepoint at which IKK DKO cells had not undergone significant levels of caspase-cleavage and hence committed to apoptotic cell death (Figure 3.9C and D).

It should be noted that the results of this RNA sequencing experiment await robust validation via qRT-PCR and chromatin immunoprecipitation (ChIP). Nevertheless, the results as they are presented confirm the importance of IKK α for canonical NF- κ B-dependent gene expression, they highlight a number of potentially novel NF- κ B-dependent genes, and they also reveal unexpected consequences of IKK β KO on the expression of genes involved in various cellular processes, including chromatin organisation, microtubule/actin cytoskeletal organisation, DNA damage and mitotic cell cycle progression.

6.2 Results

6.2.1 Assessment of RNA sample and sequencing quality

High purity total RNA was isolated from three independent clones of WT (A3, A8, E10), IKK α KO (F6, C7, A2), IKK β KO (G9, A7, A4) and IKK α / β DKO (C8, G1, E9) cells treated with 10 ng/ml recombinant, soluble human TNF α or vehicle control (0.2% BSA/PBS (w/v)) for 8 hours or TNF α for 2 hours, leading to a total of 36 samples. The individual cell clones represent the three biological replicates for each of the 12 conditions. Each of the clonal cell lines were from similar, early passages, and samples were generated in an identical manner with the same reagents, and on the same day. Efforts were made to prevent DNA contamination through the use of an on-column DNase I digestion. RNA quality was confirmed by NanoDrop and Bioanalyser (Agilent) analysis. Each sample had A260/A280 ratios > 2.00 and A260/230 ratios > 1.9 indicated high purity RNA with very little contamination from protein, phenol or other contaminants. Furthermore each of the samples exhibited RNA integrity numbers (RIN) of \geq 9.9 (out of 10), indicating exceptional RNA ‘intactness’, i.e. minimal RNA degradation (data not shown).

Illumina-compatible RNA sequencing libraries were prepared using the QuantSeq FWD 3' mRNA-Seq library preparation kit (Lexogen), which generates highly sense strand-specific next-generation sequencing (NGS) reads towards the poly(A) tail of RNA. Double-stranded cDNA libraries were sequenced on a NextSeq 500 sequencing system using a high-output, single-end read protocol of 75 cycles (to generate 75 base pair reads). The quality control of reads was performed using FastQC, which assesses the distribution of sequencing quality scores (Phred scores) across reads at each base position for each sample. Phred scores have values ranging from 1-36. The score is defined as a property which is logarithmically related to the base-calling error probabilities, such that a quality score of 30 for a base means that the probability of an incorrect base call is 1 in 1000 (i.e. a base call accuracy of 99.9%). Figure 6.1A represents a plot of the distribution of the mean read scores across all bases within each sample. It is expected that reads have a mean quality score of 30 or greater. Indeed, the distributions

exhibited peaks of mean quality scores of approximately 34, indicating that the sequencing reads for each sample were of a very high quality.

Generated reads were trimmed using TrimGalore, which trims low-quality base cells from the 3' end of reads and removes adaptor sequences. The per-sample number of sequencing reads after trimming is shown in Figure 6.1B. The average number of reads was close to the expected sequencing depth of 8-10 million reads per sample. There was a sharp drop in the number of sequencing reads at the 8 hr TNF α treatment timepoint for IKK α KO clones C7 and A2. However, the number of reads were still sufficient to detect a comparable number of genes across the samples (Figure 6.2B).

Per sequence GC content distributions (Figure 6.1C) and per base sequence contents (Figure 6.1D) were also assessed for each sample. Non-biased libraries should show a normal distribution of GC content, with the distribution centered at the overall GC content of the underlying genome (~ 40-60%). Given that the QuantSeq 3' mRNA-Seq libraries have an increase in Adenosine nucleotide content at the 3' end of the reads (Figure 6.1D), the GC content is often shifted below the overall GC content of the underlying genome, as was seen here. GC content bias resulting from technical variability in polymerase activity during library preparation can have a strong sample-specific effect on gene expression measurements that, if left uncorrected, can lead to false positives in downstream analysis (Pickrell *et al.*, 2010). Although no significant GC content bias was immediately apparent from these initial QC assessments, we decided to perform conditional quantile normalisation to remove any potential systemic bias. Such normalisation has been shown to improve precision by up to 42% without loss of accuracy (Hansen *et al.*, 2012).

Sequence duplication levels were also assessed and confirmed to be within an acceptable range (Figure 6.1E). High levels of duplication may indicate some enrichment bias, such as PCR over-amplification of a particular set of reads, or contamination. However, RNA-Seq libraries will normally show sets of reads at higher duplication bins that either correspond to highly expressed transcripts, which provide a high number of templates from the same region that are amplified and sequenced, or reads with high polyA $^+$ content, such as mitochondrial RNA and/or ribosomal RNA (particularly reads with > 1000 copies).

6.2.2 Assessment of RNA sequencing mapping and counting quality

Sequencing reads were mapped to the Ensembl *Homo sapiens* GRCh38 primary assembly (release 90) reference genome using the STAR alignment tool. Reads mapping to protein-coding genomic features (gene body) were counted using HTSeq. A feature was considered as the union of all gene exons whose genomic coordinates were determined from the annotated filtered protein-coding transcripts from the Ensembl *Homo sapiens*.GRCh38.90.gtf. An overview of the mapping quality is provided in Figure 6.2A. The reads exhibited a high enrichment within the exons of genes, as expected for a 3' mRNA directed library. The libraries also exhibited minimal rRNA contamination, indicating that the polyA-selection was successful. Also, the libraries were highly sense-strand specific as expected. The percentage of uniquely mapped reads was high (> 80%) for each sample (Figure 6.2B). Reads mapping to multiple loci (approximately 10-15% for each sample) were discarded to avoid false positives in differential expression analysis. The number of genes detected from the uniquely mapped reads were comparable for each sample (Figure 6.2B). The gene body coverage was calculated for 10 000 random genes

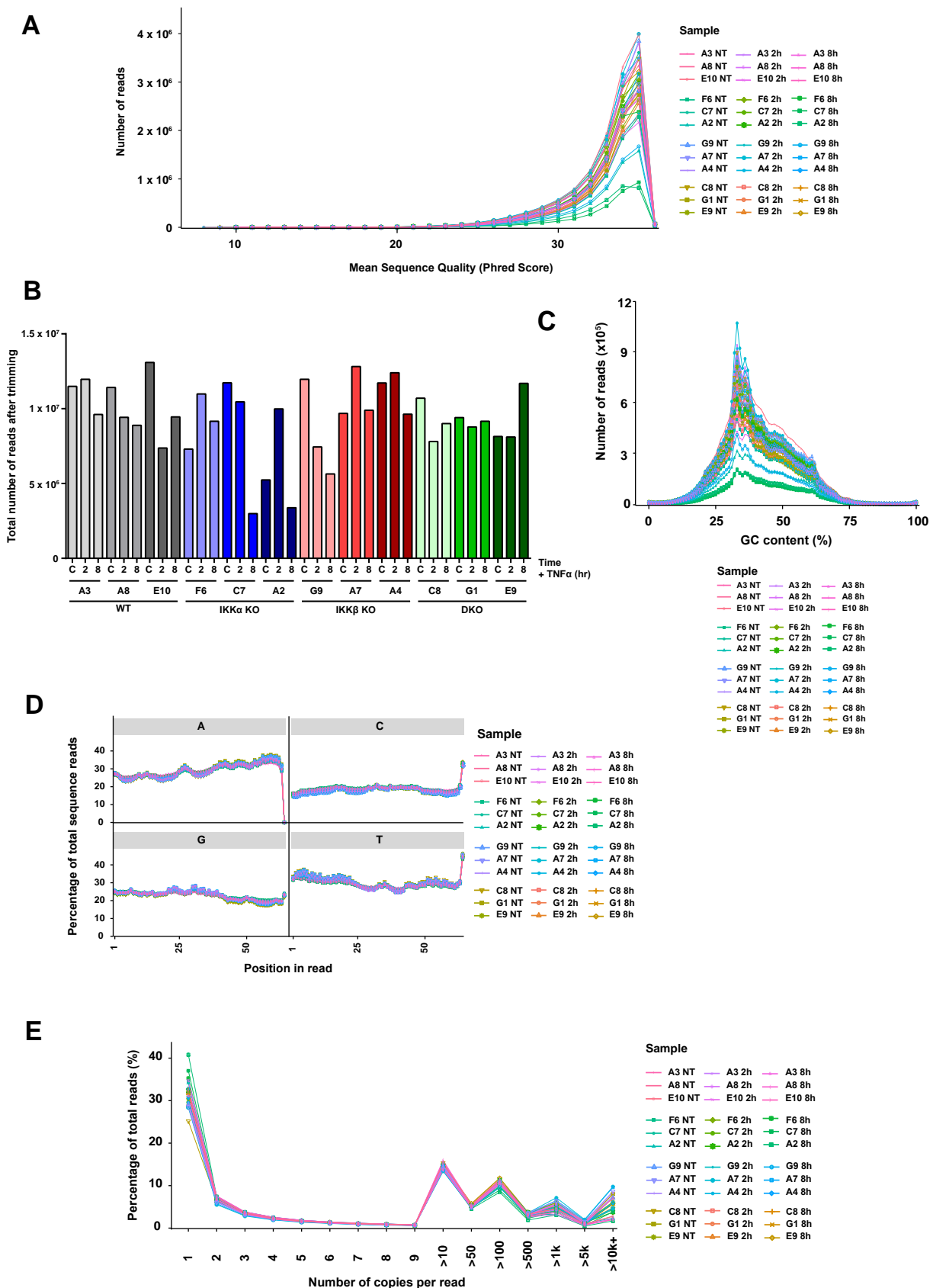
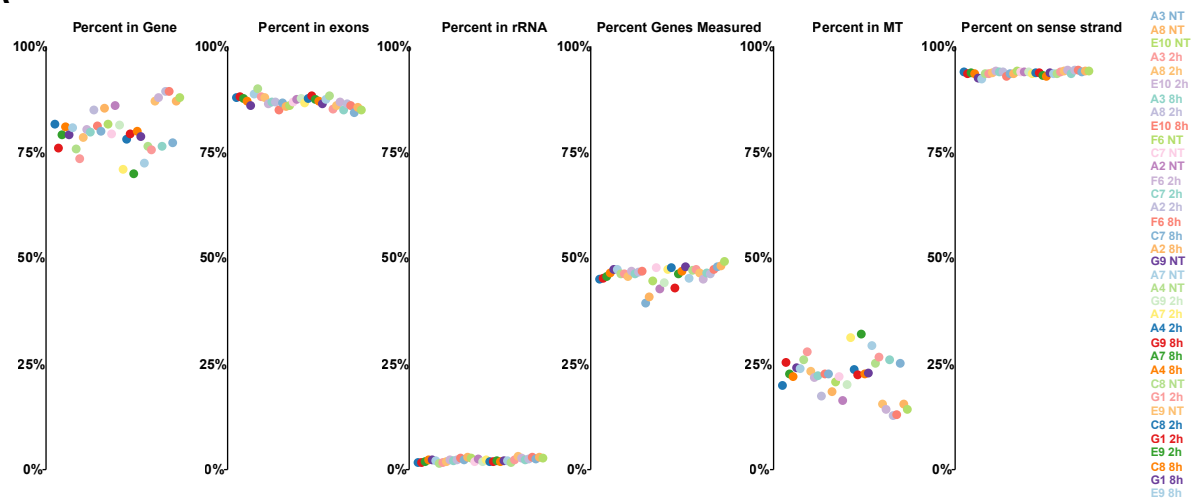


Figure 6.1. RNA sequencing quality control. **(A)** Per sequence read mean quality score for each sample (Phred score 1-36). **(B)** Number of reads per sample after trimming of low quality bases and adapters using TrimGalore. **(C)** Per sequence read percentage GC content for each sample. **(D)** Average percentage nucleotide composition across reads for each sample **(E)** Sequence duplication plot showing percentage of reads with specific number of copies. All plots generated using FastQC tool.

A**B**

Genotype	Sample	Uniquely Mapped reads(%)	Number of genes detected
WT	A3 NT	83.43	18774
	A8 NT	81.74	18930
	E10 NT	82.40	19485
	A3 2h	83.57	18477
	A8 2h	81.16	18170
	E10 2h	82.67	17741
	A3 8h	82.73	17951
	A8 8h	83.15	18211
	E10 8h	83.09	18482
IKK α KO	F6 NT	82.07	17473
	C7 NT	80.68	18326
	A2 NT	80.47	16566
	F6 2h	83.81	18613
	C7 2h	81.32	17781
	A2 2h	80.06	18035
	F6 8h	82.55	18222
	C7 8h	80.46	14873
	A2 8h	79.23	15628
IKK β KO	G9 NT	80.46	18440
	A7 NT	81.69	17708
	A4 NT	82.91	18106
	G9 2h	81.81	17213
	A7 2h	81.45	18409
	A4 2h	82.66	18349
	G9 8h	81.66	16402
	A7 8h	81.73	17454
	A4 8h	81.86	17704
DKO	C8 NT	83.78	17493
	G1 NT	82.92	17883
	E9 NT	82.97	17581
	C8 2h	83.14	17352
	G1 2h	83.61	17473
	E9 2h	82.71	17468
	C8 8h	82.62	17900
	G1 8h	81.42	17903
	E9 8h	81.67	17970

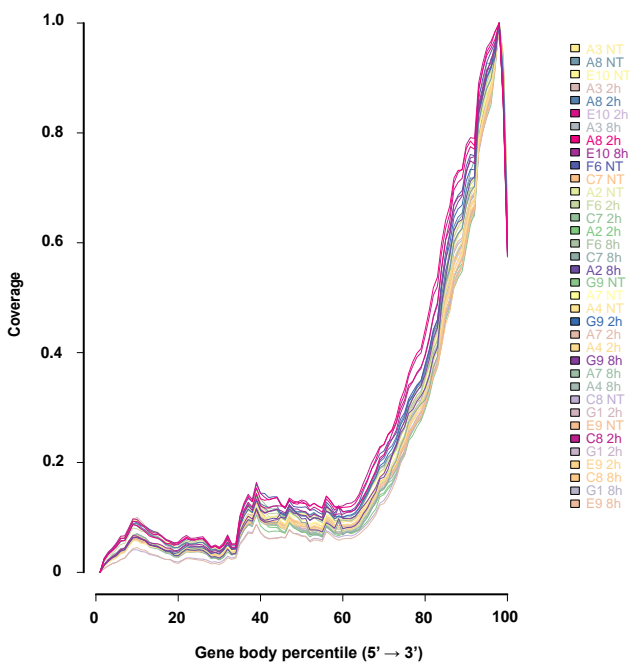
C

Figure 6.2. RNA sequencing mapping and counting quality control. (A) Sequence mapping quality control summary for each sample from SeqMonk. (B) Table summarising the results of the mapping, describing the percentage of uniquely mapped reads, and the number of genes (after filtering genes to retain those having more than 1 counts per million in at least one sample) detected in each sample. (C) Plot of read coverage along the gene body for 10 000 random genes. Generated using RSeQC v2.6.4. Reads were mapped using STAR v2.5.2a aligner. Ensembl *Homo sapiens* GRCh38 (release 90) was used as reference genome for mapping of reads, using annotated transcripts from the Ensembl *Homo sapiens* GRCh38.90.gtf. Counting of reads that map to genomic features (protein coding genes) was performed using HTSeq v0.6.0. Reads with a mapping quality less than 10, that map to multiple loci or to overlapping gene regions were discarded to avoid ambiguity and false positives.

in each sample using RSeQC, and the plots exhibited the expected 3' bias (given the 3' enrichment within the library preparation protocol) (Figure 6.2C).

Overall, the quality control assessments indicated that the RNA samples, library preparation, sequencing and mapping/counting were of a high quality.

6.2.3 Assessment of sample clustering

Principle component analysis (PCA) was performed to investigate the relationships between different groups of samples and identify any clustering of samples or sample outliers (Figure 6.3). PCA analysis is an unsupervised statistical procedure for reducing the multiple sources of variance within data sets into a set of orthogonal (i.e. that are unrelated to each other) dimensional variables, or ‘principle components,’ to reveal the simplified structures that underlie them. Samples are projected onto the 2D plane such that they spread out in the two directions that explain most of the differences between them. Similarities between data sets are correlated to the distances in the projection of the space defined by the principle component, so PCA can be used to confirm predicted relationships between samples, identify unexpected relationships (such as batch effects), and identify sample outliers. The first two components, PC1 and PC2 typically account for the majority of the variability within a data set. PCA was performed on a normalised and regularized-logarithm (rlog) transformed data matrix of read counts per gene obtained with DESeq2. Taking the log scale stabilises the variance across the mean and mitigates for the contribution of the high random noise of low count data that might otherwise overly contribute to sample-sample distances in PCA plots. In this way the distance measure has a roughly equal contribution from all genes.

The caveat with PCA analysis is that it can be difficult to identify defined clusters of samples when the data is highly dimensional, i.e. there are multiple sources of variation, both biological and technical in nature. Broadly speaking, this appears to be the case with the RNA sequencing data presented here, where there is variation resulting from IKK knockout, the effect of TNF α treatment, the length of TNF α treatment, clonal heterogeneity, and technical variation associated with the isolation of RNA and sequencing. Clustering according to genotype, length of TNF α treatment time or clonal identity was not readily apparent across the different samples. Overall, the DKO samples tended to cluster closer together than the WT or IKK KO samples (Figure 6.3A). This likely reflects the fact that TNF α treatment had a significantly reduced global impact on the expression of genes in DKO cells than WT and IKK KO cells, given the lack of NF- κ B signalling in DKO cells. It could also reflect a lower level of heterogeneity between the DKO clones than the WT and IKK KO clones. The greatest degree of separation was seen in the PC1 vs PC4 plot between DKO and WT samples, with IKK α KO and IKK β KO samples falling somewhere in between. The NT and TNF α treated samples were largely separated in the dimensions of largest variation: PC1 vs PC2, PC1 vs PC3, and PC1 vs PC4, as one would expect (Figure 6.3B). The samples also did not cluster according to clonal identity either (e.g. samples derived from clone A3), although this is not surprising as TNF α treatment was expected to have a more dominant effect on gene expression than the identity of the clone.

Subsequent PCA analysis for individual comparisons that were used to identify differential gene expression revealed that clonal heterogeneity made significant contributions to the variance within groups (e.g. Figure 6.4). Despite this apparent clonal heterogeneity there were no consistent outliers, and hence a strong case could not

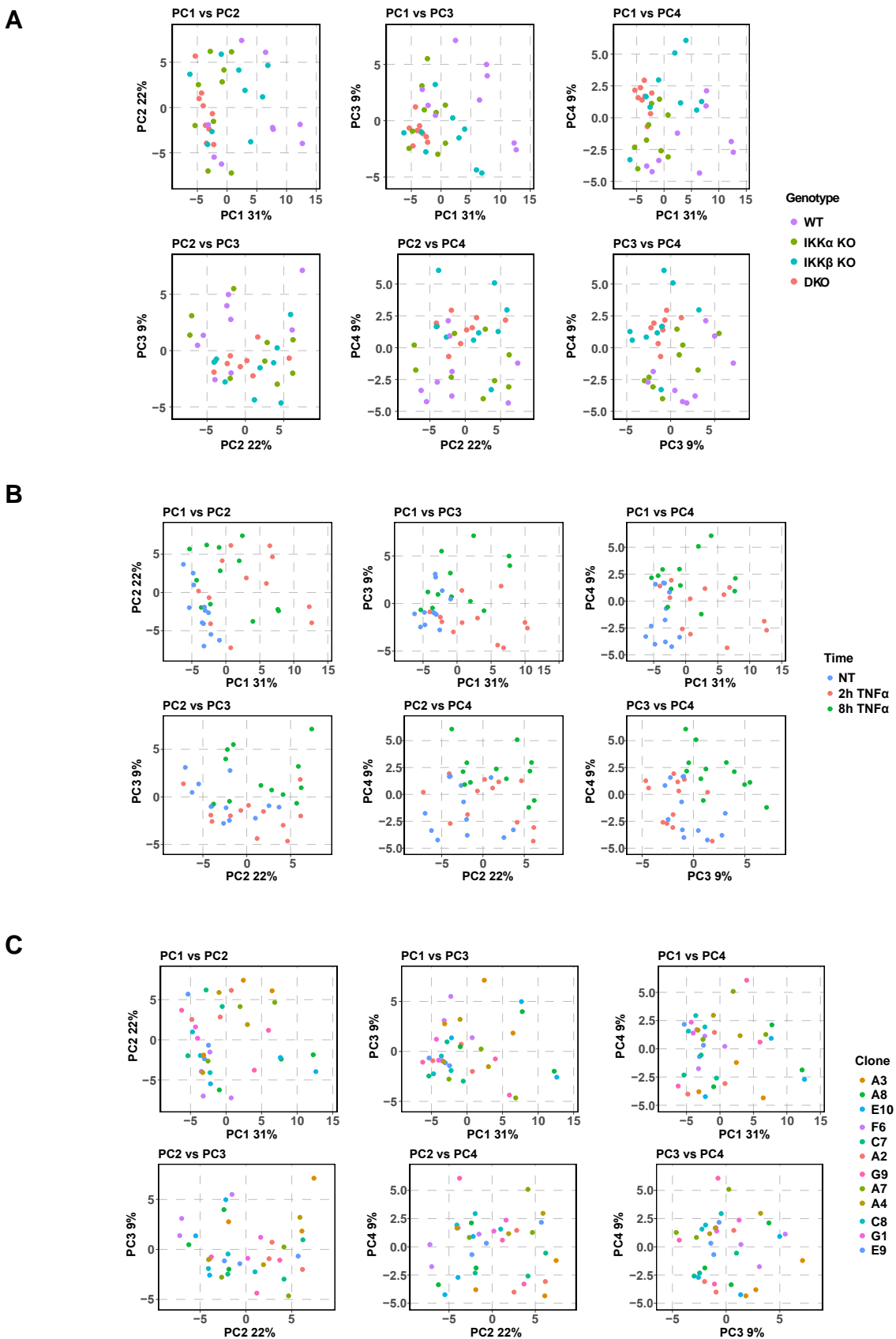


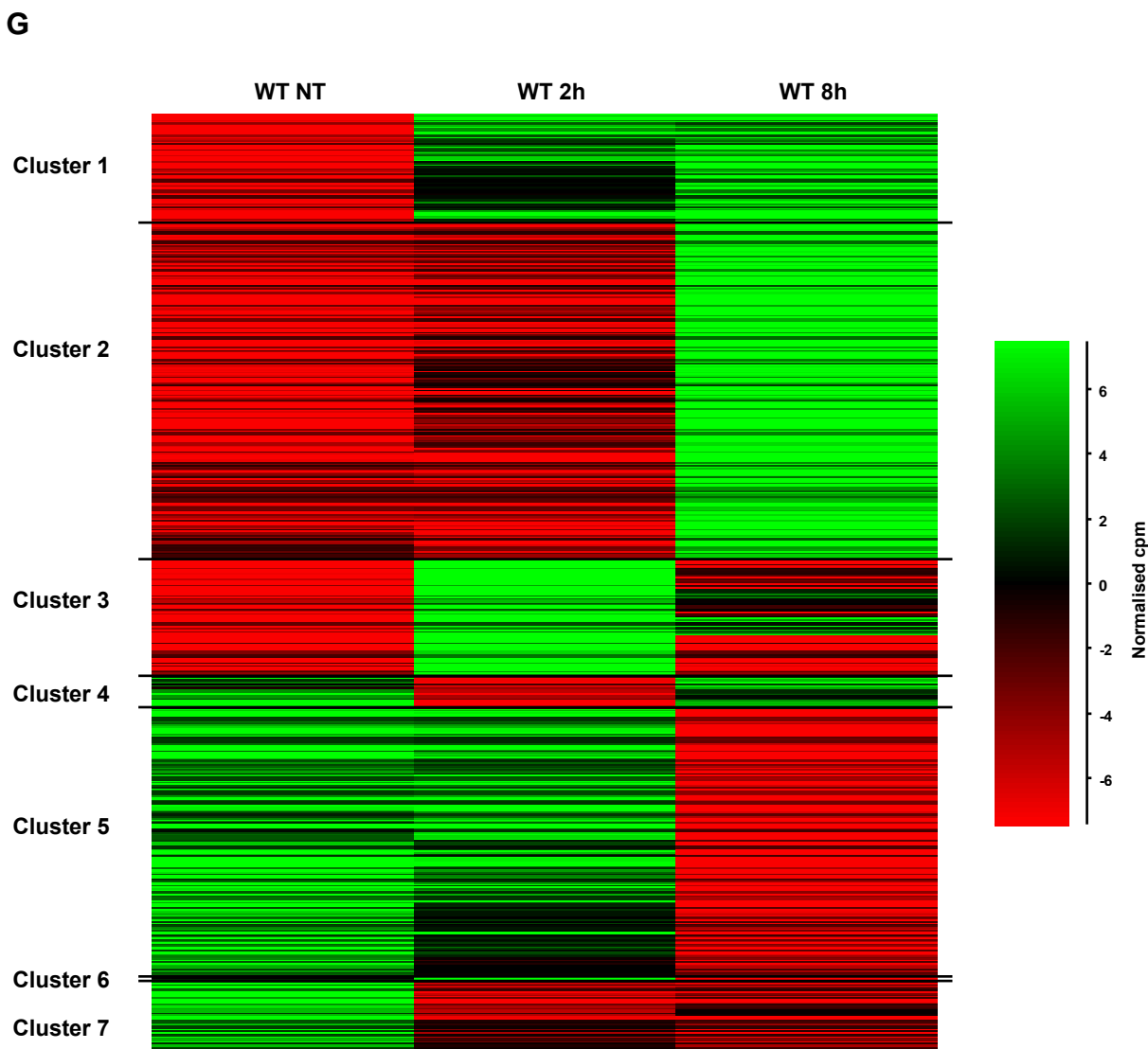
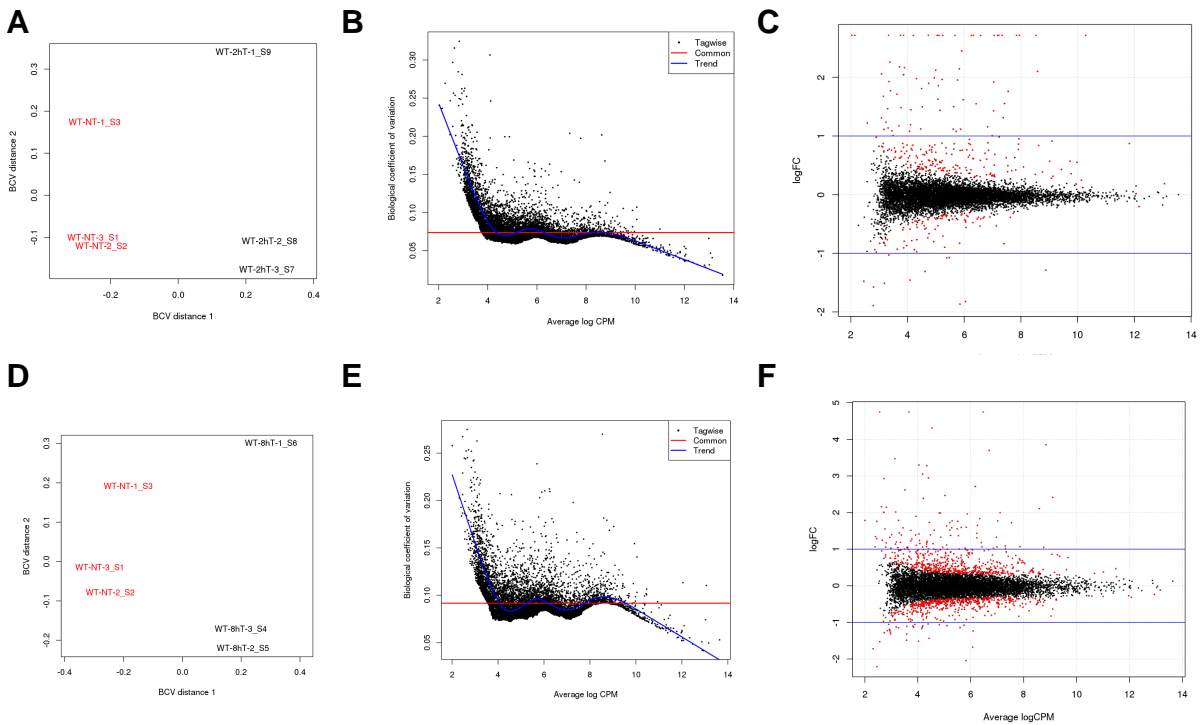
Figure 6.3. All-sample clustering analysis. Principle component analyses were based on normalised and regularized log (rlog) transformed counts obtained with DESeq2 and were performed for comparisons between genotype (**A**), treatment time (**B**) and clone identity (**C**). PC, principal components.

be made for excluding any of the samples from the subsequent analysis. Furthermore, as observed in other experiments (e.g. Chapter 3, Figure 3.6C), this clonal heterogeneity was common to all genotypes, including the WT clones. Had the heterogeneity been restricted to one group of the CRISPR-Cas9 cell lines (such as the IKK β KO clones) concerns might have been raised as to the validity of the KO's. The clonal heterogeneity common to the WT clones, however, was evidence that this heterogeneity was a consequence of the single-cell cloning process, not differences in the efficacy or off-target effects of CRISPR-Cas9 gene editing. The consequence of this clonal heterogeneity, however, was a reduced statistical power to identify differentially expressed genes, particularly in comparisons between non-treated KO clones (e.g. WT vs IKK α KO, WT vs IKK β KO and WT vs DKO) where there was no paired design to account for variance between clones as there was for comparisons between non-treated and TNF α -treated samples. As we shall see, this led to a reduced number of differentially expressed genes reaching statistical significance for the former comparisons.

6.2.4 Differential gene expression analysis of WT TNF α -treated samples identifies well-characterised patterns of gene expression and putative, novel TNF α -responsive genes

Differential gene expression (DE) analysis comparing NT with TNF α treated conditions was performed on WT samples using the R package edgeR. First, genes with low counts were filtered to reduce noise; genes having more than 10 counts per million (cpm) in at least 1 sample were kept. The sequencing libraries were also normalised to account for differences in sequencing depth and RNA composition between the samples using scaling factors calculated using the trimmed mean of M-values (TMM) between each pair of samples. This process was repeated for all further DE comparisons. Data exploration was performed on these filtered and normalised libraries using multi-dimensional scaling (MDS) plots, which show distances between samples in terms of biological coefficient of variation (BCV). BCV represents the square root of the average dispersion across genes (common dispersion). The MDS plot is therefore a type of unsupervised sample clustering. As seen in Figure 6.4A and D, the WT NT and WT TNF α treated samples exhibit a wide separation in the x-axis dimension of variation and cluster together in this dimension. Two of the three WT NT, WT 2h and WT 8h samples (corresponding to clones A8 and E10) cluster together in the y-axis of variation, with the third set of samples (corresponding to clone A3) showing a greater degree of separation. This likely reflects the heterogeneity between clones that has been discussed previously. One potential explanation for the observed differences between A3 and A8/E10 clones is the fact that A8 and E10 cell clones represent an earlier passage of cells than the A3 clone. A similar separation in clustering based on clonal passage is also observed for IKK α KO and IKK β KO clones (Figure 6.7A and 6.11A).

Irrespective of this apparent clonal heterogeneity, the variation between the samples was within the range considered reasonable to detect DE. This was highlighted in the plots of the estimated dispersion of each gene across the samples within each of the two comparisons (Figure 6.4B and E). In this plot each gene's average logCPM across samples (x-axis) is plotted against its BCV (y-axis), so each point (referred to as tagwise in the plot legend) corresponds to a gene. The blue line represents the trend through the tagwise data while the red line represents the common dispersion, which is an indication of the overall variability within the dataset. A common



H

I

2 h

8 h

UP		DOWN		UP		DOWN	
Gene	LogFC	Gene	LogFC	Gene	LogFC	Gene	LogFC
BIRC3	6.188297	ID2	-1.86625	BIRC3	5.808406	ID2	-2.04449
NFKBIA	3.440461	RGS2	-1.82216	RELB	3.696124	RGS2	-1.67644
CXCL8	6.733359	ZNF503	-1.07964	OPTN	2.710767	GRIN2B	-1.43774
IRF1	4.261792	ID1	-1.28733	NFKBIA	2.415972	CITED2	-1.51468
CXCL1	6.502161	ARL4D	-1.45784	CXCL8	4.311277	SLC2A1	-1.14331
TNFAIP3	4.588798	ID3	-0.83679	SDC4	2.107103	BDNF	-1.09125
TNFAIP2	3.697643	HES1	-1.07219	PSMB9	3.299793	BMP4	-1.07791
JUN	2.905242	AXIN2	-1.31061	IKBKE	2.946056	ARL4D	-1.16844
RELB	3.213872	KLF2	-0.89828	TNFAIP2	3.852484	TFAP2C	-1.48696
CXCL2	5.142445	BMP4	-0.82871	CD83	2.467088	ITGB4	-0.76219
EFNA1	3.35932	FOXQ1	-1.89072	TAPBP	1.774257	TCF7L2	-0.81054
ELF3	1.921044	BDNF	-0.70769	TNFAIP3	3.277688	NR2F1	-0.83304
CD83	2.751207	RNF43	-0.80008	JUN	1.995897	H1F0	-0.86561
SDC4	2.102547	FGF9	-0.97104	IFNGR2	1.720804	PRSS23	-1.04178
MAFF	2.449067	SLC30A1	-0.73674	IFIH1	3.049095	DENND5B	-0.92116
BBC3	1.761376	TET1	-1.51102	S100A3	2.385841	KANK2	-1.06315
JUNB	2.87901	TBX3	-0.90802	ETS1	1.99174	SMAD6	-1.32302
CXCL3	5.13042	GATA2	-0.93714	DTX3L	1.760196	TNS4	-1.09282
CCL20	7.947234	TIPARP	-0.86744	TAP1	1.961571	TRIM2	-0.96379
BCL3	2.14498	DBP	-1.57534	NFKB1	1.648504	THBS1	-1.12566

Figure 6.4. Characterisation of TNF α -induced gene expression profiles in WT HCT116 cells. (A) Biological coefficient of variation (BCV) multi-dimensional scaling (MDS) plot for comparison between WT non-treated (NT) and WT 2h TNF α treated samples. (B) Plot of biological coefficient of variation versus mean log counts per million (CPM) for each gene across samples within comparison from (A). Red line is the common dispersion (average dispersion across genes). (C) MA-plot of average logCPM plotted against the log fold-change (FC) for comparison between WT NT and WT 2h TNF α treated samples. Differentially expressed genes with FDR < 0.05 are highlighted in red. Blue lines are shown at logFC values of 1 and -1. (D) BCV MDS plot for comparison between WT NT and WT 8h TNF α treated samples. (E) Plot of biological coefficient of variation versus mean logCPM for each gene across samples within comparison from (D). Red line is the common dispersion (average dispersion across genes). (F) MA-plot of average logCPM plotted against the logFC for comparison between WT NT and WT 8h TNF α treated samples. Differentially expressed genes with FDR < 0.05 are highlighted in red. Blue lines are shown at logFC values of 1 and -1. (G) Hierarchical clustering heat map of differentially expressed genes (FDR < 0.05) from comparisons between WT, WT 2h TNF α -treated and WT 8h TNF α -treated clones. (H and I) Top 20 significantly differentially expressed upregulated and downregulated genes and their logFC's for WT 2h and 8h TNF α samples (ranked by FDR p value).

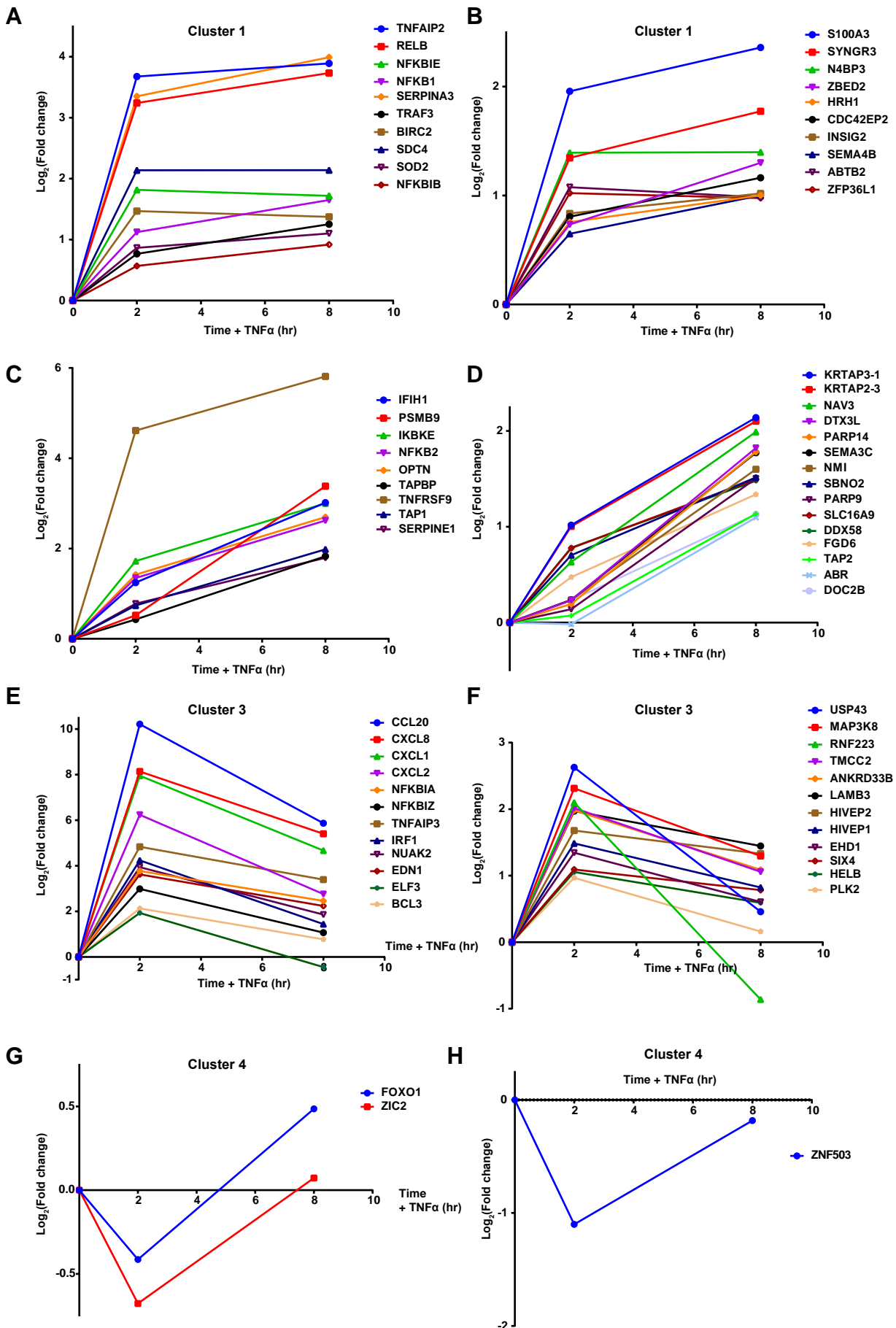
dispersion between 0.2 – 0.4 is typically considered reasonable, therefore for each of these two comparisons the variability was within the range necessary to detect differential gene expression.

DE analysis was performed, involving fitting of a negative binomial generalized linear model to estimates of common dispersions, followed by statistical testing of the coefficients (quasi-likelihood (QL) F-test) to identify statistically significant differentially expressed genes. The WT NT and WT 2h TNF and WT NT and WT 8h TNF comparisons have a paired design (each independent clone is measured before and after TNF α treatment), which improves the power of statistical testing. EdgeR applies the Benjamini-Hochberg method to *p*-values to control the false discovery rate (FDR) for multiple testing correction. Only genes with FDR < 0.05 are considered differentially expressed in subsequent analysis. A total of 332 and 1094 differentially expressed genes (DEGs) were identified in the comparison between WT NT and WT 2h TNF α , and WT NT and WT 8h TNF α samples, respectively (red dots in Figure 6.4C and F). A hierarchical clustering heatmap of the normalised average CPM across replicates for these DEGs was plotted (Figure 6.4G) and the top 20 DE upregulated and downregulated genes (ranked by FDR *p*-value) at 2h and 8h TNF α treatment tabulated (Figure 6.4H and I). A number of well-characterised TNF α -responsive, NF- κ B-dependent genes were identified as being significantly DE, including the canonical NF- κ B genes *NFKB1A* (encoding I κ B α) and *TNFAIP3* (encoding A20). The heatmap identifies seven clusters of genes with similar expression patterns across the samples. The mean log(fold change, FC) of a selection of representative well-characterised NF- κ B-dependent genes from each cluster are plotted in Figure 6.5 (left-hand panels). Also plotted are potential, novel NF- κ B-dependent genes representative of each cluster (right-hand panels). Plotted are those novel genes whose logFC are > 1.0. Identification of potential novel genes was a multi-step process. DEGs were first filtered against those DEGs from comparisons between DKO NT and DKO TNF α treated samples (Figure 6.15) to remove TNF α -responsive, non-NF- κ B-dependent genes (e.g. JUN, ATF3, MAFF, JUND etc). DEGs were also filtered against a recently curated database of 1667 NF- κ B-dependent genes (Yang *et al.*, 2016) to remove known NF- κ B-dependent genes. A literature search was then performed on remaining genes to remove other known TNF α -inducible genes. Of the 1215 unique, DEGs identified in WT samples, 220 genes were identified with no previously reported link to TNF α -dependent expression (to the best of the author's knowledge at the time of writing).

TNF α -induced NF- κ B-dependent gene expression exhibits characteristic temporal profiles, broadly segregated into early genes (peak differential expression at ~ 1h), intermediate genes (peak differential expression >2h) and late genes (peak differential expression > 8h). Reassuringly, these same gene expression profiles were observed in WT cells treated with TNF α (Figure 6.4G and 6.5). Cluster 1 represents intermediate upregulated genes, whose expression plateaus at between 2 and 8 hours. Representative known genes in this cluster are *RELB* and *NFKBIE* (encoding I κ B ϵ) (Figure 6.5A). Cluster 2 represents late upregulated genes, whose expression peaks > 8 hours. Representative known genes in this cluster are *NFKB2* (encoding p100), *OPTN* (encoding Optineurin) and *IKBKE* (encoding IKK ϵ) (Figure 6.5C). Cluster 3 represents early upregulated genes, whose expression peaks < 2h and then decreases at later timepoints. Representative known genes in this cluster are *NFKB1A* (encoding I κ B α) and the cytokines, *CXCL8*, *CXCL1* and *CXCL2* (Figure 6.5E). It is likely that at 2 hours the expression of these genes is already decreasing and their peak expression was missed. Cluster 4 represents a small subset of early downregulated genes, whose expression decreases at 2h, but increases above NT levels at 8h. Known genes in

this cluster are *FOXO1* and *ZIC2* (Figure 6.5G). Cluster 5 represents a large subset of late downregulated genes, whose expression progressively decreases between 2 and 8 hours. Known genes in this cluster are *CITED2* and *PIM1* (Figure 6.5I). Cluster 6 represents a very small subset of late downregulated genes, whose expression initially increases at 2 hours following TNF α stimulation. Known genes in this cluster are *EGR1* and *AMOTL2* (Figure 6.5J). Finally, Cluster 7 represents early downregulated genes. Known genes in this cluster are the growth factors, *BMP4* and *BDNF* (Figure 6.5K). The identification of these characteristic gene expression profiles gives us great confidence that the results obtained are of a high quality and are biologically relevant.

Validation of the putative novel NF- κ B-dependent genes awaits further work, but qRT-PCR validation of one of the identified genes, *USP43*, will be discussed in Section 6.2.5 Some of the genes identified may be TNF α -inducible but NF- κ B-independent; this will need to be investigated by ChIP experiments and promoter analysis of candidate genes. *ID2*, for example, was one of the most significantly downregulated genes in response to TNF α in WT, IKK α , IKK β and DKO cells (Figure 6.4, 6.11, 6.13 and 6.15), although the level of downregulation was lower in DKO cells. TNF α has not previously been reported to regulate the expression of *ID2*. An inspection of the genes induced by TNF α in IKK DKO cells, however, points to a mechanism by which TNF α might be able to indirectly repress *ID2*. The stress-responsive gene Activating Transcription Factor 3 (ATF3) was strongly induced by TNF α in DKO cells, in addition to WT, IKK α and IKK β cells (Figure 6.6E). This is consistent with the fact that the p38 pathway has been shown to be important in the induction of ATF3 by stress signals (Lu *et al.*, 2007). ATF3, in turn, has been proposed to cooperate with the AP-1 family TF, JunB, in the repression of *ID2* expression downstream of TGF- β signalling during EMT (Gervasi *et al.*, 2012). The involvement of JunB in repression of *ID2* in DKO cells in response to TNF α is unclear, however, given that TNF α -induced *JUNB* expression was completely absent in DKO cells (Figure 6.6D), suggesting that NF- κ B activation was required for TNF α -induced JunB expression. Indeed, JunB has been shown to contain an NF- κ B site within its promoter (Brown *et al.*, 1995b) and has been shown to be induced by TNF α , even in the absence of JNK (Ventura *et al.*, 2003). Interestingly, fellow members of the Id protein family, *ID1* and *ID3* were also downregulated in WT, IKK α and IKK β KO cells, but *not* DKO cells. *ID1* has also been proposed to be repressed by ATF3 downstream of TGF β , in this case cooperating with SMAD3 (Kang *et al.*, 2003). *SMAD3* expression was upregulated by TNF α in WT, IKK α KO and IKK β KO cells, but not DKO cells (Figure 6.6F). Confusingly, however, NF- κ B has been proposed to repress the transcription of TGF- β responsive genes, such as SMAD3 and SMAD7 (Nagarajan *et al.*, 2000). Future work will seek to characterise the signalling crosstalk that mediates the repression of Id family members. The downregulation of *ID* family expression in response to TNF α is of interest given the proposed role of ID proteins as tumour promoters in a range of cancers, including CRC (Lasorella *et al.*, 2014). For example, *ID1* and *ID3* have been proposed to sustain cancer stem cell and tumour-initiating phenotypes in colon cancer cells (O'Brien *et al.*, 2012).



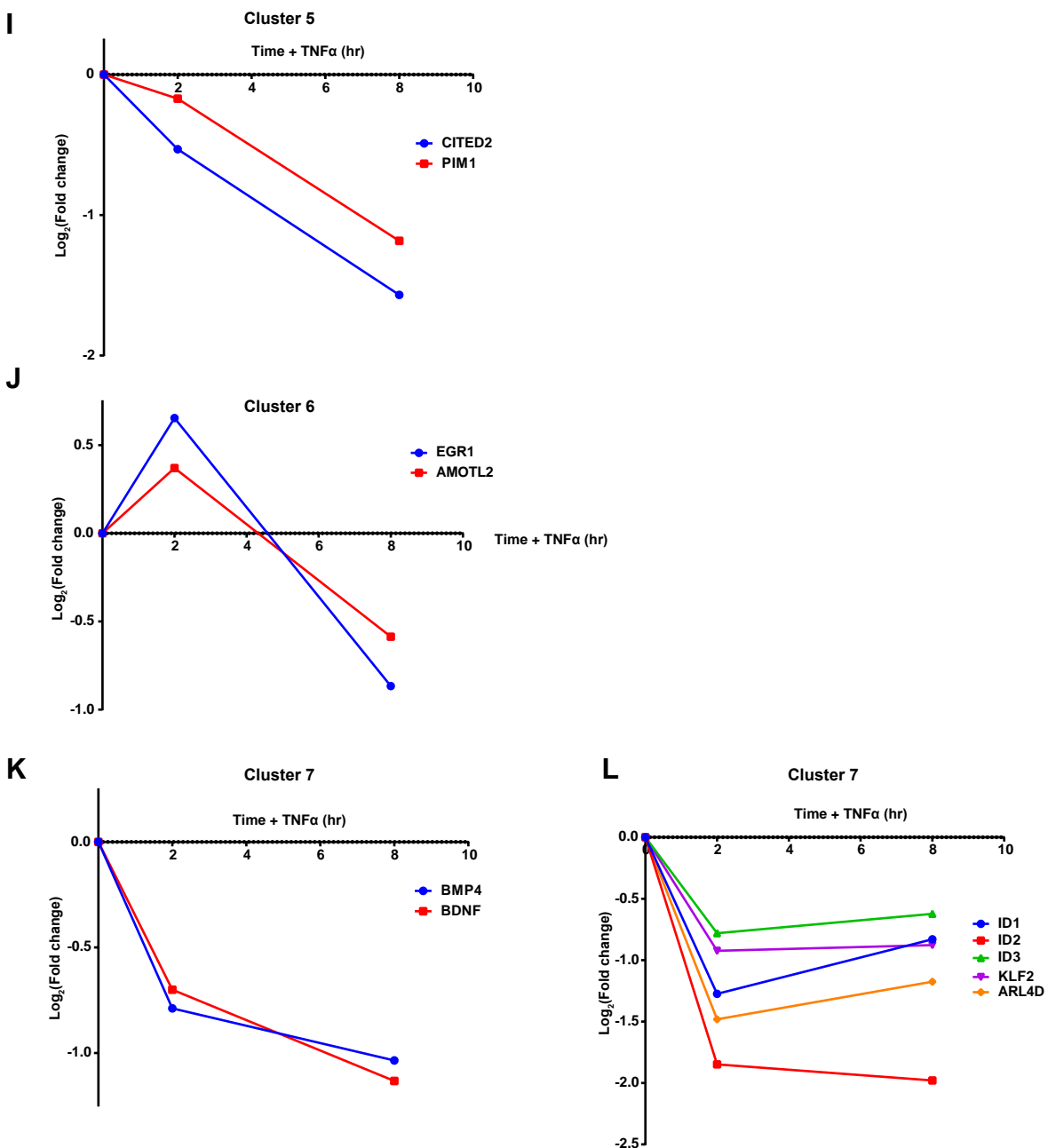


Figure 6.5. Expression profiles of a cross-section of well-characterised NF- κ B-dependent genes (A,C,E,G, I, J and K) and putative, novel TNF α -responsive genes (B, D, H, and L) from each of the clusters of differentially expressed (DE) genes identified in WT cells. Plotted are the log₂(Normalised, average fold change in gene counts per million) for a selection of DE (FDR < 0.05) genes from comparison between WT NT, WT 2h and WT 8h TNF α . The fold changes are the average of the three biological replicates. The putative, novel genes (B, D, F, I and L) represent each of the DE genes that exhibited a log₂(Fold change) > 1.0 compared to WT NT that are not already known NF- κ B-dependent or TNF α -responsive genes and were not upregulated in DKO cells treated with TNF α .

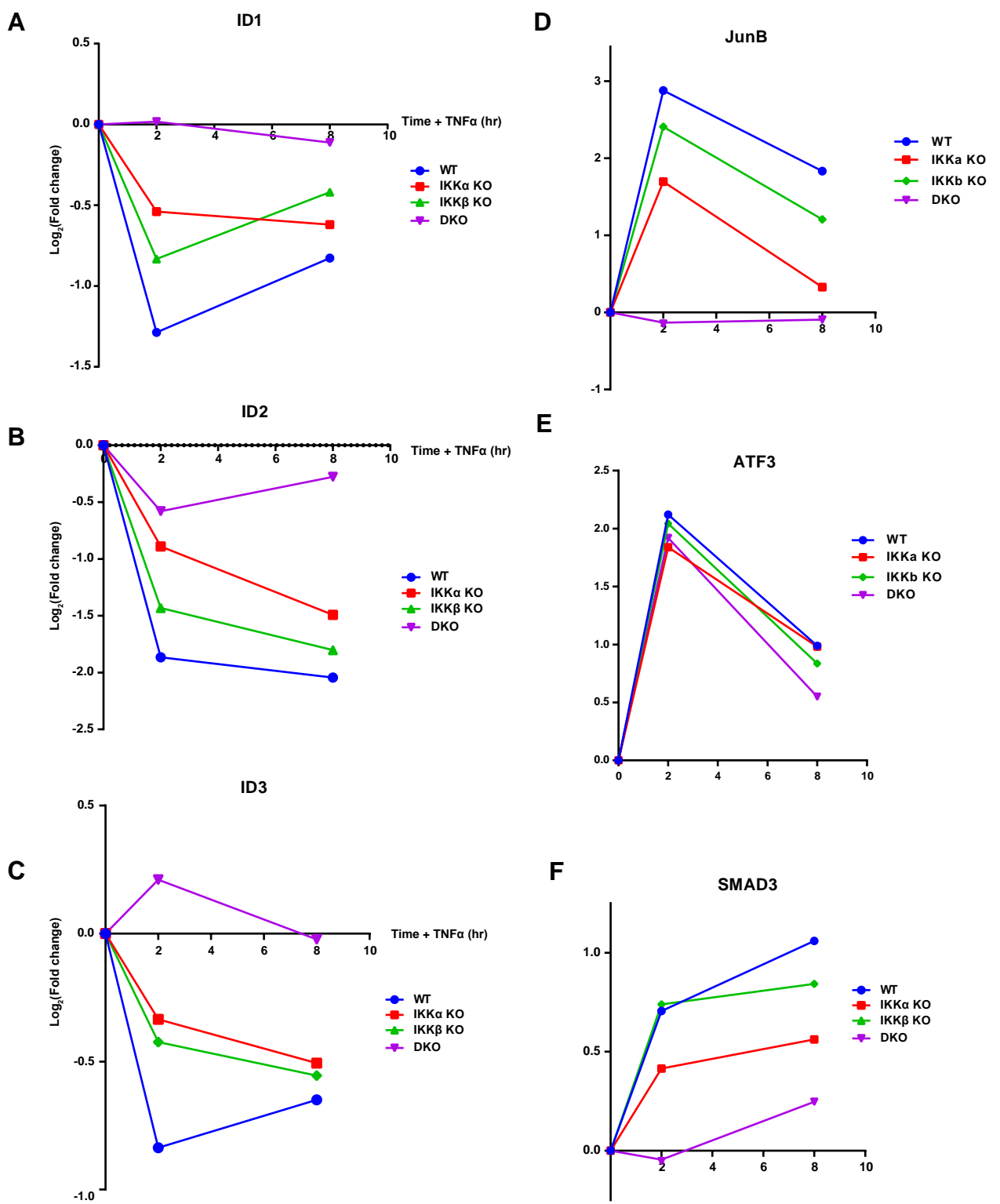


Figure 6.6. TNF α -dependent expression profiles of ID1, ID2, ID3, JunB, ATF3 and SMAD3 in WT, IKK α KO, IKK β KO and DKO cells. Plotted are the \log_2 (Normalised, average fold change in gene CPM) for the ID1 (A), ID2 (B) and ID3 (C), JunB (D) and ATF3 (E).

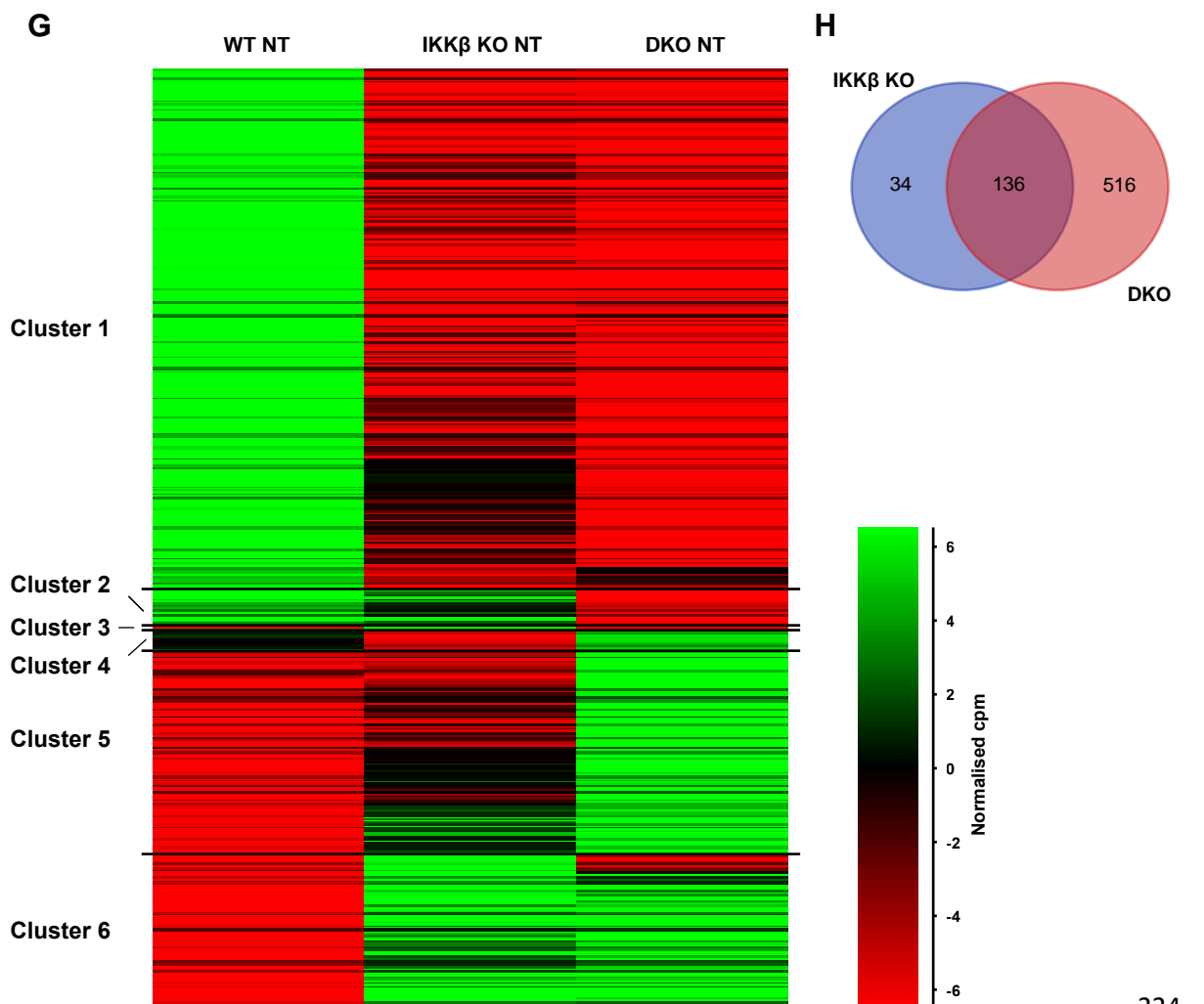
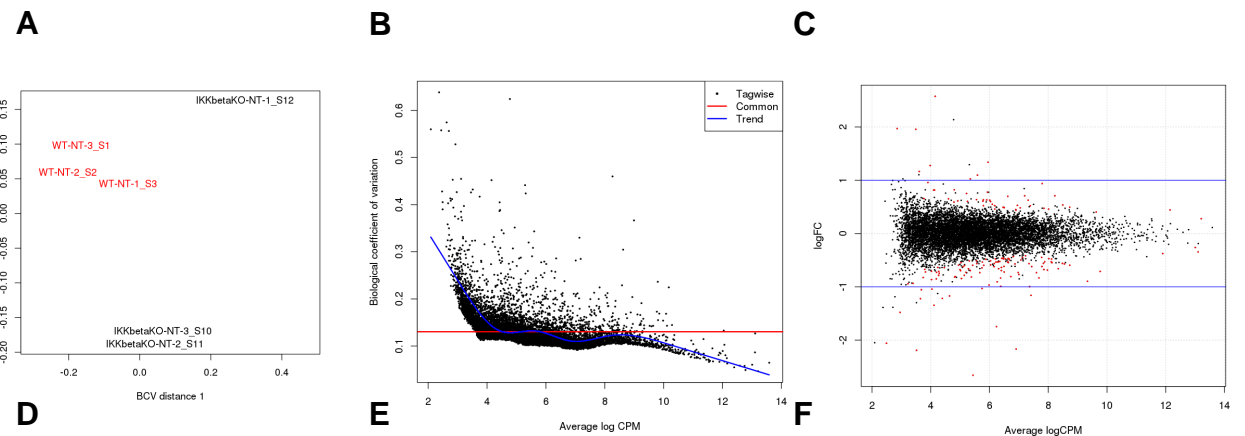
6.2.5 IKK β knockout causes the downregulation of genes involved in chromosome organisation, mitotic cell cycle progression and DNA damage repair in non-stimulated cells

To investigate the effects of IKK knockout on basal gene expression, DE analysis was performed for comparisons between WT and IKK KO NT samples. As alluded to earlier, the MDS plot for comparisons between WT NT and IKK β KO NT samples highlighted that two of the IKK β KO clones (A7 and A4) clustered close together in both dimensions of BCV, while the other (G9) exhibited separation in the BCV2 dimension (Figure 6.7A). Overall, however, the WT and IKK β KO samples separated well in the BCV1 dimension, which represents a larger proportion of the overall variance (notice the scale of the axis). The common dispersion across the samples was again within the acceptable range for DE analysis (Figure 6.7B). Meanwhile, the MDS plot for comparisons between WT NT and DKO NT samples demonstrated that WT and DKO samples separated well in the BCV1 dimension, but the DKO samples exhibited greater variance in the BCV2 dimension (Figure 6.7D). Despite this, the level of dispersion across the samples was again within the acceptable range for DE analysis.

DE analysis identified 170 genes differentially expressed between WT and IKK β KO NT samples and 652 genes differentially expressed between WT and DKO NT samples. The majority of these DEGs exhibited relatively small logFC relative to WT samples (Figure 6.7C and F). Of these genes, 136 were differentially expressed in both IKK β and DKO samples (Figure 6.7H). It should be noted that the higher number of DEGs identified in DKO cells relative to IKK β KO cells may reflect the reduced variance in the dispersion between the clonal replicates (Figure 6.7E) such that a greater number of DEGs were able to reach statistical significance (FDR p -value <0.05).

A heatmap of DEGs demonstrates that the majority of the overlapping genes were those that were downregulated in IKK β KO and DKO samples relative to WT (Figure 6.7G, Cluster 1). 11 of the top 20 DEGs downregulated relative to WT samples were common to both IKK β KO and DKO samples: *HIST1H1E*, *HIST1H2AM*, *HIST1H2AC*, *HIST1H2AH*, *APIP*, *CHRNA5*, *ARL14EP*, *ITGB3BP*, *THRA*, *RRBP1* and *FAM53B* (Figure 6.7I and J). Meanwhile, two of the top 20 DE upregulated genes were common to both IKK β KO and DKO samples: *DUSP5* and *MRPL12*. Unfortunately, *IKBKB* (encoding IKK β) was not detected in any of the samples analysed, WT, IKK β KO or otherwise, and so could not be used as additional validation of IKK β KO.

The RNA sequencing library preparation method involved a polyA-enrichment to enrich mRNA from the total RNA pool. The identification of replication-dependent Histone-encoding mRNAs was surprising, therefore, given their lack of polyA⁺ tails (Marzluff *et al.*, 2008). A total of 18 Histone genes were sequenced across the samples and exhibited a range of low to high read-counts, suggesting that Histone-encoding mRNAs were in abundance within the RNA libraries and were sequenced with comparable read-depths to other genes. In addition to the four histone genes within the top 20 DEGs in both IKK β KO and DKO samples, an additional 5 (*HIST1H2BD*, *HIST1H2AJ*, *HIST1H4C*, *HIST1H1C* and *HIST2H2AB*) were significantly downregulated in IKK β KO and DKO samples. There are circumstances under which Histone genes that typically produce mRNA's lacking polyA⁺ tails may transcribe polyadenylated mRNAs. For example, several studies indicate that polyA⁺ histone mRNA levels may increase during various cellular processes including G1 arrest caused by p53 accumulation, differentiation and tumourigenesis (Abba *et al.*, 2005; Pirngruber *et al.*, 2010; Lyons *et al.*, 2016). Furthermore, HCT116 cells have



I

J

IKK β

DKO

UP

DOWN

UP

DOWN

Gene	LogFC
MRPL12	0.937541
TFPI	1.165676
HYPK	0.708822
RPS12	0.443298
DUSP5	0.776884
CSTA	1.957084
CCAR2	1.097262
SEMA3A	2.575894
MPV17L2	0.81632
S100A14	1.338194
C19orf70	0.601634
BCAT2	0.821339
METTL15	0.636126
PSMB3	0.708795
THOC6	0.957549
PLCD3	0.626307
MCTS1	0.521385
FLYWCH2	1.276312
TSR3	0.698763
PTP4A1	0.535935

Gene	LogFC
HIST1H1E	-2.16787
HIST1H2AM	-2.65891
HIST2H2AC	-1.74756
EEF1A1	-1.15973
PRIM1	-0.99069
HIST1H2AH	-2.19095
APIP	-1.21807
CHRNA5	-1.03137
APEX1	-0.99719
ARL14EP	-0.83488
ITGB3BP	-0.76983
THRA	-0.90742
SH3D19	-1.34691
RRBP1	-0.83338
GNL3L	-0.9671
MT-ND5	-0.89617
HIST1H1C	-0.73456
CXXC5	-0.73203
PIBF1	-0.84385
FAM53B	-0.81521

Gene	LogFC
MRPL12	1.071065
SCAND1	1.220384
DUSP5	0.896507
BIRC3	2.457582
FAM122B	0.959613
PDE4B	1.173096
CPOX	0.845071
CAV2	0.901896
RPS12	0.346182
CXCL16	0.854745
PTP4A1	0.626148
ZNF761	0.915418
HES4	0.722646
NPW	0.630137
HDDC2	0.5977
RAC3	0.738293
ATP5EP2	0.717914
MPST	0.632195
AREG	0.51962
NDUFA9	0.683981

Gene	LogFC
RRBP1	-1.1656
IRF2BPL	-0.95375
HIST1H2AM	-2.63979
HIST1H2AH	-1.93609
RPL3	-0.9229
ITGB3BP	-0.84854
CHRNA5	-0.94386
HIST1H4C	-0.73428
EIF4B	-0.87437
APIP	-1.4667
PYGB	-0.90944
FAM53B	-0.87207
ARL14EP	-0.8882
ARL4D	-1.05198
ARPC1A	-0.98812
THRA	-0.86474
HIST1H1E	-2.07676
HIST2H2AC	-1.58666
IFFO2	-0.84594
GTF2I	-1.02761

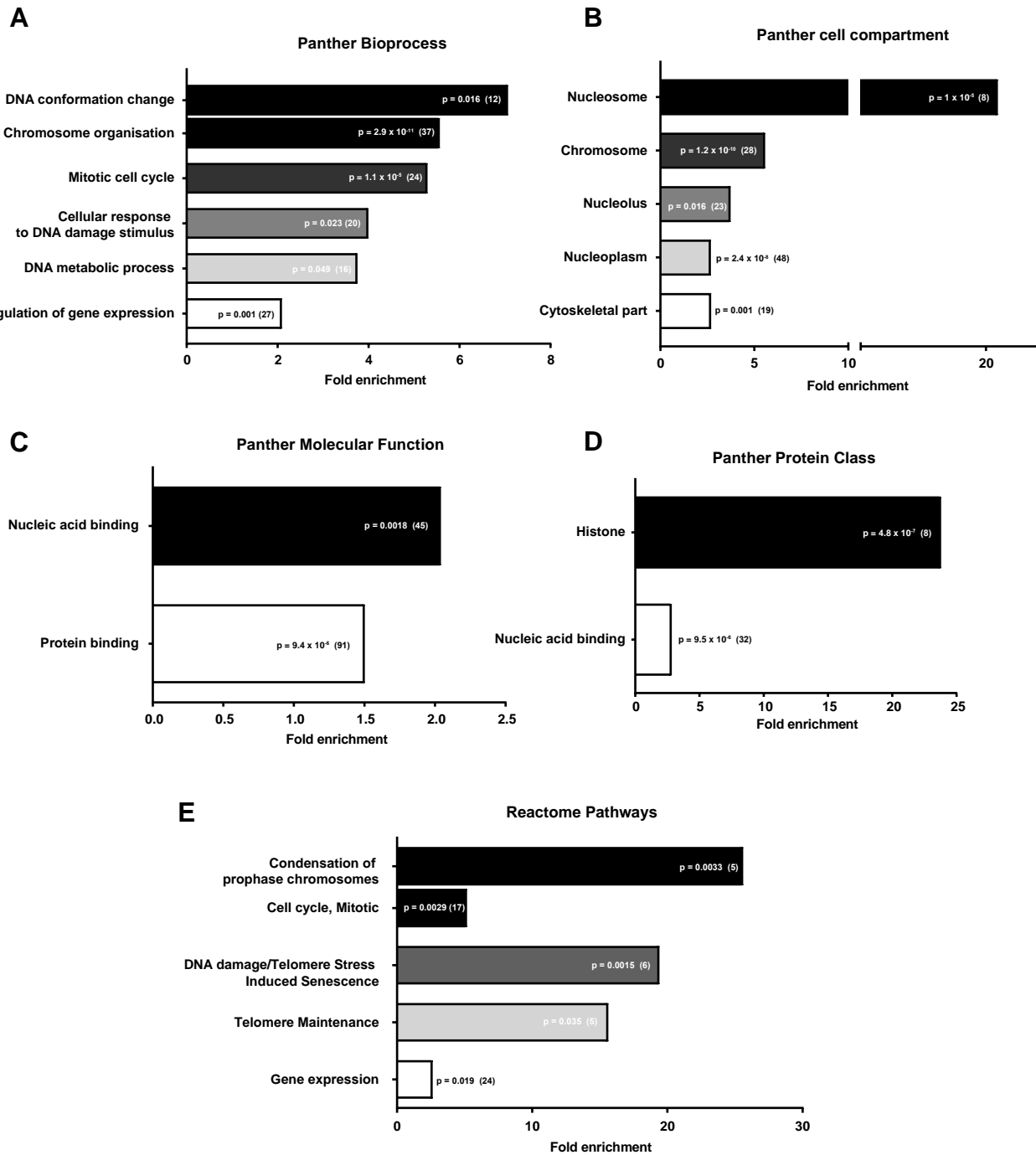
Figure 6.7. Identification of DEGs in IKK β KO NT and DKO NT cells relative to WT. (A) Biological coefficient of variation (BCV) multi-dimensional scaling (MDS) plot for comparison between WT NT and . (B) Plot of biological coefficient of variation versus mean log counts per million (CPM) for each gene across samples within comparison from (A). Red line is the common dispersion (average dispersion across genes). (C) MA-plot of average log-counts-per-million plotted against the log fold-change (FC) for comparison between WT non-treated (NT) and WT 2h TNF α treated samples. Differentially expressed genes with FDR < 0.05 are highlighted in red. Blue lines are shown at logFC values of 1 and -1. (D) Biological coefficient of variation (BCV) multi-dimensional scaling (MDS) plot for comparison between WT non-treated (NT) and WT 8h TNF α treated samples. (E) Plot of biological coefficient of variation versus mean log counts per million (CPM) for each gene across samples within comparison from (D). Red line is the common dispersion (average dispersion across genes). (F) MA-plot of average log-counts-per-million plotted against the log fold-change (FC) for comparison between WT non-treated (NT) and WT 8h TNF α treated samples. Differentially expressed genes with FDR < 0.05 are highlighted in red. Blue lines are shown at logFC values of 1 and -1. (G) Heirarchical clustering heat map of differentially expressed genes (FDR < 0.05) from comparisons between WT NT, IKK β KO NT and DKO NT samples. (H) Venn diagram showing the number of differentially expressed genes (FDR < 0.05) unique and common to IKK β KO NT and DKO NT samples. (I and J) Top 20 significantly differentially expressed upregulated and downregulated genes and their logFC's for IKK β KO and DKO samples relative to WT (ranked by FDR p value).

been shown to express significant levels of polyA+ HIST1H2BD; one of the identified DE Histone genes (Kari et al., 2013). RNA sequencing analyses using total RNA libraries have defined non-polyA+ RNAs that are typically underrepresented in polyA+ RNA libraries (Guo et al., 2015). These include histone mRNAs, small RNAs, lncRNAs, as well as a small subset of protein encoding transcripts. We compared the database of non-polyA transcripts sequenced in Guo et al., 2015 with the genes identified as DE in IKK β KO and DKO samples and, apart from the 9 Histone genes, observed no additional overlap in genes, suggesting that IKK β KO and DKO samples are not biased to express lower levels of non-polyA transcripts. However, given that we have not been able to satisfactorily resolve this apparent contradiction, nor have we yet performed any validation of the DEGs identified in IKK β KO and DKO samples, the following analyses should be regarded as preliminary.

To identify functional relationships between DEGs, gene ontology (GO) term analysis was performed separately on the upregulated (54) and downregulated (116) DEGs in IKK β KO NT samples using the PANTHER statistical overrepresentation test (Figure 6.8). A protein-encoding gene background list was used to make fold-enrichment comparisons as only protein-coding genes were counted and included in the DE analysis. Fold enrichment for identified GO terms were plotted, along with the FDR *p*-values (Bonferroni correction for multiple testing) and the number of genes representative of each GO term category in parentheses. Related ‘daughter-parent’ GO terms are grouped closer together within the bar chart (‘daughter’ refers to the more functionally specific term, and ‘parent’ to the more general parent term from which the daughter stems).

It should be noted that the 8 Histone genes that were identified as DE in IKK β KO samples have a large impact on the enrichment terms. For example, the Histone genes dominate the cell compartment and protein class GO term analyses of the DE downregulated genes. Interestingly, however, a number of other nucleic acid binding genes expressed at the chromosomes/nucleolus/nucleoplasm are also differentially downregulated (Figure 6.8B). Furthermore, of the highest enriched Bioprocess term, ‘DNA conformation change’, four of the 12 genes are Histones, but the 8 other genes include; NCAPG2 (a Condensin subunit), CENPW (a centromere-associated protein), CCNB1 (Cyclin B1), BAHCC1 (a chromatin silencing protein), ASH1L (a histone lysine N-methyltransferase), SETX (a DNA helicase), DHX9 (an RNA helicase) and ITGB3BP (a Centromere-associated protein. Furthermore, the parent GO term, ‘chromosome organisation’ was highly significantly ($p = 2.9 \times 10^{-11}$) enriched for 37 genes and included various other histone-lysine methyltransferases/demethylases (KDM1A, KDM4A, EHMT1 and NSD1) and genes involved in telomere maintenance (*POLA1* and *PRIM1*, which make up the POLA/Primase complex required for lagging strand synthesis and telomere maintenance). A number of genes involved in the DNA damage response were also downregulated, including *ATM*, the DUB *USP10*, the phosphatase *CDC14B*, the base excision repair protein *APEX1*, the nucleotide excision repair protein *RAD23A* and the translesion synthesis pathway protein *ATAD5*. Another highly significant ($p = 1.1 \times 10^{-6}$) enriched Bioprocess GO term (and Reactome pathways GO term) was ‘mitotic cell cycle,’ which included genes such as the CDK phosphatase *CDKN3*, the kinesin motor protein *KIF2A*, the phosphatase *CDC14B*, *CCNB1*, the G2/M checkpoint regulator, *GTSE1*, the centrosomal protein, *CEP55*, the mitotic spindle organisation protein, *PCNT* (Pericentrin), and the mitotic kinase, *PBK*.

Downregulated in IKK β KO



Upregulated in IKK β KO

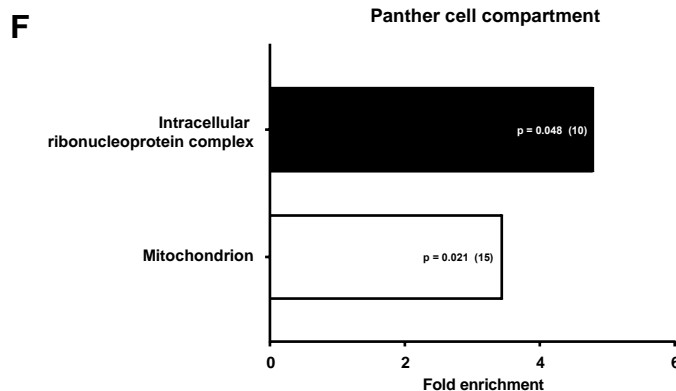


Figure 6.8. PANTHER GO:term analysis for downregulated (A, B, C, D, E) and upregulated (F) DEGs in IKK β KO NT samples. (A) Fold enrichment plot of PANTHER Bioprocess GO-terms for DE genes downregulated in IKK β KO NT samples relative to WT NT samples. (B) Fold enrichment plot of PANTHER Cell compartment GO-terms for DE genes downregulated in IKK β KO NT samples. (C) Fold enrichment plot of PANTHER Molecular function GO-terms for DE genes downregulated in IKK β KO NT samples. (D) Fold enrichment plot of PANTHER Protein class GO-terms for DE genes downregulated in IKK β KO NT samples. (E) Fold enrichment plot of Reactome pathways GO-terms for DE genes downregulated in IKK β KO NT samples. (F) Fold enrichment plot of Cell compartment GO-terms for DE genes upregulated in IKK β KO NT samples. Bonferroni method used to correct p values for multiple testing. Number of genes representative of each GO:term shown in parentheses.

GO:term analysis of the 62 upregulated genes in IKK β KO NT samples did not result in significantly enriched GO:terms, other than for proteins localised to the mitochondrion and intracellular ribonucleoprotein complexes (Figure 6.8F).

6.2.6 IKK DKO causes additional downregulation in the basal expression of genes involved in microtubule/actin cytoskeleton organisation, cell trafficking, cell junction regulation and cell differentiation

GO:term analysis was also separately performed on the upregulated (260) and downregulated (392) DEGs identified in DKO cells (Figure 6.9). A large number of significantly enriched GO:terms within the downregulated gene set were identified, many of which were also identified as being enriched within the downregulated DE gene set from DKO cells, such as ‘mitotic cell cycle’, ‘cellular response to DNA damage stimulus,’ ‘DNA conformation change,’ and its ‘parent term ‘chromosome organisation.’ Furthermore, ‘mitotic cell cycle’ and ‘chromosome organisation’ were again the most significant bioprocess GO:terms. This gave us greater confidence that the genes annotated with these terms that were commonly downregulated in both IKK β KO and DKO cells are functionally relevant groups of genes that are repressed as a result of IKK β KO. In addition, a number of GO:terms that were not identified in the IKK β KO DE gene list were identified here. Interestingly, a number of these related to regulation of the cytoskeletal network, cell junctions/projections and regulation of organisation and transport membrane-bound (endo- and exo-membrane) vesicles. For example, 55 genes whose products localise to the microtubule cytoskeleton, 50 genes whose products localise to cell junctions, 61 genes whose products localise to cell projections and 84 whose products localise to extracellular exosomes were identified. It should be noted that there may be a degree of overlap of functionally diverse genes within the different GO:terms identified. However, the number of genes identified in each GO:term category is large enough that this redundancy was not of great concern.

The most enriched Bioprocess GO:term was ‘actin filament-based transport,’ and was made up of the genes, *FNBP1L*, *ACTN4*, *MTO5A*, *SYNE2* and *SUN2*. This represents over half of the known genes with annotated actin filament-based transport function in the human genome (5 out of 9). All of these genes were also downregulated in IKK β KO clones, but only *FNBP1L* passed the FDR $p < 0.05$ threshold. The parent GO:term to which actin filament-based transport belongs, ‘cellular localisation’ was significantly enriched for 81 genes. Interestingly, 21 of the downregulated genes in DKO cells fall within the Reactome pathway annotation of RHO GTPase effectors. RHO GTPases play a pivotal role in regulating the actin cytoskeleton, microtubule dynamics and membrane transport pathways.

The second most enriched Bioprocess GO:term was ‘peptidyl-lysine dimethylation,’ and was made up of the genes, *EHMT1* (*KMT1D*), *ASH1L* (*KMT2H*), *KDM3A*, *SETD2* and *KMT2A*. This represents almost half of the known genes with annotated peptidyl-lysine demethylation function in the human genome (5 out of 12). Histone lysine methylation is controlled by lysine methyltransferases (KMTs) and lysine demethylases (KDMs) and is typically involved in transcriptionally inactive heterochromatin formation and transcriptional regulation. *EHMT1*, *ASH1L* and *KMT2A* were also significantly downregulated in IKK β KO cells, with *KDM3A* narrowly missing the significance

threshold. In addition, a number of other histone lysine methylation regulators were downregulated in both DKO and IKK β KO cells but narrowly missed the significance threshold, including *KDM5C*, *KMT5A* and *KDN4B*.

Similarly to the IKK β DE upregulated gene set, GO:term analysis of the DE upregulated genes in DKO cells was less revealing than for the downregulated genes (Figure 6.9F, G and H). The vast majority of upregulated genes were involved in ‘cellular metabolic processes’ (151 out of 260), although this reflected a marginally significant small fold enrichment over the reference gene set. Many of these genes expressed products that localised to the mitochondrion (62 out of 260), which represented a highly significant enrichment ($FDR\ p = 1.6 \times 10^{-12}$).

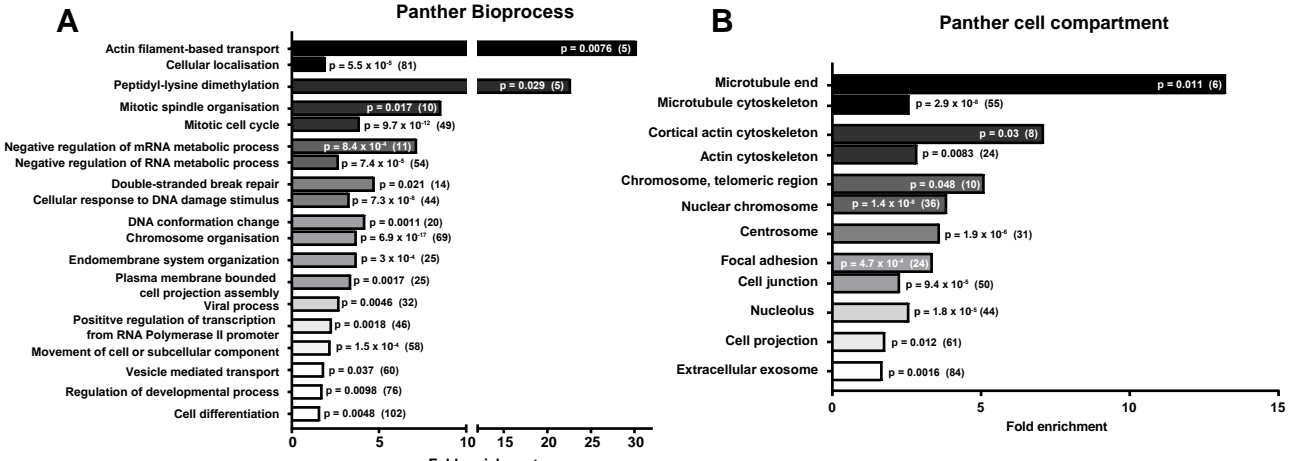
Overall the GO:term analysis indicates a wide-spread reprogramming of gene regulation in IKK β and IKK DKO cells, with downregulation of genes broadly split into the following categories: i) chromatin organisation, ii) cell cycle regulation (through mitotic spindle control) iii) DNA repair, iv) actin/microtubule cytoskeletal regulation of cell and vesicle migration and v) upregulation of genes involved in metabolism.

6.2.7 Minimal differential gene expression was detected in IKK α KO NT samples

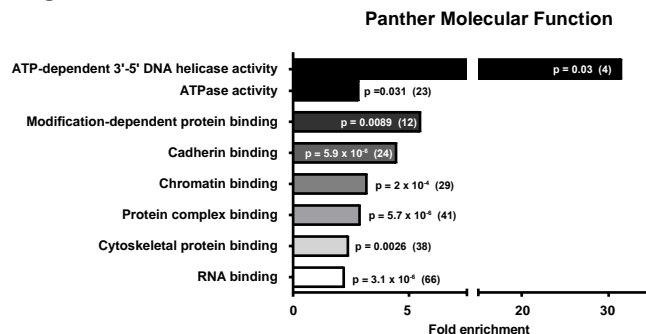
The MDS plot for comparisons between WT NT and IKK α KO NT samples highlighted a greater degree of variance between the IKK α clones than was present between IKK β and DKO clones. This is reflected in the fact that none of the IKK α KO clones clustered together, and the fact that WT and IKK α KO samples did not separate well in the BCV1 dimension. There was some separation in the BC2 dimension, however, particularly for clones 1 (F6) and 2 (C7). Questions might be raised about the other IKK α KO clone (3, A2), which clustered closer to the WT clones. Clone A2 was also a source of heterogeneity within other experiments (Figure 3.6). However, there was not sufficient evidence to label clone A2 an outlier and exclude it from subsequent analysis. Alternatively, the lack of separation in terms of BCV could simply reflect the fact that IKK α KO had minimal impact on basal gene expression relative to WT cells. Nevertheless, the result was that the common dispersion was slightly higher (closer to 0.2) within this comparison than for the comparisons between IKK β KO/DKO and WT samples. Subsequent DE analysis identified only 5 DEGs that met the $FDR\ p\text{-value} < 0.05$ threshold in the comparison between IKK α KO and WT cells. These were *RPS27A*, *DHRS2*, *ALDH3A2*, *SERINC5*, and *Conserved Helix-Loop-Helix Ubiquitous Kinase (CHUK)*, encoding IKK α) itself. This is not to say that the expression of many more genes were not affected by IKK α KO. Rather, the variance in gene expression between the three clones was too high for these genes to pass the significance threshold. To gain a rough idea of the identity of some of these DEGs, the significance threshold was lowered to a non-corrected $p\text{-value} < 0.01$ (equivalent to $FDR\ p\text{-value} < 0.41$). This identified 220 genes, a large fraction of which (approximately 40%) are statistically likely to be false-positives. The results of subsequent analysis are thus not intended to be conclusive. The gene encoding IKK α , *CHUK*, was the second most significantly downregulated gene identified, exhibiting a logFC of -1.54, adding confidence that samples were correctly labelled and sequenced.

In order to fairly compare this list of DEGs with those DEGs identified in IKK β KO and DKO cells, the significance threshold was lowered to a non-corrected $p\text{-value} < 0.01$ for the comparisons between IKK β /DKO and WT cells. This increased the number of DEGs in IKK β KO cells from 170 to 494, and the number in DKO cells from 652 to 937. The overlap between the DEGs identified from these comparisons is shown in Figure 6.10G. Of the 220 DEGs identified in IKK α KO cells, 104 exhibited overlap with the DEGs from DKO cells, and an additional 24 were

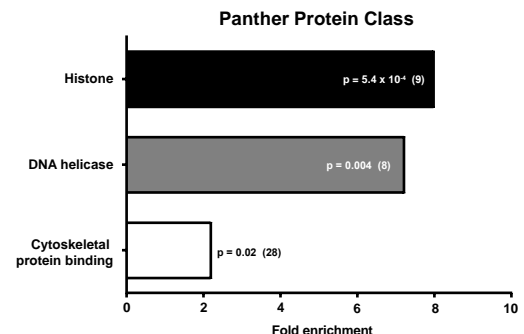
Downregulated in DKO



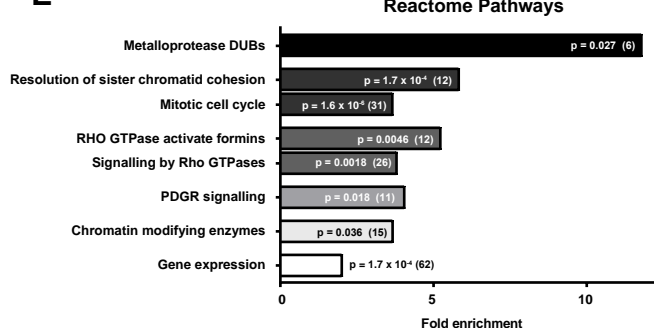
C



D

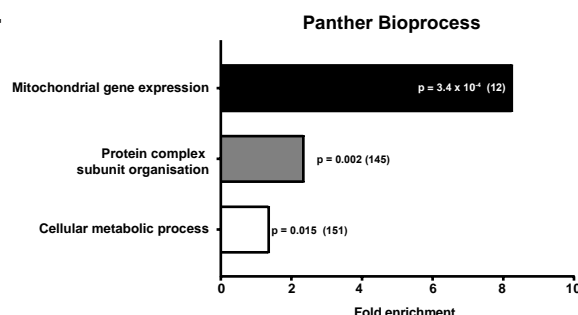


E

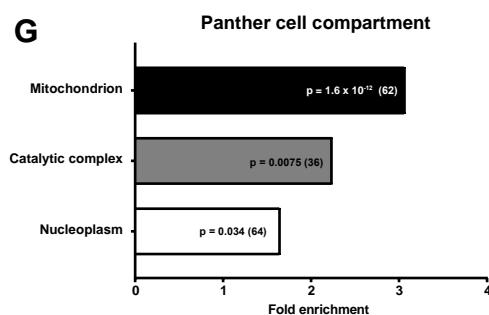


Upregulated in DKO

F



G



H

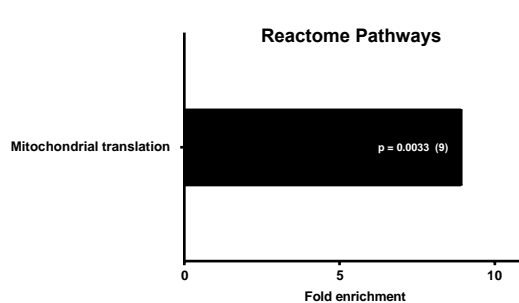
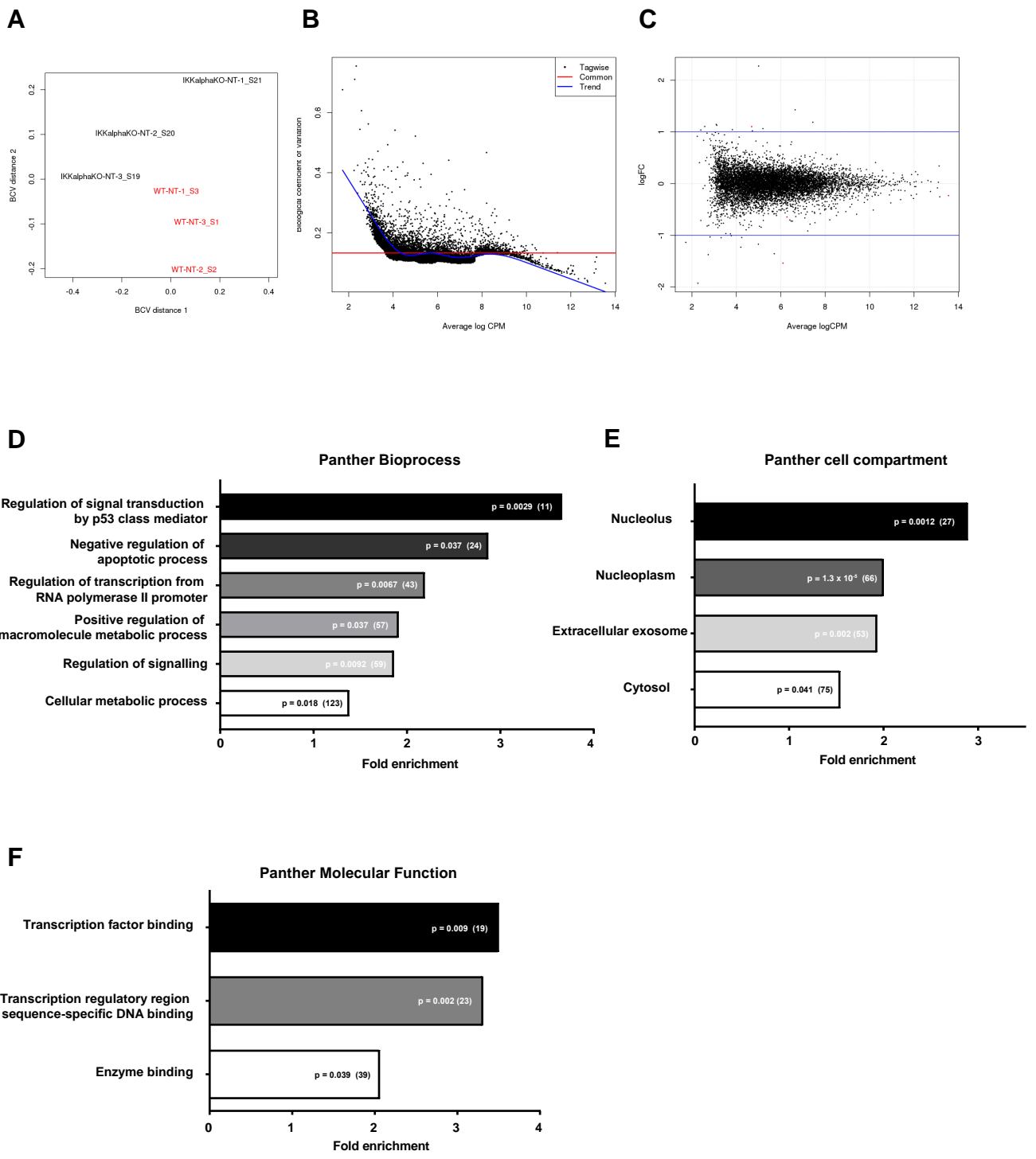


Figure 6.9. PANTHER GO:term analysis for downregulated (A, B, C, D, E) and upregulated (F) DEGs in DKO NT samples. (A) Fold enrichment plot of PANTHER Bioprocess GO-terms for DE genes downregulated in DKO NT samples relative to WT NT samples. (B) Fold enrichment plot of PANTHER Cell compartment GO-terms for DE genes downregulated in DKO NT samples. (C) Fold enrichment plot of PANTHER Molecular function GO-terms for DE genes downregulated in DKO NT samples. (D) Fold enrichment plot of PANTHER Protein class GO-terms for DE genes downregulated in DKO NT samples. (E) Fold enrichment plot of Reactome pathways GO-terms for DE genes downregulated in DKO NT samples. (F) Fold enrichment plot of Bioprocess GO-terms for DE genes upregulated in IKK β KO NT samples. (G) Fold enrichment plot of Cell compartment GO-terms for DE genes upregulated in IKK β KO NT samples. (H) Fold enrichment plot of Reactome Pathways GO-terms for DE genes upregulated in IKK β KO NT samples. Bonferroni method used to correct p values for multiple testing. Number of genes representative of each GO:term shown in parentheses.



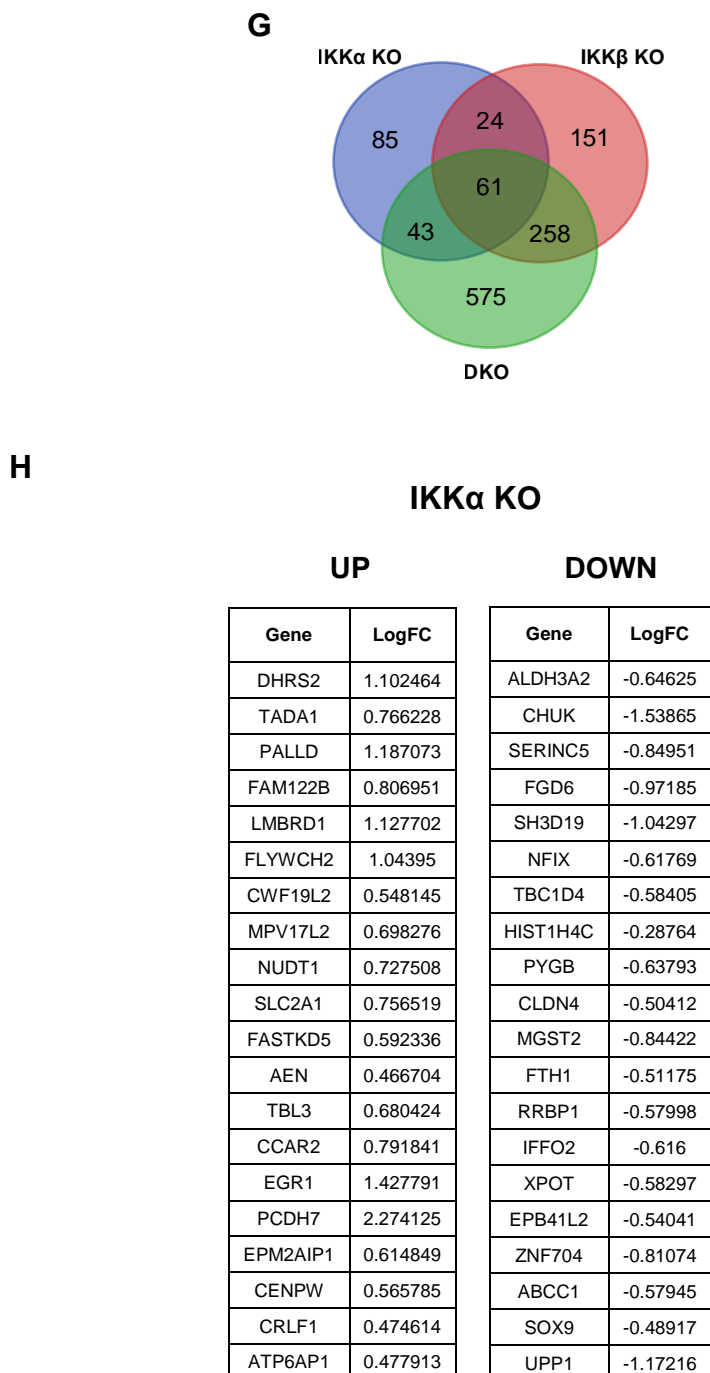


Figure 6.10. Identification of DEGs in IKK α KO NT relative to WT NT. (A) BCV MDS plot for comparison between WT NT and IKK α KO NT. (B) Plot of BCV versus mean log CPM for each gene across samples within comparison from (A). Red line is the common dispersion (average dispersion across genes). (C) MA-plot of average logCPM plotted against the logFC for comparison between WT NT IKK α KO NT. Differentially expressed genes with FDR < 0.05 are highlighted in red. Blue lines are shown at logFC values of 1 and -1. (D) Fold enrichment plot of PANTHER Bioprocess GO-terms for DE genes (up- and down-regulated) in IKK α NT samples relative to WT NT samples. (E) Fold enrichment plot of PANTHER Cell compartment GO-terms for DE genes in IKK α NT samples. (F) Fold enrichment plot of PANTHER Molecular function GO-terms for DE genes in DKO NT samples. (G) Venn diagram showing the number of differentially expressed genes (non-corrected p value < 0.01) unique and common to IKK α NT, IKK β KO NT and DKO NT samples. (H) Top 20 significantly differentially expressed ($p < 0.01$) upregulated and downregulated genes and their logFC's for IKK α KO NT samples relative (ranked by p value).

common to the DEGs from IKK β KO cells. The significant overlap with the DKO DE gene list gives us greater confidence that the $p < 0.01$ IKK α KO DE gene list contains a proportion of ‘real’ hits.

GO:term analysis was performed on the list of 220 DEGs identified in IKK α KO cells (Figure 6.10 D-F). The most significantly enriched Bioprocess GO:terms were ‘regulation of signalling’ and ‘regulation of signal transduction by p53 class mediator’. Overlap with the GO:term analysis of DKO DEGs was seen for the Bioprocess term ‘cellular metabolic process’ and genes whose products localise to the nucleolus/nucleoplasm and extracellular exosome.

6.2.8 IKK α KO cells exhibit a greater defect in TNF α -induced gene expression than IKK β KO cells, while DKO cells exhibit minimal TNF α -induced expression changes

Subsequently we performed DE analysis on IKK α KO TNF α treated samples and IKK β KO TNF α treated samples and compared the expression profiles with that identified from WT TNF α treated samples to attempt to identify genes whose expression was selectively IKK-dependent. The MDS plot for comparisons between IKK α NT and IKK α KO 2h TNF α samples once again highlighted relatively poor clustering within the IKK α KO clones according to treatment type, indicative of the high level of variance in gene expression between the IKK α KO clones (Figure 6.11A). However, the individual NT clones did separate from their paired TNF α -treated samples, and the degree of separation in the BCV2 dimension was approximately similar between the different clones (perhaps a smaller separation for clone 1 (F6)). The 8h TNF α treated samples exhibited greater clustering according to treatment type, suggesting that the expression changes were more similar between the IKK α KO clones after 8h than 2h treatment (Figure 6.11D). The low common dispersion across the samples (Figure 6.11B and C) highlights the benefit of a paired experimental design; variance in the absolute levels of gene expression between clones is cancelled out such that only the variance at the level of relative changes in gene expression are important. As such we were able to detect a reasonable number of DEGs within this comparison; a total of 97 DEGs were identified at 2h TNF α and 198 at 8h TNF α treatment (FDR p -value < 0.05) (Figure 6.11C and F). This is significantly lower than the number detected in WT cells; 332 and 1094 for 2h and 8h TNF α -treated samples, respectively. It is important to bear in mind that while this may reflect a dependency on IKK α for the TNF α -induced expression of a large number of genes, it may also partly reflect differences in the heterogeneity between the WT clones and the IKK α KO clones; greater variance between the IKK α clones may have made it more difficult for certain genes to pass the significance threshold.

After 2h TNF α treatment, the majority of the DEGs in IKK α KO cells were identical to those DEGs in WT cells; out of 97 DEGs, approximately 1 in 9 (11 genes) were unique to IKK α KO (Figure 6.11H). The proportion of unique DE expressed genes in IKK α KO cells increased dramatically at 8h TNF α treatment to approximately 1 in 3 (60 genes) (Figure 6.11I). A number of the unique DEGs in the IKK α KO 8h TNF α samples were mitochondrial genes (*MT-ND5*, *MT-ND4*, *MT-ATP8*, *MT-CO3*, *MT-CO2*). These mitochondrial genes, and others, were also upregulated in DKO cells, but not IKK β cells, treated for 8h with TNF α (Figure 6.15). The increased expression of mitochondrial biogenesis genes is a common response to oxidative stress. (Miranda *et al.*, 1999). For example, inflammatory cytokines have been shown to promote mitochondrial biogenesis under certain conditions through the production of reactive oxygen species (Cherry & Piantadosi, 2015). It will be interesting to investigate whether it

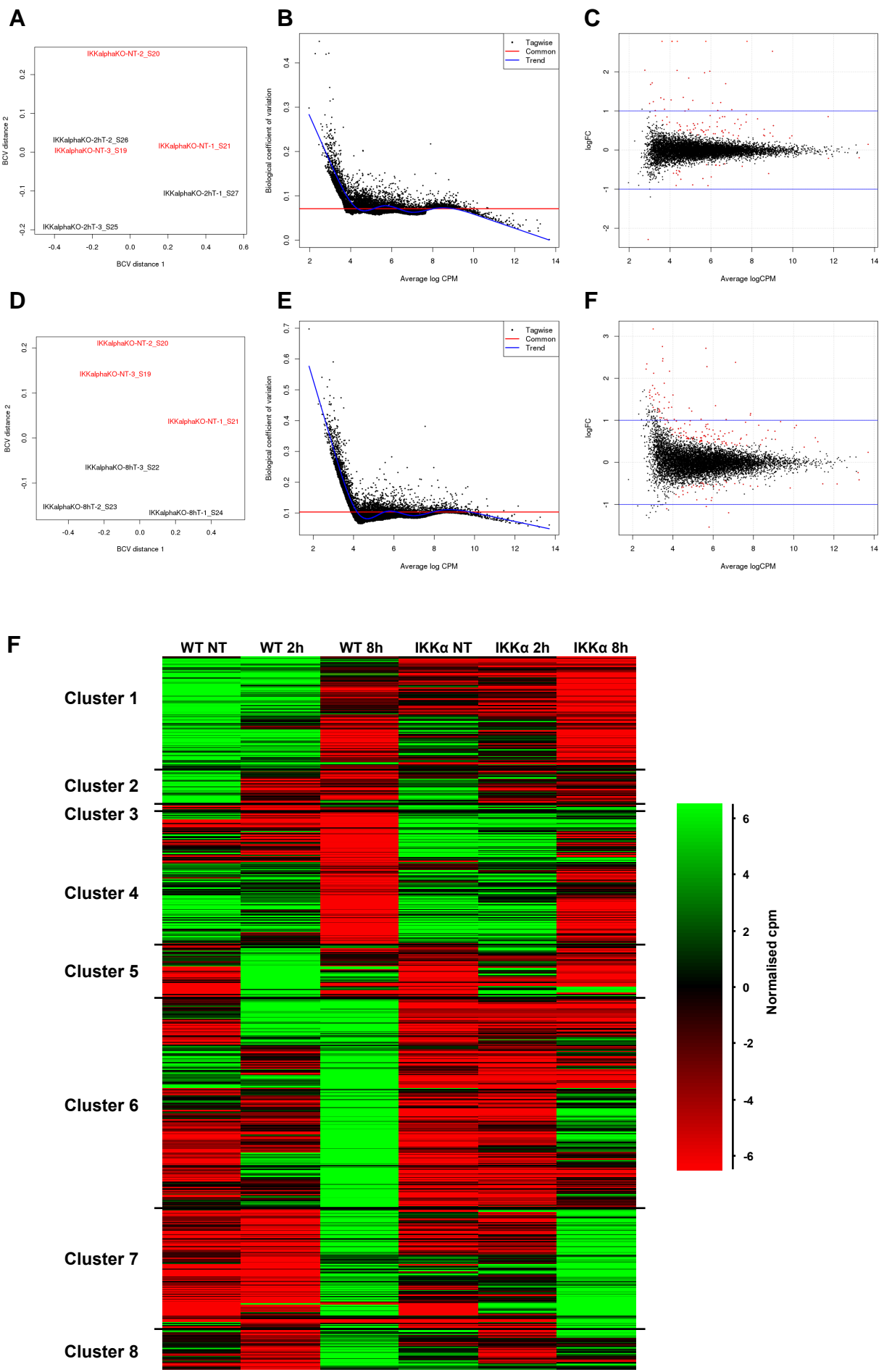
is the lack of IKK α kinase activity specifically, or the reduced downstream NF- κ B-dependent expression in IKK α KO cells that results in this apparent heightened oxidative stress response.

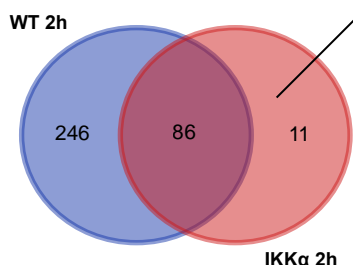
The hierarchical clustering heatmap of all DE expressed genes from comparisons between WT and IKK α KO NT, 2h and 8h TNF α samples indicates an overall damped TNF α -induced gene expression response in IKK α KO cells (Figure 6.11F). This is consistent with the reduced TNF α -induced NF- κ B nuclear translocation and NF- κ B-driven luciferase reporter activity in IKK α KO cells compared to WT discussed in Chapter 3. There are clusters of genes that exhibit similar expression changes after 2 and 8h TNF α treatment in both WT and IKK α KO cells. For example, the majority of Cluster 7 genes exhibit late upregulation at 8 h in both WT and IKK α KO cells. In addition, the majority of Cluster 4 genes exhibit late downregulation at 8 h in both WT and IKK α KO cells. The Cluster 2 genes also exhibit similar patterns of early downregulation in both WT and IKK α KO cells. Some of the biggest defects appear to be in the ‘early’ phase genes from Cluster 5, which exhibit a strong fold increase after 2 h in WT cells that is reduced in IKK α KO cell, and in the ‘intermediate’ and ‘late’ phase genes from Cluster 6 that are significantly upregulated after 2/8 hours in WT cells, but exhibit reduced or no induction at all in IKK α KO cells. There are also a relatively large subset of Cluster 1 genes that undergo downregulation after 8 hr TNF α treatment in WT cells that are lowly expressed to begin with in IKK α KO cells and are repressed even further after 8 hours treatment.

Further work is needed to identify and validate interesting genes that appear to show IKK α -dependence for expression within these different clusters. As an initial demonstration of the value of this dataset, however, we examined the expression profile of two of the genes, *ATG16L2* and *WDR90* that were identified to be DE in IKK α KO cells after 2h, but not WT cells (Figure 6.12). *ATG16L2* is a novel isoform of the autophagy protein, ATGL1, whose function has yet to be characterised, but whose mutation has been shown to be associated with Crohn’s disease (Ma *et al.*, 2016). *WDR90* is another protein whose function is currently unclear. Interestingly, both genes were only significantly upregulated in IKK α KO cells. In fact, in WT cells, both of these genes were repressed after 2h TNF α treatment. The significantly reduced induction of both genes in DKO cells suggests that their expression is at least partly NF- κ B-dependent. Perhaps IKK α kinase activity inhibits the expression of these genes independently of the requirement of NF- κ B for their expression. Further work is needed to investigate the IKK-dependence of these genes.

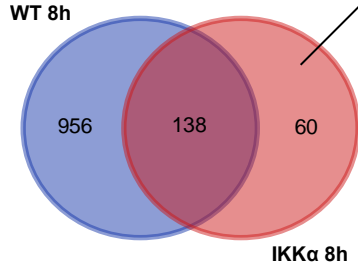
The MDS plot for comparisons between IKK β NT and IKK β KO 2h TNF α samples again highlighted relatively poor clustering within the IKK β KO NT and IKK β KO 2h TNF α clones according to treatment type (Figure 6.13A). However, the distance between paired NT and 2h TNF α treated samples was comparable between the clones. The samples exhibited greater clustering according to treatment in the comparison between IKK β KO NT and IKK β KO 8h TNF α samples, with clone 1 (G9) acting as a slight outlier as seen before (Figure 6.13D). The common trend of greater clustering after 8 h compared to 2h likely reflects the greater level of similar gene expression change overall between the different clones after 8 h compared to 2h, such that the variance among these similarly DEGs outweighs the variance in basal gene expression between the NT clones. The common dispersions for these comparisons were again of an acceptable level for DE gene analysis (Figure 6.13B and E).

A total of 152 DEGs were identified in IKK β KO cells at 2h TNF α and 132 at 8h TNF α treatment (FDR p-value < 0.05) (Figure 6.13H and I). As with IKK α KO cells, this was significantly low than the number detected in WT cells.



H

Gene	LogFC
DUSP1	1.334397
SESN2	0.504757
TNFAIP1	0.45961
RND3	0.471196
ATG16L2	0.755969
TNFRSF10A	0.355645
FAM126B	0.875625
TSC22D1	0.298079
ABL2	0.394038
FBXO46	0.41687
WDR90	0.429845

I

Gene	LogFC
MT-ND5	0.823215
MT-ND4	0.585334
FSTL3	1.299131
MT-ATP8	-0.60868
KANK1	1.436991
ADGRG1	-0.82189
MSH6	-0.5048
MT-CO3	-0.41521
ATG16L2	1.018493
MT-CO2	-0.51044
ZNF407	0.788695
RHOB	0.544378
ARHGAP32	0.63585
INO80B	0.611406
ARL3	-0.52416
C19orf44	1.716458
GABBR1	1.271178
TNFRSF21	0.486299
INPP1	0.60438
RREB1	1.207772

J**2 h**

Gene	LogFC
JUN	3.106931
NFKBIA	2.524376
RELB	2.602402
MAFF	1.97481
IRF1	2.013746
IER3	0.853697
BIRC3	3.664553
TNFAIP3	2.978333
ATF3	1.839543
JUNB	1.696667
CD83	2.03514
RHOB	1.011624
CXCL8	4.063174
BCL3	1.268818
CXCL1	3.29407
CYR61	1.030976
KLF6	0.853183
SDC4	0.905769
DUSP5	1.213733
ELF3	0.879948

DOWN

Gene	Log FC
ID2	-0.91012
ZNF503	-0.72844
RGS2	-0.68799
HES1	-0.89039
AXIN2	-0.90671
FGF9	-0.74661
HIST1H4C	-0.2129
FAM46A	-0.6343
ID1	-0.60162
ARMC7	-0.55563
KLK6	-0.59355
ADGRG1	-0.59336
JADE2	-0.53199
CRIPAK	-2.28724
CBX2	-0.38626
HIST1H1E	-0.39477
IER5L	-0.38388
ID3	-0.41617
DUSP7	-0.52619
HOXA9	-0.35201

K**8 h**

Gene	LogFC
JUN	2.378554
RELB	2.712769
OPTN	2.276576
CD83	2.167868
NFKBIA	1.162264
TSC22D1	0.953432
SBNO2	1.290902
DUSP16	2.466036
KLF6	1.018568
SDC4	1.12366
ETS1	1.601391
MT-CO1	0.879423
STC2	0.882231
DNAJB1	0.968201
S100A3	1.881222
KRTAP2-3	2.755401
NFKB1	0.896952
STEAP1	1.026118
KRTAP3-1	2.41079
ARTN	1.430232

Gene	LogFC
ID2	-1.53952
EGR1	-1.1986
BDNF	-0.84049
AMOTL2	-0.87315
RGS2	-0.90654
MT-ATP8	-0.60868
PIM1	-1.0512
BMP4	-0.6556
CXXC5	-0.5767
ADGRG1	-0.82189
MSH6	-0.5048
MT-CO3	-0.41521
TRIM2	-0.76636
MT-CO2	-0.51044
RBM14	-0.58008
PCSK9	-1.10324
THRA	-0.5685
ADM	-0.56589
DUSP6	-0.56239
KLK6	-0.76343

Figure 6.11. Identification of DEGs in IKK α KO 2h TNF α and IKK α KO 8h TNF α samples relative to IKK α KO NT

(A) BCV MDS plot for comparison between IKK α NT and IKK α KO 2h TNF α . (B) Plot of BCV versus mean log CPM for each gene across samples within comparison from (A). Red line is the common dispersion (average dispersion across genes). (C) MA-plot of average logCPM plotted against the logFC for comparison between IKK α NT and IKK α KO 2h TNF α . Differentially expressed genes with FDR < 0.05 are highlighted in red. Blue lines are shown at logFC values of 1 and -1. (D) BCV MDS plot for comparison between IKK α NT and IKK α KO 8h TNF α . (E) Plot of BCV versus mean log CPM for each gene across samples within comparison from (A). Red line is the common dispersion (average dispersion across genes). (F) MA-plot of average logCPM plotted against the logFC for comparison between IKK α NT and IKK α KO 8h TNF α . Differentially expressed genes with FDR < 0.05 are highlighted in red. Blue lines are shown at logFC values of 1 and -1. (G) Heirarchical clustering heat map of differentially expressed genes (FDR < 0.05) from comparisons between WT/IKK α NT, WT 2h and 8h TNF α -treated samples. (H) Venn diagram showing the number of differentially expressed genes (FDR < 0.05) unique and common to WT 2h TNF α and IKK α KO 2h TNF α . (I) Venn diagram showing the number of differentially expressed genes (FDR < 0.05) unique and common to WT 8h TNF α and IKK α KO 8h TNF α . The top 20 significantly DE genes out of the genes uniquely DE in IKK α KO cells are tabulated (ranked by FDR p value). (J and K) Top 20 significantly differentially expressed upregulated and downregulated genes and their logFC's for IKK α KO 2h and 8h TNF α samples (ranked by FDR p value).

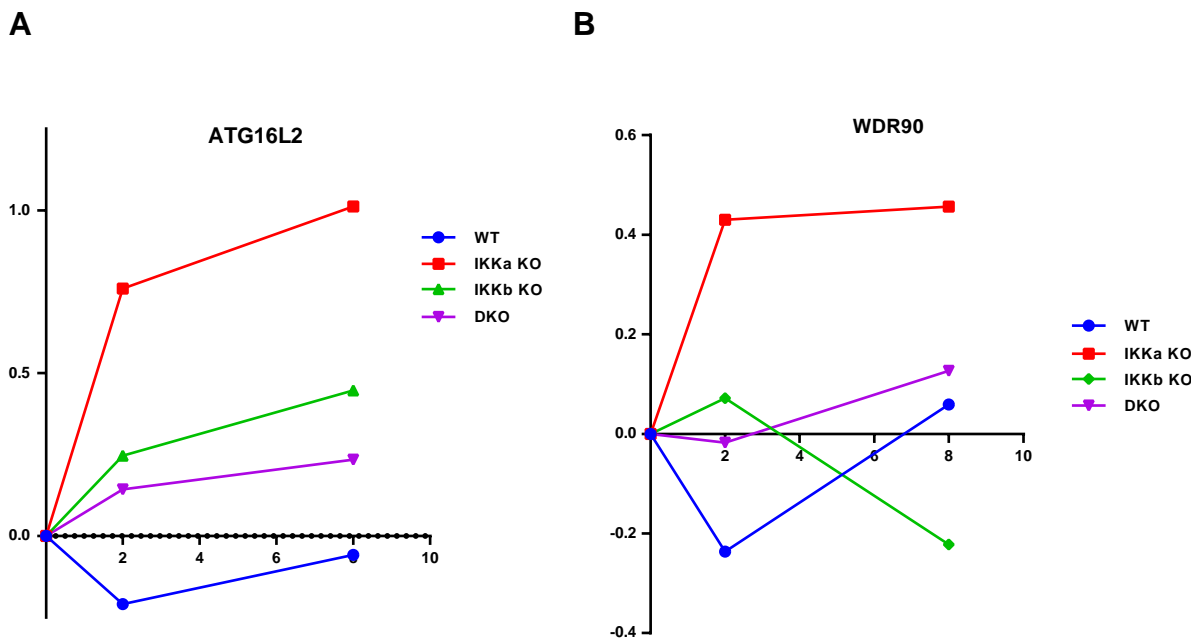
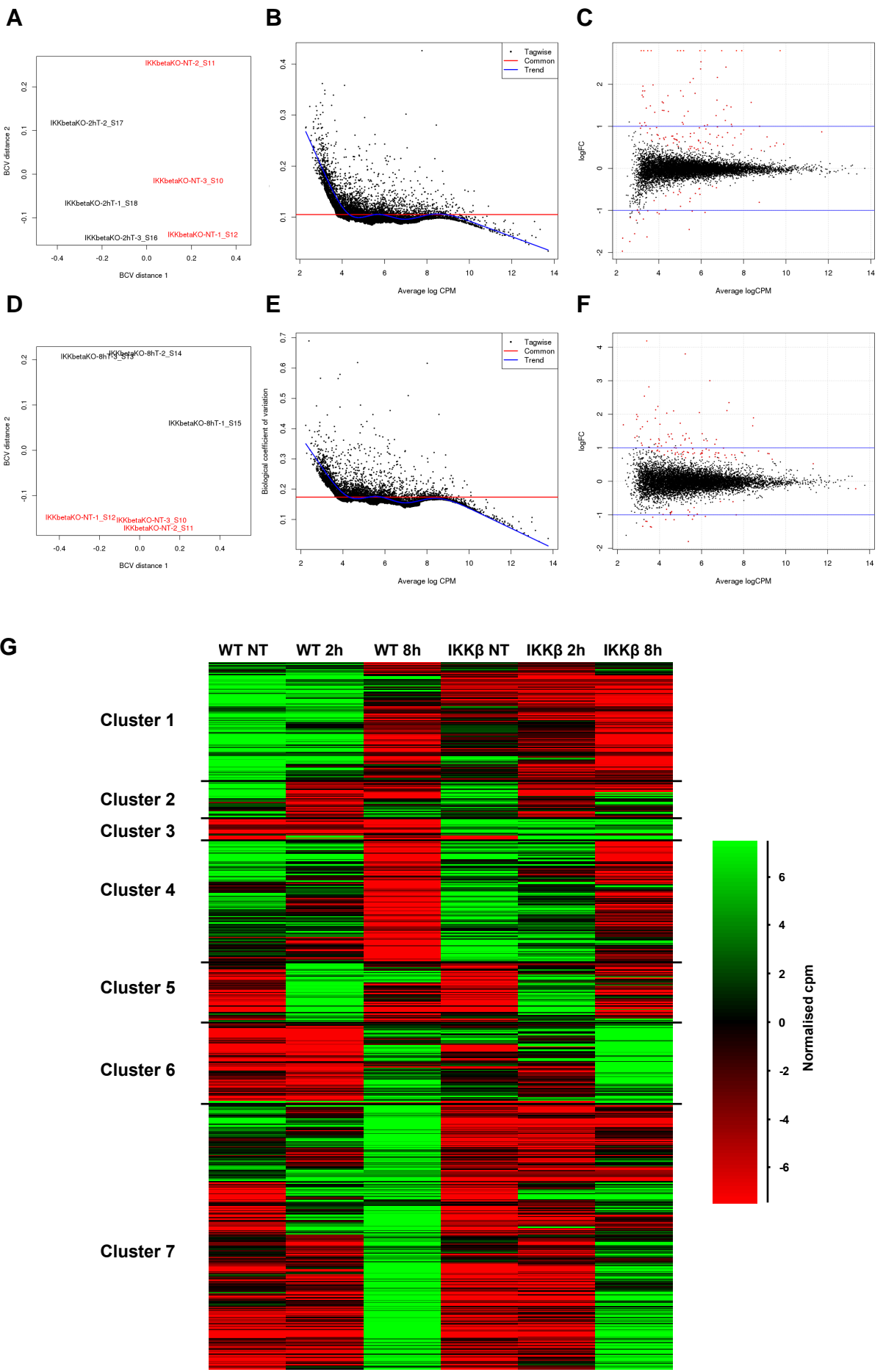


Figure 6.12. RNA sequencing data expression profiles for representative genes that are differentially expressed (FDR p -value < 0.05) in IKK α KO TNF α -treated samples, but not WT TNF α -treated samples. Plotted are the \log_2 (Normalised, average fold change in gene counts per million) for the DE (FDR < 0.05) genes ATG16L2 (A) and WDR90 (B). The fold changes are the average of the three biological replicates.



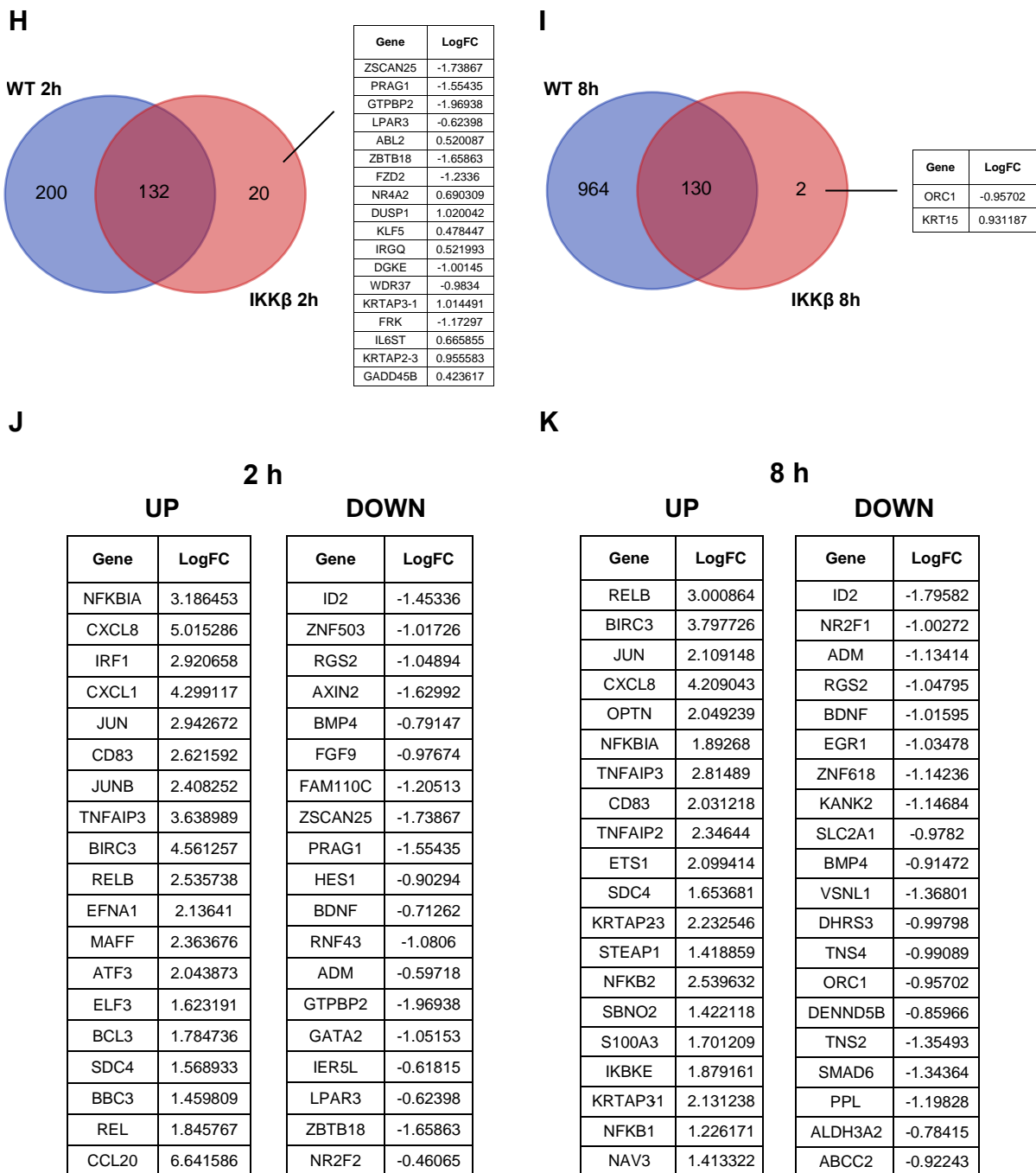


Figure 6.13. Identification of DEGs in IKK β 2h TNF α and IKK β 8h TNF α samples relative to IKK β NT (A) BCV MDS plot for comparison between IKK β KO NT and IKK β KO 2h TNF α . (B) Plot of BCV versus mean log CPM for each gene across samples within comparison from (A). Red line is the common dispersion (average dispersion across genes). (C) MA-plot of average logCPM plotted against the logFC for comparison between IKK β KO NT and IKK β KO 2h TNF α . Differentially expressed genes with FDR < 0.05 are highlighted in red. Blue lines are shown at logFC values of 1 and -1. (D) BCV MDS plot for comparison between IKK β NT and IKK β KO 8h TNF α . (E) Plot of BCV versus mean log CPM for each gene across samples within comparison from (A). Red line is the common dispersion (average dispersion across genes). (F) MA-plot of average logCPM plotted against the logFC for comparison between IKK β NT and IKK β KO 8h TNF α . Differentially expressed genes with FDR < 0.05 are highlighted in red. Blue lines are shown at logFC values of 1 and -1. (G) Heirarchical clustering heat map of differentially expressed genes (FDR < 0.05) from comparisons between WT/IKK β NT, WT 2h and 8h TNF α -treated samples. (H) Venn diagram showing the number of differentially expressed genes (FDR < 0.05) unique and common to WT 2h TNF α and IKK β KO 2h TNF α . (I) Venn diagram showing the number of differentially expressed genes (FDR < 0.05) unique and common to WT 8h TNF α and IKK β KO 8h TNF α . (J and K) Top 20 significantly differentially expressed upregulated and downregulated genes and their logFC's for IKK β KO 2h and 8h TNF α samples (ranked by FDR p value).

The hierarchical clustering heatmap of all DE expressed genes from comparisons between WT and IKK β KO, 2h and 8h TNF α samples reveals similar patterns to those seen between WT and IKK α KO, i.e. an overall dampening of the TNF α -induced gene expression response. This is highlighted by a comparison of the logFC's of some of the significantly upregulated and downregulated genes that are common to both WT and IKK β KO samples (compare Figure 6.13J and Figure 6.4H and I). For example, IRF1 is upregulated after 2h in WT cells by a logFC of 4.26, but by 2.92 in IKK β KO cells, while RelB is upregulated by a logFC of 3.2 in WT cells and 2.5 in IKK β KO cells. The genes that were significantly DE in IKK β KO cells but not WT cells were largely genes with low reads across all samples or genes that were filtered from comparisons between WT samples due to lack of expression (read counts below 10 cpm in all samples within the comparison). As such, these genes were not explored any further.

Two interesting candidate IKK-dependent genes that were followed up via qRT-PCR were *CSF1* and *USP43*. From the RNA-seq data, *CSF1* appeared to highly dependent on IKK α for TNF α -induced expression, while *USP43* induction appeared to be significantly reduced in both IKK α and IKK β KO cells (Figure 6.14A and B). qRT-PCR analysis confirmed that both genes were induced in WT cells in response to TNF α to approximately similar levels as determined from the DE analysis (Figure 6.14C and D). The kinetics of *CSF1* and *USP43* expression were also similar; *CSF1* and *USP43* expression peaked at 2 h before returning towards basal levels at 8 h. However, the qRT-PCR for *USP43* did suggest that its expression decreases below basal levels after 8 h. qRT-PCR also confirmed that both genes required IKK activity for expression as their expression was not induced in response to TNF α in DKO cells. The TNF α -induced decrease in *CSF1* expression in DKO cells after 2 hrs that was observed in the RNA sequencing data was also observed via qRT-PCR. The qRT-PCR for *USP43* also agreed well with the RNA-seq data; the induction of *USP43* was severely reduced in IKK α KO cells, to a greater extent than in IKK β KO cells. The qRT-PCR for *CSF1*, however, did not agree as well with the RNA-seq data; *CSF1* was upregulated in IKK α KO cells to a similar extent as observed for IKK β KO cells. Interestingly, however, the kinetics of *CSF1* expression appeared to be altered in IKK α KO cells relative to WT cells. Whereas *CSF1* expression increased by 6-fold after 2h then decreased by > 2-fold in WT cells, it increased by 2-fold at 2h and remained at this expression level after 8h in IKK α KO cells.

An additional reason for validating the RNA-seq data for *USP43* was that it had not previously been described as a TNF α -inducible or NF- κ B-dependent gene. *USP43* is a deubiquitinase (DUB) enzyme that removes covalently attached ubiquitin from proteins. The function of *USP43* is undefined. Of interest, however, is the fact that it was identified in a genome-wide siRNA screen for NF- κ B activation pathway components; knockdown of *USP43* impaired IKK-dependent phosphorylation of I κ B and NF- κ B nuclear translocation in response to transfection of an Epstein–Barr virus (EBV) latent membrane protein 1 (LMP1) mutant, which activates NF- κ B signalling (Gewurz *et al.*, 2012). The mechanism by which *USP43* promotes NF- κ B activation was not explored. Our RNA-seq and qRT-PCR data suggests that *USP43* is an NF- κ B-dependent gene that is significantly upregulated early in the gene expression response to TNF α . This is similar to the expression pattern of the well-characterised NF- κ B pathway DUB, *TNFAIP3* (encoding A20). Future work will seek to confirm the NF- κ B-dependence of *USP43* induction and to characterise the function of *USP43* in NF- κ B signalling.

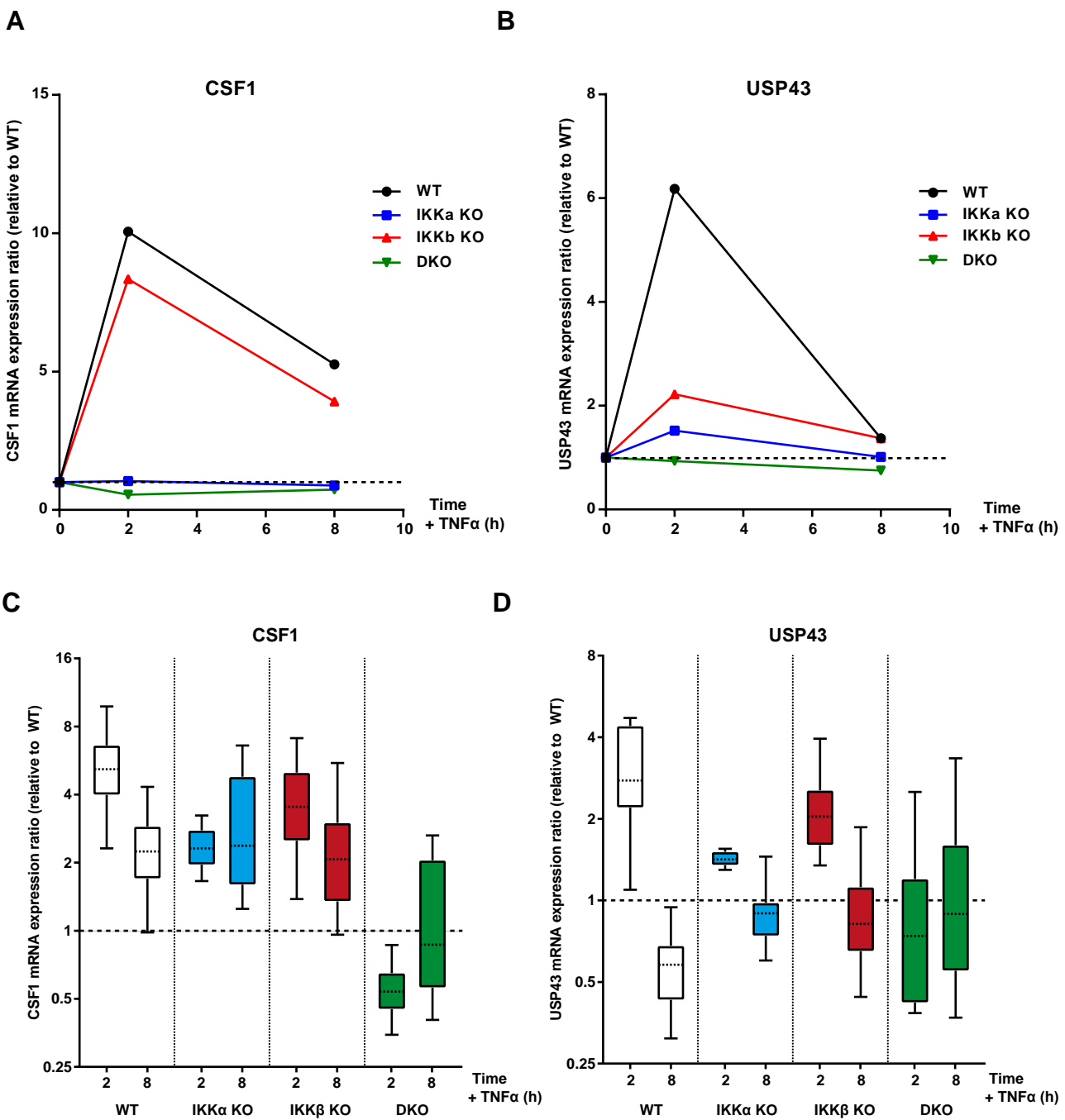
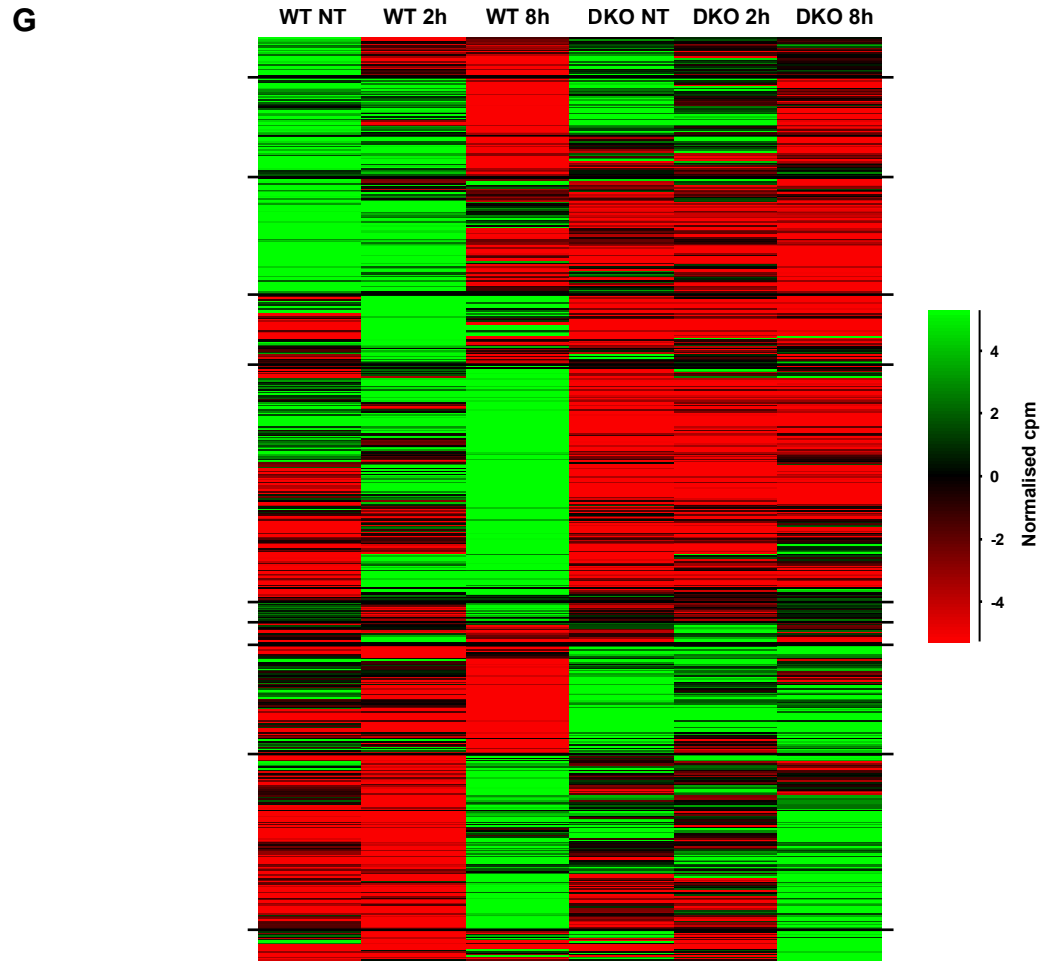
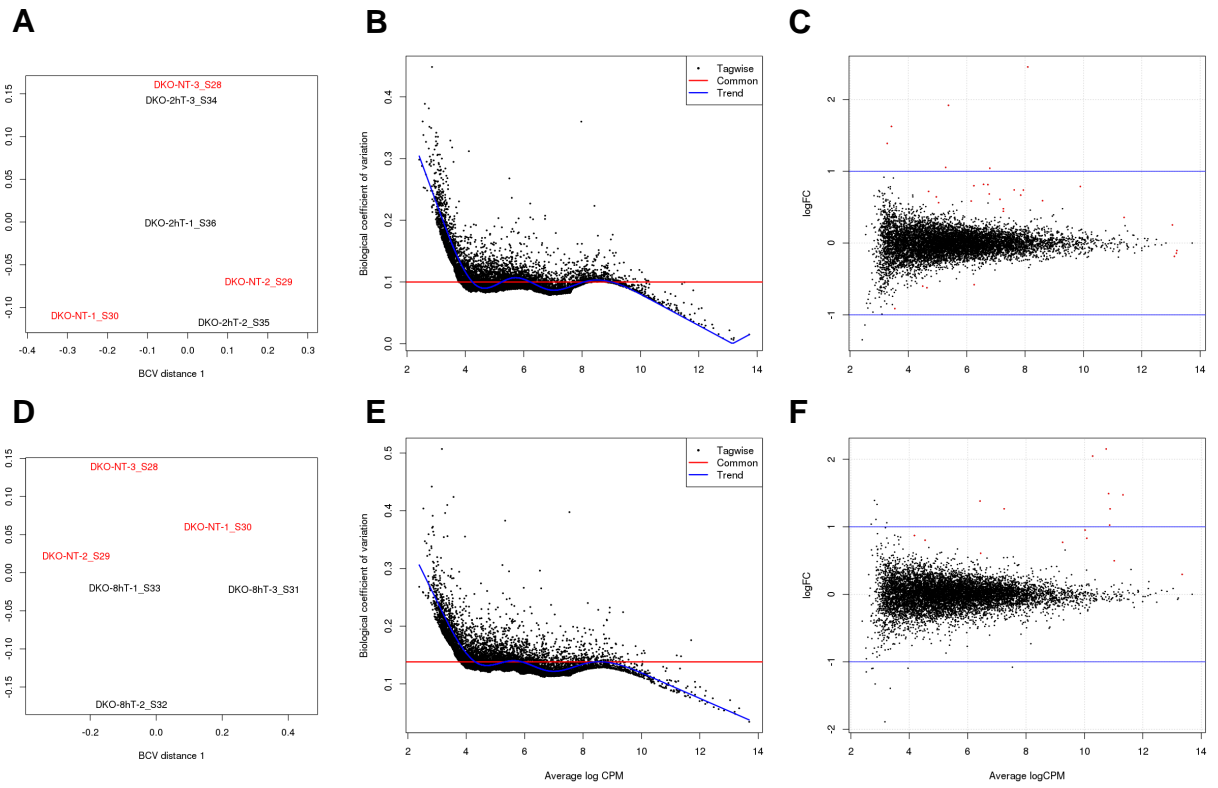


Figure 6.14. qRT-PCR validation of candidate IKK-dependent TNF α -responsive genes, CSF1 and USP43.
 Plotted are the average fold change in gene CPM for CSF1 (A) and USP43 (B). The fold changes are the average of the three biological replicates. Three independently derived WT clones and three clones each of IKK α KO, IKK β KO and DKO were seeded in normal growth medium for 48 hours prior to treatment with TNF α for 2h or 8h. Relative CSF1 (C) or USP43 (D) mRNA expression was determined by RT-qPCR, with normalisation to the geometric mean of the reference gene (*YWHAZ* and *B2M*) expression. Data are plotted on a logarithmic scale as median CSF1 expression ratios relative to the NT control samples (expression of which is represented by dotted line at expression ratio = 1). Boxes represent the interquartile range. Whiskers represent the minimum and maximum observations.

Finally, DE analysis was performed for comparisons between DKO NT and TNF α treated samples. Although the MDS plot for comparisons between DKO NT and DKO 2h and 8h TNF α samples again highlighted relatively poor clustering within the according to treatment type (Figure 6.15A), the common dispersions for these comparisons were of an acceptable level for DE gene analysis. As expected given the validated absence of stimulus-induced IKK kinase activity and NF- κ B-dependent transcriptional activity in these clones, the number of DEGs identified in the TNF α treated DKO samples was small; 27 and 19 at 2h and 8h, respectively (Figure 6.15H and I). The lack of TNF α -induced expression was clearly apparent in a heatmap of all of the DEGs identified in comparisons between NT and TNF α -treated WT and DKO samples (Figure 6.15G). A large proportion of these genes also exhibited reduced basal (NT) expression between WT and DKO cell lines suggesting that IKK expression might be important for a level of basal NF- κ B-dependent transcriptional activity that sustains the expression of certain NF- κ B-target genes at a certain level.

The genes significantly DE in both WT and DKO cells after 2h and 8h TNF α treatment contained a number of well-characterised TNF α -inducible AP-1 family transcription factors, including *JUN*, *ATF3* and *JUND*, *FOSL1* and *FOSL2* (Figure 6.15H). A number of the other genes have not been shown to be TNF α -inducible, including *ERRF1* and *PMAIP1*, although it is important to consider that the effect of TNF α on their expression may be indirect. As described earlier for IKK α KO cells, a large number of mitochondrial biogenesis genes were highly upregulated after 8h TNF α stimulation in DKO cells, consistent with an oxidative stress response in the absence of NF- κ B-dependent activation of antioxidant genes, such as SOD2.

A small subset of genes, *DUSP1*, *FOXO3*, *CSRNP1* and *KLF5* were differentially expressed in DKO cells after 2h TNF α treatment, but not in WT cells. The count data for these genes across all samples is shown in Figure 6.16. Interestingly, the phosphatase *DUSP1* was significantly upregulated in all IKK KO clones but not WT cells, suggesting perhaps that NF- κ B transcriptional activity normally suppresses *DUSP1* expression. *DUSP1* exhibits specificity towards ERK, p38 and JNK and is thought to be critical for the inactivation of p38 and JNK to promote survival in response to oxidative/heat stress and growth factors (Wu *et al.*, 2005). The increased expression of *DUSP1* in IKK KO cells relative to WT cells may, therefore, indicate a higher level of oxidative stress in these cells in response to TNF α treatment. DKO cells also exhibited a strikingly different expression profile for the tumour suppressor gene, *FOXO3*; absence of both IKK α and IKK β altered the expression profile from one typical of a 'late-induced' gene, to one more typical of an 'early' gene (Figure 6.16C). *FOXO3* has been shown to regulate NF- κ B activation, but the reverse, NF- κ B-dependent regulation of *FOXO3*, has not been reported, other than a study which has proposed that NF- κ B induces the expression of miRNA-155 that, in turn, downregulates *FOXO3* expression (Chiu *et al.*, 2016). Interestingly, oxidative stress has also been shown to induce *FOXO3* expression (Klotz *et al.*, 2015). DKO, IKK α KO and IKK β KO cells also exhibited a different TNF α -induced expression profile for the tumour suppressor transcription factor, *CSRNP1* compared to WT cells (Figure 6.16B). *CSRNP1* was significantly upregulated in DKO cells after 2h before returning to basal levels after 8h, whereas it exhibited a significant downregulation in WT cells in response to TNF α . DKO and IKK β KO cells also exhibited a stronger induction of the transcription factor, *KLF5* than WT or IKK α KO cells, possibly indicating a role for IKK β in the repression of *KLF5* expression (Figure 6.16D). The TNF α -dependent regulation of these genes will need to be investigated further in follow-up experiments.



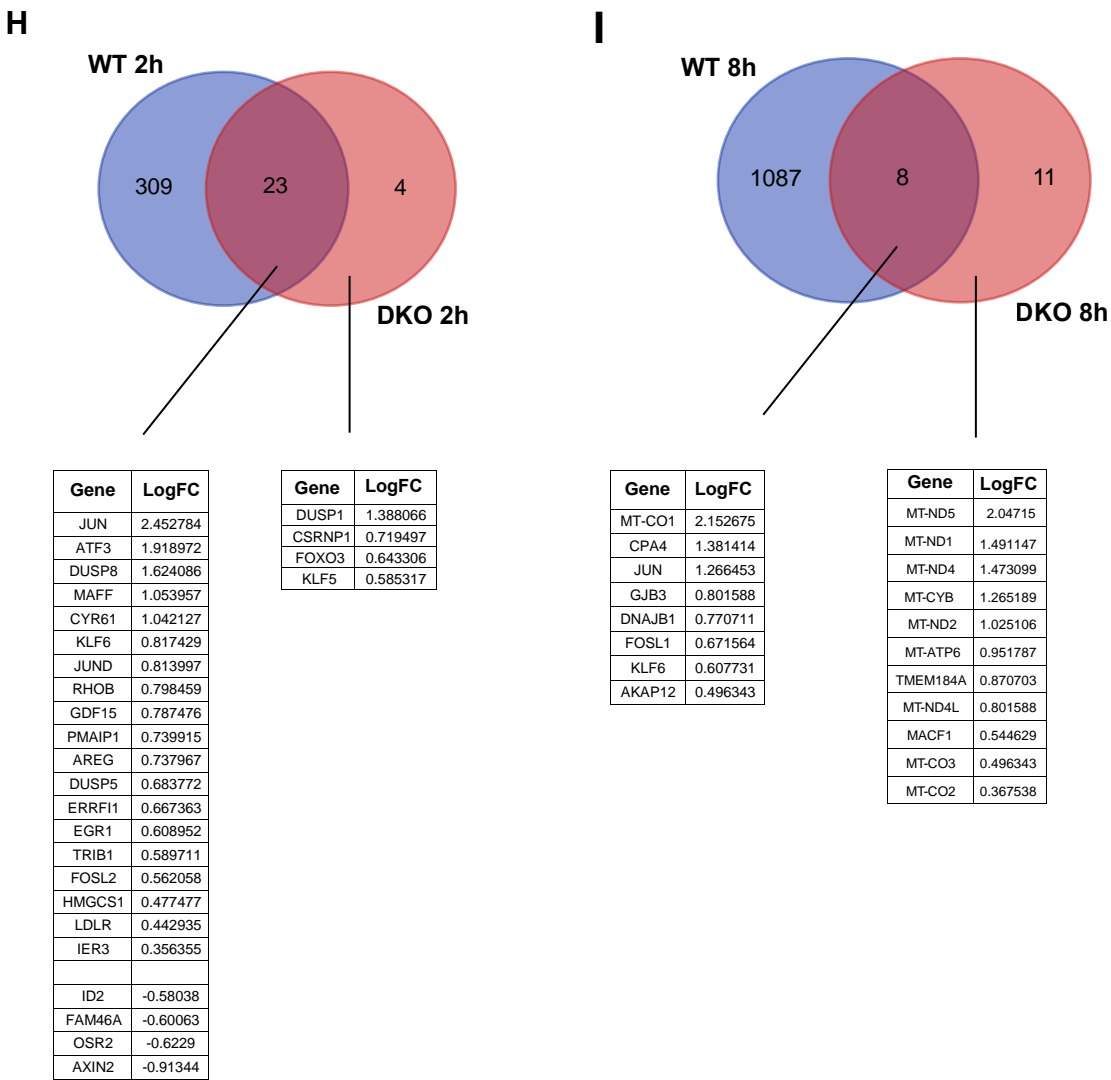


Figure 6.15. Identification of differentially expressed genes in DKO 2h TNF α and DKO 8h TNF α samples relative to DKO NT **(A)** BCV MDS plot for comparison between DKO NT and DKO 2h TNF α . **(B)** Plot of BCV versus mean log CPM for each gene across samples within comparison from (A). Red line is the common dispersion (average dispersion across genes). **(C)** MA-plot of average logCPM plotted against the logFC for comparison between DKO NT and DKO 2h TNF α . Differentially expressed genes with FDR < 0.05 are highlighted in red. Blue lines are shown at logFC values of 1 and -1. **(D)** BCV MDS plot for comparison between DKO NT and DKO 8h TNF α . **(E)** Plot of BCV versus mean log CPM for each gene across samples within comparison from (A). Red line is the common dispersion (average dispersion across genes). **(F)** MA-plot of average logCPM plotted against the logFC for comparison between DKO NT and DKO 8h TNF α . Differentially expressed genes with FDR < 0.05 are highlighted in red. Blue lines are shown at logFC values of 1 and -1. **(G)** Hierarchical clustering heat map of differentially expressed genes (FDR < 0.05) from comparisons between WT NT, 2h TNF α and 8h TNF α and DKO NT, 2h TNF α and 8h TNF α samples. **(H and I)** Venn diagrams showing the number of differentially expressed genes (FDR < 0.05) unique and common to WT 2h TNF α and DKO 2h TNF α and WT 8h TNF α and 8h TNF α samples. Also shown are tables of DE TNF α -responsive genes from DKO samples with corresponding logFC.

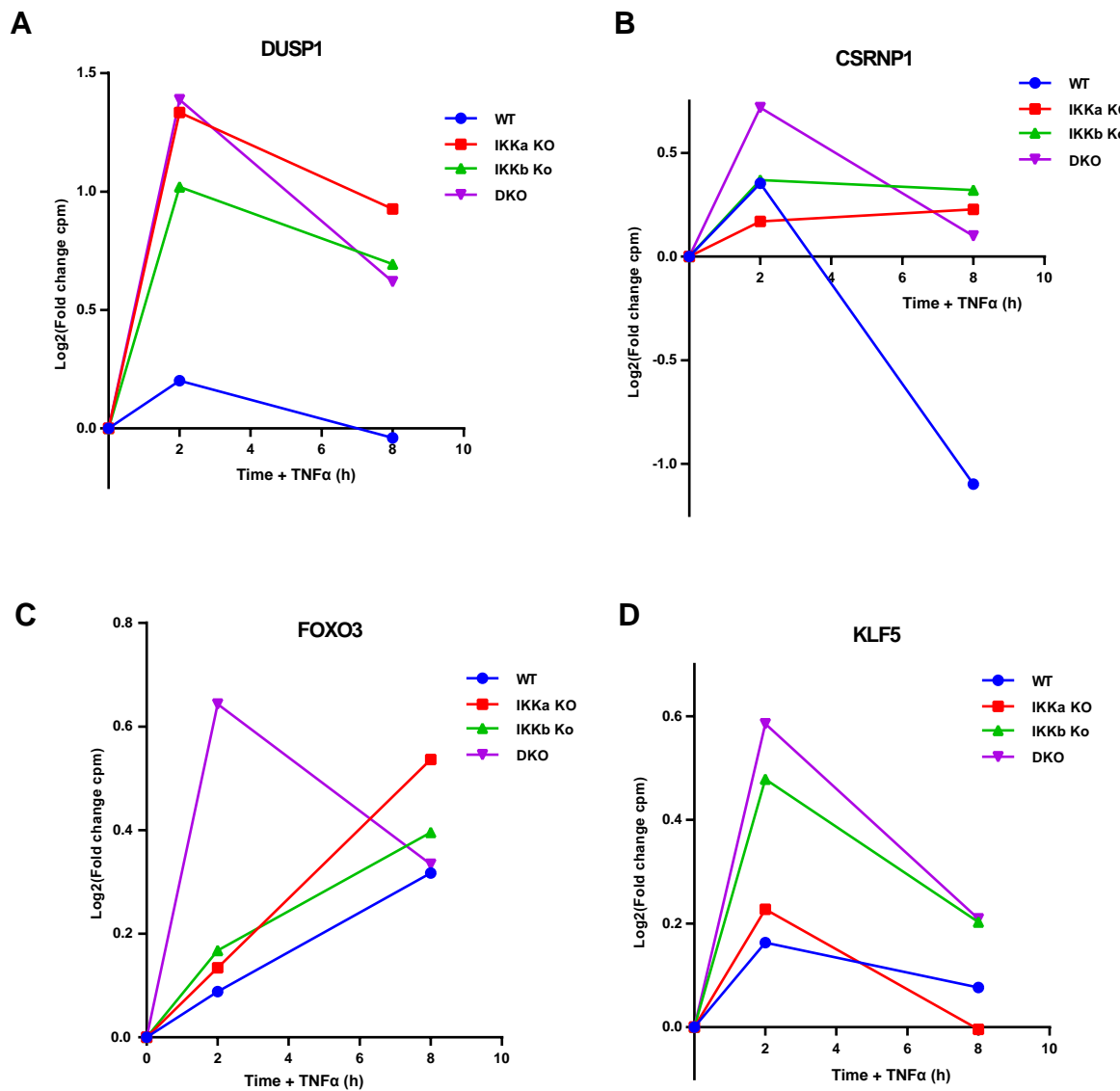


Figure 6.16. RNA sequencing data expression profiles for genes that are differentially expressed (FDR p -value < 0.05) in DKO TNF α -treated samples, but not WT TNF α -treated samples. Plotted are the \log_2 (Normalised, average fold change in gene counts per million) for the DE (FDR < 0.05) genes *DUSP1* (A), *CSRNP1* (B), *FOXO3* (C) and *KLF5*. The fold changes are the average of the three biological replicates.

6.3 Discussion

6.3.1 A detailed characterisation of the global TNF α -induced expression response in colorectal cancer cells

This large scale RNA-Seq analysis provides the most comprehensive analysis of TNF α -induced expression profiles in a CRC model to-date. The basic analysis presented here was only the first step in the utilisation of this data set. A number of follow-up studies are required to more rigorously validate the reliability of the expression changes identified, and to confirm NF- κ B- and/or selective IKK-dependence for the expression of interesting hits. Nevertheless, the results presented already justify the decision to perform this experiment and potentially identify novel aspects of IKK β function as well as IKK-dependent NF- κ B gene expression signatures.

The temporal expression changes identified in WT clones recapitulate the tri-phasic program of NF- κ B-dependent gene expression in response to TNF α that has been reported previously; early, intermediate and late expression patterns were identified for both up- and downregulated genes (Hao & Baltimore, 2009). This represented a form of quality control and underpinned confidence in our RNA-Seq data set. NF- κ B-dependent gene expression has been rigorously studied for many years, so it was no surprise that a large proportion of the DEGs were genes with varying degrees of evidence linking their expression to NF- κ B transcriptional regulation. A rudimentary filtering approach to identify potentially novel NF- κ B genes involved removing genes contained within the database of NF- κ B-dependent genes compiled by Yang *et al.*, 2016, followed by a literature search for connection to TNF α and/or NF- κ B. This resulted in a preliminary list of 220 genes. The database used for this filtering is far from definitive, so it is likely that certain previously defined NF- κ B-dependent genes passed into this list of genes. However, it is also likely that interesting genes were filtered out via this approach. A large number of genes within the database have only very loosely been connected to NF- κ B dependent transcription, some under certain specific circumstances, and some perhaps not at all. A more rigorous, candidate-based approach to identification of interesting hits will require more hands-on time with the data set than we were afforded prior to the writing of this thesis. It should also be mentioned that many of the identified DEGs may not be direct targets of NF- κ B-dependent expression, but rather their expression may be induced indirectly by TNF α through feedforward signalling, including autocrine mechanisms. Indeed, a large array of cytokine and growth factor genes, such as interferon regulatory factor 1 (*IRF1*), *CXCL8*, *CXCL3*, *CXCL2*, *CXCL1* and *PDGFB* were strongly induced after 2 h TNF α treatment in WT cells. Filtering of the gene list for known IRF1-dependent genes and/or NF- κ B/IRF1 binding site motifs may be one approach to acquire a more accurate list of genes to investigate further. It might also be interesting to follow up the expression changes of cytokines/growth factors induced by TNF α by profiling the secretome of WT cells compared to IKK KO cells using cytokine arrays (biased) or mass spectrometry (unbiased).

6.3.2 Transcriptome profiling of IKK β KO and IKK DKO cells revealed unexpected changes in the basal expression of genes involved in the regulation of numerous cellular processes

We were not expecting significant basal gene expression differences between WT and IKK KO cells, and particularly not for IKK β KO cells, for several reasons. As described in other chapters, the IKK kinases, particularly

IKK β , exhibited minimal basal phosphorylation and hence kinase activity in unstimulated HCT116 cells; although a certain level of basal IKK α activity was suggested from the loss of basal p65 phosphorylation in IKK α KO cells (Chapter 3, Figure 3.6). Furthermore, as described in Chapter 3, no obvious phenotypes were immediately apparent for IKK α and IKK β KO cells; they proliferated at similar rates to WT cells, they exhibited no striking differences in morphology and they exhibited similar cell cycle profiles and levels of basal cell death as WT cells. On the other hand, the more epithelial morphology and increased expression of E-cadherin in IKK DKO cells (Chapter 3, Figure 3.3) suggested that DKO cells might exhibit differences in gene expression relative to WT cells. IKK α KO was hypothesised to be the more likely cause of these and other potential expression changes than IKK β on the basis of the known nuclear localisation of IKK α and its previously reported involvement in transcriptional regulation independent of NF- κ B through direct phosphorylation of chromatin-bound transcriptional/epigenetic regulators, such as CBP and Histone H3 (Yamamoto *et al.*, 2003; Huang *et al.*, 2007). In contrast, IKK β is widely believed to be localised exclusively to the cytoplasm and has not been shown to play a direct role in regulation of gene expression, independently of NF- κ B.

It came as a surprise, therefore, that the more significant differential gene expression was observed in IKK β KO cells, and not IKK α KO cells. We have already explained how a greater level of heterogeneity amongst the IKK α KO clones may have precluded the identification of DEGs whose expression was perturbed by IKK α KO. This assertion is purely anecdotal, however, and has yet to be tested experimentally. A degree of heterogeneity at the level of TNF α -induced NF- κ B-dependent luciferase reporter activity had been observed between IKK α KO clones, but no more than had also been observed for WT and IKK β KO clones. One possible means to resolve this uncertainty may be to perform additional sequencing runs with other validated IKK α KO clones. Batch effects could be controlled for and are mostly restricted to the cell processing and RNA isolation steps, rather than the actual RNA sequencing procedure. Increasing the replicate number in this way may uncover subtle gene expression changes that were not of a sufficient magnitude to pass the significance threshold in the first instance. Relaxing the significance threshold to a non-corrected *p*-value of 0.01 did lead to the identification of a list of potentially IKK α -dependent genes. However, the false-positive rate within this list is so high that it was difficult to make any meaningful conclusions regarding the functions of the genes within this list.

Conversely, a large number of DEGs were identified in IKK β , and particularly, IKK DKO clones; 170 and 601, respectively. That a large proportion of the genes identified as DE in IKK β KO cells were also DE in the DKO cells gave us additional confidence in the validity of the IKK β -dependence of these genes. Concerns were raised regarding the identification of supposedly polyA⁺-tail independent Histone genes within these polyA-RNA enriched sequencing libraries. This discrepancy could not be resolved prior to the writing of this thesis. Rather than pre-emptively remove these Histone genes from the DE gene lists used for subsequent analysis, they were retained, with the caveat that, if artefactually detected, they may have biased the GO:term analysis. One of the reasons for retaining these Histone genes was the identification of numerous other nucleic acid-binding and/or nuclear-localised DEGs with functions in chromosome organisation in IKK β KO and DKO cells. In IKK β KO cells, genes involved in the regulation of the mitotic cell cycle phase and the response to DNA damage were also identified as DEGs. Importantly, all of these interesting GO:term enriched genes were downregulated in IKK β KO and DKO cells. GO:term analysis on the combined list of down- and up-regulated DEGs did not identify any

additional significantly enriched GO:terms indicating a distinct functional separation between the up- and down-regulated genes. Indeed, the upregulated genes in IKK β KO and DKO cells were largely unrelated at the functional level, apart from a significant enrichment for genes involved in metabolic regulation and mitochondrial gene expression. As previously mentioned, mitochondrial gene expression may be enhanced in response to oxidative stress. Whether IKK β KO and DKO cells exhibit a higher level of basal oxidative stress and/or higher levels of free ROS caused by loss of IKK β will require further investigation, for example by analysing basal and TNF α -stimulated ROS production using the cell permeant stain 2', 7'-dichlorofluorescin diacetate (DCFDA). Alternatively, the changes in expression of genes involved in metabolic regulation may reflect a reprogramming of cellular metabolism induced by IKK β knockout. This could be addressed in the first instance by unbiased MS-based metabolomics analysis.

The GO:term analysis of genes differentially expressed in DKO cells was consistent with a significant reprogramming of the cell structure and organisation. Consistent with the large overlap in DEGs between IKK β KO and DKO cells, many of the same GO:terms were found to be enriched, including genes involved in the cellular response to DNA damage, mitotic cell cycle control and chromosome organisation. However, a large number of additional enriched terms were also identified, possibly indicating that knockout of both IKK α and IKK β had additive effects on cell function above and beyond those induced by loss of IKK β alone. This included genes involved in the control of the microtubule and actin cytoskeletal networks, cell projections, cell junctions, endomembrane organisation and exosomes. It is tempting to speculate on the basis of these related GO:terms that IKK DKO results in changes in the cell polarity of HCT116 cells; specifically the adoption of a more polarized, epithelial-like morphology. Polarized epithelial cells, such as intestinal epithelial cells, exhibit a distinct apical-basal polarity that is important for the function of epithelial layers, such as enabling the controlled exchange of nutrients and waste between the internal and external environment. Loss of cell polarity is associated with EMT and contributes to the migration and metastatic spread of colorectal cancer cells, amongst others (Langlois *et al.*, 2010). It is interesting, therefore, that a significant enrichment of downregulated genes involved in signalling by Rho GTPases was observed; Rho GTPases are essential regulators of migration during the loss of apical-basal polarity (Hanna & El-Sibai, 2014). Furthermore, the integral polarity-promoting gene, Crumbs3 (*CRB3*) was significantly upregulated in DKO cells ($\log FC = 0.62$, FDR p -value = 0.045). The adoption of a more apical-basal morphology would be entirely consistent with the observed increase in E-cadherin expression in IKK DKO cells and their more epithelial-like morphology (Chapter 3, Figure 3.3). The differential expression of genes involved in cytoskeletal organisation, mitotic spindle organisation, cell projection assembly and endomembrane compartment organisation is also consistent with a change in polarity upon loss of IKK as these are all processes intimately linked to regulation of polarity (Martin-Belmonte & Moreno, 2012). It is also interesting within this context, that over 100 genes involved in cell differentiation were identified as significantly downregulated in DKO cells. Whether these genes are actively involved in promoting or repressing cell differentiation, or whether they are a consequence of reprogramming remains to be investigated.

The apparent downregulation of genes involved in mitotic cell cycle control is difficult to reconcile with the absence of any observed growth or cell cycle defect in IKK β KO or DKO cells. Synchronisation experiments may uncover subtle defects in the progression through mitosis that were missed in studies of the asynchronous

population. A role for IKK β in bipolar spindle assembly has previously been proposed on the basis of increased multipolar spindles and cell-cycle delay during mitosis observed following siRNA-mediated knockdown of IKK β in HeLa cells (Irelan *et al.*, 2007). It will, therefore, be worthwhile to investigate spindle morphology and chromatid separation during mitosis in IKK β KO and DKO cells. We do not believe the identification of these mitotic cell cycle gene expression changes in IKK β KO cells warrant the reconsideration of the conclusions presented in Chapter 5 regarding the findings of Blavkova *et al.*, 2007. We conclusively demonstrated that the effects of BMS-345541 on cell cycle progression were off-target since exactly the same effects were observed in IKK β KO and DKO cells. It appears to be an interesting coincidence that IKK β KO also has effects on the expression of genes involved in the regulation of mitotic cell cycle progression.

6.3.3 Comparison of TNF α -induced expression profiles in WT and IKK KO cells highlights potentially IKK-dependent genes

One of the main motivating factors for performing this RNA-Seq experiment was to attempt to identify NF- κ B-dependent genes with preferential dependence on either IKK α or IKK β , and also to investigate whether the differential effects of IKK knockout on TNF α -induced p65 and c-Rel modification and nuclear translocation translated into significant differences in the expression profiles of IKK KO cells. The identification of IKK-dependent genes involved in tumour promoting mechanisms may have provided a rational for selective therapeutic targeting of either IKK α or IKK β . On the whole, however, significant alterations in the TNF α -induced expression profiles of IKK KO cells were not observed. The identity of the top differentially expressed genes were highly similar between WT, IKK α and IKK β KO cells. Instead, a generalised reduction in the fold change expression of NF- κ B-dependent genes in IKK β KO, and particularly, IKK α KO cells was observed. The result was that a large number of genes found to be differentially expressed with small logFC's in WT cells failed to reach the significance threshold in IKK α KO and IKK β KO cells. This trend reflected the predominant importance of IKK α over IKK β in the induction of NF- κ B nuclear translocation and luciferase-reporter gene expression described in Chapter 3.

A more in-depth analysis may be necessary to stratify those genes with significantly different expression kinetics in WT and IKK KO cell lines. *CSF1* was a representative example of a gene for which the temporal regulation of expression appeared to be differentially disrupted by loss of IKK α rather than IKK β . USP43 was another highly interesting candidate TNF α -inducible gene given its reported ill-defined role in promoting activation of the NF- κ B pathway. Although obscure in function, the enhanced expression of *ATG16L2* and *WDR90* genes in IKK α KO cells will also be worthwhile exploring further. So too will the apparent IKK-dependent expression of the *DUSP1*, *FOXO3*, *CSRNP1* and *KLF5* genes. The observation that DUSP1 expression was induced in IKK α KO, IKK β KO and DKO cells, but not WT cells may have interesting consequences for regulation of the p38 and JNK signalling pathways in these cells. DUSP1 is over-expressed at different stages of tumour progression in several human cancers, including prostate, colon and bladder (Loda *et al.*, 1996). Interestingly, a dynamic interplay between NF- κ B activity and DUSP1 expression has previously been reported in prostate cancer; DUSP1 overexpression blocks NF- κ B nuclear translocation, while its expression inversely correlates with nuclear p65 in human prostate tissue specimens (Gil-Araujo *et al.*, 2014). Our data potentially support this observation. Given the increased expression of *DUSP1* in IKK KO cells it might be predicted that the kinetics of JNK and p38 signalling would be altered in these cells relative to WT. We have yet to characterise the effects of IKK KO on sustained TNF α -induced JNK/p38

activation. The increased expression of mitochondrial biogenesis genes after 8 h TNF α in IKK α KO and DKO cells, but not IKK β KO cells will also be explored further. We believe this likely reflects the accumulation of oxidative stress that results following the reduced NF- κ B-dependent expression of antioxidant proteins, such as *SOD2* and *FTH1*, the former of which did indeed show differentially reduced expression after 2h TNF α treatment in IKK α KO cells (WT logFC = 0.85, *p*-value = 1.7×10^{-11} , IKK α KO logFC = -0.003, *p*-value = 0.97, IKK β KO logFC = 0.61, *p*-value = 0.0011).

In summary, this RNA-seq analysis provided a comprehensive profile of TNF α -responsive genes in a clinically relevant CRC cell model and will provide a resource for future dissection of TNF α -dependent expression networks. A number of potentially novel NF- κ B-dependent genes were identified and will be validated in subsequent studies. An unexpected, large-scale reprogramming of basal gene expression in response to IKK β KO was uncovered. Whether this reflects a kinase-dependent or independent function of IKK β will be the subject of future investigation. Finally, comparison of TNF α -induced gene expression profiles in WT versus IKK KO cell lines confirmed the greater importance of IKK α over IKK β in mediating the activation of NF- κ B-dependent gene expression and identified a subset of genes whose expression appeared to preferentially depend on either of the two IKK kinases.

Chapter 7

Final discussion

7 Final discussion

7.1 Assessing the relative merits of targeting IKK α and IKK β in colorectal cancer

We have comprehensively demonstrated that IKK α is involved at numerous stages in the activation of TNF α and IL-1 α -induced canonical NF- κ B signalling, including the phosphorylation-dependent degradation of I κ B α , basal phosphorylation of p65 at S536, stimulus-induced phosphorylation of S536 and S468, nuclear translocation of p65 and c-Rel and activation of NF- κ B-dependent transcription. Conversely, knockout of IKK β had only a minor impact on stimulus-induced nuclear translocation of p65 and NF- κ B-dependent gene expression. These findings have important implications for the therapeutic intervention of NF- κ B signalling in colorectal cancer.

It should be stressed that the data presented most convincingly demonstrates that IKK β is less able to compensate for the loss of IKK α protein than IKK α is able to compensate for the loss of IKK β protein in the activation of canonical signalling. However, evidence was also presented that IKK α was significantly active in canonical NF- κ B in the WT state. For example, an IKK β selective inhibitor exhibited far greater potency in terms of inhibition of NF- κ B-dependent transcription in IKK α KO cells than it did in WT cells, implying that IKK α was active under these conditions (Chapter 3, Figure 3.8 and Chapter 5, Figure 5.6). However, further work will aim to more comprehensively demonstrate the importance of IKK α activation in WT cells. It is here that IKK α -selective inhibitors would be particularly useful. Characterising the effect of IKK α and IKK β siRNA-mediated knockdowns in WT treated with TNF α /IL-1 α would also strengthen confidence in the observations made with IKK KO cells.

The NF- κ B pathway has long been a therapeutic target for diseases including various forms of cancer. Interest has been driven by the large body of evidence demonstrating diverse roles for aberrant NF- κ B signalling in cancer progression. Early mouse knockout studies led to the persistent dogma that IKK β is the predominant kinase activating the canonical NF- κ B pathway. As such, the overwhelming focus of drug discovery pipelines has been centred on IKK β . The initial wave of pharmaceutical interest in IKK β inhibition has since waned, particularly as a cancer therapy, largely due to a lack of clinical success to back-up promising preclinical observations. To date, only three IKK β inhibitors have been tested in clinical trials, and not for the treatment of cancer; IMD-0354, and its prodrug IMD-1041 for the treatment of chronic obstructive pulmonary disease (COPD) and SAR113945, for the treatment of knee osteoarthritis (DiDonato *et al.*, 2012). The data presented here suggest that selective IKK β inhibition would be largely ineffective in inhibiting chronic NF- κ B signalling in colorectal cancer; assuming that CRCs exhibit a similar co-dependence on IKK α and IKK β *in vivo*. Redundancy between IKK α and IKK β at the level of canonical NF- κ B activation should also be considered in other cancer models to optimise therapeutic strategies. Furthermore, a lack of appreciation for compensatory IKK α -dependent NF- κ B activation may have led to the abandonment of pre-clinical studies with IKK β -selective inhibitors that might otherwise have exhibited promising effects.

Reduced interest in IKK β inhibitors also originates from concerns over the toxicity associated with systemic IKK β inhibition, as discussed in Chapter 1, Section 1.4.5. This toxicity stems largely from the role of IKK β -dependent NF- κ B activation in the negative control of inflammasome activation (Greten *et al.*, 2007). In contrast, there is growing interest in IKK α -selective inhibitors for the treatment of disorders where IKK α has been shown to play a

significant role in pathogenesis; prostate and pancreatic cancer being the most prominent examples. Significant evidence suggests that IKK α is highly expressed and constitutively active in poor-prognosis castration-resistant prostate cancer, where it promotes proliferation, survival and metastasis (Palayoor *et al.*, 1999; Jun-Li *et al.*, 2007; Ammirante *et al.*, 2010). This has motivated the development of first-in-class selective IKK α inhibitors by the Mackay lab who employed molecular dynamics simulations to identify differences in conformational flexibility of the homologous active sites of IKK α and IKK β that enabled rational design of selective compounds (Anthony *et al.*, 2017).

Given the importance of IKK α in canonical NF- κ B signalling in a human colorectal cancer cell model demonstrated here, selective inhibition of IKK α may prove a more attractive therapeutic strategy for the inhibition of chronic NF- κ B activation in CRC. Although preliminary, we also provided evidence that IKK α KO cells exhibited negligible activation of AKT signalling following sustained TNF α treatment compared to WT or IKK β KO cells (Chapter 3, Figure 3.18). TAM-derived IL-1 β has been proposed to activate AKT signalling and downstream Wnt signalling in an NF- κ B-dependent manner to contribute to growth and survival of colorectal cancer (Kaler *et al.*, 2009a; Kaler *et al.*, 2009b). IKK α inhibition may, therefore, offer a selective route through which to inhibit both canonical NF- κ B signalling and TME-derived AKT/Wnt-activating signals in CRC.

However, selective inhibition of IKK α is also not without significant risk. Loss of IKK α kinase activity in mouse models has also paradoxically been proposed to promote inflammation that contributes to development of certain inflammatory diseases, including pancreatitis and cancers, including spontaneous squamous cell carcinoma (SCC) of the lung (Xiao *et al.*, 2013). However, in the case of the later it was unclear whether the observed increase in tumourigenesis was due to loss of IKK α activity or loss of IKK α expression; the KD-IKK α knock-in mice also exhibited drastically reduced IKK α protein levels. Since this report, however, IKK α kinase activity has been proposed to be important in the negative regulation of the apoptosis associated speck-like protein containing a C-terminal caspase-activation-and-recruitment (CARD) domain (ASC) adaptor, which is an essential component of the NLRP3 inflammasome (Martin *et al.*, 2014). As such, bone marrow chimeric mice with a WT background that received IKK α KD bone marrow exhibited higher levels of circulation of IL-1 β indicative of inflammasome hyperactivation; a similar phenotype to that observed when IKK β is deleted in the myeloid-lineage of mice (Greten *et al.*, 2007).

Perhaps the only way to mitigate for toxicity effects associated with selective IKK α or IKK β inhibition is through careful consideration of both the dosing strategy and clinical setting to maximise any available therapeutic window. Given the evidence from the literature and the data presented here, the optimal strategy in CRC may be the use of moderate doses of a dual IKK α / β inhibitor. The combined inhibition of IKK α and IKK β may reduce canonical NF- κ B signalling in cancer cells with high levels of pathway activation sufficiently to be of therapeutic benefit, whilst retaining sufficient NF- κ B signalling in normal epithelia and cells of the immune system to prevent the toxicity associated with complete pathway inactivation.

7.2 Highlighting the discrepancies between NF-κB signalling in human cells and mouse models

A general theme that emerged from this body of work was a level of disagreement between observations made using the human CRC cells that were central to this study and evidence from studies in the literature using MEFs. One of the most striking differences was in the level of NEMO protein following loss of IKK subunits. Numerous studies have utilised IKK KO and IKK α / β DKO MEFs and, in all cases where the level of NEMO protein was measured, no change has been reported. This contrasts with the striking decrease in NEMO protein observed in IKK α / β DKO HCT116 cells (Chapter 4, Figure 4.3). We have confidence that this phenotype is not specific to CRC cells or cancer cells in general because a decrease in NEMO protein has also been reported in human fibroblasts and PBMCs from patients with a rare form of SCID caused by IKK β deficiency (Pannicke *et al.*, 2013). Another example is provided by a study that observed a striking increase in basal NIK protein in IKK α KO, IKK β KO, IKK α / β DKO and NEMO KO MEFs (Gray *et al.*, 2014). The authors proposed that this reflected a role for the IKK complex in limiting the basal pool of newly synthesised NIK. This contrasts with our observation that basal levels of NIK protein are the same in IKK KO and WT cells. Rather, we observed stabilisation of NIK protein in IKK KO cells following stimulation with TNF α . This discrepancy alludes to possible species-level differences in the mechanisms of cross-talk between canonical and non-canonical NF-κB pathways. Another important discrepancy between studies with IKK KO MEFs and the findings presented in this work relates to the function of IKK α in canonical NF-κB signalling. Although there have been conflicting observations in MEFs relating to the function of IKK α in canonical stimulus-induced NF-κB nuclear translocation and transcriptional activity, the vast majority of studies concluded that IKK α exhibits minimal TNF α -stimulated kinase activity towards I κ B α (Hu *et al.*, 1999; Li *et al.*, 1999a; Li *et al.*, 1999b; Sizemore *et al.*, 2002; Solt *et al.*, 2007). However, we clearly demonstrate that IKK α phosphorylates I κ B α in response to TNF α and IL-1 α in both IKK β KO and WT cells (Chapter 3, Figure 3.6, 3.7 and 3.8). This highlights a fundamental difference in the function of the canonical NF-κB signalling pathway in MEFs compared to human cells (at least in the case of CRCs). Any proposed explanation for the greater involvement of IKK α in canonical NF-κB signalling in human CRCs compared to MEFs would be purely speculative at this point, but it is interesting to consider that intestinal epithelial cells are the first line of defence in the mucosal immune system of the lower intestine and thus may have altered the wiring of their immune response pathways, of which the NF-κB signalling is integral, in adaptation to frequent exposure to signals from the commensal microorganisms and innate/adaptive immune cells that are abundant in the mammalian gastrointestinal tract. The greater significance of IKK α in canonical NF-κB signalling may also represent a cancer-specific adaptation. Indeed, further work will seek to demonstrate that the observations made with HCT116 cells are general to other CRCs and perhaps other cancer cell types.

It should be emphasised that some of these discrepancies could simply reflect signalling differences due to different tissues of origin, rather than species. Nonetheless, the differences are worth reflecting on. Indeed, there is a growing awareness of the limitations of the use of mouse cells and models to study human disease. In particular, there are members of the research community that argue that mouse models do not accurately mimic human inflammatory disease. For example, a systematic comparison of genomic responses associated with human inflammatory diseases of various etiologies and their corresponding mouse models demonstrated poor

correlation between two (R^2 between 0.0 and 0.1 for comparison between differentially expressed human genes and their murine orthologues) (Seok *et al.*, 2013). Furthermore, pathways involved in the propagation of intestinal inflammation are not well-conserved across the human-murine species boundary (Mestas & Hughes, 2004). For example, the profiles of T cells that reside in the intestinal epithelium vary dramatically between the two species (Gibbons & Spencer, 2011).

Mouse studies have played an integral part in the elucidation of the NF- κ B signalling pathway, and will continue to do so. However, the discrepancies within the literature described here highlight the need for caution when attempting to translate findings relating to NF- κ B signalling made in mouse models into clinically relevant settings. Furthermore, the use of human CRISPR-Cas9 cell lines is eliminating the need to study the function of signalling proteins in KO MEFs.

7.3 Regulation of structural disorder as a possible common mechanistic theme in NF- κ B signalling

Evidence was presented that NEMO exhibits significant regions of intrinsic structural disorder that in the absence of IKK interaction partners might contribute to its rapid proteasomal turnover (Chapter 4). Interestingly, various other signalling components in the NF- κ B pathway have also been shown to exhibit functionally-relevant intrinsic structural disorder. For example, a systematic analysis of intrinsic structural disorder in proteins involved in antiviral immunity and innate immunity identified a number of NF- κ B signalling components, including TAK1, IRAK-1 and RIP1, which were predicted to contain >45%, >40% and >30% disordered sequence, respectively (Xue *et al.*, 2014). Common to all of these proteins, including NEMO, is their function as adaptor proteins and their requirement to interact with numerous partners within the receptor-proximal signalling complex. In such regulatory hubs, intrinsically disordered regions facilitate promiscuous high specificity, low affinity interactions with multiple different partners to enable the rapid assembly and dissociation of signalling complexes and hence the dynamic propagation and termination of signals. In the case of RIP1 this predicted disorder has since been experimentally demonstrated to have significant functionality (Li *et al.*, 2012). RIP1 and RIP3 contain RIP homotypic interaction motifs (RHIMs) located in long regions of intrinsic disorder that upon hyperphosphorylation mediate the assembly of RIP1/3 into heterodimeric amyloid-like filamentous structures that drive programmed necrosis. IKK α and IKK β were also predicted to contain ~ 25% and 40% disordered regions, respectively (Xue *et al.*, 2014). In both cases, their C-terminal NEMO-binding domains are located in regions of intrinsic disorder. Indeed, these regions have eluded structural determination via X-ray crystallography (Xu *et al.*, 2011). As such, there is potentially conformational flexibility both at the interaction site between IKK subunits and NEMO, and between NEMO and IkB α , the interaction site for which is located in the ZNF at the flexible C-terminus of NEMO. Such conformationally heterogeneous points of contact within the IKK complex may be important in facilitating the higher-order elongated NEMO lattice structures that have been proposed to facilitate proximity-based trans-autophosphorylation and cooperative activation of NF- κ B signalling (Scholefield *et al.*, 2016).

In addition, the sequestration of intrinsically disordered, PEST motif-containing regions as a mechanism of control over ubiquitin-independent proteasomal degradation is also already an established concept of regulation within

the NF-κB pathway. The IκB α protein possesses significant regions of intrinsic disorder (Croy *et al.*, 2004; Truhlar *et al.*, 2006). Of the six ankyrin repeats (AR) within IκB α , the last two AR(5-6) are within a C-terminal intrinsically disordered region that also contains a PEST motif (Mathes *et al.*, 2008). Similar to the putative PEST motif identified in NEMO (Chapter 4, Figure 4.10F), this PEST motif is located within a flexible polyproline II helix (Mathes *et al.*, 2010). This disordered region has been shown to be important in a switch between degradation mechanisms of IκB α (Mathes *et al.*, 2008; Fortmann *et al.*, 2015). The AR(5-6) region undergoes coupled folding and binding when IκB α is in a complex with NF-κB subunits (such as p65), which contributes to the high affinity and slow dissociation rate of IκB α bound to NF-κB (Bergqvist *et al.*, 2006). Under these conditions, the half-life of NF-κB-bound IκB α is long; approximately 12 hours (O'Dea *et al.*, 2007). The characteristics of this interaction ensure that NF-κB subunits are tightly sequestered within the cytoplasm and the NF-κB pathway exhibits low basal activity. Only upon stimulus-induced ubiquitin-dependent proteasomal degradation of the IκB α subunit, mediated by an IKK-dependent phosphorylation within the N-terminal signal response element of IκB α , are NF-κB subunits able to accumulate in the nucleus (Scherer *et al.*, 1995). However, the mechanism of degradation is switched for free IκB α . When IκB α is free from NF-κB the AR(5-6) PEST motif degron is unmasked, becomes intrinsically disordered, and subsequently targets the protein for rapid signal- and ubiquitin-independent proteasomal degradation (Mathes *et al.*, 2008; Mathes *et al.*, 2010). Similar to NEMO, unbound IκB α is readily degraded in vitro by the 20S proteasome, while interaction with p65 inhibits this degradation (Alvarez-Castelao and Castaño 2005). The result is that free IκB α has a half-life of 10 minutes in the cell (O'Dea *et al.*, 2007). This short half-life contributes to maintain low cellular levels of IκB α , which is essential for robust activation of NF-κB; mutations that enhance the order of this region or disrupt the PEST motif increase the half-life of free IκB α and disrupt the function of the NF-κB pathway (Mathes *et al.*, 2008; Truhlar *et al.*, 2008; Bergqvist *et al.*, 2009; Dembinski *et al.*, 2014). The disordered C-terminal region of newly synthesised IκB α has also been proposed to facilitate the 'stripping' of p65 from the DNA to terminate the NF-κB signalling response (Bergqvist *et al.* 2009).

Binding-induced folding of disordered regions in p65 have also been proposed to contribute to the high affinity of p65 for IκB α and to the sequestration of p65 in the cytoplasm. Thermodynamic studies suggest that the p65-IκB α interaction has an extremely low dissociation rate and a high affinity, such that the complex is highly stable (Bergqvist *et al.*, 2006). The p65 NLS has been shown to be essential for this high affinity interaction. NMR studies have shown that the p65 NLS is intrinsically disordered in the absence of IκB α and folds upon binding to IκB α to generate significant favourable binding energy (Cervantes *et al.*, 2011). Furthermore, this induced-folding sequesters the NLS from recognition by Importin α , and thus inhibits nuclear translocation.

The rapid 20S-proteasome-dependent turnover of IκB α that is not bound by NF-κB ensures the minimisation of excess IκB α in the cell, such that the levels of IκB α are tightly correlated to the levels of its main interaction partner, NF-κB. This has been proposed to facilitate rapid and robust signal responsiveness. Similar principles may apply to the interaction between NEMO and the IKK kinase subunits. Rapid degradation of 'IKK-free'-NEMO may ensure that the protein levels of NEMO closely match those of its key interaction partners and prevent accumulation of excess NEMO, which could have deleterious consequences given its promiscuous binding interactions. Indeed, we and others have shown that overexpression of NEMO acts in a dominant negative manner to inhibit NF-κB signalling (Chapter 4, Figure 4.13A).

7.4 Future directions

In addition to those mentioned throughout the previous results chapters, there are a range of planned future experiments that would build upon the observations presented within this thesis. For example, the generation of various stable IKK re-expressing cell lines using the IKK α / β DKO cells as a background will provide an additional valuable set of tools with which to dissect IKK functions. This includes WT, KD and NEMO-binding-domain mutant IKK α and IKK β expressing cell lines. Such cell lines could help confirm the involvement of IKK interaction in the stabilisation of NEMO and enable a finer dissection of the relative contributions of IKK α and IKK β to the phosphorylation of NF- κ B subunits as well as NF- κ B-independent substrates. We are also highly interested in acquiring IKK α -selective inhibitors to complement the highly selective IKK β inhibitor, BIX02514, in the characterisation of the respective functions of IKK α and IKK β in NF- κ B signalling. Our KO cell lines would provide an optimal setting to validate the selectivity of candidate IKK α inhibitors and to characterise *in vivo* potency and mechanism of action.

The main area of future work will be in the additional analysis and validation of the large RNA sequencing data set described in Chapter 6. Time constraints prevented the full utilisation and extraction of biologically relevant information from this data set. Additional qRT-PCRs will be performed to validate potentially novel NF- κ B-dependent genes, and genes that show a selective dependence on IKK α or IKK β activity for robust expression. ChIP experiments will be performed to confirm the presence of NF- κ B binding sites within novel candidate target genes, such as USP43. A larger-scale ChIP-Seq experiment using the IKK KO clones to identify genome-wide IKK-dependent – κ B sites in promoters/enancers may also be highly informative. Future work will also focus on characterising the apparent effects of IKK β deficiency on the expression of genes involved in chromatin and cytoskeletal organisation, cell cycle control and DNA damage. Many of the gene expression changes associated with IKK β KO were consistent with a DNA damage/senescence response. This will be investigated through the characterisation of DNA damage and senescence markers. The upregulation of genes involved in extracellular exosome secretion was also interesting in the context of this senescence-like expression profile. The secretion profile of IKK DKO cells could be measured to further investigate this.

Another area of future work will be in the characterisation of the mechanism through which the IKK kinases protect NEMO from proteasomal degradation. Efforts will be directed towards defining the relative importance of ubiquitin-dependent or ubiquitin-independent proteasomal degradation of NEMO in the absence of the IKKs. This could be investigated by examining the half-life of NEMO mutants that are defective for known ubiquitination sites. Furthermore, knockdown of the N2 subunit of the 19S regulatory cap, which mediates the delivery of most polyubiquitinated substrates to the 26S proteasome core, has been used to propose that p21^{CIP1} is degraded in an ATP- and ubiquitin-independent manner *in vivo*; one of the few intrinsically disordered proteins for which this has been demonstrated (Chen *et al.*, 2007). A similar approach could be taken to investigate the mechanism of NEMO degradation. In the case of p21^{CIP1} and a number of other intrinsically disordered proteins the 11S family proteasomal activator REGy has been proposed to facilitate ATP- and ubiquitin-independent degradation by the 20S core proteasome (Li *et al.*, 2006; Chen *et al.*, 2007). Interestingly, REGy has been reported to be overexpressed in colorectal cancer and the level of overexpression correlates with severity of colitis-associated cancer (CAC) (Roessler *et al.*, 2006; Xu *et al.*, 2016). Furthermore, REGy deficient mice exhibited

reduced intestinal inflammation, production of cytokines/chemokines and tumourigenesis in a mouse CAC model (Xu *et al.*, 2016). REGy knockout was proposed to attenuate inflammation as a result of inhibition of NF- κ B signalling due to the decreased REGy-mediated ubiquitin-independent degradation of I κ B ϵ . It would be worthwhile exploring the involvement of REGy in the degradation of NEMO.

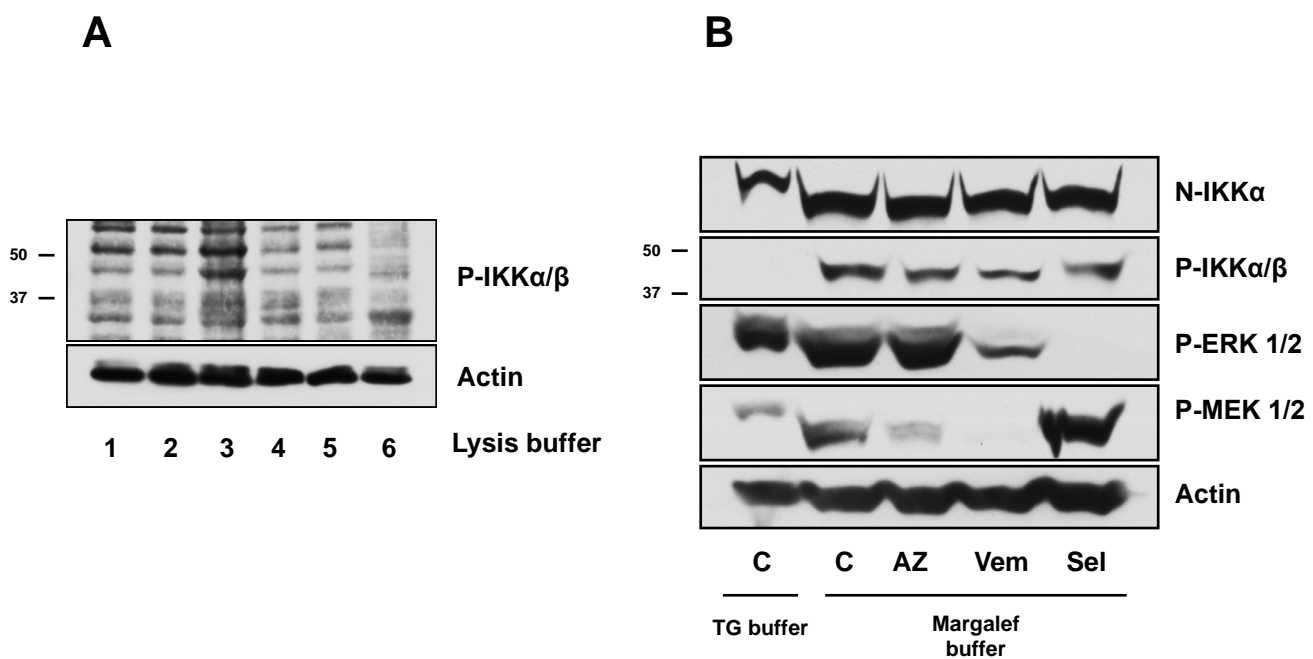
It will also be important to define the regions within NEMO that confer rapid proteasomal turnover. The disordered N-terminal region and/or the putative PEST motif-containing region would be the most logical sequences to probe initially. We will also need to investigate the ability of NEMO to fold properly in the absence of IKK interaction partners. Proteasomal targeting of misfolded NEMO protein shortly after protein synthesis could explain the lower steady state NEMO levels in IKK KO cells.

In terms of large scale future experiments, these well-validated IKK KO cell lines would be well-suited to the global quantitation of IKK α - and IKK β -specific phosphorylation sites using phosphopeptide mass spectrometry. This could potentially identify novel NF- κ B-independent functions of the IKK kinases. Additional WT and KO clones with reduced clonal heterogeneity would perhaps need to be validated prior to undertaking such experiments in order to improve the sensitivity of detection. Furthermore, mouse xenograft studies could be used to determine the requirement of IKK α and/or IKK β for *in vivo* growth of these KRAS-driven tumour cells.

7.5 Conclusions

The functions of the IKKs has been the subject of interest research since their characterisation in 1999. It is testament to the complexity of the NF- κ B signalling pathways that we were able to elucidate novel aspects of IKK α and IKK β function using CRISPR-Cas9 gene editing and small molecule inhibition approaches almost 20 years after their discovery. We report the generation, validation and characterisation of the first human CRISPR-Cas9 IKK KO cell lines. Using these cell lines we have demonstrated that small molecule inhibitors of IKK β have the potential to exhibit a common off-target selectivity profile and raised questions about the validity of reports utilising one of these widely-used commercially available inhibitors. We have uncovered a novel role for the IKKs in stabilising NEMO and preventing its rapid proteasomal degradation. Finally, we have performed a comprehensive analysis of the relative contributions of IKK α and IKK β in the canonical NF- κ B signalling response to pro-inflammatory cytokines and concluded that IKK α plays a considerably more significant role at multiple steps in the pathway than suggested from studies in mice. This work should refocus attention towards IKK α as a potential therapeutic target in colorectal cancer.

Supplementary Figures



Supplementary Figure S1. Phosphorylated p45-IKK α was only detectable using high Na₃VO₄ buffer. (A) HT29 cells were seeded for 24 hours in normal growth medium, then lysed in a range of different lysis buffers. 1 = TG lysis buffer. 2 = TG lysis buffer + cOmplete phosphatase inhibitors. 3 = Margalef lysis buffer w/ 100 mM Na₃VO₄. 4 = Margalef lysis buffer w/ 1 mM Na₃VO₄. 5 = Margalef lysis buffer with Tris buffer and 1 mM Na₃VO₄. 6 = RIPA buffer + cOmplete phosphatase inhibitors. (B) HT29 cells were seeded for 24 hours in normal growth medium then treated with DMSO vector control (C) or 2 μ M AZ628 (pan-RAF inhibitor), 3 μ M Vemurafenib (BRAF inhibitor) or 3.5 μ M Selumetinib (MEK 1/2 inhibitor) for 3 hours, then lysed in the indicated lysis buffers. Lysates were fractionated by SDS-PAGE and Western blotted with the indicated antibodies.

References

References

- Abba, M.C., Hu, Y., Sun, H., Drake, J.A., Gaddis, S., Baggerly, K., Sahin, A., and Aldaz, C.M. (2005). Gene expression signature of estrogen receptor α status in breast cancer. *BMC Genomics* 6, 37.
- Abdel-Latif, M.M.M., Kelleher, D., and Reynolds, J.V. (2015). Molecular mechanisms of constitutive and inducible NF-kappaB activation in oesophageal adenocarcinoma. *European Journal of Cancer* 51, 464-472.
- Acosta, J.C., O'Loghlen, A., Banito, A., Guijarro, M.V., Augert, A., Raguz, S., Fumagalli, M., Da Costa, M., Brown, C., Popov, N., et al. (2008). Chemokine Signaling via the CXCR2 Receptor Reinforces Senescence. *Cell* 133, 1006-1018.
- Adams, K.W., and Cooper, G.M. (2007). Rapid turnover of mcl-1 couples translation to cell survival and apoptosis. *The Journal of biological chemistry* 282, 6192-6200.
- Adli, M., Merkhofer, E., Cogswell, P., and Baldwin, A.S. (2010). IKKalpha and IKKbeta each function to regulate NF-kappaB activation in the TNF-induced/canonical pathway. *PloS one* 5, e9428.
- Adzhubei, A.A., Sternberg, M.J., and Makarov, A.A. (2013). Polyproline-II helix in proteins: structure and function. *J Mol Biol* 425, 2100-2132.
- Aggarwal, B.B. (2003). Signalling pathways of the TNF superfamily: a double-edged sword. *Nat Rev Immunol* 3, 745-756.
- Agou, F., Courtois, G., Chiaravalli, J., Baleux, F., Coic, Y.M., Traincard, F., Israel, A., and Veron, M. (2004). Inhibition of NF-kappa B activation by peptides targeting NF-kappa B essential modulator (nemo) oligomerization. *The Journal of biological chemistry* 279, 54248-54257.
- Akoulitchev, S., and Reinberg, D. (1998). The molecular mechanism of mitotic inhibition of TFIIH is mediated by phosphorylation of CDK7. *Genes Dev* 12, 3541-3550.
- Alard, A., Fabre, B., Anesia, R., Marboeuf, C., Pierre, P., Susini, C., Bousquet, C., and Pyronnet, S. (2010). NAD(P)H Quinone-Oxydoreductase 1 Protects Eukaryotic Translation Initiation Factor 4GI from Degradation by the Proteasome. *Molecular and Cellular Biology* 30, 1097-1105.
- Alessi, D.R., Andjelkovic, M., Caudwell, B., Cron, P., Morrice, N., Cohen, P., and Hemmings, B.A. (1996). Mechanism of activation of protein kinase B by insulin and IGF-1. *Embo j* 15, 6541-6551.
- Alkalay, I., Yaron, A., Hatzubai, A., Orian, A., Ciechanover, A., and Ben-Neriah, Y. (1995). Stimulation-dependent I kappa B alpha phosphorylation marks the NF-kappa B inhibitor for degradation via the ubiquitin-proteasome pathway. *Proceedings of the National Academy of Sciences* 92, 10599-10603.
- Allen, I.C., Wilson, J.E., Schneider, M., Lich, J.D., Roberts, R.A., Arthur, J.C., Woodford, R.M., Davis, B.K., Uronis, J.M., Herfarth, H.H., et al. (2012). NLRP12 suppresses colon inflammation and tumorigenesis through the negative regulation of noncanonical NF-kappaB signaling. *Immunity* 36, 742-754.
- Alt, J.R., Cleveland, J.L., Hannink, M., and Diehl, J.A. (2000). Phosphorylation-dependent regulation of cyclin D1 nuclear export and cyclin D1-dependent cellular transformation. *Genes Dev* 14, 3102-3114.
- Alvarez-Castelao, B., and Castaño, J.G. (2005). Mechanism of direct degradation of IkBa by 20S proteasome. *FEBS Letters* 579, 4797-4802.
- Ammirante, M., Luo, J.L., Grivennikov, S., Nedospasov, S., and Karin, M. (2010). B-cell-derived lymphotoxin promotes castration-resistant prostate cancer. *Nature* 464, 302-305.
- Ammirante, M., Rosati, A., Arra, C., Basile, A., Falco, A., Festa, M., Pascale, M., d'Avenia, M., Marzullo, L., Belisario, M.A., et al. (2010). IKK γ protein is a target of BAG3 regulatory activity in human tumor growth. *Proceedings of the National Academy of Sciences* 107, 7497-7502.
- Andela, V.B., Schwarz, E.M., O'Keefe, R.J., Puzas, E.J., Rosenblatt, J.D., and Rosier, R.N. (2005). A genome-wide expression profile and system-level integration of nuclear factor kappa B regulated genes reveals fundamental metabolic adaptations during cell growth and survival. *FEBS Lett* 579, 6814-6820.
- Anderson, E.M., Birmingham, A., Baskerville, S., Reynolds, A., Maksimova, E., Leake, D., Fedorov, Y., Karpilow, J., and Khvorova, A. (2008). Experimental validation of the importance of seed complement frequency to siRNA specificity. *Rna* 14, 853-861.
- Anest, V., Hanson, J.L., Cogswell, P.C., Steinbrecher, K.A., Strahl, B.D., and Baldwin, A.S. (2003). A nucleosomal function for IkappaB kinase-alpha in NF-kappaB-dependent gene expression. *Nature* 423, 659-663.
- Annunziata, C.M., Davis, R.E., Demchenko, Y., Bellamy, W., Gabrea, A., Zhan, F., Lenz, G., Hanamura, I., Wright, G., Xiao, W., et al. (2007). Frequent engagement of the classical and alternative NF-kappaB pathways by diverse genetic abnormalities in multiple myeloma. *Cancer Cell* 12, 115-130.
- Anthony, N.G., Baiget, J., Beretta, G., Boyd, M., Breen, D., Edwards, J., Gamble, C., Gray, A.I., Harvey, A.L., Hatzieremia, S., et al. (2017). Inhibitory Kappa B Kinase α (IKK α) Inhibitors That Recapitulate Their Selectivity in Cells against Isoform-Related Biomarkers. *Journal of medicinal chemistry* 60, 7043-7066.

- Antonaki, A., Demetriadis, C., Polyzos, A., Banos, A., Vatsellas, G., Lavigne, M.D., Apostolou, E., Mantouvalou, E., Papadopoulou, D., Mosialos, G., et al. (2011). Genomic Analysis Reveals a Novel Nuclear Factor- κ B (NF- κ B)-binding Site in Alu-repetitive Elements. *Journal of Biological Chemistry* 286, 38768-38782.
- Arabi, A., Ullah, K., Branca, R.M., Johansson, J., Bandarra, D., Haneklaus, M., Fu, J., Aries, I., Nilsson, P., Den Boer, M.L., et al. (2012). Proteomic screen reveals Fbw7 as a modulator of the NF- κ appaB pathway. *Nat Commun* 3, 976.
- Arenzana-Seisdedos, F., Turpin, P., Rodriguez, M., Thomas, D., Hay, R.T., Virelizier, J.L., and Dargemont, C. (1997). Nuclear localization of I kappa B alpha promotes active transport of NF- κ appa B from the nucleus to the cytoplasm. *J Cell Sci* 110 (Pt 3), 369-378.
- Ashall, L., Horton, C.A., Nelson, D.E., Paszek, P., Harper, C.V., Sillitoe, K., Ryan, S., Spiller, D.G., Unitt, J.F., Broomhead, D.S., et al. (2009). Pulsatile stimulation determines timing and specificity of NF- κ appaB-dependent transcription. *Science* 324, 242-246.
- Ashburner, B.P., Westerheide, S.D., and Baldwin, A.S. (2001). The p65 (RelA) Subunit of NF- κ B Interacts with the Histone Deacetylase (HDAC) Corepressors HDAC1 and HDAC2 To Negatively Regulate Gene Expression. *Molecular and Cellular Biology* 21, 7065-7077.
- Asher, G., Lotem, J., Sachs, L., Kahana, C., and Shaul, Y. (2002). Mdm-2 and ubiquitin-independent p53 proteasomal degradation regulated by NQO1. *Proceedings of the National Academy of Sciences* 99, 13125-13130.
- Asher, G., Tsvetkov, P., Kahana, C., and Shaul, Y. (2005). A mechanism of ubiquitin-independent proteasomal degradation of the tumor suppressors p53 and p73. *Genes & development* 19, 316-321.
- Ashkenazi, A., and Dixit, V.M. (1998). Death receptors: signaling and modulation. *Science* 281, 1305-1308.
- Auphan, N., DiDonato, J.A., Rosette, C., Helmburg, A., and Karin, M. (1995). Immunosuppression by glucocorticoids: inhibition of NF- κ appaB activity through induction of IkappaB synthesis. *Science* 270, 286.
- Authier, H., Billot, K., Derudder, E., Bordereaux, D., Rivière, P., Rodrigues-Ferreira, S., Nahmias, C., and Baud, V. (2014). IKK phosphorylates RelB to modulate its promoter specificity and promote fibroblast migration downstream of TNF receptors. *Proceedings of the National Academy of Sciences of the United States of America* 111, 14794-14799.
- Babu, M.M., van der Lee, R., de Groot, N.S., and Gsponer, J. (2011). Intrinsically disordered proteins: regulation and disease. *Current opinion in structural biology* 21, 432-440.
- Baens, M., Noels, H., Broeckx, V., Hagens, S., Fevery, S., Billiau, A.D., Vankelecom, H., and Marynen, P. (2006). The Dark Side of EGFP: Defective Polyubiquitination. *PloS one* 1, e54.
- Bagneris, C., Ageichik, A.V., Cronin, N., Wallace, B., Collins, M., Boshoff, C., Waksman, G., and Barrett, T. (2008). Crystal structure of a vFlip-IKKgamma complex: insights into viral activation of the IKK signalosome. *Molecular cell* 30, 620-631.
- Bagneris, C., Rogala, K.B., Baratchian, M., Zamfir, V., Kunze, M.B., Dagless, S., Pirker, K.F., Collins, M.K., Hall, B.A., Barrett, T.E., et al. (2015). Probing the Solution Structure of IkappaB Kinase (IKK) Subunit gamma and Its Interaction with Kaposi Sarcoma-associated Herpes Virus Flice-interacting Protein and IKK Subunit beta by EPR Spectroscopy. *The Journal of biological chemistry* 290, 16539-16549.
- Baldi, L., Brown, K., Franzoso, G., and Siebenlist, U. (1996). Critical role for lysines 21 and 22 in signal-induced, ubiquitin-mediated proteolysis of I kappa B-alpha. *The Journal of biological chemistry* 271, 376-379.
- Baldwin, A.S., Jr. (1996). The NF- κ appa B and I kappa B proteins: new discoveries and insights. *Annu Rev Immunol* 14, 649-683.
- Balkwill, F., and Mantovani, A. (2001). Inflammation and cancer: back to Virchow? *Lancet (London, England)* 357, 539-545.
- Ballard, D.W., Walker, W.H., Doerre, S., Sista, P., Molitor, J.A., Dixon, E.P., Peffer, N.J., Hannink, M., and Greene, W.C. (1990). The v-rel oncogene encodes a kappa B enhancer binding protein that inhibits NF- κ appa B function. *Cell* 63, 803-814.
- Banerjee, T., Nath, S., and Roychoudhury, S. (2009). DNA damage induced p53 downregulates Cdc20 by direct binding to its promoter causing chromatin remodeling. *Nucleic Acids Res* 37, 2688-2698.
- Bang, D., Wilson, W., Ryan, M., Yeh, J.J., and Baldwin, A.S. (2013). GSK-3 alpha Promotes Oncogenic KRAS Function in Pancreatic Cancer via TAK1-TAB Stabilization and Regulation of Noncanonical NF- κ appa B. *Cancer Discovery* 3, 690-703.
- Barbie, D.A., Tamayo, P., Boehm, J.S., Kim, S.Y., Moody, S.E., Dunn, I.F., Schinzel, A.C., Sandy, P., Meylan, E., Scholl, C., et al. (2009). Systematic RNA interference reveals that oncogenic KRAS-driven cancers require TBK1. *Nature* 462, 108-112.
- Bartek, J., and Lukas, J. (2001). Pathways governing G1/S transition and their response to DNA damage. *FEBS Letters* 490, 117-122.

- Basak, S., Kim, H., Kearns, J.D., Tergaonkar, V., O'Dea, E., Werner, S.L., Benedict, C.A., Ware, C.F., Ghosh, G., Verma, I.M., et al. (2007). A fourth IkappaB protein within the NF-kappaB signaling module. *Cell* 128, 369-381.
- Basseres, D.S., Ebbs, A., Levantini, E., and Baldwin, A.S. (2010). Requirement of the NF-kappaB subunit p65/RelA for K-Ras-induced lung tumorigenesis. *Cancer Res* 70, 3537-3546.
- Basso, A.D., Solit, D.B., Chiosis, G., Giri, B., Tsichlis, P., and Rosen, N. (2002). Akt forms an intracellular complex with heat shock protein 90 (Hsp90) and Cdc37 and is destabilized by inhibitors of Hsp90 function. *The Journal of biological chemistry* 277, 39858-39866.
- Battula, V.L., Nguyen, K., Sun, J., Pitner, M.K., Yuan, B., Bartholomeusz, C., Hail, N., and Andreeff, M. (2017). IKK inhibition by BMS-345541 suppresses breast tumorigenesis and metastases by targeting GD2+ cancer stem cells. *Oncotarget* 8, 36936-36949.
- Baud, V., Liu, Z.G., Bennett, B., Suzuki, N., Xia, Y., and Karin, M. (1999). Signaling by proinflammatory cytokines: oligomerization of TRAF2 and TRAF6 is sufficient for JNK and IKK activation and target gene induction via an amino-terminal effector domain. *Genes Dev* 13, 1297-1308.
- Baud, V., and Collares, D. (2016). Post-Translational Modifications of RelB NF-kappaB Subunit and Associated Functions. *Cells* 5.
- Baugh, J.M., Viktorova, E.G., and Pilipenko, E.V. (2009). Proteasomes Can Degrade a Significant Proportion of Cellular Proteins Independent of Ubiquitination. *Journal of Molecular Biology* 386, 814-827.
- Bednarski, B.K., Ding, X., Coombe, K., Baldwin, A.S., and Kim, H.J. (2008). Active Roles for IKK α and IKK β in NF- κ B-mediated Chemoresistance to Doxorubicin. *Molecular cancer therapeutics* 7, 1827-1835.
- Beg, A.A., Ruben, S.M., Scheinman, R.I., Haskill, S., Rosen, C.A., and Baldwin, A.S., Jr. (1992). I kappa B interacts with the nuclear localization sequences of the subunits of NF-kappa B: a mechanism for cytoplasmic retention. *Genes Dev* 6, 1899-1913.
- Beg, A.A., Finco, T.S., Nantermet, P.V., and Baldwin, A.S., Jr. (1993). Tumor necrosis factor and interleukin-1 lead to phosphorylation and loss of I kappa B alpha: a mechanism for NF-kappa B activation. *Mol Cell Biol* 13, 3301-3310.
- Beg, A.A., Sha, W.C., Bronson, R.T., Ghosh, S., and Baltimore, D. (1995). Embryonic lethality and liver degeneration in mice lacking the RelA component of NF-kappa B. *Nature* 376, 167-170.
- Beg, A.A., and Baltimore, D. (1996). An essential role for NF-kappaB in preventing TNF-alpha-induced cell death. *Science* 274, 782-784.
- Belle, A., Tanay, A., Bitincka, L., Shamir, R., and O'Shea, E.K. (2006). Quantification of protein half-lives in the budding yeast proteome. *Proceedings of the National Academy of Sciences of the United States of America* 103, 13004-13009.
- Ben-Neriah, Y., and Karin, M. (2011). Inflammation meets cancer, with NF-[kappa]B as the matchmaker. *Nat Immunol* 12, 715-723.
- Bergqvist, S., Croy, C.H., Kjaergaard, M., Huxford, T., Ghosh, G., and Komives, E.A. (2006). Thermodynamics reveal that helix four in the NLS of NF- κ B p65 anchors IkB α , forming a very stable complex. *Journal of molecular biology* 360, 421-434.
- Bergqvist, S., Alverdi, V., Mengel, B., Hoffmann, A., Ghosh, G., and Komives, E.A. (2009). Kinetic enhancement of NF- κ B-DNA dissociation by IkB α . *Proceedings of the National Academy of Sciences* 106, 19328-19333.
- Bertrand, M.J., Milutinovic, S., Dickson, K.M., Ho, W.C., Boudreault, A., Durkin, J., Gillard, J.W., Jaquith, J.B., Morris, S.J., and Barker, P.A. (2008). cIAP1 and cIAP2 facilitate cancer cell survival by functioning as E3 ligases that promote RIP1 ubiquitination. *Molecular cell* 30, 689-700.
- Bettermann, K., Vucur, M., Haybaeck, J., Koppe, C., Janssen, J., Heymann, F., Weber, A., Weiskirchen, R., Liedtke, C., Gassler, N., et al. (2010). TAK1 Suppresses a NEMO-Dependent but NF- κ B-Independent Pathway to Liver Cancer. *Cancer Cell* 17, 481-496.
- Beyette, J.R., Hubbell, T., and Monaco, J.J. (2001). Purification of 20S proteasomes. *Methods in molecular biology* (Clifton, NJ) 156, 1-16.
- Bhat-Nakshatri, P., Sweeney, C.J., and Nakshatri, H. (2002). Identification of signal transduction pathways involved in constitutive NF-kappaB activation in breast cancer cells. *Oncogene* 21, 2066-2078.
- Birbach, A., Gold, P., Binder, B.R., Hofer, E., de Martin, R., and Schmid, J.A. (2002). Signaling Molecules of the NF- κ B Pathway Shuttle Constitutively between Cytoplasm and Nucleus. *Journal of Biological Chemistry* 277, 10842-10851.
- Birmingham, A., Anderson, E.M., Reynolds, A., Ilsley-Tyree, D., Leake, D., Fedorov, Y., Baskerville, S., Maksimova, E., Robinson, K., Karpilow, J., et al. (2006). 3' UTR seed matches, but not overall identity, are associated with RNAi off-targets. *Nat Methods* 3, 199-204.
- Black, R.A., Rauch, C.T., Kozlosky, C.J., Peschon, J.J., Slack, J.L., Wolfson, M.F., Castner, B.J., Stocking, K.L., Reddy, P., Srinivasan, S., et al. (1997). A metalloproteinase disintegrin that releases tumour-necrosis factor-alpha from cells. *Nature* 385, 729-733.

- Blazkova, H., von Schubert, C., Mikule, K., Schwab, R., Anglker, N., Schmuckli-Maurer, J., Fernandez, P.C., Doxsey, S., and Dobbelaere, D.A. (2007). The IKK inhibitor BMS-345541 affects multiple mitotic cell cycle transitions. *Cell Cycle* 6, 2531-2540.
- Bloor, S. (2008). Signal processing by its coil zipper domain activates IKK γ . *Proc Natl Acad Sci USA* 105, 1279-1284.
- Boldin, M.P., Varfolomeev, E.E., Pancer, Z., Mett, I.L., Camonis, J.H., and Wallach, D. (1995). A novel protein that interacts with the death domain of Fas/APO1 contains a sequence motif related to the death domain. *Journal of Biological Chemistry* 270, 7795-7798.
- Bonizzi, G., Bebien, M., Otero, D.C., Johnson-Vroom, K.E., Cao, Y., Vu, D., Jegga, A.G., Aronow, B.J., Ghosh, G., Rickert, R.C., et al. (2004). Activation of IKK α target genes depends on recognition of specific kB binding sites by RelB:p52 dimers. *The EMBO Journal* 23, 4202-4210.
- Bours, V., Franzoso, G., Azarenko, V., Park, S., Kanno, T., Brown, K., and Siebenlist, U. (1993). The oncoprotein Bcl-3 directly transactivates through kappa B motifs via association with DNA-binding p50B homodimers. *Cell* 72, 729-739.
- Boyd, M.T., Vlatkovic, N., and Rubbi, C.P. (2011). The nucleolus directly regulates p53 export and degradation. *J Cell Biol* 194, 689-703.
- Brabletz, T., Jung, A., Reu, S., Porzner, M., Hlubek, F., Kunz-Schughart, L.A., Knuechel, R., and Kirchner, T. (2001). Variable beta-catenin expression in colorectal cancers indicates tumor progression driven by the tumor environment. *Proc Natl Acad Sci U S A* 98, 10356-10361.
- Bregman, D.B., Halaban, R., van Gool, A.J., Henning, K.A., Friedberg, E.C., and Warren, S.L. (1996). UV-induced ubiquitination of RNA polymerase II: a novel modification deficient in Cockayne syndrome cells. *Proc Natl Acad Sci U S A* 93, 11586-11590.
- Brion, J.P., Flament-Durand, J., and Dustin, P. (1986). Alzheimer's disease and tau proteins. *Lancet* (London, England) 2, 1098.
- Broemer, M., Krappmann, D., and Scheidereit, C. (2004). Requirement of Hsp90 activity for IkappaB kinase (IKK) biosynthesis and for constitutive and inducible IKK and NF-kappaB activation. *Oncogene* 23, 5378-5386.
- Brown, K., Gerstberger, S., Carlson, L., Franzoso, G., and Siebenlist, U. (1995). Control of I kappa B-alpha proteolysis by site-specific, signal-induced phosphorylation. *Science* 267, 1485-1488.
- Brown, R.T., Ades, I.Z., and Nordan, R.P. (1995). An acute phase response factor/NF-kappa B site downstream of the junB gene that mediates responsiveness to interleukin-6 in a murine plasmacytoma. *The Journal of biological chemistry* 270, 31129-31135.
- Bunting, K., Rao, S., Hardy, K., Woltring, D., Denyer, G.S., Wang, J., Gerondakis, S., and Shannon, M.F. (2007). Genome-wide analysis of gene expression in T cells to identify targets of the NF-kappa B transcription factor c-Rel. *J Immunol* 178, 7097-7109.
- Bunz, F., Dutriaux, A., Lengauer, C., Waldman, T., Zhou, S., Brown, J.P., Sedivy, J.M., Kinzler, K.W., and Vogelstein, B. (1998). Requirement for p53 and p21 to Sustain G₂ Arrest After DNA Damage. *Science* 282, 1497-1501.
- Burger, K., Muhl, B., Harasim, T., Rohrmoser, M., Malamoussi, A., Orban, M., Kellner, M., Gruber-Eber, A., Kremmer, E., Holzel, M., et al. (2010). Chemotherapeutic drugs inhibit ribosome biogenesis at various levels. *The Journal of biological chemistry* 285, 12416-12425.
- Burke, J.R., Pattoli, M.A., Gregor, K.R., Brassil, P.J., MacMaster, J.F., McIntyre, K.W., Yang, X., Iotzova, V.S., Clarke, W., Strnad, J., et al. (2003). BMS-345541 is a highly selective inhibitor of I kappa B kinase that binds at an allosteric site of the enzyme and blocks NF-kappa B-dependent transcription in mice. *The Journal of biological chemistry* 278, 1450-1456.
- Buss, H., Dorrie, A., Schmitz, M.L., Frank, R., Livingstone, M., Resch, K., and Kracht, M. (2004). Phosphorylation of serine 468 by GSK-3beta negatively regulates basal p65 NF-kappaB activity. *The Journal of biological chemistry* 279, 49571-49574.
- Cao, Y., Bonizzi, G., Seagroves, T.N., Greten, F.R., Johnson, R., Schmidt, E.V., and Karin, M. (2001). IKK α provides an essential link between RANK signaling and cyclin D1 expression during mammary gland development. *Cell* 107, 763-775.
- Carpentier, I., and Beyaert, R. (1999). TRAF1 is a TNF inducible regulator of NF- κ B activation. *FEBS Letters* 460, 246-250.
- Carswell, E.A., Old, L.J., Kassel, R.L., Green, S., Fiore, N., and Williamson, B. (1975). An endotoxin-induced serum factor that causes necrosis of tumors. *Proc Natl Acad Sci U S A* 72, 3666-3670.
- Carter, R.S., Pennington, K.N., Ungurait, B.J., and Ballard, D.W. (2003). In vivo identification of inducible phosphoacceptors in the IKK γ /NEMO subunit of human IkappaB kinase. *The Journal of biological chemistry* 278, 19642-19648.

- Catici, D.A.M., Horne, J.E., Cooper, G.E., and Pudney, C.R. (2015). Polyubiquitin Drives the Molecular Interactions of the NF- κ B Essential Modulator (NEMO) by Allosteric Regulation. *The Journal of biological chemistry* **290**, 14130-14139.
- Catici, D.A., Amos, H.E., Yang, Y., van den Elsen, J.M., and Pudney, C.R. (2016). The red edge excitation shift phenomenon can be used to unmask protein structural ensembles: implications for NEMO-ubiquitin interactions. *Febs j* **283**, 2272-2284.
- Cervantes, C.F., Bergqvist, S., Kjaergaard, M., Kroon, G., Sue, S.-C., Dyson, H.J., and Komives, E.A. (2011). The RelA nuclear localization signal folds upon binding to I κ B α . *Journal of molecular biology* **405**, 754-764.
- Chaisson, M.L., Brooking, J.T., Ladiges, W., Tsai, S., and Fausto, N. (2002). Hepatocyte-specific inhibition of NF- κ B leads to apoptosis after TNF treatment, but not after partial hepatectomy. *J Clin Invest* **110**, 193-202.
- Chan, H., Bartos, D.P., and Owen-Schaub, L.B. (1999). Activation-dependent transcriptional regulation of the human Fas promoter requires NF- κ B p50-p65 recruitment. *Mol Cell Biol* **19**, 2098-2108.
- Chao, S.H., and Price, D.H. (2001). Flavopiridol inactivates P-TEFb and blocks most RNA polymerase II transcription in vivo. *The Journal of biological chemistry* **276**.
- Chaturvedi, M.M., Sung, B., Yadav, V.R., Kannappan, R., and Aggarwal, B.B. (2011). NF- κ B addiction and its role in cancer: 'one size does not fit all'. *Oncogene* **30**, 1615-1630.
- Chen, F., Demers, L.M., Vallyathan, V., Ding, M., Lu, Y., Castranova, V., and Shi, X. (1999). Vanadate Induction of NF- κ B Involves I κ B Kinase β and SAPK/ERK Kinase 1 in Macrophages. *Journal of Biological Chemistry* **274**, 20307-20312.
- Chen, G., Cao, P., and Goeddel, D.V. (2002). TNF-induced recruitment and activation of the IKK complex require Cdc37 and Hsp90. *Molecular cell* **9**, 401-410.
- Chen, L.F., Williams, S.A., Mu, Y., Nakano, H., Duerr, J.M., Buckbinder, L., and Greene, W.C. (2005). NF- κ B RelA phosphorylation regulates RelA acetylation. *Mol Cell Biol* **25**, 7966-7975.
- Chen, X., Barton, L.F., Chi, Y., Clurman, B.E., and Roberts, J.M. (2007). Ubiquitin-Independent Degradation of Cell-Cycle Inhibitors by the REGy Proteasome. *Molecular cell* **26**, 843-852.
- Chen, P.Y., Weinmann, L., Gaidatzis, D., Pei, Y., Zavolan, M., Tuschl, T., and Meister, G. (2008). Strand-specific 5'-O-methylation of siRNA duplexes controls guide strand selection and targeting specificity. *Rna* **14**, 263-274.
- Chen, R., Wierda, W.G., Chubb, S., Hawtin, R.E., Fox, J.A., Keating, M.J., Gandhi, V., and Plunkett, W. (2009). Mechanism of action of SNS-032, a novel cyclin-dependent kinase inhibitor, in chronic lymphocytic leukemia. *Blood* **113**, 4637-4645.
- Chen, L., Peng, Z., Meng, Q., Mongan, M., Wang, J., Sartor, M., Chen, J., Niu, L., Medvedovic, M., Kao, W., et al. (2016). Loss of I κ B kinase β promotes myofibroblast transformation and senescence through activation of the ROS-TGF β autocrine loop. *Protein & Cell* **7**, 338-350.
- Cheng, J.D., Ryseck, R.P., Attar, R.M., Dambach, D., and Bravo, R. (1998). Functional redundancy of the nuclear factor kappa B inhibitors I kappa B alpha and I kappa B beta. *J Exp Med* **188**, 1055-1062.
- Cheong, R., Rhee, A., Wang, C.J., Nemenman, I., and Levchenko, A. (2011). Information Transduction Capacity of Noisy Biochemical Signaling Networks. *Science* **334**, 354-358.
- Cherry, A.D., and Piantadosi, C.A. (2015). Regulation of mitochondrial biogenesis and its intersection with inflammatory responses. *Antioxidants & redox signaling* **22**, 965-976.
- Chien, Y., Kim, S., Bumeister, R., Loo, Y.-M., Kwon, S.W., Johnson, C.L., Balakireva, M.G., Romeo, Y., Kopelovich, L., Gale, M., et al. (2006). RalB GTPase-Mediated Activation of the I κ B Family Kinase TBK1 Couples Innate Immune Signaling to Tumor Cell Survival. *Cell* **127**, 157-170.
- Chiu, C.F., Chang, Y.W., Kuo, K.T., Shen, Y.S., Liu, C.Y., Yu, Y.H., Cheng, C.C., Lee, K.Y., Chen, F.C., Hsu, M.K., et al. (2016). NF- κ B-driven suppression of FOXO3a contributes to EGFR mutation-independent gefitinib resistance. *Proc Natl Acad Sci U S A* **113**, E2526-2535.
- Choudhary, S., Kalita, M., Fang, L., Patel, K.V., Tian, B., Zhao, Y., Edeh, C.B., and Brasier, A.R. (2013). Inducible tumor necrosis factor (TNF) receptor-associated factor-1 expression couples the canonical to the non-canonical NF- κ B pathway in TNF stimulation. *The Journal of biological chemistry* **288**, 14612-14623.
- Christian, F., Smith, E.L., and Carmody, R.J. (2016). The Regulation of NF- κ B Subunits by Phosphorylation. *Cells* **5**.
- Chua, H.L., Bhat-Nakshatri, P., Clare, S.E., Morimiya, A., Badve, S., and Nakshatri, H. (2007). NF- κ B represses E-cadherin expression and enhances epithelial to mesenchymal transition of mammary epithelial cells: potential involvement of ZEB-1 and ZEB-2. *Oncogene* **26**, 711-724.
- Ciechanover, A., and Stenhill, A. (2014). The complexity of recognition of ubiquitinated substrates by the 26S proteasome. *Biochimica et Biophysica Acta (BBA) - Molecular Cell Research* **1843**, 86-96.
- Cildir, G., Low, K.C., and Tergaonkar, V. (2016). Noncanonical NF- κ B Signaling in Health and Disease. *Trends in Molecular Medicine* **22**, 414-429.

- Clark, K., Peggie, M., Plater, L., Sorcek, R.J., Young, E.R., Madwed, J.B., Hough, J., McIver, E.G., and Cohen, P. (2011). Novel cross-talk within the IKK family controls innate immunity. *The Biochemical journal* 434, 93-104.
- Claudio, E., Brown, K., Park, S., Wang, H., and Siebenlist, U. (2002). BAFF-induced NEMO-independent processing of NF-kappa B2 in maturing B cells. *Nat Immunol* 3, 958-965.
- Cohen, S., Achbert-Weiner, H., and Ciechanover, A. (2004). Dual effects of IkappaB kinase beta-mediated phosphorylation on p105: Fate: SCF(beta-TrCP)-dependent degradation and SCF(beta-TrCP)-independent processing. *Mol Cell Biol* 24, 475-486.
- Colleran, A., Ryan, A., O'Gorman, A., Mureau, C., Liptrot, C., Dockery, P., Fearnhead, H., and Egan, L.J. (2011). Autophagosomal IkappaB alpha degradation plays a role in the long term control of tumor necrosis factor-alpha-induced nuclear factor-kappaB (NF-kappaB) activity. *The Journal of biological chemistry* 286, 22886-22893.
- Colleran, A., Ryan, A., O'Gorman, A., Mureau, C., Liptrot, C., Dockery, P., Fearnhead, H., and Egan, L.J. (2011). Autophagosomal IkB α Degradation Plays a Role in the Long Term Control of Tumor Necrosis Factor- α -induced Nuclear Factor- κ B (NF- κ B) Activity. *Journal of Biological Chemistry* 286, 22886-22893.
- Colotta, F., Allavena, P., Sica, A., Garlanda, C., and Mantovani, A. (2009). Cancer-related inflammation, the seventh hallmark of cancer: links to genetic instability. *Carcinogenesis* 30, 1073-1081.
- Compagno, M., Lim, W.K., Grunn, A., Nandula, S.V., Brahmachary, M., Shen, Q., Bertoni, F., Ponzoni, M., Scandurra, M., Califano, A., et al. (2009). Mutations of multiple genes cause deregulation of NF-kappaB in diffuse large B-cell lymphoma. *Nature* 459, 717-721.
- Conroy, A., Stockett, D.E., Walker, D., Arkin, M.R., Hoch, U., Fox, J.A., and Hawtin, R.E. (2009). SNS-032 is a potent and selective CDK 2, 7 and 9 inhibitor that drives target modulation in patient samples. *Cancer chemotherapy and pharmacology* 64, 723-732.
- Cordier, F., Vinolo, E., Veron, M., Delepierre, M., and Agou, F. (2008). Solution structure of NEMO zinc finger and impact of an anhidrotic ectodermal dysplasia with immunodeficiency-related point mutation. *J Mol Biol* 377, 1419-1432.
- Cordier, F., Grubisha, O., Traincard, F., Veron, M., Delepierre, M., and Agou, F. (2009). The zinc finger of NEMO is a functional ubiquitin-binding domain. *The Journal of biological chemistry* 284, 2902-2907.
- Cortese, M.S., Uversky, V.N., and Dunker, A.K. (2008). Intrinsic disorder in scaffold proteins: getting more from less. *Progress in biophysics and molecular biology* 98, 85-106.
- Cosimo, E., McCaig, A.M., Carter-Brezinski, L.J., Whealon, H., Leach, M.T., Le Ster, K., Berthou, C., Durieu, E., Oumata, N., Galons, H., et al. (2013). Inhibition of NF-kappaB-mediated signaling by the cyclin-dependent kinase inhibitor CR8 overcomes prosurvival stimuli to induce apoptosis in chronic lymphocytic leukemia cells. *Clinical cancer research : an official journal of the American Association for Cancer Research* 19, 2393-2405.
- Courtois, G., and Gilmore, T.D. (2006). Mutations in the NF-kappaB signaling pathway: implications for human disease. *Oncogene* 25, 6831-6843.
- Coussens, L.M., and Werb, Z. (2002). Inflammation and cancer. *Nature* 420, 860.
- Cross, D.A., Alessi, D.R., Cohen, P., Andjelkovich, M., and Hemmings, B.A. (1995). Inhibition of glycogen synthase kinase-3 by insulin mediated by protein kinase B. *Nature* 378, 785.
- Croy, C.H., Bergqvist, S., Huxford, T., Ghosh, G., and Komives, E.A. (2004). Biophysical characterization of the free IkappaBalphrepeat domain in solution. *Protein Sci* 13, 1767-1777.
- Dajee, M., Lazarov, M., Zhang, J.Y., Cai, T., Green, C.L., Russell, A.J., Marinkovich, M.P., Tao, S., Lin, Q., Kubo, Y., et al. (2003). NF-kappaB blockade and oncogenic Ras trigger invasive human epidermal neoplasia. *Nature* 421, 639-643.
- Davis, R.E., Brown, K.D., Siebenlist, U., and Staudt, L.M. (2001). Constitutive nuclear factor kappaB activity is required for survival of activated B cell-like diffuse large B cell lymphoma cells. *J Exp Med* 194, 1861-1874.
- Davis, M., Hatzubai, A., Andersen, J.S., Ben-Shushan, E., Fisher, G.Z., Yaron, A., Bauskin, A., Mercurio, F., Mann, M., and Ben-Neriah, Y. (2002). Pseudosubstrate regulation of the SCF(beta-TrCP) ubiquitin ligase by hnRNP-U. *Genes Dev* 16, 439-451.
- Davis, M.I., Hunt, J.P., Herrgard, S., Ciceri, P., Wodicka, L.M., Pallares, G., Hocker, M., Treiber, D.K., and Zarrinkar, P.P. (2011). Comprehensive analysis of kinase inhibitor selectivity. *Nat Biotech* 29, 1046-1051.
- de Leon-Boenig, G., Bowman, K.K., Feng, J.A., Crawford, T., Everett, C., Franke, Y., Oh, A., Stanley, M., Staben, S.T., Starovasnik, M.A., et al. (2012). The crystal structure of the catalytic domain of the NF-kappaB inducing kinase reveals a narrow but flexible active site. *Structure* 20, 1704-1714.
- De Simone, V., Franzè, E., Ronchetti, G., Colantoni, A., Fantini, M.C., Di Fusco, D., Sica, G.S., Sileri, P., MacDonald, T.T., Pallone, F., et al. (2015). Th17-type cytokines, IL-6 and TNF-alpha synergistically activate STAT3 and NF- κ B to promote colorectal cancer cell growth. *Oncogene* 34, 3493-3503.

- de Wit, H., Dokter, W.H., Koopmans, S.B., Lummen, C., van der Leij, M., Smit, J.W., and Vellenga, E. (1998). Regulation of p100 (NFKB2) expression in human monocytes in response to inflammatory mediators and lymphokines. *Leukemia* 12, 363-370.
- Dejardin, E., Deregowski, V., Chapelier, M., Jacobs, N., Gielen, J., Merville, M.P., and Bours, V. (1999). Regulation of NF-kappaB activity by I kappaB-related proteins in adenocarcinoma cells. *Oncogene* 18, 2567-2577.
- Dejardin, E., Droin, N.M., Delhase, M., Haas, E., Cao, Y., Makris, C., Li, Z.W., Karin, M., Ware, C.F., and Green, D.R. (2002). The lymphotoxin-beta receptor induces different patterns of gene expression via two NF-kappaB pathways. *Immunity* 17, 525-535.
- Dembinski, H., Wismer, K., Balasubramaniam, D., Alverdi, V., Iakoucheva, L.M., and Komives, E.A. (2014). Predicted disorder-to-order transition mutations in IkBa disrupt function. *Physical chemistry chemical physics* : PCCP 16, 6480-6485.
- Demchenko, Y.N., Glebov, O.K., Zingone, A., Keats, J.J., Bergsagel, P.L., and Kuehl, W.M. (2010). Classical and/or alternative NF- κ B pathway activation in multiple myeloma. *Blood* 115, 3541-3552.
- Deng, Y., Ren, X., Yang, L., Lin, Y., and Wu, X. (2003). A JNK-dependent pathway is required for TNFalpha-induced apoptosis. *Cell* 115, 61-70.
- Dennis, K.L., Wang, Y., Blatner, N.R., Wang, S., Saadalla, A., Trudeau, E., Roers, A., Weaver, C.T., Lee, J.J., Gilbert, J.A., et al. (2013). Adenomatous polyps are driven by microbe-instigated focal inflammation and are controlled by IL-10-producing T cells. *Cancer Res* 73, 5905-5913.
- Derijard, B., Raingeaud, J., Barrett, T., Wu, I.H., Han, J., Ulevitch, R.J., and Davis, R.J. (1995). Independent human MAP-kinase signal transduction pathways defined by MEK and MKK isoforms. *Science* 267, 682-685.
- Derudder, E., Dejardin, E., Pritchard, L.L., Green, D.R., Korner, M., and Baud, V. (2003). RelB/p50 dimers are differentially regulated by tumor necrosis factor-alpha and lymphotoxin-beta receptor activation: critical roles for p100. *The Journal of biological chemistry* 278, 23278-23284.
- Devin, A., Cook, A., Lin, Y., Rodriguez, Y., Kelliher, M., and Liu, Z. (2000). The distinct roles of TRAF2 and RIP in IKK activation by TNF-R1: TRAF2 recruits IKK to TNF-R1 while RIP mediates IKK activation. *Immunity* 12, 419-429.
- DiDonato, J.A., Hayakawa, M., Rothwarf, D.M., Zandi, E., and Karin, M. (1997). A cytokine-responsive IkappaB kinase that activates the transcription factor NF-kappaB. *Nature* 388, 548.
- DiDonato, J.A., Mercurio, F., and Karin, M. (2012). NF-kappaB and the link between inflammation and cancer. *Immunol Rev* 246, 379-400.
- Diehl, J.A., Cheng, M., Roussel, M.F., and Sherr, C.J. (1998). Glycogen synthase kinase-3beta regulates cyclin D1 proteolysis and subcellular localization. *Genes Dev* 12, 3499-3511.
- Dinkova-Kostova, A.T., and Talalay, P. (2010). NAD(P)H:quinone acceptor oxidoreductase 1 (NQO1), a multifunctional antioxidant enzyme and exceptionally versatile cytoprotector. *Archives of biochemistry and biophysics* 501, 116-123.
- Disfani, F.M., Hsu, W.L., Mizianty, M.J., Oldfield, C.J., Xue, B., Dunker, A.K., Uversky, V.N., and Kurgan, L. (2012). MoRFpred, a computational tool for sequence-based prediction and characterization of short disorder-to-order transitioning binding regions in proteins. *Bioinformatics* 28, i75-83.
- Dixit, V.M., Green, S., Sarma, V., Holzman, L.B., Wolf, F.W., O'Rourke, K., Ward, P.A., Prochownik, E.V., and Marks, R.M. (1990). Tumor necrosis factor-alpha induction of novel gene products in human endothelial cells including a macrophage-specific chemotaxin. *The Journal of biological chemistry* 265, 2973-2978.
- Djuricovic, S., Hartmann, M.D., Habeck, M., Ursinus, A., Zwickl, P., Martin, J., Lupas, A.N., and Zeth, K. (2009). Structure and activity of the N-terminal substrate recognition domains in proteasomal ATPases. *Molecular cell* 34, 580-590.
- Dobrzanski, P., Ryseck, R.P., and Bravo, R. (1993). Both N- and C-terminal domains of RelB are required for full transactivation: role of the N-terminal leucine zipper-like motif. *Mol Cell Biol* 13, 1572-1582.
- Dobrzanski, P., Ryseck, R.P., and Bravo, R. (1994). Differential interactions of Rel-NF-kappa B complexes with I kappa B alpha determine pools of constitutive and inducible NF-kappa B activity. *The EMBO Journal* 13, 4608-4616.
- Doffinger, R. (2001). X-linked anhidrotic ectodermal dysplasia with immunodeficiency is caused by impaired NF-[kappa]B signaling. *Nature Genet* 27, 277-285.
- Dong, J., Phelps, R.G., Qiao, R., Yao, S., Benard, O., Ronai, Z., and Aaronson, S.A. (2003). BRAF oncogenic mutations correlate with progression rather than initiation of human melanoma. *Cancer Res* 63, 3883-3885.
- Dong, J., Jimi, E., Zhong, H., Hayden, M.S., and Ghosh, S. (2008). Repression of gene expression by unphosphorylated NF- κ B p65 through epigenetic mechanisms. *Genes & Development* 22, 1159-1173.
- Dosztanyi, Z., Csizmok, V., Tompa, P., and Simon, I. (2005). The pairwise energy content estimated from amino acid composition discriminates between folded and intrinsically unstructured proteins. *J Mol Biol* 347, 827-839.

- Dosztányi, Z., Mészáros, B., and Simon, I. (2009). ANCHOR: web server for predicting protein binding regions in disordered proteins. *Bioinformatics* 25, 2745-2746.
- Douillette, A., Bibeau-Poirier, A., Gravel, S.P., Clement, J.F., Chenard, V., Moreau, P., and Servant, M.J. (2006). The proinflammatory actions of angiotensin II are dependent on p65 phosphorylation by the IkappaB kinase complex. *The Journal of biological chemistry* 281, 13275-13284.
- Drew, D., Shimada, E., Huynh, K., Bergqvist, S., Talwar, R., Karin, M., and Ghosh, G. (2007). Inhibitor κB Kinase β Binding by Inhibitor κB Kinase γ. *Biochemistry* 46, 12482-12490.
- Du, C., Fang, M., Li, Y., Li, L., and Wang, X. (2000). Smac, a mitochondrial protein that promotes cytochrome c-dependent caspase activation by eliminating IAP inhibition. *Cell* 102, 33-42.
- Du, Z., Whitt, M.A., Baumann, J., Garner, J.M., Morton, C.L., Davidoff, A.M., and Pfeffer, L.M. (2012). Inhibition of type I interferon-mediated antiviral action in human glioma cells by the IKK inhibitors BMS-345541 and TPCA-1. *Journal of interferon & cytokine research : the official journal of the International Society for Interferon and Cytokine Research* 32, 368-377.
- Duan, Z., Zhang, J., Choy, E., Harmon, D., Liu, X., Nielsen, P., Mankin, H., Gray, N.S., and Hor nicek, F.J. (2012). Systematic kinome shRNA screening identifies CDK11 (PITSLRE) kinase expression is critical for osteosarcoma cell growth and proliferation. *Clinical cancer research : an official journal of the American Association for Cancer Research* 18, 4580-4588.
- Dunn, W.A. (2003). Pathways of mammalian protein degradation. *New Comprehensive Biochemistry* 38, 513-533.
- Duran, A., Linares, J.F., Galvez, A.S., Wikenheiser, K., Flores, J.M., Diaz-Meco, M.T., and Moscat, J. (2008). The Signaling Adaptor p62 Is an Important NF-κB Mediator in Tumorigenesis. *Cancer Cell* 13, 343-354.
- Dyne, J.N., Goncharov, T., Dueber, E.C., Fedorova, A.V., Izrael-Tomasevic, A., Phu, L., Helgason, E., Fairbrother, W.J., Deshayes, K., Kirkpatrick, D.S., et al. (2010). c-IAP1 and UbcH5 promote K11-linked polyubiquitination of RIP1 in TNF signalling. *Embo j* 29, 4198-4209.
- Ea, C.K., Deng, L., Xia, Z.P., Pineda, G., and Chen, Z.J. (2006). Activation of IKK by TNF[alpha] requires site-specific ubiquitination of RIP1 and polyubiquitin binding by NEMO. *Mol Cell* 22, 245-257.
- Ea, C.-K., Deng, L., Xia, Z.-P., Pineda, G., and Chen, Z.J. (2006). Activation of IKK by TNFα Requires Site-Specific Ubiquitination of RIP1 and Polyubiquitin Binding by NEMO. *Molecular cell* 22, 245-257.
- Ear, T., Cloutier, A., and McDonald, P.P. (2005). Constitutive Nuclear Expression of the IκB Kinase Complex and Its Activation in Human Neutrophils. *The Journal of Immunology* 175, 1834-1842.
- el-Deiry, W.S. (1998). Regulation of p53 downstream genes. *Seminars in cancer biology* 8, 345-357.
- Elsharkawy, A.M., Oakley, F., Lin, F., Packham, G., Mann, D.A., and Mann, J. (2010). The NF-κB p50:p50:HDAC-1 repressor complex orchestrates transcriptional inhibition of multiple proinflammatory genes. *J Hepatol* 53, 519-527.
- Emmerich, C.H., Ordureau, A., Strickson, S., Arthur, J.S.C., Pedrioli, P.G.A., Komander, D., and Cohen, P. (2013). Activation of the canonical IKK complex by K63/M1-linked hybrid ubiquitin chains. *Proceedings of the National Academy of Sciences* 110, 15247-15252.
- Emmerich, C.H., and Cohen, P. (2015). Optimising methods for the preservation, capture and identification of ubiquitin chains and ubiquitylated proteins by immunoblotting. *Biochemical and biophysical research communications* 466, 1-14.
- Enesa, K., Zakkar, M., Chaudhury, H., Luong, L.A., Rawlinson, L., Mason, J.C., Haskard, D.O., Dean, J.L.E., and Evans, P.C. (2008). NF-κB Suppression by the Deubiquitinating Enzyme Cezanne: A NOVEL NEGATIVE FEEDBACK LOOP IN PRO-INFLAMMATORY SIGNALING. *Journal of Biological Chemistry* 283, 7036-7045.
- Eraly, S.A. (2014). Striking Differences between Knockout and Wild-Type Mice in Global Gene Expression Variability. *PloS one* 9, e97734.
- Ernst, M.K., Dunn, L.L., and Rice, N.R. (1995). The PEST-like sequence of I kappa B alpha is responsible for inhibition of DNA binding but not for cytoplasmic retention of c-Rel or RelA homodimers. *Mol Cell Biol* 15, 872-882.
- Eto, A., Muta, T., Yamazaki, S., and Takeshige, K. (2003). Essential roles for NF-κB and a Toll/IL-1 receptor domain-specific signal (s) in the induction of IκB-ζ. *Biochemical and biophysical research communications* 301, 495-501.
- Evans, T., Rosenthal, E.T., Youngblom, J., Distel, D., and Hunt, T. (1983). Cyclin: a protein specified by maternal mRNA in sea urchin eggs that is destroyed at each cleavage division. *Cell* 33, 389-396.
- Fan, C.-M., and Maniatis, T. (1991). Generation of p50 subunit of NF-κB by processing of p105 through an ATP-dependent pathway. *Nature* 354, 395-398.
- Fedorov, Y., Anderson, E.M., Birmingham, A., Reynolds, A., Karpilow, J., Robinson, K., Leake, D., Marshall, W.S., and Khvorova, A. (2006). Off-target effects by siRNA can induce toxic phenotype. *RNA* 12, 1188-1196.
- Fenner, B.J., Scannell, M., and Prehn, J.H.M. (2010). Expanding the Substantial Interactome of NEMO Using Protein Microarrays. *PloS one* 5, e8799.

- Feoktistova, M., Geserick, P., Kellert, B., Dimitrova, Diana P., Langlais, C., Hupe, M., Cain, K., MacFarlane, M., Häcker, G., and Leverkus, M. (2011). cIAPs Block Ripoptosome Formation, a RIP1/Caspase-8 Containing Intracellular Cell Death Complex Differentially Regulated by cFLIP Isoforms. *Molecular cell* 43, 449-463.
- Fernandez-Majada, V., Aguilera, C., Villanueva, A., Vilardell, F., Robert-Moreno, A., Aytes, A., Real, F.X., Capella, G., Mayo, M.W., Espinosa, L., et al. (2007). Nuclear IKK activity leads to dysregulated notch-dependent gene expression in colorectal cancer. *Proc Natl Acad Sci USA* 104,
- Finco, T.S., and Baldwin, A.S. (1993). Kappa B site-dependent induction of gene expression by diverse inducers of nuclear factor kappa B requires Raf-1. *Journal of Biological Chemistry* 268, 17676-17679.
- Fishbain, S., Inobe, T., Israeli, E., Chavali, S., Yu, H., Kago, G., Babu, M.M., and Matouschek, A. (2015). Sequence composition of disordered regions fine-tunes protein half-life. *Nat Struct Mol Biol* 22, 214-221.
- Flatt, P.M., Tang, L.J., Scatena, C.D., Szak, S.T., and Pietenpol, J.A. (2000). p53 Regulation of G(2) Checkpoint Is Retinoblastoma Protein Dependent. *Molecular and Cellular Biology* 20, 4210-4223.
- Fliss, P.M., Jowers, T.P., Brinkmann, M.M., Holstermann, B., Mack, C., Dickinson, P., Hohenberg, H., Ghazal, P., and Brune, W. (2012). Viral Mediated Redirection of NEMO/IKK γ to Autophagosomes Curtails the Inflammatory Cascade. *PLoS pathogens* 8, e1002517.
- Fong, A., and Sun, S.C. (2002). Genetic evidence for the essential role of beta-transducin repeat-containing protein in the inducible processing of NF-kappa B2/p100. *The Journal of biological chemistry* 277, 22111-22114.
- Fontan, E., Traincard, F., Levy, S.G., Yamaoka, S., Veron, M., and Agou, F. (2007). NEMO oligomerization in the dynamic assembly of the IkappaB kinase core complex. *Febs j* 274, 2540-2551.
- Fortmann, K.T., Lewis, R.D., Ngo, K.A., Fagerlund, R., and Hoffmann, A. (2015). A regulated, ubiquitin-independent degron in IkBa. *Journal of molecular biology* 427, 2748-2756.
- Franzoso, G., Bours, V., Park, S., Tomita-Yamaguchi, M., Kelly, K., and Siebenlist, U. (1992). The candidate oncoprotein Bcl-3 is an antagonist of p50/NF-kappa B-mediated inhibition. *Nature* 359, 339-342.
- Fujimoto, K., Yasuda, H., Sato, Y., and Yamamoto, K. (1995). A role for phosphorylation in the proteolytic processing of the human NF-kappa B1 precursor. *Gene* 165, 183-189.
- Fujita, H., Rahighi, S., Akita, M., Kato, R., Sasaki, Y., Wakatsuki, S., and Iwai, K. (2014). Mechanism Underlying IKB Kinase Activation Mediated by the Linear Ubiquitin Chain Assembly Complex. *Molecular and Cellular Biology* 34, 1322-1335.
- Fusco, A.J., Savinova, O.V., Talwar, R., Kearns, J.D., Hoffmann, A., and Ghosh, G. (2008). Stabilization of RelB requires multidomain interactions with p100/p52. *The Journal of biological chemistry* 283, 12324-12332.
- Gamble, C., McIntosh, K., Scott, R., Ho, K.H., Plevin, R., and Paul, A. (2012). Inhibitory kappa B kinases as targets for pharmacological regulation. *British Journal of Pharmacology* 165, 802-819.
- Gardam, S., Turner, V.M., Anderton, H., Limaye, S., Basten, A., Koentgen, F., Vaux, D.L., Silke, J., and Brink, R. (2011). Deletion of cIAP1 and cIAP2 in murine B lymphocytes constitutively activates cell survival pathways and inactivates the germinal center response. *Blood* 117, 4041-4051.
- Garner, J.M., Fan, M., Yang, C.H., Du, Z., Sims, M., Davidoff, A.M., and Pfeffer, L.M. (2013). Constitutive activation of signal transducer and activator of transcription 3 (STAT3) and nuclear factor kappaB signaling in glioblastoma cancer stem cells regulates the Notch pathway. *The Journal of biological chemistry* 288, 26167-26176.
- Gautheron, J., Pescatore, A., Fusco, F., Esposito, E., Yamaoka, S., Agou, F., Ursini, M.V., and Courtois, G. (2010). Identification of a new NEMO/TRAF6 interface affected in incontinentia pigmenti pathology. *Hum Mol Genet* 19, 3138-3149.
- Geng, H., Wittwer, T., Dittrich-Breiholz, O., Kracht, M., and Schmitz, M.L. (2009). Phosphorylation of NF-kappaB p65 at Ser468 controls its COMMD1-dependent ubiquitination and target gene-specific proteasomal elimination. *EMBO Rep* 10, 381-386.
- Genovese, M.C., Cohen, S., Moreland, L., Liim, D., Robbins, S., Newmark, R., and Bekker, P. (2004). Combination therapy with etanercept and anakinra in the treatment of patients with rheumatoid arthritis who have been treated unsuccessfully with methotrexate. *Arthritis Rheum* 50, 1412-1419.
- Gentle, I.E., Wong, W.W., Evans, J.M., Bankovacki, A., Cook, W.D., Khan, N.R., Nachbur, U., Rickard, J., Anderton, H., Moulin, M., et al. (2011). In TNF-stimulated cells, RIPK1 promotes cell survival by stabilizing TRAF2 and cIAP1, which limits induction of non-canonical NF-kappaB and activation of caspase-8. *The Journal of biological chemistry* 286, 13282-13291.
- Gerlach, B., Cordier, S.M., Schmukle, A.C., Emmerich, C.H., Rieser, E., Haas, T.L., Webb, A.I., Rickard, J.A., Anderton, H., Wong, W.W., et al. (2011). Linear ubiquitination prevents inflammation and regulates immune signalling. *Nature* 471, 591-596.
- Gerondakis, S., and Siebenlist, U. (2010). Roles of the NF- κ B Pathway in Lymphocyte Development and Function. *Cold Spring Harbor Perspectives in Biology* 2, a000182.

- Gervasi, M., Bianchi-Smiraglia, A., Cummings, M., Zheng, Q., Wang, D., Liu, S., and Bakin, A.V. (2012). JunB contributes to Id2 repression and the epithelial-mesenchymal transition in response to transforming growth factor-beta. *J Cell Biol* **196**, 589-603.
- Ghalwash, M.F., Dunker, A.K., and Obradovic, Z. (2012). Uncertainty analysis in protein disorder prediction. *Mol Biosyst* **8**, 381-391.
- Gibbons, D.L., and Spencer, J. (2011). Mouse and human intestinal immunity: same ballpark, different players; different rules, same score. *Mucosal Immunol* **4**, 148-157.
- Gil-Araujo, B., Toledo Lobo, M.V., Gutierrez-Salmeron, M., Gutierrez-Pitalua, J., Ropero, S., Angulo, J.C., Chiloeches, A., and Lasa, M. (2014). Dual specificity phosphatase 1 expression inversely correlates with NF-kappaB activity and expression in prostate cancer and promotes apoptosis through a p38 MAPK dependent mechanism. *Mol Oncol* **8**, 27-38.
- Gilmore, T.D., and Herscovitch, M. (2006). Inhibitors of NF-kappaB signaling: 785 and counting. *Oncogene* **25**, 6887-6899.
- Godderz, D., Schafer, E., Palanimurugan, R., and Dohmen, R.J. (2011). The N-terminal unstructured domain of yeast ODC functions as a transplantable and replaceable ubiquitin-independent degron. *J Mol Biol* **407**, 354-367.
- Godwin, P., Baird, A.M., Heavey, S., Barr, M.P., O'Byrne, K.J., and Gately, K. (2013). Targeting Nuclear Factor-Kappa B to Overcome Resistance to Chemotherapy. *Frontiers in Oncology* **3**, 120.
- Goldman, E.H., Chen, L., and Fu, H. (2004). Activation of Apoptosis Signal-regulating Kinase 1 by Reactive Oxygen Species through Dephosphorylation at Serine 967 and 14-3-3 Dissociation. *Journal of Biological Chemistry* **279**, 10442-10449.
- Gong, J., Cai, C., Liu, X., Ku, X., Jiang, H., Gao, D., and Li, H. (2013). ChemMapper: a versatile web server for exploring pharmacology and chemical structure association based on molecular 3D similarity method. *Bioinformatics* **29**, 1827-1829.
- Gordon, A., Hart, P.A., and Young, M. (1980). Ammonia inhibits phagosome–lysosome fusion in macrophages. *Nature* **286**, 79-80.
- Goudeau, B., Huetz, F., Samson, S., Di Santo, J.P., Cumano, A., Beg, A., Israël, A., and Mémet, S. (2003). IκB α /IκB ϵ deficiency reveals that a critical NF-κB dosage is required for lymphocyte survival. *Proceedings of the National Academy of Sciences* **100**, 15800-15805.
- Gray, C.M., Remouchamps, C., McCorkell, K.A., Solt, L.A., Dejardin, E., Orange, J.S., and May, M.J. (2014). Noncanonical NF-kappaB signaling is limited by classical NF-kappaB activity. *Sci Signal* **7**, ra13.
- Grech, A.P., Amesbury, M., Chan, T., Gardam, S., Basten, A., and Brink, R. (2004). TRAF2 differentially regulates the canonical and noncanonical pathways of NF-κB activation in mature B cells. *Immunity* **21**, 629-642.
- Greten, F.R., Weber, C.K., Greten, T.F., Schneider, G., Wagner, M., Adler, G., and Schmid, R.M. (2002). Stat3 and NF-κB activation prevents apoptosis in pancreatic carcinogenesis. *Gastroenterology* **123**, 2052-2063.
- Greten, F.R., Weber, C.K., Greten, T.F., Schneider, G., Wagner, M., Adler, G., and Schmid, R.M. (2002). Stat3 and NF-kappaB activation prevents apoptosis in pancreatic carcinogenesis. *Gastroenterology* **123**, 2052-2063.
- Greten, F.R., Eckmann, L., Greten, T.F., Park, J.M., Li, Z.-W., Egan, L.J., Kagnoff, M.F., and Karin, M. (2004). IKK β Links Inflammation and Tumorigenesis in a Mouse Model of Colitis-Associated Cancer. *Cell* **118**, 285-296.
- Greten, F.R., Arkan, M.C., Bollrath, J., Hsu, L.C., Goode, J., Miething, C., Goktuna, S.I., Neuenhahn, M., Fierer, J., Paxian, S., et al. (2007). NF-kappaB is a negative regulator of IL-1beta secretion as revealed by genetic and pharmacological inhibition of IKKbeta. *Cell* **130**, 918-931.
- Grimm, S., Bauer, M.K., Baeuerle, P.A., and Schulze-Osthoff, K. (1996). Bcl-2 down-regulates the activity of transcription factor NF-kappaB induced upon apoptosis. *The Journal of cell biology* **134**, 13-23.
- Grivennikov, S., Karin, E., Terzic, J., Mucida, D., Yu, G.Y., Vallabhapurapu, S., Scheller, J., Rose-John, S., Cheroutre, H., Eckmann, L., et al. (2009). IL-6 and Stat3 are required for survival of intestinal epithelial cells and development of colitis-associated cancer. *Cancer Cell* **15**, 103-113.
- Grivennikov, S.I., Greten, F.R., and Karin, M. (2010). Immunity, inflammation, and cancer. *Cell* **140**, 883-899.
- Grivennikov, S.I., Wang, K., Mucida, D., Stewart, C.A., Schnabl, B., Jauch, D., Taniguchi, K., Yu, G.-Y., Osterreicher, C.H., Hung, K.E., et al. (2012). Adenoma-linked barrier defects and microbial products drive IL-23/IL-17-mediated tumour growth. *Nature* **491**, 254-258.
- Grollman, A.P. (1968). Inhibitors of protein biosynthesis. V. Effects of emetine on protein and nucleic acid biosynthesis in HeLa cells. *The Journal of biological chemistry* **243**, 4089-4094.
- Gsponer, J., Futschik, M.E., Teichmann, S.A., and Babu, M.M. (2008). Tight regulation of unstructured proteins: from transcript synthesis to protein degradation. *Science* **322**, 1365-1368.

- Guharoy, M., Bhowmick, P., Sallam, M., and Tompa, P. (2016). Tripartite degrons confer diversity and specificity on regulated protein degradation in the ubiquitin-proteasome system. *Nature Communications* 7, 10239.
- Guharoy, M., Bhowmick, P., and Tompa, P. (2016). Design principles involving protein disorder facilitate specific substrate selection and degradation by the ubiquitin-proteasome system. *Journal of Biological Chemistry*.
- Guinney, J., Dienstmann, R., Wang, X., de Reynies, A., Schlicker, A., Soneson, C., Marisa, L., Roepman, P., Nyamundanda, G., Angelino, P., et al. (2015). The consensus molecular subtypes of colorectal cancer. *Nat Med* 21, 1350-1356.
- Guo, B., Audu, C.O., Cochran, J.C., Mierke, D.F., and Pellegrini, M. (2014). Protein Engineering of the N-Terminus of NEMO: Structure Stabilization and Rescue of IKK β Binding. *Biochemistry* 53, 6776-6785.
- Guo, Y., Zhao, S., Sheng, Q., Guo, M., Lehmann, B., Pietenpol, J., Samuels, D.C., and Shyr, Y. (2015). RNAseq by Total RNA Library Identifies Additional RNAs Compared to Poly(A) RNA Library. *Biomed Res Int* 2015, 862130.
- Gupta, S.C., Sundaram, C., Reuter, S., and Aggarwal, B.B. (2010). Inhibiting NF- κ B Activation by Small Molecules As a Therapeutic Strategy. *Biochimica et biophysica acta* 1799, 775-787.
- Gustin, J.A., Ozes, O.N., Akca, H., Pincheira, R., Mayo, L.D., Li, Q., Guzman, J.R., Korgaonkar, C.K., and Donner, D.B. (2004). Cell type-specific expression of the IkappaB kinases determines the significance of phosphatidylinositol 3-kinase/Akt signaling to NF- κ B activation. *The Journal of biological chemistry* 279, 1615-1620.
- Guttridge, D.C., Albanese, C., Reuther, J.Y., Pestell, R.G., and Baldwin, A.S. (1999). NF- κ B controls cell growth and differentiation through transcriptional regulation of cyclin D1. *Molecular and cellular biology* 19, 5785-5799.
- Ha, S.-W., Ju, D., and Xie, Y. (2012). The N-terminal domain of Rpn4 serves as a portable ubiquitin-independent degron and is recognized by specific 19S RP subunits. *Biochemical and biophysical research communications* 419, 226-231.
- Haas, T.L., Emmerich, C.H., Gerlach, B., Schmukle, A.C., Cordier, S.M., Rieser, E., Feltham, R., Vince, J., Warnken, U., Wenger, T., et al. (2009). Recruitment of the Linear Ubiquitin Chain Assembly Complex Stabilizes the TNF-R1 Signaling Complex and Is Required for TNF-Mediated Gene Induction. *Molecular cell* 36, 831-844.
- Haber, D.A., and Settleman, J. (2007). Cancer: drivers and passengers. *Nature* 446, 145-146.
- Häcker, H., and Karin, M. (2006). Regulation and Function of IKK and IKK-Related Kinases. *Science's STKE* 2006, re13-re13.
- Hagemann, T., Lawrence, T., McNeish, I., Charles, K.A., Kulbe, H., Thompson, R.G., Robinson, S.C., and Balkwill, F.R. (2008). "Re-educating" tumor-associated macrophages by targeting NF- κ B. *The Journal of Experimental Medicine* 205, 1261-1268.
- Hanahan, D., and Weinberg, R.A. (2000). The hallmarks of cancer. *Cell* 100, 57-70.
- Hanahan, D., and Weinberg, R.A. (2011). Hallmarks of cancer: the next generation. *Cell* 144, 646-674.
- Hanna, S., and El-Sibai, M. (2013). Signaling networks of Rho GTPases in cell motility. *Cell Signal* 25, 1955-1961.
- Hansen, K.D., Irizarry, R.A., and Wu, Z. (2012). Removing technical variability in RNA-seq data using conditional quantile normalization. *Biostatistics* 13, 204-216.
- Hao, S., and Baltimore, D. (2009). The stability of mRNA influences the temporal order of the induction of genes encoding inflammatory molecules. *Nat Immunol* 10, 281-288.
- Hao, S., and Baltimore, D. (2013). RNA splicing regulates the temporal order of TNF-induced gene expression. *Proc Natl Acad Sci U S A* 110, 11934-11939.
- Hatada, E.N., Nieters, A., Wulczyn, F.G., Naumann, M., Meyer, R., Nucifora, G., McKeithan, T.W., and Scheidereit, C. (1992). The ankyrin repeat domains of the NF- κ B precursor p105 and the protooncogene bcl-3 act as specific inhibitors of NF- κ B DNA binding. *Proc Natl Acad Sci U S A* 89, 2489-2493.
- Hayden, M.S., and Ghosh, S. (2012). NF- κ B, the first quarter-century: remarkable progress and outstanding questions. *Genes Dev* 26, 203-234.
- Haynes, C., Oldfield, C.J., Ji, F., Klitgord, N., Cusick, M.E., Radivojac, P., Uversky, V.N., Vidal, M., and Iakoucheva, L.M. (2006). Intrinsic Disorder Is a Common Feature of Hub Proteins from Four Eukaryotic Interactomes. *PLOS Computational Biology* 2, e100.
- Hazan, R.B., Qiao, R., Keren, R., Badano, I., and Suyama, K. (2004). Cadherin switch in tumor progression. *Annals of the New York Academy of Sciences* 1014, 155-163.
- He, J.Q., Zarnegar, B., Oganesyan, G., Saha, S.K., Yamazaki, S., Doyle, S.E., Dempsey, P.W., and Cheng, G. (2006). Rescue of TRAF3-null mice by p100 NF- κ B deficiency. *J Exp Med* 203, 2413-2418.

- He, G., Yu, G.-Y., Temkin, V., Ogata, H., Kuntzen, C., Sakurai, T., Sieghart, W., Peck-Radosavljevic, M., Leffert, H.L., and Karin, M. (2010). Hepatocyte IKK β /NF- κ B inhibits tumor promotion and progression by preventing oxidative stress driven STAT3 activation. *Cancer cell* 17, 286-297.
- Heilker, R., Freuler, F., Vanek, M., Pulfer, R., Kobel, T., Peter, J., Zerwes, H.G., Hofstetter, H., and Eder, J. (1999). The kinetics of association and phosphorylation of IkappaB isoforms by IkappaB kinase 2 correlate with their cellular regulation in human endothelial cells. *Biochemistry* 38, 6231-6238.
- Heissmeyer, V., Krappmann, D., Hatada, E.N., and Scheidereit, C. (2001). Shared Pathways of IkB Kinase-Induced SCF β TrCP-Mediated Ubiquitination and Degradation for the NF- κ B Precursor p105 and IkBa. *Molecular and Cellular Biology* 21, 1024-1035.
- Henkel, T., Machleidt, T., Alkalay, I., Kronke, M., Ben-Neriah, Y., and Baeuerle, P.A. (1993). Rapid proteolysis of I kappa B-alpha is necessary for activation of transcription factor NF-kappa B. *Nature* 365, 182-185.
- Hettmann, T., DiDonato, J., Karin, M., and Leiden, J.M. (1999). An essential role for nuclear factor kappaB in promoting double positive thymocyte apoptosis. *J Exp Med* 189, 145-158.
- Heusch, M., Lin, L., Gelezunas, R., and Greene, W.C. (1999). The generation of nfkb2 p52: mechanism and efficiency. *Oncogene* 18, 6201-6208.
- Hinz, M., Krappmann, D., Eichten, A., Heder, A., Scheidereit, C., and Strauss, M. (1999). NF- κ B function in growth control: regulation of cyclin D1 expression and G0/G1-to-S-phase transition. *Molecular and cellular biology* 19, 2690-2698.
- Hinz, M., Stilmann, M., Arslan, S.C., Khanna, K.K., Dittmar, G., and Scheidereit, C. (2010). A cytoplasmic ATM-TRAF6-ClAP1 module links nuclear DNA damage signaling to ubiquitin-mediated NF-kappaB activation. *Molecular cell* 40, 63-74.
- Hirohashi, S. (1998). Inactivation of the E-cadherin-mediated cell adhesion system in human cancers. *Am J Pathol* 153, 333-339.
- Hochrainer, K., Racchumi, G., and Anrather, J. (2013). Site-specific phosphorylation of the p65 protein subunit mediates selective gene expression by differential NF- κ B and RNA polymerase II promoter recruitment. *Journal of Biological Chemistry* 288, 285-293.
- Hoesel, B., and Schmid, J.A. (2013). The complexity of NF- κ B signaling in inflammation and cancer. *Molecular cancer* 12, 86-86.
- Hoffmann, A., Levchenko, A., Scott, M.L., and Baltimore, D. (2002). The IkB-NF- κ B signaling module: temporal control and selective gene activation. *Science* 298, 1241-1245.
- Hoffmann, A., Leung, T.H., and Baltimore, D. (2003). Genetic analysis of NF-kappaB/Rel transcription factors defines functional specificities. *Embo j* 22, 5530-5539.
- Hsu, H., Xiong, J., and Goeddel, D.V. (1995). The TNF receptor 1-associated protein TRADD signals cell death and NF-kappa B activation. *Cell* 81, 495-504.
- Hsu, H., Huang, J., Shu, H.B., Baichwal, V., and Goeddel, D.V. (1996). TNF-dependent recruitment of the protein kinase RIP to the TNF receptor-1 signaling complex. *Immunity* 4, 387-396.
- Hsu, L.C., Enzler, T., Seita, J., Timmer, A.M., Lee, C.Y., Lai, T.Y., Yu, G.Y., Lai, L.C., Temkin, V., Sinzig, U., et al. (2011). IL-1 beta-driven neutrophilia preserves antibacterial defense in the absence of the kinase IKK beta. *Nature Immunology* 12, 144-U154.
- Hu, Y., Baud, V., Delhase, M., Zhang, P., Deerinck, T., Ellisman, M., Johnson, R., and Karin, M. (1999). Abnormal morphogenesis but intact IKK activation in mice lacking the IKKalpha subunit of IkappaB kinase. *Science* 284.
- Hu, Y., Baud, V., Oga, T., Kim, K.I., Yoshida, K., and Karin, M. (2001). IKKalpha controls formation of the epidermis independently of NF-kappaB. *Nature* 410, 710-714.
- Hu, M.C.T., Lee, D.-F., Xia, W., Golfman, L.S., Ou-Yang, F., Yang, J.-Y., Zou, Y., Bao, S., Hanada, N., Sas, H., et al. (2004). IkB Kinase Promotes Tumorigenesis through Inhibition of Forkhead FOXO3a. *Cell* 117, 225-237.
- Huang, T.T., Kudo, N., Yoshida, M., and Miyamoto, S. (2000). A nuclear export signal in the N-terminal regulatory domain of IkappaBalph controls cytoplasmic localization of inactive NF-kappaB/IkappaBalph complexes. *Proc Natl Acad Sci U S A* 97, 1014-1019.
- Huang, T.T., Feinberg, S.L., Suryanarayanan, S., and Miyamoto, S. (2002). The zinc finger domain of NEMO is selectively required for NF-kappa B activation by UV radiation and topoisomerase inhibitors. *Mol Cell Biol* 22, 5813-5825.
- Huang, T.T., Wuerzberger-Davis, S.M., Wu, Z.H., and Miyamoto, S. (2003). Sequential modification of NEMO/IKKgamma by SUMO-1 and ubiquitin mediates NF-kappaB activation by genotoxic stress. *Cell* 115, 565-576.
- Huang, W.C., Ju, T.K., Hung, M.C., and Chen, C.C. (2007). Phosphorylation of CBP by IKKalpha promotes cell growth by switching the binding preference of CBP from p53 to NF-kappaB. *Molecular cell* 26.
- Huang, W.-C., and Hung, M.-C. (2013). Beyond NF- κ B activation: nuclear functions of IkB kinase α . *Journal of Biomedical Science* 20, 3.

- Huber, M.A., Azoitei, N., Baumann, B., Grunert, S., Sommer, A., Pehamberger, H., Kraut, N., Beug, H., and Wirth, T. (2004). NF-kappaB is essential for epithelial-mesenchymal transition and metastasis in a model of breast cancer progression. *J Clin Invest* 114, 569-581.
- Hughes, G., Murphy, M.P., and Ledgerwood, E.C. (2005). Mitochondrial reactive oxygen species regulate the temporal activation of nuclear factor kappaB to modulate tumour necrosis factor-induced apoptosis: evidence from mitochondria-targeted antioxidants. *The Biochemical journal* 389, 83-89.
- Hunter, T., and Pines, J. (1994). Cyclins and cancer. II: Cyclin D and CDK inhibitors come of age. *Cell* 79, 573-582.
- Hutti, J.E., Turk, B.E., Asara, J.M., Ma, A., Cantley, L.C., and Abbott, D.W. (2007). IkappaB kinase beta phosphorylates the K63 deubiquitinase A20 to cause feedback inhibition of the NF-kappaB pathway. *Mol Cell Biol* 27, 7451-7461.
- Hutti, J.E., Turk, B.E., Asara, J.M., Ma, A., Cantley, L.C., and Abbott, D.W. (2007). I κ B Kinase β Phosphorylates the K63 Deubiquitinase A20 To Cause Feedback Inhibition of the NF- κ B Pathway. *Molecular and Cellular Biology* 27, 7451-7461.
- Huxford, T., Huang, D.B., Malek, S., and Ghosh, G. (1998). The crystal structure of the IkappaBalph/NF-kappaB complex reveals mechanisms of NF-kappaB inactivation. *Cell* 95, 759-770.
- Huynh, Q.K., Boddupalli, H., Rouw, S.A., Koboldt, C.M., Hall, T., Sommers, C., Hauser, S.D., Pierce, J.L., Combs, R.G., Reitz, B.A., et al. (2000). Characterization of the Recombinant IKK1/IKK2 Heterodimer: MECHANISMS REGULATING KINASE ACTIVITY. *Journal of Biological Chemistry* 275, 25883-25891.
- Hwang, N.S., Varghese, S., Lee, H.J., Zhang, Z., Ye, Z., Bae, J., Cheng, L., and Elisseeff, J. (2008). In vivo commitment and functional tissue regeneration using human embryonic stem cell-derived mesenchymal cells. *Proceedings of the National Academy of Sciences* 105, 20641-20646.
- Hwang, B., McCool, K., Wan, J., Wuerzberger-Davis, S.M., Young, E.W., Choi, E.Y., Cingolani, G., Weaver, B.A., and Miyamoto, S. (2015). IPO3-mediated Nonclassical Nuclear Import of NF-kappaB Essential Modulator (NEMO) Drives DNA Damage-dependent NF-kappaB Activation. *The Journal of biological chemistry* 290, 17967-17984.
- Iakoucheva, L.M., Brown, C.J., Lawson, J.D., Obradovic, Z., and Dunker, A.K. (2002). Intrinsic disorder in cell-signaling and cancer-associated proteins. *J Mol Biol* 323, 573-584.
- Ichijo, H., Nishida, E., Irie, K., ten Dijke, P., Saitoh, M., Moriguchi, T., Takagi, M., Matsumoto, K., Miyazono, K., and Gotoh, Y. (1997). Induction of apoptosis by ASK1, a mammalian MAPKKK that activates SAPK/JNK and p38 signaling pathways. *Science* 275, 90-94.
- Ikeda, F., Hecker, C.M., Rozenknop, A., Nordmeier, R.D., Rogov, V., Hofmann, K., Akira, S., Dotsch, V., and Dikic, I. (2007). Involvement of the ubiquitin-like domain of TBK1/IKK-i kinases in regulation of IFN-inducible genes. *EMBO J* 26, 3451-3462.
- Ikeda, F., Deribe, Y.L., Skåland, S.S., Stieglitz, B., Grabbe, C., Franz-Wachtel, M., van Wijk, S.J., Goswami, P., Nagy, V., and Terzic, J. (2011). SHARPIN forms a linear ubiquitin ligase complex regulating NF- κ B activity and apoptosis. *Nature* 471, 637.
- Inobe, T., Fishbain, S., Prakash, S., and Matouschek, A. (2011). Defining the geometry of the two-component proteasome degron. *Nature chemical biology* 7, 161-167.
- Inohara, N., Koseki, T., Lin, J., del Peso, L., Lucas, P.C., Chen, F.F., Ogura, Y., and Nunez, G. (2000). An induced proximity model for NF-kappa B activation in the Nod1/RICK and RIP signaling pathways. *The Journal of biological chemistry* 275, 27823-27831.
- Irelan, J.T., Murphy, T.J., DeJesus, P.D., Teo, H., Xu, D., Gomez-Ferreria, M.A., Zhou, Y., Miraglia, L.J., Rines, D.R., Verma, I.M., et al. (2007). A role for IkappaB kinase 2 in bipolar spindle assembly. *Proc Natl Acad Sci U S A* 104, 16940-16945.
- Ishida, T., and Kinoshita, K. (2007). PrDOS: prediction of disordered protein regions from amino acid sequence. *Nucleic Acids Res* 35, W460-464.
- Ivins, F.J., Montgomery, M.G., Smith, S.J., Morris-Davies, A.C., Taylor, I.A., and Rittinger, K. (2009). NEMO oligomerization and its ubiquitin-binding properties. *The Biochemical journal* 421, 243-251.
- Jacinto, E., Facchinetto, V., Liu, D., Soto, N., Wei, S., Jung, S.Y., Huang, Q., Qin, J., and Su, B. (2006). SIN1/MIP1 maintains rictor-mTOR complex integrity and regulates Akt phosphorylation and substrate specificity. *Cell* 127, 125-137.
- Jackson, A.L., Bartz, S.R., Schelter, J., Kobayashi, S.V., Burchard, J., Mao, M., Li, B., Cavet, G., and Linsley, P.S. (2003). Expression profiling reveals off-target gene regulation by RNAi. *Nat Biotechnol* 21, 635-637.
- Jackson, A.L., Burchard, J., Leake, D., Reynolds, A., Schelter, J., Guo, J., Johnson, J.M., Lim, L., Karpilow, J., Nichols, K., et al. (2006). Position-specific chemical modification of siRNAs reduces "off-target" transcript silencing. *Rna* 12, 1197-1205.
- Jacobs, M.D., and Harrison, S.C. (1998). Structure of an IkappaBalph/NF-kappaB complex. *Cell* 95, 749-758.
- Jeffrey, P.D., Russo, A.A., Polyak, K., Gibbs, E., Hurwitz, J., Massagué, J., and Pavletich, N.P. (1995). Mechanism of CDK activation revealed by the structure of a cyclinA-CDK2 complex. *Nature* 376, 313-320.

- Jia, B., Choy, E., Cote, G., Harmon, D., Ye, S., Kan, Q., Mankin, H., Hor nicek, F., and Duan, Z. (2014). Cyclin-dependent kinase 11 (CDK11) is crucial in the growth of liposarcoma cells. *Cancer Lett* 342, 104-112.
- Jiang, R., Xia, Y., Li, J., Deng, L., Zhao, L., Shi, J., Wang, X., and Sun, B. (2010). High expression levels of IKK α and IKK β are necessary for the malignant properties of liver cancer. *Int J Cancer* 126, 1263-1274.
- Jin, H.S., Lee, D.H., Kim, D.H., Chung, J.H., Lee, S.J., and Lee, T.H. (2009). cIAP1, cIAP2, and XIAP act cooperatively via nonredundant pathways to regulate genotoxic stress-induced nuclear factor- κ B activation. *Cancer Res* 69, 1782-1791.
- Jo, H., Zhang, R., Zhang, H., McKinsey, T.A., Shao, J., Beauchamp, R.D., Ballard, D.W., and Liang, P. (2000). NF- κ B is required for H-ras oncogene induced abnormal cell proliferation and tumorigenesis. *Oncogene* 19, 841-849.
- Johnson, C., Van Antwerp, D., and Hope, T.J. (1999). An N-terminal nuclear export signal is required for the nucleocytoplasmic shuttling of I κ B α . *The EMBO journal* 18, 6682-6693.
- Johnson, R.F., Witzel, I.-I., and Perkins, N.D. (2011). p53-dependent regulation of mitochondrial energy production by the RelA subunit of NF- κ B. *Cancer research* 71, 5588-5597.
- Jones, D.T., and Cozzetto, D. (2015). DISOPRED3: precise disordered region predictions with annotated protein-binding activity. *Bioinformatics* 31, 857-863.
- Julien, S., Puig, I., Caretti, E., Bonaventure, J., Nelles, L., van Roy, F., Dargemont, C., de Herreros, A.G., Bellacosa, A., and Larue, L. (2007). Activation of NF- κ B by Akt upregulates Snail expression and induces epithelium mesenchyme transition. *Oncogene* 26, 7445-7456.
- Ka Ho, H., Plevin, R., Mackay, S., and Paul, A. (2014). 193 A Novel First in Class IKK Alpha Inhibitor Abrogates Endothelial Cell Nuclear Factor Kappa B Signalling and Inflammatory Protein Expression. *Heart* 100, A107-A107.
- Kaisho, T., Takeda, K., Tsujimura, T., Kawai, T., Nomura, F., Terada, N., and Akira, S. (2001). I κ B kinase alpha is essential for mature B cell development and function. *J Exp Med* 193, 417-426.
- Kalejta, R.F., and Shenk, T. (2003). Proteasome-dependent, ubiquitin-independent degradation of the Rb family of tumor suppressors by the human cytomegalovirus pp71 protein. *Proceedings of the National Academy of Sciences* 100, 3263-3268.
- Kaler, P., Augenlicht, L., and Klampfer, L. (2009). Macrophage-derived IL-1 β stimulates Wnt signaling and growth of colon cancer cells: a crosstalk interrupted by vitamin D3. *Oncogene* 28, 3892-3902.
- Kaler, P., Godasi, B.N., Augenlicht, L., and Klampfer, L. (2009). The NF- κ B/AKT-dependent Induction of Wnt Signaling in Colon Cancer Cells by Macrophages and IL-1 β . *Cancer microenvironment : official journal of the International Cancer Microenvironment Society* 2, 69-80.
- Kamata, H., Honda, S.-i., Maeda, S., Chang, L., Hirata, H., and Karin, M. (2005). Reactive Oxygen Species Promote TNF α -Induced Death and Sustained JNK Activation by Inhibiting MAP Kinase Phosphatases. *Cell* 120, 649-661.
- Kari, V., Karpiuk, O., Tiegs, B., Kriegs, M., Dikomey, E., Krebber, H., Begus-Nahrmann, Y., and Johnsen, S.A. (2013). A Subset of Histone H2B Genes Produces Polyadenylated mRNAs under a Variety of Cellular Conditions. *PLoS one* 8, e63745.
- Karin, M., Yamamoto, Y., and Wang, Q.M. (2004). The IKK NF- κ B system: a treasure trove for drug development. *Nat Rev Drug Discov* 3.
- Karin, M., and Greten, F.R. (2005). NF- κ B: linking inflammation and immunity to cancer development and progression. *Nat Rev Immunol* 5, 749-759.
- Kawauchi, K., Araki, K., Tobiume, K., and Tanaka, N. (2008). p53 regulates glucose metabolism through an IKK-NF- κ B pathway and inhibits cell transformation. *Nat Cell Biol* 10, 611-618.
- Keats, J.J., Fonseca, R., Chesi, M., Schop, R., Baker, A., Chng, W.-J., Van Wier, S., Tiedemann, R., Shi, C.-X., Sebag, M., et al. (2007). Promiscuous Mutations Activate the Non-Canonical NF- κ B Pathway in Multiple Myeloma. *Cancer cell* 12, 131-144.
- Khoshnan, A., Kempfak, S.J., Bennett, B.L., Bae, D., Xu, W., Manning, A.M., June, C.H., and Nel, A.E. (1999). Primary Human CD4 $^{+}$ T Cells Contain Heterogeneous I κ B Kinase Complexes: Role in Activation of the IL-2 Promoter. *The Journal of Immunology* 163, 5444-5452.
- Kill, I.R. (1996). Localisation of the Ki-67 antigen within the nucleolus. Evidence for a fibrillarin-deficient region of the dense fibrillar component. *J Cell Sci* 109 (Pt 6), 1253-1263.
- Kim, S., Domon-Dell, C., Kang, J., Chung, D.H., Freund, J.-N., and Evers, B.M. (2004). Down-regulation of the Tumor Suppressor PTEN by the Tumor Necrosis Factor- α /Nuclear Factor- κ B (NF- κ B)-inducing Kinase/NF- κ B Pathway Is Linked to a Default I κ B- α Autoregulatory Loop. *Journal of Biological Chemistry* 279, 4285-4291.
- Kim, Y.-S., Morgan, M.J., Choksi, S., and Liu, Z.-g. (2007). TNF-Induced Activation of the Nox1 NADPH Oxidase and Its Role in the Induction of Necrotic Cell Death. *Molecular cell* 26, 675-687.

- Kim, J.J., Lee, S.B., Park, J.K., and Yoo, Y.D. (2010). TNF-alpha-induced ROS production triggering apoptosis is directly linked to Romo1 and Bcl-X(L). *Cell Death Differ* 17, 1420-1434.
- Kim, J.Y., Morgan, M., Kim, D.G., Lee, J.Y., Bai, L., Lin, Y., Liu, Z.G., and Kim, Y.S. (2011). TNFalpha induced noncanonical NF-kappaB activation is attenuated by RIP1 through stabilization of TRAF2. *J Cell Sci* 124, 647-656.
- Kim, J.-E., Kim, S.Y., Lim, S.Y., Kieff, E., and Song, Y.-J. (2014). Role of Ca(2+)/Calmodulin-Dependent Kinase II- IRAK1 Interaction in LMP1-Induced NF- κ B Activation. *Molecular and Cellular Biology* 34, 325-334.
- Kirisako, T., Kamei, K., Murata, S., Kato, M., Fukumoto, H., Kanie, M., Sano, S., Tokunaga, F., Tanaka, K., and Iwai, K. (2006). A ubiquitin ligase complex assembles linear polyubiquitin chains. *Embo j* 25, 4877-4887.
- Klement, J.F., Rice, N.R., Car, B.D., Abbondanzo, S.J., Powers, G.D., Bhatt, P.H., Chen, C.H., Rosen, C.A., and Stewart, C.L. (1996). IkappaBalphalpha deficiency results in a sustained NF-kappaB response and severe widespread dermatitis in mice. *Mol Cell Biol* 16, 2341-2349.
- Klotz, L.-O., Sánchez-Ramos, C., Prieto-Arroyo, I., Urbánek, P., Steinbrenner, H., and Monsalve, M. (2015). Redox regulation of FoxO transcription factors. *Redox Biology* 6, 51-72.
- KOJIMA, M., MORISAKI, T., SASAKI, N., NAKANO, K., MIBU, R., TANAKA, M., and KATANO, M. (2004). Increased nuclear factor- κ B activation in human colorectal carcinoma and its correlation with tumor progression. *Anticancer research* 24, 675-682.
- Korner, H., and Sedgwick, J.D. (1996). Tumour necrosis factor and lymphotoxin: Molecular aspects and role in tissue-specific autoimmunity. *Immunol Cell Biol* 74, 465-472.
- Kostenko, S., Dumitriu, G., Laegreid, K.J., and Moens, U. (2011). Physiological roles of mitogen-activated-protein- kinase-activated p38-regulated/activated protein kinase. *World journal of biological chemistry* 2, 73-89.
- Kovalenko, A., Chable-Bessia, C., Cantarella, G., Israel, A., Wallach, D., and Courtois, G. (2003). The tumour suppressor CYLD negatively regulates NF-kappaB signalling by deubiquitination. *Nature* 424, 801-805.
- Krappmann, D., Hatada, E.N., Tegethoff, S., Li, J., Klippel, A., Giese, K., Baeuerle, P.A., and Scheidereit, C. (2000). The I kappa B kinase (IKK) complex is tripartite and contains IKK gamma but not IKAP as a regular component. *The Journal of biological chemistry* 275, 29779-29787.
- Krause, K., Wasner, M., Reinhard, W., Haugwitz, U., Lange-zu Dohna, C., Mössner, J., and Engeland, K. (2000). The tumour suppressor protein p53 can repress transcription of cyclin B. *Nucleic Acids Research* 28, 4410-4418.
- Krause, K., Haugwitz, U., Wasner, M., Wiedmann, M., Mossner, J., and Engeland, K. (2001). Expression of the cell cycle phosphatase cdc25C is down-regulated by the tumor suppressor protein p53 but not by p73. *Biochemical and biophysical research communications* 284, 743-750.
- Krikos, A., Laherty, C.D., and Dixit, V.M. (1992). Transcriptional activation of the tumor necrosis factor alpha-inducible zinc finger protein, A20, is mediated by kappa B elements. *The Journal of biological chemistry* 267, 17971-17976.
- Kumagai, A., and Dunphy, W.G. (1991). The cdc25 protein controls tyrosine dephosphorylation of the cdc2 protein in a cell-free system. *Cell* 64, 903-914.
- Kwak, Y.T., Guo, J., Shen, J., and Gaynor, R.B. (2000). Analysis of domains in the IKKalpha and IKKbeta proteins that regulate their kinase activity. *The Journal of biological chemistry* 275, 14752-14759.
- Kwak, Y.T., Li, R., Becerra, C.R., Tripathy, D., Frenkel, E.P., and Verma, U.N. (2005). IkappaB kinase alpha regulates subcellular distribution and turnover of cyclin D1 by phosphorylation. *The Journal of biological chemistry* 280.
- Lahtela, J., Nousiainen, H.O., Stefanovic, V., Tallila, J., Viskari, H., Karikoski, R., Gentile, M., Saloranta, C., Varilo, T., Salonen, R., et al. (2010). Mutant CHUK and severe fetal encasement malformation. *The New England journal of medicine* 363, 1631-1637.
- Lam, L.T., Davis, R.E., Pierce, J., Hepperle, M., Xu, Y., Hottelet, M., Nong, Y., Wen, D., Adams, J., Dang, L., et al. (2005). Small molecule inhibitors of IkappaB kinase are selectively toxic for subgroups of diffuse large B-cell lymphoma defined by gene expression profiling. *Clinical cancer research : an official journal of the American Association for Cancer Research* 11, 28-40.
- Lam, L.T., Davis, R.E., Ngo, V.N., Lenz, G., Wright, G., Xu, W., Zhao, H., Yu, X., Dang, L., and Staudt, L.M. (2008). Compensatory IKKalpha activation of classical NF-kappaB signaling during IKKbeta inhibition identified by an RNA interference sensitization screen. *Proc Natl Acad Sci U S A* 105, 20798-20803.
- Lam, L.T., Wright, G., Davis, R.E., Lenz, G., Farinha, P., Dang, L., Chan, J.W., Rosenwald, A., Gascoyne, R.D., and Staudt, L.M. (2008). Cooperative signaling through the signal transducer and activator of transcription 3 and nuclear factor- κ B pathways in subtypes of diffuse large B-cell lymphoma. *Blood* 111, 3701-3713.
- Lamb, A., Yang, X.D., Tsang, Y.H., Li, J.D., Higashi, H., Hatakeyama, M., Peek, R.M., Blanke, S.R., and Chen, L.F. (2009). Helicobacter pylori CagA activates NF-kappaB by targeting TAK1 for TRAF6-mediated Lys 63 ubiquitination. *EMBO Rep* 10, 1242-1249.

- Lamberti, C., Lin, K.M., Yamamoto, Y., Verma, U., Verma, I.M., Byers, S., and Gaynor, R.B. (2001). Regulation of beta-catenin function by the IkappaB kinases. *The Journal of biological chemistry* 276, 42276-42286.
- Langlois, M.-J., Bergeron, S., Bernatchez, G., Boudreau, F., Saucier, C., Perreault, N., Carrier, J.C., and Rivard, N. (2010). The PTEN Phosphatase Controls Intestinal Epithelial Cell Polarity and Barrier Function: Role in Colorectal Cancer Progression. *PloS one* 5, e15742.
- Laplantine, E., Fontan, E., Chiaravalli, J., Lopez, T., Lakisic, G., Véron, M., Agou, F., and Israël, A. (2009). NEMO specifically recognizes K63-linked poly-ubiquitin chains through a new bipartite ubiquitin-binding domain. *The EMBO Journal* 28, 2885-2895.
- Lasorella, A., Benezra, R., and Iavarone, A. (2014). The ID proteins: master regulators of cancer stem cells and tumour aggressiveness. *Nat Rev Cancer* 14, 77-91.
- Lavorgna, A., De Filippi, R., Formisano, S., and Leonardi, A. (2009). TNF receptor-associated factor 1 is a positive regulator of the NF-kappaB alternative pathway. *Molecular immunology* 46, 3278-3282.
- Lavrik, I., Golks, A., and Krammer, P.H. (2005). Death receptor signaling. *J Cell Sci* 118, 265-267.
- Lawrence, T., Bebien, M., Liu, G.Y., Nizet, V., and Karin, M. (2005). IKKalpha limits macrophage NF-kappaB activation and contributes to the resolution of inflammation. *Nature* 434, 1138-1143.
- Lee, J.C., Laydon, J.T., McDonnell, P.C., Gallagher, T.F., Kumar, S., Green, D., McNulty, D., Blumenthal, M.J., Keys, J.R., Land vatter, S.W., et al. (1994). A protein kinase involved in the regulation of inflammatory cytokine biosynthesis. *Nature* 372, 739-746.
- Lee, E.G., Boone, D.L., Chai, S., Libby, S.L., Chien, M., Ladolce, J.P., and Ma, A. (2000). Failure to regulate TNF-induced NF-kappaB and cell death responses in A20-deficient mice. *Science* 289, 2350-2354.
- Lee, S.-H., and Hannink, M. (2002). Characterization of the Nuclear Import and Export Functions of IκBε. *Journal of Biological Chemistry* 277, 23358-23366.
- Lee, T.H., Shank, J., Cusson, N., and Kelliher, M.A. (2004). The Kinase Activity of Rip1 Is Not Required for Tumor Necrosis Factor-α-induced IκB Kinase or p38 MAP Kinase Activation or for the Ubiquitination of Rip1 by Traf2. *Journal of Biological Chemistry* 279, 33185-33191.
- Lee, C.H., Jeon, Y.T., Kim, S.H., and Song, Y.S. (2007). NF-kappaB as a potential molecular target for cancer therapy. *BioFactors (Oxford, England)* 29, 19-35.
- Lee, S.Y., and Choi, Y. (2007). TRAF1 and its biological functions. *Adv Exp Med Biol* 597, 25-31.
- Lee, M.H., Mabb, A.M., Gill, G.B., Yeh, E.T., and Miyamoto, S. (2011). NF-kappaB induction of the SUMO protease SENP2: A negative feedback loop to attenuate cell survival response to genotoxic stress. *Molecular cell* 43, 180-191.
- Lee, R.E., Walker, S.R., Savery, K., Frank, D.A., and Gaudet, S. (2014). Fold change of nuclear NF-kappaB determines TNF-induced transcription in single cells. *Molecular cell* 53, 867-879.
- Legler, D.F., Micheau, O., Doucey, M.A., Tschoopp, J., and Bron, C. (2003). Recruitment of TNF receptor 1 to lipid rafts is essential for TNFalpha-mediated NF-kappaB activation. *Immunity* 18, 655-664.
- Li, X., Lonard, D.M., Jung, S.Y., Malovannaya, A., Feng, Q., Qin, J., Tsai, S.Y., Tsai, M.-J., and O'Malley, B.W. The SRC-3/AIB1 Coactivator Is Degraded in a Ubiquitin- and ATP-Independent Manner by the REGγ Proteasome. *Cell* 124, 381-392.
- Li, N., and Karin, M. (1998). Ionizing radiation and short wavelength UV activate NF-kappaB through two distinct mechanisms. *Proc Natl Acad Sci U S A* 95, 13012-13017.
- Li, Q., Lu, Q., Hwang, J.Y., Buscher, D., Lee, K.F., Izpisua-Belmonte, J.C., and Verma, I.M. (1999). IKK1-deficient mice exhibit abnormal development of skin and skeleton. *Genes Dev* 13, 1322-1328.
- Li, Q., Van Antwerp, D., Mercurio, F., Lee, K.F., and Verma, I.M. (1999). Severe liver degeneration in mice lacking the IkappaB kinase 2 gene. *Science* 284, 321-325.
- Li, X., Romero, P., Rani, M., Dunker, A.K., and Obradovic, Z. (1999). Predicting Protein Disorder for N-, C-, and Internal Regions. *Genome informatics Workshop on Genome Informatics* 10, 30-40.
- Li, Z.W., Chu, W., Hu, Y., Delhase, M., Deerinck, T., Ellisman, M., Johnson, R., and Karin, M. (1999). The IKKbeta subunit of IkappaB kinase (IKK) is essential for nuclear factor kappaB activation and prevention of apoptosis. *J Exp Med* 189, 1839-1845.
- Li, Q., Estepa, G., Memet, S., Israel, A., and Verma, I.M. (2000). Complete lack of NF-kappaB activity in IKK1 and IKK2 double-deficient mice: additional defect in neurulation. *Genes Dev* 14, 1729-1733.
- Li, X., Massa, P.E., Hanidu, A., Peet, G.W., Aro, P., Savitt, A., Mische, S., Li, J., and Marcu, K.B. (2002). IKKalpha, IKKbeta, and NEMO/IKKgamma are each required for the NF-kappa B-mediated inflammatory response program. *The Journal of biological chemistry* 277, 45129-45140.
- Li, X., Massa, P.E., Hanidu, A., Peet, G.W., Aro, P., Savitt, A., Mische, S., Li, J., and Marcu, K.B. (2002). IKK α , IKK β , and NEMO/IKK γ Are Each Required for the NF- κ B-mediated Inflammatory Response Program. *Journal of Biological Chemistry* 277, 45129-45140.

- Li, Q., Lu, Q., Bottero, V., Estepa, G., Morrison, L., Mercurio, F., and Verma, I.M. (2005). Enhanced NF- κ B activation and cellular function in macrophages lacking I κ B kinase 1 (IKK1). *Proceedings of the National Academy of Sciences of the United States of America* **102**, 12425-12430.
- Li, H., Kobayashi, M., Blonska, M., You, Y., and Lin, X. (2006). Ubiquitination of RIP Is Required for Tumor Necrosis Factor α -induced NF- κ B Activation. *Journal of Biological Chemistry* **281**, 13636-13643.
- Li, W., and Miller, W.T. (2006). Role of the activation loop tyrosines in regulation of the insulin-like growth factor I receptor-tyrosine kinase. *The Journal of biological chemistry* **281**, 23785-23791.
- Li, X., Amazit, L., Long, W., Lonard, D.M., Monaco, J.J., and O'Malley, B.W. (2007). Ubiquitin- and ATP-Independent Proteolytic Turnover of p21 by the REG γ -Proteasome Pathway. *Molecular cell* **26**, 831-842.
- Li, M., and Zhang, P. (2009). The function of APC/C(Cdh1) in cell cycle and beyond. *Cell Division* **4**, 2-2.
- Li, B., Hu, Q., Xu, R., Ren, H., Fei, E., Chen, D., and Wang, G. (2012). Hax-1 is rapidly degraded by the proteasome dependent on its PEST sequence. *BMC Cell Biology* **13**, 20.
- Li, C.W., Xia, W., Huo, L., Lim, S.O., Wu, Y., Hsu, J.L., Chao, C.H., Yamaguchi, H., Yang, N.K., Ding, Q., et al. (2012). Epithelial-mesenchymal transition induced by TNF-alpha requires NF- κ B-mediated transcriptional upregulation of Twist1. *Cancer Res* **72**, 1290-1300.
- Li, J., McQuade, T., Siemer, A.B., Napetschnig, J., Moriwaki, K., Hsiao, Y.S., Damko, E., Moquin, D., Walz, T., McDermott, A., et al. (2012). The RIP1/RIP3 necosome forms a functional amyloid signaling complex required for programmed necrosis. *Cell* **150**, 339-350.
- Liang, C., Zhang, M., and Sun, S.C. (2006). beta-TrCP binding and processing of NF- κ B2/p100 involve its phosphorylation at serines 866 and 870. *Cell Signal* **18**, 1309-1317.
- Liao, G., and Sun, S.C. (2003). Regulation of NF- κ B2/p100 processing by its nuclear shuttling. *Oncogene* **22**, 4868-4874.
- Liao, G., Zhang, M., Harhaj, E.W., and Sun, S.C. (2004). Regulation of the NF- κ B-inducing kinase by tumor necrosis factor receptor-associated factor 3-induced degradation. *The Journal of biological chemistry* **279**, 26243-26250.
- Lin, L., and Ghosh, S. (1996). A glycine-rich region in NF- κ B p105 functions as a processing signal for the generation of the p50 subunit. *Mol Cell Biol* **16**, 2248-2254.
- Lin, L., DeMartino, G.N., and Greene, W.C. (1998). Cotranslational biogenesis of NF- κ B p50 by the 26S proteasome. *Cell* **92**, 819-828.
- Lin, X., Mu, Y., Cunningham, E.T., Jr., Marcu, K.B., Geleziunas, R., and Greene, W.C. (1998). Molecular determinants of NF- κ B-inducing kinase action. *Mol Cell Biol* **18**, 5899-5907.
- Lin, G., Zheng, X.-w., Li, C., Chen, Q., and Ye, Y.-b. (2012). KRAS mutation and NF- κ B activation indicates tolerance of chemotherapy and poor prognosis in colorectal cancer. *Digestive diseases and sciences* **57**, 2325-2333.
- Lind, D.S., Hochwald, S.N., Malaty, J., Rekkas, S., Hebig, P., Mishra, G., Moldawer, L.L., Copeland, E.M., 3rd, and Mackay, S. (2001). Nuclear factor- κ B is upregulated in colorectal cancer. *Surgery* **130**, 363-369.
- Linding, R., Jensen, L.J., Diella, F., Bork, P., Gibson, T.J., and Russell, R.B. (2003). Protein disorder prediction: implications for structural proteomics. *Structure* **11**, 1453-1459.
- Ling, L., Cao, Z., and Goeddel, D.V. (1998). NF- κ B-inducing kinase activates IKK-alpha by phosphorylation of Ser-176. *Proc Natl Acad Sci U S A* **95**, 3792-3797.
- Ling, J., Kang, Y., Zhao, R., Xia, Q., Lee, D.F., Chang, Z., Li, J., Peng, B., Fleming, J.B., Wang, H., et al. (2012). KrasG12D-induced IKK2/beta/NF- κ B activation by IL-1alpha and p62 feedforward loops is required for development of pancreatic ductal adenocarcinoma. *Cancer Cell* **21**, 105-120.
- Liptay, S., Weber, C.K., Ludwig, L., Wagner, M., Adler, G., and Schmid, R.M. (2003). Mitogenic and antiapoptotic role of constitutive NF- κ B/Rel activity in pancreatic cancer. *Int J Cancer* **105**, 735-746.
- Liu, Z.G., Baskaran, R., Lea-Chou, E.T., Wood, L.D., Chen, Y., Karin, M., and Wang, J.Y. (1996). Three distinct signalling responses by murine fibroblasts to genotoxic stress. *Nature* **384**, 273-276.
- Liu, B., Yang, Y., Chernishof, V., Loo, R.R.O., Jang, H., Tahk, S., Yang, R., Mink, S., Shultz, D., Bellone, C.J., et al. (2007). Proinflammatory Stimuli Induce IKK α -Mediated Phosphorylation of PIAS1 to Restrict Inflammation and Immunity. *Cell* **129**, 903-914.
- Liu, X., Jiang, H., and Li, H. (2011). SHAFTS: a hybrid approach for 3D molecular similarity calculation. 1. Method and assessment of virtual screening. *Journal of chemical information and modeling* **51**, 2372-2385.
- Liu, J., Sudom, A., Min, X., Cao, Z., Gao, X., Ayres, M., Lee, F., Cao, P., Johnstone, S., Plotnikova, O., et al. (2012). Structure of the Nuclear Factor κ B-inducing Kinase (NIK) Kinase Domain Reveals a Constitutively Active Conformation. *Journal of Biological Chemistry* **287**, 27326-27334.
- Liu, S., Misquitta, Y.R., Olland, A., Johnson, M.A., Kelleher, K.S., Kriz, R., Lin, L.L., Stahl, M., and Mosyak, L. (2013). Crystal structure of a human I κ B kinase beta asymmetric dimer. *The Journal of biological chemistry* **288**, 22758-22767.

- Liu, S., Misquitta, Y.R., Olland, A., Johnson, M.A., Kelleher, K.S., Kriz, R., Lin, L.L., Stahl, M., and Mosyak, L. (2013). Crystal structure of a human I κ B kinase β asymmetric dimer. *Journal of Biological Chemistry* 288, 22758-22767.
- Liu, X., Gao, Y., Shen, J., Yang, W., Choy, E., Mankin, H., Hor nicek, F.J., and Duan, Z. (2016). Cyclin-Dependent Kinase 11 (CDK11) Is Required for Ovarian Cancer Cell Growth In Vitro and In Vivo, and Its Inhibition Causes Apoptosis and Sensitizes Cells to Paclitaxel. *Mol Cancer Ther* 15, 1691-1701.
- Lo, Y.C., Lin, S.C., Rospigliosi, C.C., Conze, D.B., Wu, C.J., Ashwell, J.D., Eliezer, D., and Wu, H. (2009). Structural basis for recognition of diubiquitins by NEMO. *Molecular cell* 33, 602-615.
- Locksley, R.M., Killeen, N., and Lenardo, M.J. (2001). The TNF and TNF receptor superfamilies: integrating mammalian biology. *Cell* 104, 487-501.
- Loda, M., Capodieci, P., Mishra, R., Yao, H., Corless, C., Grigioni, W., Wang, Y., Magi-Galluzzi, C., and Stork, P.J. (1996). Expression of mitogen-activated protein kinase phosphatase-1 in the early phases of human epithelial carcinogenesis. *Am J Pathol* 149, 1553-1564.
- Losiewicz, M.D., Carlson, B.A., Kaur, G., Sausville, E.A., and Worland, P.J. (1994). Potent inhibition of CDC2 kinase activity by the flavonoid L86-8275. *Biochemical and biophysical research communications* 201, 589-595.
- Lu, T., Sathe, S.S., Swiatkowski, S.M., Hampole, C.V., and Stark, G.R. (2004). Secretion of cytokines and growth factors as a general cause of constitutive NF κ B activation in cancer. *Oncogene* 23, 2138-2145.
- Lu, D., Chen, J., and Hai, T. (2007). The regulation of ATF3 gene expression by mitogen-activated protein kinases. *The Biochemical journal* 401, 559-567.
- Luedde, T., Assmus, U., Wüstefeld, T., Meyer zu Vilsendorf, A., Roskams, T., Schmidt-Suprian, M., Rajewsky, K., Brenner, D.A., Manns, M.P., Pasparakis, M., et al. (2005). Deletion of IKK2 in hepatocytes does not sensitize these cells to TNF-induced apoptosis but protects from ischemia/reperfusion injury. *Journal of Clinical Investigation* 115, 849-859.
- Luedde, T., Beraza, N., Kotsikoris, V., van Loo, G., Nenci, A., De Vos, R., Roskams, T., Trautwein, C., and Pasparakis, M. (2007). Deletion of NEMO/IKK γ in Liver Parenchymal Cells Causes Steatohepatitis and Hepatocellular Carcinoma. *Cancer Cell* 11, 119-132.
- Lundberg, A.S., and Weinberg, R.A. (1998). Functional inactivation of the retinoblastoma protein requires sequential modification by at least two distinct cyclin-cdk complexes. *Mol Cell Biol* 18, 753-761.
- Lundgren, K., Walworth, N., Booher, R., Dembski, M., Kirschner, M., and Beach, D. (1991). mik1 and wee1 cooperate in the inhibitory tyrosine phosphorylation of cdc2. *Cell* 64, 1111-1122.
- Luo, J.L., Tan, W., Ricono, J.M., Korchynskyi, O., Zhang, M., Gonias, S.L., Cheresh, D.A., and Karin, M. (2007). Nuclear cytokine-activated IKK α controls prostate cancer metastasis by repressing Maspin. *Nature* 446, 690-694.
- Luo, J., Solimini, N.L., and Elledge, S.J. (2009). Principles of cancer therapy: oncogene and non-oncogene addiction. *Cell* 136, 823-837.
- Lyons, S.M., Cunningham, C.H., Welch, J.D., Groh, B., Guo, A.Y., Wei, B., Whitfield, M.L., Xiong, Y., and Marzluff, W.F. (2016). A subset of replication-dependent histone mRNAs are expressed as polyadenylated RNAs in terminally differentiated tissues. *Nucleic Acids Res* 44, 9190-9205.
- Ma, T., Wu, S., Yan, W., Xie, R., and Zhou, C. (2016). A functional variant of ATG16L2 is associated with Crohn's disease in the Chinese population. *Colorectal disease : the official journal of the Association of Coloproctology of Great Britain and Ireland* 18, O420-o426.
- Mabb, A.M., Wuerzberger-Davis, S.M., and Miyamoto, S. (2006). PIASy mediates NEMO sumoylation and NF- κ B activation in response to genotoxic stress. *Nat Cell Biol* 8, 986-993.
- Madge, L.A., and Pober, J.S. (2000). A Phosphatidylinositol 3-Kinase/Akt Pathway, Activated by Tumor Necrosis Factor or Interleukin-1, Inhibits Apoptosis but Does Not Activate NF κ B in Human Endothelial Cells. *Journal of Biological Chemistry* 275, 15458-15465.
- Madrid, L.V., Mayo, M.W., Reuther, J.Y., and Baldwin, A.S., Jr. (2001). Akt stimulates the transactivation potential of the RelA/p65 Subunit of NF- κ B through utilization of the I κ B kinase and activation of the mitogen-activated protein kinase p38. *The Journal of biological chemistry* 276, 18934-18940.
- Maeda, S., Kamata, H., Luo, J.-L., Leffert, H., and Karin, M. (2005). IKK β Couples Hepatocyte Death to Cytokine-Driven Compensatory Proliferation that Promotes Chemical Hepatocarcinogenesis. *Cell* 121, 977-990.
- Malek, S., Chen, Y., Huxford, T., and Ghosh, G. (2001). I κ B β beta, but not I κ B α lpha, functions as a classical cytoplasmic inhibitor of NF- κ B dimers by masking both NF- κ B nuclear localization sequences in resting cells. *The Journal of biological chemistry* 276, 45225-45235.
- Malhis, N., Jacobson, M., and Gsponer, J. (2016). MoRFchibi SYSTEM: software tools for the identification of MoRFs in protein sequences. *Nucleic Acids Research* 44, W488-W493.
- Mao, X., Gluck, N., Li, D., Maine, G.N., Li, H., Zaidi, I.W., Repaka, A., Mayo, M.W., and Burstein, E. (2009). GCN5 is a required cofactor for a ubiquitin ligase that targets NF- κ B/RelA. *Genes Dev* 23, 849-861.

- Margalef, P., Fernandez-Majada, V., Villanueva, A., Garcia-Carbonell, R., Iglesias, M., Lopez, L., Martinez-Iniesta, M., Villa-Freixa, J., Mulero, M.C., Andreu, M., et al. (2012). A truncated form of IKKalpha is responsible for specific nuclear IKK activity in colorectal cancer. *Cell Rep* 2, 840-854.
- Margalef, P., Colomer, C., Villanueva, A., Montagut, C., Iglesias, M., Bellosillo, B., Salazar, R., Martínez-Iniesta, M., Bigas, A., and Espinosa, L. (2015). BRAF-induced tumorigenesis is IKK α -dependent but NF- κ B-independent. *Science Signaling* 8, ra38-ra38.
- Marienfeld, R., Berberich-Siebelt, F., Berberich, I., Denk, A., Serfling, E., and Neumann, M. (2001). Signal-specific and phosphorylation-dependent RelB degradation: a potential mechanism of NF-kappaB control. *Oncogene* 20, 8142-8147.
- Marienfeld, R.B., Palkowitzsch, L., and Ghosh, S. (2006). Dimerization of the IkB Kinase-Binding Domain of NEMO Is Required for Tumor Necrosis Factor Alpha-Induced NF- κ B Activity. *Molecular and Cellular Biology* 26, 9209-9219.
- Martin, B.N., Wang, C., Willette-Brown, J., Herjan, T., Gulen, M.F., Zhou, H., Bulek, K., Franchi, L., Sato, T., Alnemri, E.S., et al. (2014). IKKalpha negatively regulates ASC-dependent inflammasome activation. *Nat Commun* 5, 4977.
- Marzluff, W.F., Wagner, E.J., and Duronio, R.J. (2008). Metabolism and regulation of canonical histone mRNAs: life without a poly(A) tail. *Nat Rev Genet* 9, 843-854.
- Massa, P.E., Li, X., Hanidu, A., Siamas, J., Pariali, M., Pareja, J., Savitt, A.G., Catron, K.M., Li, J., and Marcu, K.B. (2005). Gene Expression Profiling in Conjunction with Physiological Rescues of IKK α -null Cells with Wild Type or Mutant IKK α Reveals Distinct Classes of IKK α /NF- κ B-dependent Genes. *Journal of Biological Chemistry* 280, 14057-14069.
- Mathes, E., O'Dea, E.L., Hoffmann, A., and Ghosh, G. (2008). NF- κ B dictates the degradation pathway of IkB α . *The EMBO Journal* 27, 1357-1367.
- Mathes, E., Wang, L., Komives, E., and Ghosh, G. (2010). Flexible Regions within IkB α Create the Ubiquitin-independent Degradation Signal. *The Journal of biological chemistry* 285, 32927-32936.
- Mattes, M.J. (2007). Apoptosis assays with lymphoma cell lines: problems and pitfalls. *Br J Cancer* 96, 928-936.
- Mattioli, I., Sebald, A., Bucher, C., Charles, R.P., Nakano, H., Doi, T., Kracht, M., and Schmitz, M.L. (2004). Transient and selective NF-kappa B p65 serine 536 phosphorylation induced by T cell costimulation is mediated by I kappa B kinase beta and controls the kinetics of p65 nuclear import. *J Immunol* 172, 6336-6344.
- Mattioli, I., Geng, H., Sebald, A., Hodel, M., Bucher, C., Kracht, M., and Schmitz, M.L. (2006). Inducible Phosphorylation of NF- κ B p65 at Serine 468 by T Cell Costimulation Is Mediated by IKK ϵ . *Journal of Biological Chemistry* 281, 6175-6183.
- Mauro, C., Leow, S.C., Anso, E., Rocha, S., Thotakura, A.K., Tornatore, L., Moretti, M., De Smaele, E., Beg, A.A., Tergaonkar, V., et al. (2011). NF-kappa B controls energy homeostasis and metabolic adaptation by upregulating mitochondrial respiration. *Nature Cell Biology* 13, 1272-U1234.
- May, M.J., D'Acquisto, F., Madge, L.A., Glockner, J., Pober, J.S., and Ghosh, S. (2000). Selective inhibition of NF-kappaB activation by a peptide that blocks the interaction of NEMO with the IkappaB kinase complex. *Science* 289, 1550-1554.
- May, M.J., Marienfeld, R.B., and Ghosh, S. (2002). Characterization of the Ikappa B-kinase NEMO binding domain. *The Journal of biological chemistry* 277, 45992-46000.
- May, M.J., Larsen, S.E., Shim, J.H., Madge, L.A., and Ghosh, S. (2004). A novel ubiquitin-like domain in IkappaB kinase beta is required for functional activity of the kinase. *The Journal of biological chemistry* 279, 45528-45539.
- Mayo, M.W., Wang, C.Y., Cogswell, P.C., Rogers-Graham, K.S., Lowe, S.W., Der, C.J., and Baldwin, A.S., Jr. (1997). Requirement of NF-kappaB activation to suppress p53-independent apoptosis induced by oncogenic Ras. *Science* 278, 1812-1815.
- McClue, S.J., Blake, D., Clarke, R., Cowan, A., Cummings, L., Fischer, P.M., MacKenzie, M., Melville, J., Stewart, K., Wang, S., et al. (2002). In vitro and in vivo antitumor properties of the cyclin dependent kinase inhibitor CYC202 (R-roscovitine). *Int J Cancer* 102, 463-468.
- McCool, K.W., and Miyamoto, S. (2012). DNA damage-dependent NF- κ B activation: NEMO turns nuclear signaling inside out. *Immunological Reviews* 246, 311-326.
- Medunjanin, S., Schleithoff, L., Fiegehenn, C., Weinert, S., Zuschratter, W., and Braun-Dullaeus, R.C. (2016). GSK-3 β controls NF-kappaB activity via IKK γ /NEMO. *Scientific reports* 6, 38553.
- Mendez, M.G., Kojima, S., and Goldman, R.D. (2010). Vimentin induces changes in cell shape, motility, and adhesion during the epithelial to mesenchymal transition. *Faseb j* 24, 1838-1851.
- Mercurio, F., Murray, B.W., Shevchenko, A., Bennett, B.L., Young, D.B., Li, J.W., Pascual, G., Motiwala, A., Zhu, H., Mann, M., et al. (1999). IkappaB kinase (IKK)-associated protein 1, a common component of the heterogeneous IKK complex. *Mol Cell Biol* 19, 1526-1538.

- Mestas, J., and Hughes, C.C. (2004). Of mice and not men: differences between mouse and human immunology. *J Immunol* 172, 2731-2738.
- Mészáros, B., Simon, I., and Dosztányi, Z. (2009). Prediction of Protein Binding Regions in Disordered Proteins. *PLOS Computational Biology* 5, e1000376.
- Meylan, E., Burns, K., Hofmann, K., Blancheteau, V., Martinon, F., Kelliher, M., and Tschoopp, J. (2004). RIP1 is an essential mediator of Toll-like receptor 3-induced NF-kappa B activation. *Nat Immunol* 5, 503-507.
- Meylan, E., Dooley, A.L., Feldser, D.M., Shen, L., Turk, E., Ouyang, C., and Jacks, T. (2009). Requirement for NF-kappaB signalling in a mouse model of lung adenocarcinoma. *Nature* 462, 104-107.
- Micheau, O., Thome, M., Schneider, P., Holler, N., Tschoopp, J., Nicholson, D.W., Briand, C., and Grütter, M.G. (2002). The long form of FLIP is an activator of caspase-8 at the Fas death-inducing signaling complex. *Journal of Biological Chemistry* 277, 45162-45171.
- Micheau, O., and Tschoopp, J. (2003). Induction of TNF receptor I-mediated apoptosis via two sequential signaling complexes. *Cell* 114, 181-190.
- Michel, F., Soler-Lopez, M., Petosa, C., Cramer, P., Siebenlist, U., and Muller, C.W. (2001). Crystal structure of the ankyrin repeat domain of Bcl-3: a unique member of the IkappaB protein family. *Embo j* 20, 6180-6190.
- Milanovic, M., Kracht, M., and Schmitz, M.L. (2014). The cytokine-induced conformational switch of nuclear factor kB p65 is mediated by p65 phosphorylation. *Biochemical Journal* 457, 401-413.
- Miller, W.G., and Goebel, C.V. (1968). Dimensions of protein random coils. *Biochemistry* 7, 3925-3935.
- Miller, B.S., and Zandi, E. (2001). Complete Reconstitution of Human IkB Kinase (IKK) Complex in Yeast: ASSESSMENT OF ITS STOICHIOMETRY AND THE ROLE OF IKK γ ON THE COMPLEX ACTIVITY IN THE ABSENCE OF STIMULATION. *Journal of Biological Chemistry* 276, 36320-36326.
- Miranda, S., Foncea, R., Guerrero, J., and Leighton, F. (1999). Oxidative stress and upregulation of mitochondrial biogenesis genes in mitochondrial DNA-depleted HeLa cells. *Biochemical and biophysical research communications* 258, 44-49.
- Mizianty, M.J., Peng, Z., and Kurgan, L. (2013). MFDp2: Accurate predictor of disorder in proteins by fusion of disorder probabilities, content and profiles. *Intrinsically Disord Proteins* 1, e24428.
- Moisan, A., Larochelle, C., Guillemette, B., and Gaudreau, L. (2004). BRCA1 can modulate RNA polymerase II carboxy-terminal domain phosphorylation levels. *Mol Cell Biol* 24, 6947-6956.
- Moorthy, A.K., Savinova, O.V., Ho, J.Q., Wang, V.Y., Vu, D., and Ghosh, G. (2006). The 20S proteasome processes NF-kappaB1 p105 into p50 in a translation-independent manner. *Embo j* 25, 1945-1956.
- Mordmüller, B., Krappmann, D., Esen, M., Wegener, E., and Scheidereit, C. (2003). Lymphotoxin and lipopolysaccharide induce NF- κ B-p52 generation by a co-translational mechanism. *EMBO reports* 4, 82-87.
- Moreno, R., Sobotzik, J.-M., Schultz, C., and Schmitz, M.L. (2010). Specification of the NF- κ B transcriptional response by p65 phosphorylation and TNF-induced nuclear translocation of IKK ϵ . *Nucleic Acids Research* 38, 6029-6044.
- Morgan, D.O. (1995). Principles of CDK regulation. *Nature* 374, 131-134.
- Morgan, M.J., and Liu, Z.-g. (2011). Crosstalk of reactive oxygen species and NF- κ B signaling. *Cell Research* 21, 103-115.
- Moriguchi, T., Toyoshima, F., Masuyama, N., Hanafusa, H., Gotoh, Y., and Nishida, E. (1997). A novel SAPK/JNK kinase, MKK7, stimulated by TNFalpha and cellular stresses. *Embo j* 16, 7045-7053.
- Mousallem, T., Yang, J., Urban, T.J., Wang, H., Adeli, M., Parrott, R.E., Roberts, J.L., Goldstein, D.B., Buckley, R.H., and Zhong, X.P. (2014). A nonsense mutation in IKBKB causes combined immunodeficiency. *Blood* 124, 2046-2050.
- Mundade, R., Imperiale, T.F., Prabhu, L., Loehrer, P.J., and Lu, T. (2014). Genetic pathways, prevention, and treatment of sporadic colorectal cancer. *Oncoscience* 1, 400-406.
- Murray, A.W. (1992). Creative blocks: cell-cycle checkpoints and feedback controls. *Nature* 359, 599.
- Musacchio, A., and Salmon, E.D. (2007). The spindle-assembly checkpoint in space and time. *Nat Rev Mol Cell Biol* 8, 379-393.
- Nagarajan, R.P., Chen, F., Li, W., Vig, E., Harrington, M.A., Nakshatri, H., and Chen, Y. (2000). Repression of transforming-growth-factor- β -mediated transcription by nuclear factor kB. *Biochemical Journal* 348, 591-596.
- Nakanishi, C., and Toi, M. (2005). Nuclear factor-[kappa] B inhibitors as sensitizers to anticancer drugs. *Nature reviews Cancer* 5, 297.
- Nakano, H., Sakon, S., Koseki, H., Takemori, T., Tada, K., Matsumoto, M., Munechika, E., Sakai, T., Shirasawa, T., Akiba, H., et al. (1999). Targeted disruption of Traf5 gene causes defects in CD40- and CD27-mediated lymphocyte activation. *Proc Natl Acad Sci U S A* 96, 9803-9808.

- Nakshatri, H., Bhat-Nakshatri, P., Martin, D.A., Goulet, R.J., and Sledge, G.W. (1997). Constitutive activation of NF-kappaB during progression of breast cancer to hormone-independent growth. *Molecular and Cellular Biology* 17, 3629-3639.
- Napolitano, G., Mirra, S., Monfregola, J., Lavorgna, A., Leonardi, A., and Ursini, M.V. (2009). NESCA: a new NEMO/IKKgamma and TRAF6 interacting protein. *J Cell Physiol* 220, 410-417.
- Naumann, M., Nieters, A., Hatada, E.N., and Scheidereit, C. (1993). NF-kappa B precursor p100 inhibits nuclear translocation and DNA binding of NF-kappa B/rel-factors. *Oncogene* 8, 2275-2281.
- Nelson, D.E., Ihekwebe, A.E.C., Elliott, M., Johnson, J.R., Gibney, C.A., Foreman, B.E., Nelson, G., See, V., Horton, C.A., Spiller, D.G., et al. (2004). Oscillations in NF- κ B Signaling Control the Dynamics of Gene Expression. *Science* 306, 704-708.
- Nenci, A., Becker, C., Wullaert, A., Gareus, R., van Loo, G., Danese, S., Huth, M., Nikolaev, A., Neufert, C., Madison, B., et al. (2007). Epithelial NEMO links innate immunity to chronic intestinal inflammation. *Nature* 446, 557-561.
- Neumann, M., Klar, S., Wilisch-Neumann, A., Hollenbach, E., Kavuri, S., Leverkus, M., Kandolf, R., Brunner-Weinzierl, M.C., and Klingel, K. (2011). Glycogen synthase kinase-3beta is a crucial mediator of signal-induced RelB degradation. *Oncogene* 30, 2485-2492.
- Ng, A.H., Fang, N.N., Comyn, S.A., Gsponer, J., and Mayor, T. (2013). System-wide analysis reveals intrinsically disordered proteins are prone to ubiquitylation after misfolding stress. *Molecular & cellular proteomics : MCP* 12, 2456-2467.
- Ngadjeua, F., Chiaravalli, J., Traincard, F., Raynal, B., Fontan, E., and Agou, F. (2013). Two-sided Ubiquitin Binding of NF- κ B Essential Modulator (NEMO) Zinc Finger Unveiled by a Mutation Associated with Anhidrotic Ectodermal Dysplasia with Immunodeficiency Syndrome. *Journal of Biological Chemistry* 288, 33722-33737.
- Nieman, M.T., Prudoff, R.S., Johnson, K.R., and Wheelock, M.J. (1999). N-cadherin promotes motility in human breast cancer cells regardless of their E-cadherin expression. *J Cell Biol* 147, 631-644.
- Ninomiya-Tsuji, J., Kishimoto, K., Hiyama, A., Inoue, J., Cao, Z., and Matsumoto, K. (1999). The kinase TAK1 can activate the NIK-I kappaB as well as the MAP kinase cascade in the IL-1 signalling pathway. *Nature* 398, 252-256.
- Nishitoh, H., Saitoh, M., Mochida, Y., Takeda, K., Nakano, H., Rothe, M., Miyazono, K., and Ichijo, H. (1998). ASK1 is essential for JNK/SAPK activation by TRAF2. *Molecular cell* 2, 389-395.
- Nolan, G.P., Ghosh, S., Liou, H.C., Tempst, P., and Baltimore, D. (1991). DNA binding and I kappa B inhibition of the cloned p65 subunit of NF-kappa B, a rel-related polypeptide. *Cell* 64, 961-969.
- Nolan, G.P., Fujita, T., Bhatia, K., Huppi, C., Liou, H.C., Scott, M.L., and Baltimore, D. (1993). The bcl-3 proto-oncogene encodes a nuclear I kappa B-like molecule that preferentially interacts with NF-kappa B p50 and p52 in a phosphorylation-dependent manner. *Molecular and Cellular Biology* 13, 3557-3566.
- Nottingham, L.K., Yan, C.H., Yang, X., Si, H., Coupar, J., Bian, Y., Cheng, T.F., Allen, C., Arun, P., Gius, D., et al. (2014). Aberrant IKKalpha and IKKbeta cooperatively activate NF-kappaB and induce EGFR/AP1 signaling to promote survival and migration of head and neck cancer. *Oncogene* 33, 1135-1147.
- Nowak, D.E., Tian, B., Jamaluddin, M., Boldogh, I., Vergara, L.A., Choudhary, S., and Brasier, A.R. (2008). RelA Ser276 Phosphorylation Is Required for Activation of a Subset of NF- κ B-Dependent Genes by Recruiting Cyclin-Dependent Kinase 9/Cyclin T1 Complexes. *Molecular and Cellular Biology* 28, 3623-3638.
- Nurse, P. (1990). Universal control mechanism regulating onset of M-phase. *Nature* 344, 503-508.
- O'Brien, C.A., Kreso, A., Ryan, P., Hermans, K.G., Gibson, L., Wang, Y., Tsatsanis, A., Gallinger, S., and Dick, J.E. (2012). ID1 and ID3 regulate the self-renewal capacity of human colon cancer-initiating cells through p21. *Cancer Cell* 21, 777-792.
- Oelgeschlager, T. (2002). Regulation of RNA polymerase II activity by CTD phosphorylation and cell cycle control. *J Cell Physiol* 190, 160-169.
- Oguma, K., Oshima, H., Aoki, M., Uchio, R., Naka, K., Nakamura, S., Hirao, A., Saya, H., Taketo, M.M., and Oshima, M. (2008). Activated macrophages promote Wnt signalling through tumour necrosis factor- α in gastric tumour cells. *The EMBO Journal* 27, 1671-1681.
- Oh, W.J., Wu, C.C., Kim, S.J., Facchinetto, V., Julien, L.A., Finlan, M., Roux, P.P., Su, B., and Jacinto, E. (2010). mTORC2 can associate with ribosomes to promote cotranslational phosphorylation and stability of nascent Akt polypeptide. *Embo j* 29, 3939-3951.
- Oh, S.C., Park, Y.Y., Park, E.S., Lim, J.Y., Kim, S.M., Kim, S.B., Kim, J., Kim, S.C., Chu, I.S., Smith, J.J., et al. (2012). Prognostic gene expression signature associated with two molecularly distinct subtypes of colorectal cancer. *Gut* 61, 1291-1298.
- Ohno, H., Takimoto, G., and McKeithan, T.W. (1990). The candidate proto-oncogene bcl-3 is related to genes implicated in cell lineage determination and cell cycle control. *Cell* 60, 991-997.

- Ohno, A., Jee, J., Fujiwara, K., Tenno, T., Goda, N., Tochio, H., Kobayashi, H., Hiroaki, H., and Shirakawa, M. (2005). Structure of the UBA domain of Dsk2p in complex with ubiquitin molecular determinants for ubiquitin recognition. *Structure* 13, 521-532.
- Okazaki, T., Sakon, S., Sasazuki, T., Sakurai, H., Doi, T., Yagita, H., Okumura, K., and Nakano, H. (2003). Phosphorylation of serine 276 is essential for p65 NF- κ B subunit-dependent cellular responses. *Biochemical and biophysical research communications* 300, 807-812.
- Oldfield, C.J., Cheng, Y., Cortese, M.S., Romero, P., Uversky, V.N., and Dunker, A.K. (2005). Coupled folding and binding with alpha-helix-forming molecular recognition elements. *Biochemistry* 44, 12454-12470.
- O'Mahony, A.M., Montano, M., Van Beneden, K., Chen, L.F., and Greene, W.C. (2004). Human T-cell lymphotropic virus type 1 tax induction of biologically Active NF- κ pB requires IkappaB kinase-1-mediated phosphorylation of RelA/p65. *The Journal of biological chemistry* 279, 18137-18145.
- O'Mahony, A.M., Montano, M., Van Beneden, K., Chen, L.-F., and Greene, W.C. (2004). Human T-cell Lymphotropic Virus Type 1 Tax Induction of Biologically Active NF- κ B Requires IkB Kinase-1-mediated Phosphorylation of RelA/p65. *Journal of Biological Chemistry* 279, 18137-18145.
- Osmulski, P.A., and Gaczynska, M. (2000). Atomic force microscopy reveals two conformations of the 20 S proteasome from fission yeast. *The Journal of biological chemistry* 275, 13171-13174.
- Ozes, O.N., Mayo, L.D., Gustin, J.A., Pfeffer, S.R., Pfeffer, L.M., and Donner, D.B. (1999). NF- κ pB activation by tumour necrosis factor requires the Akt serine-threonine kinase. *Nature* 401.
- Palayoor, S.T., Youmell, M.Y., Calderwood, S.K., Coleman, C.N., and Price, B.D. (1999). Constitutive activation of IkappaB kinase alpha and NF- κ pB in prostate cancer cells is inhibited by ibuprofen. *Oncogene* 18, 7389-7394.
- Palkowitzsch, L., Leidner, J., Ghosh, S., and Marienfeld, R.B. (2008). Phosphorylation of Serine 68 in the IkB Kinase (IKK)-binding Domain of NEMO Interferes with the Structure of the IKK Complex and Tumor Necrosis Factor- α -induced NF- κ B Activity. *Journal of Biological Chemistry* 283, 76-86.
- Pannicke , U., Baumann , B., Fuchs , S., Henneke , P., Rensing-Ehl , A., Rizzi , M., Janda , A., Hese , K., Schlesier , M., Holzmann , K., et al. (2013). Deficiency of Innate and Acquired Immunity Caused by an IKBKB Mutation. *New England Journal of Medicine* 369, 2504-2514.
- Park, J.M., Greten, F.R., Wong, A., Westrick, R.J., Arthur, J.S., Otsu, K., Hoffmann, A., Montminy, M., and Karin, M. (2005). Signaling pathways and genes that inhibit pathogen-induced macrophage apoptosis--CREB and NF- κ pB as key regulators. *Immunity* 23, 319-329.
- Patel, N.M., Nozaki, S., Shortle, N.H., Bhat-Nakshatri, P., Newton, T.R., Rice, S., Gelfanov, V., Boswell, S.H., Goulet, R.J., Jr., Sledge, G.W., Jr., et al. (2000). Paclitaxel sensitivity of breast cancer cells with constitutively active NF- κ pB is enhanced by IkappaBalpa super-repressor and parthenolide. *Oncogene* 19, 4159-4169.
- Patterson, C., and Cyr, D.M. (2005). Ubiquitin-proteasome protocols, Vol 301 (Springer Science & Business Media).
- Peng, K., Radivojac, P., Vucetic, S., Dunker, A.K., and Obradovic, Z. (2006). Length-dependent prediction of protein intrinsic disorder. *BMC Bioinformatics* 7, 208-208.
- Peng, Z., and Kurgan, L. (2015). High-throughput prediction of RNA, DNA and protein binding regions mediated by intrinsic disorder. *Nucleic Acids Research* 43, e121-e121.
- Perkins, N.D., Felzien, L.K., Betts, J.C., Leung, K., Beach, D.H., and Nabel, G.J. (1997). Regulation of NF- κ pB by cyclin-dependent kinases associated with the p300 coactivator. *Science* 275, 523-527.
- Perkins, N.D. (2004). NF- κ B: tumor promoter or suppressor? *Trends in Cell Biology* 14, 64-69.
- Perkins, N.D. (2006). Post-translational modifications regulating the activity and function of the nuclear factor kappa B pathway. *Oncogene* 25, 6717.
- Persengiev, S.P., Zhu, X., and Green, M.R. (2004). Nonspecific, concentration-dependent stimulation and repression of mammalian gene expression by small interfering RNAs (siRNAs). *Rna* 10, 12-18.
- Petersen, S.L., Wang, L., Yalcin-Chin, A., Li, L., Peyton, M., Minna, J., Harran, P., and Wang, X. (2007). Autocrine TNF α Signaling Renders Human Cancer Cells Susceptible to Smac-Mimetic-Induced Apoptosis. *Cancer Cell* 12, 445-456.
- Pfeffer, K. (2003). Biological functions of tumor necrosis factor cytokines and their receptors. *Cytokine Growth Factor Rev* 14, 185-191.
- Pham, A.M., and tenOever, B.R. (2010). The IKK Kinases: Operators of Antiviral Signaling. *Viruses* 2, 55-72.
- Phelps, C.B., Sengchanthalangsy, L.L., Malek, S., and Ghosh, G. (2000). Mechanism of kappa B DNA binding by Rel/NF- κ pB dimers. *The Journal of biological chemistry* 275, 24392-24399.
- Phillips, R.J., and Ghosh, S. (1997). Regulation of IkappaB beta in WEHI 231 mature B cells. *Molecular and Cellular Biology* 17, 4390-4396.
- Picco, V., and Pages, G. (2013). Linking JNK Activity to the DNA Damage Response. *Genes & cancer* 4, 360-368.

- Pickrell, J.K., Marioni, J.C., Pai, A.A., Degner, J.F., Engelhardt, B.E., Nkadori, E., Veyrieras, J.-B., Stephens, M., Gilad, Y., and Pritchard, J.K. (2010). Understanding mechanisms underlying human gene expression variation with RNA sequencing. *Nature* **464**, 768-772.
- Ping, H., Yang, F., Wang, M., Niu, Y., and Xing, N. (2016). IKK inhibitor suppresses epithelial-mesenchymal transition and induces cell death in prostate cancer. *Oncology reports* **36**, 1658-1664.
- Pires, B.R., Mencalha, A.L., Ferreira, G.M., de Souza, W.F., Morgado-Diaz, J.A., Maia, A.M., Correa, S., and Abdelhay, E.S. (2017). NF-kappaB Is Involved in the Regulation of EMT Genes in Breast Cancer Cells. *PLoS one* **12**, e0169622.
- Pirngruber, J., and Johnsen, S.A. (2010). Induced G1 cell-cycle arrest controls replication-dependent histone mRNA 3' end processing through p21, NPAT and CDK9. *Oncogene* **29**, 2853-2863.
- Polley, S., Huang, D.-B., Hauenstein, A.V., Fusco, A.J., Zhong, X., Vu, D., Schröfelbauer, B., Kim, Y., Hoffmann, A., Verma, I.M., et al. (2013). A Structural Basis for IkB Kinase 2 Activation Via Oligomerization-Dependent Trans Auto-Phosphorylation. *PLOS Biology* **11**, e1001581.
- Polley, S., Passos, Dario O., Huang, D.-B., Mulero, Maria C., Mazumder, A., Biswas, T., Verma, Inder M., Lyumkis, D., and Ghosh, G. (2016). Structural Basis for the Activation of IKK1/α. *Cell Reports* **17**, 1907-1914.
- Polymeropoulos, M.H., Lavedan, C., Leroy, E., Ide, S.E., Dehejia, A., Dutra, A., Pike, B., Root, H., Rubenstein, J., Boyer, R., et al. (1997). Mutation in the alpha-synuclein gene identified in families with Parkinson's disease. *Science* **276**, 2045-2047.
- Pomerantz, J.L., and Baltimore, D. (1999). NF-κB activation by a signaling complex containing TRAF2, TANK and TBK1, a novel IKK-related kinase. *The EMBO Journal* **18**, 6694-6704.
- Potapova, O., Basu, S., Mercola, D., and Holbrook, N.J. (2001). Protective Role for c-Jun in the Cellular Response to DNA Damage. *Journal of Biological Chemistry* **276**, 28546-28553.
- Poyet, J.L., Srinivasula, S.M., Lin, J.H., Fernandes-Alnemri, T., Yamaoka, S., Tsichlis, P.N., and Alnemri, E.S. (2000). Activation of the Ikappa B kinases by RIP via IKKgamma /NEMO-mediated oligomerization. *The Journal of biological chemistry* **275**, 37966-37977.
- Pradère, J.-P., Hernandez, C., Koppe, C., Friedman, R.A., Luedde, T., and Schwabe, R.F. (2016). Negative regulation of NF-κB p65 activity by serine 536 phosphorylation. *Science Signaling* **9**, ra85-ra85.
- Prajapati, S., and Gaynor, R.B. (2002). Regulation of Ikappa B kinase (IKK)gamma /NEMO function by IKKbeta - mediated phosphorylation. *The Journal of biological chemistry* **277**, 24331-24339.
- Prajapati, S., Tu, Z., Yamamoto, Y., and Gaynor, R.B. (2006). IKKalpha regulates the mitotic phase of the cell cycle by modulating Aurora A phosphorylation. *Cell Cycle* **5**.
- Prakash, S., Tian, L., Ratliff, K.S., Lehotzky, R.E., and Matouschek, A. (2004). An unstructured initiation site is required for efficient proteasome-mediated degradation. *Nat Struct Mol Biol* **11**, 830-837.
- Puvvada, S.D., Funkhouser, W.K., Greene, K., Deal, A., Chu, H., Baldwin, A.S., Tepper, J.E., and O'Neil, B.H. (2010). NF-κB and Bcl-3 activation are prognostic in metastatic colorectal cancer. *Oncology* **78**, 181-188.
- Qing, G., Qu, Z., and Xiao, G. (2005). Regulation of NF-κB2 p100 Processing by Its cis-Acting Domain. *Journal of Biological Chemistry* **280**, 18-27.
- Qing, G., and Xiao, G. (2005). Essential Role of IkB Kinase α in the Constitutive Processing of NF-κB2 p100. *Journal of Biological Chemistry* **280**, 9765-9768.
- Quail, D.F., and Joyce, J.A. (2013). Microenvironmental regulation of tumor progression and metastasis. *Nature medicine* **19**, 1423-1437.
- Raasi, S., Varadan, R., Fushman, D., and Pickart, C.M. (2005). Diverse polyubiquitin interaction properties of ubiquitin-associated domains. *Nat Struct Mol Biol* **12**, 708-714.
- Rahighi, S., Ikeda, F., Kawasaki, M., Akutsu, M., Suzuki, N., Kato, R., Kensche, T., Uejima, T., Bloor, S., Komander, D., et al. (2009). Specific recognition of linear ubiquitin chains by NEMO is important for NF-kappaB activation. *Cell* **136**, 1098-1109.
- Raingeaud, J., Whitmarsh, A.J., Barrett, T., Dérijard, B., and Davis, R.J. (1996). MKK3- and MKK6-regulated gene expression is mediated by the p38 mitogen-activated protein kinase signal transduction pathway. *Molecular and Cellular Biology* **16**, 1247-1255.
- Rakkaa, T., Escude, C., Giet, R., Magnaghi-Jaulin, L., and Jaulin, C. (2014). CDK11(p58) kinase activity is required to protect sister chromatid cohesion at centromeres in mitosis. *Chromosome research : an international journal on the molecular, supramolecular and evolutionary aspects of chromosome biology* **22**, 267-276.
- Rakoff-Nahoum, S., and Medzhitov, R. (2007). Regulation of Spontaneous Intestinal Tumorigenesis Through the Adaptor Protein MyD88. *Science* **317**, 124-127.
- Ramakrishna, S., Suresh, B., Lim, K.H., Cha, B.H., Lee, S.H., Kim, K.S., and Baek, K.H. (2011). PEST motif sequence regulating human NANOG for proteasomal degradation. *Stem cells and development* **20**, 1511-1519.

- Ran, R., Lu, A., Zhang, L., Tang, Y., Zhu, H., Xu, H., Feng, Y., Han, C., Zhou, G., Rigby, A.C., et al. (2004). Hsp70 promotes TNF-mediated apoptosis by binding IKK gamma and impairing NF-kappa B survival signaling. *Genes Dev* 18, 1466-1481.
- Rao, H., and Sastry, A. (2002). Recognition of Specific Ubiquitin Conjugates Is Important for the Proteolytic Functions of the Ubiquitin-associated Domain Proteins Dsk2 and Rad23. *Journal of Biological Chemistry* 277, 11691-11695.
- Rao, P., Hayden, M.S., Long, M., Scott, M.L., West, A.P., Zhang, D., Oeckinghaus, A., Lynch, C., Hoffmann, A., Baltimore, D., et al. (2010). IkappaBbeta acts to inhibit and activate gene expression during the inflammatory response. *Nature* 466, 1115-1119.
- Raskatov, J.A., Meier, J.L., Puckett, J.W., Yang, F., Ramakrishnan, P., and Dervan, P.B. (2012). Modulation of NF- κ B-dependent gene transcription using programmable DNA minor groove binders. *Proceedings of the National Academy of Sciences* 109, 1023-1028.
- Raskatov, J.A., Meier, J.L., Puckett, J.W., Yang, F., Ramakrishnan, P., and Dervan, P.B. (2012). Modulation of NF- κ B-dependent gene transcription using programmable DNA minor groove binders. *Proc Natl Acad Sci U S A* 109, 1023-1028.
- Ratner, J.N., Balasubramanian, B., Corden, J., Warren, S.L., and Bregman, D.B. (1998). Ultraviolet radiation-induced ubiquitination and proteasomal degradation of the large subunit of RNA polymerase II. Implications for transcription-coupled DNA repair. *The Journal of biological chemistry* 273, 5184-5189.
- Razani, B., Zarnegar, B., Ytterberg, A.J., Shiba, T., Dempsey, P.W., Ware, C.F., Loo, J.A., and Cheng, G. (2010). Negative feedback in noncanonical NF- κ B signaling modulates NIK stability through IKKalpha-mediated phosphorylation. *Sci Signal* 3, ra41.
- Razani, B., Reichardt, A.D., and Cheng, G. (2011). Non-canonical NF- κ B signaling activation and regulation: principles and perspectives. *Immunol Rev* 244, 44-54.
- Rechsteiner, M., and Rogers, S.W. (1996). PEST sequences and regulation by proteolysis. *Trends in Biochemical Sciences* 21, 267-271.
- Reichling, T., Goss, K.H., Carson, D.J., Holdcraft, R.W., Ley-Ebert, C., Witte, D., Aronow, B.J., and Groden, J. (2005). Transcriptional profiles of intestinal tumors in Apc(Min) mice are unique from those of embryonic intestine and identify novel gene targets dysregulated in human colorectal tumors. *Cancer Res* 65, 166-176.
- Religa, T.L., Sprangers, R., and Kay, L.E. (2010). Dynamic regulation of archaeal proteasome gate opening as studied by TROSY NMR. *Science* 328, 98-102.
- Renner, F., Moreno, R., and Schmitz, M.L. (2010). SUMOylation-Dependent Localization of IKKE in PML Nuclear Bodies Is Essential for Protection against DNA-Damage-Triggered Cell Death. *Molecular cell* 37, 503-515.
- Rickard, J.A., Anderton, H., Etemadi, N., Nachbur, U., Darding, M., Peltzer, N., Lalaoui, N., Lawlor, K.E., Vanyai, H., Hall, C., et al. (2014). TNFR1-dependent cell death drives inflammation in Sharpen-deficient mice. *eLife* 3, e03464.
- Riedlinger, T., Dommerholt, M.B., Wijshake, T., Kruit, J.K., Huijkman, N., Dekker, D., Koster, M., Kloosterhuis, N., Koonen, D.P.Y., de Bruin, A., et al. (2017). NF- κ B p65 serine 467 phosphorylation sensitizes mice to weight gain and TNF α -or diet-induced inflammation. *Biochimica et Biophysica Acta (BBA) - Molecular Cell Research* 1864, 1785-1798.
- Rock, K.L., Gramm, C., Rothstein, L., Clark, K., Stein, R., Dick, L., Hwang, D., and Goldberg, A.L. (1994). Inhibitors of the proteasome block the degradation of most cell proteins and the generation of peptides presented on MHC class I molecules. *Cell* 78, 761-771.
- Rockx, D.A., Mason, R., van Hoffen, A., Barton, M.C., Citterio, E., Bregman, D.B., van Zeeland, A.A., Vrieling, H., and Mullenders, L.H. (2000). UV-induced inhibition of transcription involves repression of transcription initiation and phosphorylation of RNA polymerase II. *Proc Natl Acad Sci U S A* 97, 10503-10508.
- Roessler, M., Rollinger, W., Mantovani-Endl, L., Hagmann, M.L., Palme, S., Berndt, P., Engel, A.M., Pfeffer, M., Karl, J., Bodenmuller, H., et al. (2006). Identification of PSME3 as a novel serum tumor marker for colorectal cancer by combining two-dimensional polyacrylamide gel electrophoresis with a strictly mass spectrometry-based approach for data analysis. *Molecular & cellular proteomics : MCP* 5, 2092-2101.
- Rogers, S., Wells, R., and Rechsteiner, M. (1986). Amino acid sequences common to rapidly degraded proteins: the PEST hypothesis. *Science* 234, 364-368.
- Rojo, F., Gonzalez-Perez, A., Furriol, J., Nicolau, M.J., Ferrer, J., Burgues, O., Sabbaghi, M., Gonzalez-Navarrete, I., Cristobal, I., Serrano, L., et al. (2016). Non-canonical NF- κ B pathway activation predicts outcome in borderline oestrogen receptor positive breast carcinoma. *Br J Cancer* 115, 322-331.
- Romero, P., Obradovic, Z., Li, X., Garner, E.C., Brown, C.J., and Dunker, A.K. (2001). Sequence complexity of disordered protein. *Proteins* 42, 38-48.

- Rosebeck, S., Madden, L., Jin, X., Gu, S., Apel, I.J., Appert, A., Hamoudi, R.A., Noels, H., Sagaert, X., Van Loo, P., et al. (2011). Cleavage of NIK by the API2-MALT1 fusion oncoprotein leads to noncanonical NF-kappaB activation. *Science* 331, 468-472.
- Rothwarf, D.M., Zandi, E., Natoli, G., and Karin, M. (1998). IKK-gamma is an essential regulatory subunit of the IkappaB kinase complex. *Nature* 395, 297-300.
- Rovillain, E., Mansfield, L., Caetano, C., Alvarez-Fernandez, M., Caballero, O.L., Medema, R.H., Hummerich, H., and Jat, P.S. (2011). Activation of nuclear factor-kappa B signalling promotes cellular senescence. *Oncogene* 30, 2356-2366.
- Rubbi, C.P., and Milner, J. (2003). Disruption of the nucleolus mediates stabilization of p53 in response to DNA damage and other stresses. *Embo j* 22, 6068-6077.
- Rubin, D.C., Shaker, A., and Levin, M.S. (2012). Chronic intestinal inflammation: inflammatory bowel disease and colitis-associated colon cancer. *Frontiers in Immunology* 3, 107.
- Rudolph, D., Yeh, W.C., Wakeham, A., Rudolph, B., Nallainathan, D., Potter, J., Elia, A.J., and Mak, T.W. (2000). Severe liver degeneration and lack of NF-kappaB activation in NEMO/IKKgamma-deficient mice. *Genes Dev* 14, 854-862.
- Ruocco, M.G., Maeda, S., Park, J.M., Lawrence, T., Hsu, L.-C., Cao, Y., Schett, G., Wagner, E.F., and Karin, M. (2005). IKB kinase (IKK) β , but not IKK α , is a critical mediator of osteoclast survival and is required for inflammation-induced bone loss. *The Journal of Experimental Medicine* 201, 1677-1687.
- Rushe, M., Silvian, L., Bixler, S., Chen, L.L., Cheung, A., Bowes, S., Cuervo, H., Berkowitz, S., Zheng, T., Guckian, K., et al. (2008). Structure of a NEMO/IKK-Associating Domain Reveals Architecture of the Interaction Site. *Structure* 16, 798-808.
- Russo, A.A., Jeffrey, P.D., and Pavletich, N.P. (1996). Structural basis of cyclin-dependent kinase activation by phosphorylation. *Nature Structural & Molecular Biology* 3, 696-700.
- Rustgi, A.K. (2007). The genetics of hereditary colon cancer. *Genes Dev* 21, 2525-2538.
- Ryan, A.E., Colleran, A., O'Gorman, A., O'Flynn, L., Pindjacova, J., Lohan, P., O'Malley, G., Nosov, M., Mureau, C., and Egan, L.J. (2015). Targeting colon cancer cell NF-kappaB promotes an anti-tumour M1-like macrophage phenotype and inhibits peritoneal metastasis. *Oncogene* 34, 1563-1574.
- Ryseck, R.P., Bull, P., Takamiya, M., Bours, V., Siebenlist, U., Dobrzanski, P., and Bravo, R. (1992). RelB, a new Rel family transcription activator that can interact with p50-NF-kappa B. *Mol Cell Biol* 12, 674-684.
- Saccani, S., Pantano, S., and Natoli, G. (2003). Modulation of NF- κ B Activity by Exchange of Dimers. *Molecular cell* 11, 1563-1574.
- Saito, K., Kigawa, T., Koshiba, S., Sato, K., Matsuo, Y., Sakamoto, A., Takagi, T., Shirouzu, M., Yabuki, T., Nunokawa, E., et al. (2004). The CAP-Gly domain of CYLD associates with the proline-rich sequence in NEMO/IKKgamma. *Structure* 12, 1719-1728.
- Saitoh, T., Nakayama, M., Nakano, H., Yagita, H., Yamamoto, N., and Yamaoka, S. (2003). TWEAK Induces NF- κ B2 p100 Processing and Long Lasting NF- κ B Activation. *Journal of Biological Chemistry* 278, 36005-36012.
- Sakamoto, K., Maeda, S., Hikiba, Y., Nakagawa, H., Hayakawa, Y., Shibata, W., Yanai, A., Ogura, K., and Omata, M. (2009). Constitutive NF-kappaB activation in colorectal carcinoma plays a key role in angiogenesis, promoting tumor growth. *Clinical cancer research : an official journal of the American Association for Cancer Research* 15, 2248-2258.
- Sakamoto, K., Hikiba, Y., Nakagawa, H., Hirata, Y., Hayakawa, Y., Kinoshita, H., Nakata, W., Sakitani, K., Takahashi, R., Akanuma, M., et al. (2013). Promotion of DNA repair by nuclear IKK[math]\beta phosphorylation of ATM in response to genotoxic stimuli. *Oncogene* 32, 1854-1862.
- Sakon, S., Xue, X., Takekawa, M., Sasazuki, T., Okazaki, T., Kojima, Y., Piao, J.H., Yagita, H., Okumura, K., Doi, T., et al. (2003). NF-kappaB inhibits TNF-induced accumulation of ROS that mediate prolonged MAPK activation and necrotic cell death. *Embo j* 22, 3898-3909.
- Sakurai, H., Chiba, H., Miyoshi, H., Sugita, T., and Toriumi, W. (1999). IkappaB kinases phosphorylate NF-kappaB p65 subunit on serine 536 in the transactivation domain. *The Journal of biological chemistry* 274, 30353-30356.
- Sandhu, K.S., and Dash, D. (2006). Conformational flexibility may explain multiple cellular roles of PEST motifs. *Proteins* 63, 727-732.
- Sandra, F., Matsuki, N.A., Takeuchi, H., Ikebe, T., Kanematsu, T., Ohishi, M., and Hirata, M. (2002). TNF inhibited the apoptosis by activation of Akt serine/threonine kinase in the human head and neck squamous cell carcinoma. *Cell Signal* 14, 771-778.
- Sanjo, H., Zajonc, D.M., Braden, R., Norris, P.S., and Ware, C.F. (2010). Allosteric regulation of the ubiquitin:NIK and ubiquitin:TRAF3 E3 ligases by the lymphotoxin-beta receptor. *The Journal of biological chemistry* 285, 17148-17155.
- Sarbassov, D.D., Guertin, D.A., Ali, S.M., and Sabatini, D.M. (2005). Phosphorylation and regulation of Akt/PKB by the rictor-mTOR complex. *Science* 307, 1098-1101.

- Sasaki, C.Y., Barberi, T.J., Ghosh, P., and Longo, D.L. (2005). Phosphorylation of RelA/p65 on serine 536 defines an I κ B α -independent NF- κ B pathway. *The Journal of biological chemistry* **280**, 34538-34547.
- Savinova, O.V., Hoffmann, A., and Ghosh, G. (2009). The NfkB1 and NfkB2 Proteins p105 and p100 Function as the Core of High-Molecular-Weight Heterogeneous Complexes. *Molecular cell* **34**, 591-602.
- Saxena, S., Jonsson, Z.O., and Dutta, A. (2003). Small RNAs with imperfect match to endogenous mRNA repress translation. Implications for off-target activity of small inhibitory RNA in mammalian cells. *The Journal of biological chemistry* **278**, 44312-44319.
- Scacheri, P.C., Rozenblatt-Rosen, O., Caplen, N.J., Wolfsberg, T.G., Umayam, L., Lee, J.C., Hughes, C.M., Shanmugam, K.S., Bhattacharjee, A., Meyerson, M., et al. (2004). Short interfering RNAs can induce unexpected and divergent changes in the levels of untargeted proteins in mammalian cells. *Proc Natl Acad Sci U S A* **101**, 1892-1897.
- Scheinman, R.I., Beg, A.A., and Baldwin, A.S. (1993). NF- κ B p100 (Lyt-10) is a component of H2TF1 and can function as an I κ B-like molecule. *Molecular and Cellular Biology* **13**, 6089-6101.
- Scherer, D.C., Brockman, J.A., Chen, Z., Maniatis, T., and Ballard, D.W. (1995). Signal-induced degradation of I κ B α requires site-specific ubiquitination. *Proceedings of the National Academy of Sciences of the United States of America* **92**, 11259-11263.
- Schlicker, A., Beran, G., Chresta, C.M., McWalter, G., Pritchard, A., Weston, S., Runswick, S., Davenport, S., Heathcote, K., and Castro, D.A. (2012). Subtypes of primary colorectal tumors correlate with response to targeted treatment in colorectal cell lines. *BMC medical genomics* **5**, 66.
- Schmidt-Suprian, M., Bloch, W., Courtois, G., Addicks, K., Israel, A., Rajewsky, K., and Pasparakis, M. (2000). NEMO/IKK gamma-deficient mice model incontinentia pigmenti. *Molecular cell* **5**, 981-992.
- Schmitz, M.L., Stelzer, G., Altmann, H., Meisterernst, M., and Baeuerle, P.A. (1995). Interaction of the COOH-terminal transactivation domain of p65 NF- κ B with TATA-binding protein, transcription factor IIB, and coactivators. *The Journal of biological chemistry* **270**, 7219-7226.
- Scholefield, J., Henriques, R., Savulescu, A.F., Fontan, E., Boucharat, A., Laplantine, E., Smahi, A., Israel, A., Agou, F., and Mhlanga, M.M. (2016). Super-resolution microscopy reveals a preformed NEMO lattice structure that is collapsed in incontinentia pigmenti. *Nat Commun* **7**, 12629.
- Schrofelbauer, B., Polley, S., Behar, M., Ghosh, G., and Hoffmann, A. (2012). NEMO ensures signaling specificity of the pleiotropic IKK β by directing its kinase activity toward I κ B α . *Molecular cell* **47**, 111-121.
- Schuster, M., Annemann, M., Plaza-Sirvent, C., and Schmitz, I. (2013). Atypical I κ B proteins – nuclear modulators of NF- κ B signaling. *Cell Communication and Signaling : CCS* **11**, 23-23.
- Schwabe, R.F., and Sakurai, H. (2005). IKK β phosphorylates p65 at S468 in transactivaton domain 2. *Faseb j* **19**, 1758-1760.
- Schwamborn, J., Lindecke, A., Elvers, M., Horejschi, V., Kerick, M., Rafigh, M., Pfeiffer, J., Prüllage, M., Kaltschmidt, B., and Kaltschmidt, C. (2003). Microarray analysis of tumor necrosis factor α induced gene expression in U373 human glioblastoma cells. *BMC Genomics* **4**, 46.
- Schwitalla, S., Fingerle, Alexander A., Cammareri, P., Nebelsiek, T., Göktuna, Serkan I., Ziegler, Paul K., Canli, O., Heijmans, J., Huels, David J., Moreaux, G., et al. (2013). Intestinal Tumorigenesis Initiated by Dedifferentiation and Acquisition of Stem-Cell-like Properties. *Cell* **152**, 25-38.
- Senderowicz, A.M., and Sausville, E.A. (2000). Preclinical and clinical development of cyclin-dependent kinase modulators. *J Natl Cancer Inst* **92**, 376-387.
- Senftleben, U., Cao, Y., Xiao, G., Greten, F.R., Krähn, G., Bonizzi, G., Chen, Y., Hu, Y., Fong, A., and Sun, S.-C. (2001). Activation by IKK α of a second, evolutionary conserved, NF- κ B signaling pathway. *Science* **293**, 1495-1499.
- Seok, J., Warren, H.S., Cuenca, A.G., Mindrinos, M.N., Baker, H.V., Xu, W., Richards, D.R., McDonald-Smith, G.P., Gao, H., Hennessy, L., et al. (2013). Genomic responses in mouse models poorly mimic human inflammatory diseases. *Proceedings of the National Academy of Sciences* **110**, 3507-3512.
- Shaked, H., Hofseth, L.J., Chumanovich, A., Chumanovich, A.A., Wang, J., Wang, Y., Taniguchi, K., Guma, M., Shenouda, S., Clevers, H., et al. (2012). Chronic epithelial NF- κ B activation accelerates APC loss and intestinal tumor initiation through iNOS up-regulation. *Proceedings of the National Academy of Sciences* **109**, 14007-14012.
- Shao, Diane D., Xue, W., Krall, Elsa B., Bhutkar, A., Piccioni, F., Wang, X., Schinzel, Anna C., Sood, S., Rosenbluh, J., Kim, Jong W., et al. (2014). KRAS and YAP1 Converge to Regulate EMT and Tumor Survival. *Cell* **158**, 171-184.
- Shembade, N., Ma, A., and Harhaj, E.W. (2010). Inhibition of NF- κ B signaling by A20 through disruption of ubiquitin enzyme complexes. *Science* **327**, 1135-1139.

- Shembade, N., Pujari, R., Harhaj, N.S., Abbott, D.W., and Harhaj, E.W. (2011). The kinase IKKalpha inhibits activation of the transcription factor NF-kappaB by phosphorylating the regulatory molecule TAX1BP1. *Nat Immunol* 12, 834-843.
- Shi, C.S., and Kehrl, J.H. (1997). Activation of stress-activated protein kinase/c-Jun N-terminal kinase, but not NF-kappaB, by the tumor necrosis factor (TNF) receptor 1 through a TNF receptor-associated factor 2- and germinal center kinase related-dependent pathway. *The Journal of biological chemistry* 272, 32102-32107.
- Shi, C.S., Leonardi, A., Kyriakis, J., Siebenlist, U., and Kehrl, J.H. (1999). TNF-mediated activation of the stress-activated protein kinase pathway: TNF receptor-associated factor 2 recruits and activates germinal center kinase related. *J Immunol* 163, 3279-3285.
- Shi, R.X., Ong, C.N., and Shen, H.M. (2004). Luteolin sensitizes tumor necrosis factor-alpha-induced apoptosis in human tumor cells. *Oncogene* 23, 7712-7721.
- Shibata, W., Takaishi, S., Muthupalani, S., Pritchard, D.M., Whary, M.T., Rogers, A.B., Fox, J.G., Betz, K.S., Kaestner, K.H., Karin, M., et al. (2010). Conditional deletion of IkappaB-kinase-beta accelerates helicobacter-dependent gastric apoptosis, proliferation, and preneoplasia. *Gastroenterology* 138, 1022-1034.e1021-1010.
- Shibata, Y., Oyama, M., Kozuka-Hata, H., Han, X., Tanaka, Y., Gohda, J., and Inoue, J. (2012). p47 negatively regulates IKK activation by inducing the lysosomal degradation of polyubiquitinated NEMO. *Nat Commun* 3, 1061.
- Shih, V.F.-S., Kearns, J.D., Basak, S., Savinova, O.V., Ghosh, G., and Hoffmann, A. (2009). Kinetic control of negative feedback regulators of NF- κ B/RelA determines their pathogen- and cytokine-receptor signaling specificity. *Proceedings of the National Academy of Sciences* 106, 9619-9624.
- Shimada, T., Kawai, T., Takeda, K., Matsumoto, M., Inoue, J.-i., Tatsumi, Y., Kanamaru, A., and Akira, S. (1999). IKK-i, a novel lipopolysaccharide-inducible kinase that is related to I κ B kinases. *International immunology* 11, 1357-1362.
- Shukla, S., MacLennan, G.T., Fu, P., Patel, J., Marengo, S.R., Resnick, M.I., and Gupta, S. (2004). Nuclear Factor- κ B/p65 (Rel A) Is Constitutively Activated in Human Prostate Adenocarcinoma and Correlates with Disease Progression. *Neoplasia* (New York, NY) 6, 390-400.
- Siggers, T., Chang, A.B., Teixeira, A., Wong, D., Williams, K.J., Ahmed, B., Ragoussis, J., Udalova, I.A., Smale, S.T., and Bulyk, M.L. (2012). Principles of dimer-specific gene regulation revealed by a comprehensive characterization of NF-[kappa] B family DNA binding. *Nature immunology* 13, 95-102.
- Singh, G.P., Ganapathi, M., Sandhu, K.S., and Dash, D. (2006). Intrinsic unstructuredness and abundance of PEST motifs in eukaryotic proteomes. *Proteins* 62, 309-315.
- Singh, A., Sweeney, M.F., Yu, M., Burger, A., Greninger, P., Benes, C., Haber, D.A., and Settleman, J. (2012). TAK1 inhibition promotes apoptosis in KRAS-dependent colon cancers. *Cell* 148, 639-650.
- Sizemore, N., Lerner, N., Dombrowski, N., Sakurai, H., and Stark, G.R. (2002). Distinct Roles of the I κ B Kinase α and β Subunits in Liberating Nuclear Factor κ B (NF- κ B) from I κ B and in Phosphorylating the p65 Subunit of NF- κ B. *Journal of Biological Chemistry* 277, 3863-3869.
- Sizemore, N., Agarwal, A., Das, K., Lerner, N., Sulak, M., Rani, S., Ransohoff, R., Shultz, D., and Stark, G.R. (2004). Inhibitor of κ B kinase is required to activate a subset of interferon γ -stimulated genes. *Proceedings of the National Academy of Sciences of the United States of America* 101, 7994-7998.
- Sledz, C.A., Holko, M., de Veer, M.J., Silverman, R.H., and Williams, B.R. (2003). Activation of the interferon system by short-interfering RNAs. *Nat Cell Biol* 5, 834-839.
- Smahi, A., Courtois, G., Vabres, P., Yamaoka, S., Heuertz, S., Munnich, A., Israel, A., Heiss, N.S., Klauck, S.M., Kioschis, P., et al. (2000). Genomic rearrangement in NEMO impairs NF-kappaB activation and is a cause of incontinentia pigmenti. The International Incontinentia Pigmenti (IP) Consortium. *Nature* 405, 466-472.
- Smahi, A., Courtois, G., Rabia, S.H., Doffinger, R., Bodemer, C., Munnich, A., Casanova, J.L., and Israel, A. (2002). The NF-kappaB signalling pathway in human diseases: from incontinentia pigmenti to ectodermal dysplasias and immune-deficiency syndromes. *Hum Mol Genet* 11, 2371-2375.
- Sobecki, M., Mrouj, K., Camasses, A., Parisi, N., Nicolas, E., Lleres, D., Gerbe, F., Prieto, S., Krasinska, L., David, A., et al. (2016). The cell proliferation antigen Ki-67 organises heterochromatin. *Elife* 5, e13722.
- Solan, N.J., Miyoshi, H., Carmona, E.M., Bren, G.D., and Paya, C.V. (2002). RelB cellular regulation and transcriptional activity are regulated by p100. *The Journal of biological chemistry* 277, 1405-1418.
- Solt, L.A., Madge, L.A., Orange, J.S., and May, M.J. (2007). Interleukin-1-induced NF- κ B activation is NEMO-dependent but does not require IKK β . *Journal of Biological Chemistry* 282, 8724-8733.
- Solt, L.A., Madge, L.A., and May, M.J. (2009). The nemo binding domains of both IKKalpha and IKKbeta regulate IKK complex assembly and classical NFkappaB activation. *Journal of Biological Chemistry*.

- Song, Y.J., Jen, K.Y., Soni, V., Kieff, E., and Cahir-McFarland, E. (2006). IL-1 receptor-associated kinase 1 is critical for latent membrane protein 1-induced p65/RelA serine 536 phosphorylation and NF-kappaB activation. *Proc Natl Acad Sci U S A* **103**, 2689-2694.
- Spiegelman, V.S., Stavropoulos, P., Latres, E., Pagano, M., Ronai, Z., Slaga, T.J., and Fuchs, S.Y. (2001). Induction of beta-transducin repeat-containing protein by JNK signaling and its role in the activation of NF-kappaB. *The Journal of biological chemistry* **276**, 27152-27158.
- Spriggs, D., Imamura, K., Rodriguez, C., Horiguchi, J., and Kufe, D.W. (1987). Induction of tumor necrosis factor expression and resistance in a human breast tumor cell line. *Proceedings of the National Academy of Sciences* **84**, 6563-6566.
- Staal, J., Bekaert, T., and Beyaert, R. (2011). Regulation of NF- κ B signaling by caspases and MALT1 paracaspase. *Cell Research* **21**, 40-54.
- Staudt, L.M. (2010). Oncogenic activation of NF-kappaB. *Cold Spring Harb Perspect Biol* **2**, a000109.
- Steinman, R.M., Mellman, I.S., Muller, W.A., and Cohn, Z.A. (1983). Endocytosis and the recycling of plasma membrane. *J Cell Biol* **96**, 1-27.
- Stilmann, M., Hinz, M., Arslan, S.Ç., Zimmer, A., Schreiber, V., and Scheidereit, C. A Nuclear Poly(ADP-Ribose)-Dependent Signalosome Confers DNA Damage-Induced IκB Kinase Activation. *Molecular cell* **36**, 365-378.
- Stock, J.K., Giadrossi, S., Casanova, M., Brookes, E., Vidal, M., Koseki, H., Brockdorff, N., Fisher, A.G., and Pombo, A. (2007). Ring1-mediated ubiquitination of H2A restrains poised RNA polymerase II at bivalent genes in mouse ES cells. *Nat Cell Biol* **9**, 1428-1435.
- Strausfeld, U., and Labbe, J. (1991). Dephosphorylation and Activation of a p34 (cdc2)/Cyclin B Complex in vitro by Human CDC25 Protein. *Nature* **351**, 242.
- Suman, S., Kurisetty, V., Das, T.P., Vadodkar, A., Ramos, G., Lakshmanaswamy, R., and Damodaran, C. (2014). Activation of AKT signaling promotes epithelial–mesenchymal transition and tumor growth in colorectal cancer cells. *Molecular carcinogenesis* **53**.
- Sumitomo, M., Tachibana, M., Nakashima, J., Murai, M., Miyajima, A., Kimura, F., Hayakawa, M., and Nakamura, H. (1999). An essential role for nuclear factor kappa B in preventing TNF-alpha-induced cell death in prostate cancer cells. *The Journal of urology* **161**, 674-679.
- Sun, S.C., Ganchi, P.A., Ballard, D.W., and Greene, W.C. (1993). NF-kappa B controls expression of inhibitor I kappa B alpha: evidence for an inducible autoregulatory pathway. *Science* **259**, 1912-1915.
- Sun, S.C., Ganchi, P.A., Beraud, C., Ballard, D.W., and Greene, W.C. (1994). Autoregulation of the NF-kappa B transactivator RelA (p65) by multiple cytoplasmic inhibitors containing ankyrin motifs. *Proc Natl Acad Sci U S A* **91**, 1346-1350.
- Sun, S.-C. (2011). Non-canonical NF- κ B signaling pathway. *Cell Research* **21**, 71-85.
- Suskiewicz, M.J., Sussman, J.L., Silman, I., and Shaul, Y. (2011). Context-dependent resistance to proteolysis of intrinsically disordered proteins. *Protein Science : A Publication of the Protein Society* **20**, 1285-1297.
- Syljuasen, R.G., Sorensen, C.S., Hansen, L.T., Fugger, K., Lundin, C., Johansson, F., Helleday, T., Sehested, M., Lukas, J., and Bartek, J. (2005). Inhibition of human Chk1 causes increased initiation of DNA replication, phosphorylation of ATR targets, and DNA breakage. *Mol Cell Biol* **25**, 3553-3562.
- Tada, K., Okazaki, T., Sakon, S., Kobayai, T., Kurosawa, K., Yamaoka, S., Hashimoto, H., Mak, T.W., Yagita, H., Okumura, K., et al. (2001). Critical roles of TRAF2 and TRAF5 in tumor necrosis factor-induced NF-kappa B activation and protection from cell death. *The Journal of biological chemistry* **276**, 36530-36534.
- Tai, D.I., Tsai, S.L., Chang, Y.H., Huang, S.N., Chen, T.C., Chang, K.S., and Liaw, Y.F. (2000). Constitutive activation of nuclear factor κ B in hepatocellular carcinoma. *Cancer* **89**, 2274-2281.
- Takeda, K., Takeuchi, O., Tsujimura, T., Itami, S., Adachi, O., Kawai, T., Sanjo, H., Yoshikawa, K., Terada, N., and Akira, S. (1999). Limb and skin abnormalities in mice lacking IKKalpha. *Science* **284**.
- Talbot, L.J., Bhattacharya, S.D., and Kuo, P.C. (2012). Epithelial-mesenchymal transition, the tumor microenvironment, and metastatic behavior of epithelial malignancies. *International Journal of Biochemistry and Molecular Biology* **3**, 117-136.
- Tanaka, K., Babic, I., Nathanson, D., Akhavan, D., Guo, D., Gini, B., Dang, J., Zhu, S., Yang, H., De Jesus, J., et al. (2011). Oncogenic EGFR signaling activates an mTORC2-NF-kappaB pathway that promotes chemotherapy resistance. *Cancer Discov* **1**, 524-538.
- Tang, X., Liu, D., Shishodia, S., Ozburn, N., Behrens, C., Lee, J.J., Hong, W.K., Aggarwal, B.B., and Wistuba, II (2006). Nuclear factor-kappaB (NF-kappaB) is frequently expressed in lung cancer and preneoplastic lesions. *Cancer* **107**, 2637-2646.
- Tao, Z., Fusco, A., Huang, D.-B., Gupta, K., Young Kim, D., Ware, C.F., Van Duyne, G.D., and Ghosh, G. (2014). p100/IkB δ sequesters and inhibits NF- κ B through kappaBsome formation. *Proceedings of the National Academy of Sciences* **111**, 15946-15951.

- Taraswi, B., Nath, S., and Roychoudhury, S. (2008). Repression of the spindle assembly checkpoint gene CDC20 by p53 upon DNA damage. *Cancer Research* 68, 2597-2597.
- Tay, S., Hughey, J.J., Lee, T.K., Lipniacki, T., Quake, S.R., and Covert, M.W. (2010). Single-cell NF-[kgr]B dynamics reveal digital activation and analogue information processing. *Nature* 466, 267-271.
- Taylor, W.R., and Stark, G.R. (2001). Regulation of the G2/M transition by p53. *Oncogene* 20, 1803-1815.
- Tegethoff, S., Behlke, J., and Scheidereit, C. (2003). Tetrameric Oligomerization of IκB Kinase γ (IKK γ) Is Obligatory for IKK Complex Activity and NF-κB Activation. *Molecular and Cellular Biology* 23, 2029-2041.
- Tenesa, A., and Dunlop, M.G. (2009). New insights into the aetiology of colorectal cancer from genome-wide association studies. *Nat Rev Genet* 10, 353-358.
- Tennagels, N., Bergschneider, E., Al-Hasani, H., and Klein, H.W. (2000). Autophosphorylation of the two C-terminal tyrosine residues Tyr1316 and Tyr1322 modulates the activity of the insulin receptor kinase in vitro. *FEBS Lett* 479, 67-71.
- Tergaonkar, V., Correa, R.G., Ikawa, M., and Verma, I.M. (2005). Distinct roles of IκappaB proteins in regulating constitutive NF-κappaB activity. *Nat Cell Biol* 7, 921-923.
- Terzić, J., Grivennikov, S., Karin, E., and Karin, M. Inflammation and Colon Cancer. *Gastroenterology* 138, 2101-2114.e2105.
- Thakur, S., Lin, H.C., Tseng, W.T., Kumar, S., Bravo, R., Foss, F., Gelinas, C., and Rabson, A.B. (1994). Rearrangement and altered expression of the NFκB-2 gene in human cutaneous T-lymphoma cells. *Oncogene* 9, 2335-2344.
- Theillet, F.X., Kalmar, L., Tompa, P., Han, K.H., Selenko, P., Dunker, A.K., Daughdrill, G.W., and Uversky, V.N. (2013). The alphabet of intrinsic disorder: I. Act like a Pro: On the abundance and roles of proline residues in intrinsically disordered proteins. *Intrinsically Disord Proteins* 1, e24360.
- Thiery, J.P. (2002). Epithelial-mesenchymal transitions in tumour progression. *Nat Rev Cancer* 2, 442-454.
- Thiery, J.P., Acloque, H., Huang, R.Y., and Nieto, M.A. (2009). Epithelial-mesenchymal transitions in development and disease. *Cell* 139, 871-890.
- Thrower, J.S., Hoffman, L., Rechsteiner, M., and Pickart, C.M. (2000). Recognition of the polyubiquitin proteolytic signal. *Embo j* 19, 94-102.
- Tian, B., Nowak, D.E., and Brasier, A.R. (2005). A TNF-induced gene expression program under oscillatory NF-κappaB control. *BMC Genomics* 6, 137.
- Tian, B., Nowak, D.E., Jamaluddin, M., Wang, S., and Brasier, A.R. (2005). Identification of direct genomic targets downstream of the nuclear factor-κappaB transcription factor mediating tumor necrosis factor signaling. *The Journal of biological chemistry* 280, 17435-17448.
- Ting, A.T., Pimentel-Muiños, F.X., and Seed, B. (1996). RIP mediates tumor necrosis factor receptor 1 activation of NF-κappaB but not Fas/APO-1-initiated apoptosis. *Embo j* 15, 6189-6196.
- Ting, A.T., Pimentel-Muiños, F.X., and Seed, B. (1996). RIP mediates tumor necrosis factor receptor 1 activation of NF-κappaB but not Fas/APO-1-initiated apoptosis. *The EMBO Journal* 15, 6189-6196.
- Tokunaga, F., Sakata, S., Saeki, Y., Satomi, Y., Kirisako, T., Kamei, K., Nakagawa, T., Kato, M., Murata, S., Yamaoka, S., et al. (2009). Involvement of linear polyubiquitylation of NEMO in NF-κappaB activation. *Nat Cell Biol* 11, 123-132.
- Tokunaga, F., Nakagawa, T., Nakahara, M., Saeki, Y., Taniguchi, M., Sakata, S., Tanaka, K., Nakano, H., and Iwai, K. (2011). SHARPIN is a component of the NF-κappaB-activating linear ubiquitin chain assembly complex. *Nature* 471, 633-636.
- Tomita, K., van Bokhoven, A., van Leenders, G.J., Ruijter, E.T., Jansen, C.F., Bussemakers, M.J., and Schalken, J.A. (2000). Cadherin switching in human prostate cancer progression. *Cancer Res* 60, 3650-3654.
- Tornatore, L., Sandomenico, A., Raimondo, D., Low, C., Rocci, A., Tralau-Stewart, C., Capece, D., D'Andrea, D., Bua, M., Boyle, E., et al. (2014). Cancer-selective targeting of the NF-κappaB survival pathway with GADD45beta/MKK7 inhibitors. *Cancer Cell* 26, 495-508.
- Tosolini, M., Kirilovsky, A., Mlecnik, B., Fredriksen, T., Mauger, S., Bindea, G., Berger, A., Bruneval, P., Fridman, W.H., Pages, F., et al. (2011). Clinical impact of different classes of infiltrating T cytotoxic and helper cells (Th1, Th2, Treg, Th17) in patients with colorectal cancer. *Cancer Res* 71, 1263-1271.
- Traenckner, E., Pahl, H.L., Henkel, T., Schmidt, K., Wilk, S., and Baeuerle, P. (1995). Phosphorylation of human I kappa B-alpha on serines 32 and 36 controls I kappa B-alpha proteolysis and NF-κappa B activation in response to diverse stimuli. *The EMBO journal* 14, 2876.
- Trembley, J.H., Loyer, P., Hu, D., Li, T., Grenet, J., Lahti, J.M., and Kidd, V.J. (2004). Cyclin dependent kinase 11 in RNA transcription and splicing. *Progress in nucleic acid research and molecular biology* 77, 263-288.
- Truhlar, S.M., Croy, C.H., Torpey, J.W., Koeppe, J.R., and Komives, E.A. (2006). Solvent accessibility of protein surfaces by amide H/2H exchange MALDI-TOF mass spectrometry. *Journal of the American Society for Mass Spectrometry* 17, 1490-1497.

- Truhlar, S.M.E., Mathes, E., Cervantes, C.F., Ghosh, G., and Komives, E.A. (2008). Pre-folding I κ B α Alters Control of NF- κ B Signaling. *Journal of Molecular Biology* 380, 67-82.
- Tsuchiya, Y., Asano, T., Nakayama, K., Kato Jr, T., Karin, M., and Kamata, H. (2010). Nuclear IKK β Is an Adaptor Protein for I κ B α Ubiquitination and Degradation in UV-Induced NF- κ B Activation. *Molecular cell* 39, 570-582.
- Tsuchiya, H., Otake, F., Arai, N., Kaiho, A., Yasuda, S., Tanaka, K., and Saeki, Y. (2017). In Vivo Ubiquitin Linkage-type Analysis Reveals that the Cdc48-Rad23/Dsk2 Axis Contributes to K48-Linked Chain Specificity of the Proteasome. *Molecular cell* 66, 488-502.e487.
- Tsvetkov, P., Asher, G., Paz, A., Reuven, N., Sussman, J.L., Silman, I., and Shaul, Y. (2008). Operational definition of intrinsically unstructured protein sequences based on susceptibility to the 20S proteasome. *Proteins* 70, 1357-1366.
- Tsvetkov, P., Reuven, N., and Shaul, Y. (2009). The nanny model for IDPs. *Nature chemical biology* 5, 778-781.
- Umar, S., Sarkar, S., Wang, Y., and Singh, P. (2009). Functional Cross-talk between β -Catenin and NF κ B Signaling Pathways in Colonic Crypts of Mice in Response to Progastrin. *The Journal of biological chemistry* 284, 22274-22284.
- Vallabhapurapu, S., Matsuzawa, A., Zhang, W., Tseng, P.H., Keats, J.J., Wang, H., Vignali, D.A., Bergsagel, P.L., and Karin, M. (2008). Nonredundant and complementary functions of TRAF2 and TRAF3 in a ubiquitination cascade that activates NIK-dependent alternative NF- κ B signaling. *Nat Immunol* 9, 1364-1370.
- Vallabhapurapu, S., and Karin, M. (2009). Regulation and function of NF- κ B transcription factors in the immune system. *Annu Rev Immunol* 27, 693-733.
- Van den Heuvel, S., and Harlow, E. (1993). Distinct roles for cyclin-dependent kinases in cell cycle control. *SCIENCE-NEW YORK THEN WASHINGTON-*, 2050-2050.
- van der Lee, R., Buljan, M., Lang, B., Weatheritt, R.J., Daughdrill, G.W., Dunker, A.K., Fuxreiter, M., Gough, J., Gsponer, J., Jones, D.T., et al. (2014). Classification of intrinsically disordered regions and proteins. *Chemical reviews* 114, 6589-6631.
- van der Lee, R., Lang, B., Kruse, K., Gsponer, J., Sánchez de Groot, N., Huynen, Martijn A., Matouschek, A., Fuxreiter, M., and Babu, M M. (2014). Intrinsically Disordered Segments Affect Protein Half-Life in the Cell and during Evolution. *Cell Reports* 8, 1832-1844.
- Varfolomeev, E., Blankenship, J.W., Wayson, S.M., Fedorova, A.V., Kayagaki, N., Garg, P., Zobel, K., Dynek, J.N., Elliott, L.O., Wallweber, H.J., et al. (2007). IAP antagonists induce autoubiquitination of c-IAPs, NF- κ B activation, and TNFalpha-dependent apoptosis. *Cell* 131, 669-681.
- Vermeulen, L., De Wilde, G., Van Damme, P., Vanden Berghe, W., and Haegeman, G. (2003). Transcriptional activation of the NF- κ B p65 subunit by mitogen- and stress-activated protein kinase-1 (MSK1). *Embo j* 22, 1313-1324.
- Viatour, P., Merville, M.P., Bouris, V., and Chariot, A. (2005). Phosphorylation of NF- κ B and I κ B proteins: implications in cancer and inflammation. *Trends Biochem Sci* 30, 43-52.
- Viemann, D., Goebeler, M., Schmid, S., Nordhues, U., Klimmek, K., Sorg, C., and Roth, J. (2006). TNF induces distinct gene expression programs in microvascular and macrovascular human endothelial cells. *J Leukoc Biol* 80, 174-185.
- Vietor, I., Schwenger, P., Li, W., Schlessinger, J., and Vilcek, J. (1993). Tumor necrosis factor-induced activation and increased tyrosine phosphorylation of mitogen-activated protein (MAP) kinase in human fibroblasts. *The Journal of biological chemistry* 268, 18994-18999.
- Vince, J.E., Wong, W.W.-L., Khan, N., Feltham, R., Chau, D., Ahmed, A.U., Benetatos, C.A., Chunduru, S.K., Condon, S.M., McKinlay, M., et al. IAP Antagonists Target cIAP1 to Induce TNFα-Dependent Apoptosis. *Cell* 131, 682-693.
- Vlantis, K., Wullaert, A., Polykratis, A., Kondylis, V., Dannappel, M., Schwarzer, R., Welz, P., Corona, T., Walczak, H., Weih, F., et al. (2016). NEMO Prevents RIP Kinase 1-Mediated Epithelial Cell Death and Chronic Intestinal Inflammation by NF- κ B-Dependent and -Independent Functions. *Immunity* 44, 553-567.
- von Mikecz, A. (2006). The nuclear ubiquitin-proteasome system. *J Cell Sci* 119, 1977-1984.
- Wajant, H., Pfizenmaier, K., and Scheurich, P. (2003). Tumor necrosis factor signaling. *Cell Death Differ* 10, 45-65.
- Wallenfang, M.R., and Seydoux, G. (2002). cdk-7 Is required for mRNA transcription and cell cycle progression in *Caenorhabditis elegans* embryos. *Proc Natl Acad Sci U S A* 99, 5527-5532.
- Walsh, I., Martin, A.J., Di Domenico, T., and Tosatto, S.C. (2012). ESpritz: accurate and fast prediction of protein disorder. *Bioinformatics* 28, 503-509.
- Wan, F., and Lenardo, M.J. (2009). Specification of DNA Binding Activity of NF- κ B Proteins. *Cold Spring Harbor Perspectives in Biology* 1, a000067.
- Wang, C. (2001). TAK1 is a ubiquitin-dependent kinase of MKK and IKK. *Nature* 412, 346-351.
- Wang, L., Du, F., and Wang, X. (2008). TNF-alpha induces two distinct caspase-8 activation pathways. *Cell* 133, 693-703.

- Wang, H., Moreau, F., Hirota, C.L., and MacNaughton, W.K. (2010). Proteinase-activated receptors induce interleukin-8 expression by intestinal epithelial cells through ERK/RSK90 activation and histone acetylation. *Faseb j* 24, 1971-1980.
- Wang, Y., Lu, J.-j., He, L., and Yu, Q. (2011). Triptolide (TPL) Inhibits Global Transcription by Inducing Proteasome-Dependent Degradation of RNA Polymerase II (Pol II). *PloS one* 6, e23993.
- Wang, Y., Mo, X., Piper, M.G., Wang, H., Parinandi, N.L., Guttridge, D., and Marsh, C.B. (2011). M-CSF induces monocyte survival by activating NF-kappaB p65 phosphorylation at Ser276 via protein kinase C. *PloS one* 6, e28081.
- Wang, David J., Ratnam, Nivedita M., Byrd, John C., and Guttridge, Denis C. (2014). NF- κ B Functions in Tumor Initiation by Suppressing the Surveillance of Both Innate and Adaptive Immune Cells. *Cell Reports* 9, 90-103.
- Wang, K., Kim, M.K., Di Caro, G., Wong, J., Shalapour, S., Wan, J., Zhang, W., Zhong, Z., Sanchez-Lopez, E., Wu, L.W., et al. (2014). Interleukin-17 receptor a signaling in transformed enterocytes promotes early colorectal tumorigenesis. *Immunity* 41, 1052-1063.
- Wang, B., Wei, H., Prabhu, L., Zhao, W., Martin, M., Hartley, A.V., and Lu, T. (2015). Role of Novel Serine 316 Phosphorylation of the p65 Subunit of NF-kappaB in Differential Gene Regulation. *The Journal of biological chemistry* 290, 20336-20347.
- Wang, K., and Karin, M. (2015). Chapter Five-Tumor-Elicited Inflammation and Colorectal Cancer. *Advances in cancer research* 128, 173-196.
- Wang, V.Y.-F., Li, Y., Kim, D., Zhong, X., Du, Q., Ghassemian, M., and Ghosh, G. (2017). Bcl3 Phosphorylation by Akt, Erk2, and IKK Is Required for Its Transcriptional Activity. *Molecular cell* 67, 484-497.e485.
- Watanabe, N., Broome, M., and Hunter, T. (1995). Regulation of the human WEE1Hu CDK tyrosine 15-kinase during the cell cycle. *The EMBO Journal* 14, 1878-1891.
- Weil, R., Laurent-Winter, C., and Israel, A. (1997). Regulation of IkappaBbeta degradation. Similarities to and differences from IkappaBalph. *The Journal of biological chemistry* 272, 9942-9949.
- Weinberg, R.A. (1995). The retinoblastoma protein and cell cycle control. *Cell* 81, 323-330.
- Weinstein, I.B., and Joe, A. (2008). Oncogene addiction. *Cancer Res* 68, 3077-3080; discussion 3080.
- Wertz, I.E., O'rourke, K.M., Zhou, H., and Eby, M. (2004). De-ubiquitination and ubiquitin ligase domains of A20 downregulate NF-kappaB signalling. *Nature* 430, 694.
- Wharry, C.E., Haines, K.M., Carroll, R.G., and May, M.J. (2009). Constitutive non-canonical NFkappaB signaling in pancreatic cancer cells. *Cancer Biol Ther* 8, 1567-1576.
- Whiteside, S.T., Epinat, J.C., Rice, N.R., and Israel, A. (1997). I kappa B epsilon, a novel member of the I kappa B family, controls RelA and cRel NF-kappa B activity. *Embo j* 16, 1413-1426.
- Whitmarsh, A.J., and Davis, R.J. (1996). Transcription factor AP-1 regulation by mitogen-activated protein kinase signal transduction pathways. *Journal of molecular medicine (Berlin, Germany)* 74, 589-607.
- Whittaker, S.R., Te Poel, R.H., Chan, F., Linardopoulos, S., Walton, M.I., Garrett, M.D., and Workman, P. (2007). The cyclin-dependent kinase inhibitor seliciclib (R-roscovitine; CYC202) decreases the expression of mitotic control genes and prevents entry into mitosis. *Cell Cycle* 6, 3114-3131.
- Wicovsky, A., Henkler, F., Salzmann, S., Scheurich, P., Kneitz, C., and Wajant, H. (2009). Tumor necrosis factor receptor-associated factor-1 enhances proinflammatory TNF receptor-2 signaling and modifies TNFR1-TNFR2 cooperation. *Oncogene* 28, 1769-1781.
- Wiebusch, L., and Hagemeier, C. (2010). p53-and p21-dependent premature APC/C-Cdh1 activation in G2 is part of the long-term response to genotoxic stress. *Oncogene* 29, 3477.
- Wiggins, C.M., Tsvetkov, P., Johnson, M., Joyce, C.L., Lamb, C.A., Bryant, N.J., Komander, D., Shaul, Y., and Cook, S.J. (2011). BIM(EL), an intrinsically disordered protein, is degraded by 20S proteasomes in the absence of poly-ubiquitylation. *J Cell Sci* 124, 969-977.
- Windheim, M., Stafford, M., Peggie, M., and Cohen, P. (2008). Interleukin-1 (IL-1) induces the Lys63-linked polyubiquitination of IL-1 receptor-associated kinase 1 to facilitate NEMO binding and the activation of I[kappa]B[alpha] kinase. *Mol Cell Biol* 28, 1783-1791.
- Wood, L.D., Parsons, D.W., Jones, S., Lin, J., Sjöblom, T., Leary, R.J., Shen, D., Boca, S.M., Barber, T., Ptak, J., et al. (2007). The genomic landscapes of human breast and colorectal cancers. *Science* 318, 1108-1113.
- Wu, J.J., and Bennett, A.M. (2005). Essential Role for Mitogen-activated Protein (MAP) Kinase Phosphatase-1 in Stress-responsive MAP Kinase and Cell Survival Signaling. *Journal of Biological Chemistry* 280, 16461-16466.
- Wu, C.J., Conze, D.B., Li, T., Srinivasula, S.M., and Ashwell, J.D. (2006). Sensing of Lys 63-linked polyubiquitination by NEMO is a key event in NF-[kappa]B activation. *Nature Cell Biol* 8, 398-406.
- Wu, Z.H., Shi, Y., Tibbetts, R.S., and Miyamoto, S. (2006). Molecular linkage between the kinase ATM and NF-kappaB signaling in response to genotoxic stimuli. *Science* 311, 1141-1146.

- Wu, Z.H., and Miyamoto, S. (2008). Induction of a pro-apoptotic ATM-NF-kappaB pathway and its repression by ATR in response to replication stress. *Embo J* 27, 1963-1973.
- Wu, Y., Deng, J., Rychahou, P.G., Qiu, S., Evers, B.M., and Zhou, B.P. (2009). Stabilization of snail by NF-kappaB is required for inflammation-induced cell migration and invasion. *Cancer Cell* 15, 416-428.
- Wu, L., Shao, L., Li, M., Zheng, J., Wang, J., Feng, W., Chang, J., Wang, Y., Hauer-Jensen, M., and Zhou, D. (2013). BMS-345541 sensitizes MCF-7 breast cancer cells to ionizing radiation by selective inhibition of homologous recombinational repair of DNA double-strand breaks. *Radiation research* 179, 160-170.
- Wuerzberger-Davis, S.M., Chang, P.Y., Berchtold, C., and Miyamoto, S. (2005). Enhanced G2-M arrest by nuclear factor-{kappa}B-dependent p21waf1/cip1 induction. *Molecular cancer research : MCR* 3, 345-353.
- Wulczyn, F.G., Naumann, M., and Scheidereit, C. (1992). Candidate proto-oncogene bcl-3 encodes a subunit-specific inhibitor of transcription factor NF-kappa B. *Nature* 358, 597-599.
- Xia, Z.P., Sun, L., Chen, X., Pineda, G., Jiang, X., Adhikari, A., Zeng, W., and Chen, Z.J. (2009). Direct activation of protein kinases by unanchored polyubiquitin chains. *Nature* 461, 114-119.
- Xia, Y., Yeddula, N., Leblanc, M., Ke, E., Zhang, Y., Oldfield, E., Shaw, R.J., and Verma, I.M. (2012). Reduced cell proliferation by IKK2 depletion in a mouse lung-cancer model. *Nat Cell Biol* 14, 257-265.
- Xia, Y., Shen, S., and Verma, I.M. (2014). NF- κ B, an active player in human cancers. *Cancer immunology research* 2, 823-830.
- Xiao, G., Harhaj, E.W., and Sun, S.C. (2001). NF-kappaB-inducing kinase regulates the processing of NF-kappaB2 p100. *Molecular cell* 7, 401-409.
- Xiao, Z., Jiang, Q., Willette-Brown, J., Xi, S., Zhu, F., Burkett, S., Back, T., Song, N.Y., Datla, M., Sun, Z., et al. (2013). The pivotal role of IKKalpha in the development of spontaneous lung squamous cell carcinomas. *Cancer Cell* 23, 527-540.
- Xie, H., Vucetic, S., Iakoucheva, L.M., Oldfield, C.J., Dunker, A.K., Obradovic, Z., and Uversky, V.N. (2007). Functional anthology of intrinsic disorder. 3. Ligands, post-translational modifications, and diseases associated with intrinsically disordered proteins. *J Proteome Res* 6, 1917-1932.
- Xu, X., Prorock, C., Ishikawa, H., Maldonado, E., Ito, Y., and Gelinas, C. (1993). Functional interaction of the v-Rel and c-Rel oncoproteins with the TATA-binding protein and association with transcription factor IIB. *Mol Cell Biol* 13, 6733-6741.
- Xu, M., Skaug, B., Zeng, W., and Chen, Z.J. (2009). A Ubiquitin Replacement Strategy in Human Cells Reveals Distinct Mechanisms of IKK Activation by TNF α and IL-1 β . *Molecular cell* 36, 302-314.
- Xu, G., Lo, Y.C., Li, Q., Napolitano, G., Wu, X., Jiang, X., Dreano, M., Karin, M., and Wu, H. (2011). Crystal structure of inhibitor of kappaB kinase beta. *Nature* 472, 325-330.
- Xu, J., Zhou, L., Ji, L., Chen, F., Fortmann, K., Zhang, K., Liu, Q., Li, K., Wang, W., Wang, H., et al. (2016). The REGgamma-proteasome forms a regulatory circuit with IkappaBvarepsilon and NFkappaB in experimental colitis. *Nat Commun* 7, 10761.
- Xue, W., Meylan, E., Oliver, T.G., Feldser, D.M., Winslow, M.M., Bronson, R., and Jacks, T. (2011). Response and Resistance to NF- κ B Inhibitors in Mouse Models of Lung Adenocarcinoma. *Cancer Discovery*.
- Xue, B., Blocquel, D., Habchi, J., Uversky, A.V., Kurgan, L., Uversky, V.N., and Longhi, S. (2014). Structural disorder in viral proteins. *Chemical reviews* 114, 6880-6911.
- Yamaguchi, T., Kimura, J., Miki, Y., and Yoshida, K. (2007). The deubiquitinating enzyme USP11 controls an IkappaB kinase alpha (IKKalpha)-p53 signaling pathway in response to tumor necrosis factor alpha (TNFalpha). *The Journal of biological chemistry* 282, 33943-33948.
- Yamamoto, A., Tagawa, Y., Yoshimori, T., Moriyama, Y., Masaki, R., and Tashiro, Y. (1998). Bafilomycin A1 prevents maturation of autophagic vacuoles by inhibiting fusion between autophagosomes and lysosomes in rat hepatoma cell line, H-4-II-E cells. *Cell structure and function* 23, 33-42.
- Yamamoto, M., Yamazaki, S., Uematsu, S., Sato, S., Hemmi, H., Hoshino, K., Kaisho, T., Kuwata, H., Takeuchi, O., Takeshige, K., et al. (2004). Regulation of Toll/IL-1-receptor-mediated gene expression by the inducible nuclear protein IkappaBzeta. *Nature* 430, 218-222.
- Yamaoka, S., Courtois, G., Bessia, C., Whiteside, S.T., Weil, R., Agou, F., Kirk, H.E., Kay, R.J., and Israël, A. (1998). Complementation Cloning of NEMO, a Component of the I κ B Kinase Complex Essential for NF- κ B Activation. *Cell* 93, 1231-1240.
- Yang, T., Buchan, H.L., Townsend, K.J., and Craig, R.W. (1996). MCL-1, a member of the BLC-2 family, is induced rapidly in response to signals for cell differentiation or death, but not to signals for cell proliferation. *J Cell Physiol* 166, 523-536.
- Yang, J., and Weinberg, R.A. (2008). Epithelial-mesenchymal transition: at the crossroads of development and tumor metastasis. *Dev Cell* 14, 818-829.
- Yang, J., Splittergerber, R., Yull, F.E., Kantrow, S., Ayers, G.D., Karin, M., and Richmond, A. (2010). Conditional ablation of Ikk β inhibits melanoma tumor development in mice. *The Journal of Clinical Investigation* 120, 2563-2574.

- Yang, Y., Wu, J., and Wang, J. (2016). A database and functional annotation of NF- κ B target genes. *Int J Clin Exp Med* 9, 9.
- Yao, Z., Zhou, G., Wang, X.S., Brown, A., Diener, K., Gan, H., and Tan, T.H. (1999). A novel human STE20-related protein kinase, HGK, that specifically activates the c-Jun N-terminal kinase signaling pathway. *The Journal of biological chemistry* 274, 2118-2125.
- Ye, J., Xie, X., Tarassishin, L., and Horwitz, M.S. (2000). Regulation of the NF- κ B activation pathway by isolated domains of FIP3/IKKgamma, a component of the IkappaB-alpha kinase complex. *The Journal of biological chemistry* 275, 9882-9889.
- Yeh, W.C., Shahinian, A., Speiser, D., Kraunus, J., Billia, F., Wakeham, A., de la Pompa, J.L., Ferrick, D., Hum, B., Iscove, N., et al. (1997). Early lethality, functional NF- κ B activation, and increased sensitivity to TNF-induced cell death in TRAF2-deficient mice. *Immunity* 7, 715-725.
- Yewdell, J.W., Lacsina, J.R., Rechsteiner, M.C., and Nicchitta, C.V. (2011). Out with the Old, In with the New? Comparing Methods for Measuring Protein Degradation. *Cell biology international* 35, 457-462.
- Yin, Q., Lamothe, B., Darnay, B.G., and Wu, H. (2009). Structural basis for the lack of E2 interaction in the RING domain of TRAF2. *Biochemistry* 48, 10558-10567.
- Yoon, M.-K., Mitrea, D.M., Ou, L., and Kriwacki, R.W. (2012). Cell cycle regulation by the intrinsically disordered proteins p21 and p27 (Portland Press Limited).
- Yoshikawa, A., Sato, Y., Yamashita, M., Mimura, H., Yamagata, A., and Fukai, S. (2009). Crystal structure of the NEMO ubiquitin-binding domain in complex with Lys 63-linked di-ubiquitin. *FEBS Lett* 583, 3317-3322.
- Yoshimori, T., Yamamoto, A., Moriyama, Y., Futai, M., and Tashiro, Y. (1991). Bafilomycin A1, a specific inhibitor of vacuolar-type H(+)-ATPase, inhibits acidification and protein degradation in lysosomes of cultured cells. *Journal of Biological Chemistry* 266, 17707-17712.
- Yu, H.-G., Yu, L.-L., Yang, Y., Luo, H.-S., Yu, J.-P., Meier, J.J., Schrader, H., Bastian, A., Schmidt, W.E., and Schmitz, F. (2003). Increased Expression of RelA/Nuclear Factor- κ B Protein Correlates with Colorectal Tumorigenesis. *Oncology* 65, 37-45.
- Yu, H., Kago, G., Yellman, C.M., and Matouschek, A. (2016). Ubiquitin-like domains can target to the proteasome but proteolysis requires a disordered region. *Embo j* 35, 1522-1536.
- Yuasa, T., Ohno, S., Kehrl, J.H., and Kyriakis, J.M. (1998). Tumor necrosis factor signaling to stress-activated protein kinase (SAPK)/Jun NH2-terminal kinase (JNK) and p38. Germinal center kinase couples TRAF2 to mitogen-activated protein kinase/ERK kinase kinase 1 and SAPK while receptor interacting protein associates with a mitogen-activated protein kinase kinase kinase upstream of MKK6 and p38. *The Journal of biological chemistry* 273, 22681-22692.
- Zaph, C., Troy, A.E., Taylor, B.C., Berman-Booty, L.D., Guild, K.J., Du, Y., Yost, E.A., Gruber, A.D., May, M.J., Greten, F.R., et al. (2007). Epithelial-cell-intrinsic IKK-[bgr] expression regulates intestinal immune homeostasis. *Nature* 446, 552-556.
- Zarnegar, B., Yamazaki, S., He, J.Q., and Cheng, G. (2008). Control of canonical NF- κ B activation through the NIK-IKK complex pathway. *Proc Natl Acad Sci U S A* 105, 3503-3508.
- Zarnegar, B.J., Wang, Y., Mahoney, D.J., Dempsey, P.W., Cheung, H.H., He, J., Shiba, T., Yang, X., Yeh, W.C., Mak, T.W., et al. (2008). Noncanonical NF- κ B activation requires coordinated assembly of a regulatory complex of the adaptors cIAP1, cIAP2, TRAF2 and TRAF3 and the kinase NIK. *Nat Immunol* 9, 1371-1378.
- Zeng, Y., and Cullen, B.R. (2003). Sequence requirements for micro RNA processing and function in human cells. *Rna* 9, 112-123.
- Zhang, J., Chang, C.C., Lombardi, L., and Dalla-Favera, R. (1994). Rearranged NFKB2 gene in the HUT78 T-lymphoma cell line codes for a constitutively nuclear factor lacking transcriptional repressor functions. *Oncogene* 9, 1931-1937.
- Zhang, Q., Didonato, J.A., Karin, M., and McKeithan, T.W. (1994). BCL3 encodes a nuclear protein which can alter the subcellular location of NF- κ B proteins. *Mol Cell Biol* 14, 3915-3926.
- Zhang, K., Zhao, J., Liu, X., Yan, B., Chen, D., Gao, Y., Hu, X., Liu, S., Zhang, D., and Zhou, C. (2011). Activation of NF-B upregulates Snail and consequent repression of E-cadherin in cholangiocarcinoma cell invasion. *Hepato-gastroenterology* 58, 1-7.
- Zhang, J., Clark, K., Lawrence, T., Peggie, M.W., and Cohen, P. (2014). An unexpected twist to the activation of IKK β : TAK1 primes IKK β for activation by autophosphorylation. *Biochemical Journal* 461, 531-537.
- Zheng, C., Kabaleeswaran, V., Wang, Y., Cheng, G., and Wu, H. (2010). Crystal Structures of the TRAF2: cIAP2 and the TRAF1: TRAF2: cIAP2 Complexes: Affinity, Specificity, and Regulation. *Molecular cell* 38, 101-113.
- Zheng, C., Yin, Q., and Wu, H. (2011). Structural studies of NF- κ B signaling. *Cell Res* 21, 183-195.
- Zhong, H., Voll, R.E., and Ghosh, S. (1998). Phosphorylation of NF- κ B p65 by PKA stimulates transcriptional activity by promoting a novel bivalent interaction with the coactivator CBP/p300. *Molecular cell* 1, 661-671.

- Zhou, A., Scoggin, S., Gaynor, R.B., and Williams, N.S. (2003). Identification of NF-kappa B-regulated genes induced by TNFalpha utilizing expression profiling and RNA interference. *Oncogene* 22, 2054-2064.
- Zhou, B.P., Deng, J., Xia, W., Xu, J., Li, Y.M., Gunduz, M., and Hung, M.C. (2004). Dual regulation of Snail by GSK-3beta-mediated phosphorylation in control of epithelial-mesenchymal transition. *Nat Cell Biol* 6, 931-940.
- Zhou, Y., Han, C., Li, D., Yu, Z., Li, F., Li, F., An, Q., Bai, H., Zhang, X., Duan, Z., *et al.* (2015). Cyclin-dependent kinase 11(p110) (CDK11(p110)) is crucial for human breast cancer cell proliferation and growth. *Scientific reports* 5, 10433.
- Zins, K., Abraham, D., Sioud, M., and Aharinejad, S. (2007). Colon cancer cell-derived tumor necrosis factor-alpha mediates the tumor growth-promoting response in macrophages by up-regulating the colony-stimulating factor-1 pathway. *Cancer Res* 67, 1038-1045.